AD NUMBER
ADB010468
LIMITATION CHANGES

TO:

Approved for public release; distribution is unlimited.

FROM:

Distribution authorized to U.S. Gov't. agencies only; Test and Evaluation; 23 APR 1976. Other requests shall be referred to Supersonic Transport Office, Washington, DC 20590.

AUTHORITY

FAA ltr, 26 Apr 1977

SUPERSONIC TRANSPORT NOISE REDUCTION

TECHNOLOGY PROGRAM

PHASE II
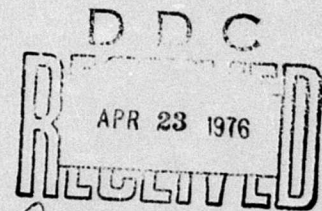
VOLUME I

J.T.BLOZY   R.B.MISHLER

V.L.DOYLE   R.L.NEBUDA

S.B.KAZIN   E.J.STRINGAS

A.R. SIECKMAN

GROUP ENGINEERING DIVISION
Aircraft Engine Group
General Electric Company
Cincinnati, Ohio 45215

FINAL REPORT

SEPTEMBER, 1975

ADB010468

DDC FILE COPY

AD No.

DDC
RECEIVED
APR 23 1976
B

The contents of this report reflect the views of the
General Electric Company, which is responsible for
the facts and the accuracy of the data presented
herein. The contents do not necessarily reflect the
official views or policy of the Department of
Transportation. This report does not constitute a
standard, specification, or regulation.

1. Report No. FAA-SS-73-29-1	2. Government Accession No.	3. Recipient's Catalog No.

4. Title and Subtitle	5. Report Date
Supersonic Transport Noise Reduction Technology Program - Phase II, Volume I.	September, 1975
	6. Performing Organization Code

7. Author(s)	8. Performing Organization Report No.
S.B. Kazin and E.J. Stringas (Program Technical Directors) J.T. Blozy, V.L. Doyle, R.B. Mishler, R.L. Nebuda, A.R. Sieckman	R75AEG362 Vol-1

9. Performing Organization Name and Address	10. Work Unit No.
Group Engineering Division Aircraft Engine Group General Electric Company Cincinnati, Ohio 45215	478 p.
	11. Contract or Grant No. DOT-FA72WA-2894 new

12. Sponsoring Agency Name and Address	13. Type of Report and Period Covered
Department of Transportation Federal Aviation Administration Supersonic Transport Office Washington, D.C. 20590	Final rept.
	14. Sponsoring Agency Code

15. Supplementary Notes

16. Abstract

The Supersonic Transport Noise Reduction Technology Program, sponsored by the Federal Aviation Administration, was conducted as a follow-on effort after cancellation of the SST Program to finalize selected noise technology areas and summarize results of the SST Program. Using initial effects of the SST Program, as summarized in Phase I of The Supersonic Transport Noise Reduction Technology Program, the Phase II contract was issued to the General Electric Company (and Boeing to continue this important work. The overall program objective was to provide additional acoustic technology necessary to design high speed aircraft systems, recognizing future acceptable noise levels. General Electric's effort was divided into the acoustic technology areas of jet noise reduction, turbomachinery noise reduction, and aircraft system integration.

Jet noise reduction technology work was achieved through analytical studies, model tests, and J79 engine tests. Selected suppression systems identified during the SST Program were further refined (multispoke/chute suppressors or annular plug nozzles). Novel advanced concepts of suppression were identified, and extensive aerodynamic (static and wind-on) performance tests and hot-jet acoustic tests were performed.

Both compressor and turbine noise were studied in the turbomachinery noise reduction areas. A 3-stage low pressure compressor with variable-flap inlet guide vanes was tested at General Electric's outdoor test site. A hybrid inlet, which employs airflow acceleration suppression in combination with wall acoustic treatment, was investigated as the suppression device for all three noise monitoring point operating conditions. The effect of auxiliary inlets on noise leakage and suppression was studied for takeoff mode. Also, variable inlet guide vane flaps were used to reduce area and generate high passage Mach numbers as another means of compressor noise suppression. Turbine noise was studied using a J85 engine with massive inlet suppressor and open nozzle to unmask the turbine. Second-stage turbine blade/nozzle spacing and exhaust acoustic treatment were investigated as means of turbine noise suppression.

The best performing components from noise suppression work performed under the jet and turbomachinery noise reduction tasks were integrated into a viable-type aircraft-engine system study. Overall system noise was evaluated from EPNL estimates of the suppressed and unsuppressed SST systems relating to the current FAR Part 36 Noise Regulations.

17. Key Words (Suggested by Author(s))	18. Distribution Statement
Jet Noise, High Velocity Suppression, Aircraft Engine Suppression, Turbomachinery Noise, Hybrid Inlet Aircraft Engine Suppression Integration	Approved for U.S. Government only. Transmittal of this document outside the U.S. Government must have prior approval of the Supersonic Transport Office.

19. Security Classif. (of this report)	20. Security Classif. (of this page)	21. No. of Pages	22. Price*
Unclassified	Unclassified	849	

403 468

PREFACE

TABLE OF CONTENTS

VOLUME I

VOLUME II

TABLE OF CONTENTS (concluded)

LIST OF ILLUSTRATIONS

VOLUME I

LIST OF ILLUSTRATIONS (Continued)

LIST OF ILLUSTRATIONS (Continued)

LIST OF ILLUSTRATIONS (Continued)

LIST OF ILLUSTRATIONS (Continued)

LIST OF ILLUSTRATIONS (Continued)

LIST OF ILLUSTRATIONS (Continued)

LIST OF ILLUSTRATIONS (Continued)

LIST OF ILLUSTRATIONS (Continued)

LIST OF ILLUSTRATIONS (Continued)

LIST OF ILLUSTRATIONS (Continued)

LIST OF ILLUSTRATIONS (Continued)

LIST OF ILLUSTRATIONS (Continued)

VOLUME II

LIST OF ILLUSTRATIONS (Continued)

LIST OF ILLUSTRATIONS (Continued)

LIST OF ILLUSTRATIONS (Continued)

LIST OF ILLUSTRATIONS (Continued)

LIST OF ILLUSTRATIONS (Continued)

LIST OF ILLUSTRATIONS (Continued)

LIST OF ILLUSTRATIONS (Concluded)

LIST OF TABLES

VOLUME I

VOLUME II

LIST OF TABLES (Continued)

LIST OF TABLES (Continued)

LIST OF TABLES (Continued)

LIST OF TABLES (Concluded)

NOMENCLATURE

Symbol	Description	Units
A	Area	$(in.^2, ft^2)$
A_8	Physical primary nozzle exit (throat) plane area	$(in.^2), (ft^2)$
A_{e8}	Effective throat area	$(in.^2), (ft^2)$
A_9	Nozzle exit plane area	$(in.^2), (ft^2)$
A_{18}	Fan stream exit area	$(in.^2), (ft^2)$
A_B	Blocked area	$(in.^2), (ft^2)$
AR_d	Area ratio: ratio of total area (annulus for plug nozzles, plane for 2-D nozzles) to physical flow area	- - -
a	Ellipse semimajor axis	(in.)
AST	Advanced supersonic transport	- - -
B	Turbine blade	- - -
BID	Blow-in-door	- - -
BPF	Blade passing frequency	(Hz)
b	Ellipse semiminor axis	(in.)
C	Coefficient	- - -
C_1, C_2, etc	Compressor rotor	- - -
$C_1 - F_2$	Compressor rotor - 2nd harmonic	(Hz)
C_{fg}	Nozzle gross thrust coefficient (static and wind-on)	- - -
C_D	Nozzle discharge coefficient (ratio of actual to ideal flow rates) or inlet area coefficient (ratio of actual to physical flow area)	
C_x	Axial balance readout	counts
C_{pp}	Normalized cross-correlation function in-jet to far-field	- - -
c	Speed of sound	(ft/sec)
D	Diameter	(in.), (ft)
D_F	Aerodynamic drag force	lb_f
D_o	Nozzle physical outer dia.	(in.)
D_t	Tube internal diameter	(in.)
D_{Td}	Circumscribed tube bundle diameter	(in.)
D_8	Internal diameter of conical primary nozzle at primary exit, plane 8	(in.)
D_9	Internal diameter of nozzle at plane 9	(in.)
dm	Outer shroud diameter	(in.)
dB	Decibel, re 0.0002 dyne/in.^{2}	(dB)
Dv	Discharge valve	- - -
EGT	Exhaust gas temperature	(° R)
EPNL	Effective perceived noise level	(EPNdB)
EPNdB	Unit of effective perceived noise level	
F	Sabbl separation parameter	- - -
Fg, fg	Measured gross thrust (stream)	(lb_f)
F_N	Net thrust	(lb_f)

Symbol	Description	Units
f	Frequency	(Hz)
G	Real-gas stream thrust correlation factor	- - -
H	Axial thrust	(lb)
H_x	Axial balance force	(lb)
H_8	2-D nozzle throat height (normal)	(in.)
H_p	2-D ramp (plug) rize	(in.)
$\bar{H}$	2-D immersion depth parameter	(in.)
HPT	High pressure turbine	- - -
$\bar{h}$	Conical ejector annulus height (mean)	(in.)
h_1, h_2	2-D suppressor height	(in.)
h	2-D primary flow passage height	(in.)
H	Height	(in.)
h	Pressure altitude	(ft)
IGV	Inlet guide vane	- - -
j	$\sqrt{-1}$ imaginary number	
$jX/\rho c$	Normalized reactance (imaginary part of complex acoustic impedance)	- - -
K_{cr}	Critical flow factor	$\sqrt{^\circ R}$/sec
K_e	Fan-core (dual-flow) exit plane offset distance ~ 5.75"	(in.)
k	Isentropic ratio of specific heats (1.4)	
L	Calibration load	(lb)
L	Length	in., ft
L_p	Axial length of 2-D ramp	(in.)
L_z	Axial reference location of variable position inlet centerbody	
L_s	Shroud internal length	(in.)
L_t	Tube external diameter	(in.)
LPC	Low pressure compressor	- - -
LPT	Low pressure turbine	- - -
M	Mach number	- - -
M_o	Freestream Mach number	- - -
M_j	Jet stream Mach number	- - -
$M_{a/c}$	Aircraft Mach number	- - -
MPT	Multiple pure tone	- - -
m	Mass flow rate	(lbm/sec)
M_{th}	Throat Mach number	- - -
N	Nozzle	- - -
N	Rotational speed	rpm
$\%N_c$	Percent corrected speed	%
$N/\sqrt{\theta}$	Corrected speed	rpm
n	Number	- - -
NR	Narrowband	- - -
NOY	Annoyance weight SPL; used to calculate PNL	(NOY)

Symbol	Description	Units
OB	Octave band	- - -
OAPWL	Overall sound power level re 10^{-13} watts	dB
OAJPL	Overall jet pressure level(aerodynamic pressure, rms)	dB
OASPL	Overall sound pressure level	dB
P	Pressure	psia, psig
P_o	Ambient free stream pressure	psia, psig
P_b	Suppressor base static pressure	psia, psig
P_s	Static pressure (surface)	psia, psig
P_w	Wall surface pressure	psia, psig
P_r	Pressure ratio	- - -
PT8	Nozzle exit total pressure	psia
ΔP	Static pressure difference	psi
PWL	Sound power level, re 10^{-13} watts	dB
$(\Delta P_T/P_T)_{Max.}$	Inlet total pressure distortion =	$\dfrac{(P_{TMax} - P_{TMin.})}{P_{TAv}}$
PNL	Perceived noise level	PNdB
PNdB	Unit of perceived noise level	- - -
P_F	Sound pressure in far field	(psi)
$P_j(t)$	Sound pressure in jet	(psi)
qc	Compressible dynamic pressure,	$P_T - P_S$
R	Resistance	
R	Radius	
R_o	Outer flowpath contour radius	(in.)
R_i	Inner flowpath contour radius	(in.)
$R/\rho c$	Normalized resistance (real part of complex acoustic impedance)	(in.)
RPM	Revolutions per minute	- - -
R1	Rotor one – 1st stage rotor	rpm
R_N	Reynolds number	- - -
r	Radial distance	- - -
RH	Relative humidity	(in.)
r_i	Immersion radius	%
r_o	Outer (tip) radius	(in.)
r_h	Hub (inner) radius	(in.)
S	Distance between $\mathcal{L}$ of tube rows	(in.)
S_j	In-jet Strouhal number fD/V	(in.)
$S_j^2 \cdot \overline{P_F\,P_j}(t)$	Source function distribution	- - -
SPL	Sound pressure level	- - -
SL	Sideline distance	dB
SDOF	Single degree of freedom	- - -
SST	Supersonic transport	- - -
SABBL	Stratford and Beavers boundary layer analysis – computer program	- - -

Symbol	Description	Units
SM	Compressor stall margin	%
STC	Streamtube curvature – compressible potential flow computer program	- - -
T	Temperature	°R
T_{T8}	Nozzle exit total temperature	°R
T_1, T_2	Turbine Stage 1, Stage 2, etc.	- - -
U	Rotor tangential velocity	ft/sec
U_t, V_T	Rotor tip speed	ft/sec
$\underline{u}'$	Turbulent particle velocity	ft/sec
$\underline{u}$	Mean particle velocity	ft/sec
V, v	Velocity	ft/sec
V_c	Core stream velocity	ft/sec
V_F	Fan bypass stream velocity	ft/sec
V_J, V_j	Fully expanded ideal jet velocity	ft/sec
VSF	Vortex shedding frequency	Hz
W, ω	Weight flow rate	lb/sec
w	Width	(in.)
W_e, W_{ej}	Secondary entrained flow	lb/sec
W_8	Nozzle primary flow	lb/sec
W_T	Total primary and secondary flow	lb/sec
W_2	Induced flow	lb/sec
WFB	Flow width at basis (hub)	(in.)
WFT	Flow width at tip (casing)	(in.)
x	Axial distance	(in.)
X	Reactance	- - -
Y	Ramp normal coordinate direction	(in.)
Z	Axial coordinate from geometric 2-D unsuppressed nozzle throat	(in.)
Z	Aerodynamic axial calculation station	(in.)
10 log ρA	Normalizing factor (SPL and PNL) for size & test condition variance (deg)	
α	Angle of attack	(deg)
β	Bypass ratio	- - -
β	Orifice coefficient	- - -
θ	Angle between a straight line from source to microphone and engine or nozzle ₵ ; ref to inlet or exhaust (acoustic angle)	(deg)
θ	Diffusion angle	(deg)
θ	Corrected total temperature $(\frac{T_{act}}{T_o})$	
δ	Corrected total pressure $(\frac{P_{act}}{P_o})$	
ρ	Jet stream density	lbm/ft^3
∂	Ratio of specific heats	- - -
Δ	Incremental quantity	- - -
λ	Pressure ratio's wave length	(ft)
η_R	Inlet total pressure recovery factor	- - -

NOMENCLATURE (Concluded)

Symbol	Description	Units

Subscripts

AMB, a	Ambient	
ANN	Annulus	
Av	Average	
B	Blocked	
BID	Blow-in-door	
b	Base	
C	Core	
CH	Chute	
D	Subsonic diffuser	
d	Discharge	
e	Effective	
e	Exit	
EN	Entrance	
EQ	Equivalent	
Ex	Exit	
F	Fan	
I	Inlet	
i	Ideal	
j,	Jet	
H	Hub	
Max.	Maximum	
Min.	Minimum	
O	Freestream or ambient condition	
Overall	Combined primary & BID performance	
PRI	Primary inlet	
SP	Spoke	
S	Static condition	
t,T	Total conditions	
T	Tip	
TE	Trailing edge	
th, TH	Throat	
Total	Sum of primary & BID properties	
Venturi	Venturi-measured flowrate	
w	Wall	
.5	Compressor entrance station	
1	Metering nozzle station - wind tunnel	
2	Diffuser exit (aero-traverse) station	
2.5C	Compressor discharge station	
3	Flexible seal station - wind tunnel	
7	Measurement plane for nozzle throat P_T and T_T	
8	Nozzle throat plane	
9	Nozzle exit plane	
18	Fan bypass exhaust throat plane	

1.0 INTRODUCTION

1.1 BACKGROUND

In 1964 General Electric entered the competition to provide the power-plant for the United States Supersonic Transport and, ultimately, was awarded the contract in late 1966 to develop the engines for the prototype aircraft.

At the initial conception of the Supersonic Transport Program, noise (especially as it affects the community around airports) was a matter of concern but did not dominate in the engine selection and design. The initial approach was one of establishing the most economically attractive engine/airframe combination and then identifying the operational procedures which provided the minimum community noise intrusion. As the SST program progressed, the impact of noise became more pronounced; and, for Phase III of the program, noise goals both at takeoff and approach were set as requirements.

The original engine proposed by General Electric in 1966 (designated GE4) was a 475 lbs/sec, fully augmented turbojet with a two-stage ejector nozzle. To meet the quoted noise goals at the community and approach location, the exhaust nozzle was operated on an open area schedule with the inlet choked.

During the course of the program, although the engine cycle remained relatively constant, the engine increased in size; and, the power settings at takeoff and approach were raised to be consistent with increases in aircraft weight and modified design. These changes, in conjunction with a reduction in the acceptable noise levels as community reaction to noise became more evident, caused a rapid increase in emphasis in technology to control the supersonic jet noise and turbomachinery noise as the program progressed.

Based upon analysis and a vast background of engine, component, and model scale testing, it was shown that the limiting noise source at the sideline monitoring point was the jet; the turbomachinery was the major noise contributor at approach. At the community monitoring point, both jet and turbomachinery noise could be important, the dominance depending upon engine size and exact power setting.

Research and development in support of the suppressed GE4 exhaust system necessitated an extensive effort in the field of basic supersonic jet noise technology and its application to the development of a viable jet noise suppressor. Major categories of concepts tested were:

- High-flow ejectors
- Primary rod, tab, and chute systems
- Secondary ejectors with rod, flap, and chute systems

1

- Fluid injection

- Multispoke-chute and tube systems for conical and similar nozzle systems

During the later phases of the Supersonic Transport Program, it became evident that current jet noise suppression technology could not develop a fully augmented turbojet engine capable of meeting acceptable noise levels. Mutual agreements among Boeing, DOT, the Airlines, and General Electric (continually reassessing the B2707-300 aircraft noise goals) kept reducing the allowable noise (see Table 1), with each change more closely aligned with the new subsonic aircraft noise limitations. The GE4 augmented turbojet was reconfigured in line with the earlier goals; however, achieving the final noise goals required a substantial engine modification and advanced suppression techniques. Thorough design studies of high-airflow engines and noise suppression systems were conducted. These studies were supported by scale model acoustic and aerodynamic test programs. The recommended engine configuration at the conclusion of the program was a high-flow turbojet engine operating without augmentation at takeoff.

The suppressor concepts which provided the most favorable combination of high jet noise suppression for given thrust and weight penalties were in the form of multielement spoke/chute plug nozzle geometries. The systems were designed to be the most beneficial in the lift-off exhaust nozzle velocity range of 2300-2500 ft/sec for the high-flow engines. The suppressor elements could be deployed from a stowed position within the central plug and form the throat of the nozzle, sealing with the translating annular shroud. Therefore, the retractable suppressors would not penalize the cycle when suppression was not required at the important cruise condition.

An extensive model acoustic and wind tunnel aerodynamic test program was conducted (see Reference 1). By proper selection of spoke/chute plug nozzle geometric parameters, 8.5 EPNL gross suppression with a 6% thrust loss was thought attainable. Several of these suppressor configurations, with a direct application to the high-flow engine/exhaust system concept, were subjected to in-flight acoustic testing at J85 scale on an F-106 aircraft. The results of these in-flight tests are reported in Reference 2.

The demonstrated suppression level was intended to satisfy the dry turbojet requirements in late 1970 necessary to meet a 112-EPNL sideline goal. Further Airline/Boeing/General Electric meetings established that, in line with this new concept, the subsonic aircraft FAR Part 36 noise regulations would be the new GE4/B2707-300 goals. This would be accomplished through jet suppressor refinement to meet 108-110 EPNL sideline noise levels as shown in Table 1, early in 1971.

While jet noise was known to pose a severe problem for the SST, particularly at the sideline measuring condition, the turbomachinery noise problem at the approach and community monitoring points was not clearly defined. In fact, the magnitude of noise reduction required and the complexity of the approach to the solution was not understood until acoustic testing of the choked inlet on a full-scale GE4 engine had been conducted. The results

2

Table 1. GE4/B2707-300 Noise Goals.

| Time Period | EPNL Noise Goals | | | Engine Configuration |
	0.35 n mi Sideline	3.5 n mi Takeoff	1.0 n mi Approach	
Early 1970	124	108	108	• 633 lbs/sec Augmented Turbojet • 4.5 PNdB Jet Suppressor (TSEN Nozzle) • Turbomachinery (T/M) Noise Suppression
Mid 1970	116	108	108	• Preliminary Design of High-Airflow Dry Turbojet and Bypass Turbojet Engines • Jet and T/M Noise Suppression
Late 1970	112	108	108	• 900 lbs/sec Dry Turbojet • Multielement Jet Suppressor • T/M Noise Suppression
Early 1971	110	107	105	• High-Flow Engine • Advanced Multiengine Spoke/Chute Suppressor • To Meet 108/108/108 Goals with Trades • T/M Noise Reduction

3

from these plus other diagnostic tests showed that reduction of turbomachinery noise was clearly a requirement to meet the approach and community noise goals. The advantage of beating the requirements at one or both of these monitoring points, in order to take advantage of the trading aspects of the FAR Part 36 regulation, was also realized. Technologies being developed on related noise programs (such as the General Electric NASA Quiet Engine Program, General Electric CF6 development, etc.) needed to be adapted to engine configurations suitable for supersonic transport systems. Full utilization of these approaches would impact on the design of the engine component through:

- Acoustic treatment on most available flow surfaces
- Blade row spacing
- Blade/vane ratio
- Flow acceleration (choking or partial choking)
- Leaned vanes
- Use of IGV's to restrict upstream noise propagation

In early 1971 when the noise objectives for the SST had been redefined to meet the FAA subsonic transport noise goals with trades of 108 EPNdB (for an aircraft of over 600,000 pounds TOGW), the engine design was set as a dry turbojet of approximately 800 lbs/sec weight flow. This design was arrived at after extensive optimization studies, including acoustic inputs. Also based upon aeroacoustic inputs, the nozzle design was an annular convergent/divergent system with a multichute suppressor. Turbomachinery noise reduction anticipated the use of extensive acoustic treatment in the compressor and turbine areas, along with optimizing turbine rotor/stator spacing. Presuming a continued technology development in both jet noise and turbomachinery noise suppression, it was predicted that this engine, in conjunction with the Boeing B2707-300 aircraft with high-life devices, had the potential of meeting the required airport noise levels.

The Department of Transportation issued a contract to General Electric and Boeing after the cancellation of the SST Program which was to finalize selected noise technology areas and summarize the results of the program.

Phase I of the Supersonic Transport Noise Reduction Technology Program (Contract No. FA-SS-71-13) was completed in December, 1972. The program covered several critical areas in the noise reduction of a Supersonic Transport Propulsion System. It encompassed work in both the jet noise and turbomachinery noise fields. Results of the Phase I effort are documented in References 1 and 3, which include a summary of the jet noise suppression work conducted during the SST program. The Phase I jet noise summary provided a data base for continued and new suppressor development in the DOT Phase II program.

4

1.2 PROGRAM OBJECTIVES

Using the initial efforts of the SST program as a starting point, the FAA/DOT issued the Phase II contract to GE in order to continue this important work. The effort was divided into three major areas: 1) Jet Noise Reduction, 2) Turbomachinery Noise Reduction, and 3) Aircraft/Engine System Integration.

The work carried out in this program, as the overall objective, had to provide the additional acoustic technology necessary to design high speed aircraft systems recognizing future acceptable noise levels. The program approach was to develop basic data on the two major noise sources that must be controlled, specifically jet noise and turbomachinery noise. The work was carried out on scale models and moderate-to-large sized engines, with the range of variables employed to permit application to a variety of possible advanced aircraft engine sizes and systems.

The program intent was broad enough to allow exploration of new concepts and provide basic data adaptable to a range of possible advanced engine systems, in addition to carrying out the development of specific concepts through the system evaluation phase. The program built directly on the work performed during the SST engine development program and the Supersonic Transport Noise Reduction Technology Program (Phase I) and was integrated with the effort of the NASA-Lewis AST Program (Reference 4) in evaluating likely suppressor configurations and SST engine cycles.

The overall objective of the Supersonic Transport Noise Reduction Technology Program was to advance noise suppression technology so as to permit development of future supersonic commercial aircraft unhampered by major noise problems. The program goal was to develop component and jet noise suppressor technology such that future supersonic aircraft could meet or possibly better Federal noise regulations for subsonic aircraft.

1.3 METHOD OF ACCOMPLISHMENT

1.3.1 Jet Noise Reduction

The jet noise reduction documented herein was achieved through analytical studies, model tests, and J79 engine tests. The work was accomplished in the following tasks:

- Continued development of the most promising configurations identified during the SST Program

- Evaluation of additional advanced concepts which showed promise of high suppression capability with reasonable aerodynamic and mechanical compromise

- Refinement of the most promising approaches based on work above

- Evaluation of acoustically treated ejectors to match selected suppressor systems

5

1.2 PROGRAM OBJECTIVES

Using the initial efforts of the SST program as a starting point, the FAA/DOT issued the Phase II contract to GE in order to continue this important work. The effort was divided into three major areas: 1) Jet Noise Reduction, 2) Turbomachinery Noise Reduction, and 3) Aircraft/Engine System Integration.

The work carried out in this program, as the overall objective, had to provide the additional acoustic technology necessary to design high speed aircraft systems recognizing future acceptable noise levels. The program approach was to develop basic data on the two major noise sources that must be controlled, specifically jet noise and turbomachinery noise. The work was carried out on scale models and moderate-to-large sized engines, with the range of variables employed to permit application to a variety of possible advanced aircraft engine sizes and systems.

The program intent was broad enough to allow exploration of new concepts and provide basic data adaptable to a range of possible advanced engine systems, in addition to carrying out the development of specific concepts through the system evaluation phase. The program built directly on the work performed during the SST engine development program and the Supersonic Transport Noise Reduction Technology Program (Phase I) and was integrated with the effort of the NASA-Lewis AST Program (Reference 4) in evaluating likely suppressor configurations and SST engine cycles.

The overall objective of the Supersonic Transport Noise Reduction Technology Program was to advance noise suppression technology so as to permit development of future supersonic commercial aircraft unhampered by major noise problems. The program goal was to develop component and jet noise suppressor technology such that future supersonic aircraft could meet or possibly better Federal noise regulations for subsonic aircraft.

1.3 METHOD OF ACCOMPLISHMENT

1.3.1 Jet Noise Reduction

The jet noise reduction documented herein was achieved through analytical studies, model tests, and J79 engine tests. The work was accomplished in the following tasks:

- Continued development of the most promising configurations identified during the SST Program

- Evaluation of additional advanced concepts which showed promise of high suppression capability with reasonable aerodynamic and mechanical compromise

- Refinement of the most promising approaches based on work above

- Evaluation of acoustically treated ejectors to match selected suppressor systems

5

- System evaluation of the best suppression approaches with acoustically treated ejectors by evaluating the aeroacoustic effects, and weight penalties, on the performances of an advanced high speed transport aircraft

- Design and test of a final configuration based on all the above work with evaluation to include model acoustic and aero tests plus incorporation into an engine exhaust system for test in the engine environment

Scale models were used for acoustic testing at General Electric's Jet Engine Noise Outdoor Test Stand (JENOTS). Static aerodynamic performance tests, as well as with external flow, were carried out using approximately the same scale model size in tests at the FluiDyne Engineering Corporation and the NASA-Lewis wind tunnel facilities.

The analytical work was supported by direct measurements of the jet plume details (for example, the velocity and turbulence distributions) using the General Electric Laser Doppler Velocimeter developed under USAF/ DOT Supersonic Jet Exhaust Noise Investigation Program (Reference 5).

The large scale engine evaluation of the final suppression system was carried out at the General Electric facilities at Edwards Air Force Base on a modified J79-8/15 engine. The tests were jointly conducted with Task 1 and Task 3 of the DOT High Velocity Jet Noise Source Location and Reduction Program (Contract No. DOT-OS-30034), Reference 6.

1.3.2 Turbomachinery Noise Reduction

Both primary contributors to SST turbomachinery noise were investigated, i.e., turbine noise and compressor noise. Turbine noise identification and reduction was studied using a YJ85 engine. Testing was conducted at General Electric Laboratories at Edwards Air Force Base. A massive inlet suppressor was used to suppress the J85 compressor noise, and an open nozzle was used to reduce jet noise. This approach was successful in unmasking and identifying the turbine noise. Two methods for suppressing the turbine noise were investigated, i.e., increasing the second (final) stage spacing and wall plus mid-duct splitter acoustic treatment. Both internal and far-field acoustic data were recorded during the tests. The aerodynamic performance of the turbine and other engine components was also monitored. Thus a representative high pressure turbine was used to identify the impact of turbine noise on an SST engine system and to investigate two practical ways of reducing this form of turbomachinery noise in the far field.

An advanced three-stage low pressure compressor (LPC) was used in the compressor noise investigation. This 26.3-inch diameter (first stage rotor) was considered quite representative of the first compressor system which would be utilized in future SST engines and, in fact, serves as the basic model in the current NASA-Lewis AST Program cycle/system study efforts being conducted at General Electric. The compressor has a design pressure ratio

6

of 4.1 at a first rotor tip speed of 1534 ft/sec. Testing of the compressor was conducted at General Electric's outdoor sound field at Peebles, Ohio. The LM1500 gas generator drive system and jet noise were highly suppressed in order to isolate the compressor noise. Two basic approaches to suppressing the radiated compressor noise were investigated. They were: (1) a "hybrid" inlet, and (2) high Mach number IGV's. The variable geometry inherent in a supersonic tranport engine inlet and nozzle makes it well suited to the hybrid inlet concept, which employs moderate airflow acceleration suppression in addition to wall acoustic treatment suppression (and thus avoids the performance problems associated with hard choking the inlet). The basic design was quite similar to the SST/GE4 inlet, and was representative of an axisymmetric mixed compression, translating centerbody inlet designed for supersonic cruise at M_o = 2.5. The characteristic sharp lip was replaced with a bellmouth forebody to simulate inflow conditions during low speed flight. The inlet was fitted with replaceable treatment panels in order to isolate the effects of the wall acoustic treatment. In addition, an effort to evaluate the effect of blow-in-door auxiliary inlets, a necessary part of any SST inlet, on take-off noise was accomplished, with an attempt in the design to suppress the noise leakage through the doors. A baseline cylindrical inlet also was tested to evaluate the basic source noise characteristics of the compressor, to isolate the acceleration suppression and to perform the High Mach Number IGV Test. The variable flap IGV's of the compressor were particularly suited to the high Mach Number IGV test in that the flaps were remotely controllable to reduce the IGV passage area and thus increase the Mach number. Both near- and far-field noise measurements were made in addition to aerodynamic performance measured for both the inlet and compressor.

1.3.3 Aircraft System Integration

In order to assess the effectiveness of the model and engine noise suppression work performed under the Jet Noise Reduction and Turbomachinery Noise Reduction Tasks of the program, the best performing components were integrated into a viable type aircraft-engine system. The evaluation was based on trades between aeroacoustic and mechanical considerations of the suppressor configurations and on the most current understanding of relative velocity effects on EPNL suppression. The engine cycle selection and baseline airplane were established from current technology being developed under the NASA-Lewis AST Program. Results of the integration work included comparisons of fully suppressed and unsuppressed engine-aircraft systems. The effectiveness of the jet and turbomachinery suppression are shown in terms of EPNL at the FAR Part 36 monitoring points for the sideline, community, and approach conditions and in terms of noise footprints under the flight path.

7

2.0 PROGRAM HIGHLIGHTS AND SUMMARY

2.1 JET NOISE REDUCTION

The suppression technology developed under the jet noise reduction task of this program was a continuation of the jet noise suppression development studies initiated during the GE4/SST design effort.

The overall objective of the jet noise portion of this program was to advance jet noise suppression technology in order to permit the development of future supersonic aircraft unhampered by major jet noise problems. The program goal was to develop jet noise suppressor technology such that future supersonic aircraft would meet or exceed current Federal Noise Regulations for subsonic aircraft. This development work on jet noise suppression was accomplished through scale model tests, J79 engine tests, and analytical studies.

The scale model suppressor development effort was directed at a number of specific areas. Hot jet acoustic and wind-on aerodynamic performance tests were performed on most of the suppressor configurations. The program built directly on the work accomplished in Phase I of this program, particularly in the area of multielement (spoke/chute) suppressors on annular plug nozzles. Table 2 provides a summary of the jet noise suppressors investigated in the course of this program along with the key results.

The multielement suppressor concept, with solid spoke or ventilated-chute-type elements mounted on the annulus of a plug nozzle, showed that high levels of suppression could be attained with acceptable performance degradation in the suppressed mode. In the unsuppressed mode, the supersonic cruise performance was enhanced by the presence of the plug which provided stowage space for the suppressor elements. These suppressor systems were further refined during this program. Tests were conducted on suppressor configurations derived from parametric tests (element number, area ratio, planform and cant angle variation) conducted on similar suppressor models during Phase I.

As seen in Figures 1 and 2 radically different aeroacoustic results were obtained on the multielement (chute) annular plug suppressors. These differences were subsequently related to the nozzle geometry, seen in Figure 3, by thoroughly evaluating the results from these and previous acoustic, laser velocimeter, and wind tunnel tests. Key geometric parameters effecting multichute suppressor aeroacoustic performance include: 1) exit planform, 2) exit plane cant angle, and 3) depth of chute.

● Exit Planform - controls the primary flow distribution around the annulus of the plug nozzle. It is directly related to the hub to tip flow-width parameter. Limiting our discussion to the primary flow passage between the chute, the test results suggest that high flow-width ratios (>1.5) result in wide spacings at the hub and narrow spacings at the tip. Aerodynamically, this is attractive since this pressurizes the plug surface and reduces or eliminates the drag associated with low

8

Table 2. Summary of Jet Suppressor Major Test Results.

Suppressor Category	ΔPNL at 2128-ft SL	ΔPNL / ΔC_{f_g} *
1. Multispoke/Chute Suppressors on Annular Plug Nozzles		
▪ 40 Spoke	8.1	0.61
▪ 40 Chute	14.0	0.94
▪ 36 Chute	8.5	2.12
▪ 36 Chute + Hardwall Ejector 1	9.5	2.71
▪ 36 Chute + Hardwall Ejector 2	9.5	1.76
▪ 36 Chute + Treated Ejector 1	10.5	---
▪ 36 Chute + Treated Ejector 2	10.5	---
▪ 32 Chute (Phase I – Model)	11.5	1.64
(Acoustic Baseline: Conical Nozzle)		
2. Multitube/Annular Plug Suppressors		
▪ 72 Tube	13	---
▪ 66 Tube	12	---
▪ 66 Tube + Hardwall Ejector 2	12	---
▪ 66 Tube + Treated Ejector 2	12	---
(Acoustic Baseline: Conical Nozzle)		
3. Advanced Concepts		
▪ Asymmetric 2-D Unsuppressed Nozzle	1.5	---
** ● Unsuppressed 2-D + Sidewalls	1.5	---
▪ Unsuppressed 2-D + Hardwall Ejector	3.0	---
▪ Unsuppressed 2-D + Ejector Wing	8.0	---
+ ● Dual-Flow Nozzle, Noncoplanar $A_{Core}/A_{Fan} = 1.32$	---	---
4. Parametric Refinements		
▪ Dual-Flow Nozzle, Noncoplanar, $A_{Core}/A_{Fan} = 1.0$	5.5	---
● Dual-Flow Nozzle, Noncoplanar, $A_{Core}/A_{Fan} = 1.5$	6.5	---
▪ Dual-Flow Nozzle, Coplanar $A_{Core}/A_{Fan} = 1.5$	4.0	---
▪ Unsuppressed 2-D + Hardwall Ejector	3.0	10
▪ Unsuppressed 2-D + Treated Ejector	3.0	---
▪ Suppressed 2-D + Hardwall Ejector	9.0	.53
▪ Suppressed 2-D + Treated Ejector	10.5	---
▪ (Aeroacoustic Baseline Unsuppressed 2-D)		
5. Final Model Tests		
▪ 32 Deep Chute	12.0	2.11
● 32 Deep Chute + Hardwall Ejector	12.0	2.45
▪ 32 Deep Chute + Treated Ejector	12.5	---
6. Final Engine Tests		
● 32 Deep Chute	12.0	---
● 32 Deep Chute + Treated Ejector	12.0	---

---

* ΔPNL at V_j = 2500 ft/sec, $P_{T8}/P_0 \sim 3.0$, and M_0 = 0, re Acoustic Baseline ΔC_{f_g} at M_0 = .36, $P_{T8}/P_0 \sim 3.0$ re Unsuppressed Plug Nozzle; Assumes ΔPNL (Static) = ΔPNL (Flight).

** ΔPNL for 2-D Nozzle re Unsuppressed 2-D.

+ ΔPNL For Dual-Flow re to Suppressed Core Alone.

9
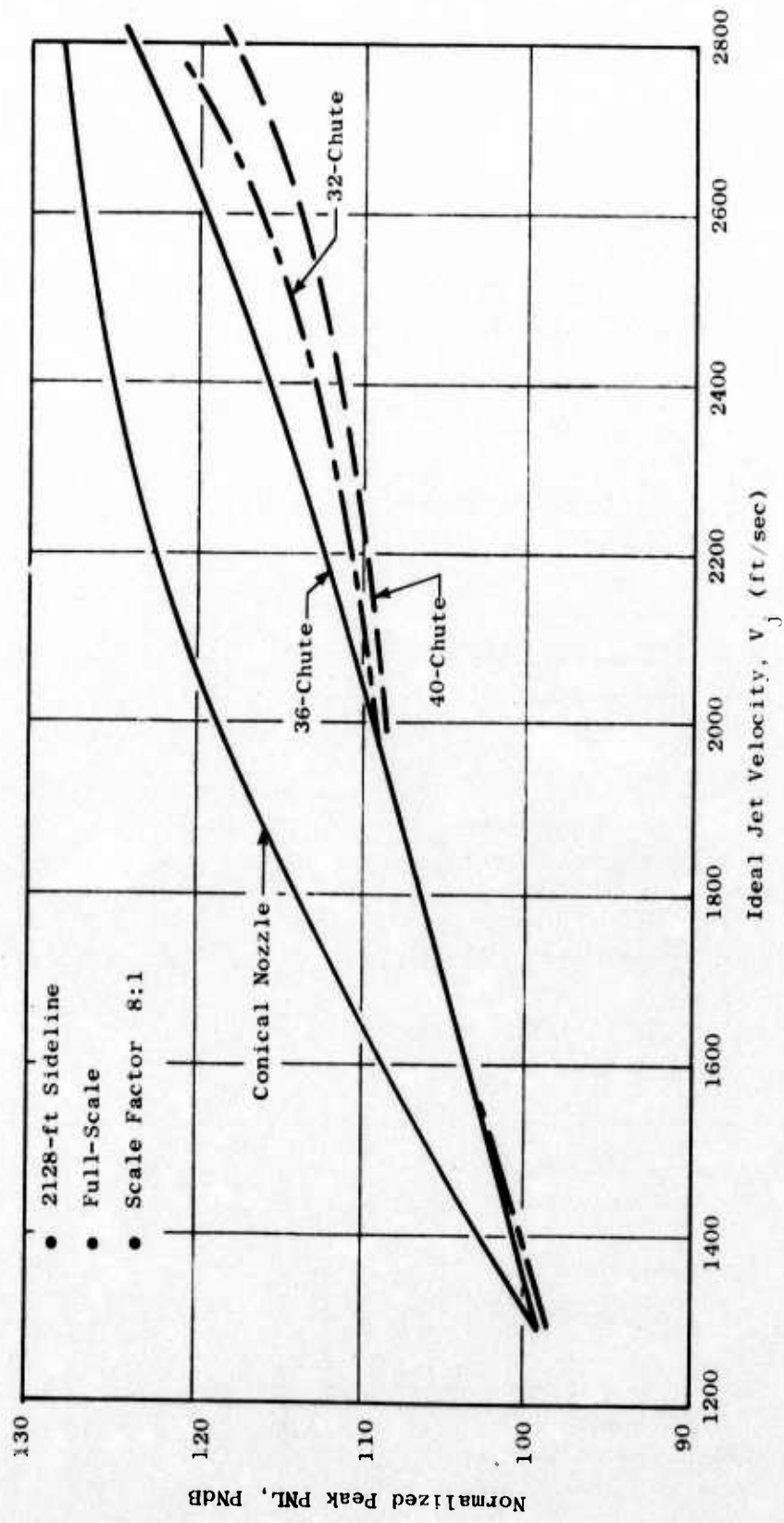
Figure 1. Peak PNL Comparisons of Multichute Suppressors.
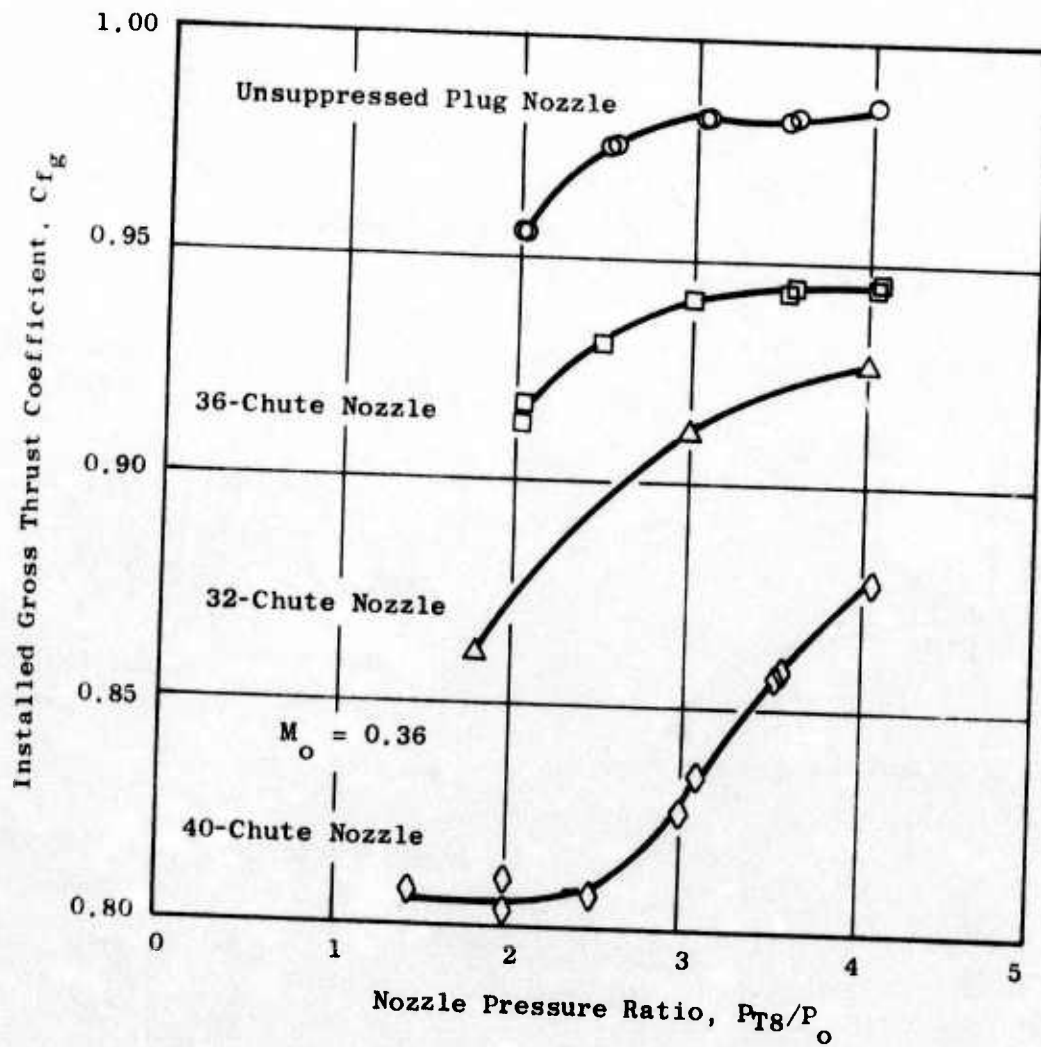
Figure 2. Wind-On Performance Comparisons of Multichute Suppressors.
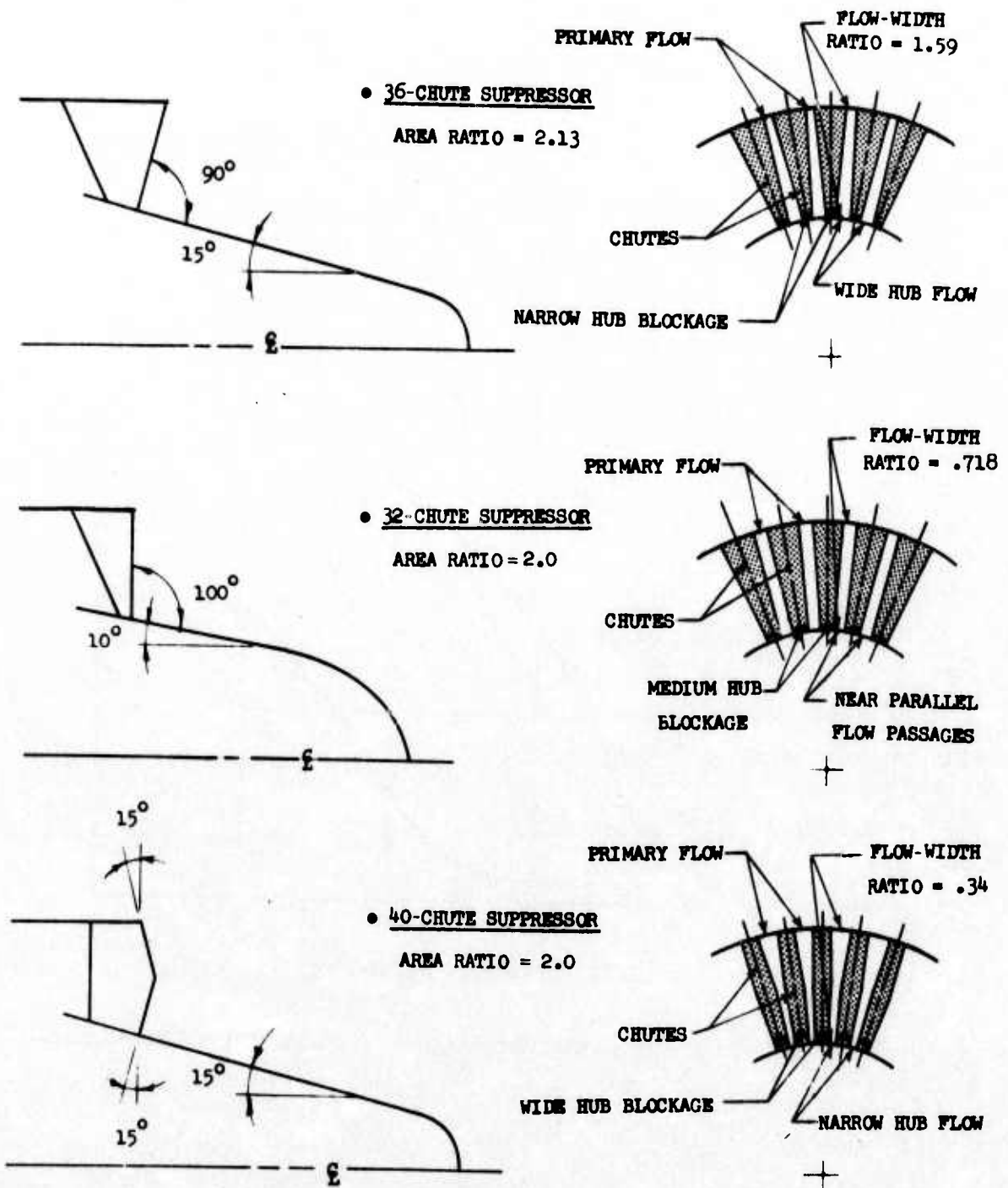
Figure 3. Schematic of Multichute Geometric Characteristics.

pressures. Acoustically, however, the effect is detrimental since it distributes a large amount of high velocity flow at the hub where it can merge quickly to a coalesced jet without sufficient time to entrain enough ambient air to reduce the velocity, thus resulting in high noise levels.

The opposite effect can be seen with a very low hub-to-tip flow-width ratio (<0.5), which results in narrow hub spacings and wide tip spacings. Aerodynamically, this effect is seen to starve the plug surface, increasing the plug drag and overall performance loss. Acoustically, this is beneficial since a minimum amount of high velocity flow is concentrated at the hub the majority of the flow is distributed to the outer annulus where sufficient mixing with ambient entrained air can take place.

Obviously, these extremes are to be avoided if a realistic suppressor is to be designed. An attractive compromise appears to be one with intermediate hub-to-tip flow-width ratios (0.7 - 1.0). This provides a primary flow passage that is nearly parallel and uniformly distributes the flow at e exit plane.

● Exit Plane Cant Angle - influences the initial direction that the primary flow takes after leaving the nozzle exit plane. The tendency of the flow is to move in a direction normal to the exit plane angle. Canting the exit plane angle normal to the plug surface tends to focus the flow along the plug and coalesces it to a single jet at the plug end. The effect on aeroacoustic performance is similar to the effect of high hub-to-tip flow-width ratio on exit planform.

If the exit plane is canted away from the plug, the tendency of the flow is to move outward and off the plug surface, inhibiting aerodynamic performance by increasing plug drag and enhancing acoustic suppression by moving the high energy streams to a larger diameter and allowing better aerodynamic mixing to take place.

Again, these are two extremes which must be compromised for effective multichute nozzle design. A compromise on exit cant angle for suppressors without ejectors can be reached with axial flow from the exit plane. In this case the exit cant angle is zero or normal to the nozzle axis. If a secondary ejector is employed, consideration must be given to select the exit cant angle which will allow the flow to enter the ejector without impinging on the inlet or flowing around the outside of the ejector.

● Depth of Chute - controls the amount of ambient air available to mix with the primary flow elements. Large deep chutes (depth / height $\geq$1) allow sufficient entrainment to pressurize the base of the chute so that fewer, wider chutes can be used to segment the primary flow.

13

Multitube suppressors were investigated to determine their effectiveness when incorporated in an annular plug nozzle configuration. The results of these tests (on 72- and 66-tube suppressors discussed in Section 3.2.2) showed that both nozzles were close in suppression levels (Figure 4), even though the suppressor geometries were somewhat different (the 72-tube was designed for high suppression, while the 66-tube was designed for ease of mechanical implementation and stowage in the plug). Favorable agreement with previous multitube test data was obtained, which suggested that the multitube/annular plug system (with moderate radius ratios) has limited capability for increased suppression. The addition of a treated ejector in the multitube annular plug nozzle system may aid suppression with judicious selection of the multitube and ejector geometries. However, the added complexity and weight to the overall system is likely to offset any gains typically achieved with ejector systems (~2 - 4 dB).

A look at a few of the advanced suppressor concepts (discussed in Section 3.2.4) thought to have potential as high suppression systems included test effort on three concepts: 1) asymmetric 2-D nozzles, 2) dual-flow exhaust nozzle with suppressed core, and 3) orderly structure. Asymmetric 2-dimensional nozzles, unsuppressed and suppressed, mounted over a simulated wing to take advantage of both wing shielding and asymmetry effects on jet noise, were tested during this phase of the program. The acoustic characteristics of the over-the-wing, asymmetric nozzles, exhibited potential for high suppression gains as illustrated in Figure 5.

A dual-flow exhaust nozzle concept was tested to evaluate the suppression effect from aerodynamic shielding of a cold fan stream around a hot suppressed core. Some suppression (~4 dB) was obtained (Figure 6) with the addition of the cold unsuppressed fan stream. However, the performance penalty due to the increased base drag resulting from isolating the internal suppressed core from the ambient was excessive.

A third concept which underwent investigation during this phase of the jet noise reduction task was the "orderly structure" experiment. This was an exploratory test to determine the effect of inhibiting plume radial growth and its impact on reducing the generation of jet noise. Although results from this test did exhibit some suppression on an OASPL basis, the idealized nature of this work prohibited further investigations during the remainder of the program.

An aeroacoustic parametric refinement of two suppressor concepts based on the results of the advanced suppressor concept studies was subsequently conducted (see Section 3.2.5). The two advanced concepts selected were the asymmetric and dual-flow nozzle systems. The asymmetric nozzle system underwent further evaluation with both acoustic and wind-on performance tests of a suppressed and unsuppressed primary with a long treated ejector. Results of these tests showed this type of system to be capable of high suppression with reasonable aerodynamic performance (Figure 7). Implementation of such a system, however, requires a detailed aircraft-engine systems integration study in order to more fully realize the benefits and limitations of such a system.

14
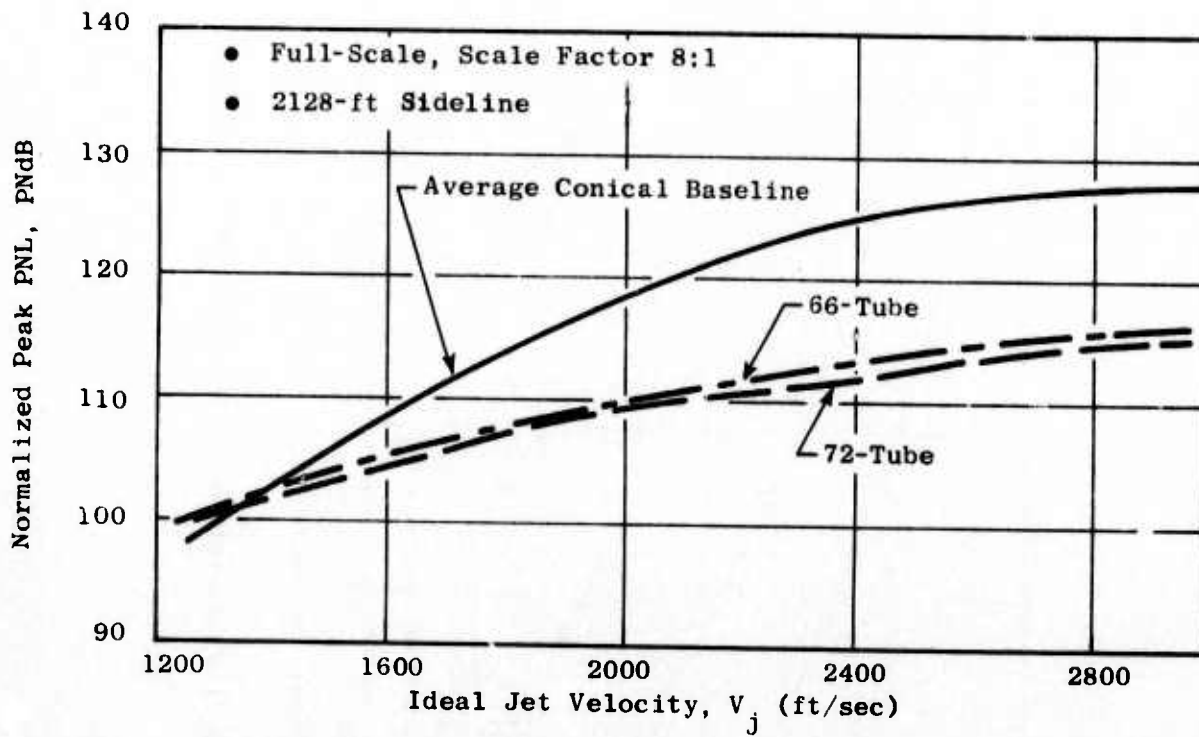
Figure 4.   Peak PNL Comparisons of Multitube/Annular Plug Suppressors.

15
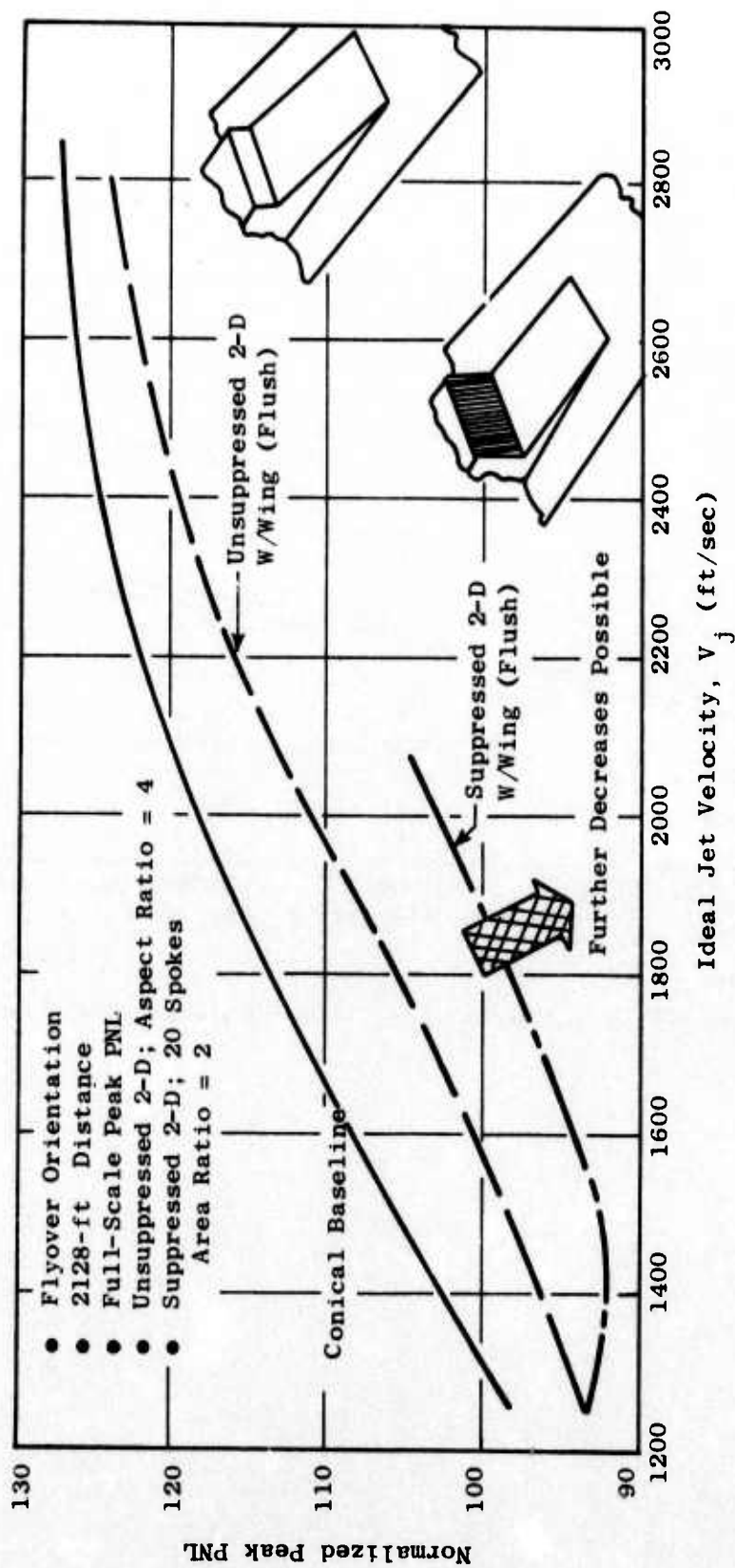
Figure 5. Asymmetric Nozzle Over-the-Wing Acoustic Characteristics.

- Flyover Orientation
- 2128-ft Distance
- Full-Scale Peak PNL
- Unsuppressed 2-D; Aspect Ratio = 4
- Suppressed 2-D; 20 Spokes
  Area Ratio = 2

Conical Baseline

Unsuppressed 2-D
W/Wing (Flush)

Suppressed 2-D
W/Wing (Flush)

Further Decreases Possible

Normalized Peak PNL

Ideal Jet Velocity, V_j (ft/sec)

16
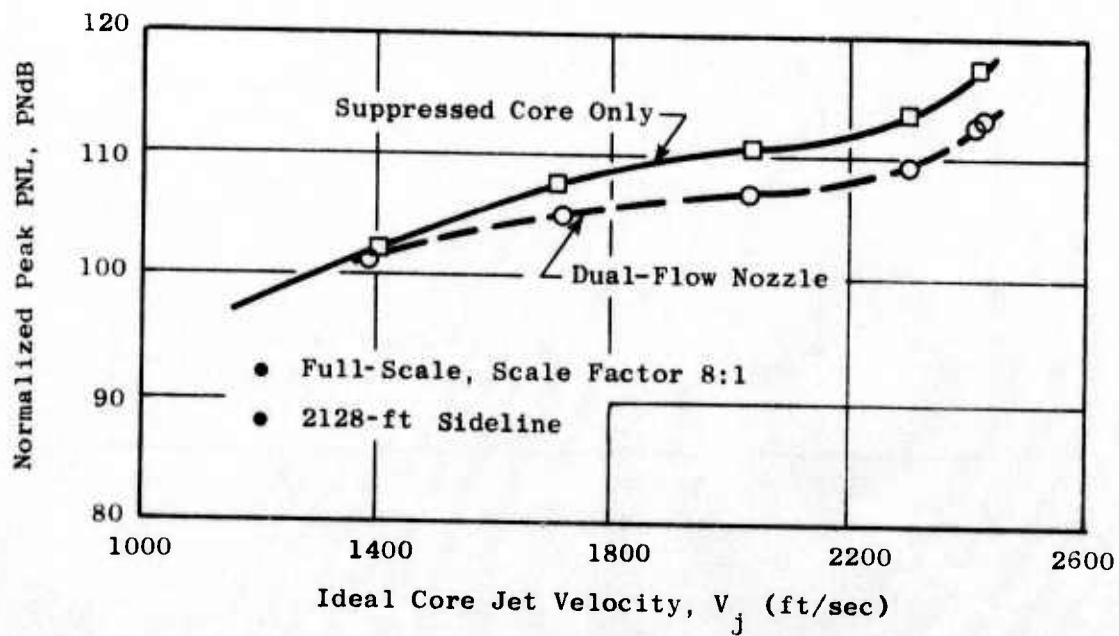
Figure 6. Peak PNL Comparison of Dual-Flow Nozzle with Suppressed Core.

- 2128-ft Sideline

- Scaled Data
    Unsuppressed (8:1)
    Suppressed (10:1)
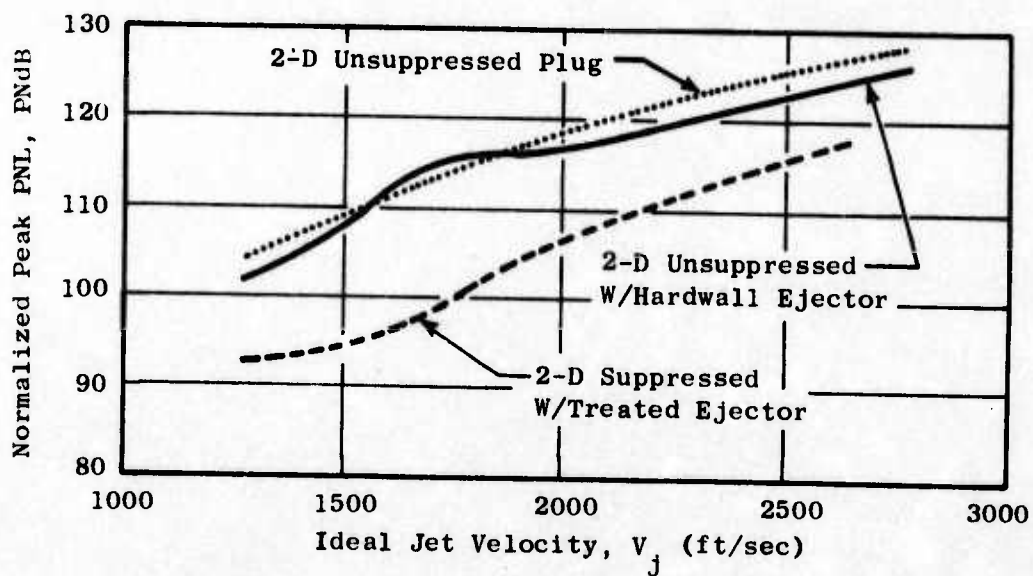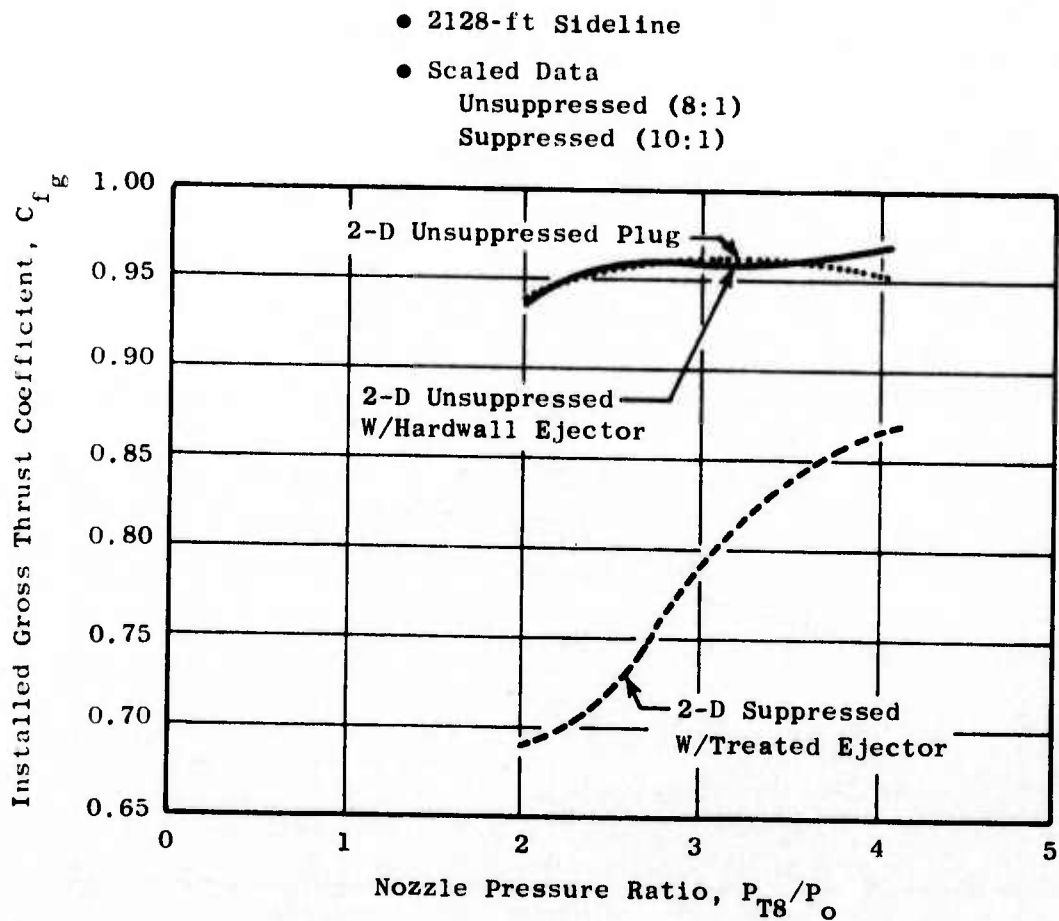
Figure 7. Asymmetric 2-D Nozzle System Aeroacoustic Evaluation.

18

The Dual-Flow Exhaust Nozzle System underwent acoustic testing and aero-
dynamic evaluation during the parametric refinement phase to determine the
effect of suppressed core-to-fan area ratio variation, and non-coplanar-to-
coplanar exit plane influence on PNL suppression. Comparisons of suppression
levels obtained from the different area ratio, non-coplanar nozzles indicated
no major differences in PNL level. The area ratio of 1.5 appeared to give
a lower spectrum level than the other configurations. Differences resulting
from coplanar and non-coplanar exit planes were insignificant.

In contrast to the above suppressed core results, substantial gains in
suppression (~10 dB) have recently been observed with a high core-to-fan
area ratio, low bypass ratio, duct-burning configuration having both fan and
core streams unsuppressed. At General Electric these configurations were
recently tested under the Acoustic Tests of Duct-Burning Turbofan Jet Noise
Simulation Program (NAS3-18008) Reference 7, sponsored by NASA-Lewis.

Selection of the final suppressor configuration (see Section 3.3) which
was to be tested in both model scale and J79 engine size was made after con-
sidering four key parameters: 1) identification of the type of engine flow
system (single-flow cycle), 2) suppressor system mechanical feasibility with
appropriate aeroacoustic trades, 3) review of the suppressor systems tested
during the program, and 4) application to currently envisioned advanced
supersonic transport technology systems. From these considerations, a 32-
deep-chute annular plug suppressor system was designed for the final model
and engine demonstration phase of the program. An alternate configuration
included the addition of a treated ejector as a means of obtaining increased
suppression and static thrust augmentations.

The results of the final model (Section 3.4.1) and engine suppressor
tests (Section 3.4.2) showed the 32-deep-chute suppressor to exhibit good
static PNL suppression (12 dB at 2128-ft SL) in the 2300 to 2500 ft/sec ideal
jet velocity range with a correspondingly attractive C_{fg} of 0.924 at Mo = 0.36,
P_{T8}/P_o = 3.0, which results in a $\Delta PNL/\Delta C_{fg}$ trade in excess of 2.1.

Comparison of the model and engine results (Section 3.4.3) indicate
exceptionally good agreement on a PNL basis (Figure 8). Directivity and
spectral comparisons show similar results. Laser velocimeter mean velocity
profile measurements of the model and engine suppressors shown in Figure 9
also indicate close agreement. These acoustic scaling analyses strongly
suggest that diameter (geometric) scaling can yield favorable trends
especially on a PNL basis.

Related technology pertinent to a more thorough understanding of what
effects jet noise reduction is discussed in Section 3.5. A summary of a paper
by Dr. R.A. Kantola of the General Electric Company's Research and Develop-
ment Center reviews his work under this program with jet and suppressor cor-
relation measurements in which he attempted to cross-correlate in-jet
fluctuating static pressure measurements with the far-field acoustic pressures
for two typical scale model annular plug suppressors.
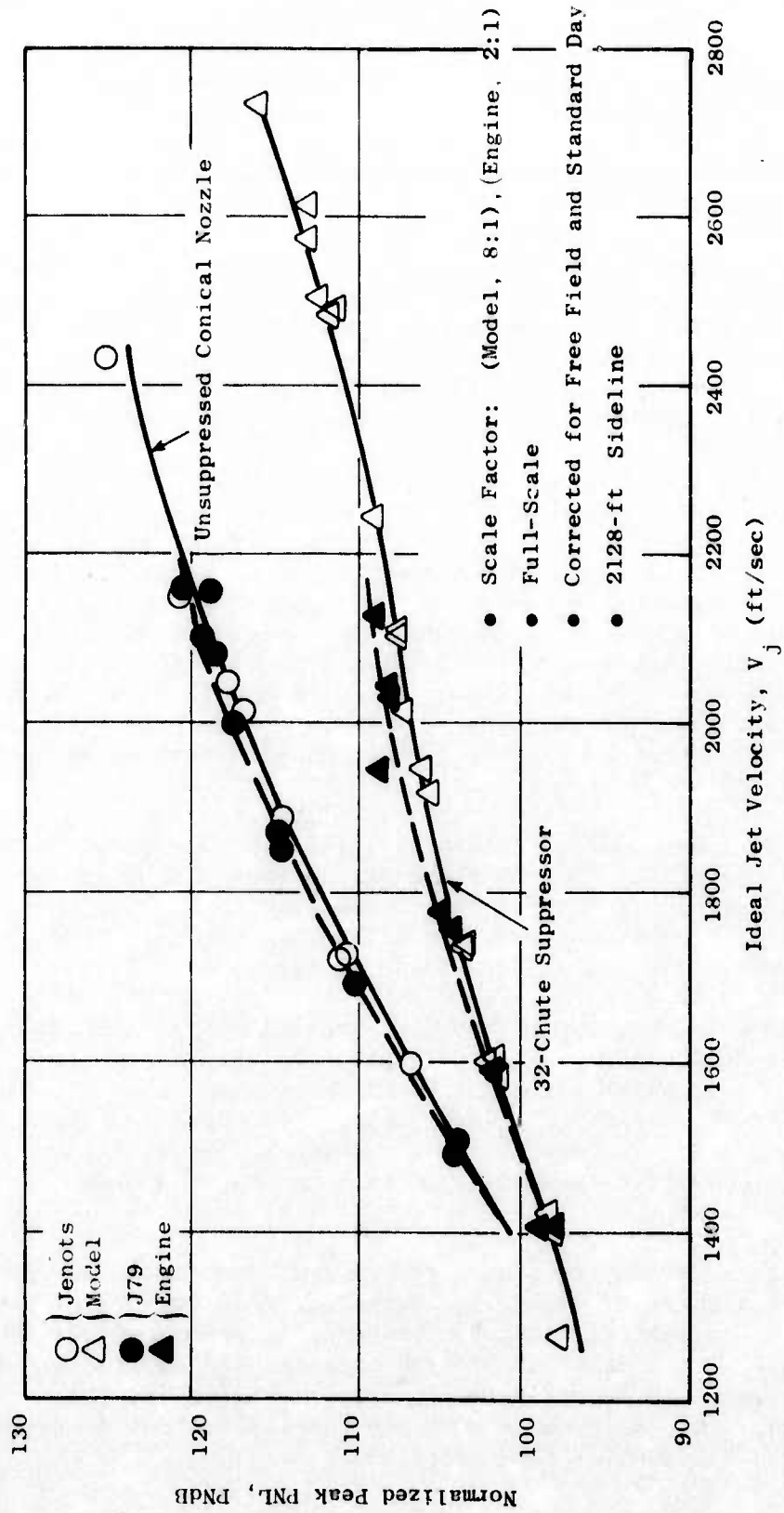
Figure 8. Model-to-Engine Peak PNL Comparison.

20
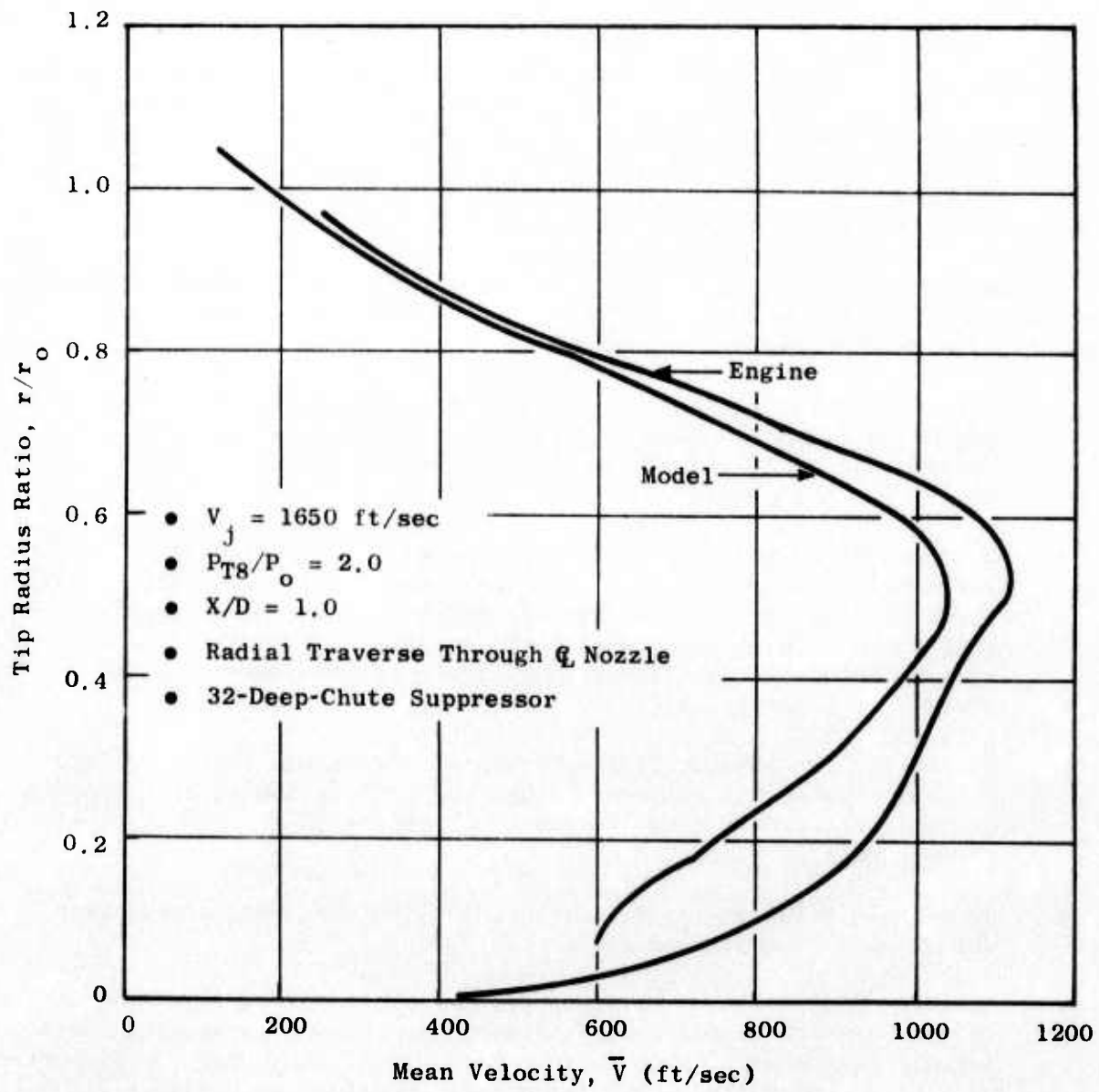
Figure 9. Mean Velocity Profile Comparisons for Model and Engine
Suppressors.

Another area of study was directed toward an assessment of the far-field acoustic signature as influenced by nozzle underexpansion, i.e., shocks. Several rudimentary diagnostic tests were conducted in a effort to identify the shock contribution to the total noise signature measured in the far field. Emphasis was directed in the forward quadrant, since the shock contribution may exert an undesirable influence during flight.

To summarize, the jet noise reduction technology on mid- to high-velocity jets resulting from the work conducted under this program has led to the following observations and conclusions:

- The program has provided an acoustic and aerodynamic data bank on a number of advanced technology suppressor configurations, complimenting the already-extensive jet suppression data bank acquired during the SST program.

- A number of unique suppression schemes were identified as having potentially high suppression benefit. Among these, are the over-the-wing asymmetric 2-D suppressed nozzle systems which appeared attractive from an aeroacoustic standpoint, but require a more comprehensive systems integration effort for implementation to advanced technology aircraft.

- The multichute annular plug suppressor concept was developed into a viable system for advanced technology application as an outgrowth of the test results from the model and engine 32-deep-chute suppressor configurations.

- Acceptable model-to-engine acoustic scaling was demonstrated from the results of model and engine tests.

- Although some of the suppressor systems evaluated in this program show promise of higher levels of suppression with acceptable aerodynamic performance, considerably more development work, complemented by better definition of the jet noise generation mechanisms, is required if current subsonic Federal Noise Requlations are to be met by advanced supersonic aircraft.

- To more clearly understand in-flight effects on suppression and their relationship with static model and large-scale suppressor test results, the J79 engine suppressor configuration should undergo wind-on acoustic testing.

2.2 TURBOMACHINERY NOISE REDUCTION

As discussed earlier, both major contributors to SST engine turbomachinery noise were investigated as part of this program; namely, turbine and compressor noise. Turbine noise was studied using a YJ85 engine. Two approaches to reducing turbine noise in the far field were examined.

First, the spacing between the second stage turbine nozzle and turbine blades was increased from 0.34 to 1.0 nozzle tip chords. This resulted in an average turbine tone PWL reduction in the far field of 5.6 dB. Scaling studies were performed to indicate the magnitude of turbine noise reductions to be expected from spacing in an SST application. On a 300-foot sideline, peak PNL's (110° inlet angle) were reduced 8.6 and 4.3 PNdB at takeoff (100% rpm) and approach (80% rpm), respectively.

Second, a turbine noise suppressor, one turbine exit diameter in length with a treated splitter was tested. This is shown schematically in combination with the spaced configuration in Figure 10. Also indicated are the important design parameters of the SDOF treatment. A nominal tuning frequency of 16 KHz was selected in order to: (1) suppress the stage 1 noise (not directly affected by spacing), and (2) to utilize the broadband suppression characteristics of SDOF to furthur reduce the stage 2 noise in the far field. SDOF treatment was selected because Phase I (Reference 3) studies determined it should be used in high temperature applications due to its predictable acoustic behavior in the turbine environment and its superior mechanical characteristics. The length of one diameter was selected as an upper limit on the amount of treatment that might be utilized in an engine application. Testing the YJ85 with maximum exhaust treatment thus provided an estimate of the upper limit for turbine noise suppression; selection of the amount of treatment required to meet any systems goals could then be determined by interpolation rather than extrapolation. The treatment reduced the turbine tone second-stage power by 23.5 dB relative to the spaced configuration. Jet noise and casing radiation created a floor in the far field for the YJ85, particularly at take-off conditions which limited the apparent treatment effectiveness in the far field for this vehicle. At approach, full-scale results indicated a 9.1 PNdB reduction relative to the spaced configuration in the 300-foot sideline peak PNL with the treatment. While the application of treatment to the turbine exhaust has greater noise reduction potential than does spacing, it carries with it a relatively greater penalty as well. Moderate application of either spacing and/or treatment appear to be practical approaches to turbine noise reduction.

Other results and conclusions from the turbine noise investigation are summarized below:

- A strong dependence of the turbine noise on the turbine pressure ratio and/or energy extraction was suggested.

- The baseline turbine noise in the far field was a modulated tone (Figure 11).

23

Resonator Depth = 0.125"

Face Plate Porosity = 6.5%

Hole Diameter = 0.04"

Face Plate Thickness = 0.015"

Cell Size = 0.20" - 0.225"

L/D_{tip} = 1.0

L/H = 9.85

Tuning Frequency = 16 KHz (Nominal)

H/λ = 1.39

Treatment Area = 2600 in.^{2}
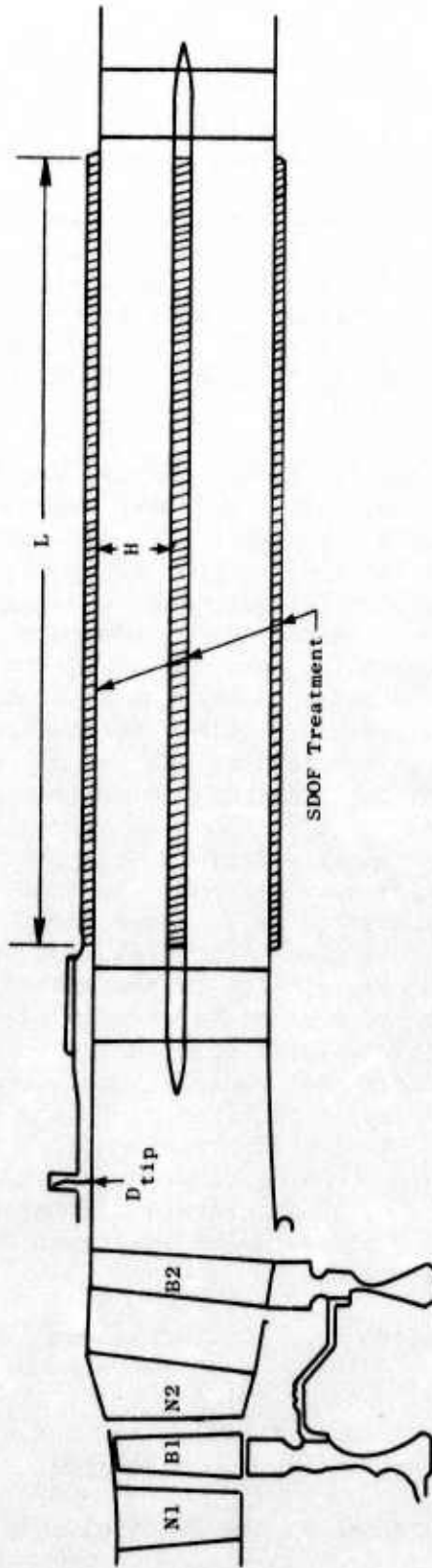
Figure 10. YJ85 Turbine Spacing + Treatment.

24
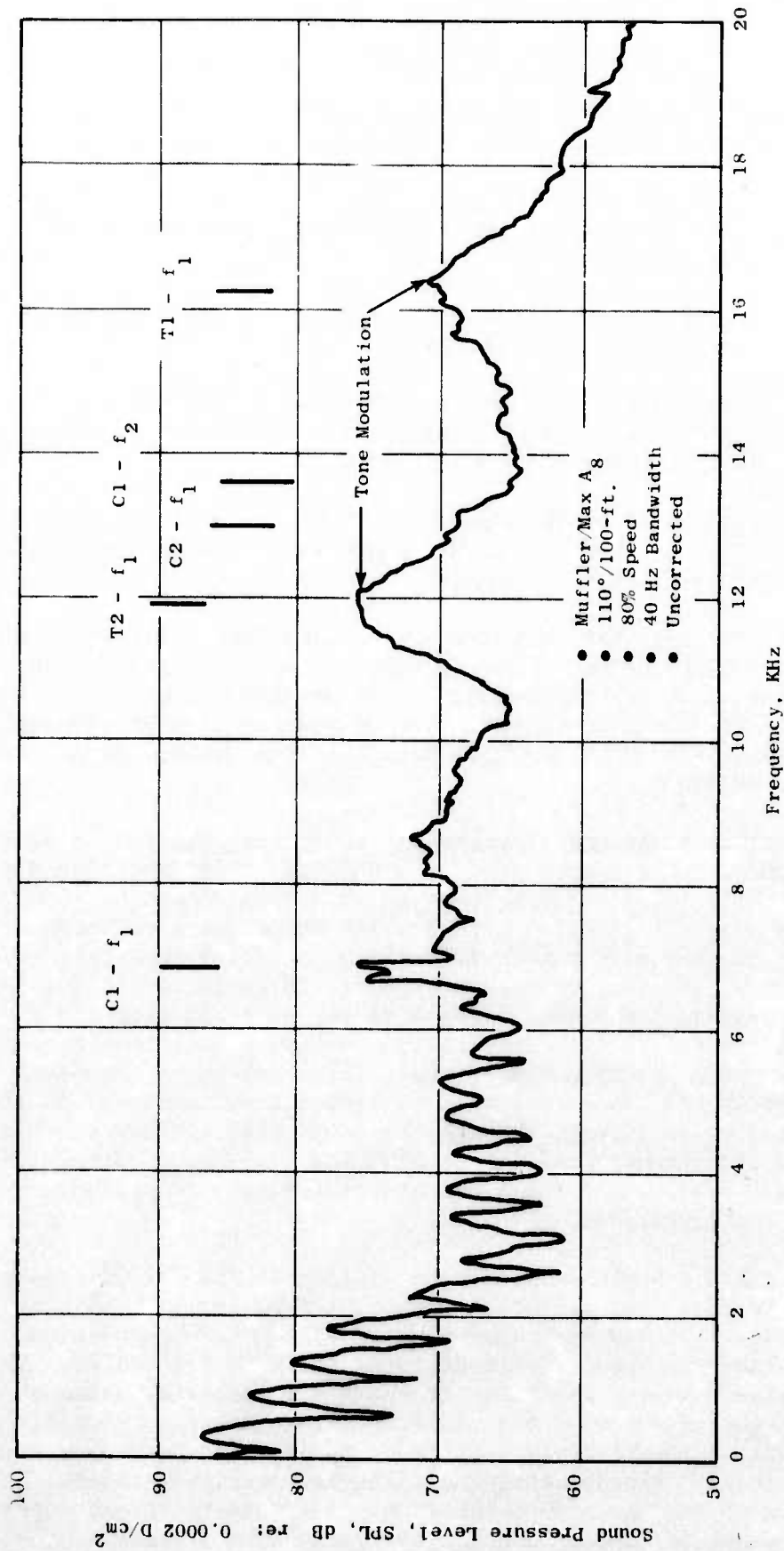
Figure 11. Far-Field Narrowband Spectrum, Inlet Suppressor/Max. A_8.

25

- Measured turbine directivities were consistant with previously published results (such as Smith and Bushel, Reference 8, see Figure 12).

- Both spacing and treatment suppressed turbine noise over a broad frequency range (Figure 13).

- Far-field turbine directivities were similar for the suppressed and unsuppressed turbine (Figure 14).

- The spacing results are consistant with Phase I (Reference 3) results; the curve of Figure 15 can be used for preliminary design studies of turbine noise suppression with spacing.

- The design goal of 20 dB suppression by the treatment was met; for the preliminary design studies, the suppression due to treatment versus length (L/D) shown in Figure 16 may be used.

Compressor noise and suppression studies were conducted using an advanced three-stage low pressure compressor (LPC) considered representative of the first compression unit in future SST engines. The design pressure ratio was 4.1 at a Rotor 1 tip speed of 1534 ft/sec. The 26.3-inch-diameter compressor had inlet guide vanes (IGV's) with variable trailing edge flaps, and all three stator sets were variable.

The characteristics of the basic compressor noise were studied as well as two different suppression concepts namely, a "hybrid" inlet and high Mach number IGV's. The hybrid inlet concept is based on a combination of suppression from a moderate amount of airflow acceleration suppression and wall acoustic treatment, and thus avoids the performance penalties associated with hard choking the inlet. The test vehicle was particularly suited to the high Mach number IGV suppression technique, because of the variable flap IGV's which could be closed to reduce flow area in the passage. At take-off conditions, the effect of auxiliary blow-in-door (BID) inlets, a necessary part of any SST inlet system, were investigated. An attempt was made in the design to suppress the noise leakage through the doors with airflow acceleration. Inlet and fan aerodynamic performance also was measured to determine the penalties of the various suppression techniques. Figure 17 provides a summary of the test configurations.

The hybrid inlet had a basic design quite similar to the SST/GE4 inlet, but had a bellmouth forebody to simulate low-speed-flight inflow conditions during the static tests. It was basically a model of a mixed-compression, axisymmetric translating centerbody inlet designed for $M_o = 2.5$ cruise. The centerbody was adjustable to two positions (takeoff and approach) using a spool piece inserted just forward of the six inlet frame struts. Four different segments of wall acoustic treatment were used in order to suppress a wide range of frequencies. Approximately half the treatment was located between the blow-in door and the compressor to provide some treatment suppression to noise which might be leaked through the doors. The treatment panels were replaceable with hardwall panels so that acoustic treatment suppression could be isolated.

26
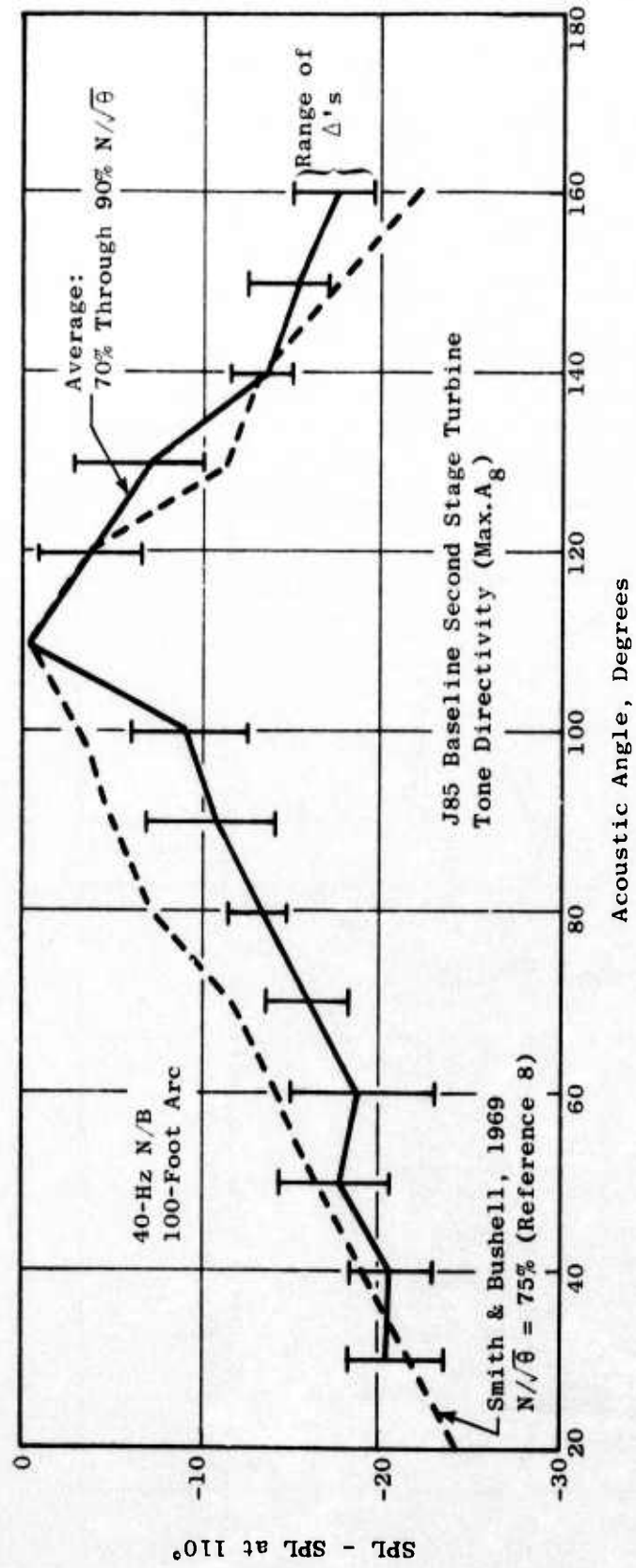
Figure 12. J85 Directivity Compared with Prior Results.

27
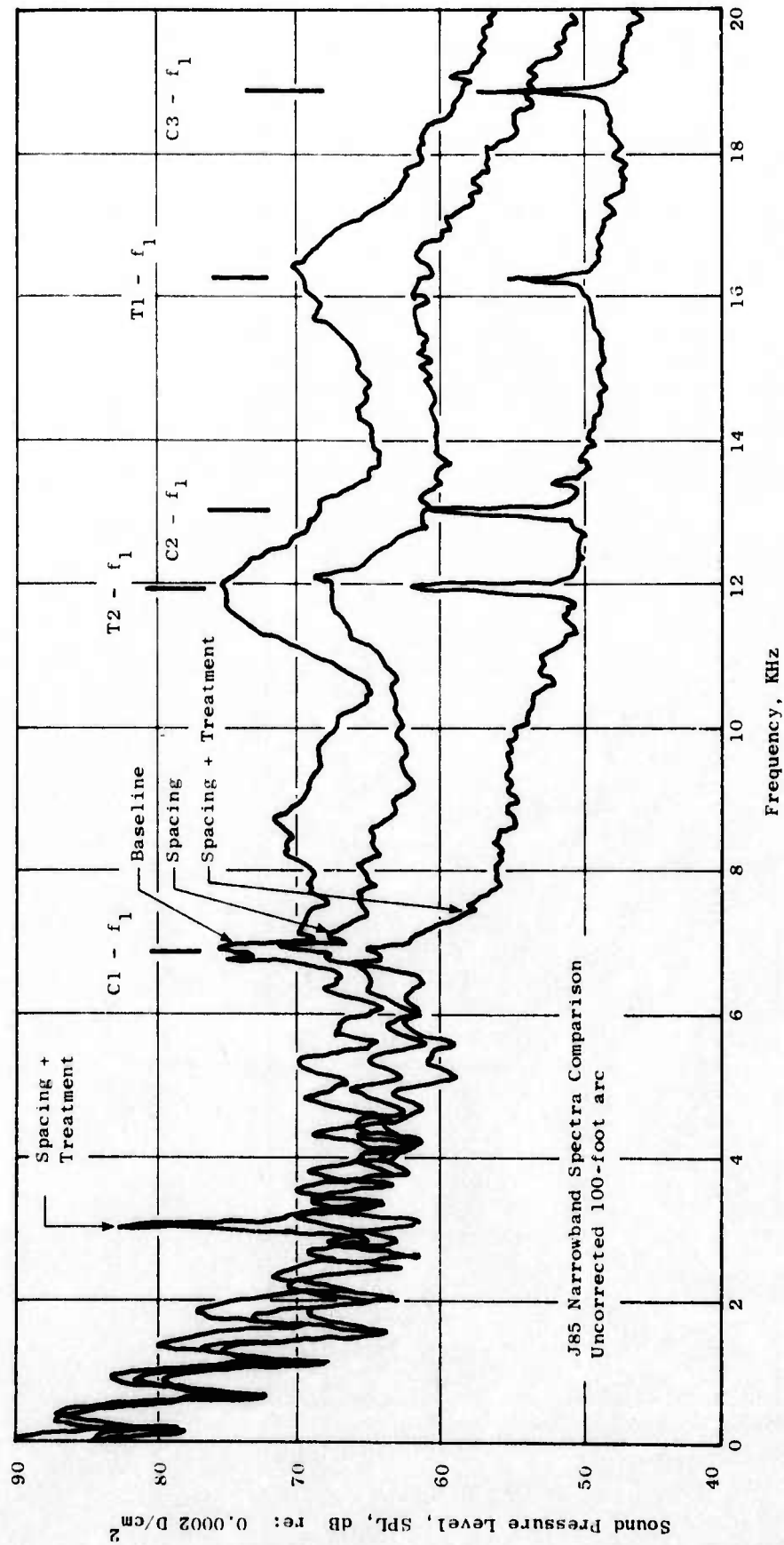
Figure 13. J85 Turbine Test, 80% Speed, 110° to Inlet, U_{tip} = 945 ft/sec.

28
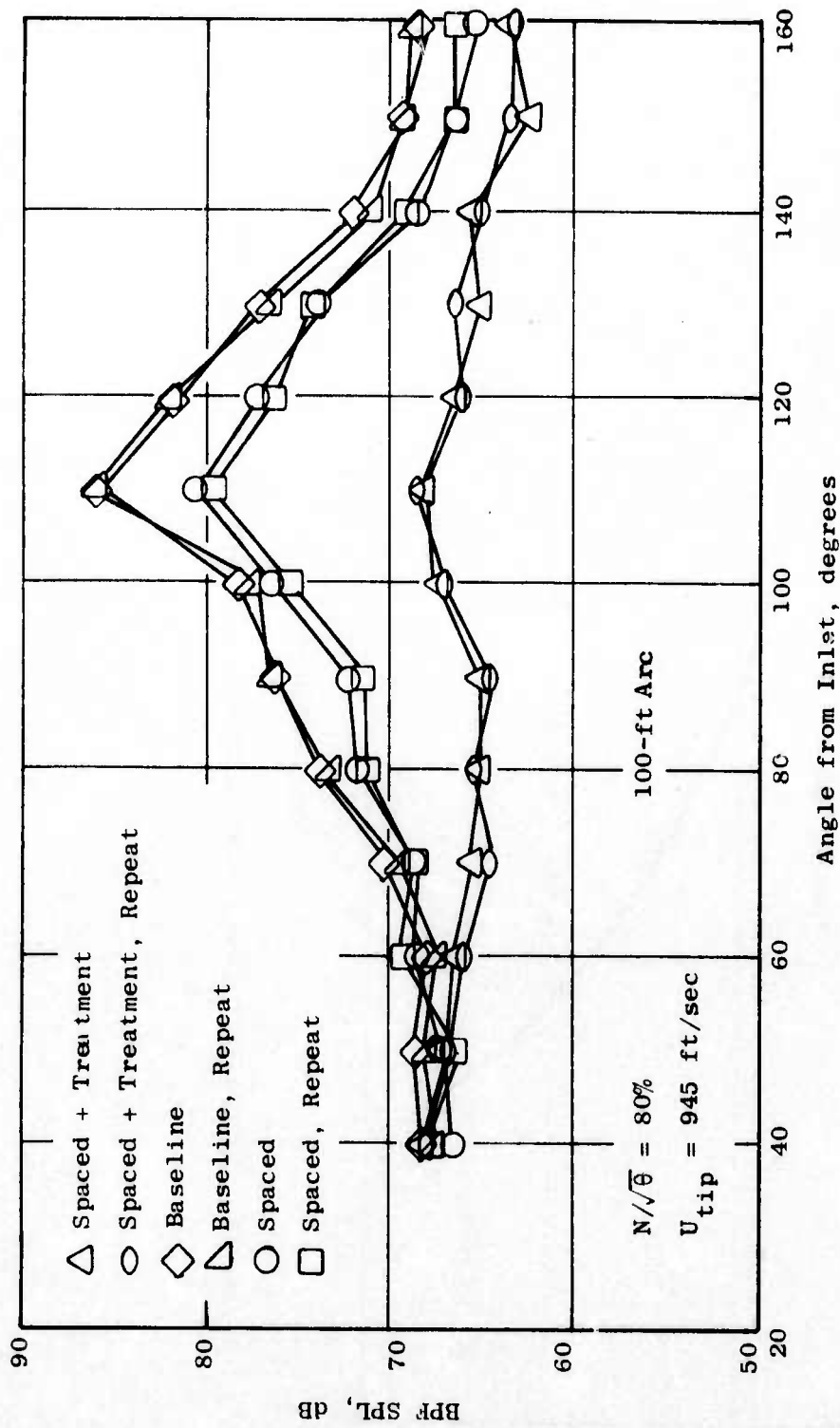
Figure 14. 1/3 Octave Second Stage Turbine Tone Directivity.
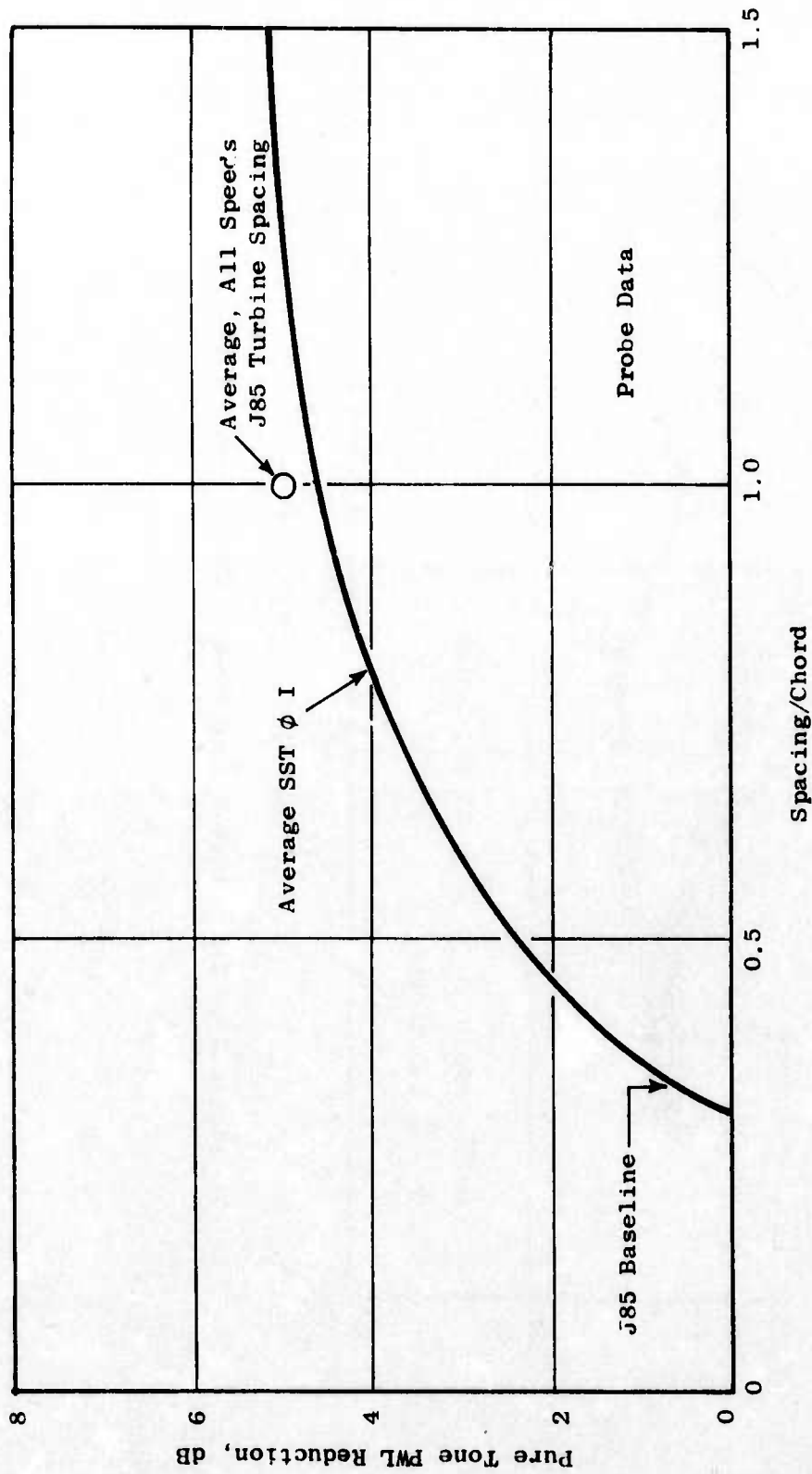
Figure 15. Effect of Spacing on High Pressure Turbine Noise, J85 and Phase I.

30
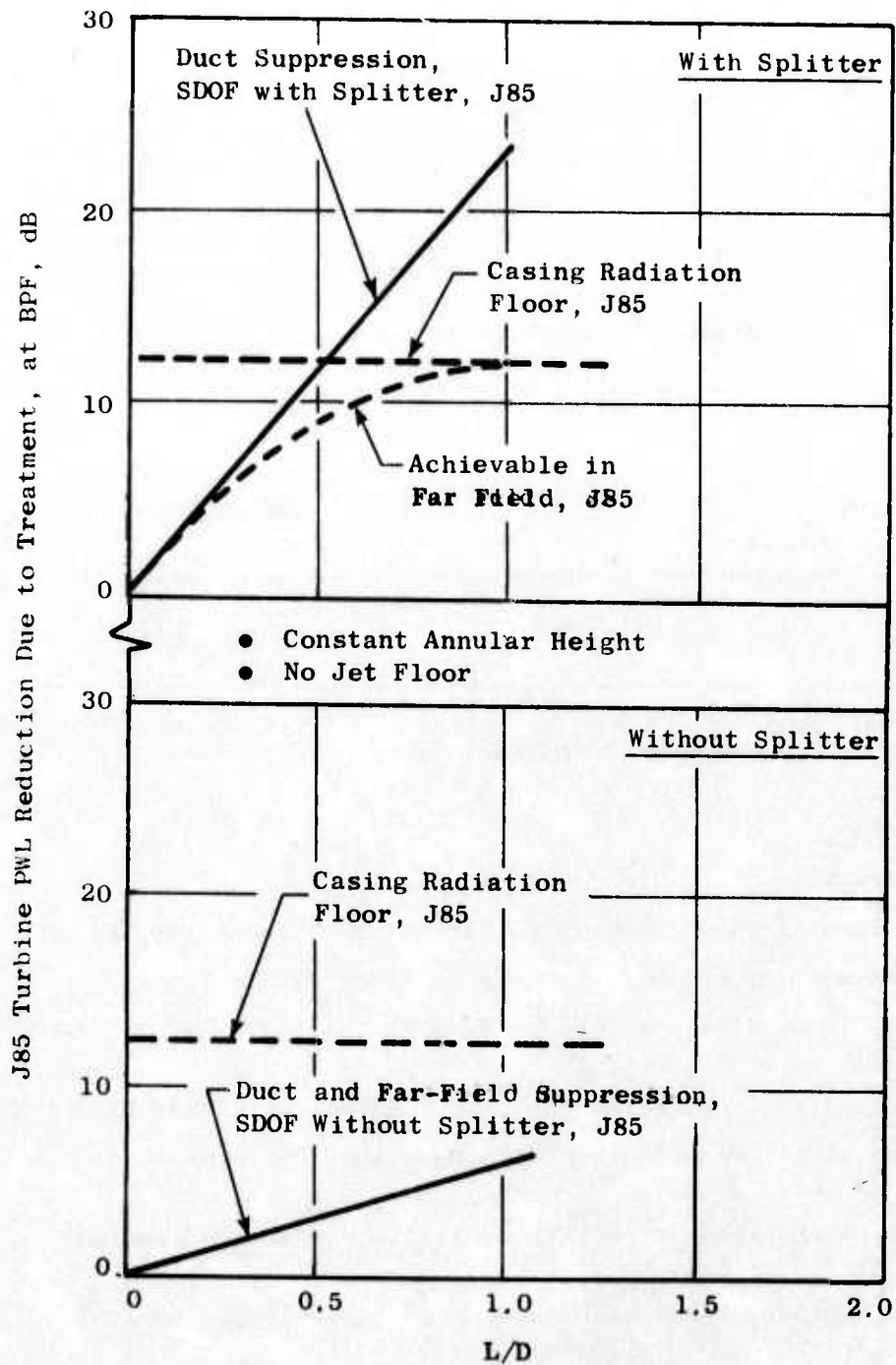
Figure 16. Effect of Acoustic Treatment on Turbine Far-Field Noise, J85.

31
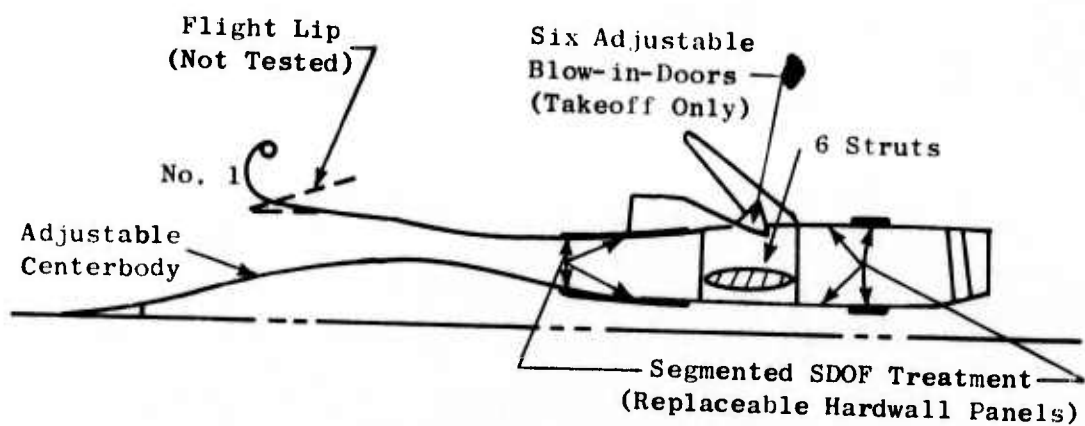
Hybrid Inlet Description
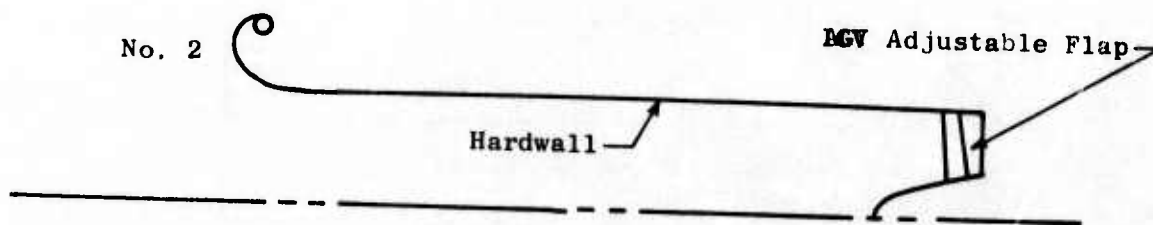
Baseline Cylindrical Inlet

Test Configurations

1. Baseline hardwall cylindrical inlet (Inlet No. 2)

2. Accelerating inlet with approach centerbody position (Inlet No. 1)

3. Hybrid inlet with approach centerbody position (Inlet No. 1)

4. Accelerating inlet with take-off centerbody position; BID closed (Inlet No. 1)

5. Hybrid inlet with take-off centerbody position; BID closed (Inlet No. 1)

6. Hybrid inlet with take-off centerbody position; BID nominal (Inlet No. 1)

7. Hybrid inlet with take-off centerbody position; BID 114% nominal (Inlet No. 1)

8. Hybrid inlet with take-off centerbody position; BID 81% nominal (Inlet No. 1)

9. High Mach IGV test (Inlet No. 2)

    Note: Accelerating inlet implies hardwall
           Hybrid inlet implies treated walls plus acceleration

Figure 17. Description of Compressor Test Configurations.

32

A baseline cylindrical inlet was also tested to evaluate the basic source noise characteristics of the compressor, to isolate the acceleration suppression, and to perform the High-Mach-Number IGV test.

The unsuppressed perceived noise level, PNL, of the compressor was found to be dominated at all speeds by either the Rotor 1 blade passing frequency (BPF) or its second harmonic. This is shown in Figure 18 which compares the full-scale (1045-1bm/sec engine) PNL and BPF sound pressure level versus speed trends. The 1/3-octave dominance of the BPF noise at all speeds is attributed primarily to the existance of the IGV's and the close spacing of all the compressor components. The IGV's not only have the effect of generating some pure tone noise but also delay the onset of multiple pure tones (MPT's) at high speed and limit their strength. On a 200-foot sideline, the unsuppressed PNL was observed to peak at a 40° inlet angle at all speeds.

The performance of the accelerating and hybrid inlet in the approach mode is summarized in Figure 19. In Part A, the full-scale PNL at a 200-foot sideline is plotted versus Rotor 1 tip speed. Superimposed is the one-dimensional average throat Mach number (based on throat corrected airflow and physical area) M_{th}, of the accelerating and hybrid inlets. At low speed, prior to the onset of acceleration suppression, there was a reduction of 3 to 4 PNdB due to inlet configuration differences between the baseline and the acceleration inlets. An additional reduction of 2-4 PNdB was provided by the wall treatment. The high throat Mach number design operating condition was selected based on the inlet performance shown in Part B of Figure 19. Thus, a throat Mach number of 0.78 was selected so as to avoid any significant performance penalty associated with the hybrid inlet suppression technique. At this Mach number, the hybrid inlet provided 11.5 PNdB suppression in maximum perceived noise relative to the baseline cylindrical hardwall inlet. Of this, 4 PNdB were due to the wall acoustic treatment.

The performance of the accelerating and hybrid inlets in the take-off mode is summarized in Figure 20. In Part A, the measured maximum PNL is compared to the baseline with the blow-in-doors closed. At the selected design operating condition, which again was based on inlet performance, the PNL reduction was 15.5 PNdB. Of this, only 0.5 PNdB was due to the treatment. With regard to inlet performance, it should be noted that, both for takeoff and approach, there was no penalty associated with the wall acoustic treatment, as determined by no difference in pressure recovery between the hardwall and treated inlets.

The effect of the blow-in doors on acoustic and inlet aerodynamic performance in summarized in Figure 21. The blow-in doors were tested with the hybrid inlet only. At low speed and low M_{th}, there was no noise level increase attributed to leakage through the doors. Thus, the wall treatment between the compressor and doors was fairly successful in limiting the noise leakage. With the doors open, the compressor could operate to higher tip speeds before high throat Mach numbers were generated in the primary inlet. This is, of course, the purpose of the doors, which provided a much more realistic compressor speed/flow operating condition for takeoff than did the doors-closed configuration. The M_{th} of the primary inlet is superimposed on the abscissa
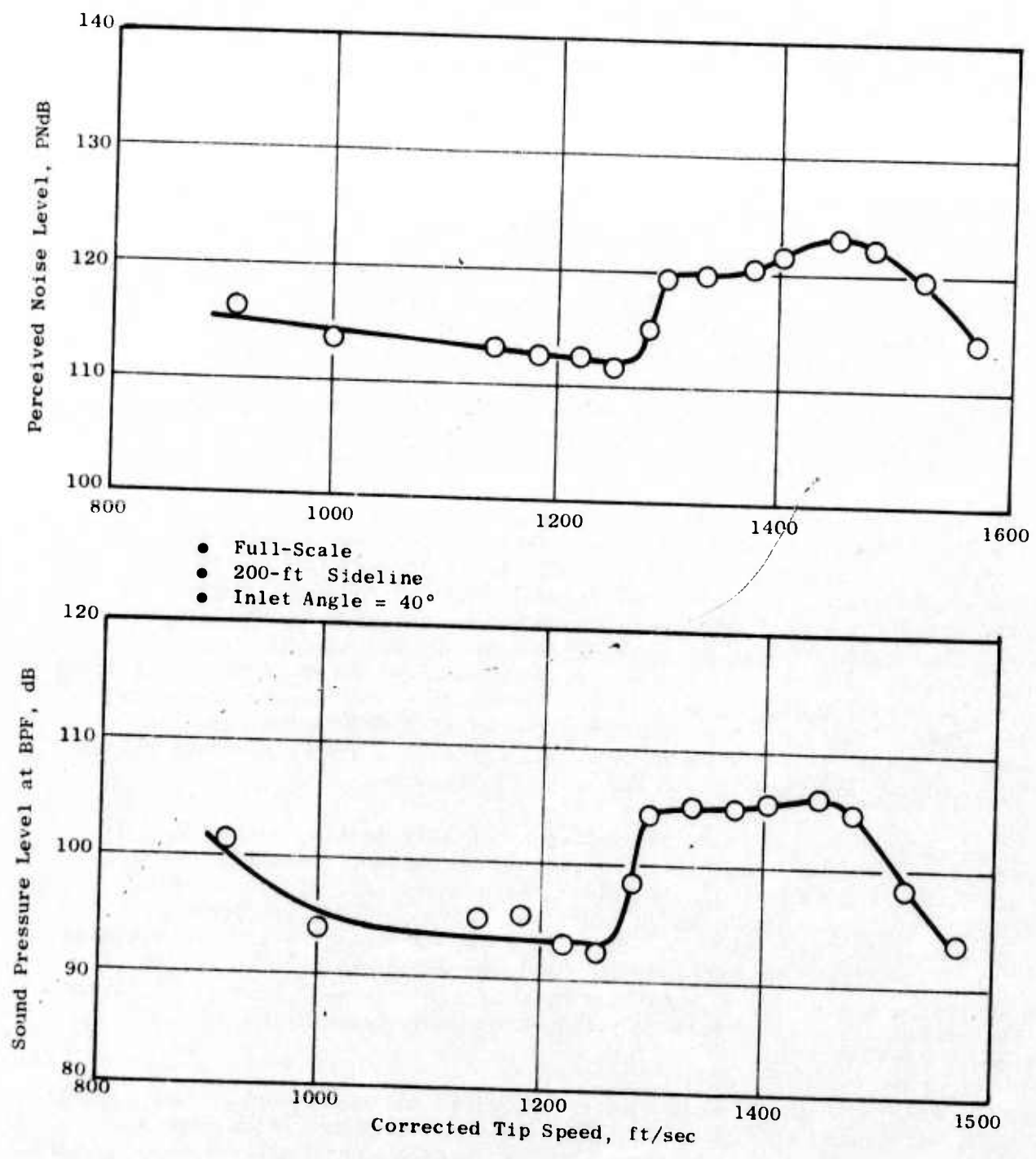
Figure 18. Character of Unsuppressed Compressor Noise.

34
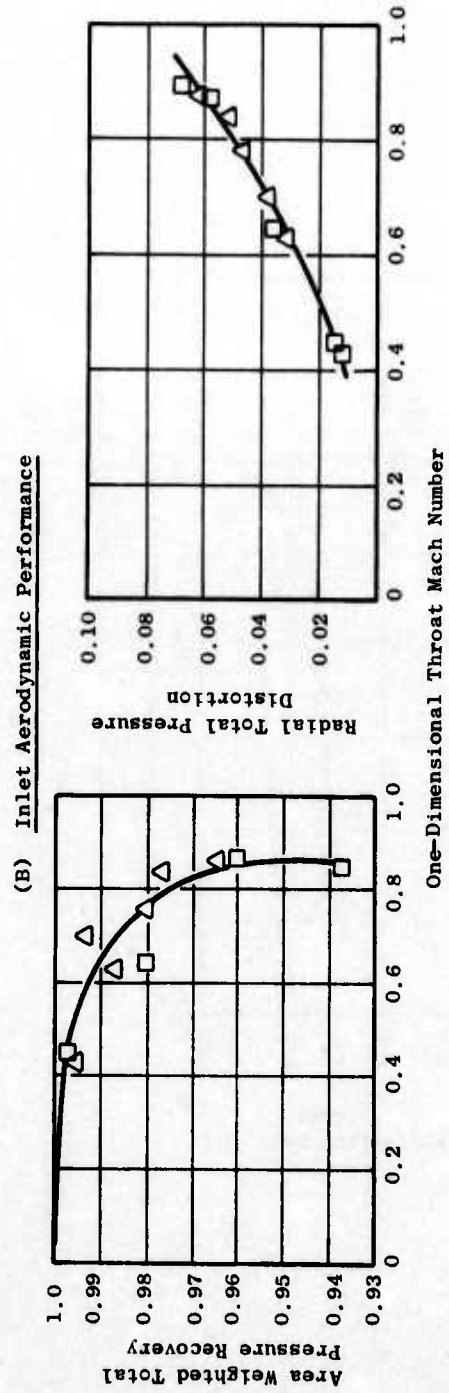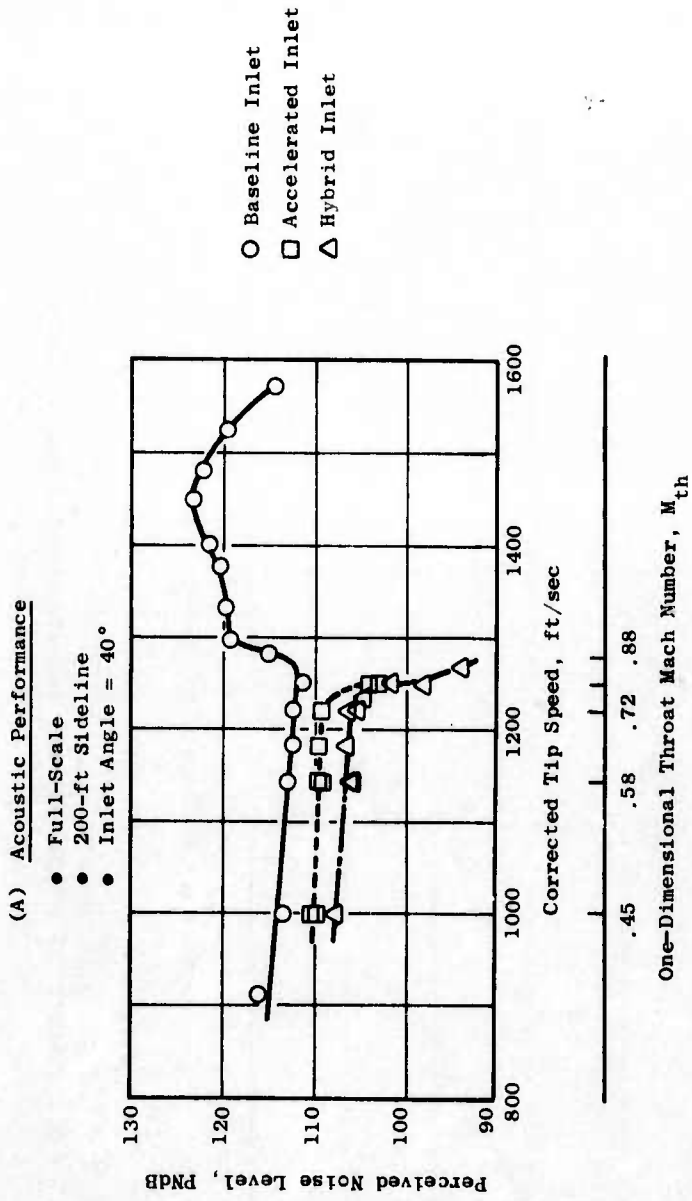
Figure 19. Performance of Hybrid and Accelerated Inlets at Approach.

35
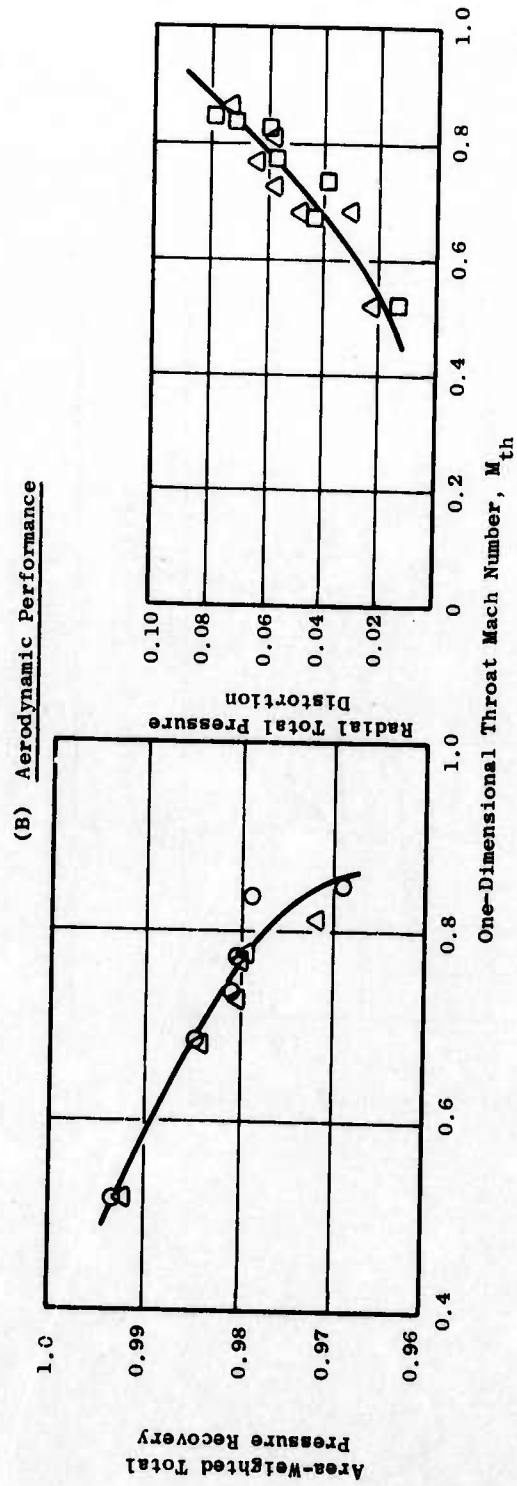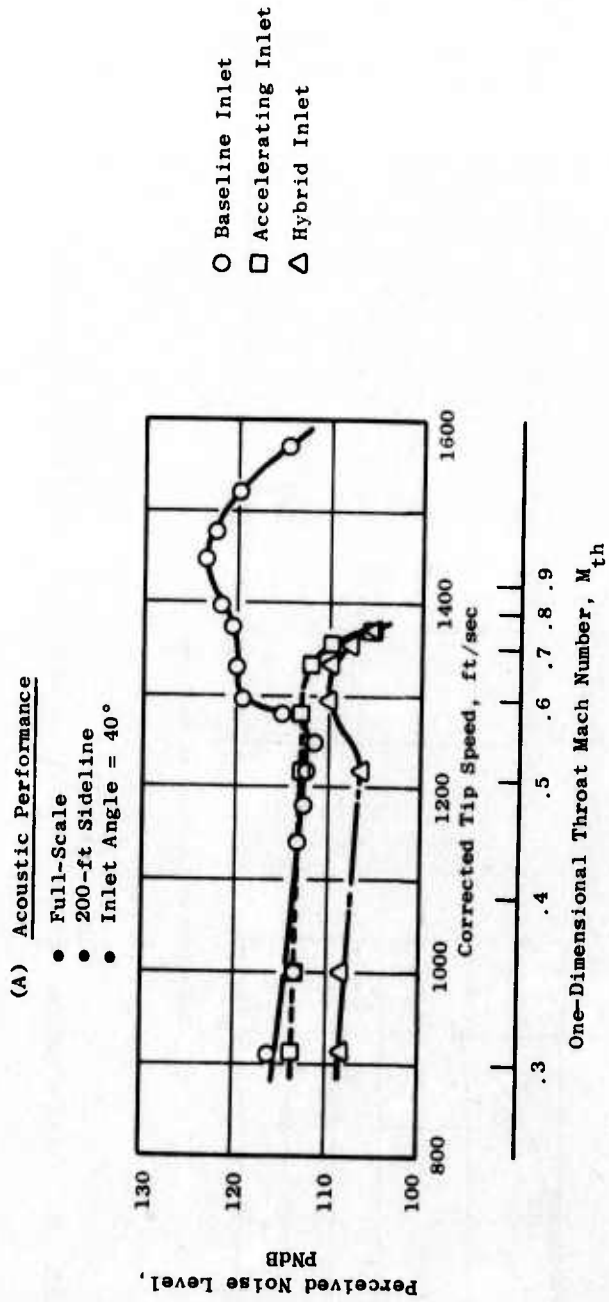
Figure 20. Performance of Hybrid and Accelerating Inlets at Takeoff.
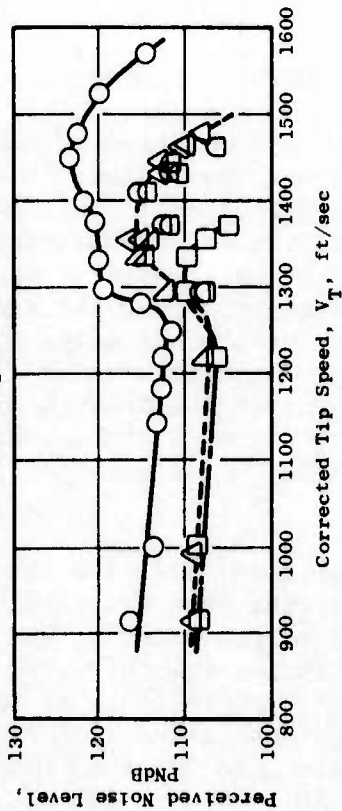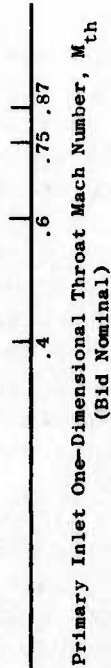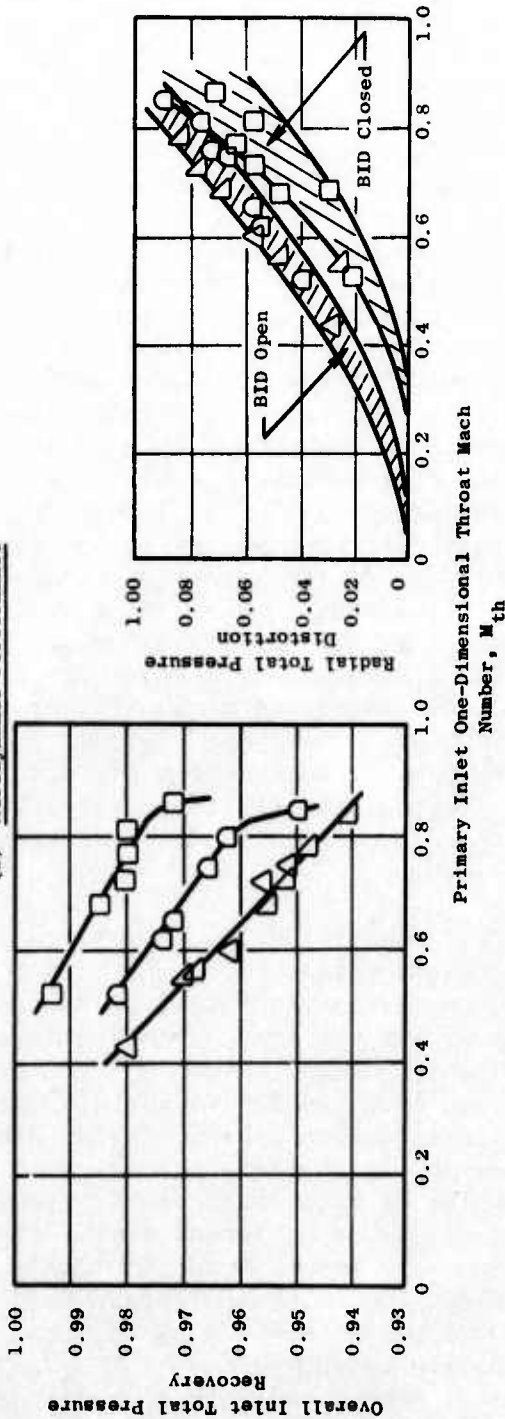
Figure 21. Summary of Hybrid Inlet Performance with Blow-In Doors at Takeoff.

37

in Part A of Figure 21 for the nominal BID position. It is seen that, for the most part, the maximum PNL was about the same regardless of BID position, although the 81% nominal position tended to produce somewhat lower values. This was not the design intent, and, in fact, the 81% position was the only one which operated according to prediction. More specifically, the blow-in doors were designed aerodynamically to produce different levels of passage Mach numbers relative to the primary inlet, as shown in Part A of Figure 22. This was intended to define both the leakage and suppression obtainable as a function of BID passage Mach number. However, the doors actually operated as shown in Part B of Figure 22. That is, they all produced about the same average passage throat Mach number for a given primary inlet throat Mach number, with the 81% position performing about as designed. The failure of the doors to operate as expected is suspected of being associated with poor flow quality caused primarily by the sharp side-plate corners. With the exception of the side plates, the BID flowpath entrance was rounded to the extent practical to provide good performance during static testing. Part B of Figure 21 shows that overall inlet performance was poorer with the doors open when compared on the basis of primary inlet throat Mach number, with the 81% position providing somewhat better recovery than the other two. Despite the fact that the door passage throat never attained high Mach numbers, noise levels on the order of 15 PNdB lower than the baseline were measured at high primary throat Mach numbers, as indicated in Figure 21 A. These lower levels were probably due to the large impedance change across the blow-in doors and the acoustic treatment between the flow-in doors and the IGV's. Surprisingly, no major change in the directional characteristics of the compressor noise was measured as a result of opening the doors. In summary, opening the blow-in doors did not result in a significant noise increase at the simulated take-off operating condition. Further investigations are recommended to improve upon blow-in-door design for static testing, so that the initial objectives of providing airflow acceleration suppression through the doors may be realized, and additional noise reductions relative to the baseline may be obtained.

High Mach Number IGV tests were run with the cylindrical baseline inlet at two compressor speeds (92.5 and 100% $N/\sqrt{\theta}$). These speeds were selected to provide enough airflow so that high Mach numbers could be generated in the IGV passage within the area variation made possible with the remotely variable trailing edge IGV flaps. Prior to testing, significant flow rollback of the compressor was expected due to the off-design operation associated with closing the IGV flaps to reduce passage throat area. The results, in terms of both acoustic and fan aerodynamic performance, are summarized in Figure 23. The IGV passage throat Mach number superimposed on the abscissa is the average one-dimensional value estimated from fairly detailed calculations of passage physical area as a function of flap angle. There is a general trend of noise reduction with flap angle (increased Mach number) as shown in Part A of Figure 23. Total reductions between the nominal and fully closed flap setting were 9.0 and 5.5 PNdB in PNL_{Max}, for the 92.5 and 100% $N/\sqrt{\theta}$ speed conditions, respectively. Associated with increasing the flap angle beyond the nominal fan operating value was a critical loss in fan performance, as seen in Parts B and C of Figure 23. The trend witnessed in the loss of pressure ratio and airflow was akin to deceleration along the nominal fan operating line. These

38
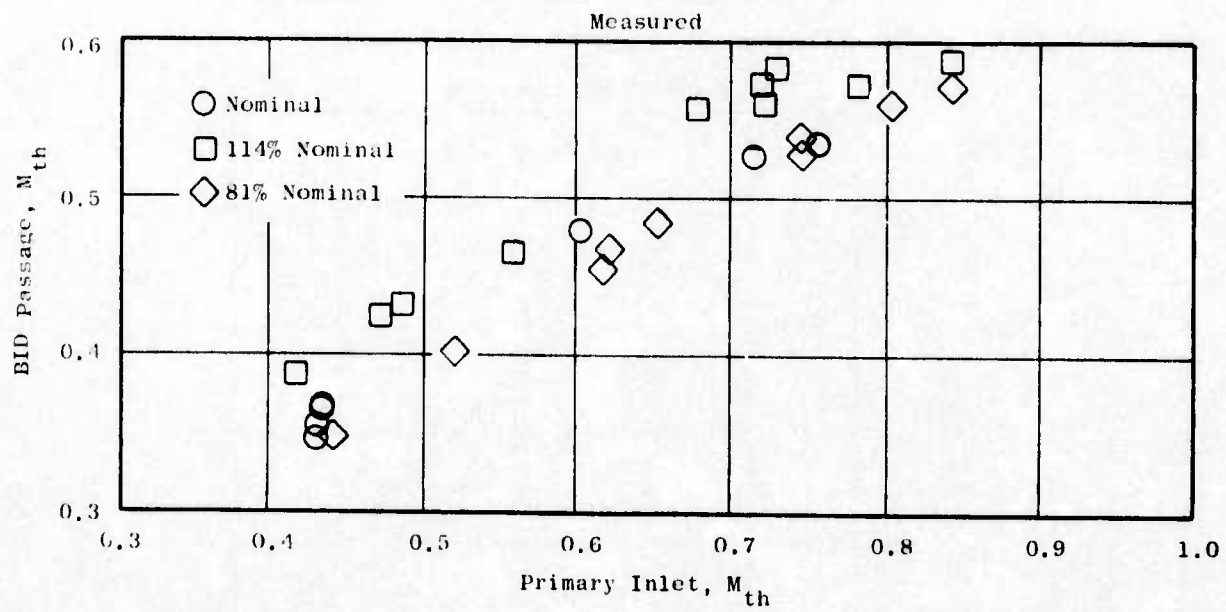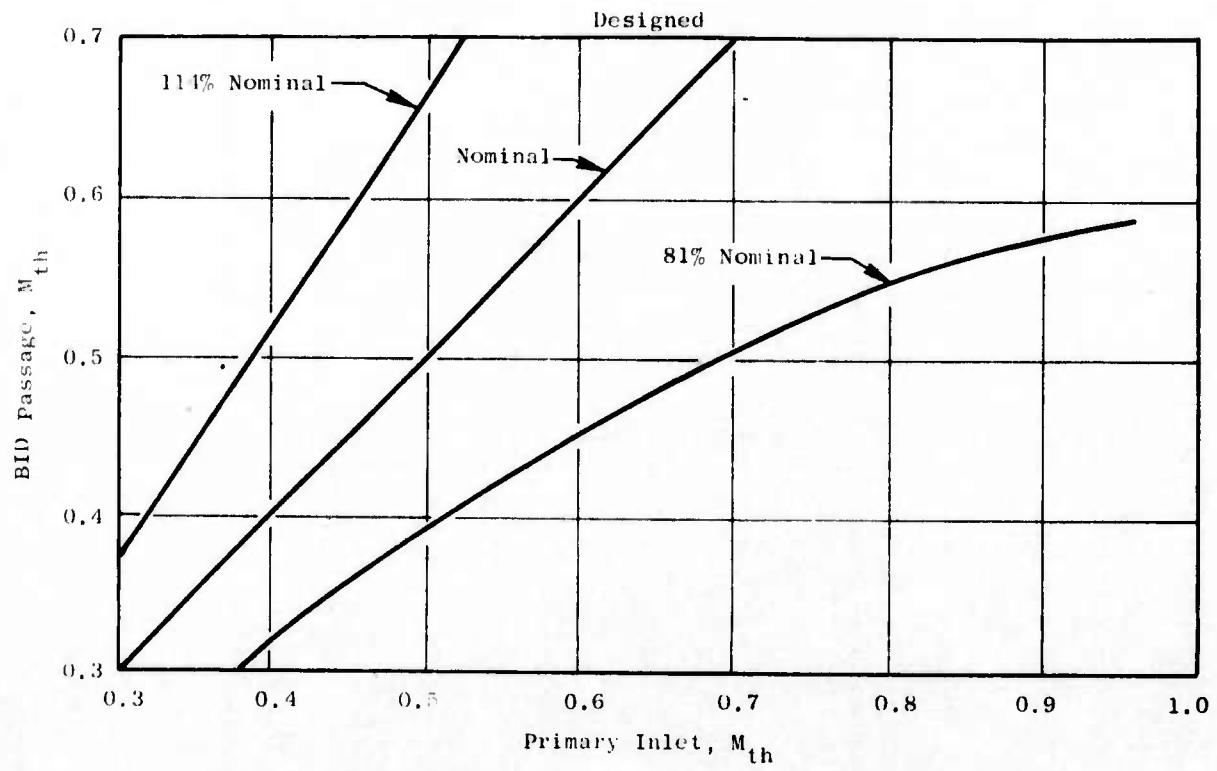
Figure 22. Variation of Blow-In-Door Passage M_{th} with Primary Inlet M_{th}, Designed Versus Measured.

39
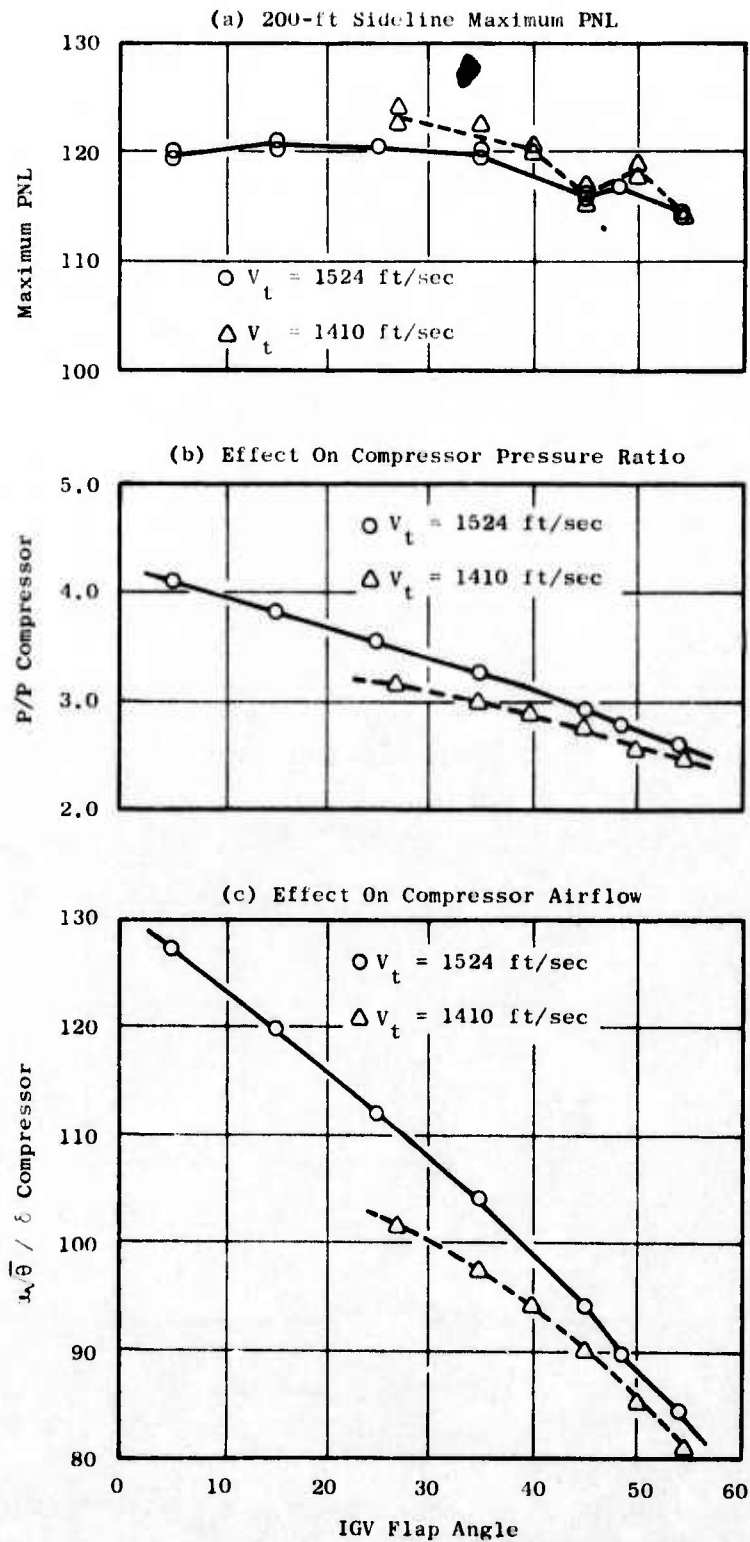
Figure 23. Summary of High Mach IGV Performance.

40

performance losses render impractical the high Mach number IGV technique for noise suppression in any operating condition requiring high thrust. Application of the technique to the approach operating condition might be possible.

In summary, the hybrid inlet approach to compressor noise reduction was shown to be a practical noise suppression device at all noise monitoring conditions. Large suppressions were obtained with minimum system penalty by making use of the variable geometry inherent in an SST engine inlet/nozzle system. Even with auxiliary inlets open, which provided a potential noise leakage path, significant noise reductions below the unsuppressed baseline were obtained for the take-off operating condition. The isolation of turbine noise in a J85 engine was demonstrated, and two practical approaches (spacing and treatment) to the suppression of turbine noise were demonstrated. The turbomachinery acoustic technology developed in this program will be useful in the development of any future SST engine, as well as other types of axial flow turbomachinery.

2.3 AIRCRAFT/ENGINE INTEGRATION AND SYSTEM EVALUATION

An overall SST system noise evaluation was performed on a representative aircraft/engine configuration. System EPNL calculations were performed at each of the noise monitoring points according to the current FAR Part 36 regulation for subsonic transport aircraft. In addition, PNL and EPNL contributions made by each major engine component (jet, turbine, combustor and compressor) were evaluated at these conditions. Footprint areas of 90 EPNdB contours were calculated for the suppressed SST and compared to an unsuppressed subsonic transport with four low bypass turbofan engines. Some practical aspects of applying component noise suppression to the SST system were addressed. The results of this study indicate that a suppressed SST system as defined by the systems integration work has the potential for meeting the current FAR-36 noise requirements; although additional work would be necessary before the actual levels could be achieved.

The SST system model used consisted of an airplane with an arrow wing and tail and four low bypass ($\beta=0.43$) turbojet engines mounted under the wing in axisymmetric nacelles. The projected takeoff gross weight of the aircraft was on the order of 900,000 pounds and could carry 292 passengers slightly in excess of 3400 nautical miles in an all supersonic cruise mission. The engine design airflow was 1045 lb/sec with a takeoff thrust of 61,400 pounds per engine. The engine was selected based on the results of a preliminary design study (Reference 4) which showed a low bypass turbojet to be one of the two most practical conventional type SST engines.

The method used in evaluating the system noise employed for the most part static acoustic data from the component tests conducted during the program. Conical (unsuppressed) and 32 chute suppressor jet noise data were utilized. Turbine noise reduction was obtained by increasing the second stage spacing. The YJ85 turbine tests were used to define the turbine noise reduction. Unsuppressed three stage low pressure compressor spacing and hybrid inlet data were employed for the compressor noise model. An estimate of the unsuppressed combustor noise was made from core engine estimates on turbofans which were tempered by some available data on a JT8D engine (Reference 64). These test results were used in a flyover noise prediction computer program which applied extra ground attenuation corrections, Doppler shift, noise scaling, distance extrapolations and General Electric's current understanding of jet relative velocity effects. No inlet flight effect corrections were applied.

As shown below, the estimated SST system noise exceeded the current FAR36 regulation level (for subsonic transports) by 1.1 EPNdB after employing the trading criteria. (Note that design tolerances must be considered when evaluating the results.)

	Current FAR36	Suppressed SST System	Traded FAR36	Traded ΔEPNL
Sideline	108	111.1	109.1	+ 1.1
Community (Cutback)	108	107.8		
Approach	108	106.5		

As expected, the jet noise dominated the system noise at the sideline (see Figure 24) and community (Figure 25) conditions. At approach (Figure 26), the jet suppressor was assumed stowed. The combustor was unsuppressed for all conditions. In the approach operating condition, the compressor noise dominated the unsuppressed system noise. However, when the turbomachinery noise was suppressed, significant contributions to system noise were made by all components, with the suppressed turbine making the least contribution. This indicated that obtaining further system noise reductions at the approach condition would be a complicated problem, requiring additional suppression on each of the major components.

The feasibility and practicality of the component noise suppression methods studied in this program and applied to the SST system were addressed. The 32 chute jet suppressor in combination with a translating shroud/annular plug nozzle was determined to be particularly attractive for SST engines. The plug assembly provides a convenient space for housing a retractable (32 chute) jet suppressor. The 32 chute suppressor used exhibited a good trade between PNL suppression and thrust loss, resulting in a design point $\Delta PNL/\Delta C_{fg}$ of greater than 2.1 to 1.0 (assuming no change in suppression due to flight effects). The hybrid inlet used for compressor noise suppression is also well suited for an SST application, in that it makes effective use of the variable geometry (inlet and nozzle) inherent in the system. Suppressions large enough to cause the suppressed turbine noise to emerge as dominant at approach were obtained with the hybrid inlet, while maintaining inlet pressure recovery at about 0.98 and steady state distortion levels at about 6.0 to 8.0% $(P_{Tmax} - P_{Tmin})/P_{Tavg}$. This was with a bellmouth inlet designed to simulate flight inflow conditions during static testing. Turbine second stage increased spacing (from 0.34 to 1.0 chord) was used to provide moderate amounts of turbine suppression, particularly on the tone. Such a spacing increase would result in a minimum penalty to an SST system. Greater suppression could have been obtained with turbine exhaust treatment, with a corresponding higher system penalty. This did not appear warranted, however, since the other components were making an equal or greater contribution to the system noise.

Ninety EPNdB contours were calculated for the suppressed SST engine and the enclosed area compared to that of typical unsuppressed narrow-bodied subsonic transports with four turbojet engines. At approach, the SST area was estimated to be about half that of the narrow-bodied transport, but was about 36% greater at the takeoff condition without cutback (see Figure 27). With cutback, the suppressed SST sideline noise area was about the same as the unsuppressed aircraft, suggesting a realistic takeoff operation over water where the large area along the flight path might have little influence on the surrounding populace.

The component acoustic technology developed in this program showed significant gains in terms of noise level and footprint area for a representative SST system employing viable suppression devices. The system has shown the potential for meeting the current FAR-36 noise requirements, although it is apparent that additional research and development is required to meet the present noise goals jet noise at the takeoff (sideline) condition is the most critical problem, but jet noise at the community (cutback) point and turbomachinery noise at approach are high enough to warrant continued attention. The combustor is also a source of concern, especially at approach.
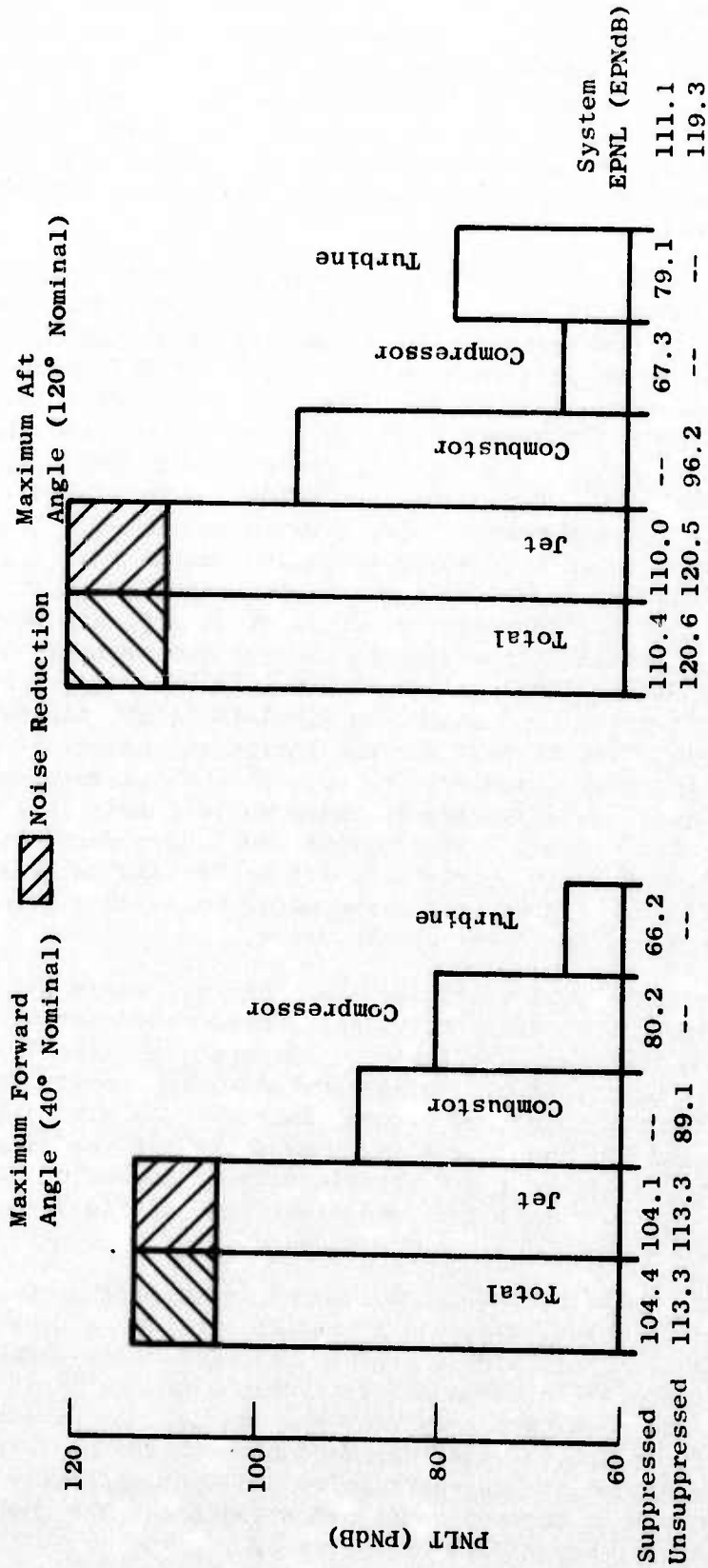
Figure 24. Component Noise Comparison at Takeoff (Sideline).

Figure 25. Component Noise Comparison at Cutback (Community).

- 4 Engines
- TOGW = 900,000 lb
- Cutback Thrust = 35,000 lb/Engine
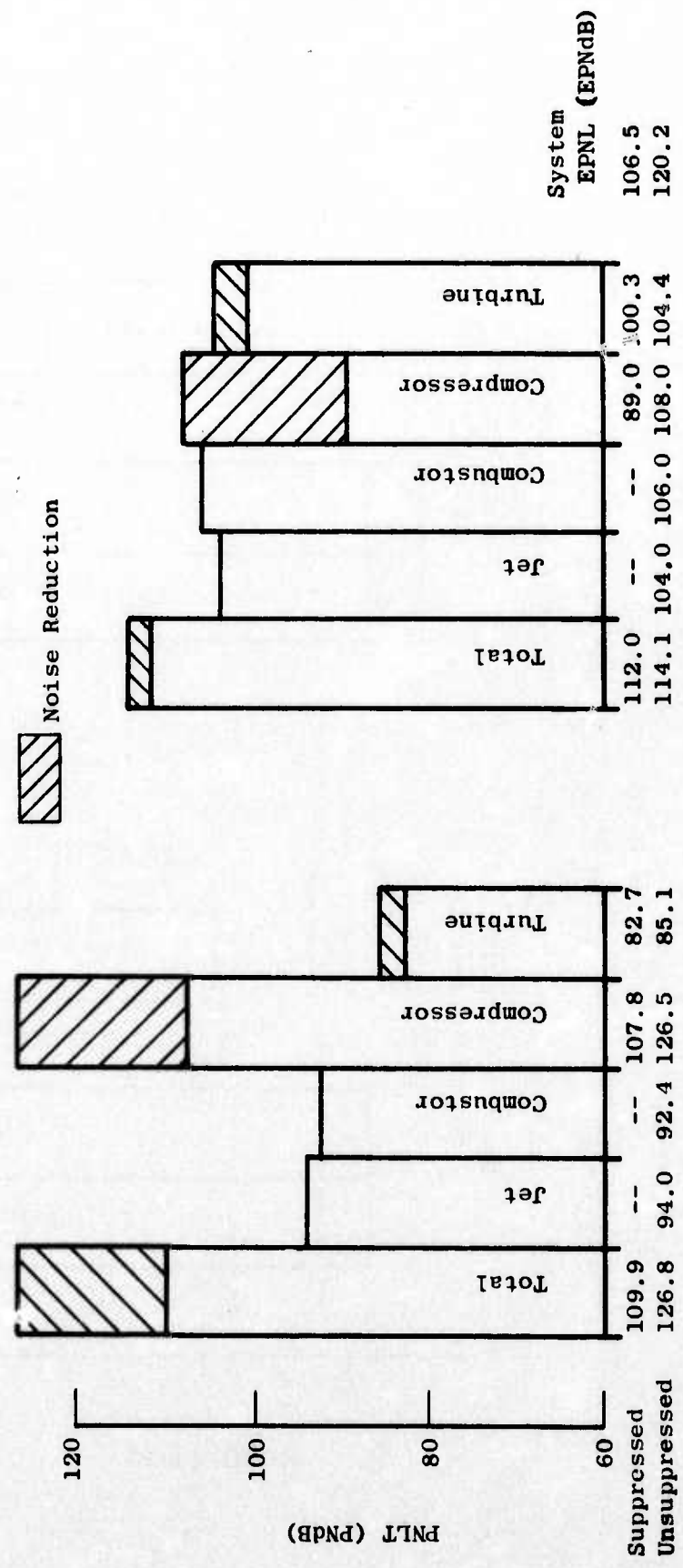
Figure 26. Component Noise Comparison at Approach.

90 - EPNL Footprint Areas

	Suppressed SST	Unsuppressed Narrow-Bodied Subsonic Transport
Takeoff	67.6 sq n mi	49.8 sq n mi
Cutback	80.8 sq n mi	----
Approach	5.5 sq n mi	11.3 sq n mi

• 4 Engine Aircraft

Figure 27. Comparisons of 90-EPNL Noise Contours.

47

3.0 JET NOISE REDUCTION TECHNOLOGY

3.1 INTRODUCTION

3.1.1 Background

The Jet Noise Reduction Technology effort conducted in this program is intended to provide basic aeroacoustic data for application to a range of possible advanced engine systems with prime emphases on high-flow turbojets, and to investigate new suppression concepts, identifying those that showed high potential for more detailed evaluation. The work in the Jet Noise Reduction Phase was carried out through a series of scale model and engine tests which were preceded by aeroacoustic design studies. The selection of the most promising suppressor concept was made based on the results obtained during the overall system trade studies. Model scale and large scale engine demonstrations were conducted, and the overall system was evaluated in the aircraft systems integration phase of the program (see Section 5.0).

3.1.2 Approach

The Jet Noise Reduction Technology effort was, in part, a continuation of the Jet Noise Suppression work conducted under the original SST program. During that time (1966-1970), General Electric had conducted a multitude of suppressor investigations and acoustic and aerodynamic tests on a variety of suppressor concepts including multielement suppressors with and without secondary ejector systems. This extensive background, as reported in Reference 1, provided a wealth of information which aided in the selection and evaluation of new suppressor systems. Toward the closing days of the SST contract, annular plug nozzle systems appeared to provide a viable means of implementing the multielement (spoke/chute) suppressor systems by stowing them in the translating plug while providing attractive aerodynamic performance during the subsonic and supersonic legs of the mission. In addition, the attractiveness of the relatively simple multispoke/chute annular plug suppressor system was also apparent from an acoustic standpoint, since moderately high PNL suppression levels ($\sim$ 13 dB) had been demonstrated.

The multielement concept achieves suppression by segmenting the high velocity jet into a number of smaller jets, thus shortening the length of the jet's potential core. Turbulent mixing of entrained ambient air (down the back of the spokes and chutes) with the elementized primary flow tends to reduce the overall jet velocity and reduce the noise. The chute (ventilated spoke) is an aerodynamic improvement of the solid-element spokes, in that the backside of the chute forms a channel for air entrainment.'

This system was subsequently identified for development in this program, since it showed the greatest potential for meeting the FAR Part 36 noise requirements. Multitube nozzles also were selected for continued development

48

since the tube cluster nozzles had previously demonstrated high suppression levels. The development effort in this program had as its principle objective, the extension of multitube technology and performance to annular plug nozzle types while still maintaining high suppression and improving aerodynamic performance.

New concepts in jet suppression also were studied to identify advanced suppressor systems for possible SST application. Injector tests with several different suppressor systems provided additional background in hardwall and acoustically treated ejector effects.

Model and engine tests of the final suppressor configuration, determined from overall considerations of the aircraft/engine system, provided the basis for model-to-engine size scaling comparisons of a practical suppressor design.

Figure 28 illustrates the approach followed in the jet noise reduction technology effort to carry out the program objectives.

3.2 MODEL SUPPRESSOR AEROACOUSTIC TESTS

3.2.1 Scope and Data Presentation

The jet suppressors tested in this program are categorized by type and major investigative effort (as shown in Figure 28). Only the studies and tests prior to the selection of the final suppressor configuration are included in Section 3.2. The final configuration selection is described in Section 3.3, while subsequent tests of the final configuration are described in Section 3.4.

The categories in Section 3.2 include;

Multispoke/Chute Suppressors (3.2.2)

The continued development and refinements to the multielement (spoke/chute) suppressor system are discussed. This section includes aeroacoustic test results of:

- 40-spoke and 40-chute suppressors

- 36-chute suppressor with and without ejectors

- Comparisons of 32-, 36-, and 40-chute suppressors

Multitube/Annular Plug Suppressors (3.2.3)

The implementation of multitube suppressors to annular plug nozzle systems is discussed. Included are aeroacoustic test results of:
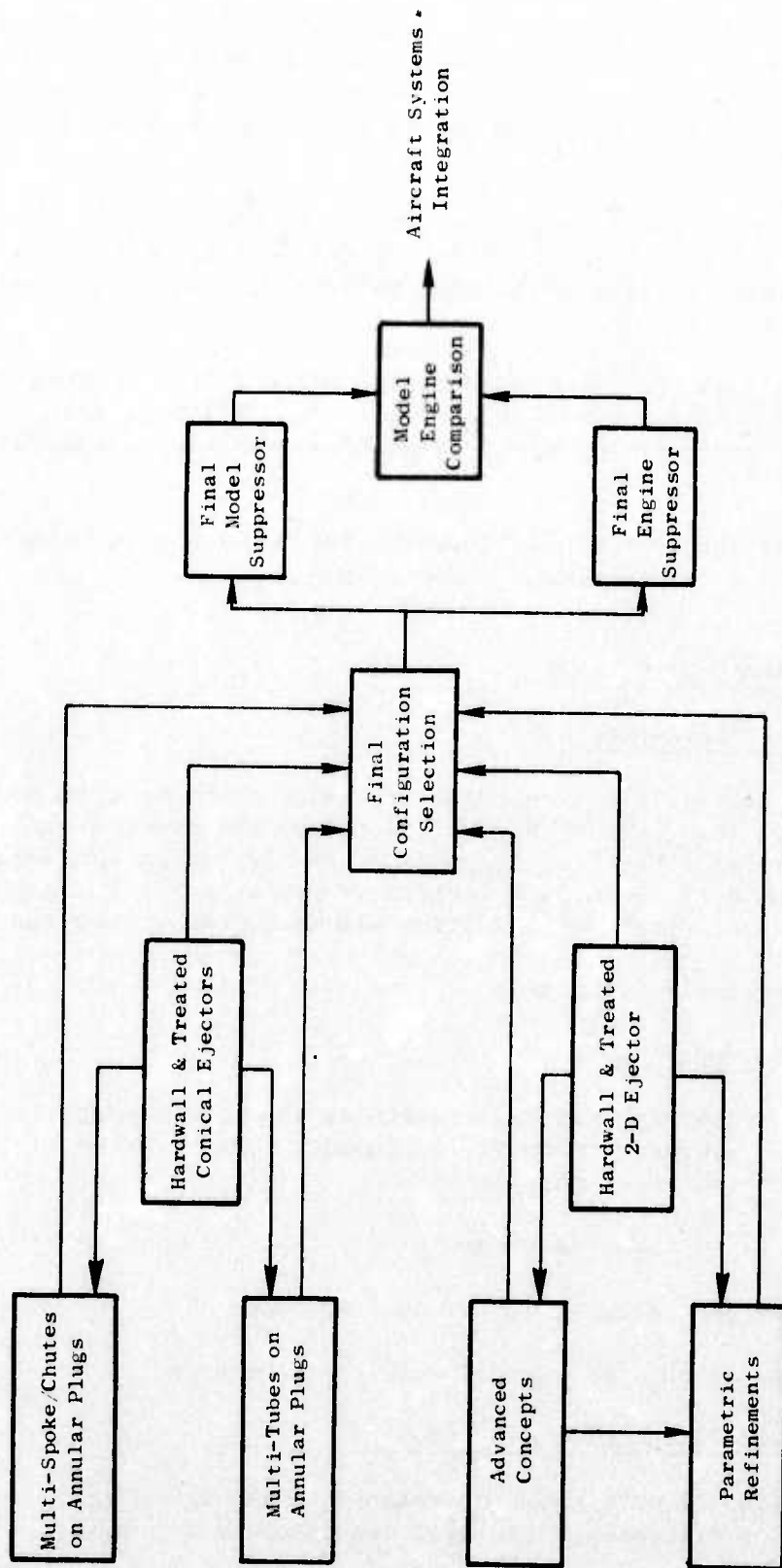
Figure 28. Approach for Jet Noise Reduction Technology.

50

- 72-tube and 66-tube suppressors on annular plug nozzles

- 66-tube with ejector

Advanced Concepts (3.2.4)

The search for advanced or novel exhaust nozzle concepts which had potential for high suppression is discussed. Presented are the preliminary evaluations of:

- Asymmetric 2-D nozzle systems

- Dual-flow exhaust nozzles

- The orderly structure experiment

Parametric Refinements (3.2.5)

The selection and refinements of two suppressor systems which had potential for high suppression are discussed. Included are the final evaluations of:

- Dual-flow exhaust nozzles

- Asymmetric 2-D nozzles

The acoustic data are presented as full-scale in size and frequency range except where noted (i.e., near-field measurements are presented as measured, model data; the orderly structure test results in Section 3.2.4 are model scale results).

Acoustic results are presented in the form of tabulations and plots of normalized peak perceived noise level (PNL), measured in PNdB, around an arc and at specific sideline distances. Tabulation summaries of the acoustic results are included in a separate appendix (Appendix C). The model data, taken on a 40-ft arc, were scaled by a factor of 8:1 (10:1 for suppressed 2-D in Section 3.2.5) to obtain full-scale data on a 320-ft arc with sideline extrapolations to 300, 1500, and 2128 feet. PNL suppression comparisons at 300-, 1500- and 2128-foot sidelines (relative to a baseline conical nozzle or other baseline reference configuration), are included. Frequency spectra and PNL directivity at selected increments of velocity also are included for many of the nozzle categories. The normalization factor, 10 log ρA, was used to adjust for small changes in the physical model areas which are reflected in the full-size area when scaled by a common scale factor. In no case is it intended to be used as a means of normalizing scale model with large scale engine test results.

51

No free-field corrections were made on the acoustic data of Section 3.2 taken on the JENOTS facility. The final model and engine data found in Section 3.4.3 are corrected for free-field per the method described in Reference 3.

The test conditions specified for the majority of the jet suppressor configurations were based on a simulated operating line for the GE4 supersonic transport engine over an ideal jet velocity range from 1000 to 3150 ft/sec which is representative of typical AST cycle studies.

Selected laser velocimeter measurements of the jet plume were taken on several of the suppressor configurations to assist in pinpointing some of the more critical aerodynamic flow characteristics which would influence the far-field acoustic data (e.g., point of element coalescense, maximum turbulence intensity regions, etc., as the geometry was varied). The results are presented as radial and axial distributions of mean and turbulent velocities.

Aerodynamic static performance and wind tunnel tests were conducted on the majority of the suppressor configurations tested to determine static and installed gross thrust coefficients, respectively. Base pressure measurements also were obtained with most suppressor configurations which are presented as base pressure radial profiles and base drag coefficients.

3.2.2 Multispoke/Chute Suppressors on Annular Plug Nozzles

3.2.2.1 40-Spoke and 40-Chute/Annular Plug Suppressors

Preliminary Review of Aeroacoustic Data

During the SST program (FA-SS-67-7), the spoke/chute jet noise suppressor system was developed through a series of scale model tests and several J85 engine suppressor tests. These suppressors were integrated with a cylindrical translating shroud plug nozzle applied to a high flow, nonaugmented at takeoff engine cycle.

Parallel acoustic and aerodynamic test programs evaluated variable geometric parameters of element number, area ratio, element planform, insertion angle relative to the gas stream, and solid spoke versus ventilated chute. The program made available the initial test data and minimal analysis before the SST program was terminated.

The spoke/chute jet noise suppressor concept, when applied to the high airflow J6H2 engine cycle, showed the GE4/SST system capable of meeting the FAR Part 36 noise regulation within an acceptable thrust penalty. Therefore, the system was considered for further development and refinement during this program. The data obtained during the SST program were analyzed more

thoroughly, and correlations were made in a fashion suitable for use in aeroacoustic predictions.

From this analysis, major geometric parameters influencing both acoustic and aerodynamic performance were identified. A series of new models was defined for study, incorporating the favorable aeroacoustic trade mechanisms identified in the data analysis. Aerodynamic and acoustic performance estimates were made for the suppressors.

Spoke/Chute Acoustic Data Review

Figures 29 through 33 show schematically the spoke/chute model designs tested during the original program, the acoustic suppression performance, and the aerodynamic wind tunnel measurements. Details of the tests and results can be found in the DOT/FAA Phase I Final Report (Reference 1). The acoustic performance is in terms of 2128-foot (0.35 n mi) sideline delta Perceived Noise Level (ΔPNL) relative to a conical convergent nozzle baseline.

Figure 29 is for spoke nozzle area ratio variation, defined as total annulus area divided by flow area. Figure 30 is for element number variations; models tested with 24, 32, 48, and 64 elements acoustically and at 24, 32, and 48 elements aerodynamically. Figure 31 is for cant angle variation; that is, the angle of spoke penetration within the gas stream. Three positions were used, namely, inclining the spoke exit such that the flow was directed down the 10° half angle plug (-10° position), parallel to the nozzle centerline (90° position), and away from the plug (+10° position). Figure 32 shows solid spoke versus ventilated chute, indicating that the entrained secondary flow through the chutes was only slightly beneficial acoustically, but improved aerodynamic performance substantially due to higher base pressure and corresponding lower base drag. Figure 33 shows the effect of spoke planform, parallel spokes versus tapered spokes. The parallel-sided spokes directed the major portion of flow through the outer annulus region and had better acoustic performance but with an accompanying high thrust decrement. Reviewing Figures 29, 30, and 33, a major parameter influencing acoustic design is the apportionment of flow with radial location within the annulus. Thus, the individual increments of increased suppression resulting from each geometry change, as seen in Figures 29 through 33, cannot be lumped for future model predictions without consideration of flow distribution. These data subsequently were reviewed from a suppression/performance tradeoff point of view to assist in the selection of new suppressor nozzles. Although spoke nozzles exhibited fairly high suppression, their suppression/performance characteristics were poor. The long chute configuration, however, did yield suppressions in the order of 11-13 PNdB with corresponding suppression/performance levels greater than one to one.

Based on these data, the design point of the new nozzles was chosen as $P_{T8}/P_0 = 3.0$, $V_j = 2500$ ft/sec with the goal of achieving higher suppression than previously demonstrated with more favorable aerodynamic/acoustic trade.
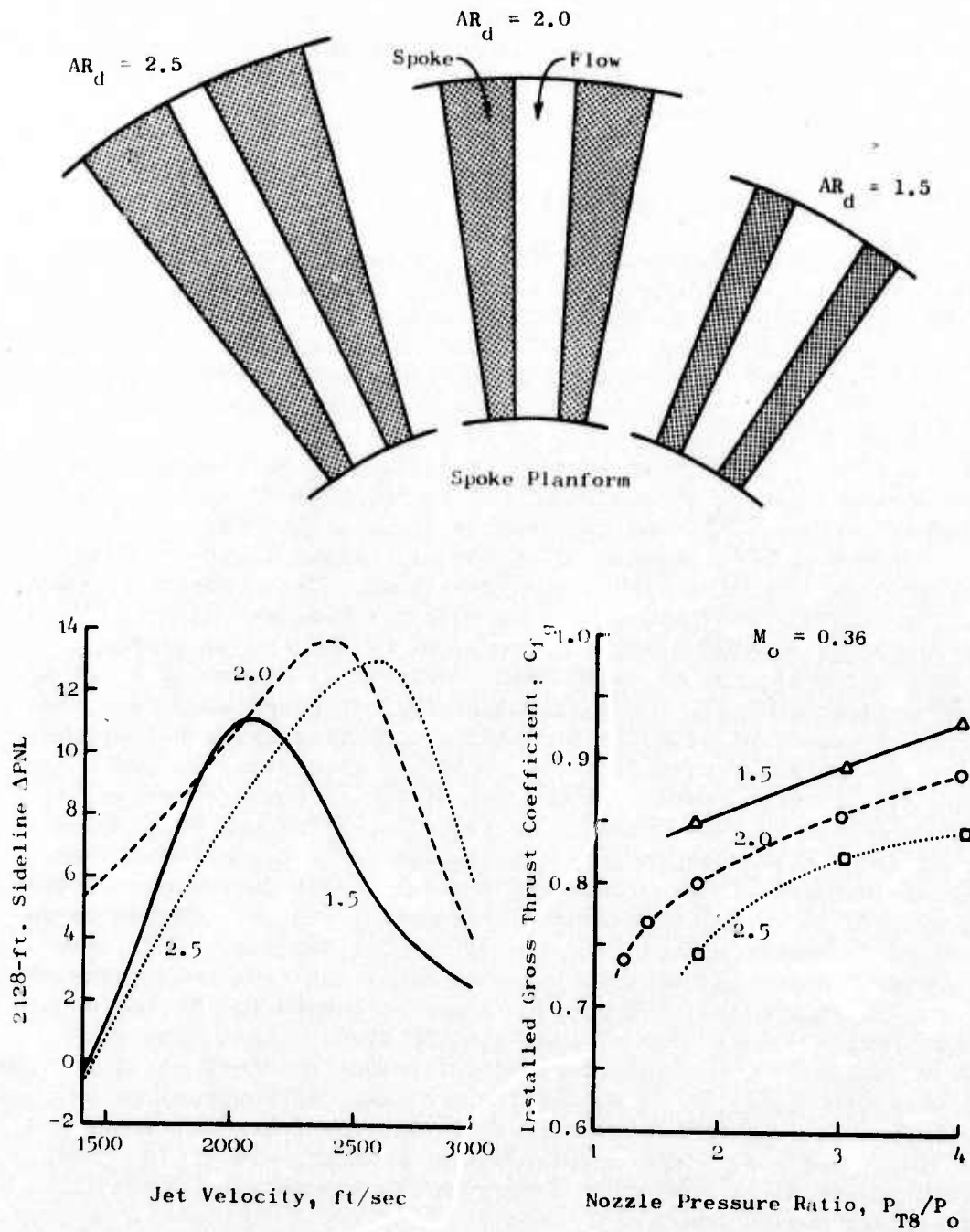
Figure 29. Spoke Nozzle Area Ratio Variation.
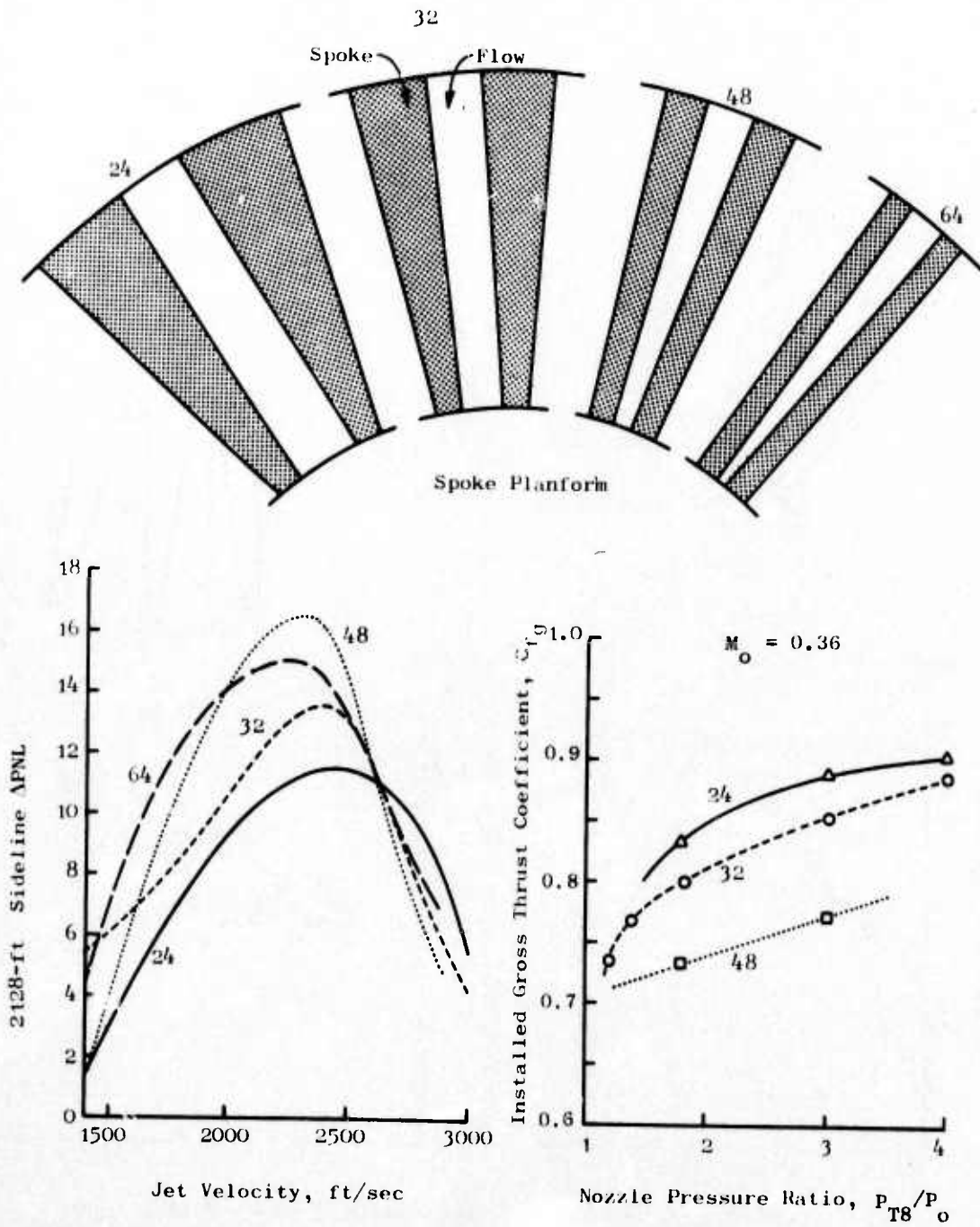
Figure 30. Spoke Nozzle Element Number Variation.

55
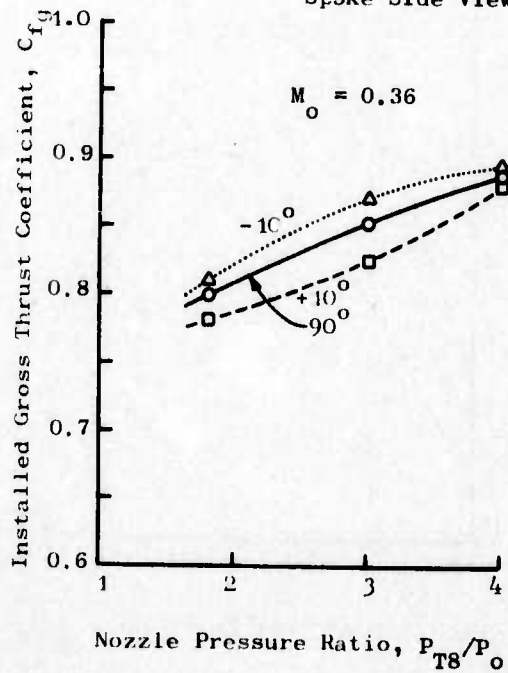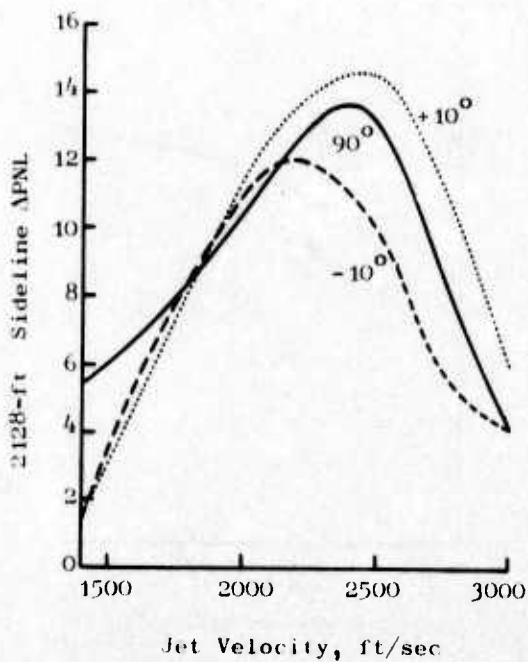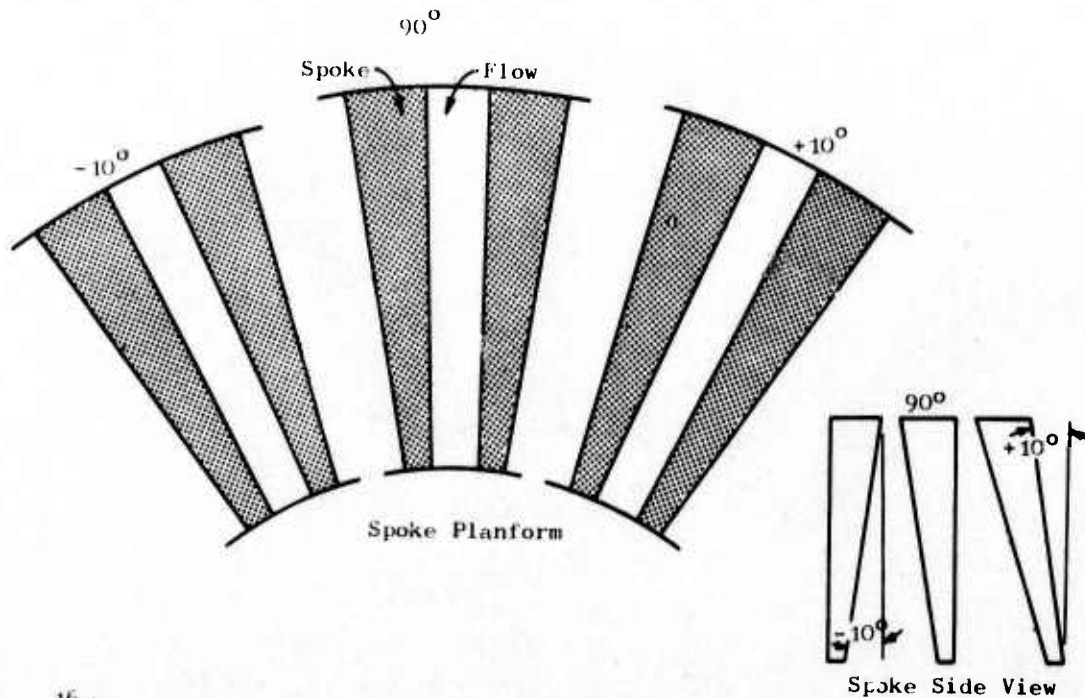
Figure 31. Spoke Nozzle Cant Angle Variation.

- 32 Elements @ $90°$ to Nozzle $\mathcal{C}$
- $AR_d = 2.0$

Spoke/Chute Planform

Chute   Spoke

Jet Velocity, ft/sec

Nozzle Pressure Ratio, P_{T8}/P_o
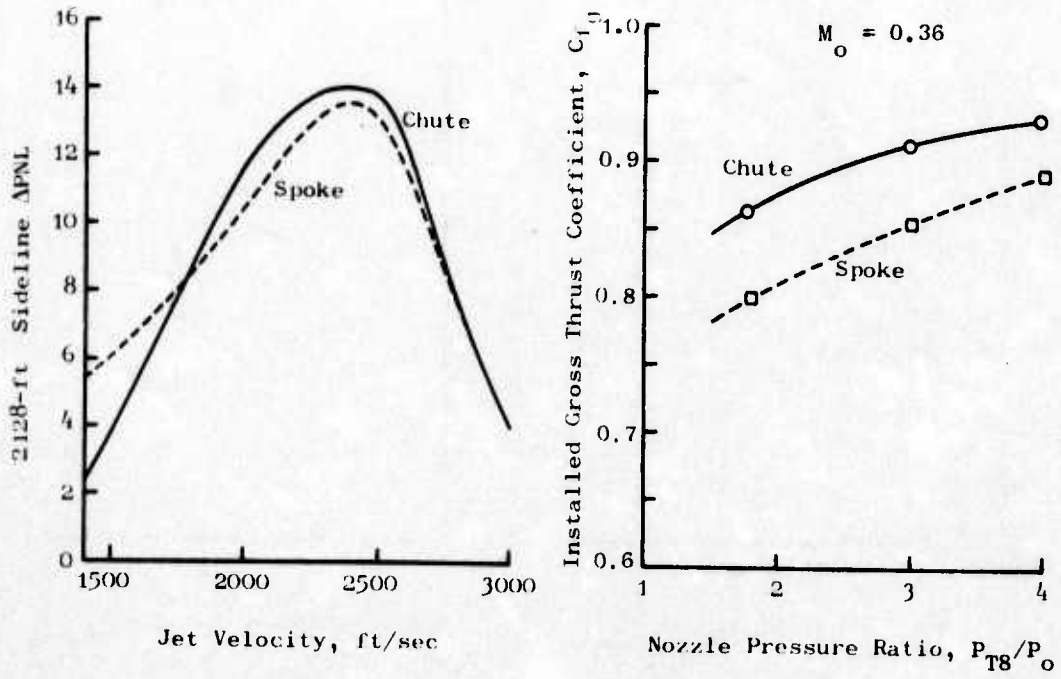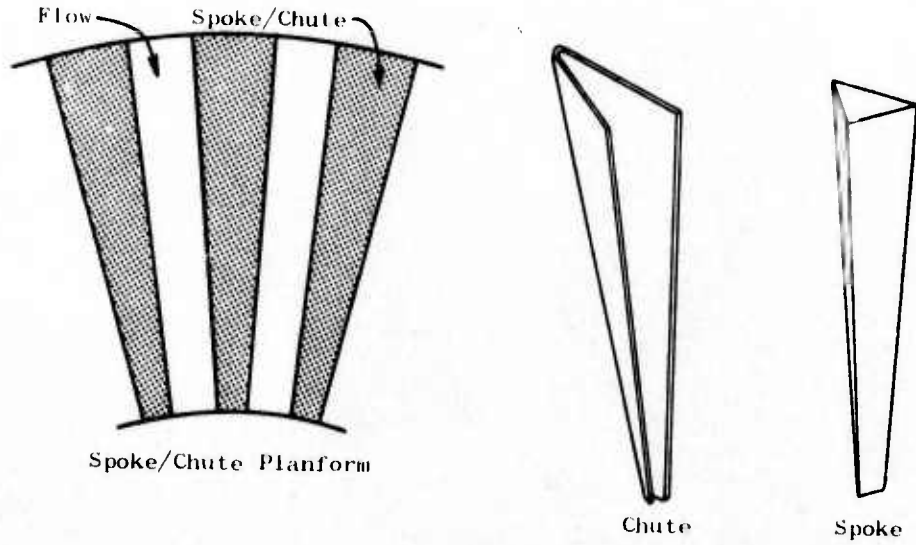
Figure 32.   Spoke Versus Chute.
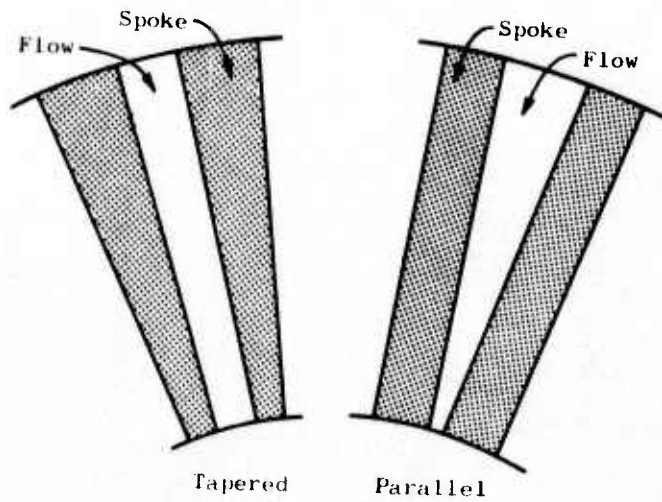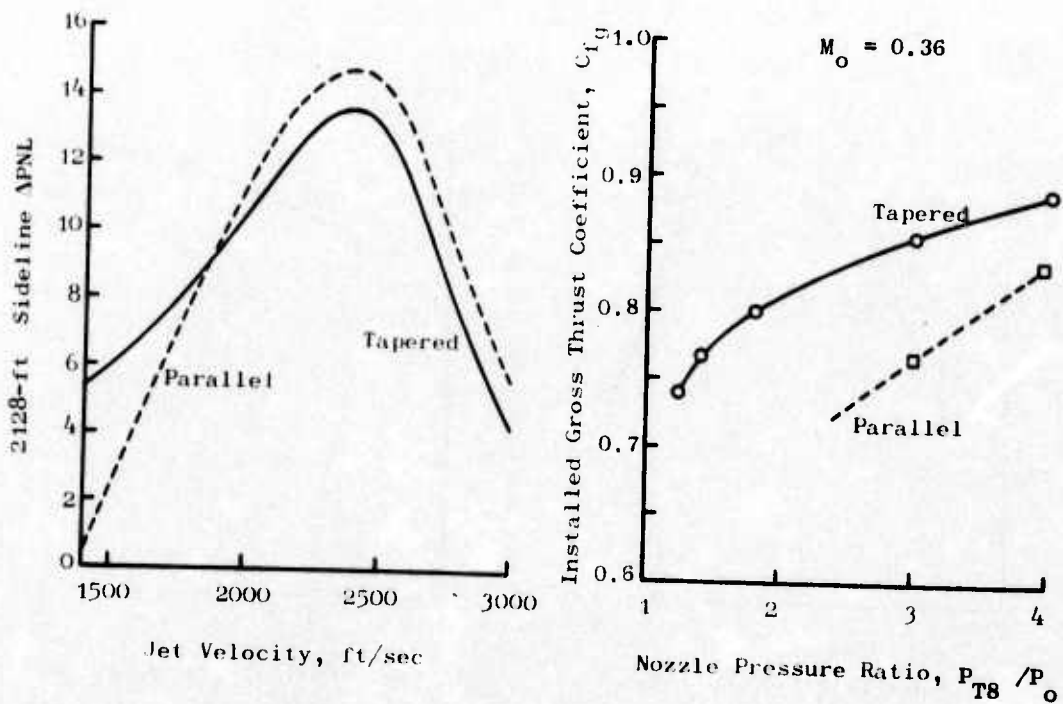
Figure 33. Spoke Nozzle Planform Variation.

Spoke/Chute Aerodynamic Data Review

The experimental data used in the investigation of the spoke and chute aerodynamic nozzle losses also were accumulated during the last scale-model nozzle aerodynamic test program under the SST program. In this experimental program, nine spoke and three chute configurations were tested both statically and in a wind tunnel with an external flow Mach number of 0.36. Table 3 summarizes the gross geometric throat parameters for these 12 configurations.

The first nine models listed in the table (Configurations 1 through 10, excluding number 6) are identical in geometry to the acoustic models discussed in the acoustic data review.

The losses incurred from the insertion of spokes or chutes at the nozzle throat are significant. For both the static, $M = 0$, and the wind tunnel conditions, $M = 0.36$, each configuration's spoke or chute base pressure drag was calculated at a nozzle pressure ratio of 3.0. The conditions, $M = 0.36$ and $P_{T8}/P_0 = 3.0$, simulate the take-off cycle of the J6H2 nonaugmented engine. In Table 4, each configuration's thrust loss resulting from the pressure drag on the spokes or chutes is compared with the sum of all its other losses. For the spoke models (Configurations 1 through 9 and 22), the spoke thrust loss, at best, is equivalent to the sum of all the other nozzle losses and, at worst, is as much as nine times greater than the sum of all other losses. For the chute models analyzed (Configurations 20 and 21), the chute losses were of the same order, or smaller, than the sum of all the other nozzle losses.

Once the magnitude and, consequently, the importance of the spoke/chute base pressure drags had been established, a correlation method was needed to allow the losses resulting from a spoke or chute geometry to be predicted. After careful examination of the spoke pressure distributions, a general cause-and-effect relationship was noted. The spoke losses follow, in general, the flow area distributions. The configuration with the greatest flow area near the plug has the smallest thrust loss due to spoke drag; and, conversely, the model with the least flow area near the plug has the highest spoke thrust loss. The most successful correlating parameter of the many investigated was the ratio of the flow width between two spokes at the plug to the flow width between two spokes at the shroud, WFB/WFT. This parameter represents, to some extent, the flow area distribution effect which was noted. This flow width ratio was plotted against the nondimensional, average spoke pressure for a $P_{T8}/P_0 = 3.0$ in Figure 34 at both Mach numbers. The trends indicated by this plot tend to confirm the earlier flow area distribution findings and were used as the basis for future model aerodynamic predictions.

The aforementioned correlation of spoke element losses as a function of flow width ratio was extended to the chute models and to nozzle pressure ratios of 2.0, 2.5, and 3.5. The static and wind tunnel correlations of the spoke losses are presented in Figures 35 and 36, respectively. The static and wind tunnel chute pressure losses are correlated in Figures 37 and 38, respectively. The difference in values of Figures 35 through 38 are twofold. First,

Table 3. Spoke/Chute Nozzles, A Comparison of the Nozzle Thrust Losses at $P_{T8}/P_0 = 3.0$.
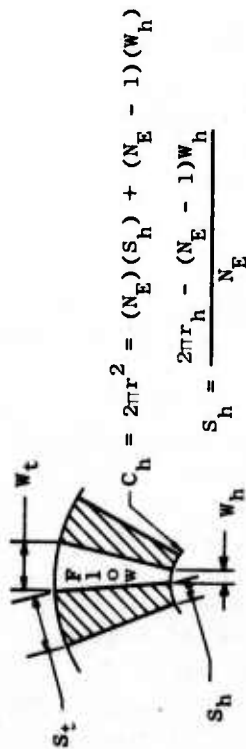
$$C_h = 2\pi r^2 = (N_E)(S_h) + (N_E - 1)(w_h)$$

$$S_h = \frac{2\pi r_h - (N_E - 1)w_h}{N_E}$$

Configuration Number	(N_E) Number of Spokes/Chutes	(r_h) Inner Radius (inches)	(r_t) Outer Radius (inches)	(w_h) Elemental Flow Width at Plug (inch)	(w_t) Elemental Flow Width at Shroud (inch)	Total Flow Area (inches^2)	Total Spoke/Chute Area (inches^2)	Area Ratio	Remarks
1 (Spokes)	32	1.760	3.535	0.2266	0.3048	15.099	14.428	1.956	
2 (Spokes)	24	1.760	3.535	0.3310	0.3642	14.820	14.707	1.992	
3 (Spokes)	48	1.760	3.536	0.1038	0.2400	14.657	14.892	2.016	
4 (Spokes)	32	1.814	3.536	0.237	0.306	15.199	13.975	1.934	Acoustic Configuration
5 (Spokes)	32	1.703	3.537	0.221	0.315	15.984	14.455	1.919	
7 (Spokes)	32	1.760	3.535	0.103	0.424	14.975	14.551	1.972	
8 (Spokes)	32	1.760	3.855	0.222	0.239	15.458	21.498	2.391	
9 (Spokes)	32	1.760	3.187	0.225	0.432	15.012	7.166	1.477	
10 (Chutes)	32	1.760	3.535	0.215	0.301	14.661	14.866	2.014	
20 (Chutes)	32	2.325	3.602	0.327	0.368	14.709	9.569	1.673	Aerodynamic Performance Only
21 (Chutes)	24	2.325	3.602	0.482	0.444	14.705	9.573	1.674	
22 (Spokes)	24	2.351	3.667	0.489	0.668	18.938	6.581	1.36	

Table 4. Spoke/Chute Nozzles - A Comparison of the Nozzle Thrust Losses at $P_{T8}/P_o = 3.0$.

Config. No.	M = 0 Thrust Losses		M = 0.36 Thrust Losses	
	Spoke Loss %	Other %	Spoke Loss %	Other %
1	7.89	2.56	11.86	2.75
2	2.42	2.45	6.40	4.68
3	19.14	1.55	20.08	2.71
4	4.04	3.01	8.07	4.63
5	9.22	3.16	12.20	5.00
7	15.80	4.98	16.54	6.22
8	6.86	3.10	12.22	5.60
9	6.12	3.04	6.68	3.80
10	---	---	No Analysis Made	
20	1.00	2.05	3.10	2.82
21	0.35	2.04	1.64	3.19
22	3.69	3.71	4.26	4.07
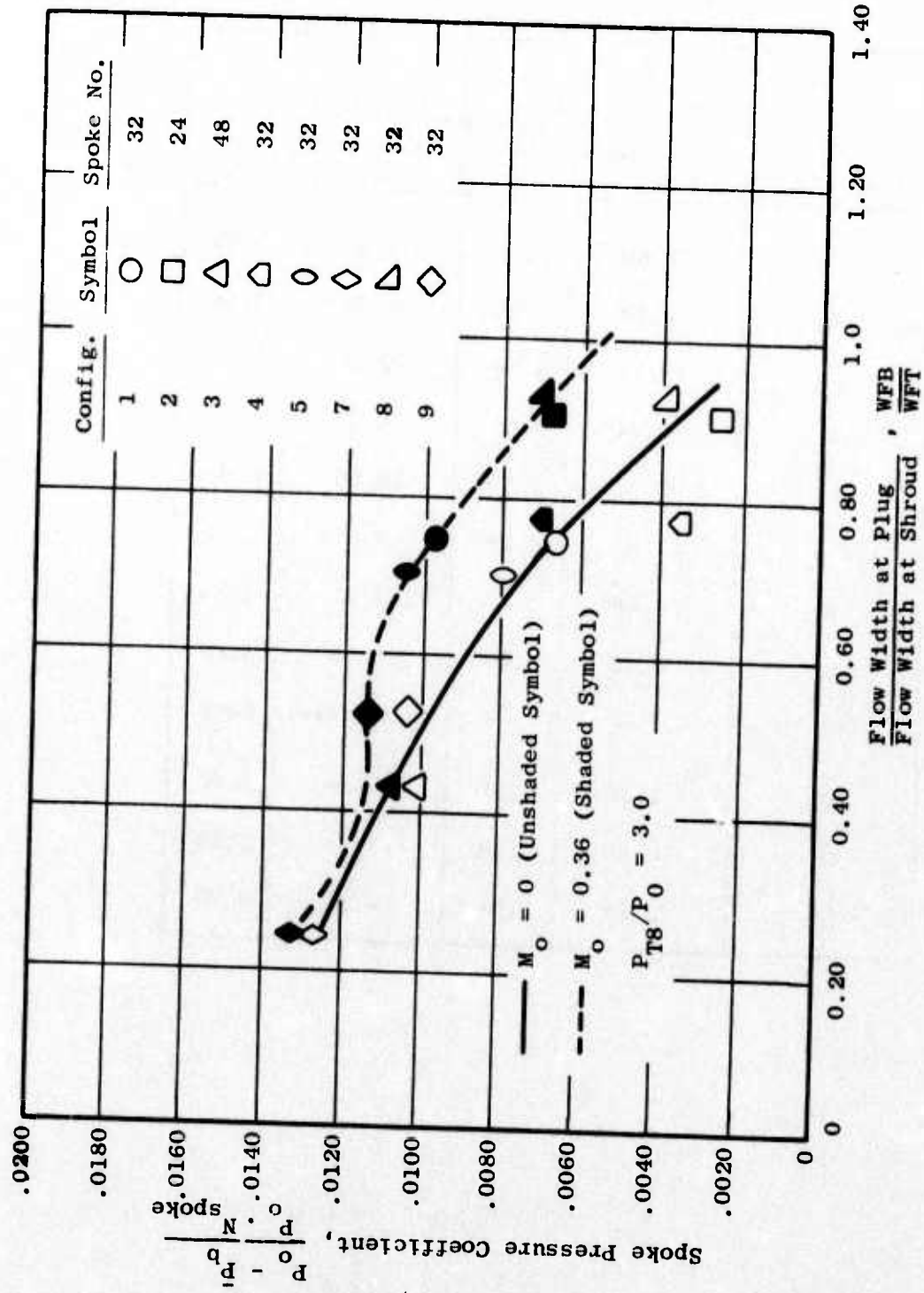
Figure 34. Spoke Aerodynamic Correlation, Pressure Loss Per Spoke.

62
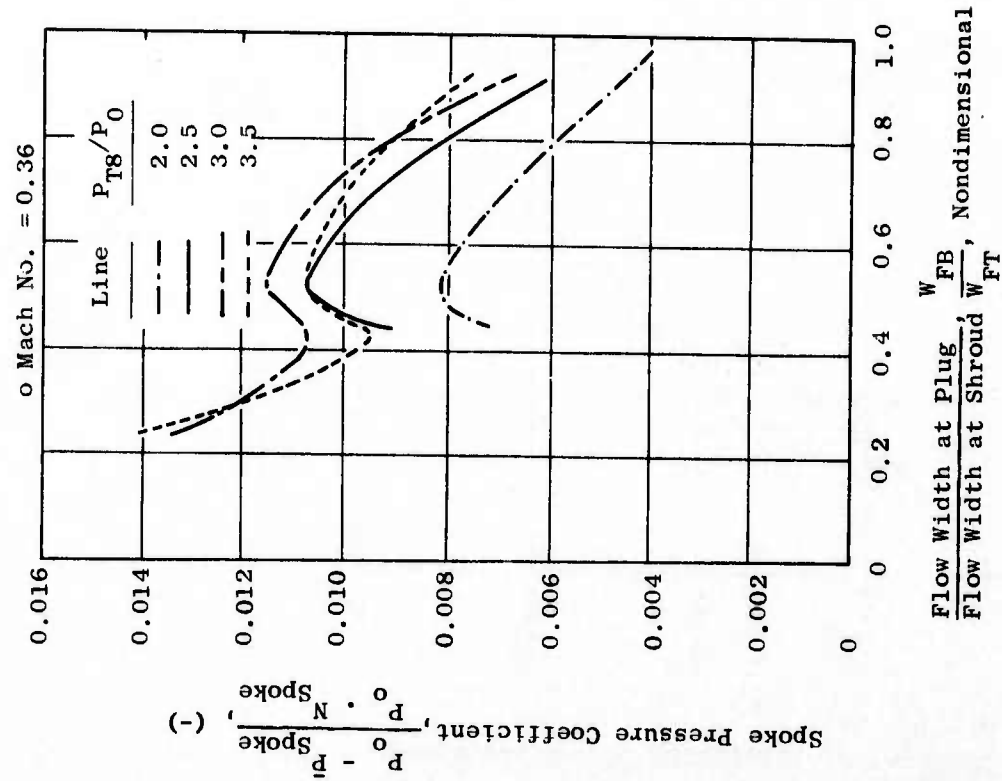
Figure 36. Pressure Loss Per Spoke at Mach No. = 0.36.
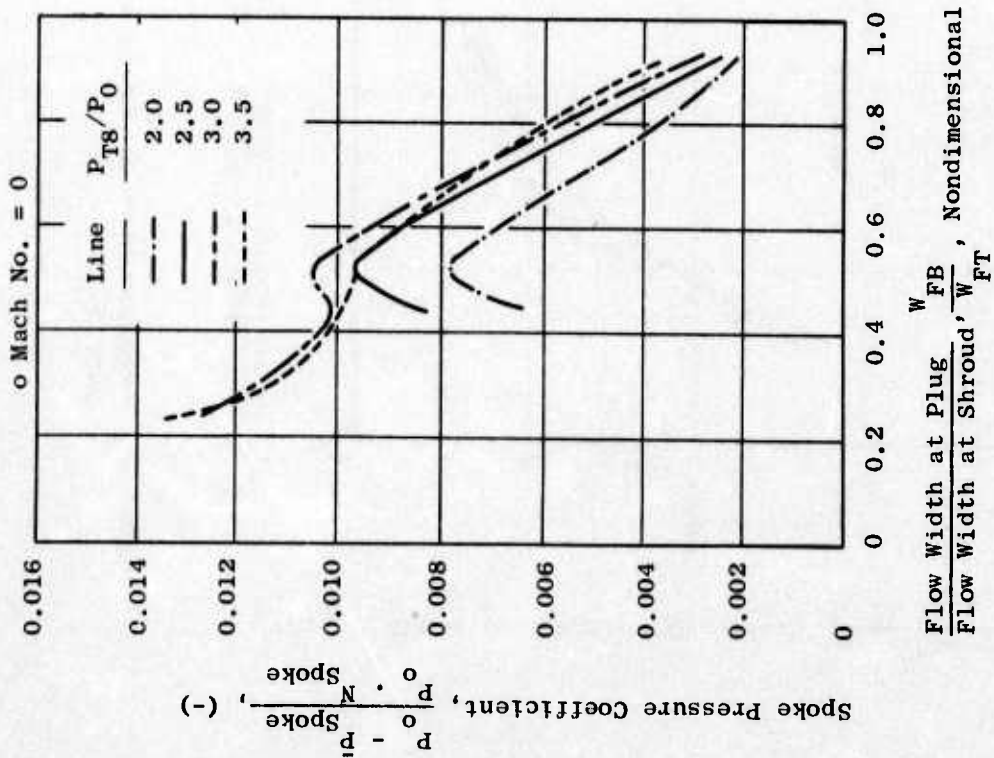
Figure 35. Pressure Loss Per Spoke at Mach No. = 0.

63
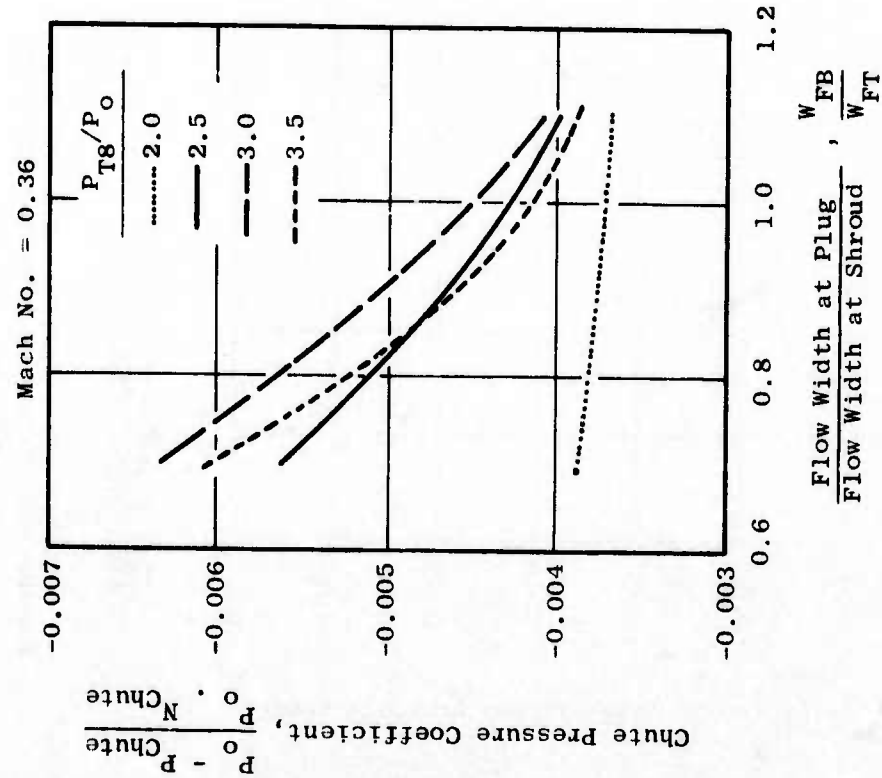
Figure 38. Pressure Loss Per Chute at Mach Number = 0.36.
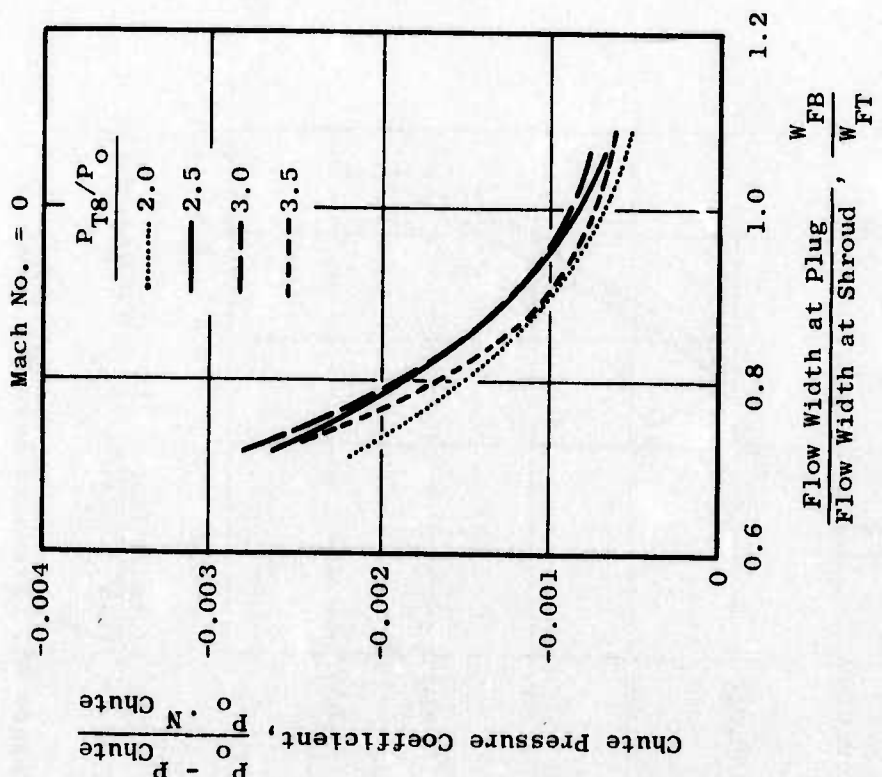
Figure 37. Pressure Loss Per Chute at Mach Number = 0.

the derivative of the pressure loss as a function of the flow width ratio can be determined from these plots. This derivative is indicative of the sensitivity of the pressure loss as a function of the flow width parameter. Second, it is possible to calculate the absolute magnitude of the thrust loss per spoke (chute) for a given spoke geometry and, consequently, the total spoke base thrust loss, as follows:

$$\Delta C_{fg} = \frac{\text{Area}_{SP}\,(P_o - P_b)\,dA_b}{(M_o V_{IDEAL})}$$

$$\Delta C_{fg} = \frac{A_{b\,Total} \cdot N_{SPOKE}}{\dfrac{Fip}{P_{T8} \cdot A_{8e}} \cdot \dfrac{P_{T8}}{P_o} \cdot C_{D8} \cdot A_8} \cdot \frac{P_o - \overline{P}_b}{P_o \cdot N_{SPOKE}}$$

where:

A_b	—	Total Projected Spoke (Chute) Area
N_{SPOKE}	—	Number of Spokes (Chutes)
C_{D8}	—	Throat Discharge Coefficient
A_8	—	Geometric Throat Area
P_{T8}	—	Throat Total Pressure
Fip	—	Ideal Thrust
$\dfrac{P_o - P_b}{P_o \cdot N_{SPOKE}}$		Correlated Spoke (Chute) Element Pressure Loss

Design of the 40-Spoke/Annular Plug Suppressor

For the first phase of the spoke/chute system refinement activity, two new models were designed and fabricated for aerodynamic, acoustic, and laser velocimeter testing. The first configuration was a low discharge coefficient (C_D) spoke design. The concept was based on the assumption that aerodynamic blockage is as effective in noise reduction as physical blockage, allowing for better aerodynamic performance through a reduced physical base area. The reduced physical base area would provide less base drag than the conventional high C_D spoke design and would also reduce suppressor weight.

A schematic of the concept, compared to a high C_D spoke configuration, and corresponding aerodynamic data are shown in Figure 39. The high C_D configuration has greater thrust loss than the low C_D model due to additional base drag with the greater physical blockage.

The suppressor was designed with 40 elements slanted 15° aft with respect to the normal to the nozzle centerline. The elements were designed as sharp-cornered flat plates to provide the low C_D. The nozzle effective area ratio of 2.0 was chosen, defined as:

$$\text{ARd}_{eff} = (A_8 + A_B)/A_{e8}$$

where:

A_8 = Physical flow area

A_B = Physical blocked area

A_{e8} = Effective flow area

The high element number, 15° aft slant, and near-parallel spoke planform were chosen for their beneficial acoustic characteristics. In addition to the lower base area for beneficial aerodynamic performance, the deployed suppressor could be positioned axially in a region of low projected plug area to reduce overexpansion losses on the plug surface.

The photograph of the low C_D acoustic model hardware is shown in Figure 40. The aerodynamic models were similar except with clean external flowpaths. The acoustic models were built to withstand high test temperatures, with water-cooled centerbody and adapter jackets and with bulk external flanges and externally mounted instrumentation.

The low C_D spoke configuration had 40 elements of rectangular cross section at its throat. The cross-sectional shape of the low C_D spoke was determined after aerodynamic and stress studies were performed. The element was required to withstand high gas loading at the elevated test temperatures in the acoustic model and to have the same low C_D in both the aerodynamic and the acoustic models. The acoustic model's spokes are made of Hastelloy X.

The discharge coefficient of the low C_D spoke model would not be radially constant in the flow channel between spokes. The discharge coefficients in the regions of the smooth plug and shroud would be greater than the discharge coefficient between the sharp-cornered spokes. The average C_D was estimated at 0.80.

Design of the 40-Chute/Annular Plug Suppressor Model

The second model was a refined chute suppressor, chosen at an area ratio of 2.0 and with 40 elements. The chutes had a double exit cant of ± 15° from the normal to the nozzle centerline. The design intent was to allow the flow
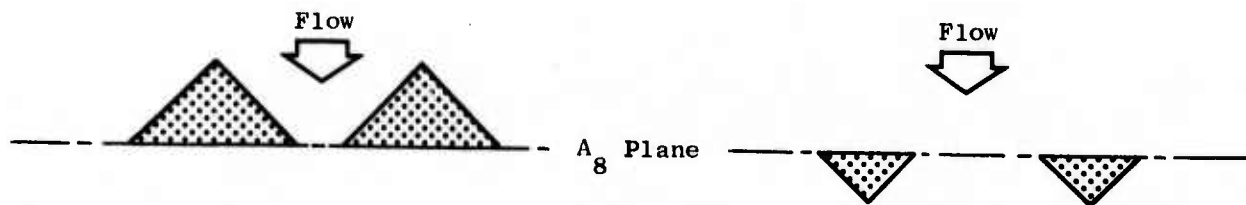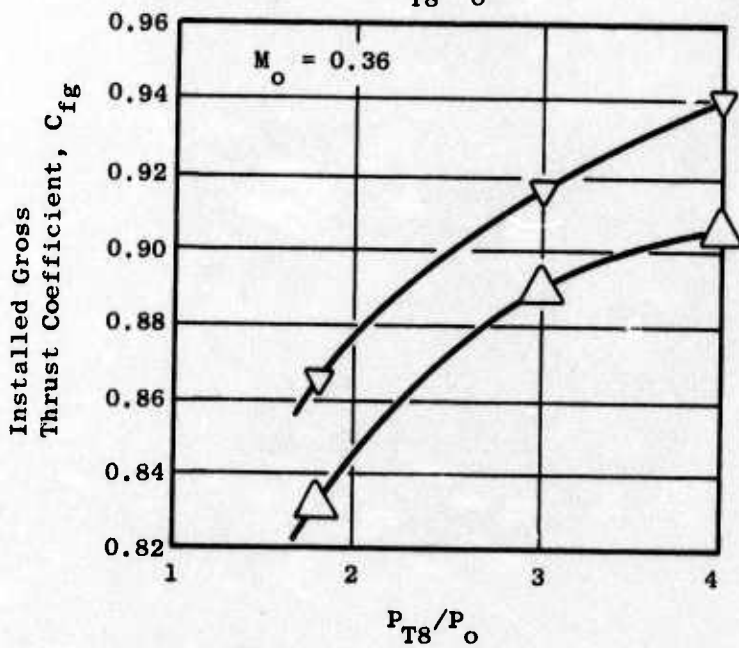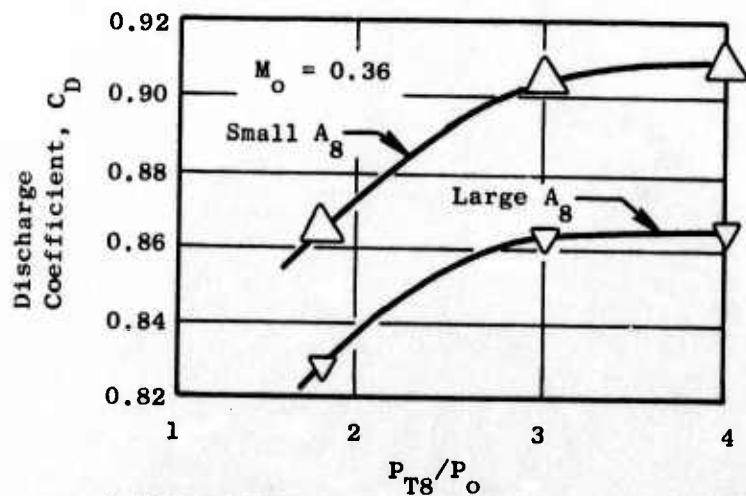
Figure 39. High C_D - Low C_{f_g} Versus Low C_D - High C_{f_g} Models.

67
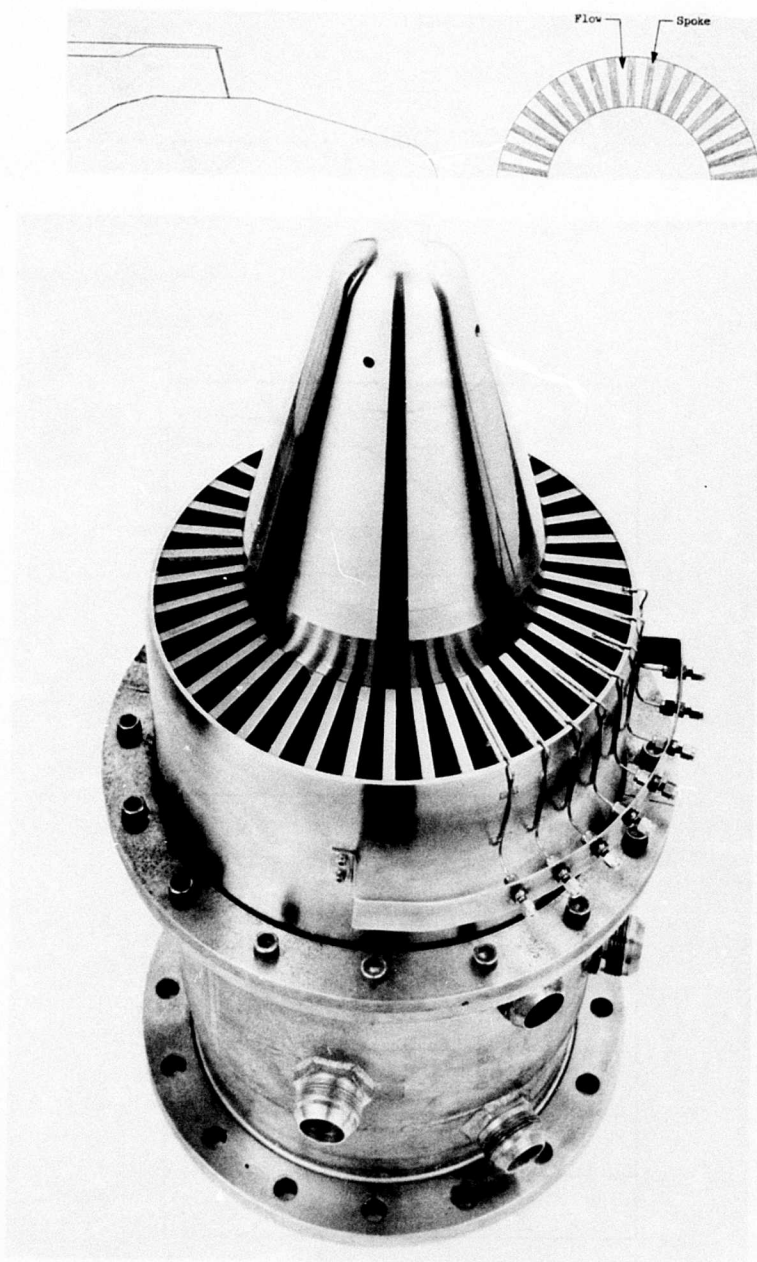
Figure 40. Low C_D 40-Spoke/Annular Plug Model Suppressor Hardware.

68

within the inner annulus to be directed down the plug to reduce expansion losses and the flow within the outer annulus to further separate before coalescence for beneficial acoustic performance. The deep-chute cross section over the full radial length was chosen to improve ventilation and decrease base drag. A near-parallel-sided, chute exit plane planform was chosen for better acoustic suppression, and was not anticipated to be aerodynamically detrimental when incorporated within a deep-chute design. A photograph of the final hardware is shown in Figure 41. The photograph shows the details of the deep chutes, made of Hastelloy X, with support pins for strength during hot acoustic tests.

Preliminary Aeroacoustic Performance Estimates

Utilizing the results of the available spoke/chute suppressor data and the previously discussed aerodynamic correlation, thrust loss for the suppressors was anticipated to be of the order of 12% and 9%, respectively, for the spoke and chute/plug configurations (relative to an unsuppressed plug nozzle at Mach 0.36 and nozzle pressure ratio of 3.0). Using the acoustic correlations as typically shown in Figures 29 through 33, 2128-foot sideline, the resulting suppression/performance levels estimated would be better than 1:1.

The sources of the thrust loss of the spoke/chute configurations are: (1) spoke or chute base pressure drag, (2) flow angularity, (3) friction, and (4) expansion. The spoke or chute base pressure losses were calculated from the empirical, spoke/chute base pressure drag correlation presented previously. The angularity, friction, and expansion losses are determined from experimental, unsuppressed plug results.

Acoustic Tests

The initial phase of the 40-spoke/chute annular plug suppressor test series also included tests with the 5.7-inch-diameter (D_8) baseline conical nozzle. The suppressor nozzles were 1/8th scale of full-size engine hardware design, being equivalent to 6-inch-D_8 nozzles in flow area.

Far-field acoustic data measurements were taken on the JENOTS facility (see Appendix A) while operating the nozzles through exhaust cycle conditions to (a) simulate a smooth operating line of a GE4-J6H2 engine from 1300 through 3000 ft/sec ideal jet exhaust velocity, and (b) traverse a matrix of P_{T8}/P_o of 2.0, 2.5, 3.0, and 3.5 and a T_{T8} of 1400° to 2000° R to investigate temperature dependence at constant pressure on suppression.

In addition to the standard microphone setup (15.93 feet high), described in Appendix A, microphones were also located at 55 inches above the ground plane (nozzle centerline height) at 105°, 115°, 125°, 135°, and 150° from the inlet axis for measurements during the baseline conical nozzle test (see Figure 42). These measurements would assure continuity of data between the
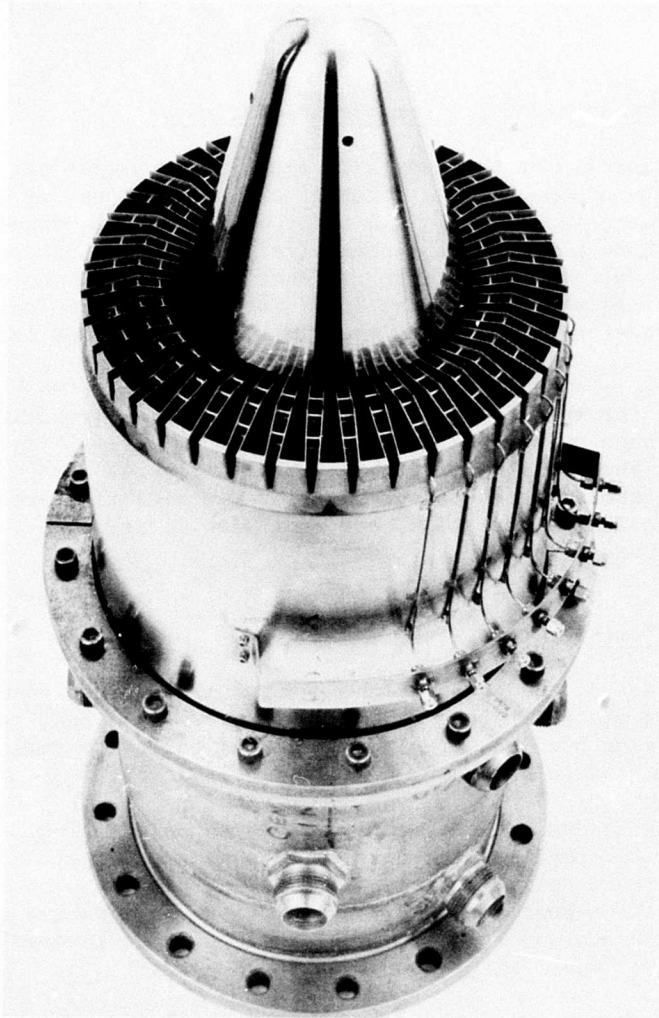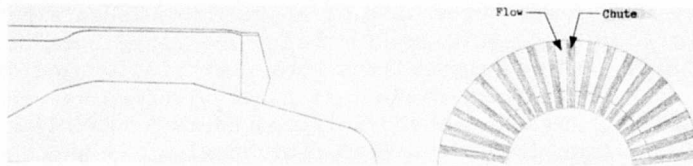
Figure 41. 40-Chute/Annular Plug Model Suppressor
Hardware.

- PLAN VIEW

Microphones on this arc are 55" above ground plane and on a 40 foot radius to the nozzle center point.

40.0' R @ Nozzle Centerline Height

38.4' R @ Nozzle Centerline Height

Microphones on this arc are 15.93 foot above ground plane and on a 40 foot hemispherical radius to the nozzle center point

Nozzle Exit Plane
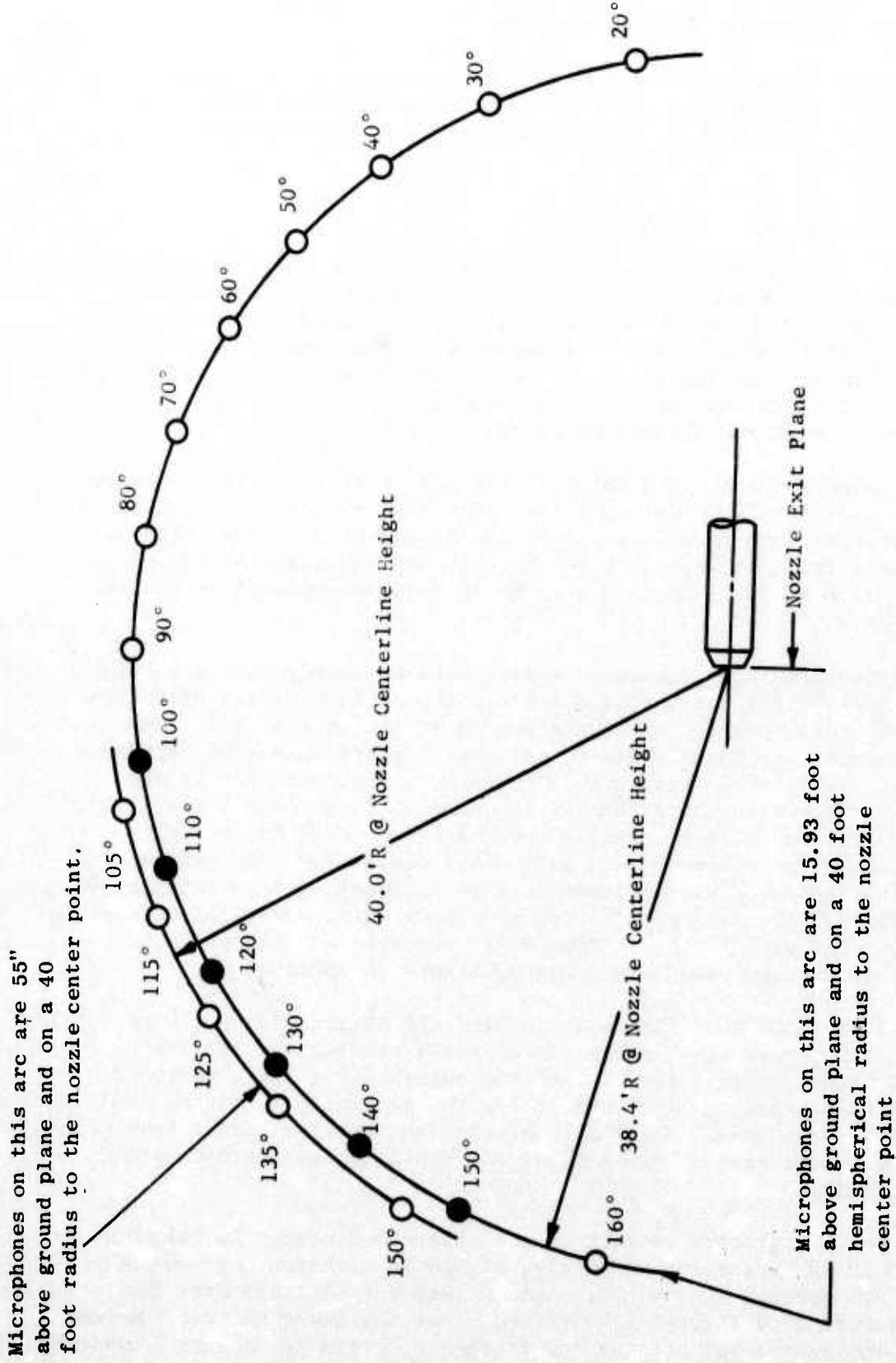
Figure 42. Microphone Array for the Acoustic Tests at JENOTS.

71

current test series and the acoustic tests on the previous spoke and chute suppressors taken during the GE4/SST program.

To obtain sufficient acoustic information to completely document the performance of the suppressor nozzles in their range of application, the test schedule shown in Figure 43 was followed for all three nozzles.

Acoustic Results and Analysis

The acoustic data were obtained from 50 Hz to 40 KHz using a 14-channel Sangamo tape recorder (Appendix A). The acoustic data were corrected to standard conditions and scaled by a factor of 8:1 to engine size, using the technique described in Appendix B. The analysis of the data from this series of tests established: (a) continuity of data from the microphones at 15.93-foot height with previous data at the 55-inch-microphone height, and (b) the acoustic suppression levels of the 40-spoke and 40-chute nozzles.

A typical comparison of data taken at the 150° position relative to the inlet axis is shown in Figure 44. The two spectra were from the microphones located at 55 inches and 15.93 feet above the ground plane. The shift in location of the first null frequency is observed and the shape of the spectra from the microphone at 15.93 feet is seen to be more representative of free-field measurements.

Since the baseline and suppressed models were of nearly equivalent flow diameter (5.7-inch-D_8 for the baseline and approximately 6.0-inch-D_8 for the chute and spoke), all acoustic data were scaled by a factor of 8:1. The 40-foot model measuring arc, therefore, was quivalent to an engine reference arc of 320 feet. The model frequency range of 400 Hz through 40 KHz was scaled to an equivalent engine frequency range of 50 Hz through 5 KHz. (For subsequent acoustic tests, measurements were taken up to 80 KHz as more sophisticated recording equipment was made available.) From the reference arc of 320 feet, data were extrapolated in one-third octave band form to 300-, 1500-, and 2128-foot (0.35-nautical-mile) sidelines using spherical divergence and 59° F, 70% relative humidity, standard day atmospheric absorption. Summary tables of the test conditions are contained in Appendix C.

Figure 45 presents the 2128-foot sideline PNL directivity patterns for the conical baseline nozzle, 40-chute and 40-spoke nozzles, respectively. Sharp changes in the directivity patterns are observed for the suppressed configurations referenced to the baseline nozzle, particularly at the low exhaust velocity conditions. For the high velocity baseline nozzle test points, Figure 45a, the spikes seen at the exhaust and the inlet angles were attributed to shock noise.

To gauge the 1/3 spectra content of the suppressed nozzle in relation to each other and to the unsuppressed nozzle, Figure 46 compares the 300-foot-sideline peak PNL spectra at the four nominal velocity settings over the operating line from 1650 through 2790 ft/sec. For the lower velocity points on Figure 46, the suppressor nozzles low frequency merged jet spectral content
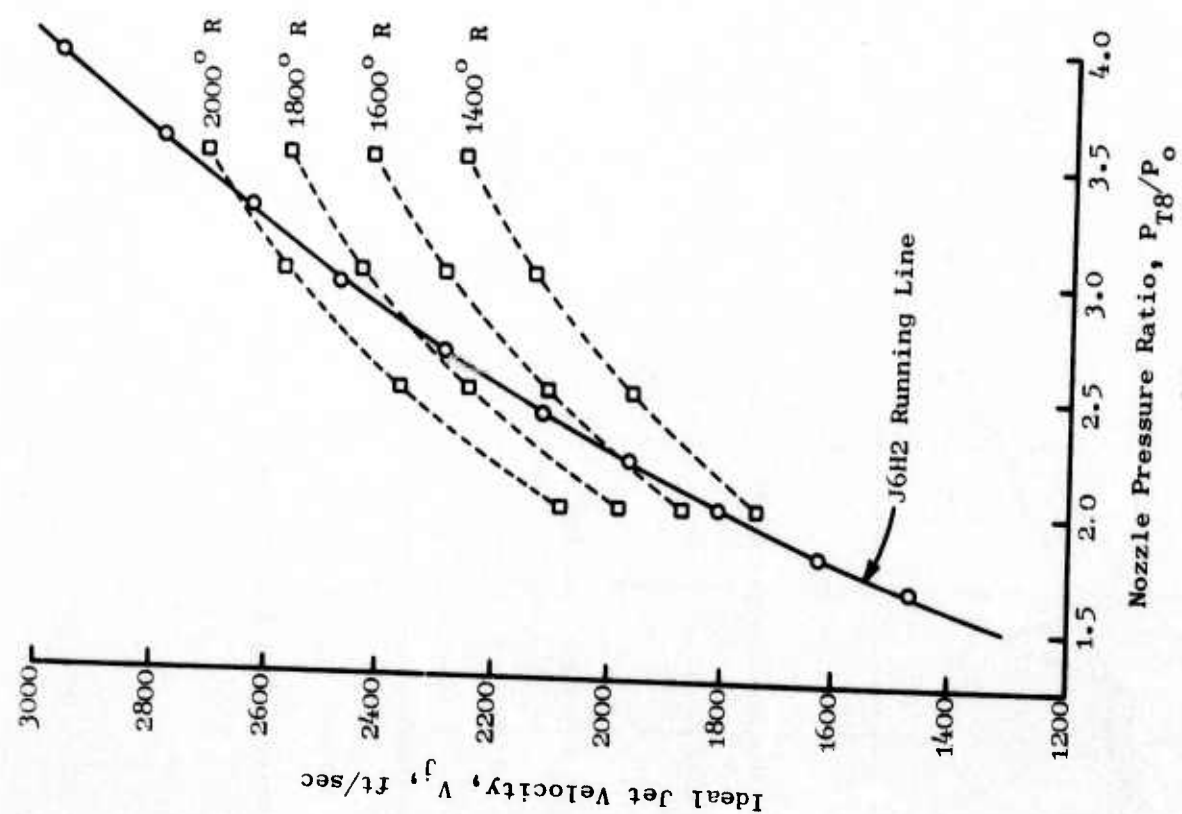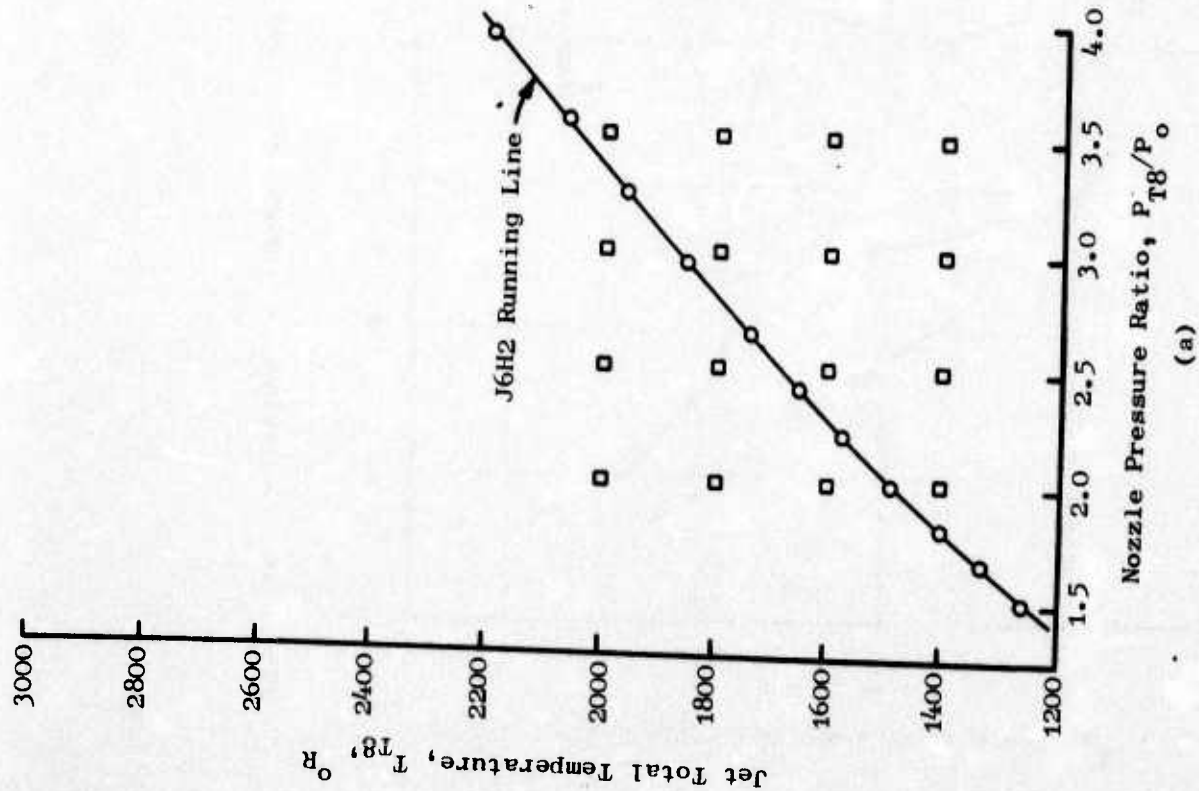
Figure 43. Test Point Matrix for Acoustic Evaluation of Spoke/Chute Models.

73
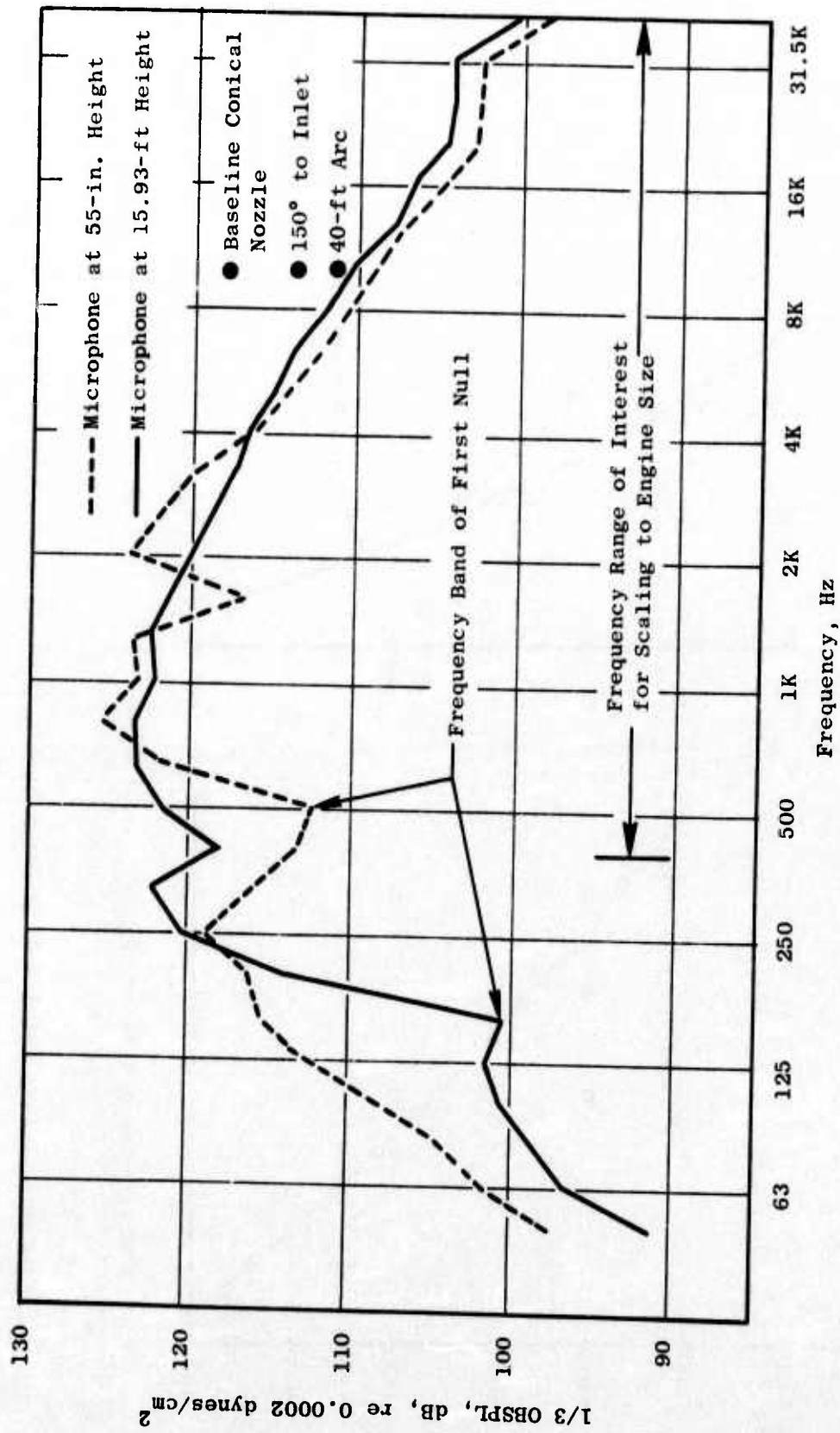
Figure 44. Comparison of Ground Reflection Patterns for Microphone Systems of the JENOTS Facility.

74

Rdg.	$V_j \sim$ fps
11	2926
8	2431
5	1970
3	1598

(a) Conical Convergent Baseline Nozzle

Rdg.	$V_j \sim$ fps
11	2959
8	2487
5	2003
3	1670

(b) 40-Chute/Annular Plug Suppressor

Rdg.	$V_j \sim$ fps
11	2972
8	2464
5	2028
3	1708

(c) 40-Spoke/Annular Plug Suppressor
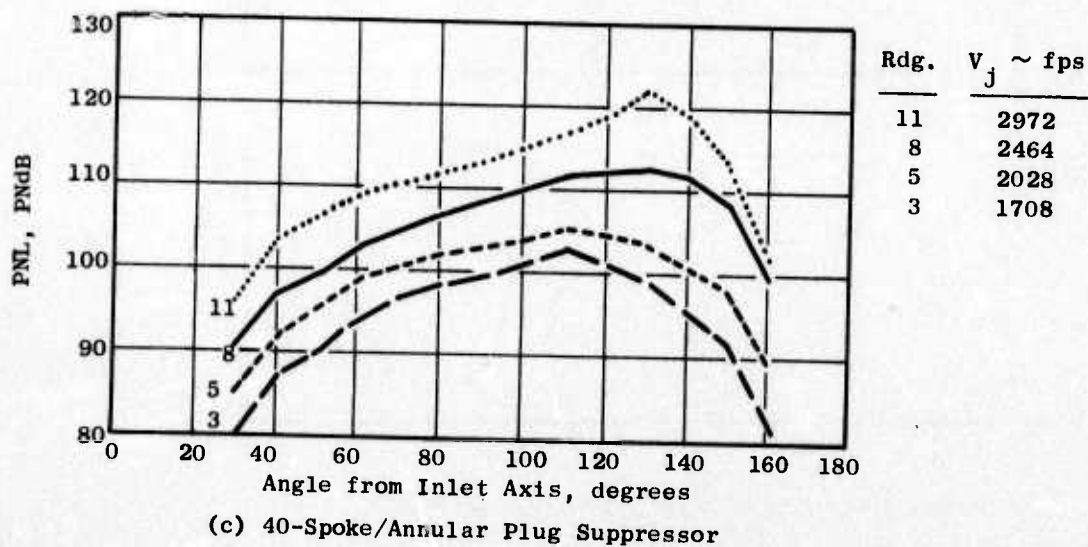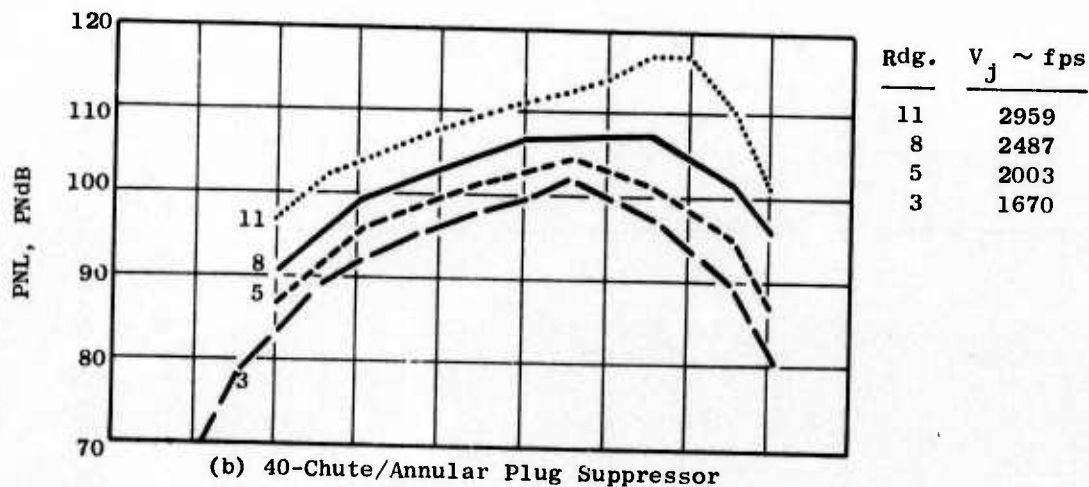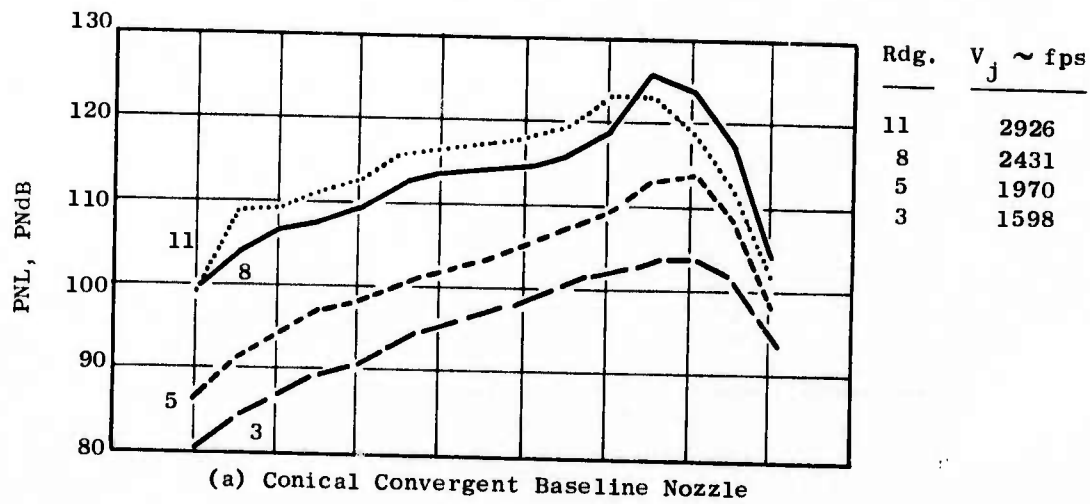
Figure 45.   2128-Foot Sideline PNL Directivity.

75
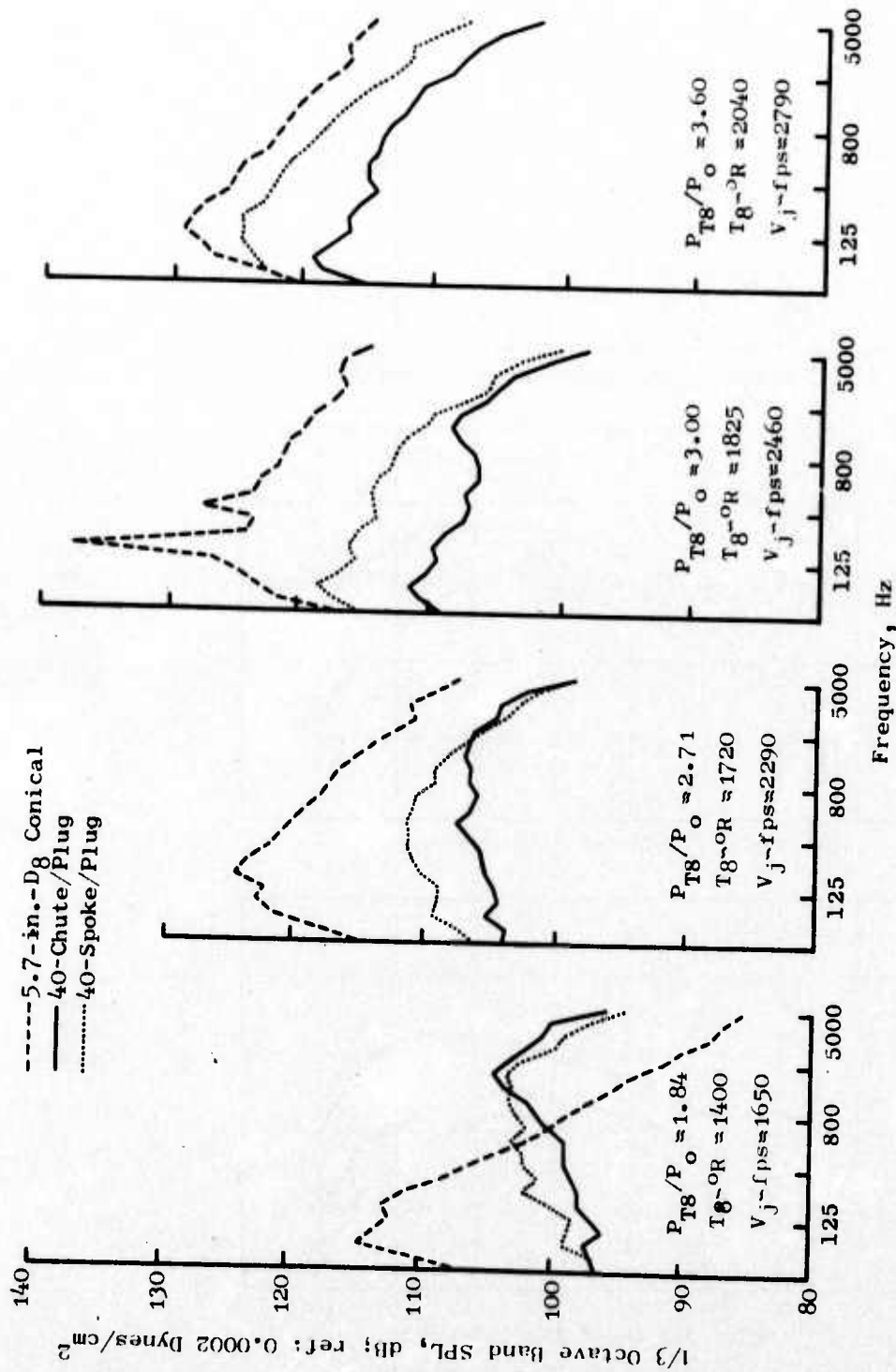
Figure 46. 300-Foot Sideline Spectra Comparisons at Angle of Peak PNL.

and the high frequency individual immerged jet spectra contributions are discernible. The suppressed jet spectra differ drastically in shape from the unsuppressed jet due to the two source contributions, and typify spectra of previously tested multielement suppressed jets. The suppressed jet spectra shapes change gradually as jet velocity increases, and (at high jet velocity) match the unsuppressed jet spectra shape which is indicative of the merged (coalesced) jet's noise dominance.

PNL suppression performance of the chute and spoke configurations referenced to the baseline nozzle are presented in Figures 47a and 47b, respectively. The plots are composites of:

- PNL suppression on the 32-foot arc and at the 300-, 1500-, and 2128-foot sidelines; all data are scaled by the scale factor of 8:1. These data show the dependency of PNL suppression on distance of extrapolation.

- PNL suppression of the unscaled measurements on the model 40-foot arc to show the PNL suppression dependency on acoustic scale factor/technique.

Observations from Figure 47 show that peak PNL suppression values of 16.8 and 13.1 were obtained for the chute and spoke nozzles, respectively, for the unscaled measurements on the model 40-foot arc. Scaling the data to engine size, frequency, and location, lowered the peak suppressions to 13.3 and 11.4 dB, respectively, on the 320-foot arc. Additional lowering of peak suppressions, and shifting of suppression patterns with jet velocity, are seen as the data are extrapolated to the 300-foot sideline from the 320-foot arc. PNL suppression levels generally tend to increase as extrapolation distance was increased from the 300-foot sideline to the 1500- and 2128-foot sidelines. This is due to the high frequency spectra attenuation with distance and the relative shift of PNL dominance of that high frequency spectra content between the baseline and suppressed configurations.

In addition to acoustic data, the JENOTS tests produced base pressure measurements from the static taps mounted on the base of the suppressor elements of the spoke and chute nozzles, respectively. This instrumentation was added to the acoustic model to ensure continuity of aerodynamic performance between the aerodynamic model tests in the NASA-Lewis 8' × 6' wind tunnel and the outdoor acoustic tests at the JENOTS facility. Typical results are shown in Figure 48 for the spoke nozzle and Figure 49 for the chute nozzle, in the form of P_{base}/P_o ratio as a function of tap radial location.

As a diagnostic test to aid in establishing the flow vectoring of the 40-chute nozzle, a flow visualization check was also performed on the JENOTS rig. Using a sheet metal baffle between two chutes, centrally located within the jet flow sector, lampblack dots were applied. Ambient temperature gas flow was used at several nozzle pressure ratio settings, the plate being photographed at each test condition. Typical patterns resulting from the test are shown in Figure 50 at nozzle P_{T8}/P_o settings of 2.5 and 3.0,

and the high frequency individual immerged jet spectra contributions are discernible. The suppressed jet spectra differ drastically in shape from the unsuppressed jet due to the two source contributions, and typify spectra of previously tested multielement suppressed jets. The suppressed jet spectra shapes change gradually as jet velocity increases, and (at high jet velocity) match the unsuppressed jet spectra shape which is indicative of the merged (coalesced) jet's noise dominance.

PNL suppression performance of the chute and spoke configurations referenced to the baseline nozzle are presented in Figures 47a and 47b, respectively. The plots are composites of:

- PNL suppression on the 32-foot arc and at the 300-, 1500-, and 2128-foot sidelines; all data are scaled by the scale factor of 8:1. These data show the dependency of PNL suppression on distance of extrapolation.

- PNL suppression of the <u>unscaled</u> measurements on the model 40-foot arc to show the PNL suppression dependency on acoustic scale factor/technique.

Observations from Figure 47 show that peak PNL suppression values of 16.8 and 13.1 were obtained for the chute and spoke nozzles, respectively, for the unscaled measurements on the model 40-foot arc. Scaling the data to engine size, frequency, and location, lowered the peak suppressions to 13.3 and 11.4 dB, respectively, on the 320-foot arc. Additional lowering of peak suppressions, and shifting of suppression patterns with jet velocity, are seen as the data are extrapolated to the 300-foot sideline from the 320-foot arc. PNL suppression levels generally tend to increase as extrapolation distance was increased from the 300-foot sideline to the 1500- and 2128-foot sidelines. This is due to the high frequency spectra attenuation with distance and the relative shift of PNL dominance of that high frequency spectra content between the baseline and suppressed configurations.

In addition to acoustic data, the JENOTS tests produced base pressure measurements from the static taps mounted on the base of the suppressor elements of the spoke and chute nozzles, respectively. This instrumentation was added to the acoustic model to ensure continuity of aerodynamic performance between the aerodynamic model tests in the NASA-Lewis 8' × 6' wind tunnel and the outdoor acoustic tests at the JENOTS facility. Typical results are shown in Figure 48 for the spoke nozzle and Figure 49 for the chute nozzle, in the form of P_{base}/P_o ratio as a function of tap radial location.

As a diagnostic test to aid in establishing the flow vectoring of the 40-chute nozzle, a flow visualization check was also performed on the JENOTS rig. Using a sheet metal baffle between two chutes, centrally located within the jet flow sector, lampblack dots were applied. Ambient temperature gas flow was used at several nozzle pressure ratio settings, the plate being photographed at each test condition. Typical patterns resulting from the test are shown in Figure 50 at nozzle P_{T8}/P_o settings of 2.5 and 3.0,

a) 40-Chute/Annular Plug Suppressor

Ideal Jet Velocity, V_j, ft/sec
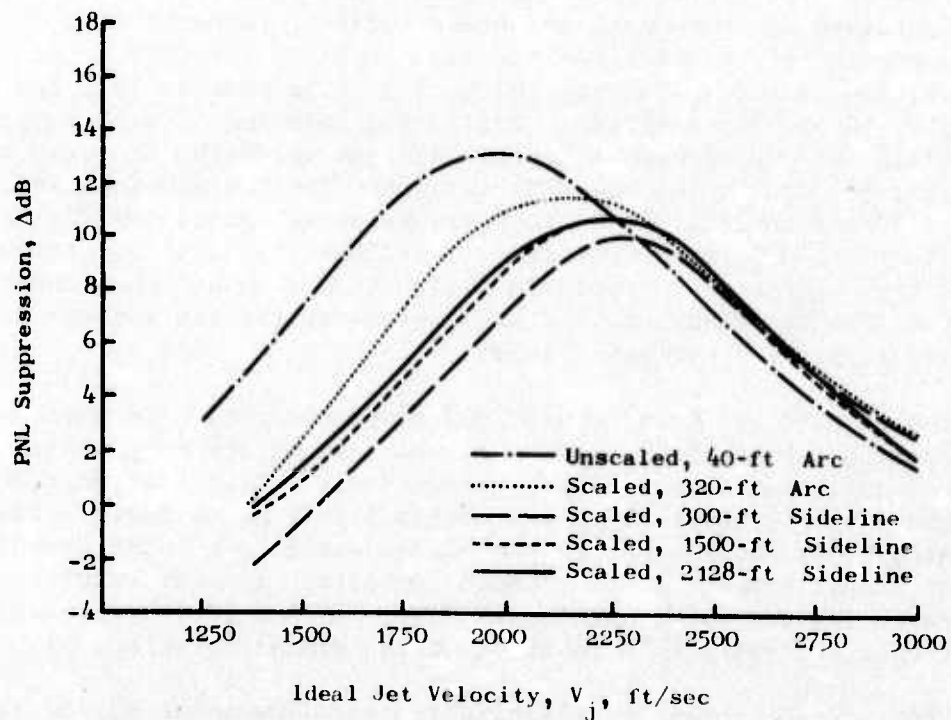
b) 40-Spoke/Annular Plug Suppressor

Figure 47. Peak PNL Suppression Referenced to Unsuppressed Conical
Baseline Nozzle.
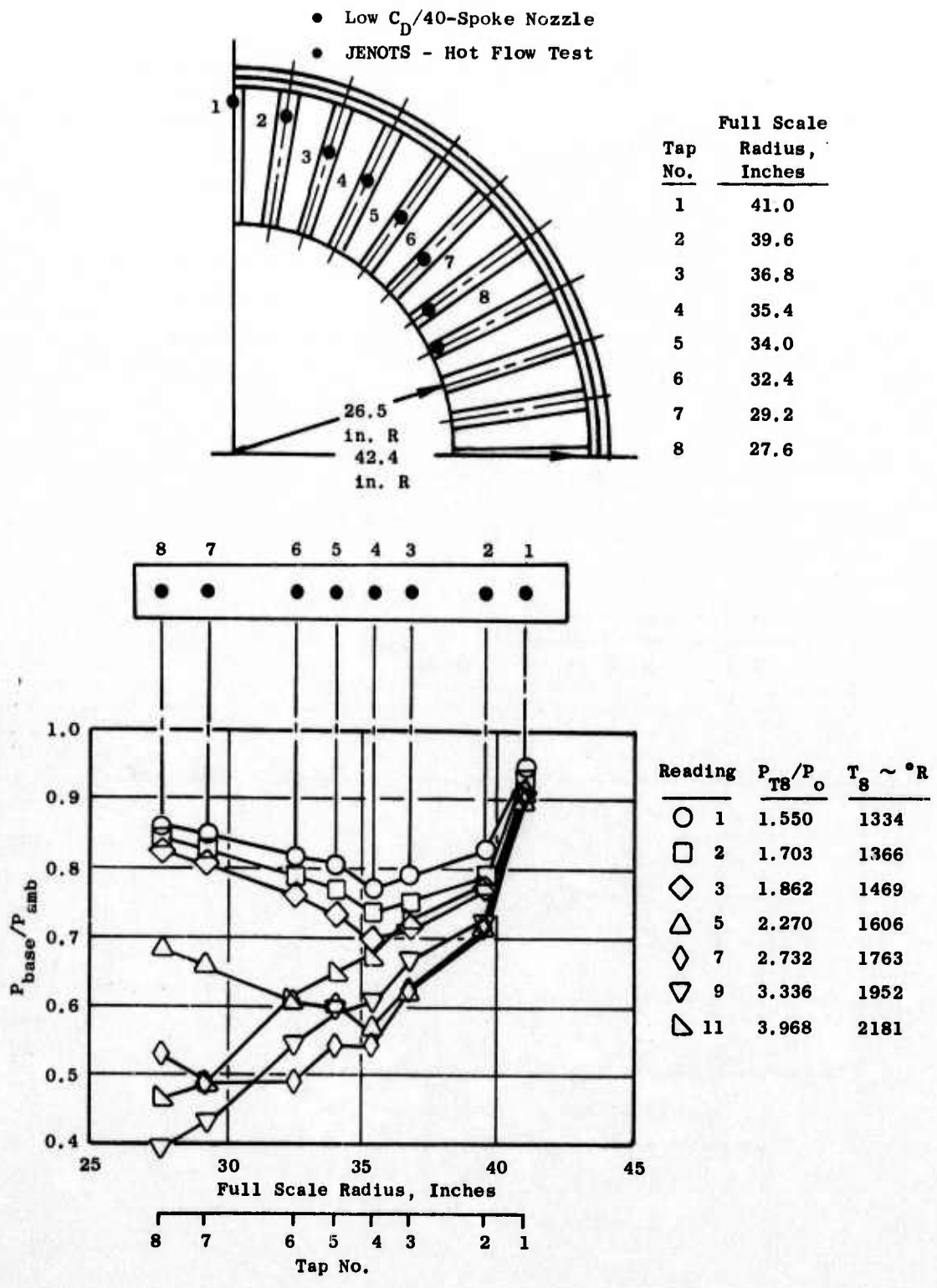
Figure 48. Base Pressure Data for 40-Spoke Nozzle from JENOTS Tests.
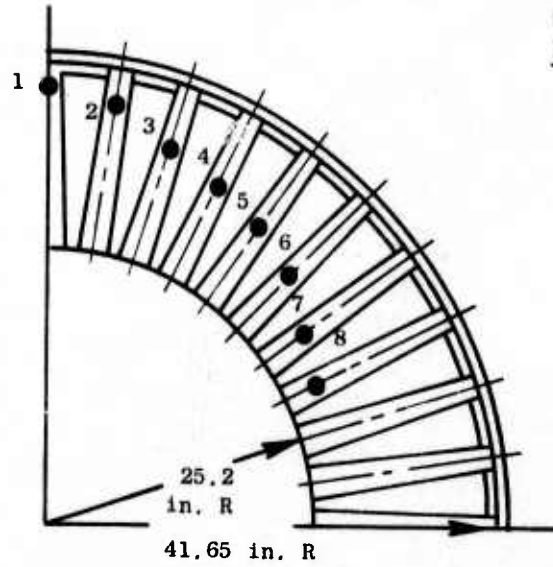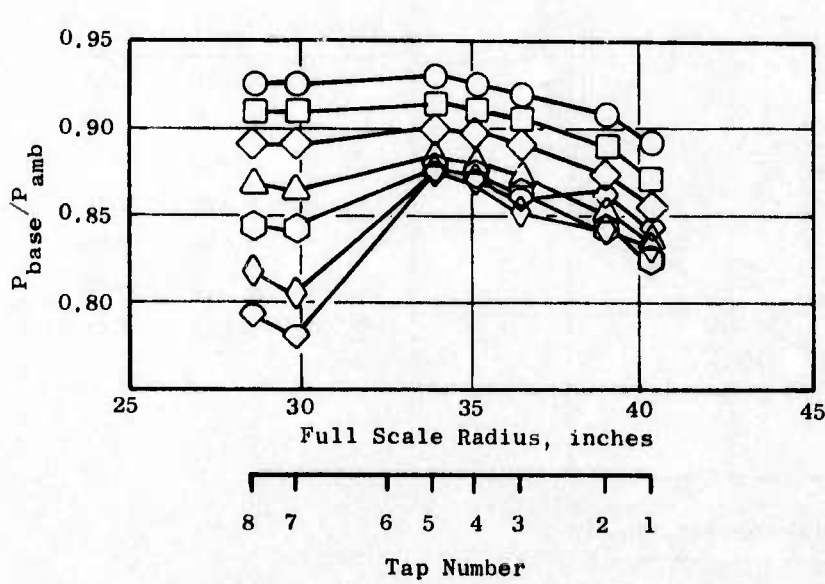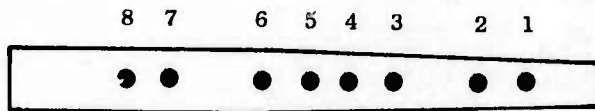
Figure 49. Base Pressure Data for 40-Chute Nozzle from JENOTS Tests.

a) $P_{T8}/P_o = 2.5$
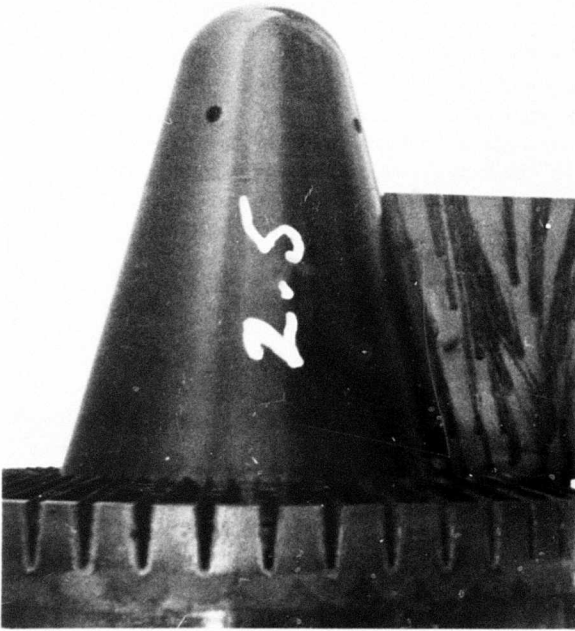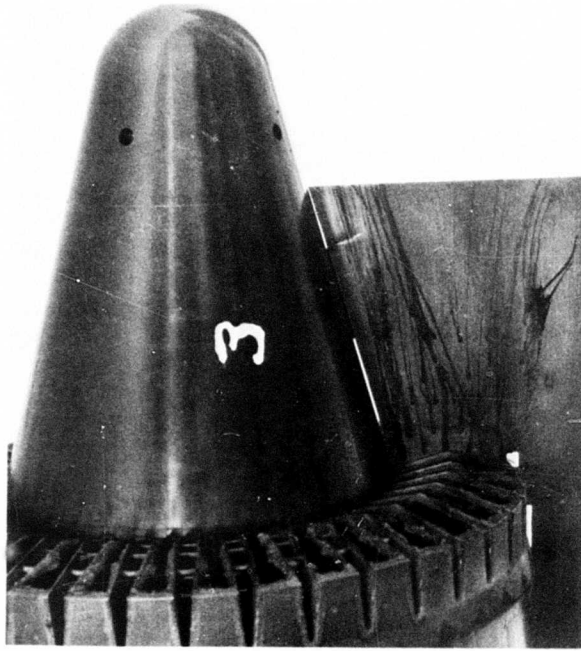
b) $P_{T8}/P_o = 3.0$

Figure 50. Flow Visualization of 40-Chute Nozzle at JENOTS.

respectively, which indicate that the chute design did focus a portion of the flow down the plug surface while the majority of the stream was vectored to a larger plume diameter.

Aerodynamic Performance Tests

The initial aerodynamic test phase of the spoke/chute development program was conducted in the NASA-Lewis 8' × 6' wind tunnel and included four test models: a Supersonic Tunnel Association (STA) standard nozzle, a baseline unsuppressed plug nozzle, the low C_D/40-spoke suppressor, and the 40-chute suppressor. Each of these models was tested statically and with external flow for the following quantities: thrust coefficient, discharge coefficient, boattail and spoke or chute pressure drags, and plug pressure coefficient distribution. The quantities were calculated in the NASA data reduction computer program from the measured model pressures, temperatures and forces. (See Reference 9 for complete details of test and results.)

A description of the NASA-Lewis 8' × 6' facility can be found in Appendix A. A view of the system in the test section is shown in Figure 51 with the STA nozzle affixed. The support and force balance systems remained the same throughout the test program. The nozzle was the only section changed. The baseline unsuppressed plug nozzle is shown in Figure 52. The aerodynamic suppressor models tested are displayed in wind tunnel installation photographs, Figures 53 and 54.

Each model was tested statically in the tunnel at nozzle pressure ratios of 1.5, 2, 2.5, 3, 3.5, and 4.0. All of the model nozzles were tested at freestream Mach numbers of 0, 0.36, 0.40 and 0.45. The STA nozzle and baseline unsuppressed plug underwent additional testing at freestream Mach numbers of 0.8 and 0.9. In order to ensure no entrainment flow over the model at M = 0 conditions, a plywood blocker door was fitted across the test section. Once the static data were judged acceptable, the blocker door was removed and the wind tunnel runs were made. The test sequence for each model, at a given Mach number, included the recording of data at particular values of P_{T8}/P_o as the nozzle pressure ratio was increased and then the recording of repeat data as the nozzle pressure ratio was decreased.

Aerodynamic Performance Results and Analysis

The rationale for running the STA and the baseline unsuppressed plug was to assure the accuracy of the NASA/FluiDyne system. The STA and the unsuppressed plug had been tested previously at FluiDyne. The results of these earlier tests were available to compare with the NASA-Lewis results. The comparative thrust coefficients of the two different test series for both the STA and the unsuppressed plug nozzles agreed within 0.3%. The STA and the unsuppressed plug thrust coefficients for the FluiDyne and the NASA-Lewis tests are compared in Figures 55 and 56, respectively.

82
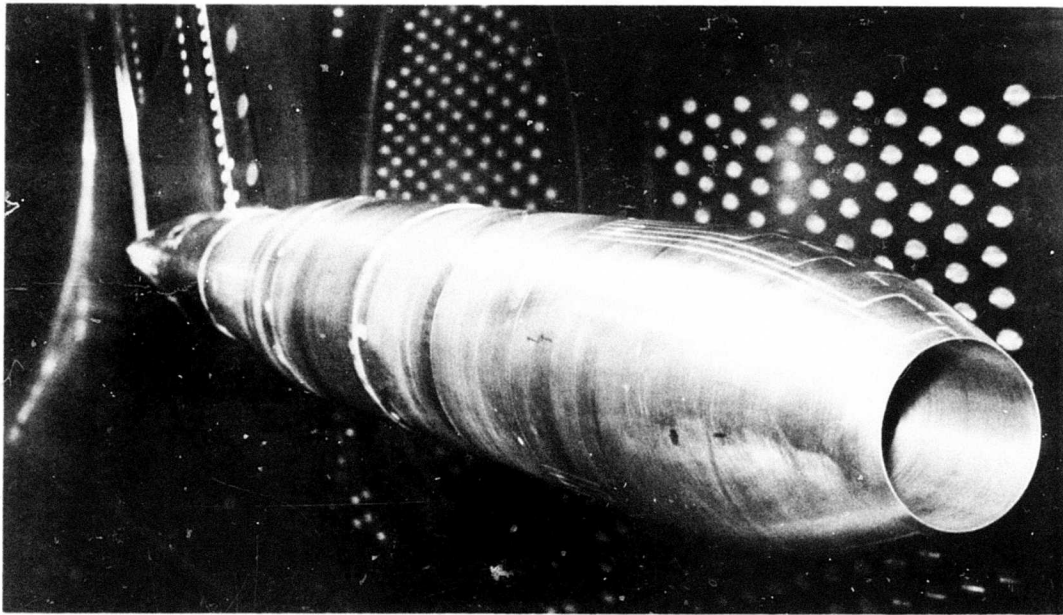
Figure 51.   STA Nozzle Mounted in NASA Wind Tunnel (Aft View).
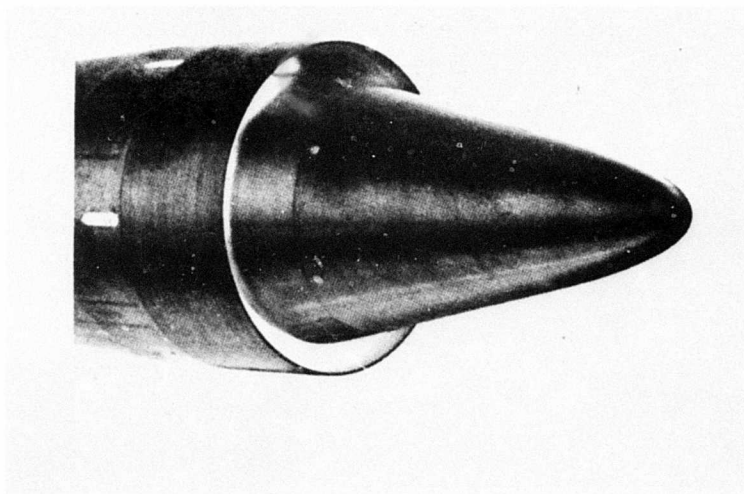
Figure 52.   Baseline Unsuppressed Plug Nozzle.
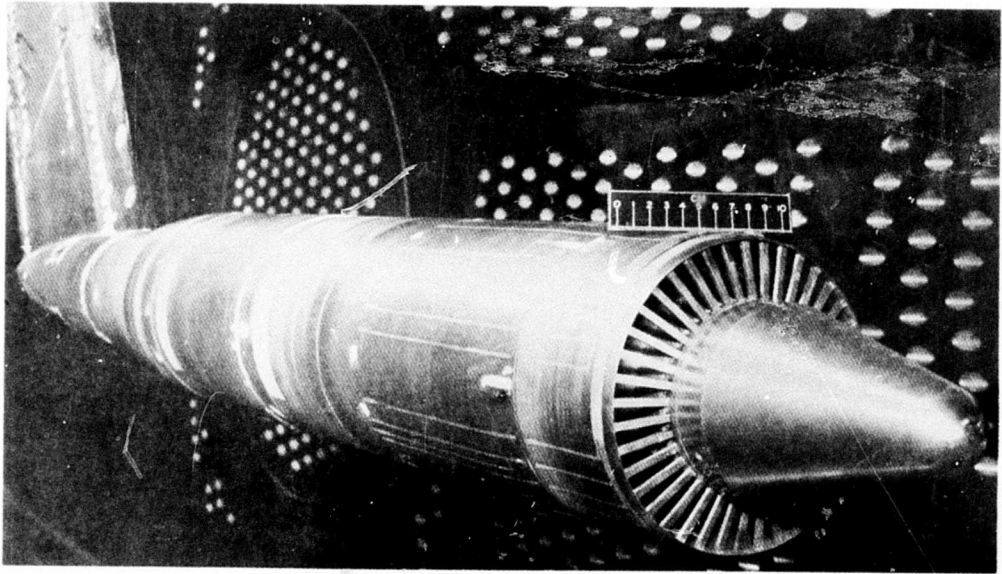
Figure 53. Low C_D 40-Spoke Suppressor Mounted in NASA-Lewis Wind Tunnel.
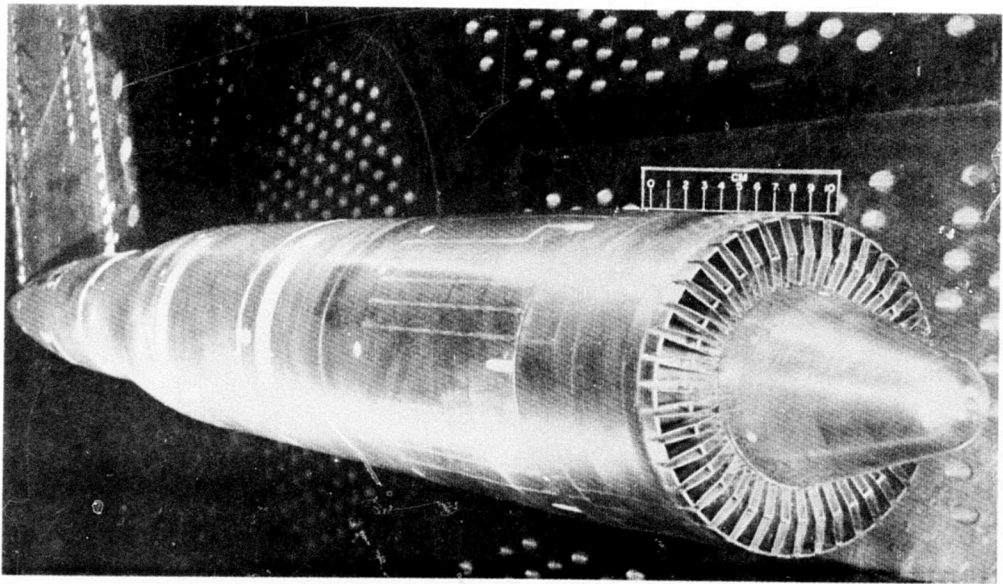
Figure 54. 40-Chute Suppressor Mounted in NASA-Lewis Wind Tunnel.

Figure 56. Unsuppressed Plug Nozzle Performance.

Figure 55. Standard Nozzle Static Performance.

Thrust coefficients for the spoke and chute configurations at static and Mach number 0.36 conditions are presented in Figures 57 and 58, respectively. As previously discussed, one of the most important areas in this investigation involved the spoke and chute base drags. Spoke thrust losses are presented in Figure 59 for static and $M_O = 0.36$ conditions. On this same figure, the predicted spoke losses at the same conditions are plotted. These results indicate that the 15° outward lean of the spoke increases the spoke pressure drag at static conditions and that the shroud extension over the top of the spoke eliminates the external flow effects on the spoke pressures. The base pressure profiles of the 40-spoke and 40-chute nozzles for $M_O = 0$ and 0.36 are presented in Figures 60 and 61, respectively. Plug surface pressure distributions for the unsuppressed plug nozzle are shown in Figure 62, while Figures 63 and 64 show similar distributions for the 40-spoke and 40-chute suppressor nozzles, respectively.

The thrust-minus-drag coefficients of the unsuppressed plug, the multi-spoke suppressor, and the multichute suppressor nozzles are presented as a function of nozzle pressure ratio in Figure 65 at Mach numbers of 0, 0.36, 0.40, and 0.45. For static tunnel conditions, the two suppressors have internal nozzle performances (Figure 65a) which are approximately equal at pressure ratios equal to or greater than three. The chute suppressor sustained somewhat greater losses with external flow than did the spoke suppressor. The thrust-minus-drag coefficients of both suppressors at free-stream Mach numbers of 0.36, 0.40, and 0.45 are presented in Figures 65b, 65c, and 65d, respectively. The thrust-minus-drag coefficients of the unsuppressed plug at Mach numbers of 0.80 and 0.90 are plotted in Figures 65e and 65f.

The thrust-minus-drag coefficients of the unsuppressed plug and the two suppressor plug nozzles are presented as a function of free-stream Mach number in Figure 66 at a nozzle pressure ratio of three. At the assumed take-off conditions, a nozzle pressure ratio of 3.0, and an external Mach number of 0.36, the thrust-minus-drag coefficients of the unsuppressed plug and the suppressor nozzles were 0.98 and 0.835, respectively.

The largest pressure drag components of the unsuppressed plug, the 40-spoke suppressor, and the 40-chute suppressor nozzles are presented in Figure 67. The nozzle thrust losses resulting from the boattail pressure drag of the unsuppressed plug are plotted in Figure 67a at the free-stream Mach numbers tested. The nozzle thrust loss from the low C_D, 40-spoke, base pressure drag was insensitive to external flow over the Mach number range of $M_O = 0$ to 0.45 (Figure 67b). However, the 40-chute base pressure drag increased approximately the same amount over the no-external-flow condition at all Mach numbers tested. The thrust loss from the chute base pressure drag is presented in Figure 67c.

Another loss mechanism which was investigated in the two suppressor plug nozzles was flow angularity. The flow angularity probe was positioned down-stream of the spoke suppressor in the outer radial position. Angularity data were measured statically for three nozzle pressure ratios (2.5, 3.0, 3.5) at three radial positions. In Figure 68, the nozzle exit planes and the angularity probe positions of the spoke and the chute suppressors are drawn to scale. At each of the hub, pitch, and shroud probe positions on the figure, a ray

Figure 58. Chute Suppressor Installed Performance.

Figure 57. Spoke Suppressor Installed Performance.

87
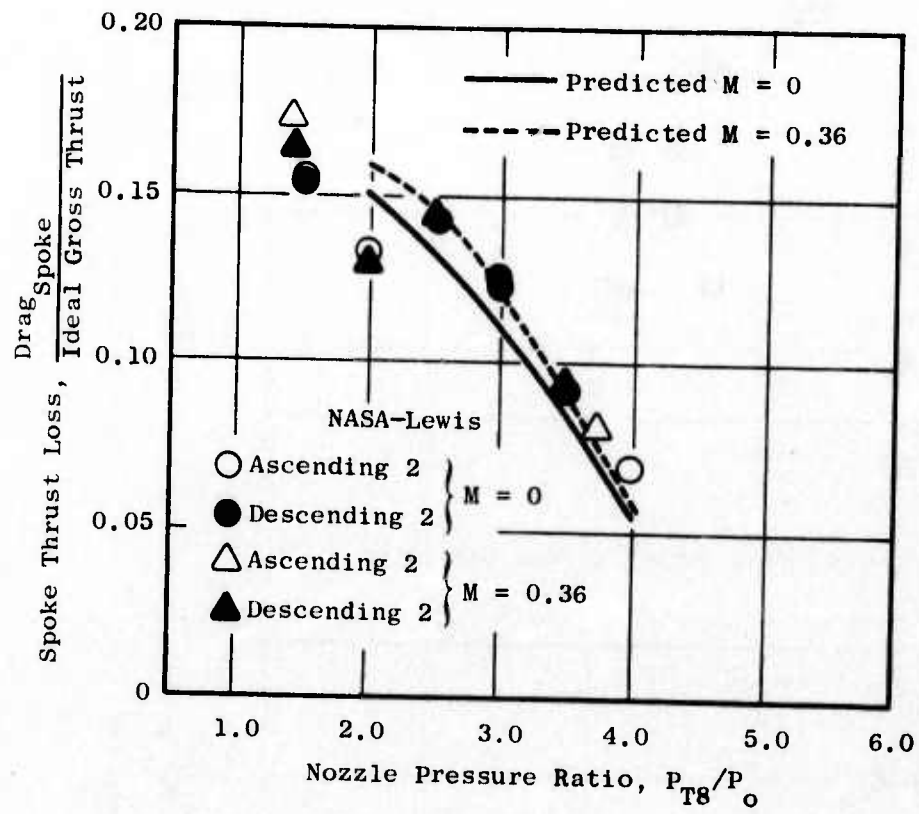
Figure 59. Spoke Base Pressure Losses.
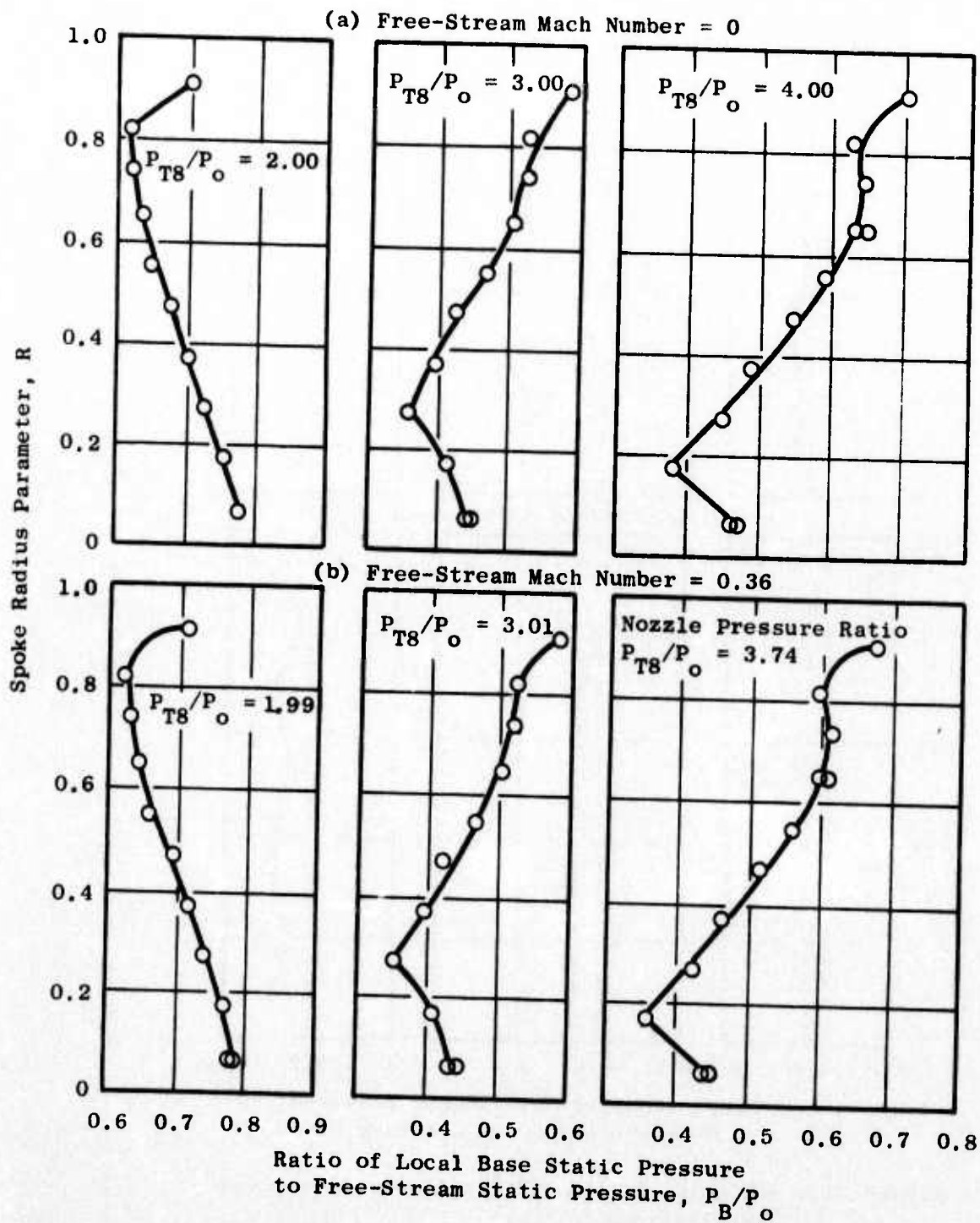
Figure 60. 40-Spoke, Plug Nozzle, Spoke-Base Pressure Distributions.

89

Figure 61. 40-Chute, Plug Nozzle, Spoke-Base Pressure Distributions.
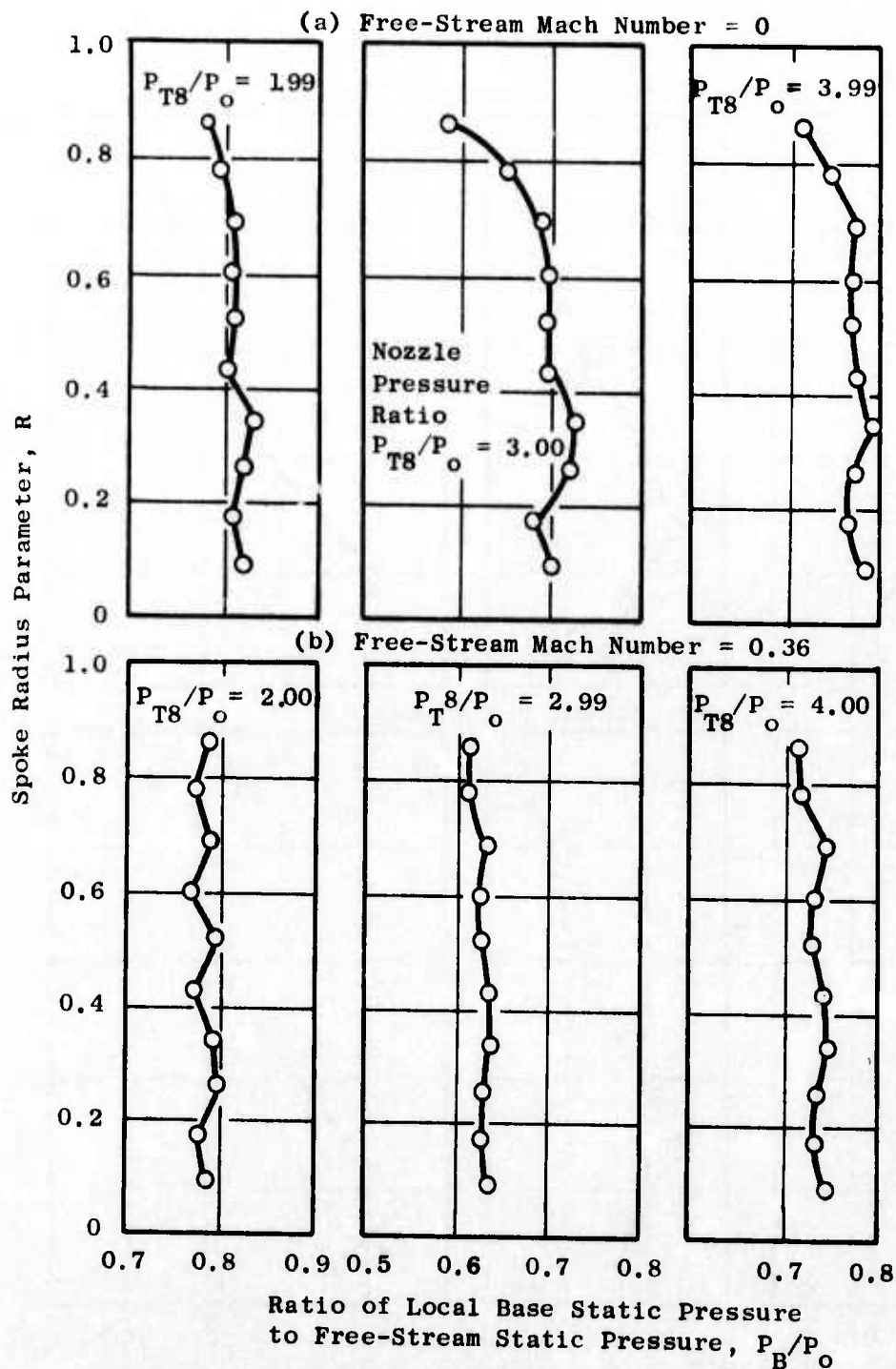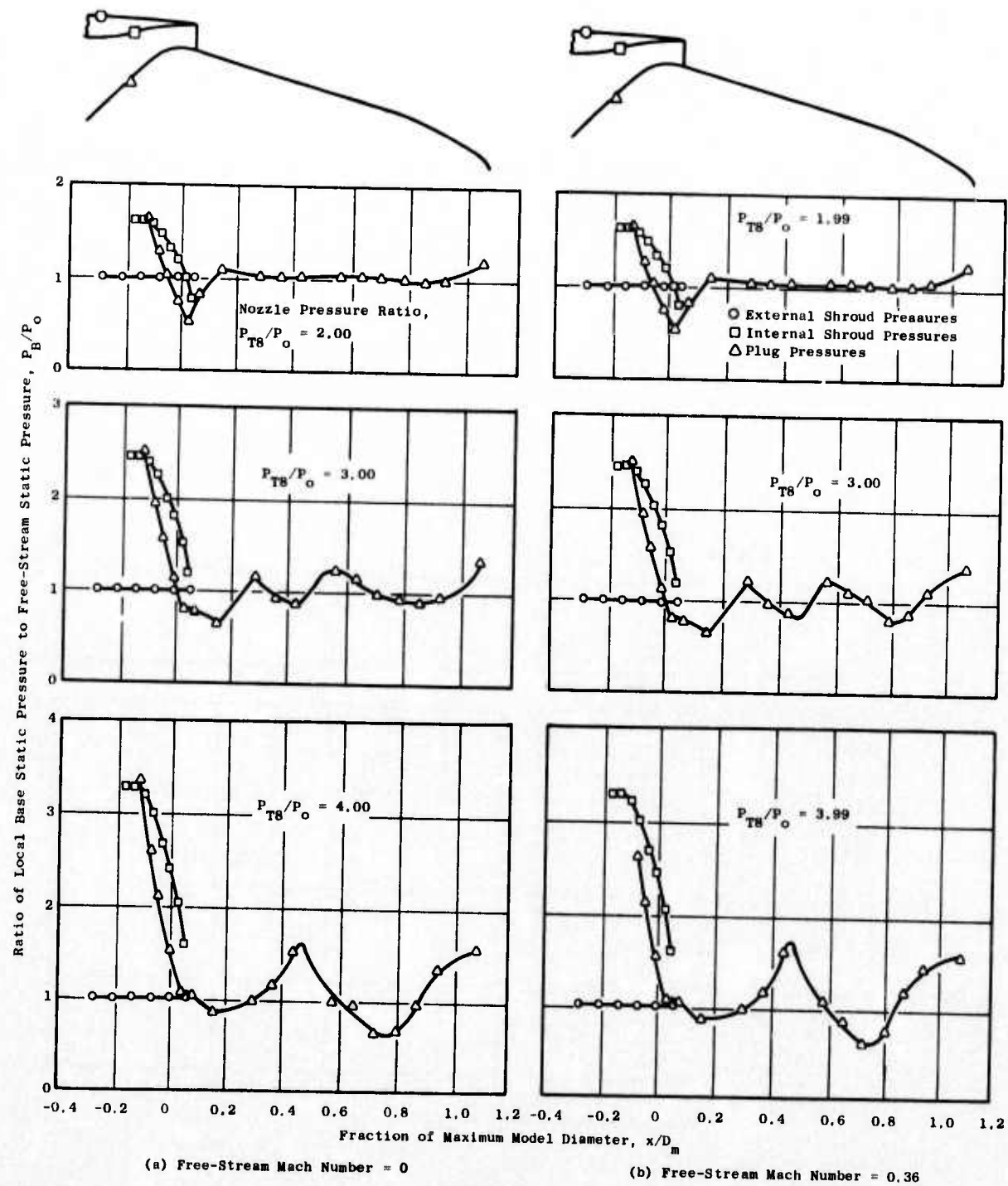
Figure 62. Unsuppressed Plug Nozzle Surface Pressure Distributions.
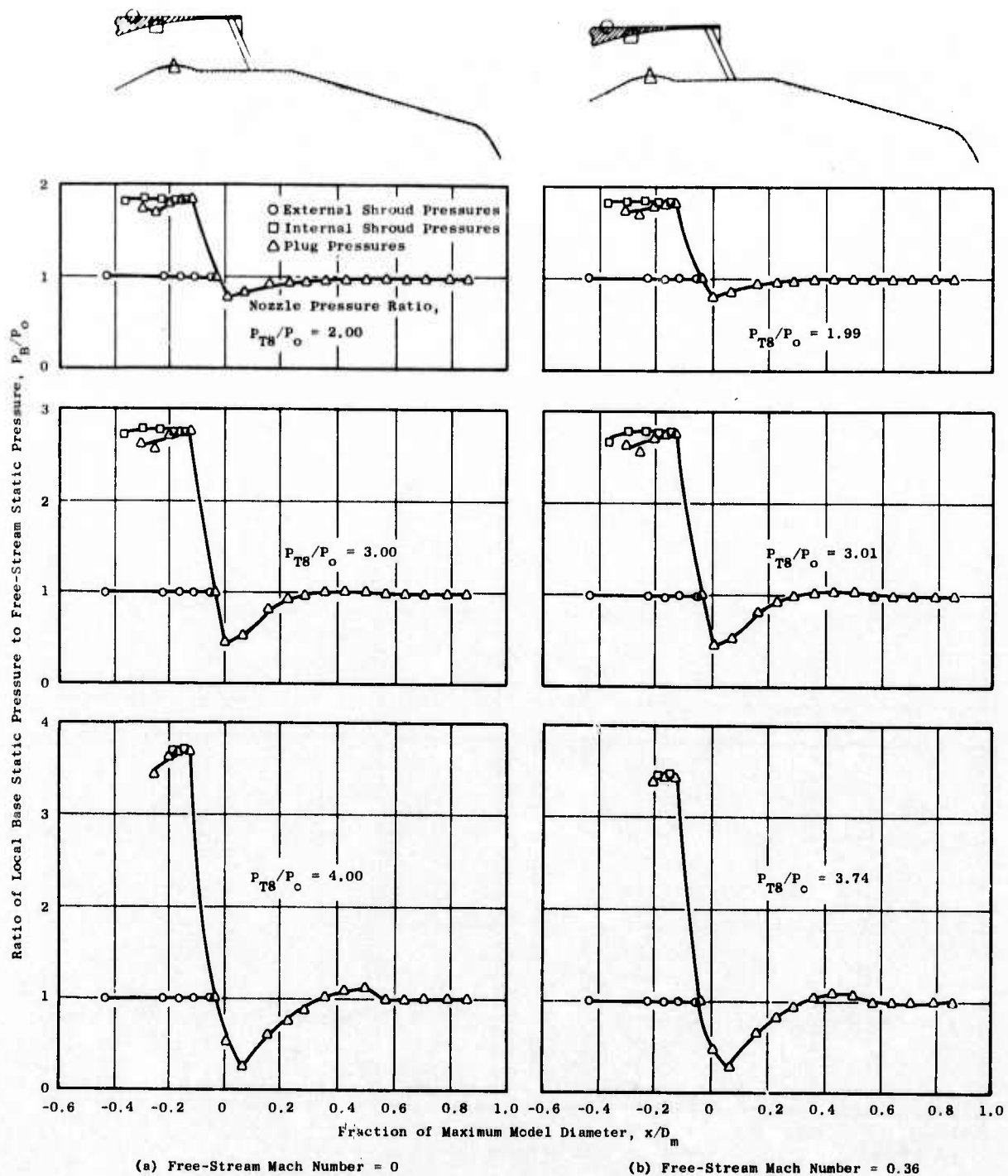
Figure 63. 40-Spoke, Plug Nozzle Surface Pressure Distributions.
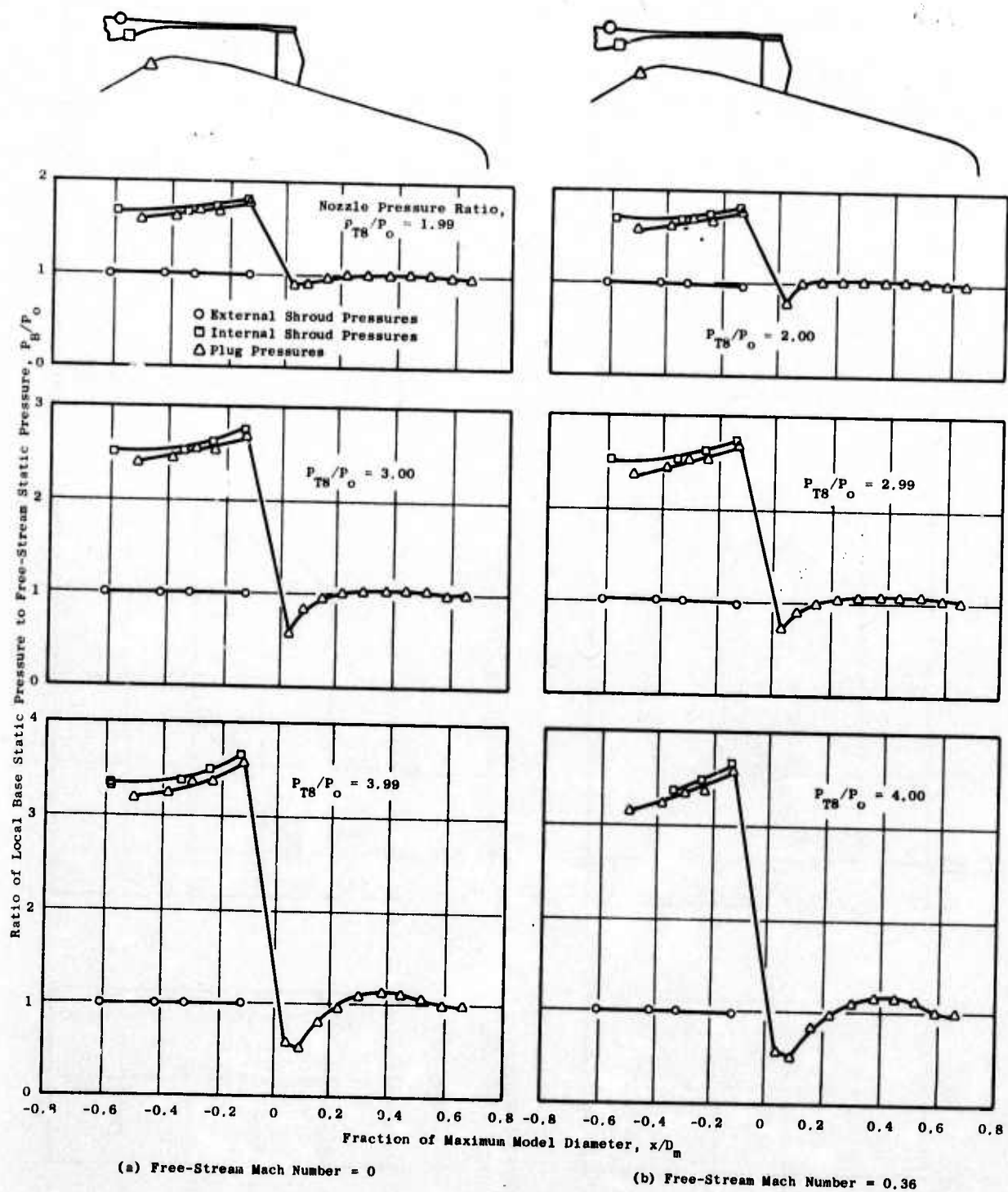
Figure 64.   40-Chute, Plug Nozzle Surface Pressure Distributions.

93
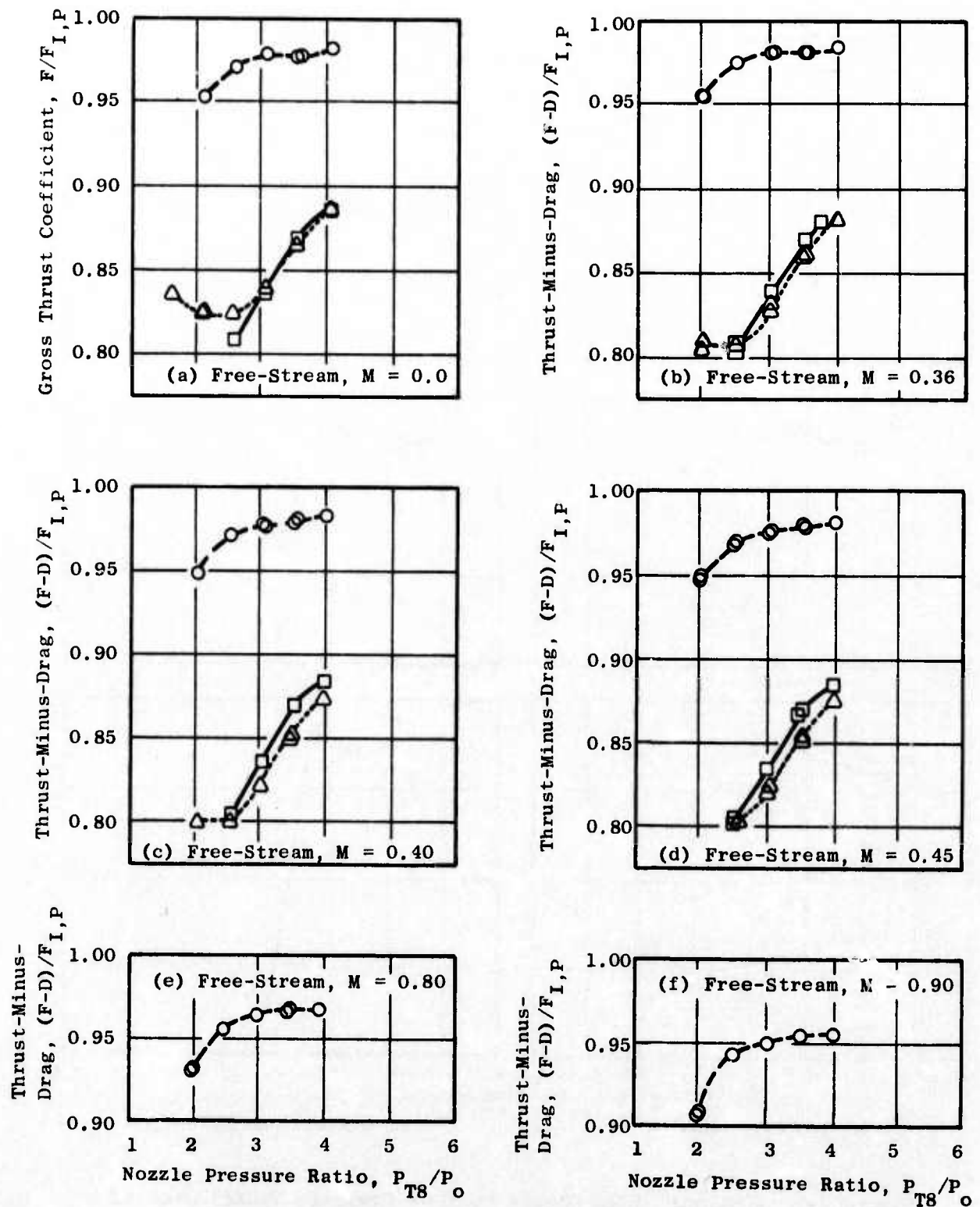
Figure 65. Comparison of Unsuppressed Plug Nozzle Performance with Suppressed Nozzle Performance.
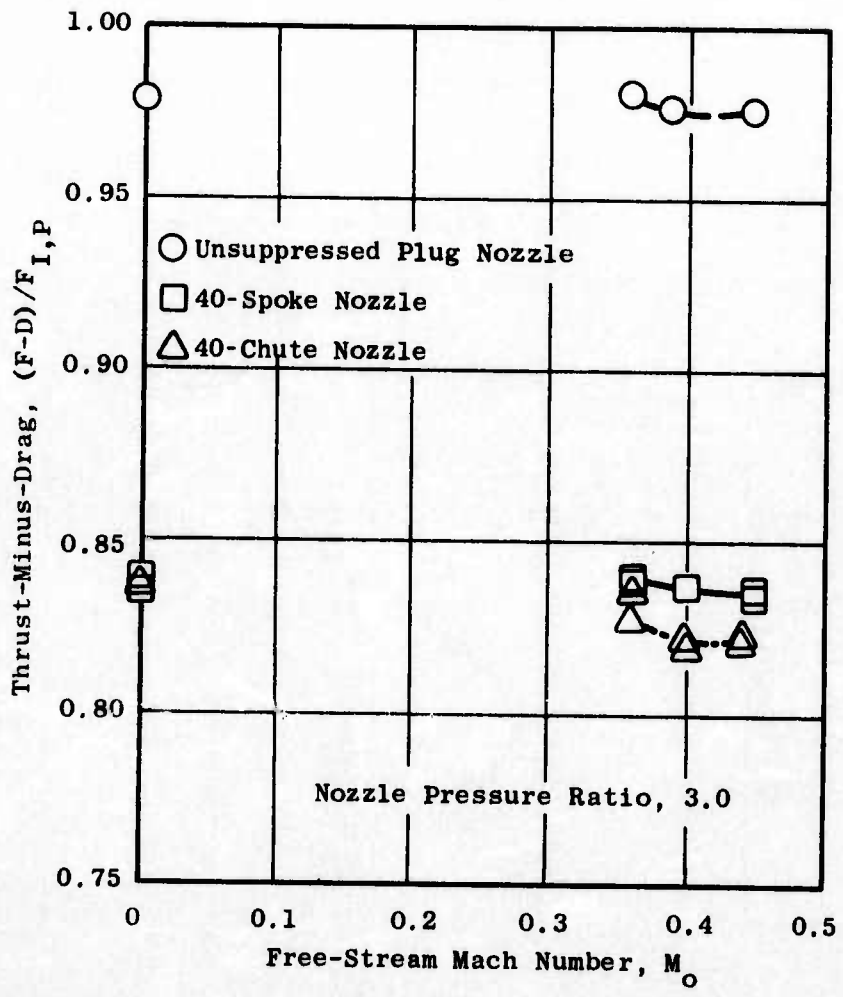
Figure 66. External Flow Effects on Nozzle Performance.
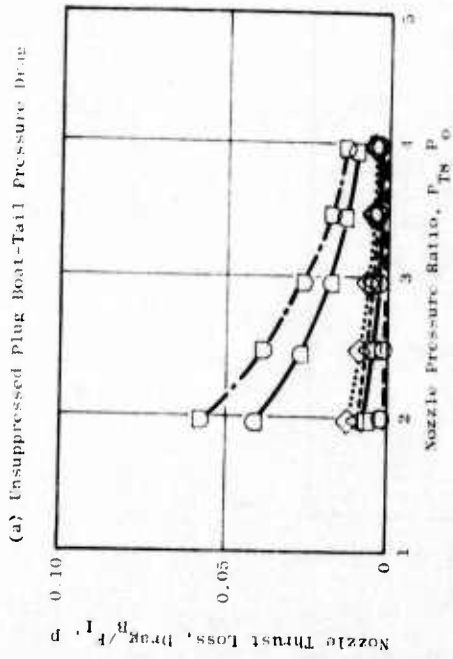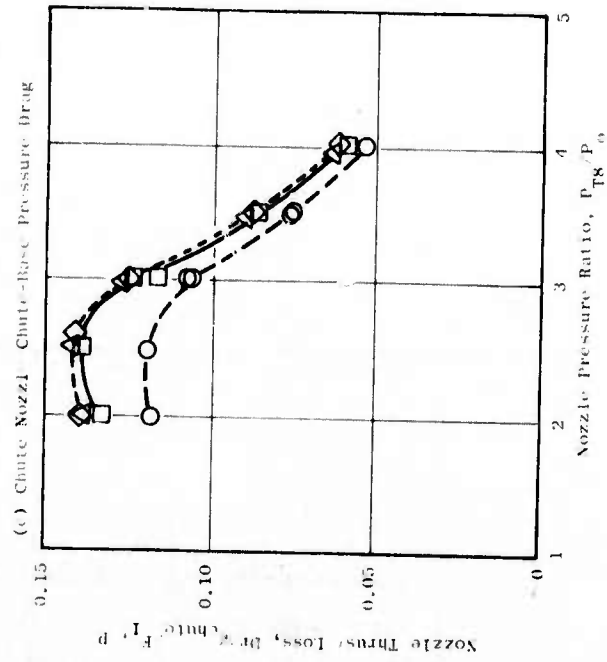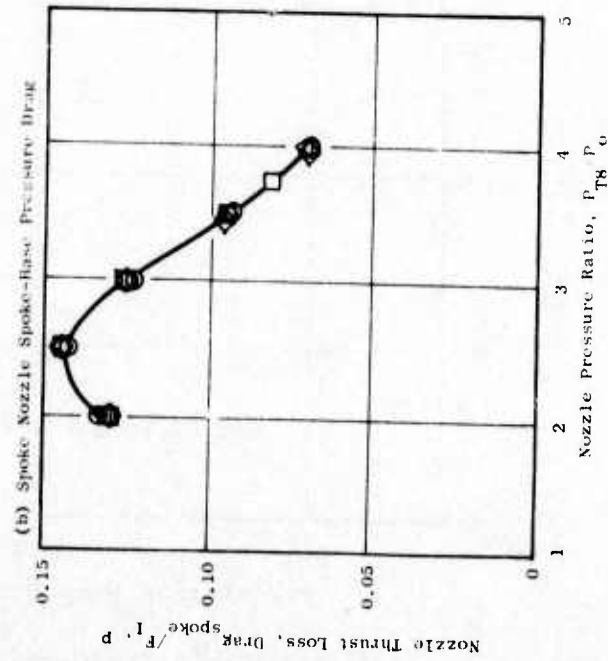
Figure 67. Nozzle Thrust Loss from One Drag Component.
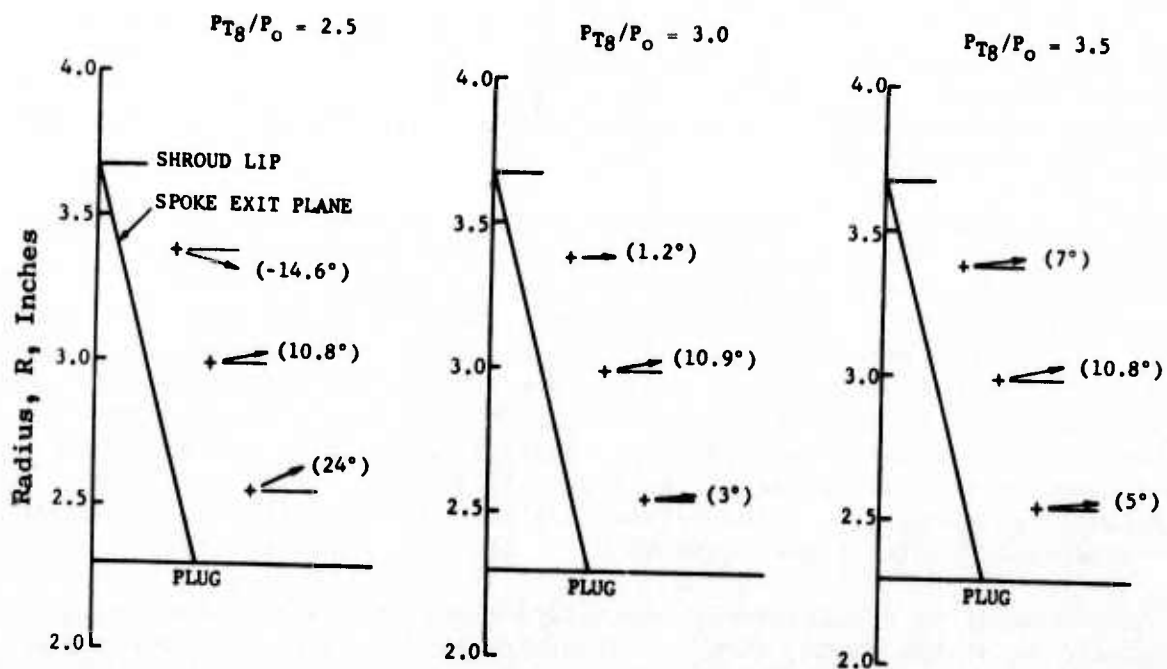
(a) Low C_D/40-Spoke Suppressor
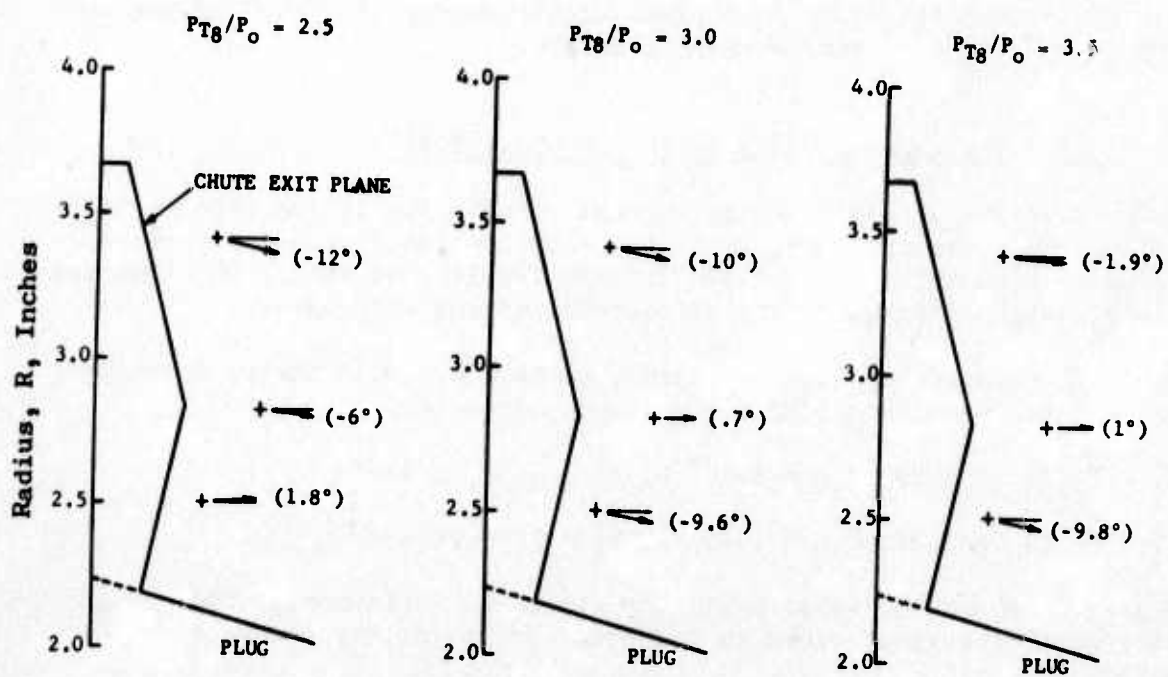
(b) 40-Chute Suppressor

Figure 68. Flow Angularity at Mach No. = 0.

and a number indicating flow direction are presented. For the 40-spoke suppressor plug nozzle, the flow angles at the outer radial probe position were smaller than one-half the outward physical cant angle of the spokes at the nozzle exit plane (Figure 68a). The 40-chute suppressor flow angles at the outer radial position were all negative which indicated the flow was directed down the plug (Figure 68b).

The nozzle discharge coefficients of the unsuppressed plug, the 40-spoke suppressor, and the 40-chute suppressor nozzles are presented in Figure 69. The increase in discharge coefficient with nozzle pressure ratio was attributed to the increase in turbulence level upstream of the flow metering nozzle where the upstream total pressure and the total temperature were measured. The high turbulence levels were a result of the dumping of the flow from the tubes in the strut into the flow bottle in the sting. This turbulence and the limited upstream instrumentation prevented achieving the desired accuracy in total pressure and temperature. The nozzle discharge coefficient, by the nature of the system, was much more sensitive to upstream total pressure and total temperature than was the thrust coefficient.

In an attempt to qualitatively understand the flow field in the region of the backside of the chute, flow visualization studies were made using a glycerin-lampblack mixture. The entrainment of the external flow between the primary flow passages, documented in Figure 70, was at static conditions and at a nozzle pressure ratio of three. The external flow behind the chute did not penetrate to the plug but was turned axially approximately two-thirds down the chute substantiating to a considerable degree the "why" of the poor performance exhibited by the chute/plug nozzle.

Laser Velocimeter Tests of the 40-Chute Nozzle

To support the acoustic and aerodynamic evaluation of the multispoke/chute nozzle suppression characteristics, detailed laser velocimeter experiments also were conducted at the JENOTS test facility to assess the turbulent flow field characteristics of the 40 deep-chute/plug suppressor.

Two cycle conditions were selected for the laser velocimeter investigations on the 40 deep-chute/plug suppressor; they were:

a) $P_{T8}/P_o = 3.25$, $T_{T8} = 1960°$ R, $V_j = 2635$ ft/sec

b) $P_{T8}/P_o = 2.20$, $T_{T8} = 1565°$ R, $V_j = 1968$ ft/sec

Figure 71 shows the axial measuring stations for investigation. Figure 72 shows the axial locations close to the nozzle exit for the 40-chute suppressor.

Laser velocimeter measurements of the jet plume were conducted at each axial station, in-plane. Figure 73 illustrates the in-plane measurement positions for two stations, $X/D = 0$ and 0.5, close to the nozzle exit. Similar in-plane measurements were taken at axial stations further downstream.

98
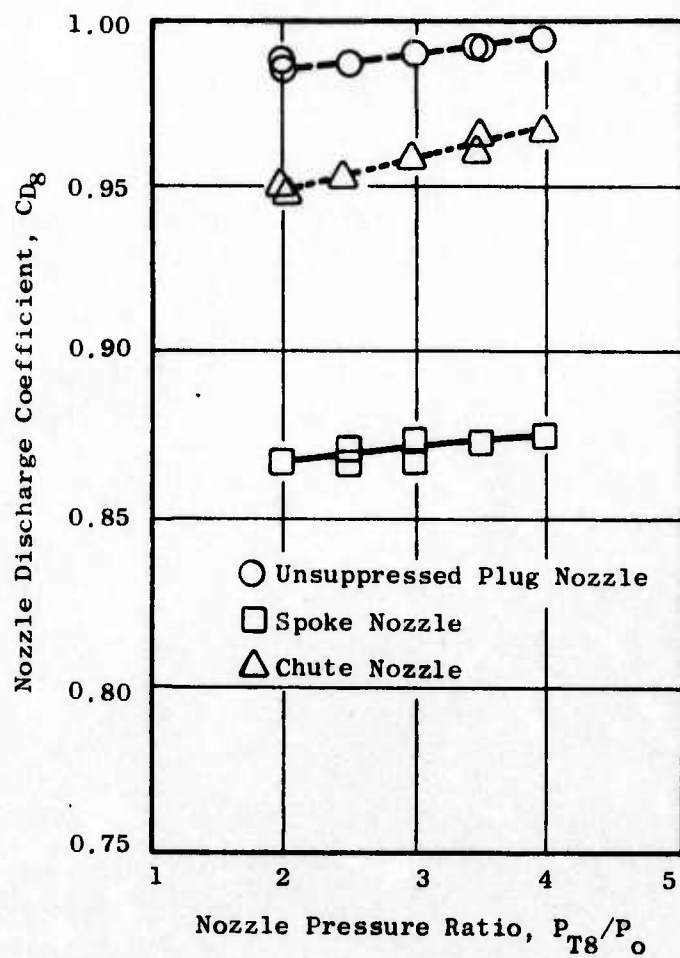
Figure 69. Nozzle Discharge Coefficient.
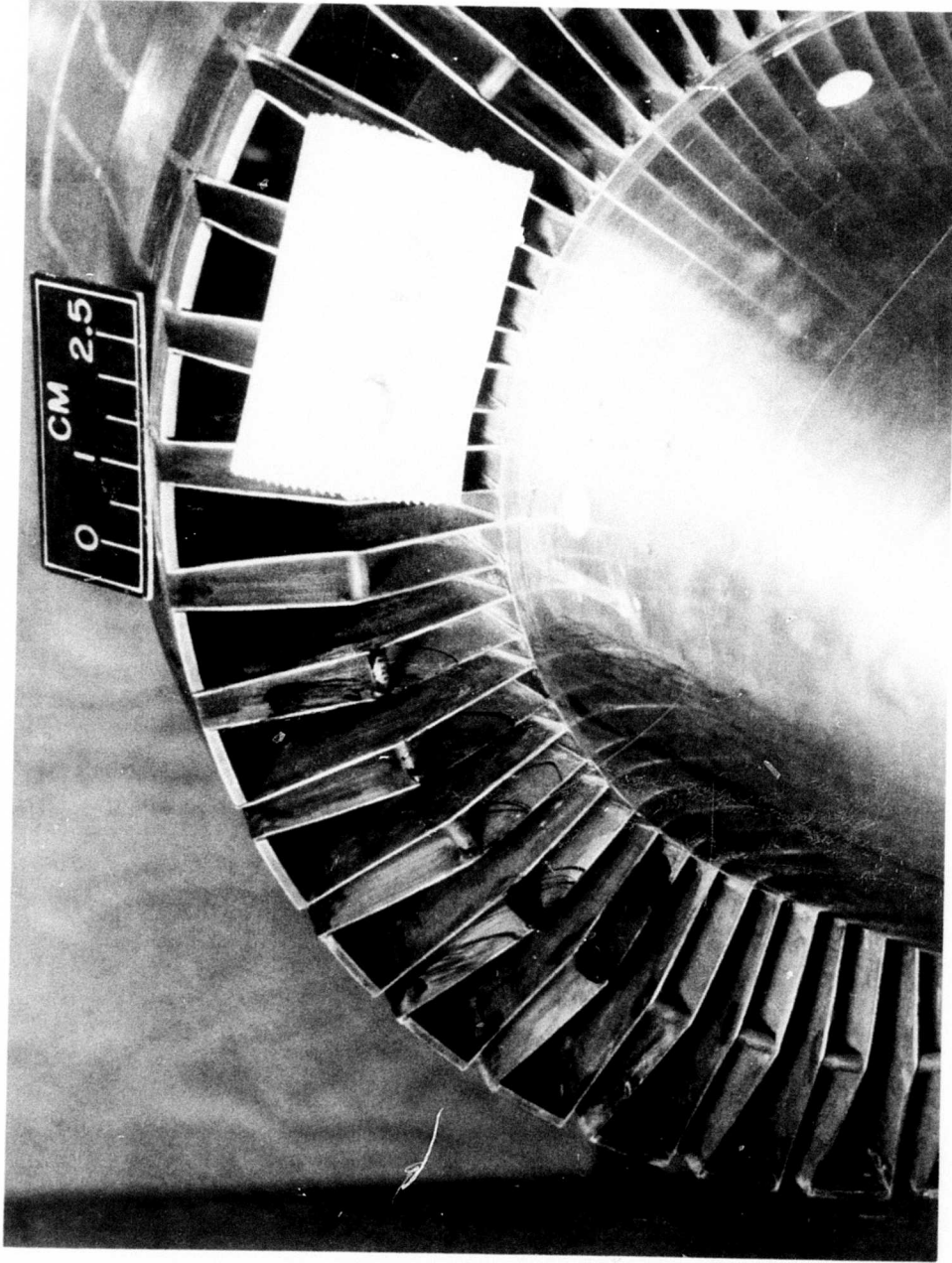
Figure 70. Flow Visualization on 40-Chute Suppressor Showing External Flow Entrainment.
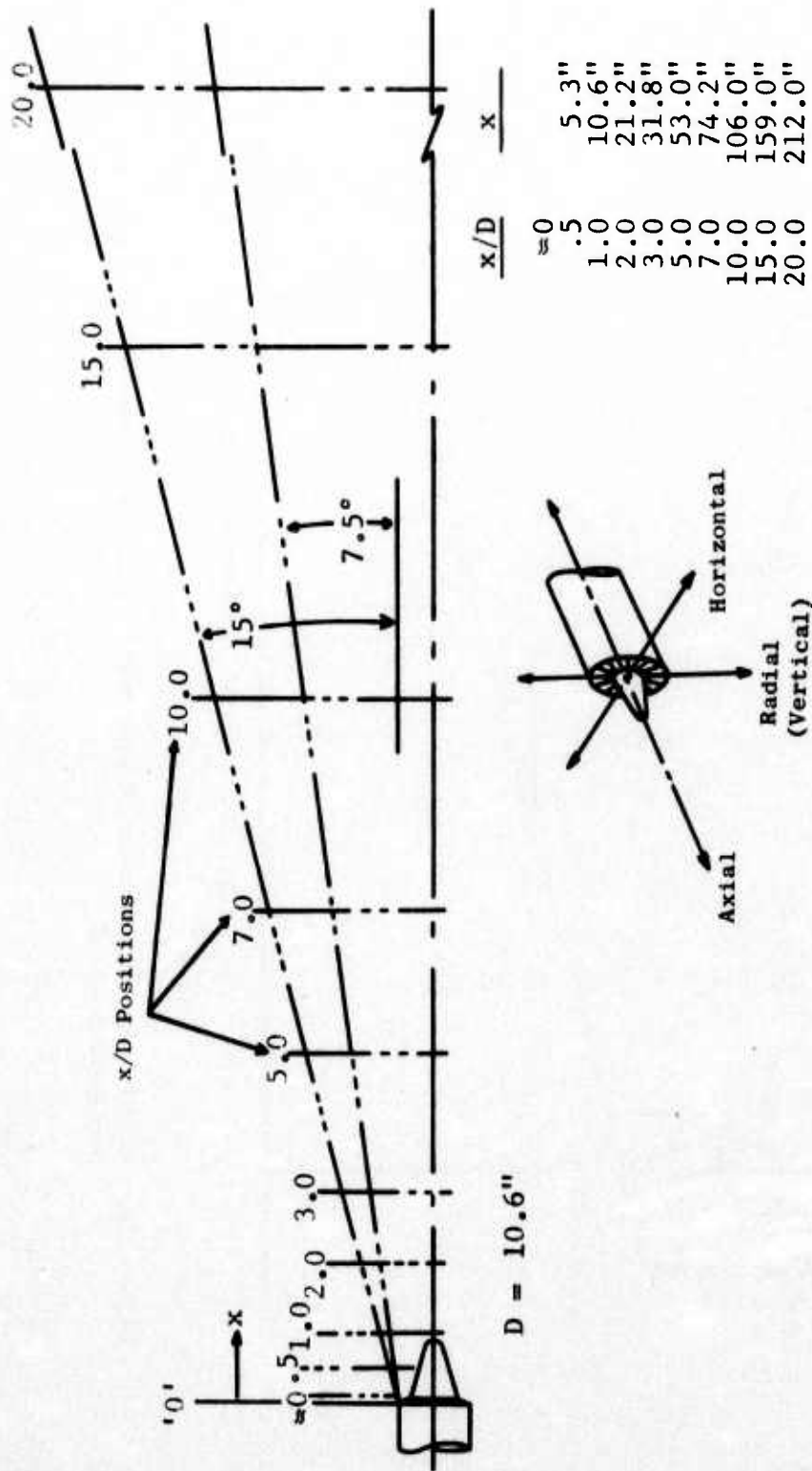
Figure 71. Axial Stations for Laser Velocimeter Measurements on 40-Chute Nozzle.
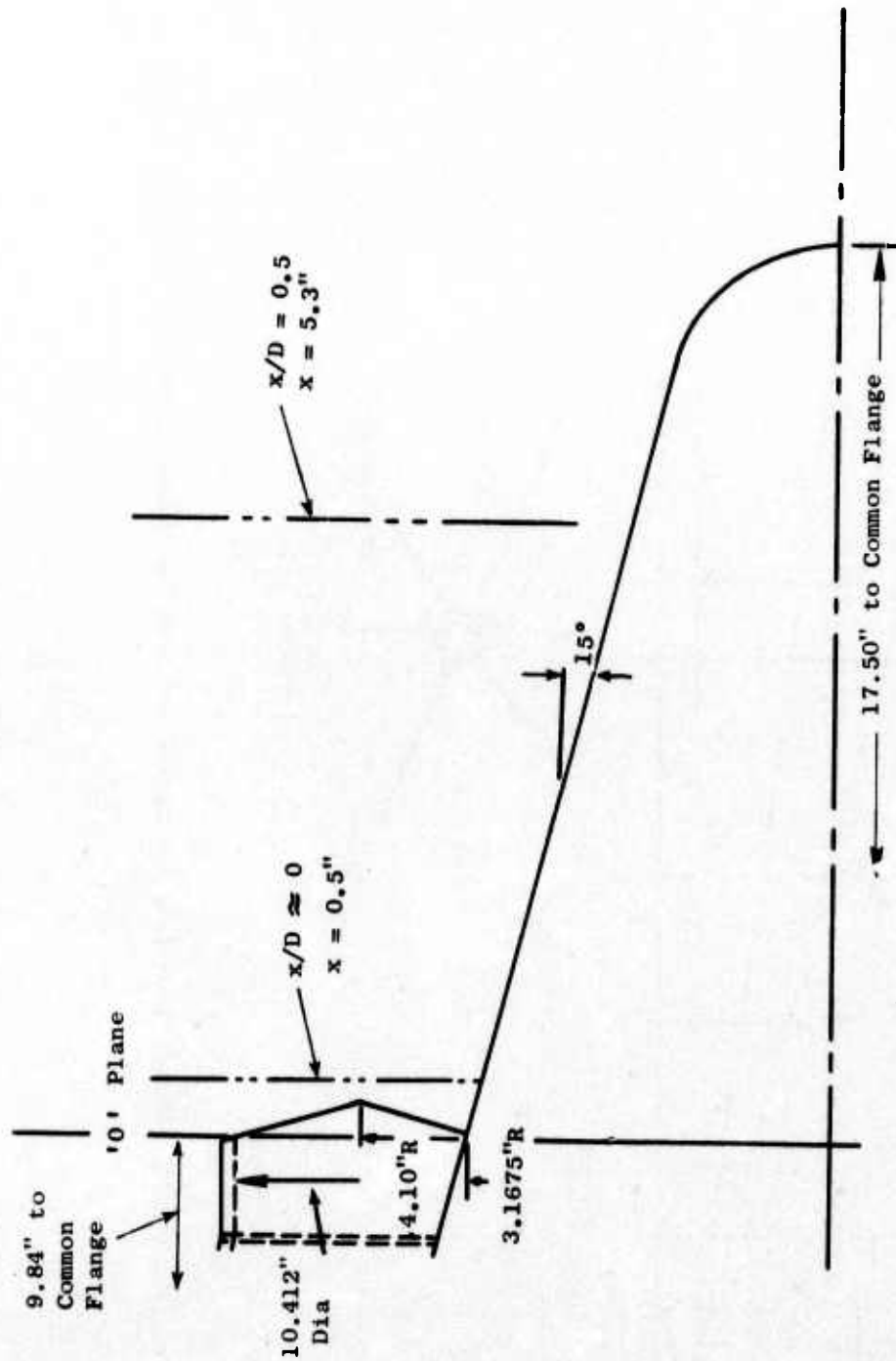
Figure 72. Axial Laser Velocimeter Measurement Stations Close to Exit Plane of 40-Chute Nozzle.

102

6.7"R at 15° expansion angle at x/D = .5

Flow

Chute

1.7"R at plug at x/D = .5

x/D = .5
x = 5.3"
✕ Locations for histograms

6.70"
5.70"
4.70"
3.70"
2.70"

b) x/D = .5

5.45"R at 15° expansion angle

Chute

Flow

3.05"R at plug at x/D ≅ "0"

x/D ≅ 0
x = .5"
✕ Locations for histograms

5.45"
4.68"
4.32"
3.76"
3.2"
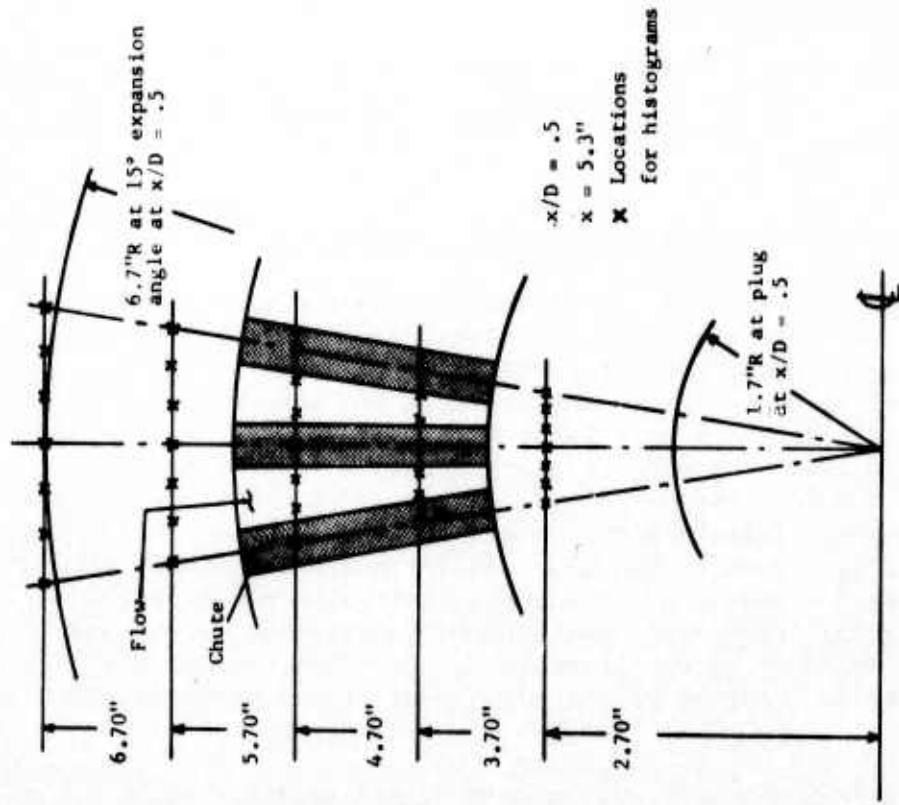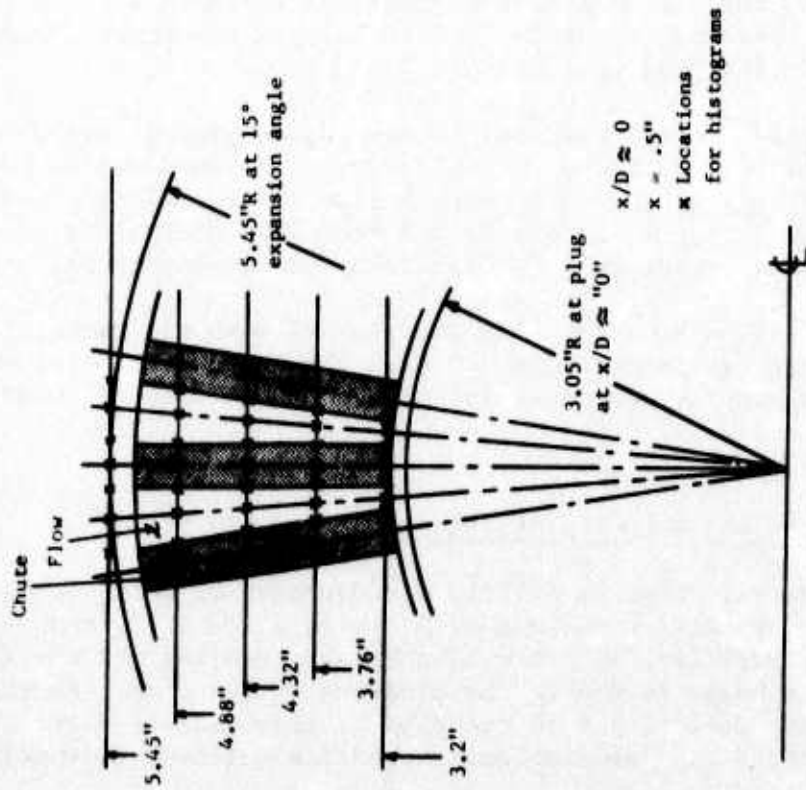
a) x/D ≅ 0.

Figure 73. Laser Velocimeter In-Plane Measurement Locations for 40-Deep-Chute Nozzle.

Laser Measurement Evaluation

Some of the results of measurements of axial and radial surveys close to the nozzle exit plane, as well as far downstream of the nozzle exit plane, are presented below for $P_{T8}/P_o = 3.3$, $T_{T8} = 1950°$ R.

● Mean and Turbulent Velocity Distribution within X/D = 1

Figures 74, 75, and 76 show results of axial decay profiles of mean and turbulent velocity in the open flow area for radial locations of r/r_o = 0.657, 0.829, and 0.941, respectively. All measurements were taken within the first diameter of the flow field. From these measurements the mean velocity at the smallest r/r_o locations maintain a relatively high mean flow of 2000 ft/sec. At the larger r/r_o locations, the mean velocity decay is seen to become steeper; and, at $r/r_0 = 0.941$, the velocity has decayed to 400 ft/sec within the first diameter length. These measurements indicated a rather uniform jet plume with very little jet spread. The increased turbulence velocity generation due to the increased velocity decay and gradients also was observed with an increase in radial locations. The action of the chute to mix and rapidly decay the jet velocity in the plume (and, therefore, reduce the exhaust jet noise) also is observed by the high local turbulent intensity ($u'/\bar{u}$) profiles.

Figures 77 and 78 show measured mean and turbulent velocity axial decays behind the solid (or blocked) area behind the chute for radial locations of r/r_0 = 0.711, 0.826, and 0.937. From these measurements, it can be observed that, within X/D = 0.4, the flow behind the chute and the open area of the jet are fully merged. As expected, the values of turbulence are higher than in the open flow areas close to the exit planes.

Figure 79 shows axial decay traverses in the edge region of the chute. Although fewer data points were taken for this survey, as compared to the data taken in the open flow region, the same general flow characteristics were observed for both cases (compare Figures 75 and 79). This similarity seems to indicate that there is significant jet spreading downstream of the chutes.

Figures 80 and 81 illustrate the flow profiles of mean and turbulent velocities at the nozzle exit across two chutes. The typical velocity defect behind the chuted area and the attendant increase of turbulence is readily observed.

● Mean and Turbulent Velocity Distributions for X/D > 1

Figure 82 shows radial velocity profile measurements of mean velocity and turbulent velocity at axial locations of X/D = 1, 2, 3, 5, 7, and 10. From the mean velocity profiles, at X/D = 1, a bulging profile off the centerline is observed. This bulge is due to the presence of the plug. At the centerline, the velocity deficit due to the plug is also readily seen. With increasing axial locations, the mean velocity profiles are seen to smooth out
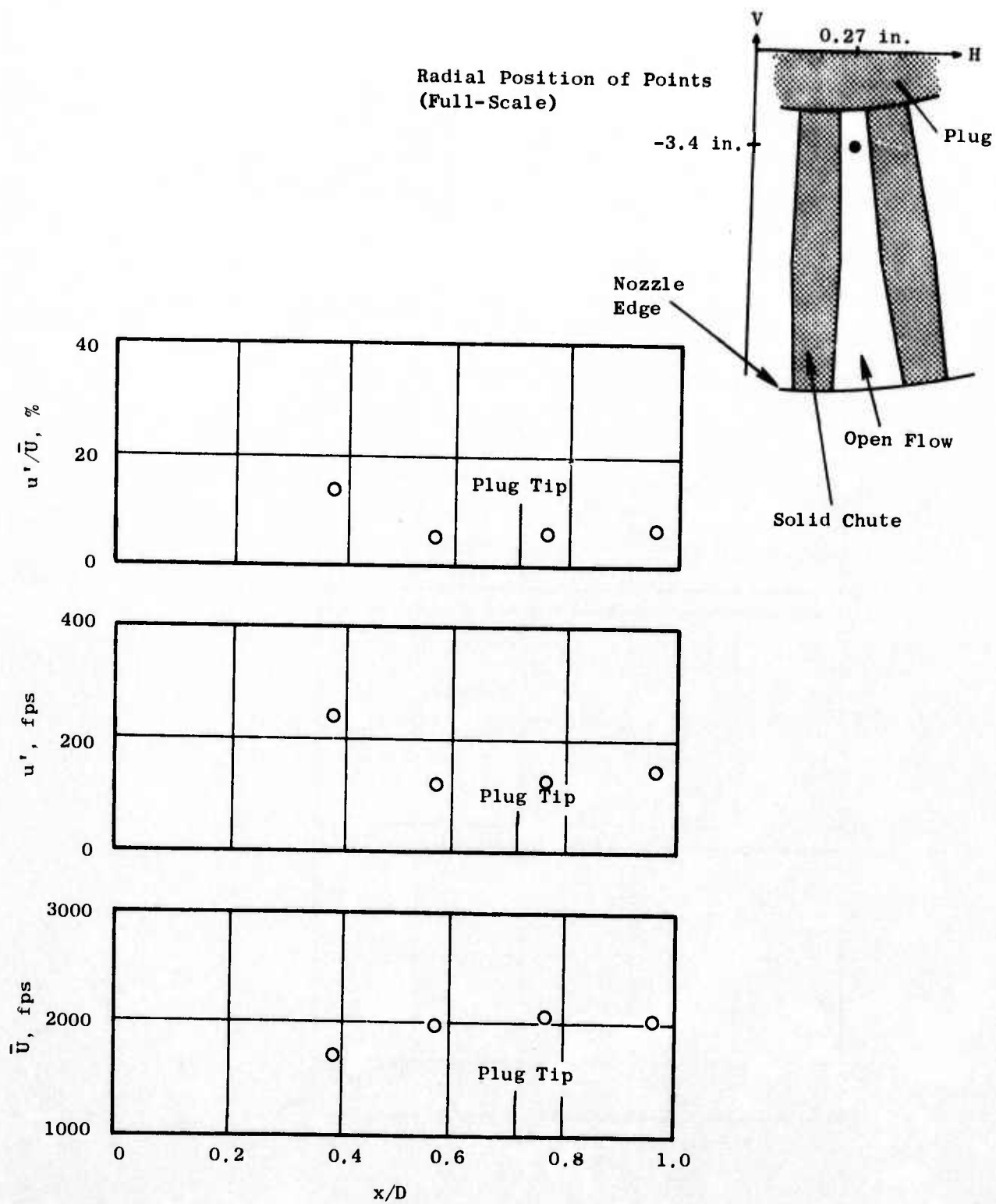
Figure 74. Axial Decay of Mean and Turbulent Velocity at $r/r_o = 0.657$ (Open Flow Area).
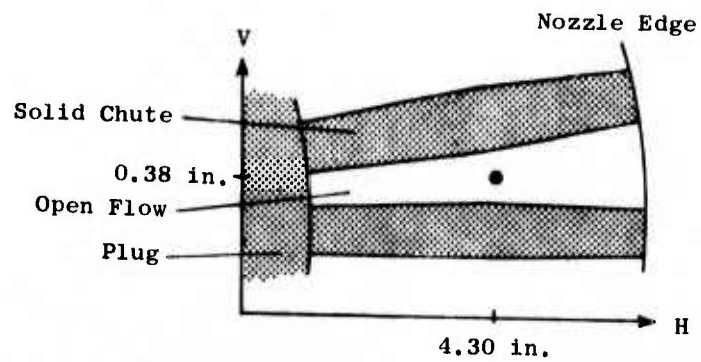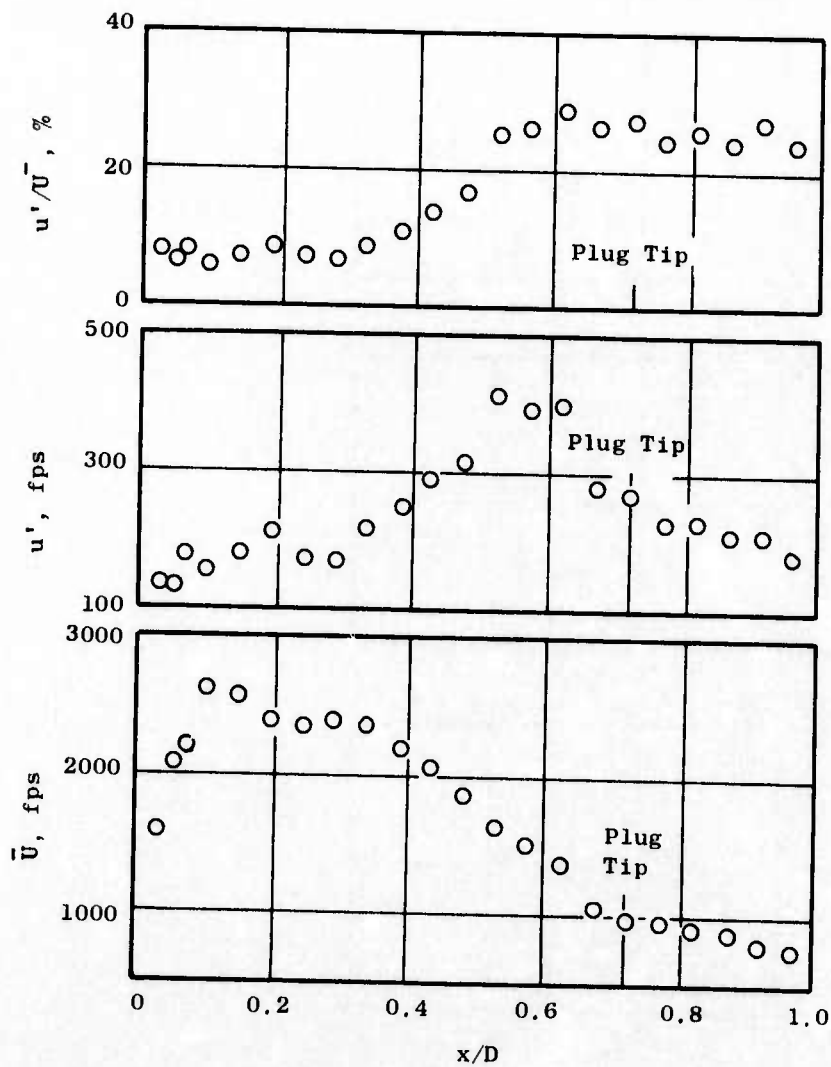
Figure 75. Axial Decay of Mean and Turbulent Velocity at $r/r_o = 0.829$ (Open Flow Area).
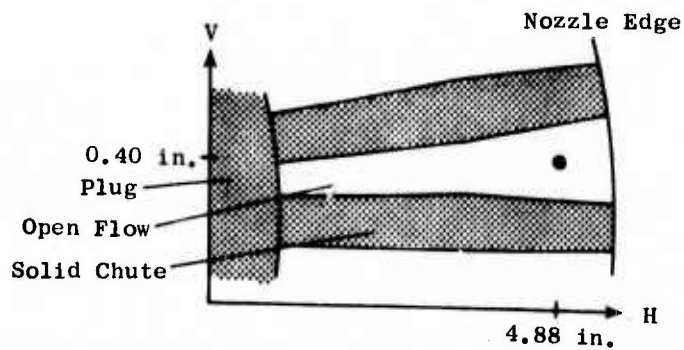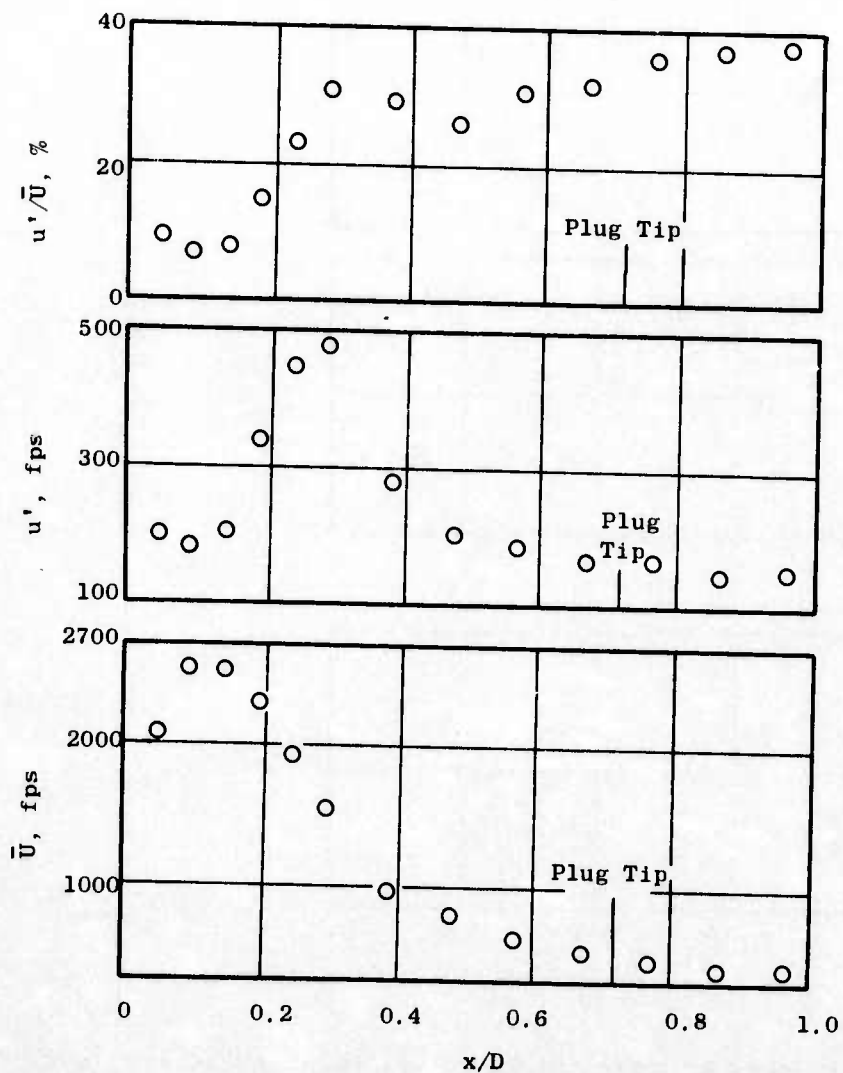
Figure 76. Axial Decay of Mean and Turbulent Velocity at $r/r_o =$ 0.941 (Open Flow Area).

107
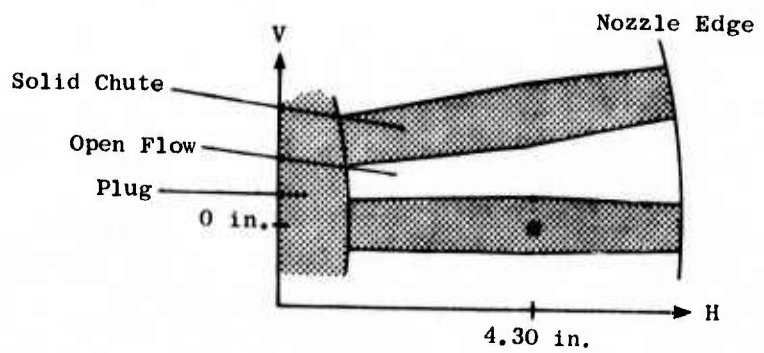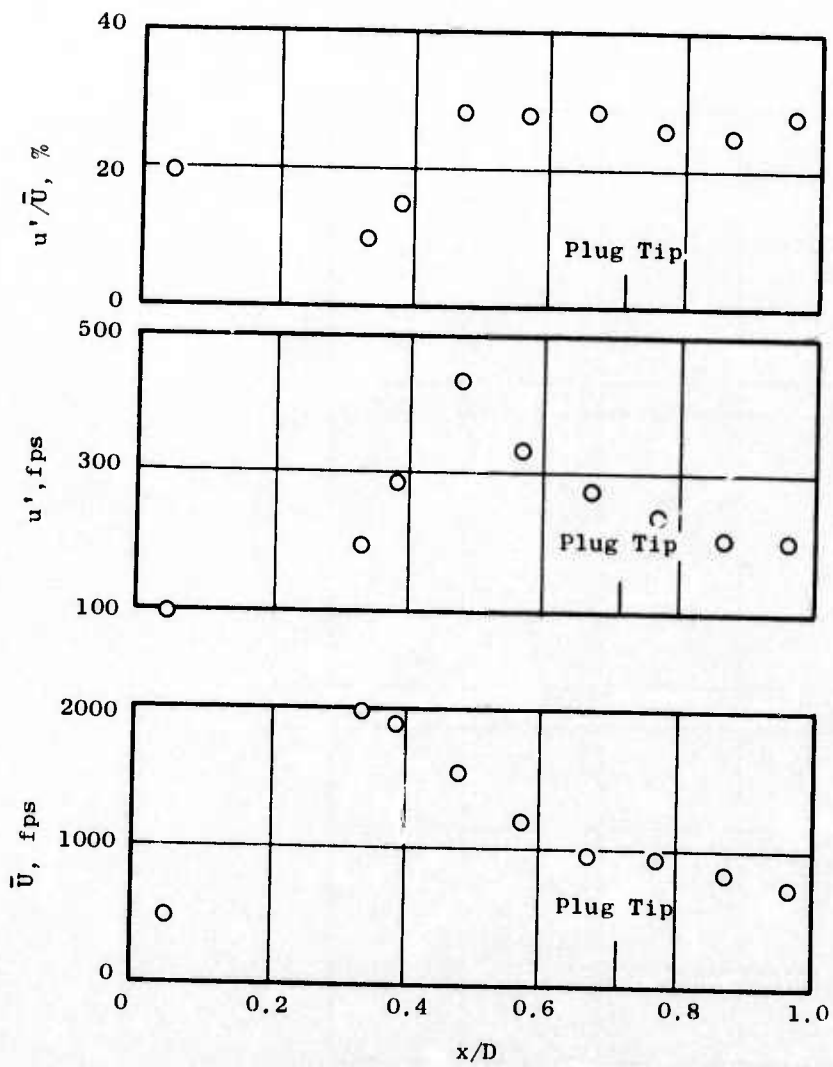
Figure 77. Axial Decay of Mean and Turbulent Velocity at $r/r_o = 0.826$ (Behind the Chute).
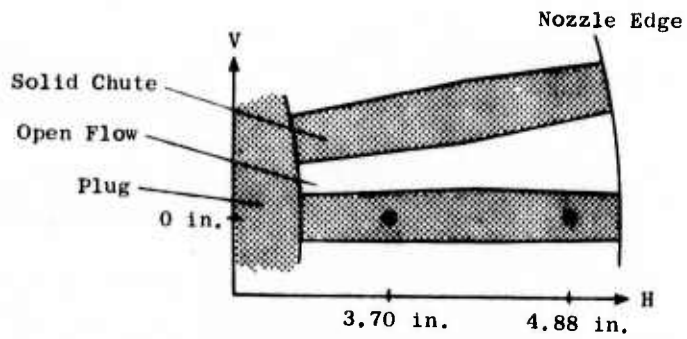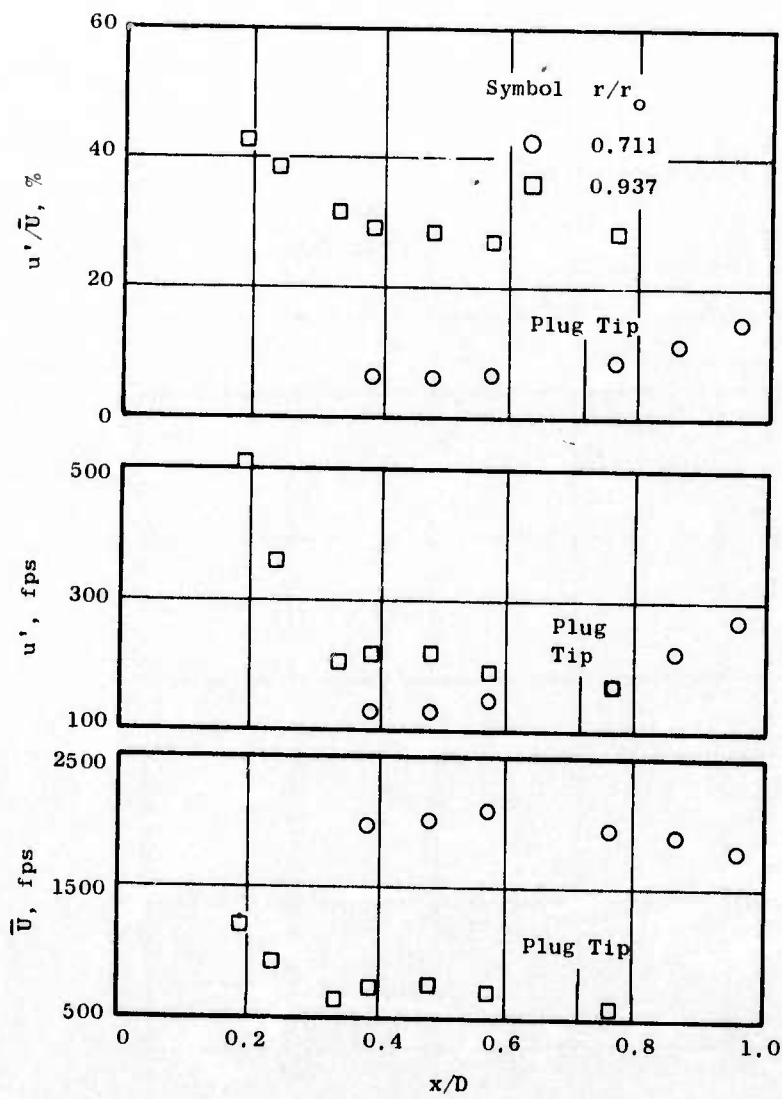
Figure 78. Axial Decay of Mean and Turbulent Velocity at r/r_o = 0.711 and 0.937 (Behind the Chute).
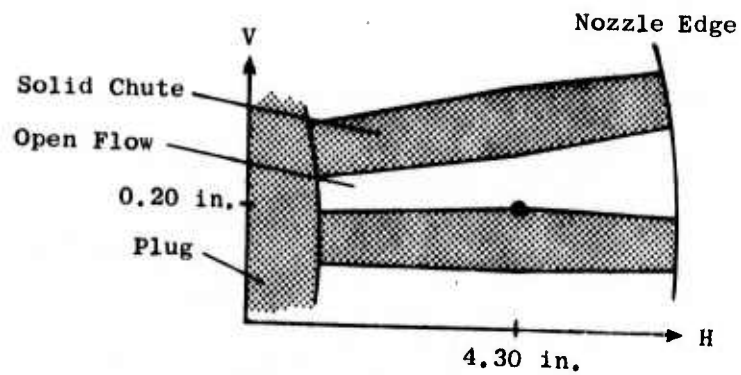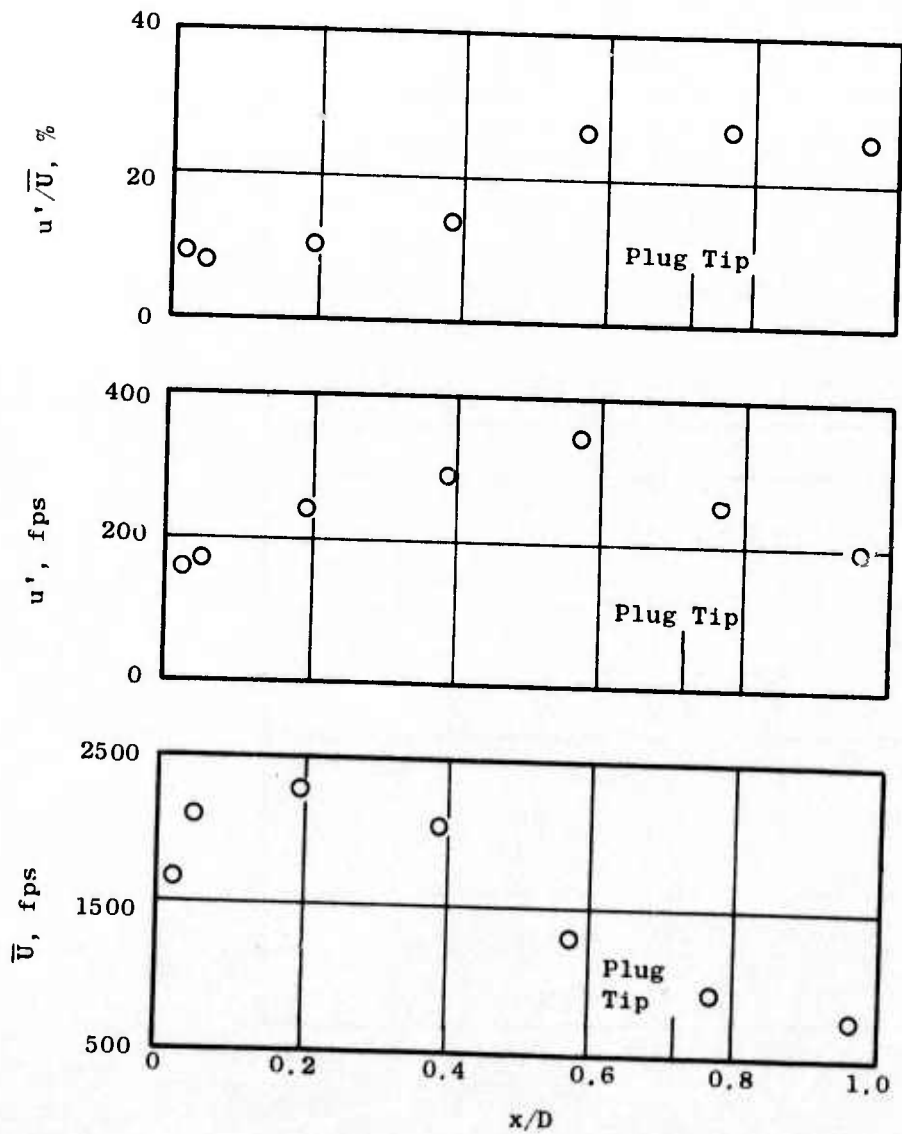
Figure 79. Axial Decay of Mean and Turbulent Velocity at $r/r_o = 0.827$ (Edge of Chute).

110
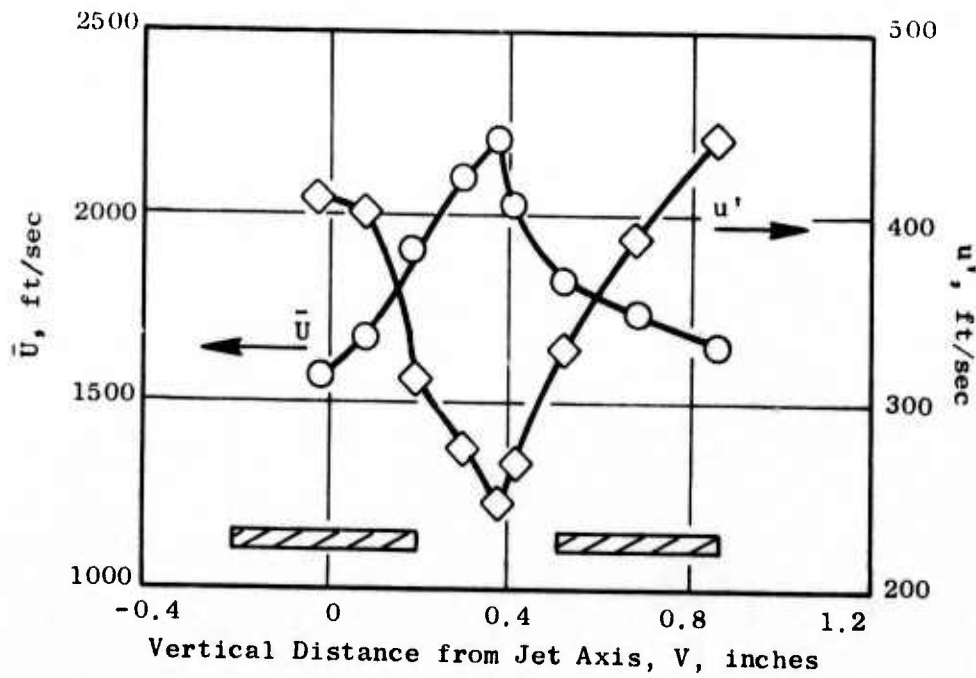
Figure 80. Mean and Turbulent Velocity Profiles Across the Chute at $r/r_o \sim 0.829$.
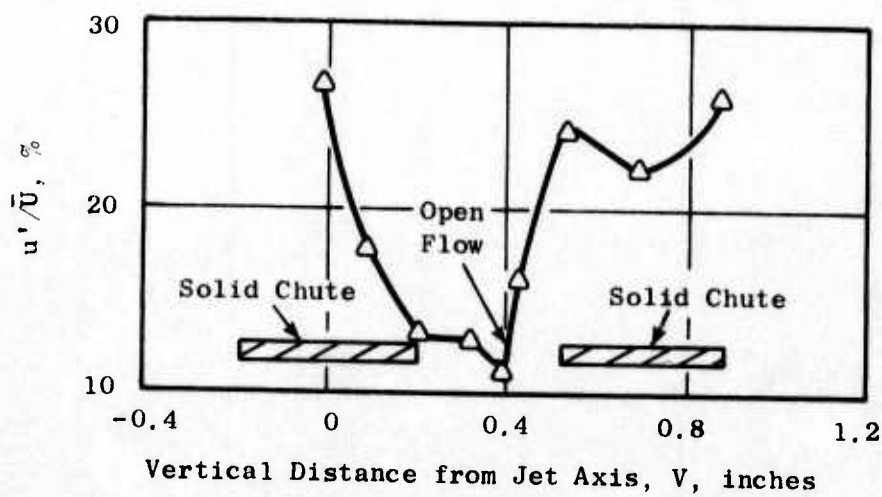
Figure 81. Turbulence Intensity Profile Across the Chute at $r/r_o \sim 0.829$.

111
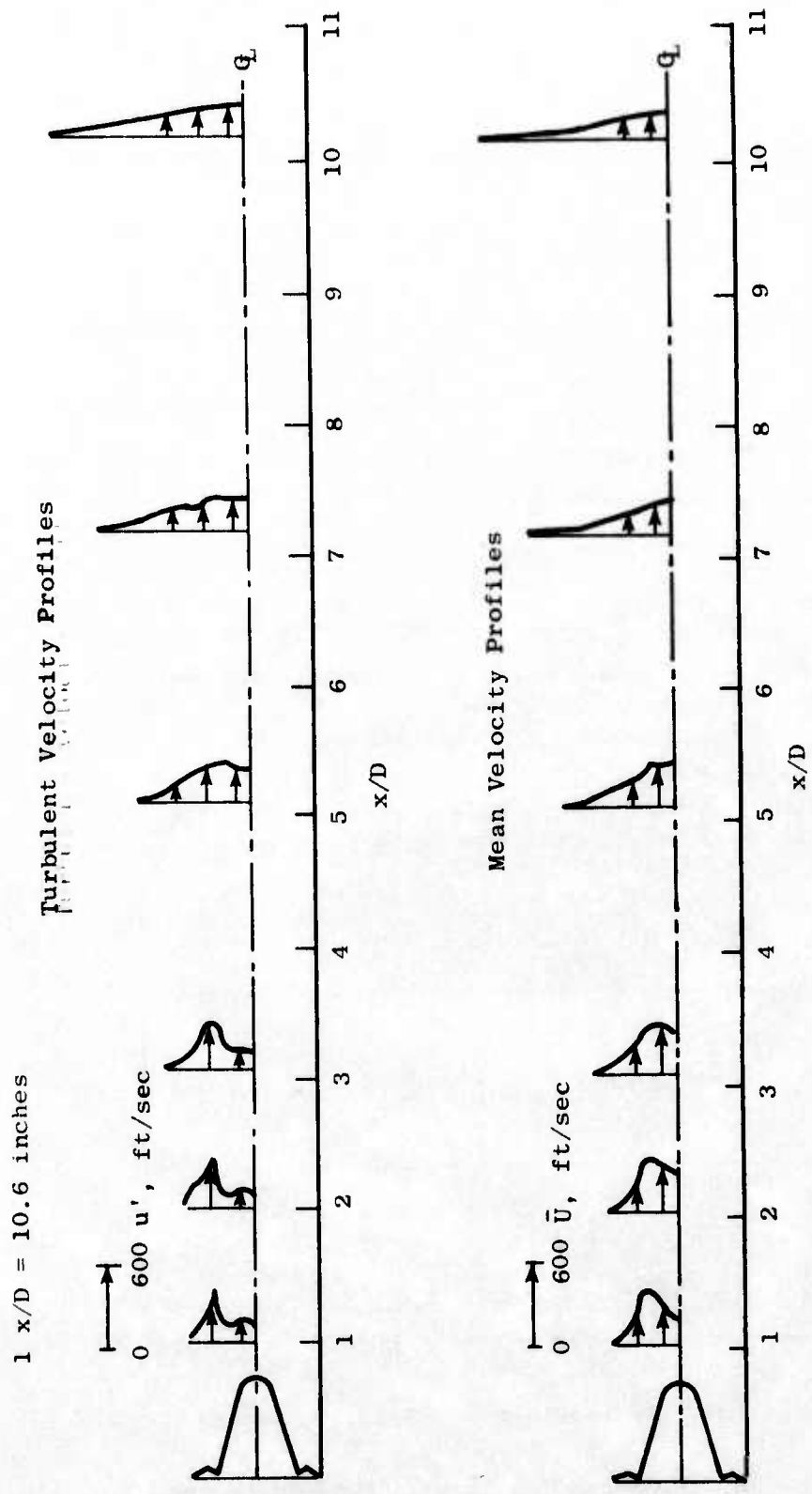
Figure 82. Measured Laser Velocimeter Turbulent and Mean Velocity Profiles of a 40-Chute Plug Nozzle Suppressor ($P_{T8}^i/P_o \sim 3.3$; $T_{T8} \sim 1950°$ R).

112

until, at X/D ∿ 7, the profiles look much like what would be expected from a simple conical nozzle. From Figure 82, the general shape of the jet boundary can be inferred. Within the first 2 and 2-1/2 diameters, the jet plume is uniform. After this location a gradual jet spread is seen, as would be observed for a conical jet.

From the radial turbulence velocity profiles at X/D = 1, 2, 3, 5, 7 and 10, the striking feature observed was the high turbulence velocities at a radial location corresponding to the junction of the plug and the chutes. This feature persists out to the first three diameters. At axial locations of X/D = 5 and larger, the turbulence profiles smoothed out and appeared more regular in nature.

The data were subsequently reduced to a contour form of isovelocity curves. An example of this analysis, Figure 83, shows isovelocity contours for the first five diameters of the jet exhaust plume. The results indicate the generation of some concentrated islands of turbulence in the 40-chute suppressor as well as a rapid reduction in mean velocity.

Test Series Evaluation

The results of the 40-spoke and 40-chute annular plug nozzle aeroacoustic/ LV tests indicated that the 40-spoke system did not achieve the hoped-for aeroacoustic results, primarily from the suppression point of view. The 40-chute nozzle system, however, did show a relatively high level of suppression (13-14 PNdB at the 2128-foot sideline) but exhibited a disappointingly low thrust coefficient (∿0.85) even though the chute design had allowed for good base ventilation. The overall evaluation of the spoke and chute systems indicated that the chute concept, specifically deep chutes, had the most potential for improvement in further development work.

3.2.2.2 36-Chute/Annular Plug Suppressor with and without Ejectors

The definition of a second series of multielement/annular plug suppressors was an outgrowth of the results from the 40-spoke/40-chute tests. It was apparent from a review of the aerodynamic performance and acoustic results on these models that spoke-type elements did not achieve the desired $\Delta PNL/\Delta C_{f_g}$ trades. Suppression levels were well below anticipated goals and previously demonstrated levels with similar spoke suppressors. The chute elements, however, did show some improvement in base ventilation over the spokes, even though thrust losses were well below anticipated levels for the chute model.

Since extensive parametric tests had been previously conducted on annular spoke suppressors, and because of the inherent aerodynamic advantage of the chute suppressor (better base ventilation), the remaining development effort in this task was directed toward chute-type suppressors, specifically deep-chutes with chute depth-to-height ratios near 1.0 or greater.

113
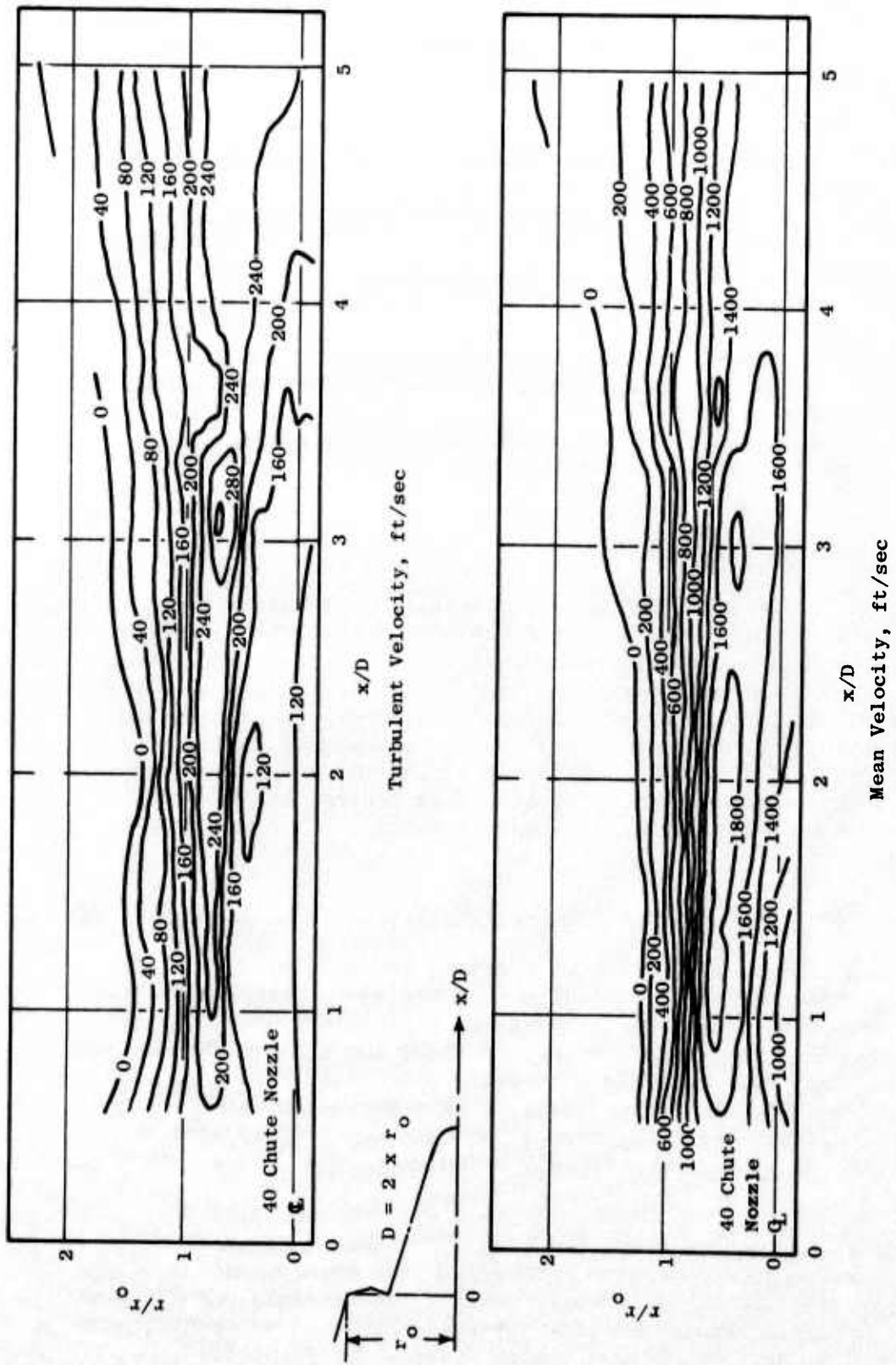
Figure 83. Isovelocity Contours Determined from Laser Measurements.

Design of the 36-Chute Suppressor Configurations

The deep-chute concept had initially been tried on the 40-chute model, but acoustic biases in exit plane geometry negated any aerodynamic performance improvement as discussed in the previous section. The acoustic results, however, were very good, having achieved better than 13 PNdB suppression (statically) at the 2128-foot-sideline for the design jet velocity of 2500 ft/sec, which might be considered as near the upper boundary on the acoustic improvement for the chute suppressor.

Due to the limited amount of annular chute suppressor data available, additional chute development effort was initiated. Since the 40-chute suppressor had provided a good acoustic upper boundary, the new suppressor design intent was to establish a high level of aerodynamic performance (~ 0.94 C_{fg}) (previously demonstrated during the GE4/SST program, but without comparable acoustic model tests) while trying to maintain reasonable suppression.

Aeroacoustic trade studies were conducted by reviewing previous multi-spoke parametric results, considering mechanical constraints, and evolving a design which was the 36-chute. This suppressor was designed for an area ratio of 2.2, with 36 deep chutes having a depth-to-height ratio of 1.0. The exit plane was canted 15° normal to the plug surface, and the exit planform maintained a flow-width parameter (casing-to-hub-width ratio) of 1.59.

An ejector (hardwall and acoustically treated) was integrated with this annular nozzle configuration to identify the effectiveness of such a system. Two ejector systems were identified. The ejectors were designed to have a conical contour for adaptability to acoustic treatment. The inlet area and exit area of the ejector annular flowpath were the same to prevent over-expansion losses on the plug. Two different size ejectors were employed. The first having an approximate $L/2h = 1.165$; and a larger one with an $L/2h = 0.905$, (where h is the average annulus height between the plug surface and the conical ejector and L is ejector length). Both ejectors were relatively short, ending just forward of the end of the plug for ease of mechanical implementation. The design of the ejectors was based on an aeroacoustic review of the Boeing Company's parametric variations (Reference 10) of ejector-suppressor spacing and ejector, L/D, and on previous General Electric ejector data (Reference 1). This review, combined with a consideration of the mechanical complexities of adapting the conical ejector to the annular plug system lead to the ejector design.

The smaller ejector (Ejector 1) was designed specifically for the 36-chute suppressor to form a viable system for application. The larger ejector (Ejector 2, the large inlet ejector) was designed to be used with the 36-chute suppressor (and also with a 66-tube/annular plug suppressor discussed in Section 3.2.3 in an attempt to evaluate overall suppression effectiveness of the multitube/annular plug system).

Separate acoustic and aerodynamic model hardware was fabricated for hot jet acoustic suppression tests at JENOTS and installed performance tests at the NASA-Lewis 6' × 8' wind tunnel facility.

Design of Acoustic Treatment

The acoustic treatment used to line the conical ejectors, as well as the rectangular ejector, for testing with the asymmetric 2-D nozzle systems (Section 3.2.5), was designed from an evaluation of sound pressure measurements taken (in the case of the 2-D nozzle/ejector system) on near-field microphones and ejector kulite probes. The intent of the study was to review the 2-D ejector data and apply the results to the design selection of acoustic treatment to be used in the 2-D ejector and in both the annular ejectors. Type of material, thickness of material and faceplate, porosity of faceplate, and hole size were defined.

The liner designs were based on a combination of approximate theoretical considerations and available experimental results. The liner material was designed to withstand high temperatures in the nozzle exhaust environment. The liners possessed good sound absorption properties within a reasonably wide range of frequencies. Fibrous bulk absorbers like Kaowool, Monoblock, and Cerafelt met these requirements. Temperature requirements also were to be met by the faceplate material.

Ejector design flow conditions were estimated as follows:

- Ejector Surface Temperature

    $T_s)_{inlet} \sim 300°$ F, $T_s)_{exit} \sim 600°$ F

- Ejector Surface Mach Number

    $M_s)_{inlet} \sim .3$, $M_s)_{exit} \sim .6$

- Average Stream Total Temperature

    $\bar{T}_T \sim 1400°$ R (940° F)

Table 5 shows the parameters defining the ejector wall liners, the approximate frequency ranges within which significant sound absorption by the liners is desired, the tuning frequencies, and representative average ejector wall temperatures.

The approximate frequency ranges for the considered ejector types were based primarily upon sideline (1500-foot) maximum aft angle SPL spectra and associated NOY-weighted spectra. The parameters in Table 5 refer to the scale model ejectors.

Typical SPL NOY-weighted spectra for the suppressed annular plug nozzles are shown in Figures 84a and 84b.

Obviously, the far-field spectra are only an approximate representation of the sound spectra distributions incident upon the ejector wall liners. The uncertainty in the spectral sound distribution may be of significant consequence, since, as found experimentally, liner effectiveness depends to a large extent upon the sound spectral content within the ejector.

116

Table 5. Tuning Frequencies and Parameters Defining Acoustic Treatment for the Scale Model Ejectors.

Ejector Type	Model Frequency Range, Hz	Model Tuning Frequency, Hz	Cavity Depth, in.	Model Tuning Frequency, Hz	Cavity Depth, in.
Two-Dimensional					
Inner & Sidewall Surfaces	800 - 8000	3200	1.40 ± 0.1	4000	1.10 ± 0.1
Nozzle Exit Ramp Surface	800 - 8000	3200	1.90 ± 0.2	4000	1.50 ± 0.2
Annular	8000 - 32000	16000	0.28 ± 0.03	12000	0.37 ± 0.03

Faceplate

- Thickness, in.   0.020 ± 0.002
- Hole Diameter, in. 0.045 ± 0.002
- Open Area Ratio   0.37 ± 0.02

117

(a) SPL Spectra
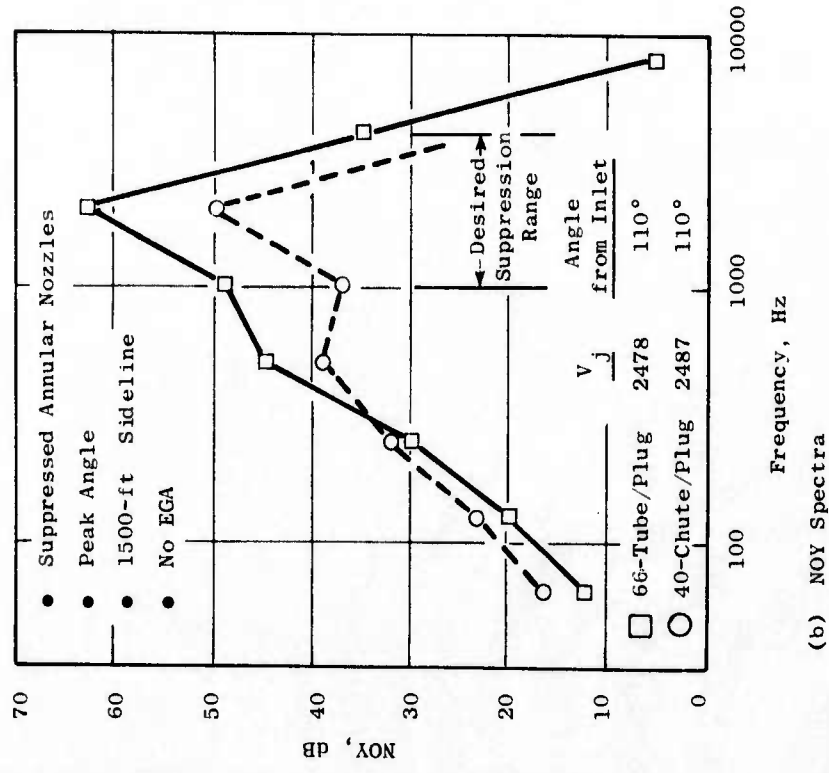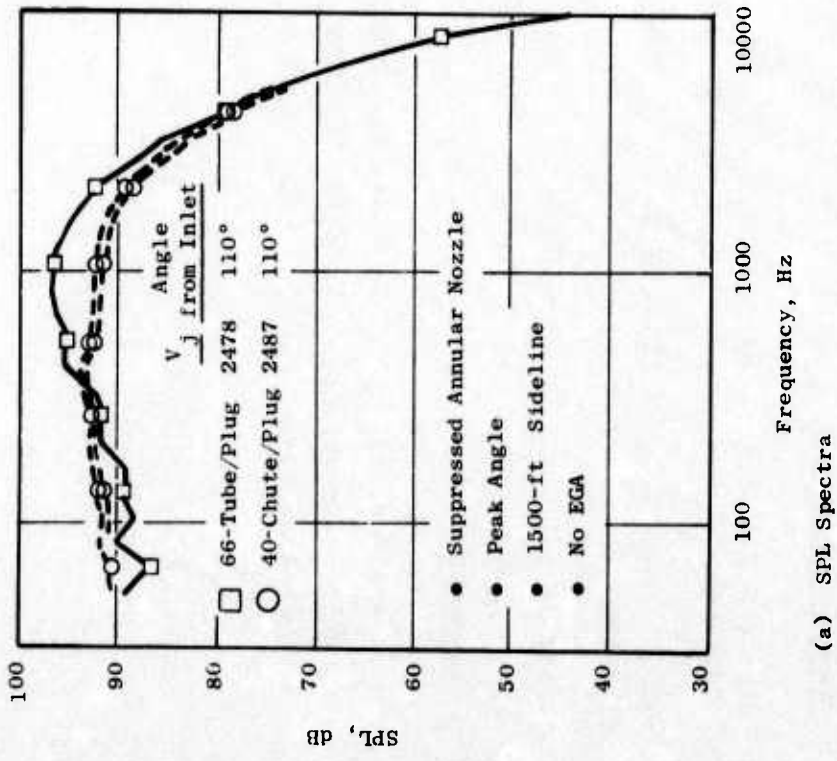
(b) NOY Spectra

Figure 84. SPL and NOY Spectra at Sideline Maximum Aft Angle Utilized for the Conical Ejector.

118

It is to be noted that two sets of tuning frequencies and, correspondingly, two sets of cavity depths are shown in Table 5. Both sets of the tuning frequencies appear to be equally reasonable from an engineering viewpoint. The cavity depths should be interpreted as the thicknesses of the fibrous bulk absorber, like Kaowool, with a density of 3 lbs/cu ft. The space behind the perforated faceplate was divided into approximately 2-inch by 2-inch-square compartments (cells) and filled with the Kaowool fibrous absorber of the appropriate thickness.

An evaluation of several combinations of bulk absorber and perforated faceplate were tested at ambient conditions in the General Electric Acoustic Laboratory one-inch-diameter impedance tube. Each sample was tested with a perforated plate of 37% open area (0.045-inch-diameter holes, 225 holes/in.^{2}, 24 gage 304 SS). The bulk absorber, which filled the cavity, consisted of combined thicknesses of a ceramic blanket fiber (1 in. thick, 3 lbs/ft^3) and sintered foam metal sheets (60-70 cgs rayls, NiCr $\sim$ 0.08 - 0.10 in. thick). The samples were tested over a range of frequencies (i.e., 1000, 1250, 1600, 2500, 3150, 4000, 5000, and 6300 Hz) to determine the nulls and maximum amplitudes of each frequency characteristic of the absorber. Results of the tests were processed into the normalized resistance (R/ρc) and reactance (jX/ρc) components of the impedance.

The criteria for comparison were (1) a flat characteristic curve for both the resistance and reactance, which was synonymous with broadband suppression, (2) a level of resistance near 1.0 at the temperature of operation ($\sim$ 1200° F), and (3) zero reactance at that temperature.

The test results, briefly summarized, indicated that the first sample, which had the cavity completely filled with KAOWOOL 1 in. thick, gave the best acoustic characteristics but mechanically would not hold up in the high velocity hot jet environment. A second sample consisting of stacked layers of foam metal gave little hope of any acoustic suppression. A combination of KAOWOOL (2 in. compressed to 1 in.) and foam metal (1 layer $\sim$ 0.10 in. thick) showed the closest approximation to the characteristic curves of the first sample. This combination was incorporated into the acoustic liner of the model conical Ejector 1 (see Figure 85) for the JENOTS hot jet test.

Acoustic Tests

The far-field acoustic tests of the baseline conical nozzle, the 36-deep-chute suppressor, and hardwall ejector systems were conducted on the JENOTS facility over a range of conditions simulating a J6H2 turbojet engine operating line.

Figure 86 is a photograph of the 36-chute suppressor on the JENOTS facility. Photographs of the annular plug suppressor-ejector configurations tested in this series are shown in Figure 87 for hardwall Ejectors 1 and 2. These hardwall ejectors included inlet bellmouths for the static acoustic testing to simulate in-flight flow conditions (Figure 88). Treated ejector tests of the 36-chute suppressor also were conducted.

119
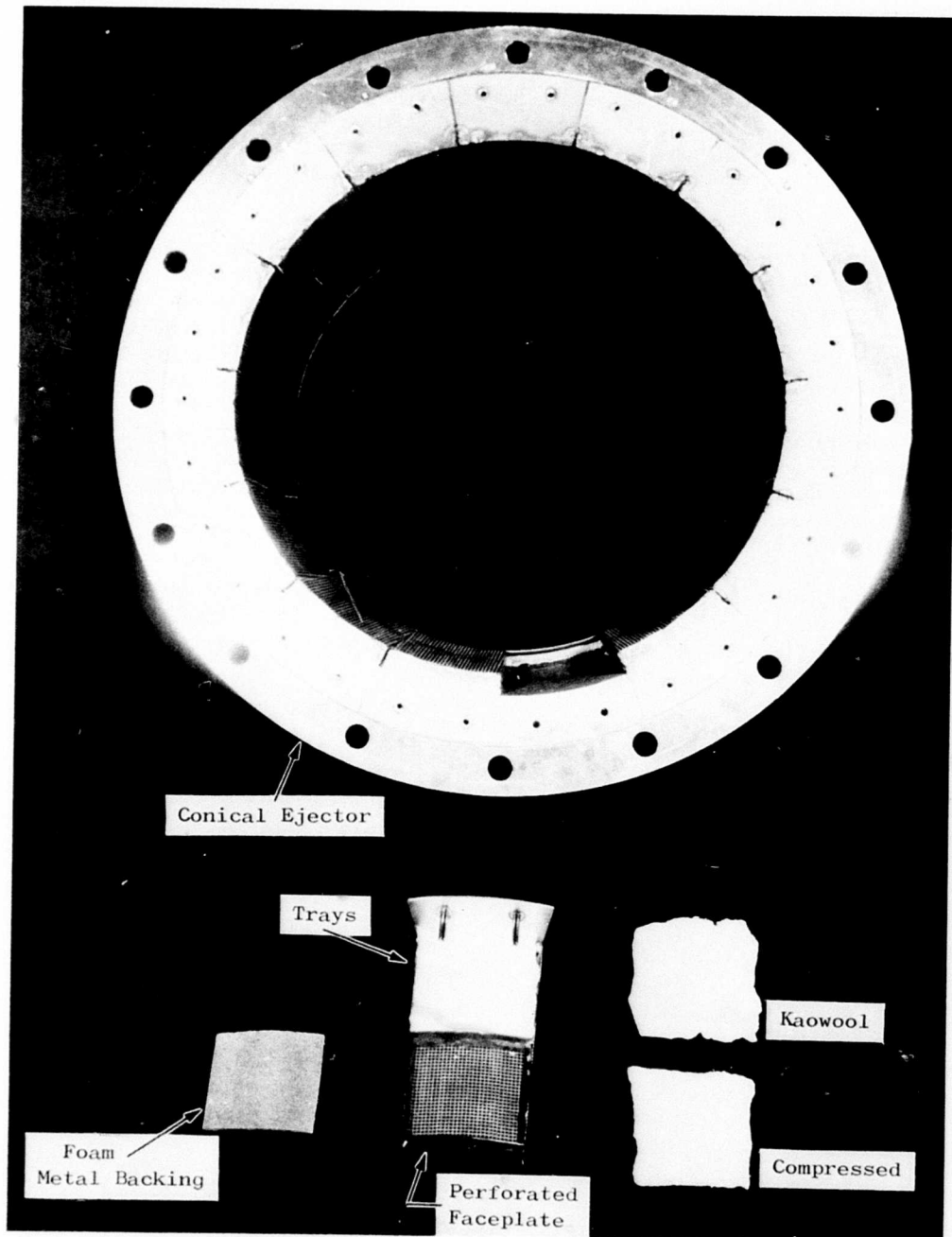
Figure 85. Conical Ejector Acoustic Liner.

120

36 DEEP CHUTE
ANNULAR PLUG SUPPRESSOR
AREA RATIO = 2.2

WATER COOLED ADAPTERS

Figure 86.   36-Chute/Annular Plug Suppressor on JENOTS Facility.

121
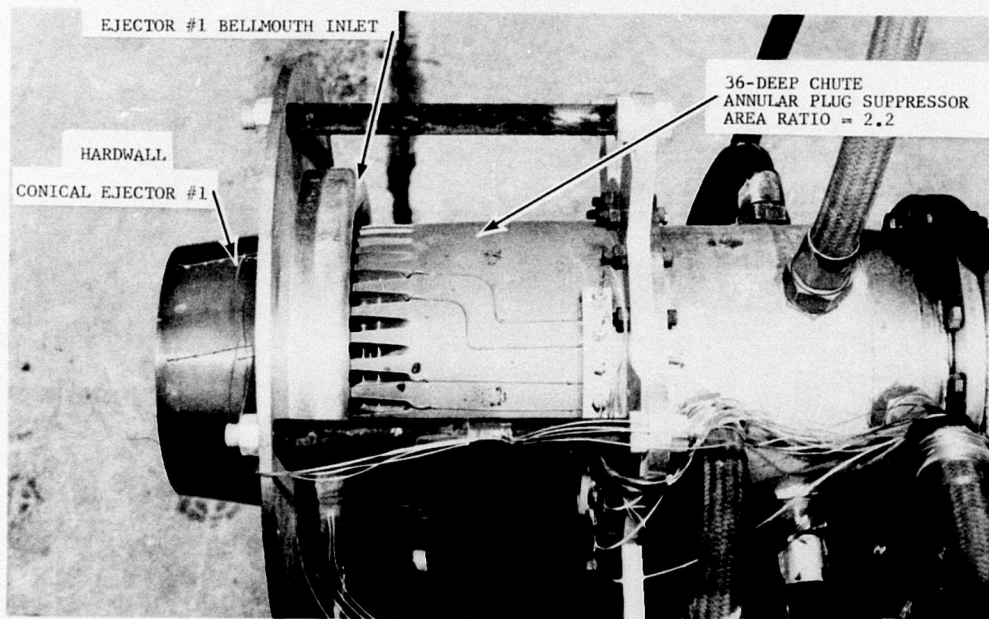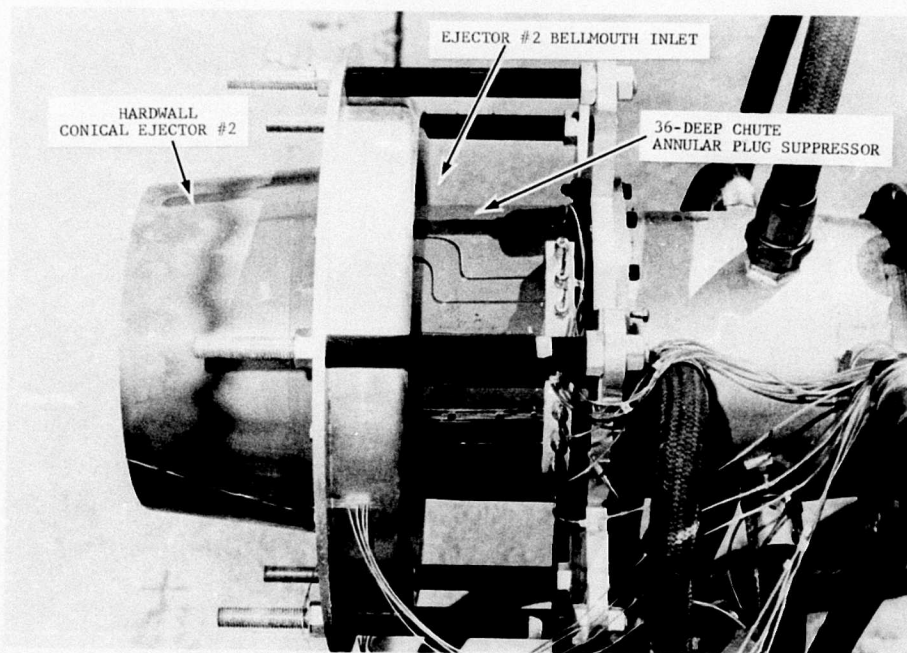
Figure 87. 36-Chute/Annular Plug Suppressor with Conical Ejectors 1 and 2 on the JENOTS Facility.

- 36-Deep-Chute/Annular Plug Suppressor
  with Ejector No. 1
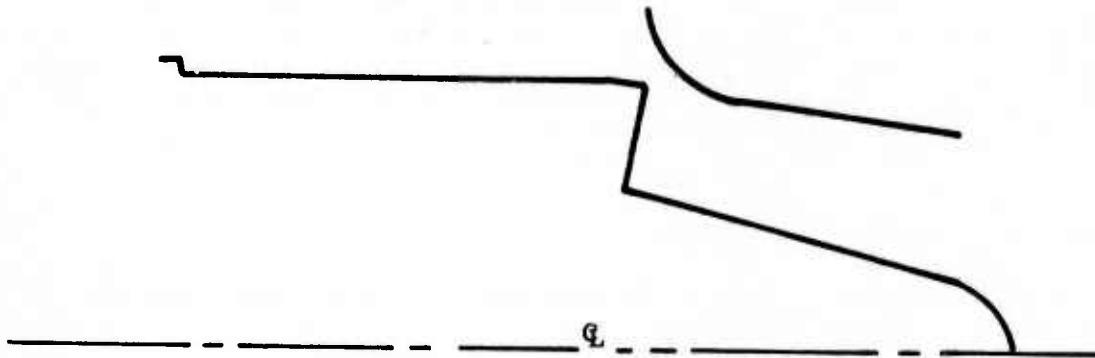
C͟L

- 36-Deep-Chute/Annular Plug Suppressor
  with Ejector No. 2

Ejector Bellmouth Used
for Acoustic Tests Only

C͟L

- 66-Tube/Annular Plug Suppressor with Ejector No. 2

C͟L
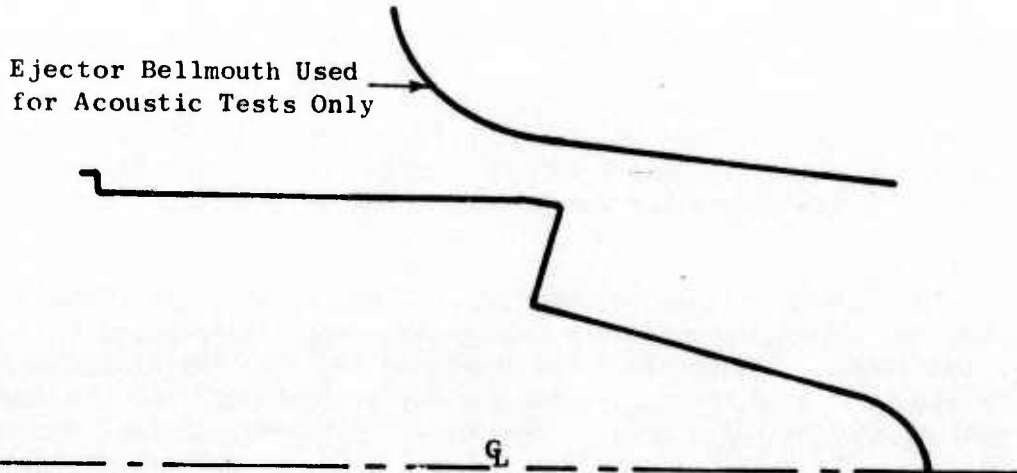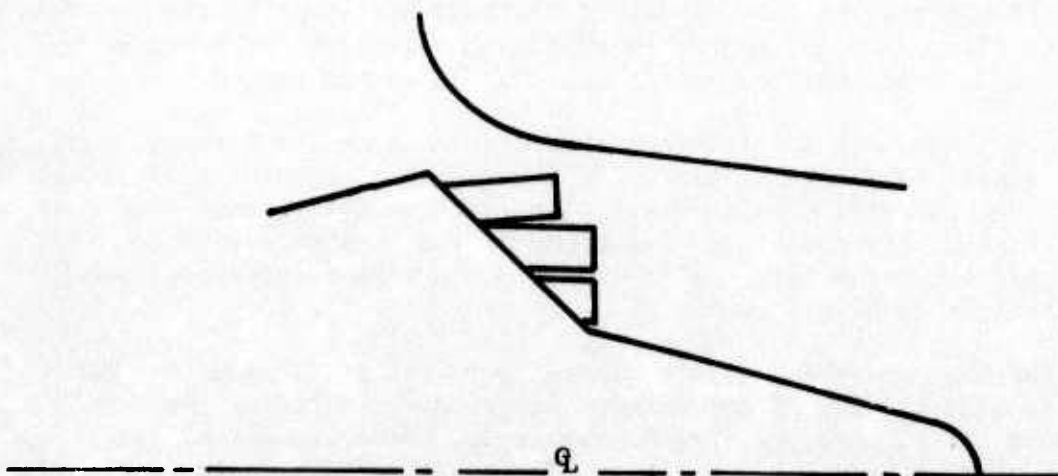
Figure 88. Suppressed Annular Nozzles with Ejectors.

123

The sound field for this series of tests employed only the 15 high (~ 16 ft) microphones on the 40-ft hemispherical arc equally spaced from 20° to 160° from jet inlet. The 5-ft microphones were not required, since testing on the 40-spoke/chute nozzle series had shown that the two microphone systems gave compatible results when scaled to full size.

Acoustic Results and Analysis

A summary of the acoustic results of each model tested, along with the test conditions, is found in Appendix C.

Results of the tests conducted on the 36-chute/annular plug suppressor configurations showed that peak PNL suppression of 8-9 PNdB was achieved for the suppressor alone (without ejectors) at a 2128-foot sideline without EGA for the design jet velocity of 2500 ft/sec.

Comparisons of the conical Ejectors 1 and 2 on the 36-chute suppressor are illustrated in Figures 89 through 94. The variations of peak PNL over the velocity range of interest are compared at the 2128-foot sideline for the chute suppressor with and without ejectors in Figure 89. The PNL suppression obtained from the 36-chute suppressor at the design jet velocity is approximately 8.5 PNdB with the hardwall ejectors providing an additional 1.0 dB of suppression.

Plots of the 2128-foot sideline PNL directivity for Ejectors 1 and 2 are seen in Figures 90 and 91, respectively, while 320-foot arc spectral directivity plots are similarly shown in Figures 92 and 93. The PNL distributions are about the same for both ejectors, peaking out at 100°-110° for the low velocities with a gradual shift aft, closer to the jet axis, at 130° for the higher velocities. The design jet velocity (2500 ft/sec) spectral directivites showed trends similar to the PNL directivity.

Comparisons of peak angle spectra at the 300-foot sideline for the multi-chute/annular plug suppressor with hardwall ejectors are shown in Figures 94a, b, and c. They illustrate the degree of shielding effectiveness provided by the hardwall ejectors at selected velocities over the range tested.

The SPL levels for Ejector 2 appear higher than those for Ejector 1 over the frequency range for all ideal jet velocities tested. Ejector 1 exhibited typical suppressor spectral characteristics over the velocity range from 1200 to 2000 ft/sec. Low frequency domination of the spectra starts to occur at 2200 ft/sec, while full low frequency domination is apparent from 2485 ft/sec through the high V_j end.

Reasons for the less-than-desired ejector acoustic performance may be due to the premature merging of the primary suppressor individual jet elements to form the high energy, low frequency dominated, coalesced jet, typical of an unsuppressed conical nozzle. The ejectors were designed for lengths consistent with the predominantly high frequencies found in a well-suppressed jet. The noise sources may be forced downstream, out of the region

124
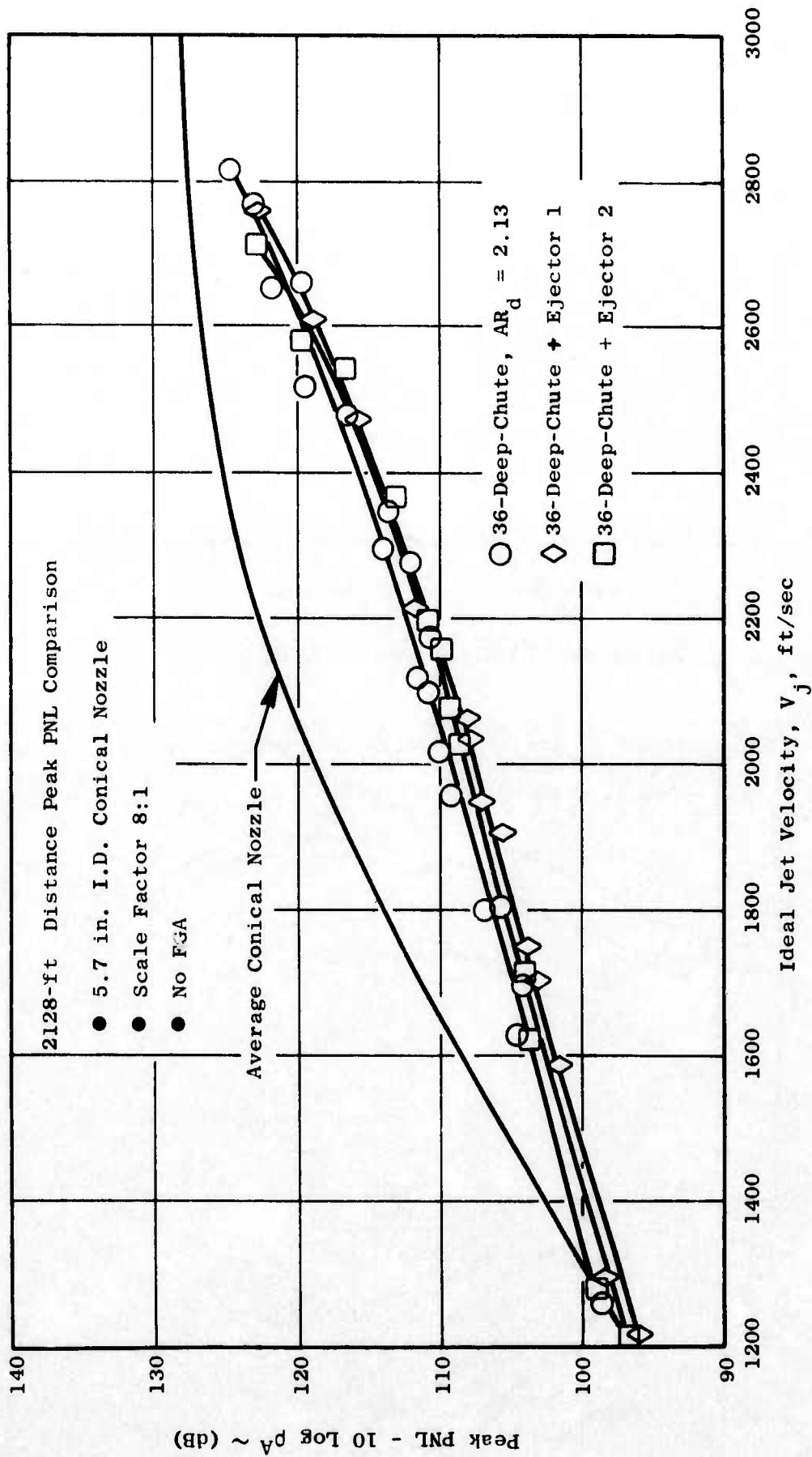
Figure 89. Peak PNL Comparison of Multichute/Annular Plug Suppressor with Hardwall Ejectors.

125

V_j ft/sec	P_{T8}/P_o
2760	3.55
2477	2.99
2217	2.68
2065	2.52
1909	2.24
1591	1.82
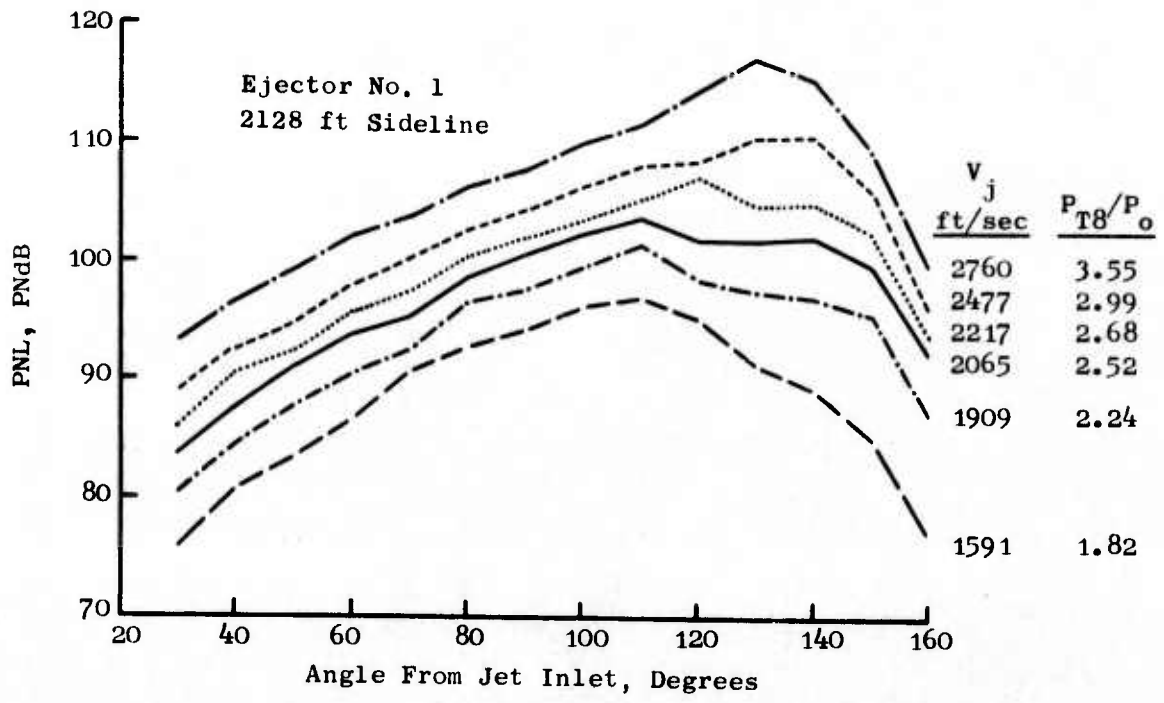
Figure 90. PNL Directivity, Ejector 1.

V_j ft/sec	P_{T8}/P_o
2714	3.54
2544	3.03
2370	2.64
2203	2.52
1624	1.82
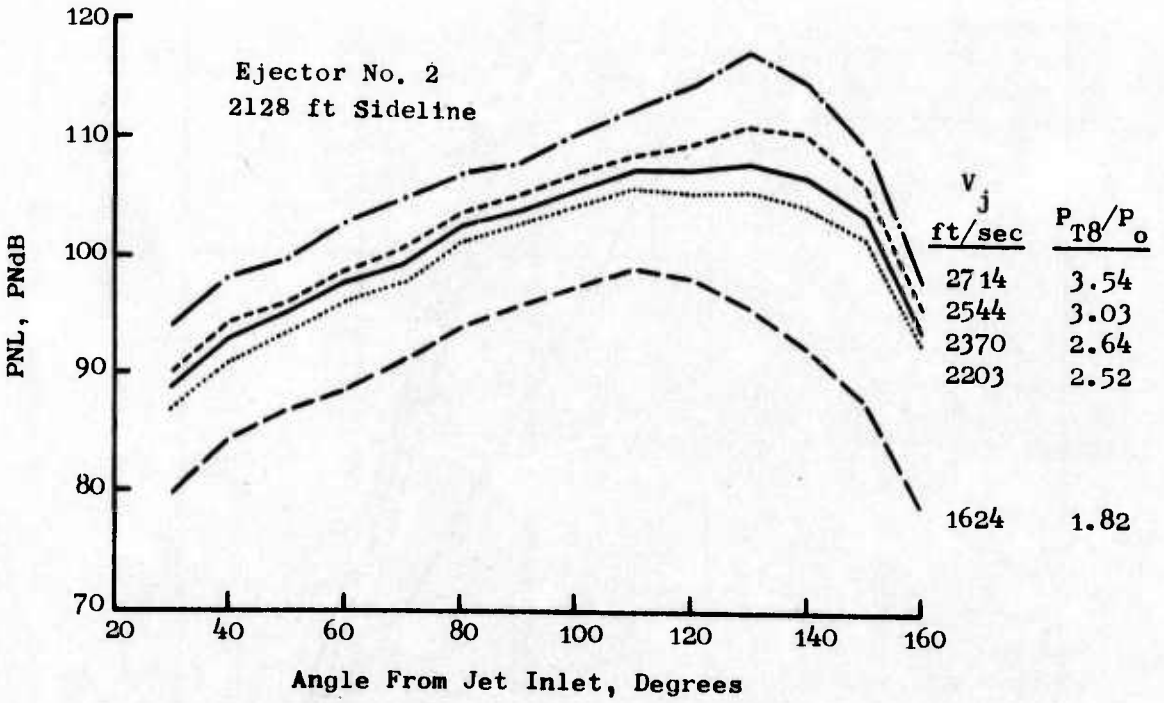
Figure 91. PNL Directivity, Ejector 2.

126
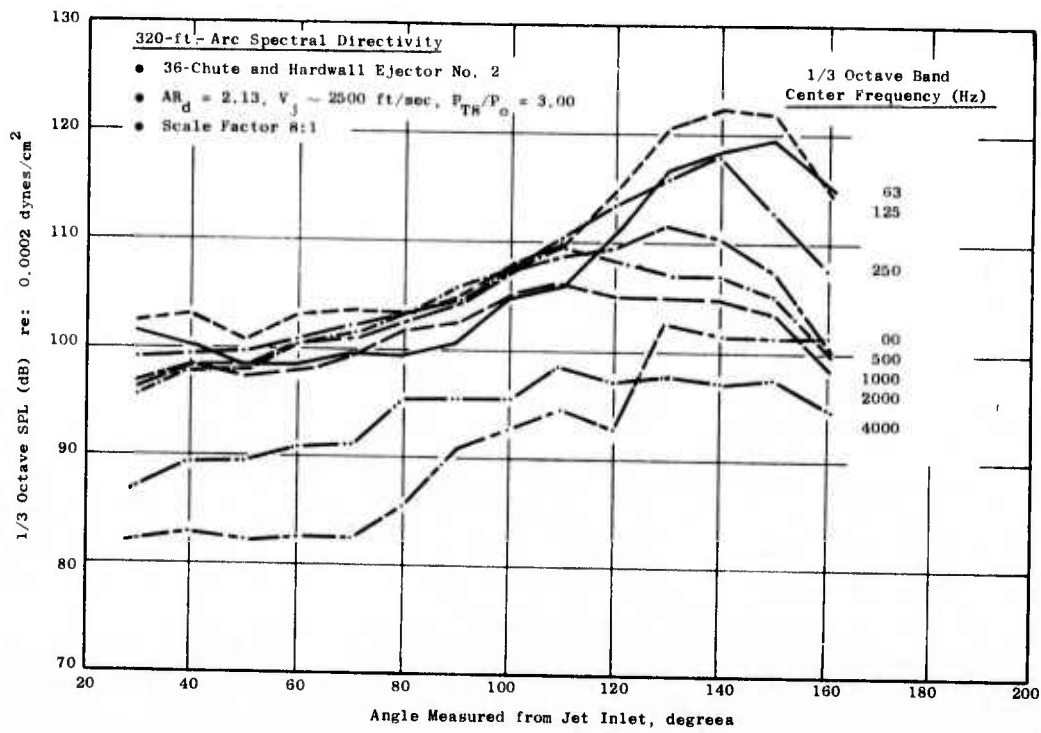
Figure 92. Spectral Directivity for Multichute/Annular Plug
Suppressor with Hardwall Ejector 1.
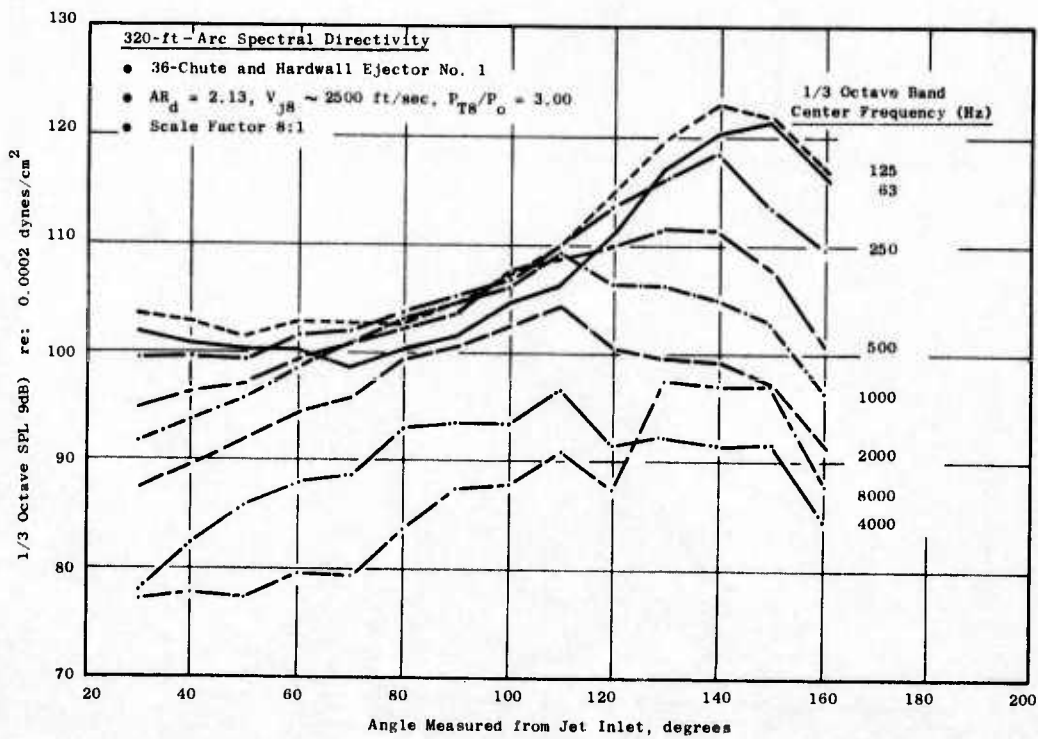
Figure 93. Spectral Directivity for Multichute/Annular Plug
Suppressor with Hardwall Ejector 2.

127
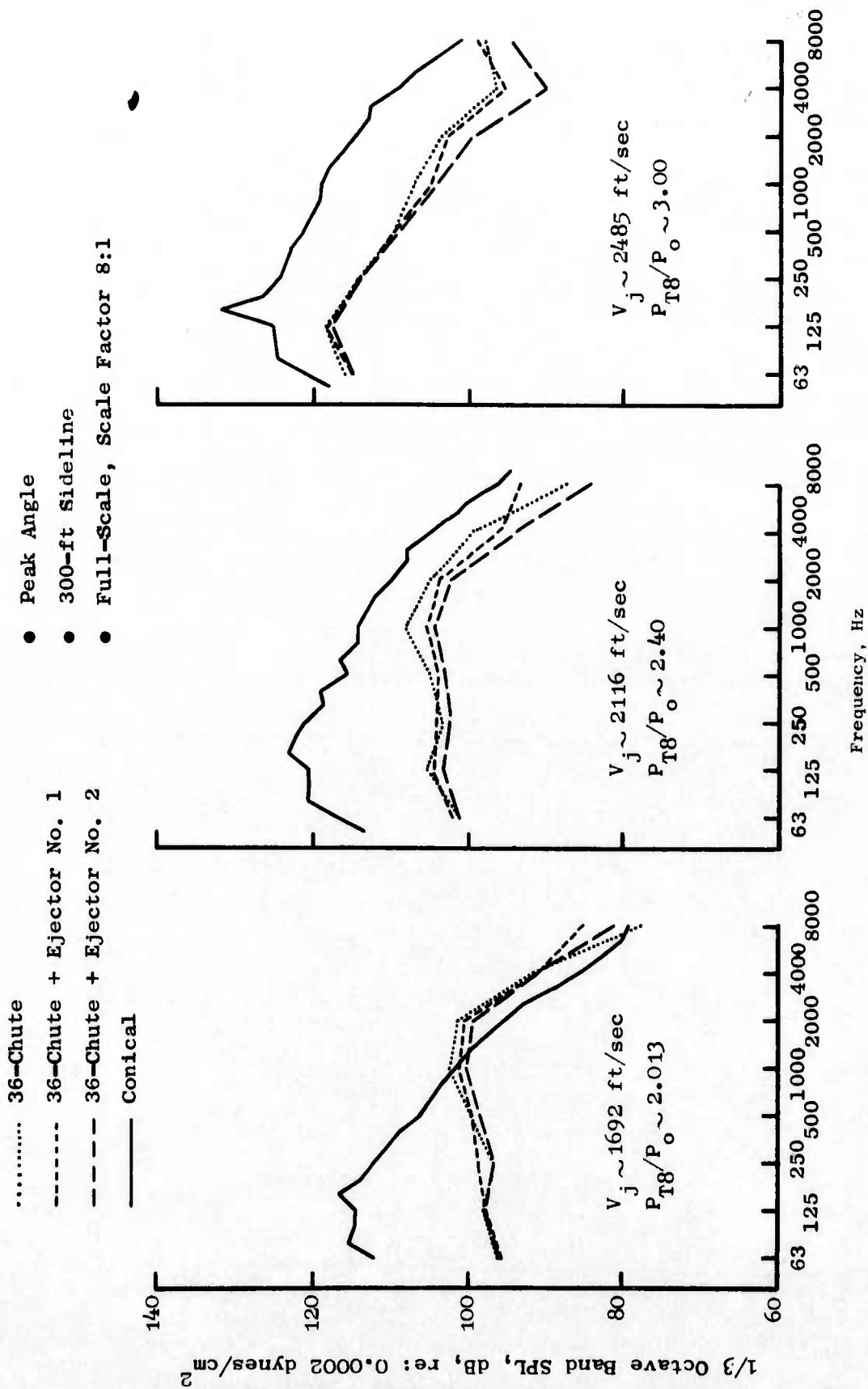
Figure 94. SPL Spectra Comparisons with Hardwall Ejectors.

of ejector influence, as a result of the suppressors ability (or inability) to mix out and lower the core flow velocity.

Acoustic (Treated) Ejector Tests

Acoustic tests were conducted on the 36-chute suppressor and acoustically treated conical ejector configurations to investigate the acoustic benefits obtained over the hardwall ejector tests as well as evaluating the acoustic-mechanical effectiveness of two combinations of the bulk absorber.

The conical ejectors tested on the 36-chute suppressor employed two different combinations of acoustic liner. The acoustic liners were the broadband bulk absorber type designed for effectiveness in the full-scale frequency range of 1000 to 5000 Hz. The first liner consisted of a single layer of ceramic fiber packed into the perforated sheet metal trays that surrounded the ejector inner surface. This formed a lightweight configuration. The second liner consisted of a double layer of ceramic fiber plus the addition of a single layer of sintered foam metal next to the perforated sheet metal for increased liner rigidity.

Testing was performed in the same manner as with the previously discussed 36-chute test series over the same ranges of ideal jet velocity and nozzle pressure ratio. Figure 95 shows a typical acoustic test facility setup with an acoustically treated conical ejector and 36-chute suppressor mounted on the JENOTS single-flow stand.

Acoustic (Treated) Ejector Results and Analysis

The results of the conical ejector tests are presented and compared as tested on the 36-chute suppressor. The acoustic results and operating conditions are summarized in Appendix C for the configurations tested. All the acoustic data presented have been scaled to full J6H2 size and frequency range.

Minimal difference in PNL suppression was observed between the treated Ejector 1 (original treatment and repacked with second treatment) and treated Ejector 2. The results shown in Figure 96 indicate that a maximum of only 1 dB difference occurred over the entire operating range.

Acoustic results of the conical Ejector 1 tests are illstrated in Figure 97 which shows the 2128-foot sideline peak PNL variations on the 36-chute with treated Ejector 1 with ideal jet velocity. The PNL comparison with the hardwall ejector and 36-chute suppressor alone also are shown. Suppression gains of 2.5 to 4.5 PNdB were obtained with the treated ejectors relative to the multichute suppressor alone. The maximum suppression occurred at velocities below 2000 ft/sec and was reduced at higher velocities. The ejector effectiveness is the result of the 36-chute suppressor spectral characteristics which show the low frequency domination of the merged jet to occur at velocities above 2300 ft/sec. In this case, the frequencies which

129

ACOUSTIC TREATMENT
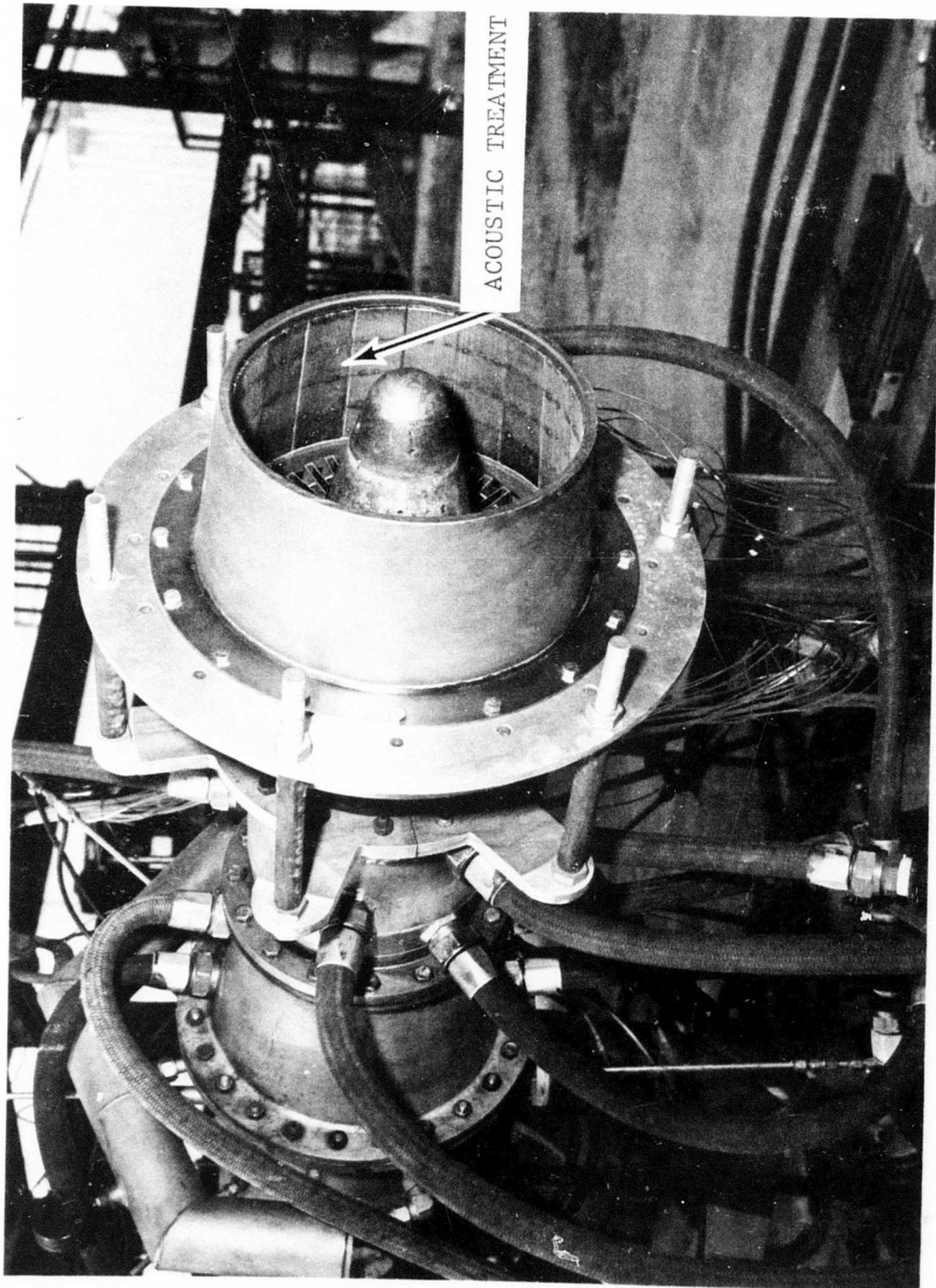
Figure 95. Multichute/Annular Plug Suppressor with Treated Ejector.

- 36-Deep-Chute, AR_d = 2.13
- Treated Ejectors 1 and 2
- 5.7 in. I.D. Conical Nozzle
- Scale Factor 8:1
- No EGA
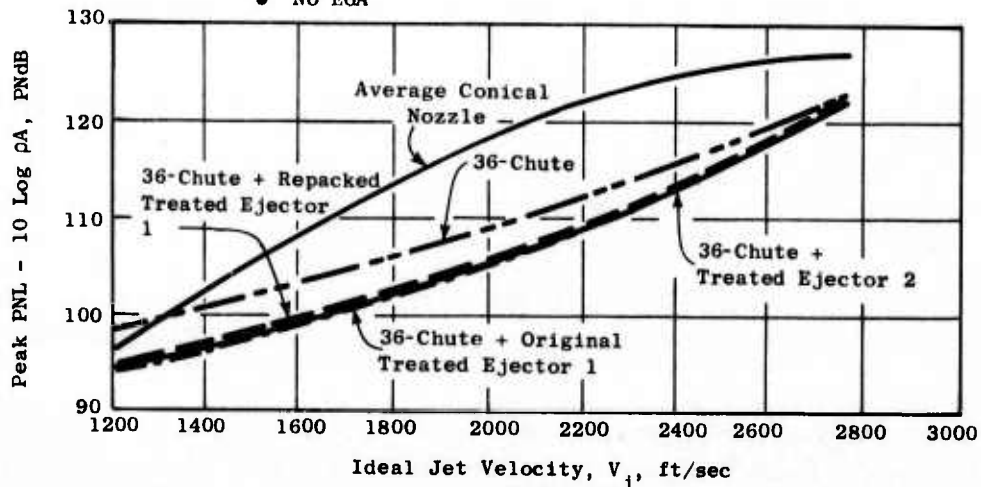
Figure 96.   Peak PNL Comparisons of Multichute/Annular Plug
Suppressor with Treated Ejectors.

2128-ft. Distance Peak PNL Comparison of
Multi-Chute/Annular Plug Models

- 36-Deep-Chute, AR_d = 2.13
- Hardwall and Treated Ejector 1
- Scale Factor 8:1
- No EGA
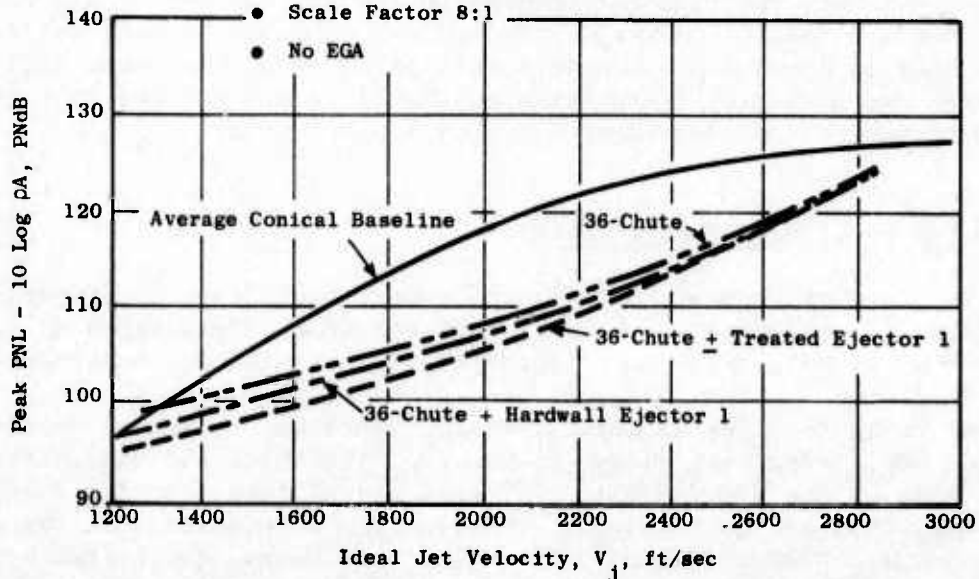
Figure 97.   Peak PNL Comparisons of Multichute/Annular Plug
Suppressor with Hardwall and Treated Ejectors.

131

the ejector treatment was designed to suppress are generated downstream of the ejector region of influence, and therefore limit the ejector effectiveness.

The PNL directivity for the treated (repacked) Ejector 1 configuration is presented on the 2128-foot sideline in Figure 98. The plot shows the peak angle shift from 110° to 130° with increasing V_j strongly suggesting that coalescence of the smaller elemental jets has occurred between 2184 and 2474 ft/sec.

The spectral directivity at the 320-foot arc is shown in Figure 99 for the $V_j \sim 2500$ ft/sec, $P_{T8}/P_o \sim 3.00$ conditi 1. Figure 99 illustrates the 1/3 octave band SPL center frequency angular distributions which show the low frequencies becoming dominant in the aft angles, characteristic of a coalesced jet.

Figures 100a, b, and c illustrate SPL spectra comparisons for the 36-chute suppressor with and without hardwall and acoustically treated Ejector 1. The SPL spectra show that the hardwall and treated ejectors reduce the SPL levels at the low V_j conditions in the frequency range between 500 to 2000 Hz. Additional high frequency suppressions of 4 to 6 dB at 1000 Hz are apparent at V_j's from 1200 to 2200 ft/sec for the treated ejector. Peak angle for all three configurations occurred at 110° for this same V_j range of 1200 to 2200 ft/sec indicative of multielement suppressors wherein the premerged region was dominating. While at V_j's of 2485 ft/sec and above, the spectra were low-frequency-dominated and the peak angles shifted aft to 130°. This effect again indicated that the postmerged region of the multielement suppressor had occurred and coalesced to a single jet.

Posttest examination of treated Ejector 1 tested with the 36-chute suppressor proved that the flow environment in the jet exhaust nozzle was too hostile for the original (lightweight configuration) acoustic bulk absorber used in the treated Ejector 1. Acoustic results on each liner were similar; the second one was mechanically superior to the first and was the type selected for use on the full-scale suppressor - engine demonstration.

Aerodynamic Performance Tests

The objectives of these series of performance tests were to determine the installed gross thrust losses, and to investigate what effect depth of chute had on base drag as well as assessing ejector air entrainment characteristics.

Wind tunnel testing for aerodynamic performance was conducted on six annular, 36-chute configurations and on two facility check-out models. Testing was done at the NASA-Lewis 6' × 8' wind tunnel (see Appendix B for facility description and typical model setup). Complete details of the test and results can be found in Reference 11. The configurations, tested at free-stream Mach numbers of 0, 0.36, and 0.45, are listed below:
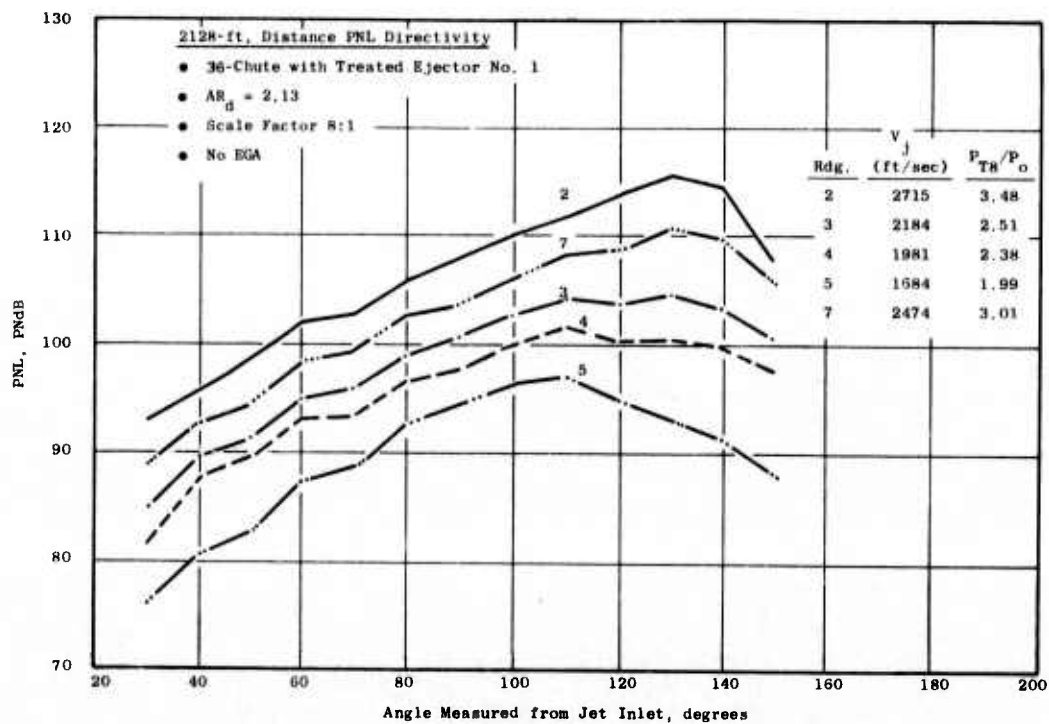
Figure 98. PNL Directivity for Multichute/Annular Plug Suppressor with Treated Ejector.
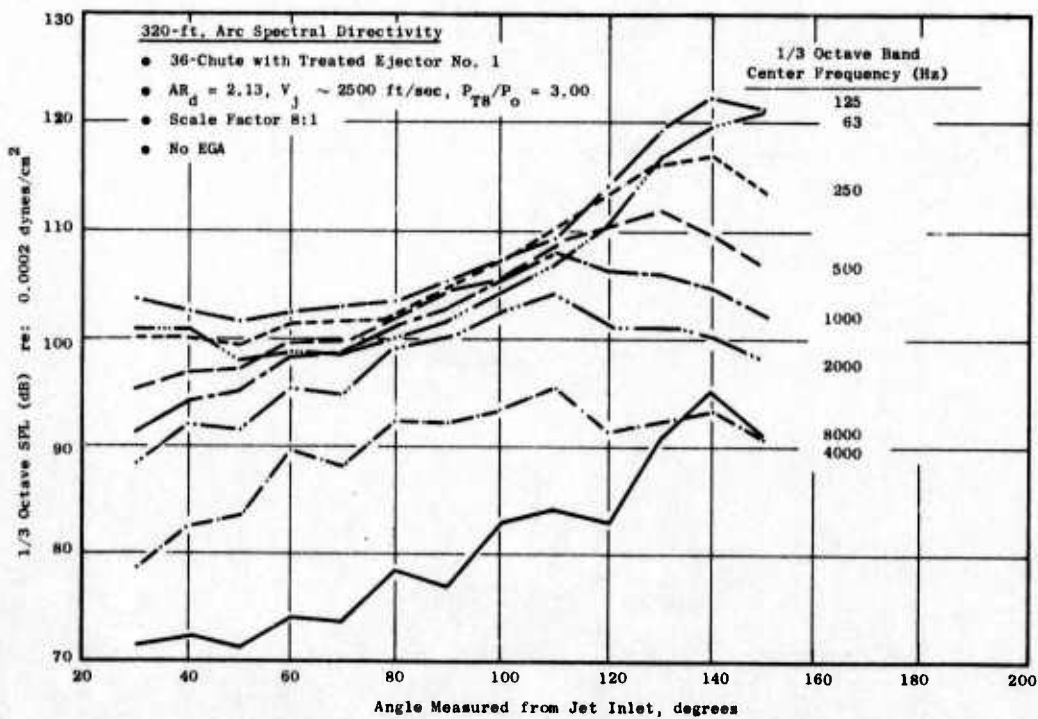
Figure 99. Specular Directivity for Multichute/Annular Plug Suppressor with Treated Ejector.

133
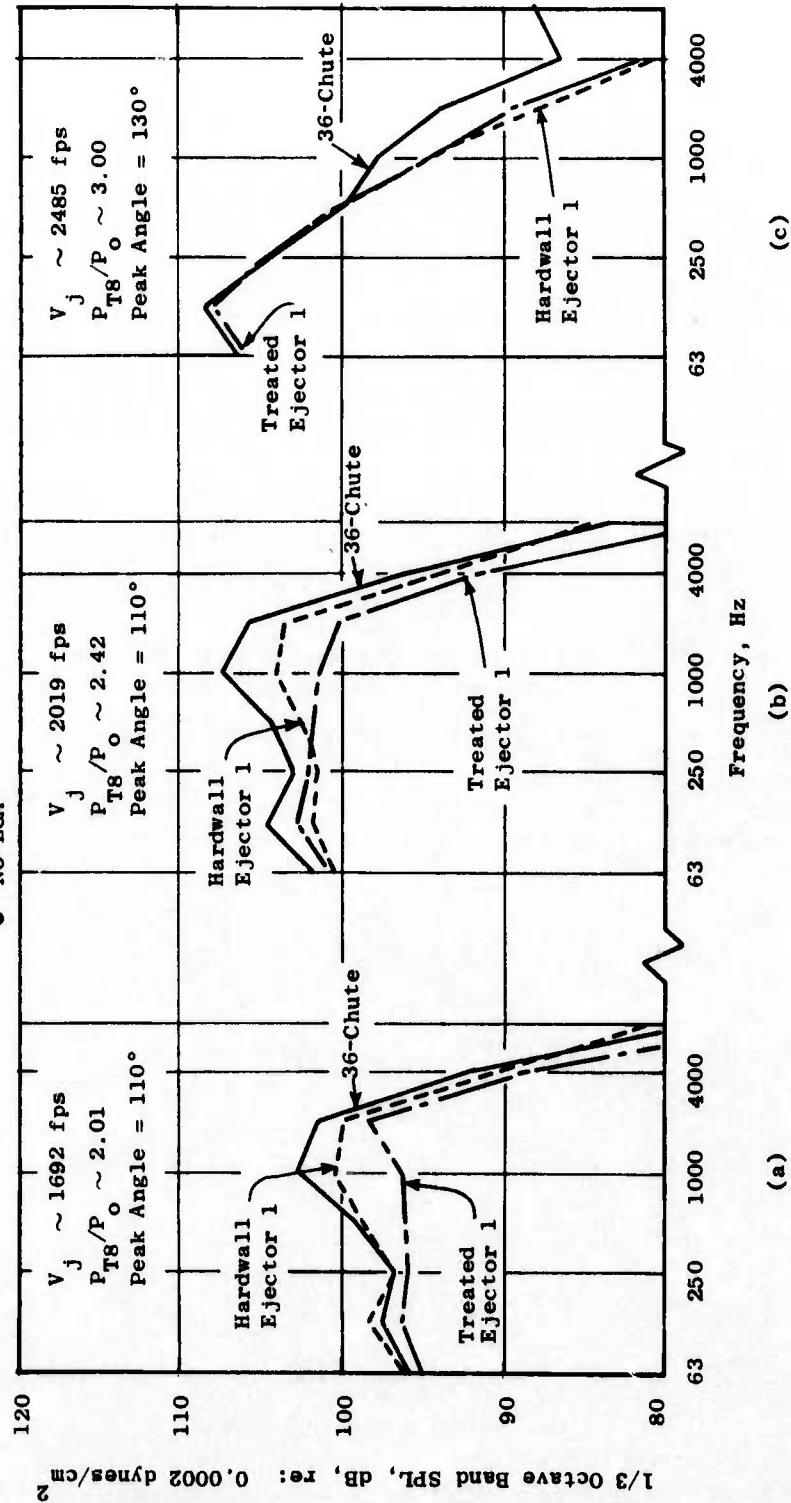
Figure 100. Spectral Comparison for Multichute/Annular Plug Suppressor with Hardwall and Treated Ejectors.

134

- Supersonic Tunnel Association (STA) Reference Nozzle

- 36-Deep-Chute Nozzle

- 36-Deep-Chute/Setback Ejector 1 Nozzle

- 36-Deep-Chute/Large Inlet Area Ejector 2 Nozzle

- 36-Shallow-Chute Nozzle

- 36-Shallow-Chute/Setback Ejector 1 Nozzle

- 36-Shallow-Chute/Large-Inlet-Area Ejector 2 Nozzle

- Boundary Layer Shroud

All but the boundary layer shroud were tested at nozzle pressure ratios of 1.5, 2.0, 2.5, 3.0, 3.5, and 4.0.

Figures 101 a, b, and c are schematic illustrations of the basic suppressor systems tested and relative locations of the nozzle charging station. Figure 101 shows the 36-deep-chute suppressor assembly, while Figure 101b illustrates the variations in depth of the chutes. Figure 101c shows the 36-chute suppressor with the smaller Ejector (1). The large inlet ejector is not shown. Both ejectors employed flight-type inlets (as opposed to the bellmouth inlets used for static acoustic tests).

Figure 102 jointly displays two of these suppressor configurations, the deep-chute nozzle and the shallow-chute nozzle. The chute depth of the deep-chute nozzle and its derivatives can be seen from two chutes in the upper left-of-center region of the photograph. The other chutes in the figure contain inserts which allow a parametric investigation of the effect of chute depth on nozzle performance. Two ejector shrouds were tested on both the deep- and shallow-chute nozzles. The setback ejector (Ejector 1) and the large inlet ejector (Ejector 2) are shown on the deep-chute nozzle in the tunnel in Figures 103a and b, respectively.

Aerodynamic Performance Results and Analysis

The nozzle efficiencies of the deep-chute suppressor nozzles, with and without the two ejector shrouds, are presented as a function of nozzle pressure ratio at Macn numbers of 0 and 0.36 in Figures 104a and b, respectively. In addition to the performance of the three deep-chute configurations on each plot, an unsuppressed plug nozzle's performance is included for comparative purposes. Statically, the deep-chute/setback ejector nozzle had the best performance. This ejector had a peak nozzle efficiency of 1.004 at a nozzle pressure ratio of 3.25. At a Mach number of 0.36 this ejector had the highest performance level of the suppressor configurations for pressure ratios greater than 3.0. A tabulation of the nozzle efficiencies for the six multichute suppressors and the unsuppressed plug nozzle are presented in
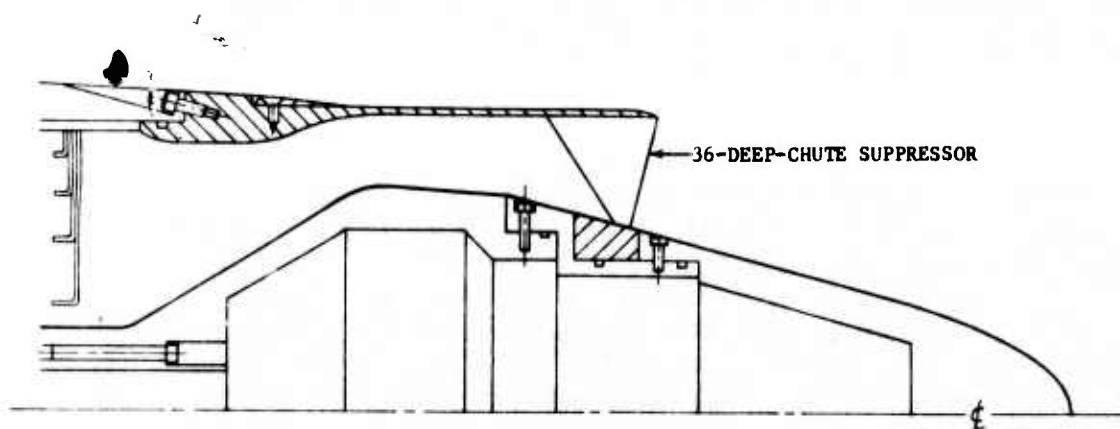
(a) Deep-Chute Suppressor
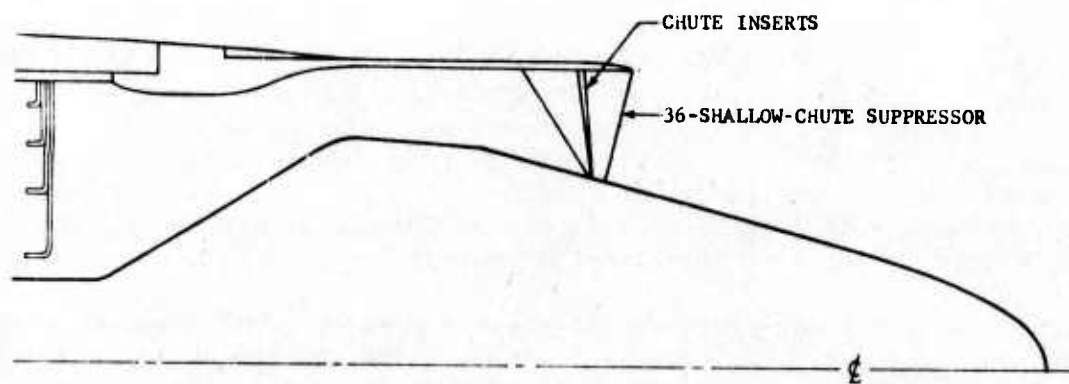
(b) Shallow-Chute Suppressor
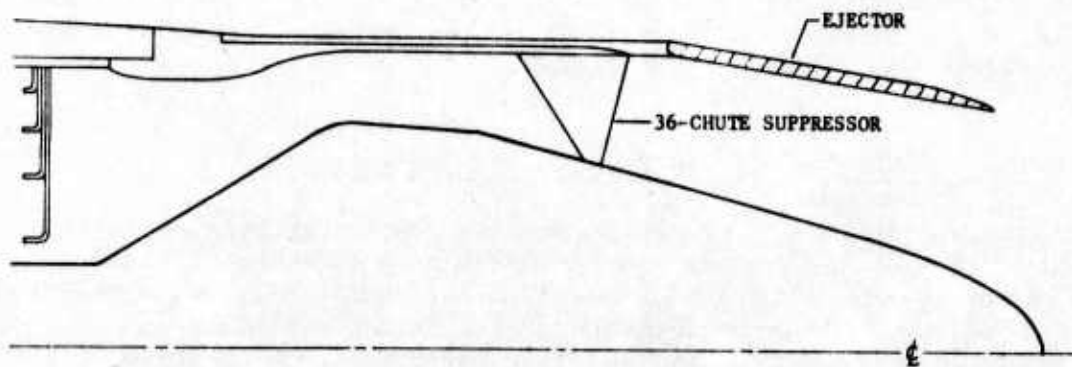
(c) Deep-Chute Suppressor with Setback Ejector

Figure 101. Schematic Illustrations of the Basic Suppressor
Systems Tested at NASA-Lewis.
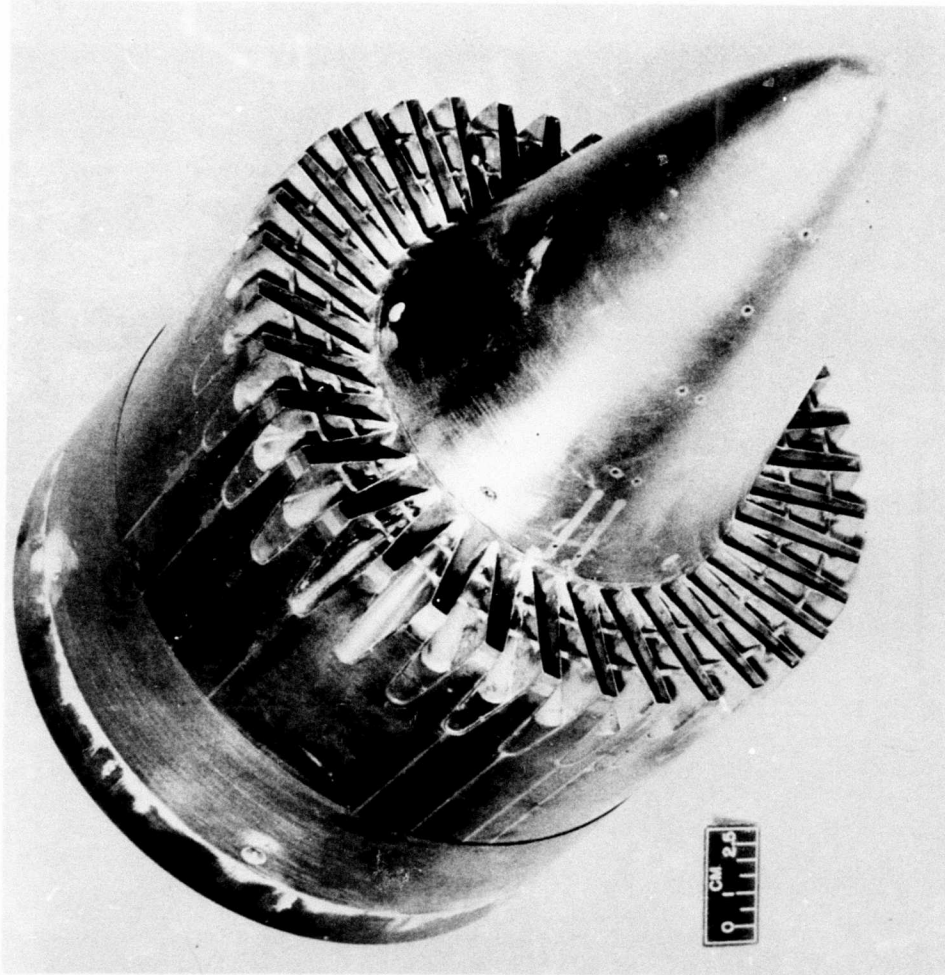
Figure 102. 36-Chute Annular Plug Nozzle Aerodynamic Model Hardware.

137
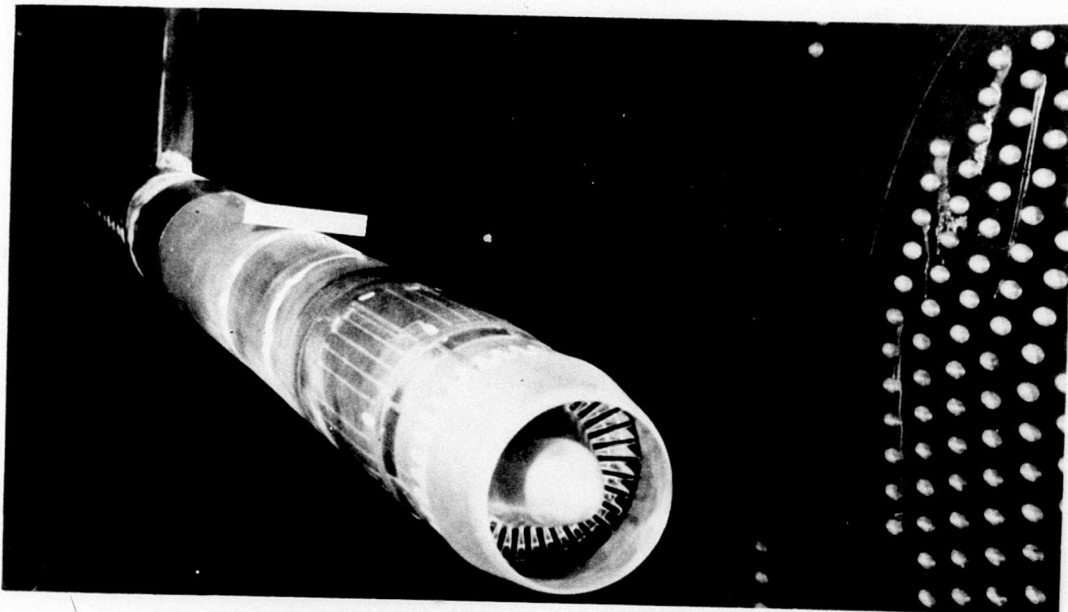
36-Deep-Chute Suppressor with Setback Ejector
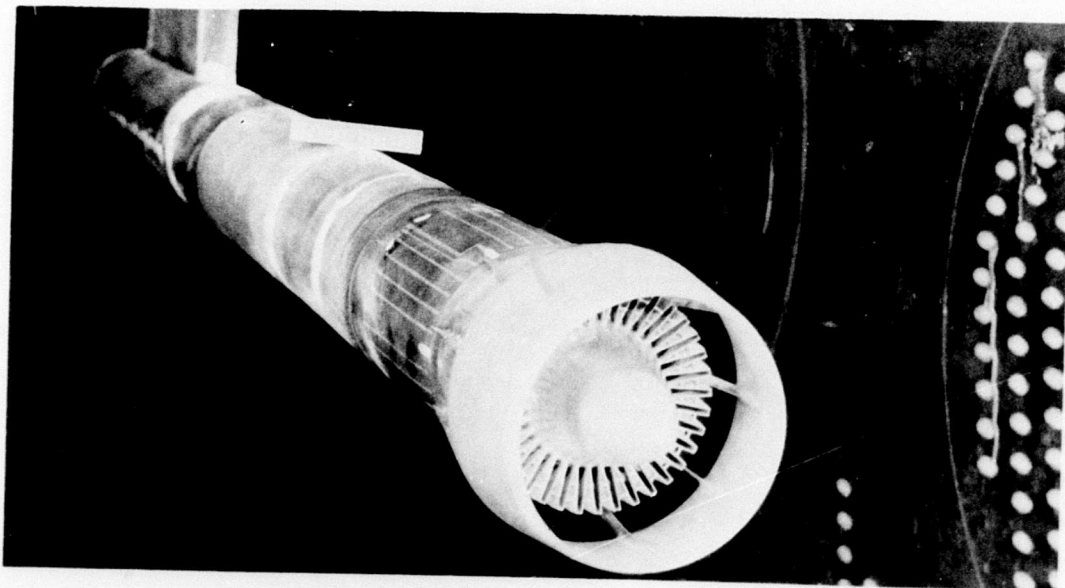
36-Deep-Chute Suppressor with Large Inlet Ejector

Figure 103. 36-Deep-Chute Suppressor, Comparison of Setback Ejector and Large Inlet Ejector.

138

Figure 104. Comparison of Performance for Unsuppressed Plug Nozzle and 36-Deep-Chute Suppressor Nozzle with and without Ejector Shrouds; Axisymmetric Nozzles.
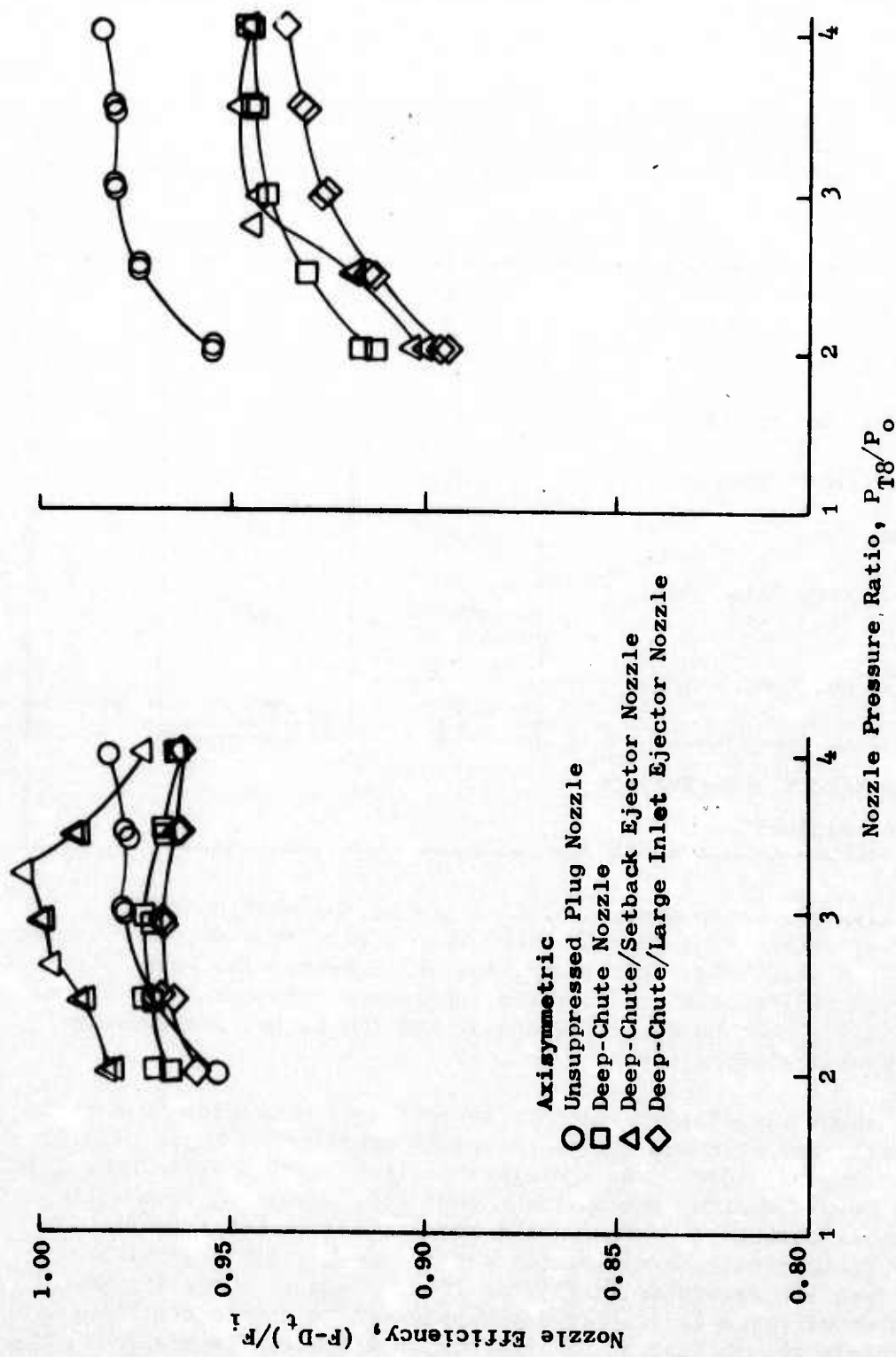
a) Free-Stream Mach Number = 0.0   b) Free-Stream Mach Number = 0.36

139

Table 6. for both Mach numbers at the assumed take-off nozzle pressure ratio of 3.0.

Table 6.   Summary of Nozzle Efficiencies for the Seven Configurations Tested at NASA-Lewis.

Configuration	$M=0$ $(F-D_t)/F_i$	$M=0.36$ $(F-D_t)/F_i$	$\dfrac{\Delta PNL}{\Delta C_{fg}}$
Unsuppressed Plug	.978	.981	---
Deep-Chute Nozzle	.972	.941	2.12
†Deep-Chute/Setback Ejector Nozzle	1.000	.946	2.86
†Deep-Chute/Large Inlet Ejector	.968	.927	1.94
*Shallow-Chute Nozzle	.964	.913	---
*Shallow-Chute/Setback Inlet Ejector Nozzle	.979	.900	---
*Shallow-Chute/Large Inlet Ejector Nozzle	.940	.889	---
†Uses Treated Ejector PNL Results *Not Tested Acoustically			

In Figures 105a and b the nozzle efficiencies of the shallow-chute suppressor nozzles, with and without the same two ejector shrouds, are plotted at Mach numbers of 0 and 0.36. Statically, the shallow-chute/setback ejector nozzle had the best performance of the three suppressor nozzles. However, at a Mach number of 0.36, the shallow-chute nozzle had the higher performance over the nozzle pressure range investigated.

It has been found empirically that the largest loss mechanism in a chute suppressor nozzle at low pressure ratios (take-off conditions, $P_{T8}/P_o \approx 3.0$) is the chute base pressure drag. As a diagnostic tool in evaluating this loss as a function of nozzle design, the nozzle thrust loss resulting from chute pressure drag was calculated for each of the six multichute suppressor configurations. These nozzle thrust losses for the deep-chute suppressor and its two ejectors are presented in Figures 106a, b and c, while Figures 107a, b, and c present these losses for the shallow-chute nozzle and its two ejectors. The nozzle thrust losses from the chutes for both the deep- and the shallow-chute models at Mach number 0.36 are greatest with the setback ejector and smallest with no ejector at all for nozzle pressure ratios up to 3.25. In this range the large inlet ejector nozzle fell, in both cases,
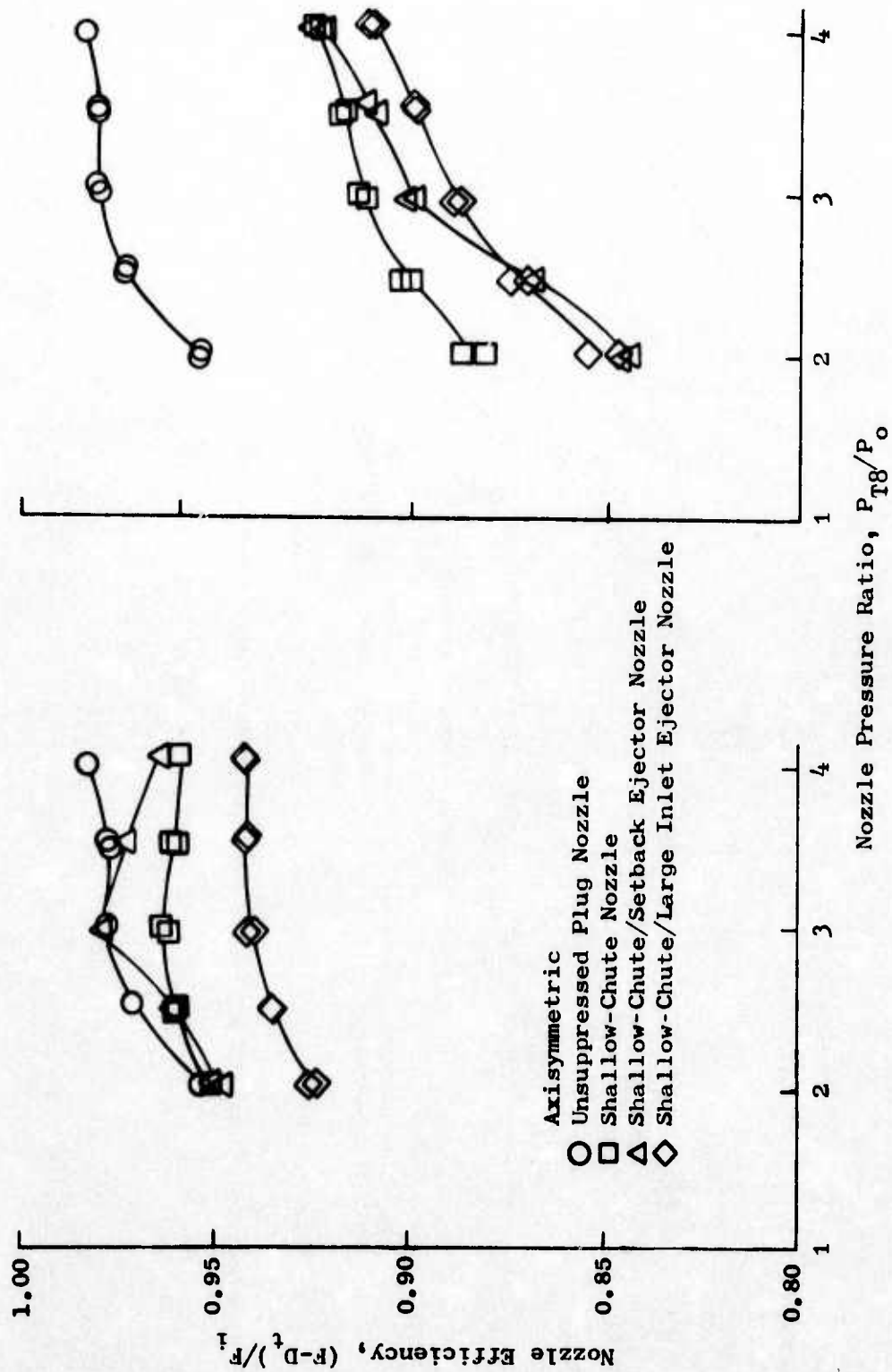
Figure 105. Comparison of Performance for the Unsuppressed Plug Nozzle and the 36-Shallow-Chute Suppressor Nozzle with and without Ejector Shrouds; Axisymmetric Nozzles.

141
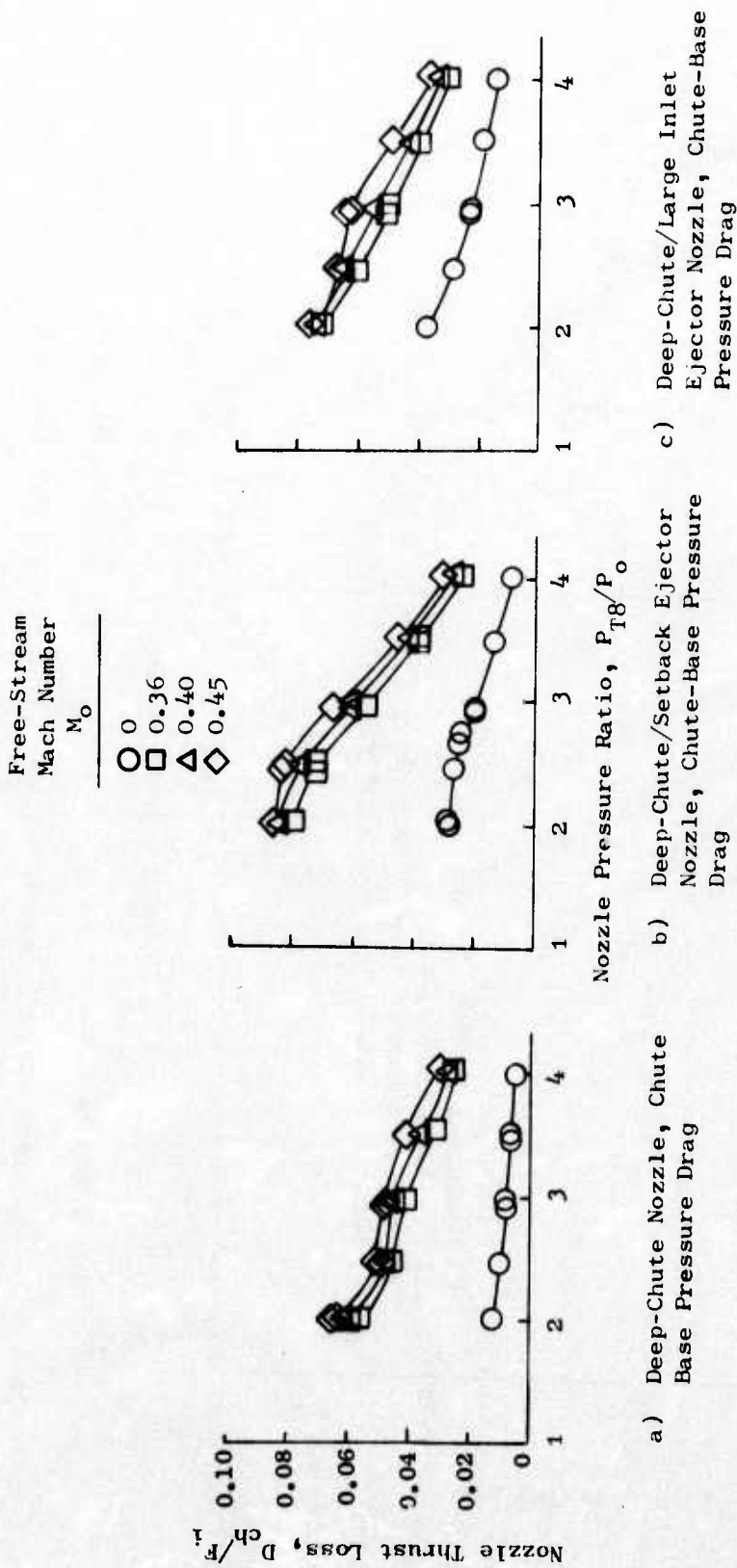
Figure 106. Nozzle Thrust Loss from Deep-Chute Base Pressure Drag; Axisymmetric Nozzle.

Free-Stream Mach Number M_o

○ 0
□ 0.36
△ 0.40
◇ 0.45

Nozzle Pressure Ratio, P_{T8}/P_o

a) Deep-Chute Nozzle, Chute Base Pressure Drag

b) Deep-Chute/Setback Ejector Nozzle, Chute-Base Pressure Drag

c) Deep-Chute/Large Inlet Ejector Nozzle, Chute-Base Pressure Drag

Nozzle Thrust Loss, D_{ch}/F_i

Free-Stream
Mach Number
M_o

	M_o
$\bigcirc$	0
$\square$	0.36
$\triangle$	0.40
$\diamond$	0.45

Nozzle Thrust Loss, D_{ch}/F_i

Nozzle Pressure Ratio, P_{T8}/P_o

a) Shallow-Chute Nozzle, Chute Base Pressure Drag

b) Shallow-Chute/Setback Ejector Nozzle, Chute Base Pressure Drag

c) Shallow-Chute/Large Inlet Ejector Nozzle, Chute Base Pressure Drag

Figure 107. Nozzle Thrust Loss from Shallow Chute Base Pressure Drag; Axisymmetric Nozzle.

143

in the middle. However, the setback ejector had better performance in all cases than the large inlet ejector.

In Figures 108a and b the external flow effects on the deep-chute and shallow-chute nozzles are presented at the assumed take-off pressure ratio of 3.0. Under this condition the deep-chute and the deep-chute/setback ejector nozzles have the same performance over the Mach number range of 0.36 to 0.45. The performance of both is greater than that of the deep-chute/large inlet ejector nozzle. For the shallow-chute configurations, the performance of the basic shallow-chute nozzle is greater, over the Mach number range of 0.36 to 0.45 than either of the two ejector models. The performance superiority of the deep-chute over the shallow-chute is clearly demonstrated in Figure 108.

At the assumed take-off conditions, $P_{T8}/P_0 = 3.0$ and $M = 0.36$, the deep-chute nozzle has 2.8% higher performance than the shallow-chute nozzle.

The ratio of the peak PNL suppression at the 2128-foot sideline ($V_j = 2500$ ft/sec) to the ΔC_{fg} at $M_0 = 0.36$ and $P_{T8}/P_0 = 3.0$ for the deep-chute suppressor configurations shows that both the 36-chute with and without the setback ejector achieve $\Delta PNL/\Delta C_{fg}$ trades above 2.0, which is desirable from a systems standpoint.

Test Series Evaluation

Aerodynamic wind-tunnel performance on these models yielded thrust coefficients in the 0.93 - 0.94 class. The combined $\Delta PNL/\Delta C_{fg}$ tradeoff for this system (36 deep chutes, area ratio of approximately 2.2) was in the 2.0 plus category. Although this was a good tradeoff for a suppressor system, the need to improve the basic suppression level was clearly demonstrated.

The addition of the treated ejector showed that suppression gains could be achieved at the low-to-mid velocity range with this type of system.

3.2.2.3 Comparison Tests on Multichute/Annular Plug Suppressors

To more thoroughly understand the effects of multichute/annular plug suppressor geometry changes on aeroacoustic interaction of the jet plume, a series of acoustic and Laser Velocimeter tests was conducted on the 40-chute and 36-chute suppressors, and on a 32-chute/suppressor model previously tested during the original SST program (See Reference 1). The immediate intent of this investigation was to identify the possible causes of the low PNL suppression obtained on the 36-chute suppressor and to decide on an approach for another multichute/annular plug suppressor configuration.

A review of the nozzle geometries was conducted to include area ratio, element number, planform, and exit plane cant angle. Demonstrated suppression levels achieved with each model were correlated with planform characteristics, and trends were established which served as design guides for the final model

144
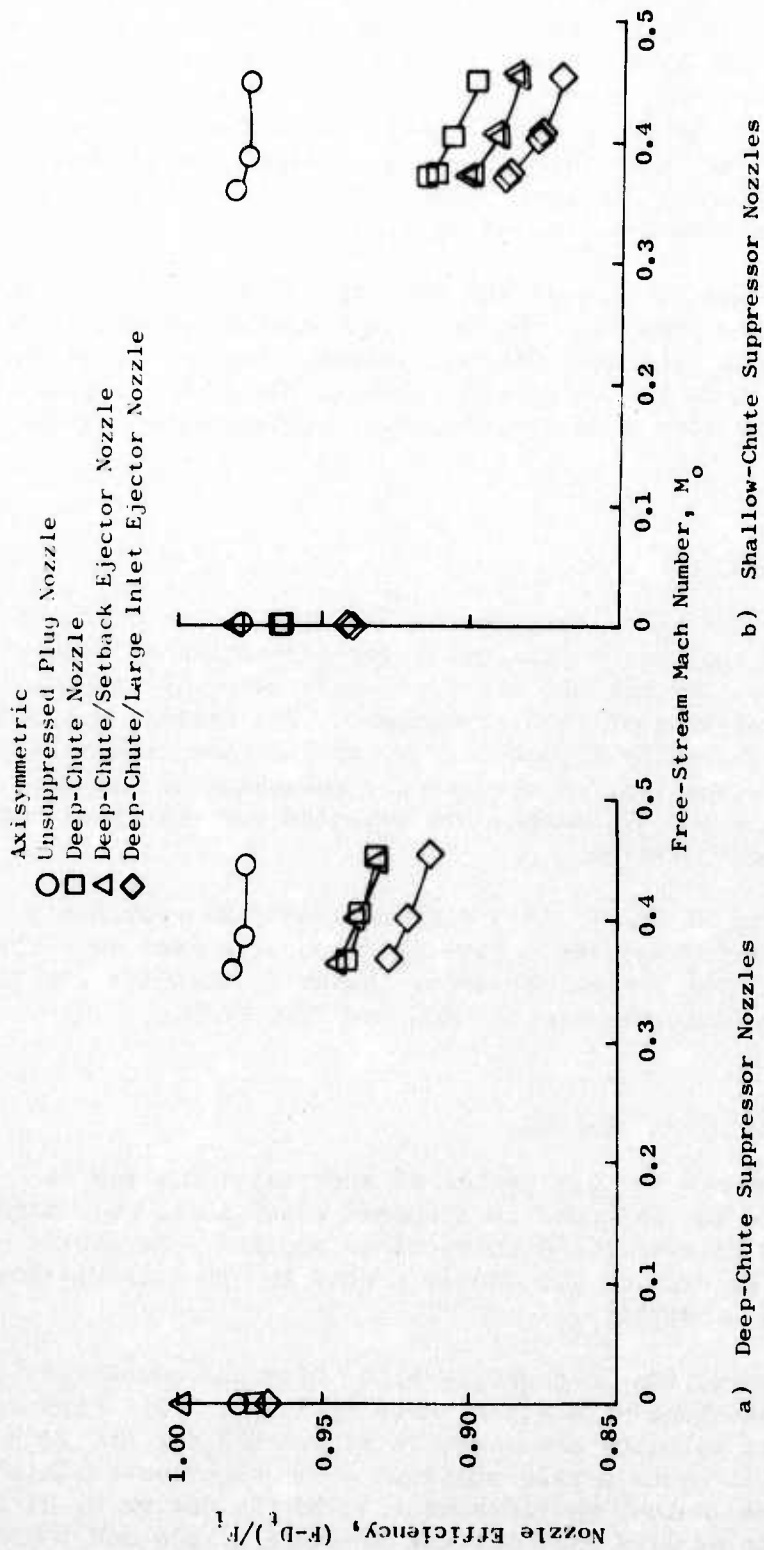
Figure 108. External Flow Effects on Axisymmetric Nozzle Performance; Nozzle Pressure Ratio = 3.0.

configuration. Figure 109 schematically illustrates the geometric differences between the three nozzles. All three multichute suppressors had similar area ratios (2.13 for the 36-chute and 2.0 for the 32- and 40-chute nozzles). The 36- and 40-chute nozzles used common plug hardware geometry (plug angle of 30°), while the 32-chute suppressor employed a 20° included-angle plug centerbody. The exit plane geometry, as illustrated in Figure 109 shows the 36-chute with the nozzle exit normal to the plug surface, the 32-chute nozzle exit normal to the nozzle axis, and the 40-chute exit plane with a ± 15° cant relative to the normal to the suppressor axis.

The planform comparisons of Figure 109 show the 36-chute to have a large amount of open primary flow area near the hub and a smaller amount at the tip, while the 40-chute planform maintains minimum primary flow area near the hub but has a large amount in the outer tip region. The 32-chute planform is more uniform in primary flow area distribution, having near-parallel-sided primary flow elements.

Acoustic/LV Tests

Concurrent acoustic and Laser Velocimeter (LV) tests were performed on each of these multichute suppressor nozzles at jet velocities of interest along the operating line. The results of these tests supported the earlier apparent trends, characteristic of each suppressor. The merging patterns of the jet plume were graphically illustrated by the LV measurements taken on each nozzle. This information was used in the selection of the next multichute model design, which ultimately was selected for the final model and engine suppressor configuration.

Testing was conducted at JENOTS in a similar manner as previously discussed for the single-flow systems. Far-field acoustic data were obtained at all points tested over the operating range. Laser Velocimeter testing was conducted at three jet velocities between 2200 and 2600 ft/sec.

Acoustic Results and Analysis

The results of the tests on this series of suppressor nozzles is presented as full-scale data corrected to standard conditions, but without extra ground attenuation or free-field corrections applied. Pertinent acoustic results are summarized for each of the models tested in Appendix C, along with a tabulation of the test conditions.

A summary comparison of the 36-chute results, with the concurrent test results of the 32- and 40-chute models, is shown in Figure 110. Peak PNL variations with ideal jet velocity are shown in Figure 110 for the 2128-foot sideline distance. The 36-chute nozzle achieved a PNL suppression level of 8.5 PNdB, relative to the conical nozzle baseline, at the design V_j of 2500 ft/sec. PNL suppressions of 11.0 PNdB for the 32-chute nozzle and 13.5 PNdB for the 40-chute suppressor were observed.
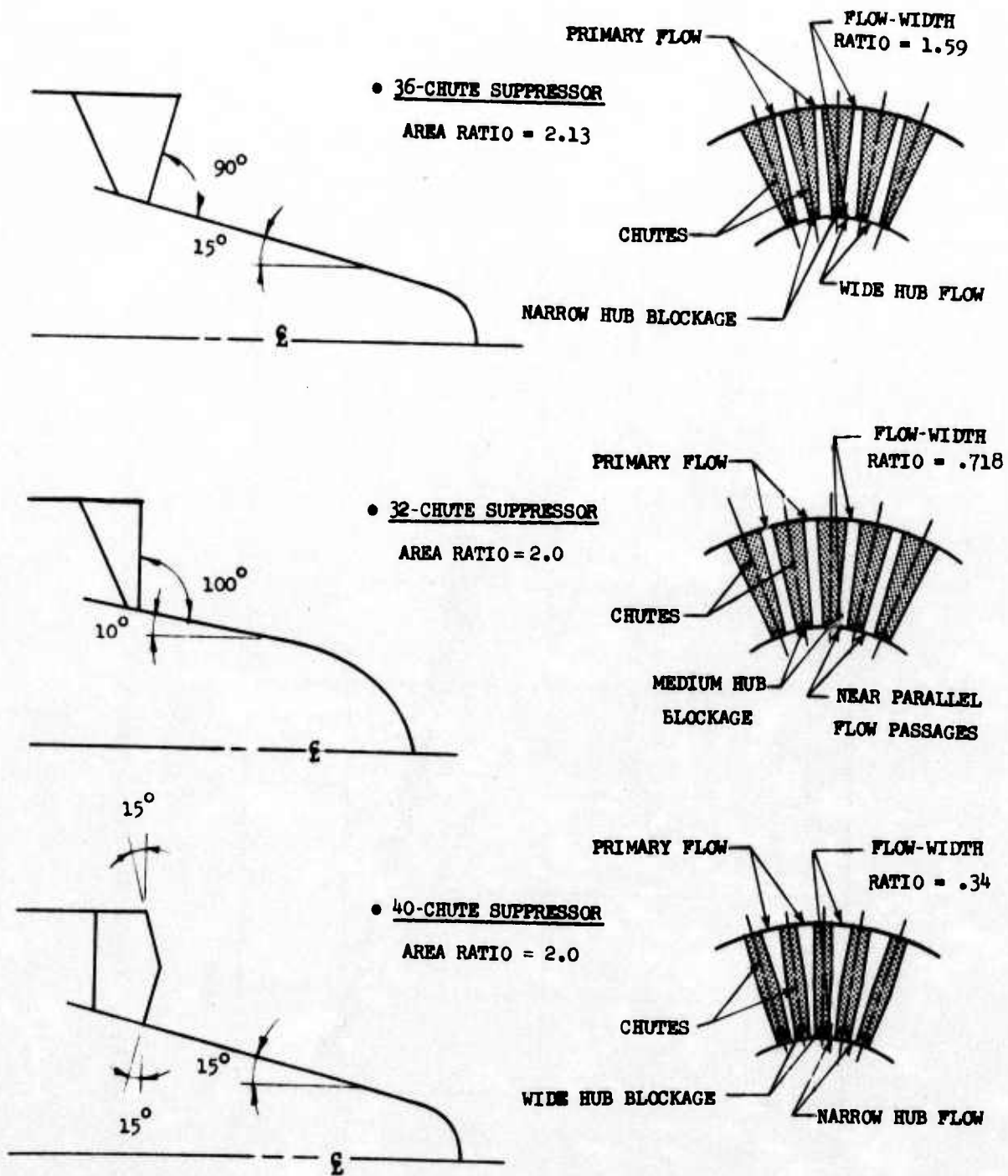
Figure 109. Schematic of Multichute Geometric Characteristics.

147
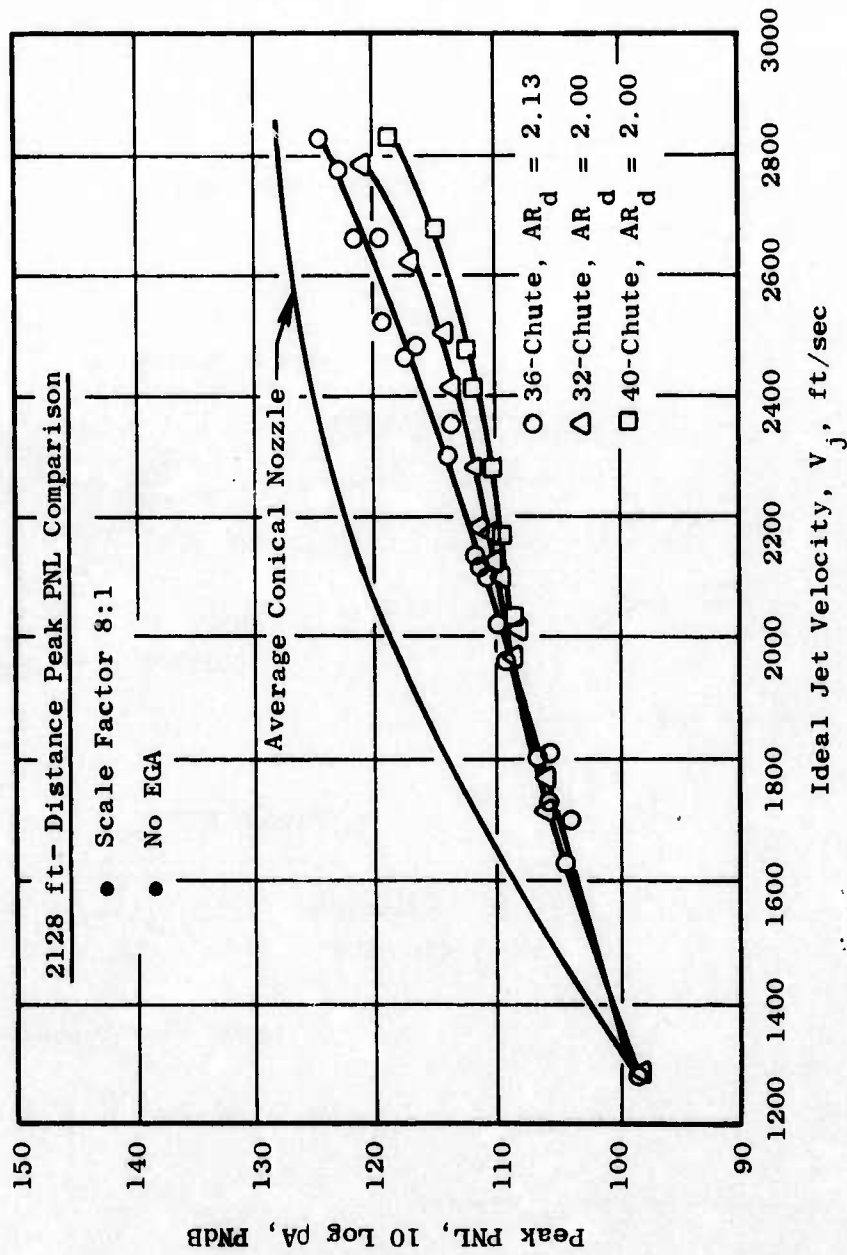
Figure 110. Peak PNL Comparison of Multichute/Annular Plug Suppressors.

148

A comparison of the PNL directivity at the 2128-foot sideline (Figure 111a), shows a constant peak angle of 130° (relative to the jet inlet) for the 36-chute nozzle for jet velocities ranging from 2347 to 2769 ft/sec, while the characteristics of the 32-chute (Figure 111b) and 40-chute (Figure 111C) suppressors indicate a shift in peak angle, with increasing velocity, from 110° to 140°.

Spectral comparisons of the three multichute suppressors at 110°, 130°, and 150° on the 320-foot arc are shown in Figure 112 at the design ideal jet velocity of 2500 ft/sec. Figures 113a, b, and c compare the individual nozzle effects on SPL spectra at constant angle (130°) over the velocity range tested.

The spectra show the 36-chute to become low-frequency-dominated much sooner than either the 32-chute or 40-chute models. The results indicate that rapid merging of the primary flow elements of the 36-chute suppressor occurs somewhere around 2300 ft/sec, since the spectra show complete low-frequency domination at the 2500 ft/sec jet velocity.

Laser Velocimeter Evaluation

The peak measured values of a number of mean velocity axial traverses, as measured by the laser velocimeter, are illustrated in Figure 114. If indeed the mean velocity effects on jet noise are proportional to V_j the figure shows that when the $V_j \sim 2300$ ft/sec and $P_{T8}/P_o = 2.7$, the 40-chute suppressor should have been quieter than either the 36- or 32-chute, since the mean velocity decays rapidly in 3 nozzle diameters. The 36-chute, on the other hand, maintains a near-constant mean velocity through that distance; while the 32-chute is between the two extremes.

The velocity profiles obtained from the laser velocimeter surveys are shown in Figures 115a, b, and c. They illustrate the merging characteristics of each multichute nozzle and suggest why the 36-chute nozzle achieved less suppression than either the 32- or 40-chute models of comparable area ratios.

The results of these tests indicate that the effects of planform and exit plane cant angle are the dominating factors contributing to the suppression differences. The 36-chute, high-exit, aftward-cant angle and high flow-width ratio planform (characteristic of narrow hub blockage) combined to focus the primary flow elements down the plug surface, coalescing them to a high energy stream more rapidly than either the 32- or 40-chute models. The planform of the 32-chute nozzles did not converge the primary flow elements as rapidly as the 36-chute did, while the 40-chute planform maintained the annular flow contour.

The more rapid coalescence, without the benefit of adequate mixing, results in a low-frequency dominated spectrum (e.g., typical of a high velocity conical nozzle) for the 36-chute at the design jet velocity of 2500 ft/sec.

149

(a) 36-Chute, $AR_d = 2.13$

Reading	V_j ft/sec	P_{T8}/P_o
4	2769	3.54
2	2482	2.98
5	2347	2.88
1	2278	2.66
3	2664	3.33

(b) 32-Chute, $AR_d = 2.0$

Reading	V_j ft/sec	P_{T8}/P_o
13	2780	3.59
11	2507	3.03
14	2413	2.91
10	2283	2.70
12	2620	3.28

(c) 40-Chute, $AR_d = 2.0$

Reading	V_j ft/sec	P_{T8}/P_o
13	2826	3.56
11	2472	2.85
15	2411	2.89
10	2277	2.69
1	2677	3.28

Angle Measured from Jet Inlet, Degrees
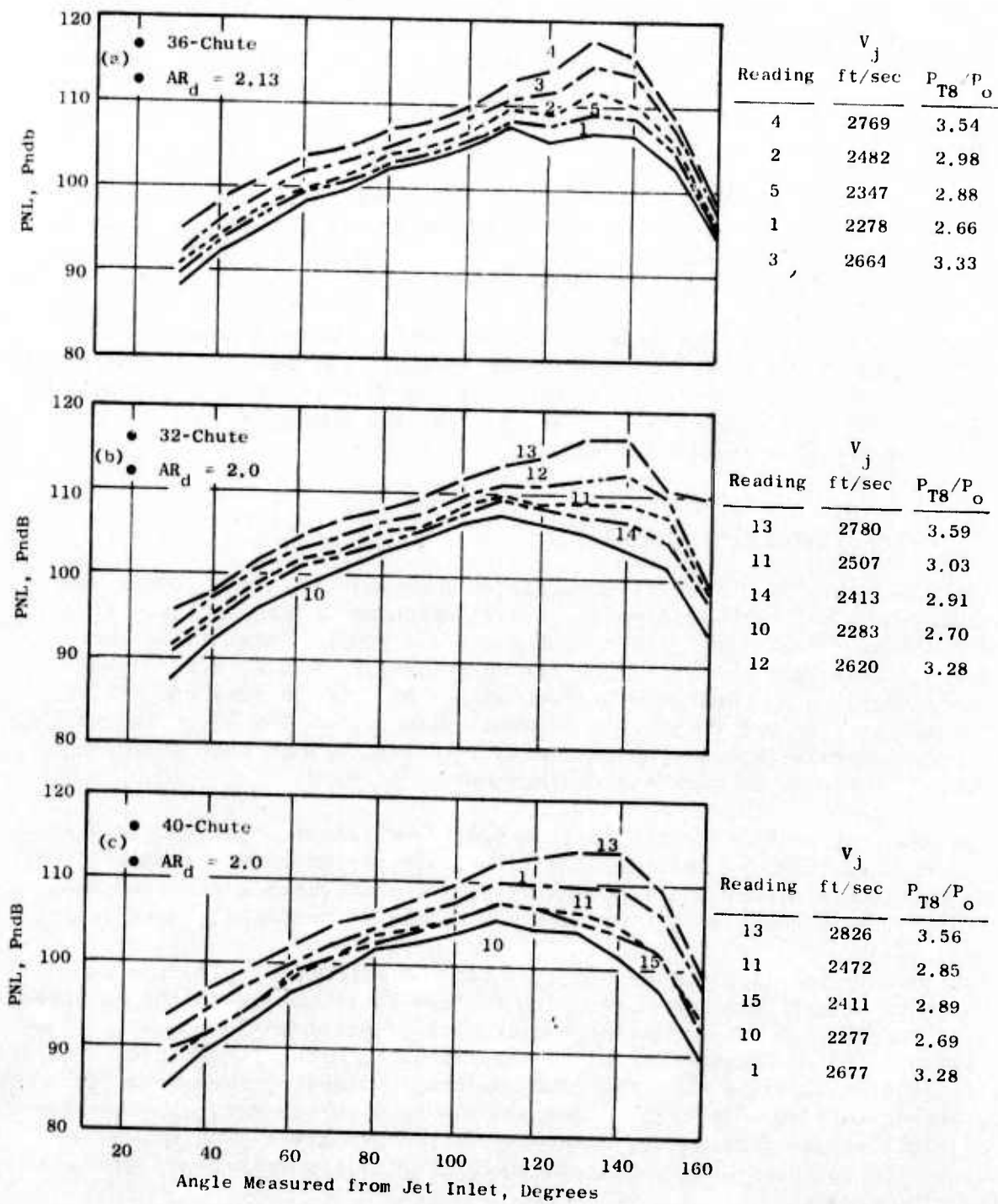
Figure 111. Full-Scale PNL Directivity for Multichute/Annular Plug Suppressors at the 2128-foot Sideline.

150
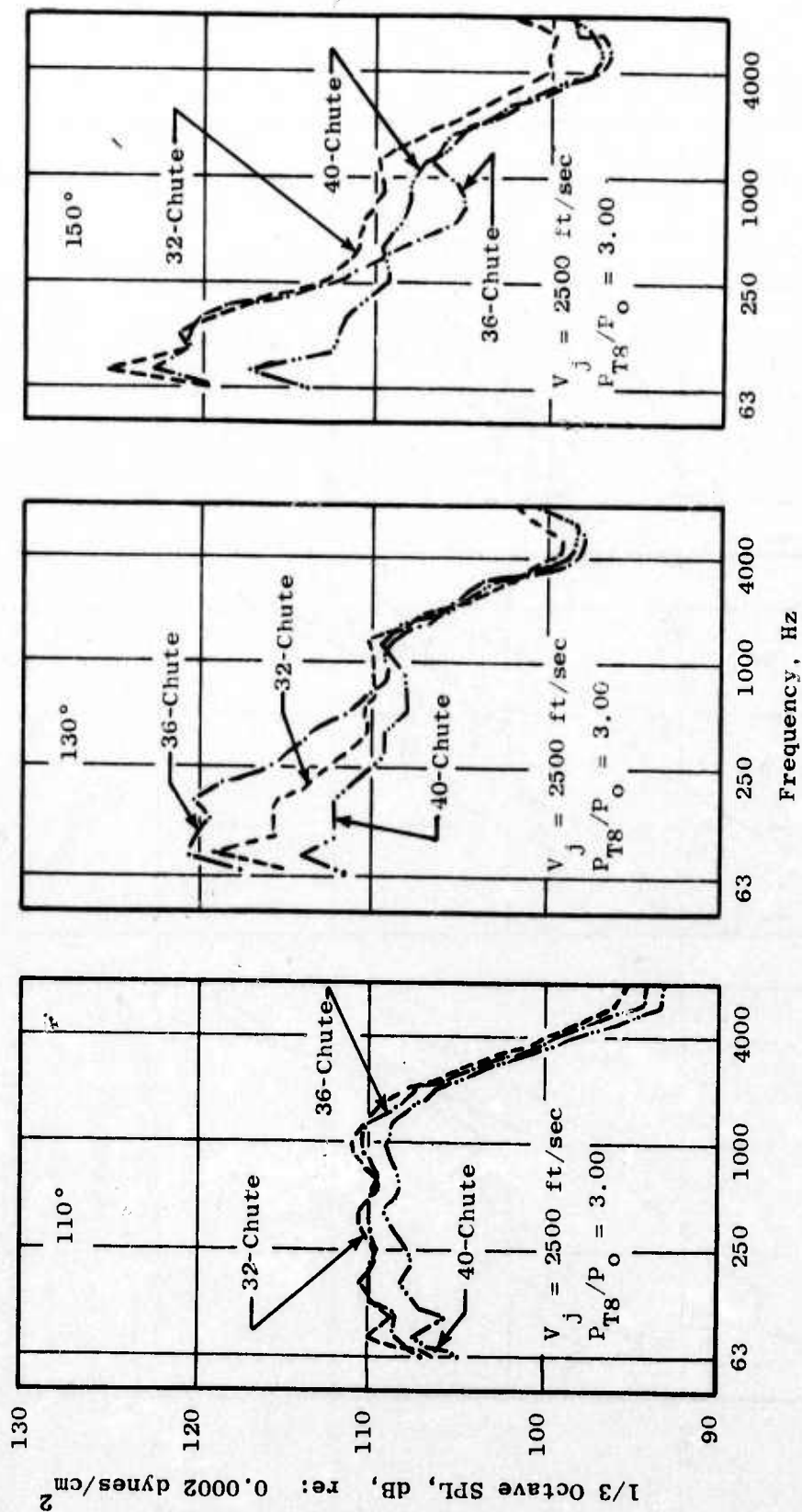
Figure 112. Spectra Comparison for Multichute/Annular Plug Suppressors.

151
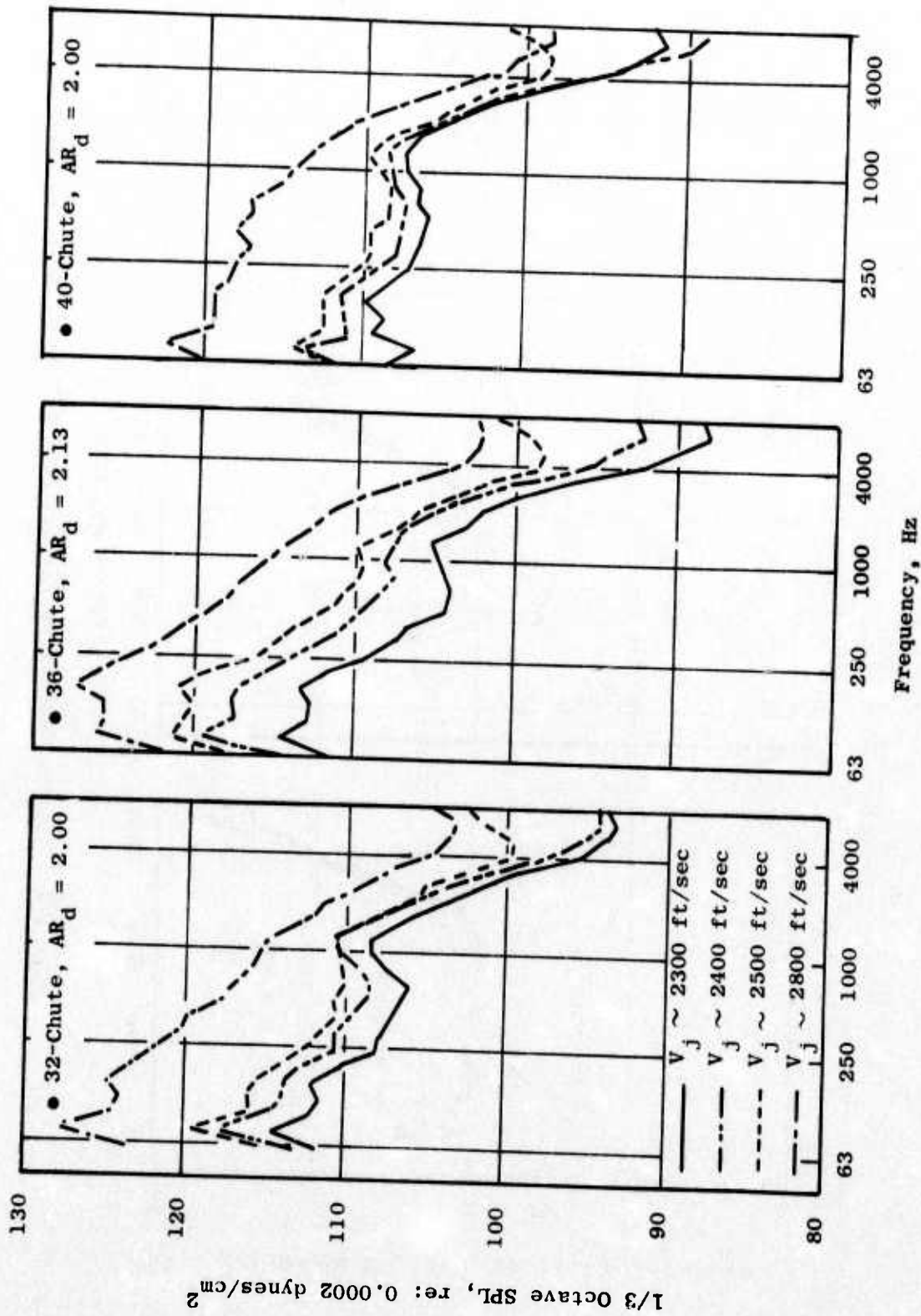
Figure 113. Spectra Comparison for Multichute/Annular Plug Suppressors.
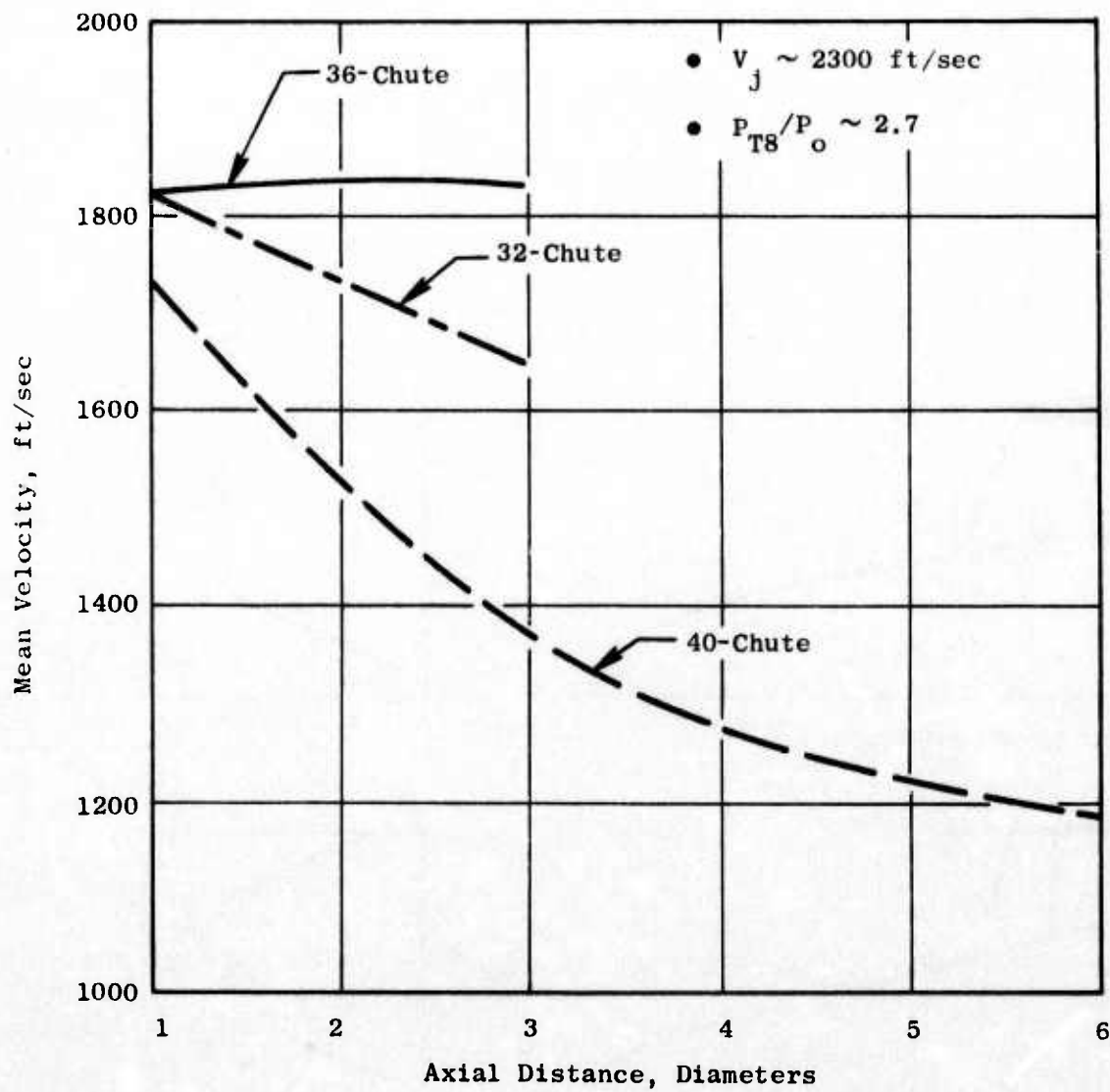
Figure 114. Mean Velocity Trends from LV Measurements.

(a) 36-Chute Suppressor

$V_j \sim 2256$ ft/sec

$P_{T8}/P_o \sim 2.68$

(b) 32-Chute Suppressor

$V_j \sim 2310$ ft/sec

$P_{T8}/P_o \sim 2.68$
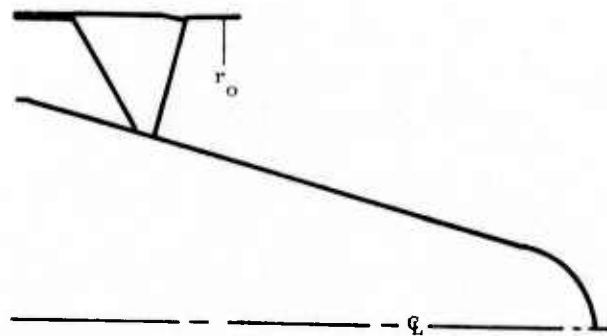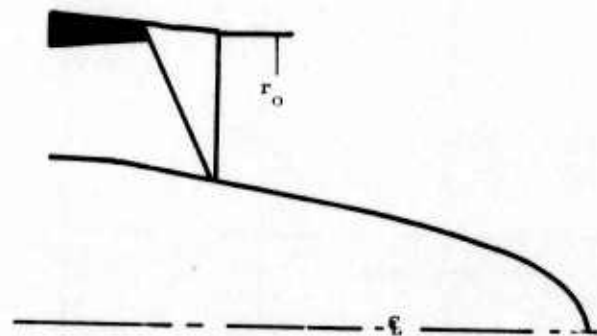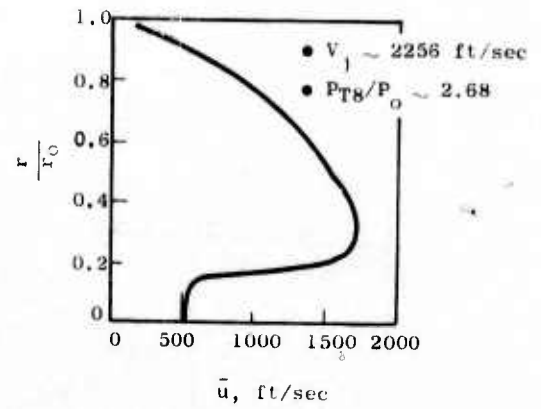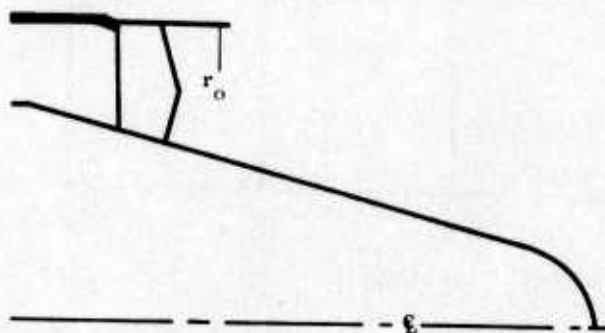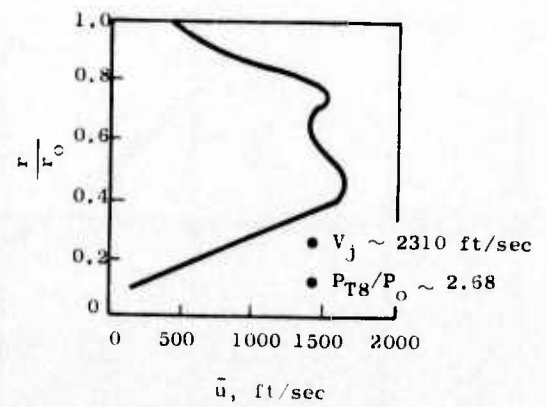
(c) 40-Chute Suppressor

$V_j \sim 2249$ ft/sec

$P_{T8}/P_o \sim 2.68$
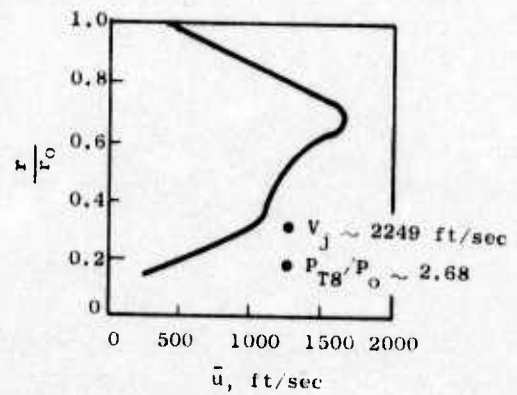
Figure 115. Multichute Mean Jet Velocity Profiles.

Aerodynamic Performance Comparisons

A review of previous aerodynamic wind-on ($M_o \sim 0.36$) performance results on the 32- and 40-chute nozzles was conducted to compare with the favorable results obtained with the 36-deep-chute nozzle. A comparison of the ΔPNL/ C_{fg} trades for the three multichute suppressors is shown in Figure 116. The 40-chute aerodynamic performance from previous testing was undesirable ($C_{fg} \sim 0.84$) from a systems viewpoint, while the 32-chute produced a favorable combination of aerodynamic ($C_{fg} \sim 0.91$) and acoustic (ΔPNL ~ 11.0 PNdB) performance trades.

Test Series Evaluation

The results of this series of acoustic and Laser Velocimeter tests on the 36-, 32-, and 40-chute suppressors more clearly identified the geometric parameters that influenced the aeroacoustic performance of multichute nozzle systems. The key geometric parameters which have major impact on multichute aeroacoustic performance are:

- Exit planform (flow-width ratio)

- Exit-plane cant angle

- Chute depth

Those with lesser impact but nevertheless having some effect include area ratio variation and element number; both of these are keenly influenced by mechanical constraints of the system.

The effects of the key geometric parameters for a given area ratio and element number are described as follows:

Exit Planform - controls the primary flow distribution around the annulus of the plug nozzle. It is directly related to the hub-to-tip flow-width parameter. Limiting our discussion to the primary flow passage between the chute, the test results suggest that high flow-width ratios (>1.5) result in wide spacings at the hub and narrow spacings at the tip. Aerodynamically, this is attractive, since this pressurizes the plug surface and reduces or eliminates the drag associated with low plug pressures. Acoustically, however, the effect is detrimental, since it distributes a large amount of high velocity flow at the hub where it can merge quickly to a coalesced jet without sufficient time to entrain enough ambient air to reduce the velocity resulting in high noise levels.

The opposite effect can be seen with a very low hub-to-tip flow-width ratio (<0.5), which results in narrow hub spacings and wide tip spacings. Aerodynamically, this effect is seen to starve the plug surface, increasing

155

- M_o = 0.36
- P_{T8}/P_o = 3.0
- V_j = 2500 ft/sec
- Peak PNL at 2128-ft Sideline
- Relative Velocity Effects Not Included on Suppression
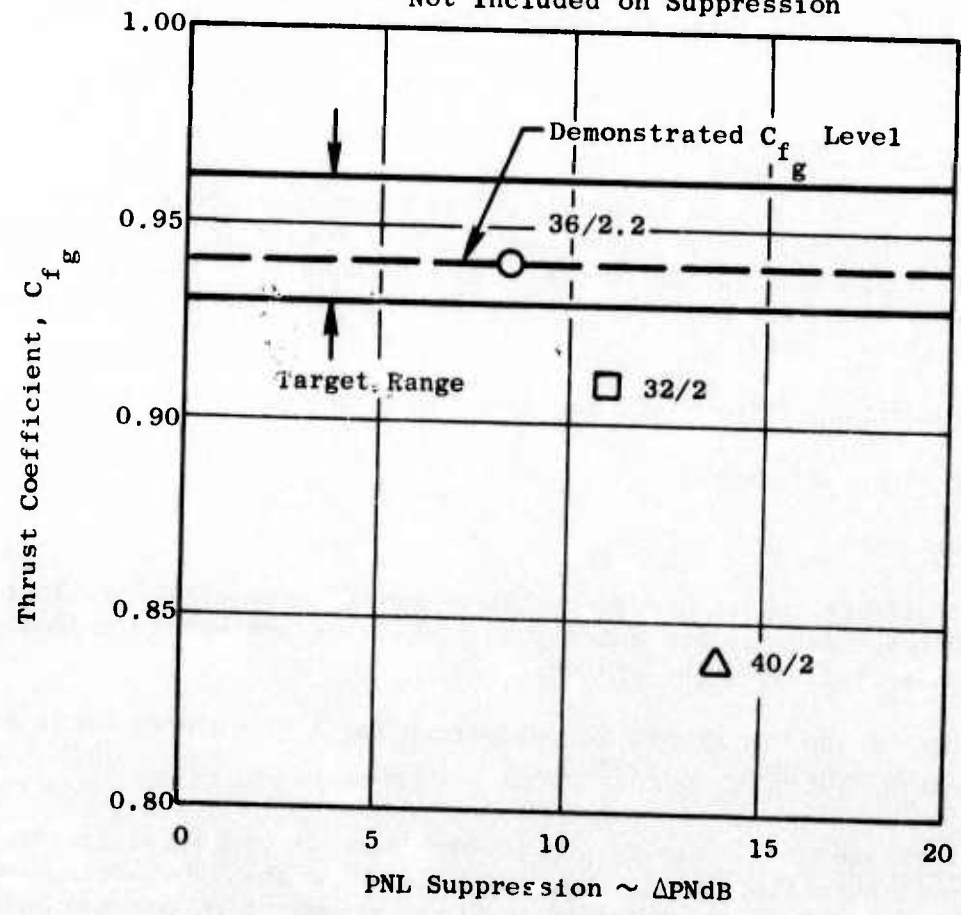
Figure 116. Multichute Suppressor Design Background.

the plug drag and overall performance loss. Acoustically, this is beneficial, since a minimum amount of high velocity flow is concentrated at the hub, and the majority of the flow is distributed to the outer annulus where sufficient mixing with ambient entrained air can take place.

Obviously, these extremes are to be avoided if a realistic suppressor is to be designed. An attractive compromise appears to be one with intermediate hub-to-tip flow-width ratios (.7 - 1.0). This provides a primary flow passage that is nearly parallel and uniformly distributes the flow at the exit plane.

Exit Plane Cant Angle - influences the initial direction that the primary flow takes after leaving the nozzle exit plane. The tendency of the flow is to move in a direction normal to the exit plane angle. Canting the exit plane angle normal to the plug surface tends to focus the flow along the plug and coalesces it to a single jet at the plug end. The effect on aeroacoustic performance is similar to the effect of a high hub-to-tip flow-width ratio on the exit planform.

If the exit plane is canted away from the plug, the tendency of the flow is to move outward and off the plug surface, inhibiting aerodynamic performance by increasing plug drag and enhancing acoustic suppression by moving the high energy streams to a larger diameter and allowing better aerodynamic mixing to take place.

Again, these are two extremes which must be compromised for effective multichute nozzle design. A compromise on exit cant angle for suppressors without ejectors can be reached with axial flow from the exit plane. In this case, the exit cant angle is zero or normal to the nozzle axis. If a secondary ejector is employed, consideration must be given to select the exit cant angle which will allow the flow to enter the ejector without impinging on the inlet or flowing around the outside of the ejector.

Chute Depth - controls the amount of ambient air available to mix with the primary flow elements. Large deep chutes (depths/height ≥ 1) allow sufficient entrainment to pressurize the base of the chute so that fewer, wider chutes can be used to segment the primary flow.

A consideration of all of these key parameters was undertaken prior to arriving at the next (and final) multichute/annular plug suppressor system to be tested.

157

3.2.3 Multitube/Annular Plug Suppressor Nozzles

3.2.3.1 Concept Feasibility Studies

During Phase I of the Department of Transportation's Supersonic Transport Noise Reduction Technology Program, multitube exhaust nozzles were shown to provide high levels of exhaust jet noise suppression at thrust loss values which were not too severe. In this light, one of the objectives of Phase II of the program was to further develop multitube suppressors/nozzles and, if possible, extend the state of the art to higher suppression and suppression per thrust-loss levels.

A large number of multitube configurations had been tested previously by both Boeing and General Electric (References 12 and 1). Data from these tests were used to correlate the acoustic suppression levels with the numerous nozzle parameters which affect the thrust-loss mechanisms. Examples of the more important variables include suppressor area ratio, tube number, length, convergence, and geometrical arrangement, as well as tube exit plane, tube cant angle, and baseplate stagger angle. Parametric studies were conducted separately on noise suppression and nozzle performance and later combined to produce suppression/thrust-loss trades in the regions of high values of noise suppression. The results were used to design and integrate the "best" multitube suppressor with a typical translating shroud annular plug nozzle. Such annular plug nozzles are attractive for supersonic transport application because of their inherent high installed performance over a wide range of nozzle pressure ratios. The particular engine cycle chosen to use for design guidelines was the GE4/J6H2 engine. During the suppressor designs, it became obvious that the mechanical design of the system, particularly stowage problems, would dictate many limitations to any suppressor system. Since it was beyond the scope of the program to conduct parametric mechanical design studies in order to make the best suppressor design compatible with all mechanical considerations, and it also was not desirable to use existing mechanical designs and thus seriously compromise the suppression qualities of the nozzle, it was decided that two models would be tested. The first model was designed using only the aeroacoustic critera in an attempt to give the "most optimum" suppressor and was not consistent with any existing mechanical design. A second model combined the aeroacoustic trade studies with previous mechanical designs to give a mechanically feasible design while sacrificing suppressor performance.

Early Multitube Suppressor Studies

A multitube suppressor within an annular plug nozzle system had been tested early in the tube nozzle work of the SST/GE4 contract. It showed promising suppression but was not pursued further until just prior to the contract termination.

At that time, preliminary design activity identified a feasible mechanical system for incorporating the multitube suppressor within the translating shroud annular plug nozzle as stowable within the plug centerbody.

158

The system was conceived for the high-flow engine operating at a low cycle pressure ratio at lift-off and within the jet exhaust velocity range where multitubes are considered most effective.

Acoustic data for the single multitube annular plug nozzle tested were reviewed and analyzed for application to further designs. A preliminary evaluation of the system conceived for the high-flow engine cycle of the J6H2 engine was undertaken and indicated that a static thrust coefficient of approximately 89% could be attained at the design point. Base pressure losses were calculated using the correlation curve presented in Figure 117.

Preliminary Concept Review

Available data were reviewed on the noise suppression achieved by multitube nozzles designed for conical ejector systems and the corresponding thrust decrement imposed, as a function of the key design parameters. These data seemed to indicate that relatively high suppression (>15 PNdb) could be achieved with as little as 10% loss in static thrust by means of the multitube nozzle approach. This approach warranted continued effort to optimize the suppression/thrust trade-offs.

General conclusions derived from the review of the multitube suppressor data are summarized below:

- Multitube suppressor configurations generally exhibit a double-humped noise spectrum at low and intermediate velocities. The higher frequency hump is associated with the individual tubes or premerged region and the lower frequency hump with the merged flow.

- The level of the high-frequency noise is much less than would have been estimated by summing the noise from the particular number of individual jet tubes. The level of the low-frequency noise appears to be well correlated by the velocity and diameter of the stream where the flow merges from the individual jets.

- An area ratio (total area/flow area) in the range of 3 to 5 yields maximum PNL reduction at high jet velocities. Increasing the area ratio also tends to reduce the thrust loss by increasing the baseplate ventilation.

- Longer tubes result in less thrust loss without appreciably affecting the noise suppression.

- Configuration of the tube ends has little effect insofar as conical or round-convergent ends are concerned. Greatrex ends improve suppression but increase the thrust loss.

- Increased numbers of tubes reduces noise for as many as up to 150 tubes, however, at the expense of thrust.
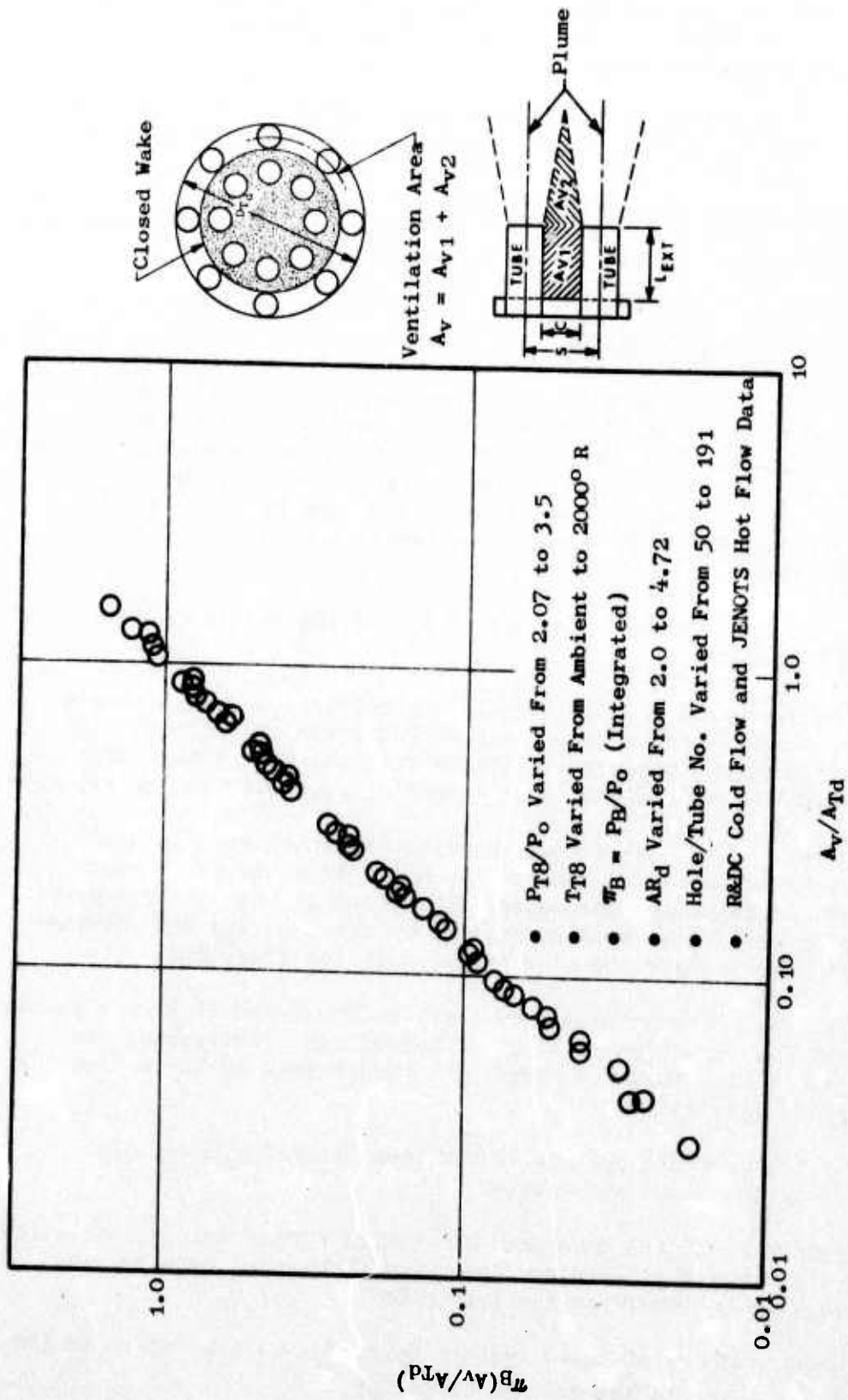
Figure 117. Normalized Base Ratio for Multielement Suppressor Systems.

160

Development of Multitube Prediction Technique

These data provided information which could be compared with predictions developed from noise data from individual jets at supersonic exhaust velocities and from clustered rockets. The basic information which was needed, and the approach used for the prediction procedure, included:

1) The maximum angle OASPL and octave band spectral distributions as determined from simple nozzle geometry. These data were used for an individual tube (premerged) based on the nozzle exit condition and, for the merged jet, based on the calculated flow conditions and area of the jet when fully coalesced.

2) Noise was then calculated for the flow from the tubes, prior to merging, as follows:

   a. The axial location of peak noise generation was calculated for each octave band.

   b. The axial location at which noise was no longer generated by flow from the individual tubes was predicted for each octave band.

   c. Based on the results of (a) and (b) above, and using the predicted axial distribution of noise, the SPL relative to the overall octave band SPL (determined in Step 1) was then determined to establish the SPL in the octave band for noise from an individual tube.

   d. The noise from all the tubes was then determined using the predicted effective number of tubes which radiate sound to the far field.

3) Noise from the merged flow (determined in Step 1) then was added to that from the individual tubes (Step 2) for each octave band. These data then were used to determine the Perceived Noise Level (PNL) by standard procedures.

The results of this prediction procedure were checked against typical measured data. Representative comparisons at low and high area ratios are shown in Figures 118a and b.

The program was restricted to predicting the noise from multitube bundles or clusters in which the tubes were of equal length and diameter, uniformly spaced, and parallel to the jet axis. Contributions from other geometric characteristics were estimated separately from previous test results with similar type configurations.

Using this prediction scheme, a parametric study was performed to establish a range of flow and geometric conditions from which a good design could be selected.
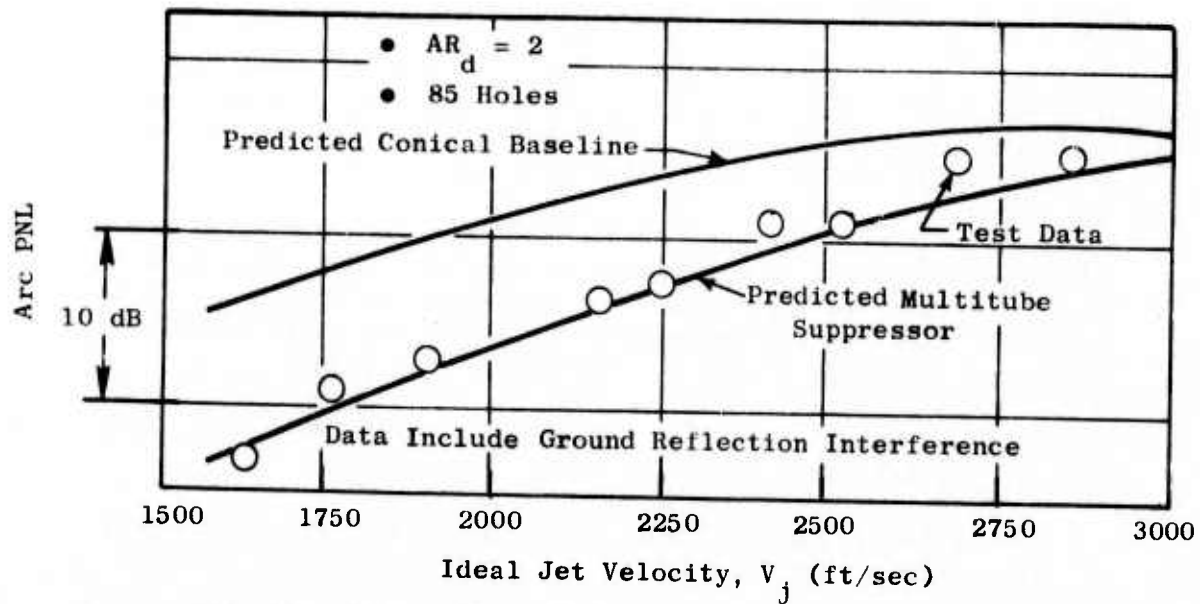
(a) Area Ratio, $AR_d = 2.0$
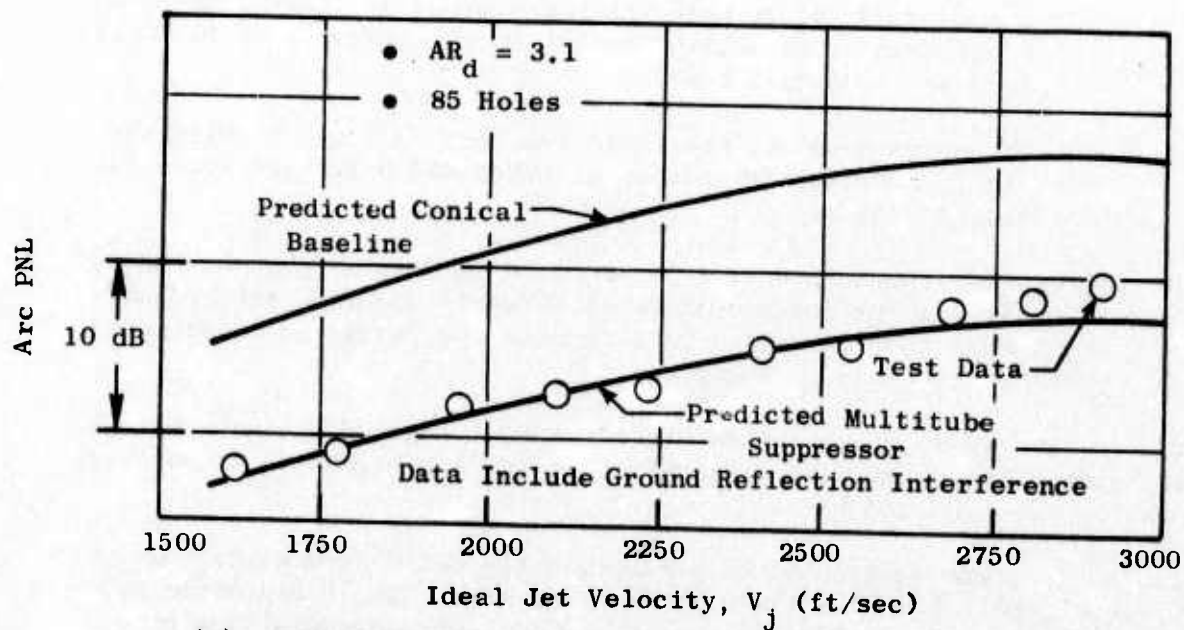
(b) Area Ratio, $AR_d = 3.1$

Figure 118. GE 85-Hole Nozzle PNL Comparisons.

162

Multitube/Annular Plug Suppressor Design Approach

Two model scale multitube suppressor configurations on an annular plug were planned for this task. These suppressors were designed for acoustic and static performance benefits with the nozzle configurations representative of viable mechanical systems as far as the limited practical studies would allow.

The evaluation of multitube suppressor systems on annular plug nozzles was carried out in two basic steps. The first step consisted of establishing aeroacoustic trends for varying geometric parameters on plain multitube suppressors without a plug; the second step was adapting these results to an annular plug configuration.

Multitube Acoustic Parametric Studies - The design selection of the multitube annular plug model configurations was preceded by a parametric study and evaluation of the geometric characteristics that had acoustic and aerodynamic influence on the nozzle effectiveness.

The acoustic parametric evaluation was conducted as part of the two-phase effort in the development of the multitube annular plug nozzle density combinations of area ratio and tube number, which yielded maximum levels of PNL suppression. The results of this study were combined with the results of a similar aerodynamic investigation (to be discussed later) conducted on multitube suppressors to establish ΔPNL and ΔC_{fg} tradeoffs for final application to configurations of multitubes on annular plug nozzles.

The initial phase of the acoustic study was conducted over a range of area ratios from 2.0 to 3.5 with tube number variations of 7, 40, 55, 64, 70, 76, 85, and 100 tubes. The selections were based on area ratio and tube number combinations that were deemed aerodynamically and mechanically feasible, as well as acoustically beneficial.

The jet velocity range of interest for the multitube/annular plug suppressor operation was set from 2000 to 2500 ft/sec. The design point selected for this study was based on the GE4/JoH2 engine operating line at conditions of P_{T8}/P_o = 3.0, T_{T8} = 1884° R, and V_j = 2485 ft/sec.

Results of the Phase I study showed that, for a V_j design point of 2485 ft/sec, suppression increased wth increasing area ratio at a constant tube number (N_t = 40 to 85) up to AR_d's of 2.7 to 3.1. Suppression also increased with increasing tube numbers at constant area ratios above 2.4. At low area ratios ($AR_d \approx 2.0$) changes in tube number did not appreciably affect suppression.

Further parametric studies on multitube nozzles are conducted using the multitube prediction technique to: 1) verify the predicted trends established in Phase I of the study, and 2) define the most effective area ratio and tube number combinations for incorporation into the multitube/annular plug nozzle configurations under consideration.

Figures 119 and 120 show a comparison of the ratio of merged jet velocity to jet core velocity, V_m/V_j, with area ratio and tube number, respectively. The V_m/V_j ratio is an indication of the tube spacing and length of supersonic core interaction. The figures indicate that increasing area ratios decreased V_m/V_j from 0.78 to 0.55 for all tube numbers. For a constant area ratio, the effect of varying tube number had little effect on the V_m/V_j ratio.

Peak PNL of the merged jet and that attributed to the individual tubes is plotted as a function of area ratio for different tube numbers in Figure 121. "Optimum" area ratios were obtained for each number of tubes based on intersections of merged jets with the sum of the jets from the individual tubes. These area ratios are seen to form a smooth locus of points as shown in Figure 121. The peak suppression attainable occurs at optimum area ratios for the given number of tubes at the design-point ideal jet velocity of 2485 ft/sec. The total PNL from the sum of the merged jets with the individual jets yields a similar locus of area ratios for any number of tubes at the cycle conditions investigated. These results are shown in Figure 122.

At area ratios between 2.7 and 3.2, varying the tube number from 55 to 100 (Figure 122) changed the level of suppression by only 2 dB. These predicted trends were substantiated by numerous model tests conducted with multitube suppressors.

Selection of acoustically optimum area ratio and tube number was tentatively confined to a range of AR_d's from 2.7 to 3.1 with the tube numbers varying from 55 to 80.

Conclusions reached from the Phases I and II acoustic parametric studies are as follows:

1) The multitube prediction technique yielded suppression levels in close agreement with experience.

2) Trends established in the Phase I studies did not change appreciably in Phase II.

    •   Optimum area ratio range was defined between 2.6 to 2.8 for the design condition specified ($V_j \sim 2500$ ft/sec, $P_{T8}/P_o \sim 3.0$).

    •   Tube numbers (N_t) of 61-72 yield the same ΔPNL values at an area ratio of 2.8.

    •   Locus of optimum multitube area ratios (AR_d) is nearly linear over the range of AR_d's and N_t's considered.

Multitube Aerodynamic Performance Studies - To support the multitube plug suppressor nozzle design selection, parametric aerodynamic performance studies of multitube nozzles were conducted over a wide range of variables. Key parameters included area ratio, tube number and length, angle of inclin-

164

Figure 120. Effect of Tube Number on Merged Jet to Jet Core Velocity Ratio.
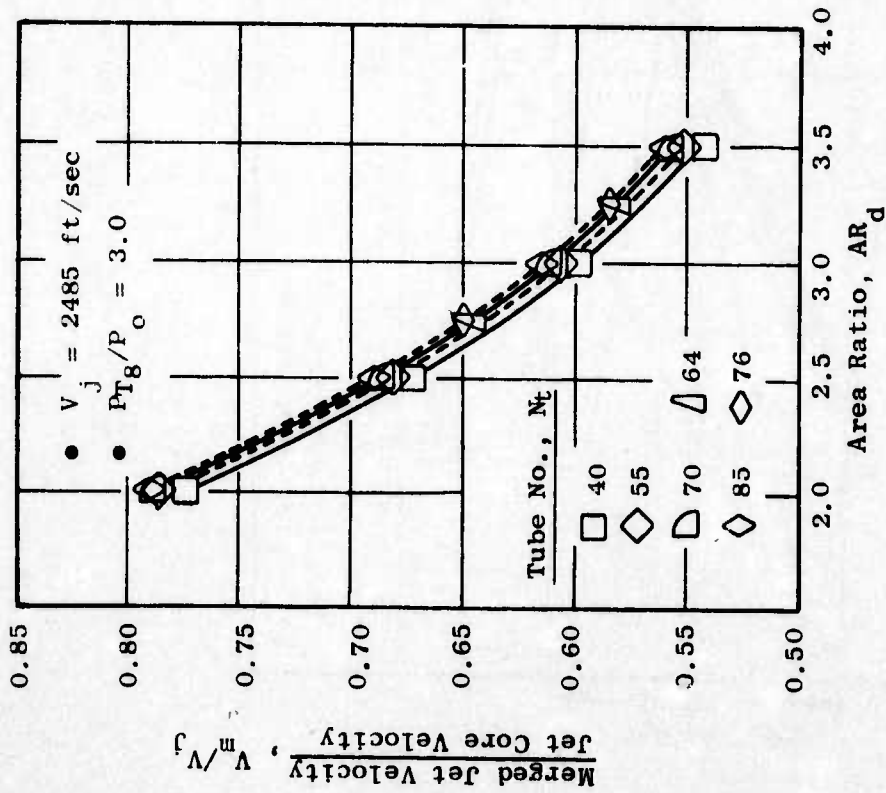
Figure 119. Effect of Area Ratio on Merged Jet to Jet Core Velocity Ratio.

165
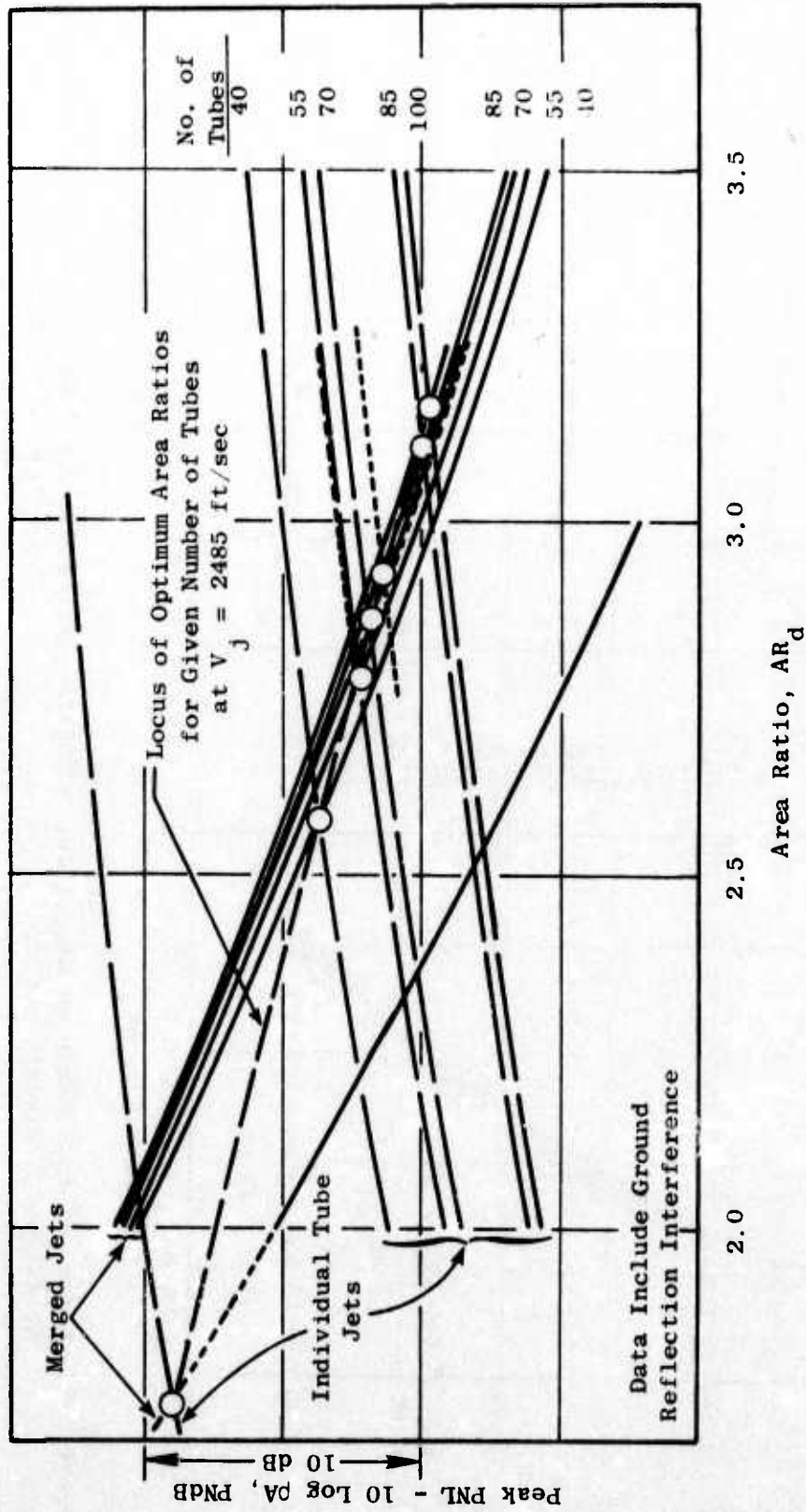
Figure 121. Phase I Multitube Prediction Results, Peak PNL.

166
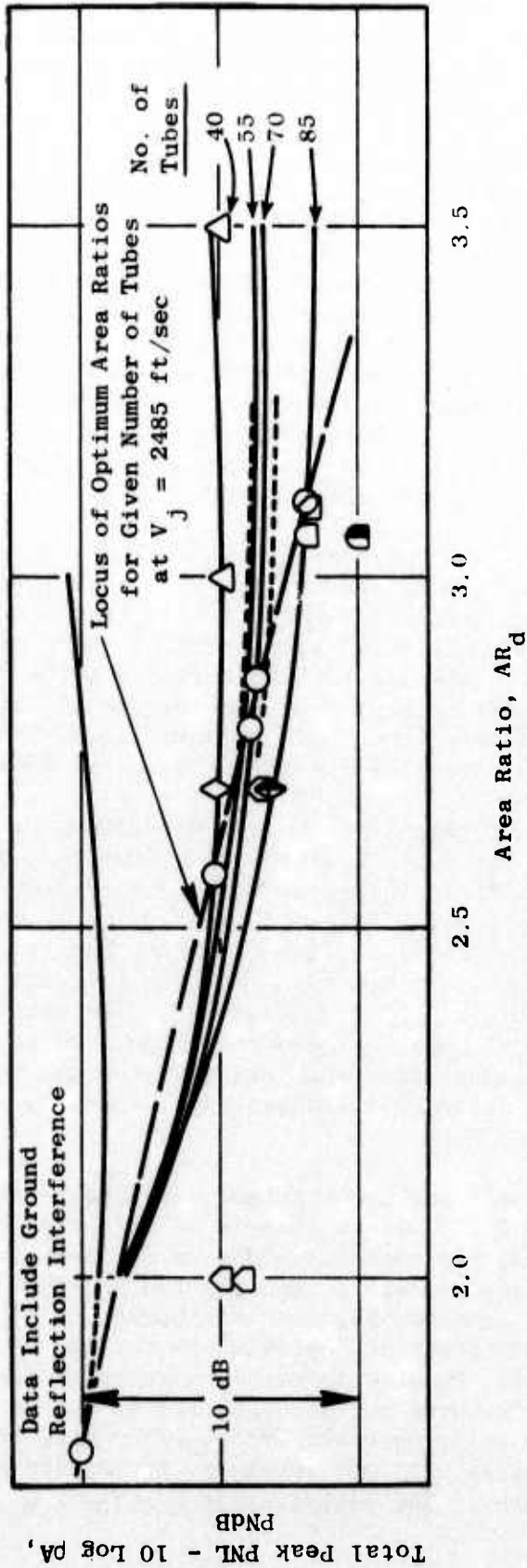
Figure 122. Phase I Multitube Prediction Results, Total PNL.

167

ation of base plate and tubes, and tube spacing. Aerodynamic performance penalties for the suppressors were based on internal losses, consisting of tube entrance and friction losses, and external losses consisting of pressure and friction drag.

During Phase I of the program, static performance tests were run on a large number of multitube noise suppressor designs. In general, the single most significant thrust-loss mechanism was the pressure drag on the base area of the suppressor. This pressure drag, in terms of average base pressure, proved to be a function of several parameters, namely, tube length and spacing, tube exit stagger angle, nozzle pressure ratio, and tube diameter relative to total exit area. Figure 123 illustrates these various parameters. It should be noted that all the previous configurations tested by GE had tubes arranged such that all tubes were equally spaced from adjoining tubes, thus yielding a hexagonal-type array. These data were used to analyze the effect of the above-named parameters, but it has been demonstrated that the tube arrangement also affects the level of the base pressure.

The average base pressures for a large number of test configurations were correlated against the key model parameters, as shown in Figure 123. The correlation parameter, $[S^2 + (L/\cos\theta)^2] / A_8$ is an indication of the amount of base ventilation area available with respect to the nozzle area. The existing data are seen to collapse quite well for lines of equal nozzle pressure ratio, noting that some degree of inaccuracy is expected simply due to the nature of the base pressure calculation which consists of integrating test pressures over a calculated base area.

Other significant loss mechanisms are tube internal friction and the sudden contraction of the flow from the upstream flowpath into the tubes. Because these losses could not be readily measured in a test, the effect of varying parameters was studied using semiempirical methods. Tube skin friction was analyzed using turbulent boundary layer theory and average skin friction coefficients. The skin friction is a function of tube length, diameter, and flow Mach number. The entrance loss was calculated using classical empirical sudden-contraction loss factors and was dependent on contraction area ratio and upstream and downstream Mach numbers. Examples of the parametric evaluation of these two losses are shown in Figures 124 and 125.

Combining these primary loss mechanisms in terms of thrust coefficient, Figure 126 shows an example of this type of parametric study. Based on these studies, two configurations were chosen for test. The first configuration, designated Model 1, incorporated all the features shown to be advantageous from a combined aeroacoustic basis during the parametric studies, thus giving an upper limit of "optimum" to the state-of-the-art multitube suppressor concept. Model 2 incorporated many of the desirable suppression and performance features but also sacrificed others in an attempt to produce a mechanically workable system. The main item compromised was the hexagonal tube array. It was necessary to utilize a more radial array in order to stow the tubes. The radial configuration lowered the predicted suppression

168
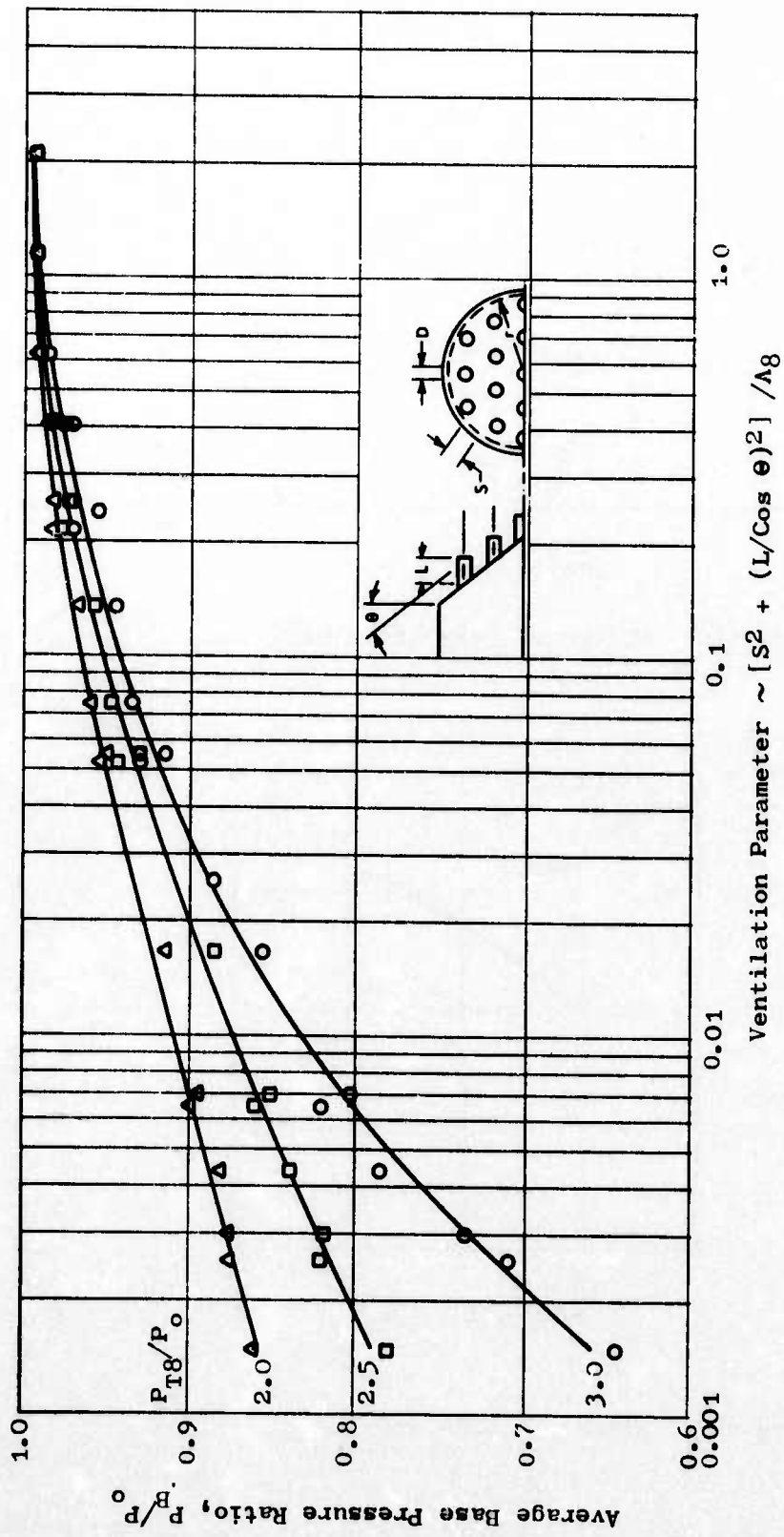
Figure 123. Multitube Base Pressures at Mach No. = 0.
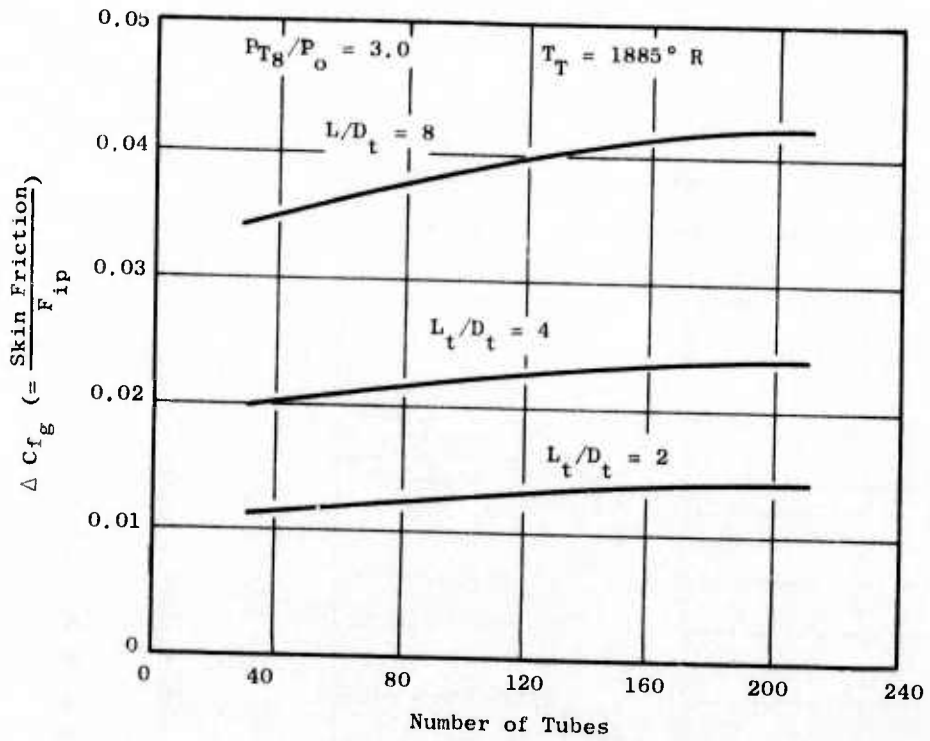
Figure 124. Effect of Skin Friction.
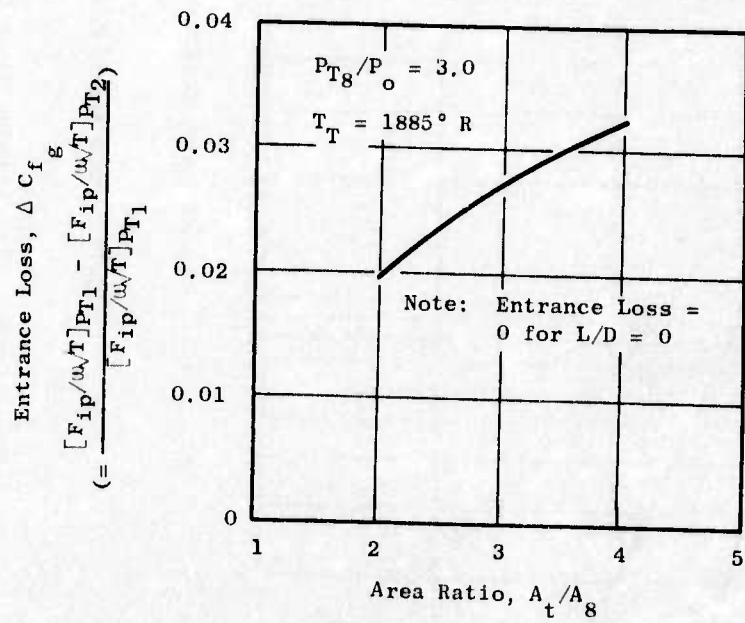
Figure 125. Effect of Entrance Loss.

170
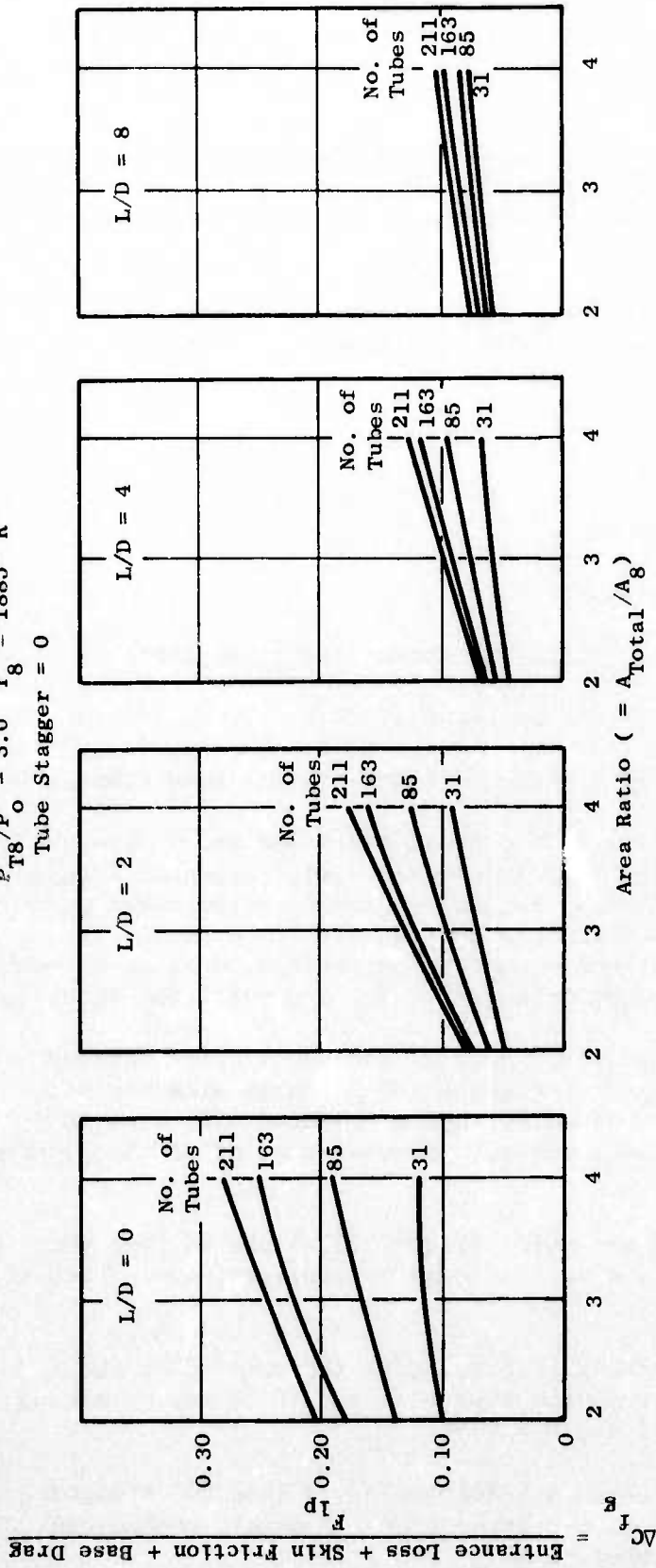
Figure 126. Combined Effects of Entrance Loss, Skin Friction, and Base Drag.

effectiveness by several dB. Additional mechanical studies may permit stowage of a more evenly spaced tube arrangement; but, for this test, an existing design was used.

Aeroacoustic Trade Studies on Nozzle Geometric Features - Design selections of 72 and 66 tubes at an area ratio of approximately 2.8 were chosen as a result of the aeroacoustic parametric studies on multitube suppressor nozzles.

In addition to optimizing the area ratio and number of tubes for the basic multitube suppressor system, consideration also was given to:

- Baseplate stagger

- Tube exit plane stagger

- Tube length-to-diameter ratio

- Tube orientation (cant angle)

- Tube exit configuration (plain, Greatrex, and convergent)

- Tube size and spacing (equal to unequal)

- Estimating the effect of a plug centerbody in the tube cluster

Noise estimates of these parameters on the basic multitube array were obtained from available test data. Acoustic-aerodynamic trades were made on each of these parameters using similar estimates made on aerodynamic performance. The final result was to obtain the best available aeroacoustic $(\Delta PNL/\Delta C_{fg}$ trade-off estimates of the geometric parameters in order to combine them with the optimum area ratio and tube number for the multitube suppressor.

The tube cant angle variation (Figure 127a) was empirically derived from multispoke data which showed that canting the blockage elements aft, relative to the nozzle exit outer diameter, had a positive effect on the PNL suppression but caused increased losses. Forward canting of the elements had the opposite effect.

The tube exit plane stagger variation (Figure 127b) showed that the least change in thrust loss for a given increase in suppression was between exit angles of 30° to 0°.

The variation of the tube number (Figure 127c) indicated that the predicted maximum suppression occurred with approximately 70 tubes, resulting in a corresponding thrust loss of about 0.065.

The base stagger variation (Figure 127d) indicated that 60° stagger angles were most beneficial from a ΔPNL standpoint. However, mechanical considerations dictated a compromise to 45°.
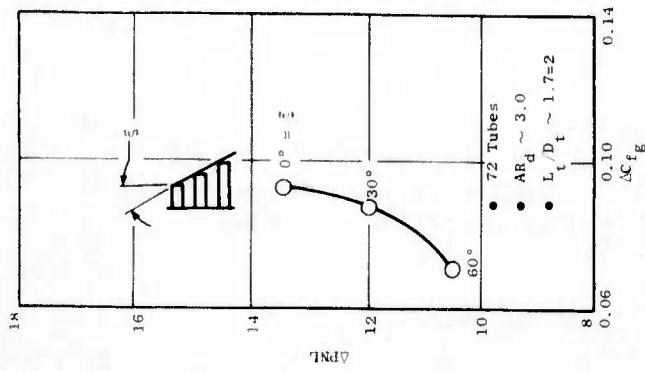
172
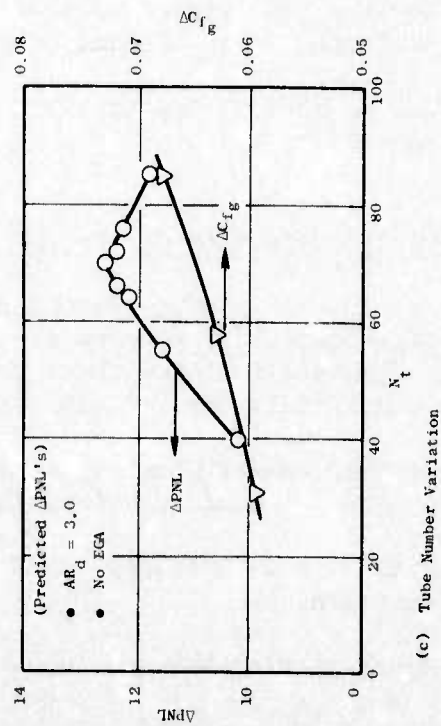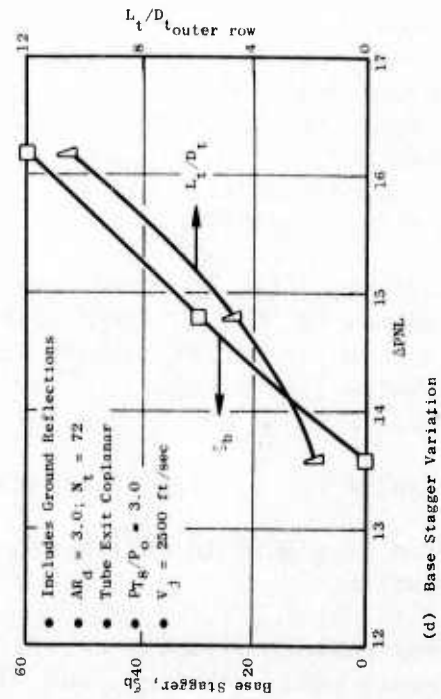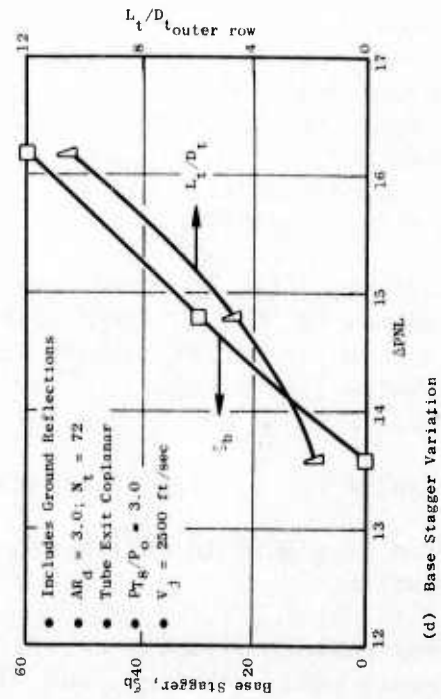
Figure 127. Multitube $\Delta PNL/\Delta C_{f_g}$ Trade-offs.

With the trade-offs completed on the multitube suppressor configuration
without the plug, the final step was the selection of the best plug centerbody
design. The selection of the optimum plug design for the multitube suppres-
sors was decided upon from a search of available literature on unsuppressed
and suppressed plug nozzles. A limited amount of multitube/annular plug data
were available (acoustic only) from some early (1967) model testing. The
conclusions reached from the plug-design selection survey indicated that the
maximum acoustic benefit could be achieved using a plug with a 20° cone angle
(10° half angle), a short plug extension, and a blunt (not full conical) end.
Mechanical considerations would employ a 30° cone angle (15° half angle) but
would otherwise be similar.

A review of available literature (References 13 and 14) was conducted to
gain information on the PNL suppression effects of annular plug nozzles
relative to an unsuppressed conical nozzle. Aerodynamic wind-on performance
tests (Reference 1) had shown the unsuppressed plug nozzle to yield
attractive C_{fg}'s (0.981 at $M_O = 0.36$).

The results of the literature search revealed that:

- The plug aids in suppression (0.5-3 dB) relative to a conical
  nozzle.

- For maximum acoustic benefit, use a plug with a 20° cone angle,
  short plug extension, and blunt (truncated) end.

- Shallow plug angles provide favorable aerodynamic effects - less
  projected area, reduced drag.

- For mechanical feasibility, use a plug with a 30° cone angle -
  reduces length.

Design Selection of 72- and 66-Tube/Annular Plug Nozzles

Using the design studies described in the preceding paragraphs, prelimi-
nary $\Delta PNL/\Delta C_{fg}$ trade-offs were made. The purpose was to define "optimum"
aeroacoustic geometric values which could be mechanically designed and
applied to a multitube annular plug system.

A multitube/annular plug suppressor initially considered is shown in
Figure 128. The geometric constraints were as follows:

- Shallow plug cone angles of 20° or less (dependent on mechanical
  restraints)

- Equal spacing between tubes

- Canted tube rows of less than 10°

- High base stagger angles of around 60° with coplanar tube exit

174

Figure 128. Sketch of Initial Multitube/Annular Plug Suppressor Configuration.

- $N_t = 72$, $AR_d = 3.0$
- $A_8 = 2014$ in.^{2} (Full-Scale)
  Plane 8

175

- L_t/D_t of four or more in outer row

- Area ratio, $AR_d = 3.0$ at exit plane

- Tube number, N_t, around 70

These initial trade-offs and limitations were further refined, and mechanical feasibility restraints were set.

The final selection of the multitube/annular plug suppressor configurations was based on two considerations. The first was acoustic/aerodynamic technology; the intent was to build and test a multitube/annular plug nozzle system to establish a benchmark of aero/acoustic ($\Delta PNL/\Delta C_{fg}$) performance (upper limit) for this type of suppressor system. The suppressor would employ the best trades of aeroacoustic parameters determined from predicted results and trends of empirical data. Mechanical feasibility would be investigated in the model design but would not be restrictive.

The second consideration was the mechanical feasibility of the multitube/annular plug system. Using current mechanical technology, the aeroacoustic estimates were relaxed slightly in order to define a multitube/annular plug system that would establish a second benchmark - a level of $\Delta PNL/C_{fg}$ for a multitube/annular plug nozzle with engine application. Based on this nozzle selection rationale, the multitube/annular plug nozzle configurations were fabricated.

Multitube/annular plug suppressor Model 1 contained 72 tubes (~3 rows) in a modified hexagonal array around a plug with a 20° included angle. The tubes were mounted in a 45° staggered baseplate with a coplanar tube exit. The inner and outer rows were canted ±5° (toward plug; away from plug) forming an area ratio of 2.95 at the exit plane. Convergent tube ends were provided for the outer two rows of tubes. The inner row had plain ends.

The second suppressor configuration, Model 2, contained 66 tubes (3 rows) in a pattern which would allow the tube bundle to be collapsed and stowed in a plug centerbody with a 30° included cone angle. This resulted in non-uniform spacing of tubes and a non-coplanar tube exit. The tubes, mounted in a 45° staggered baseplate, were parallel; the outer row was provided with convergent tube ends (inner rows had plain ends) which gave an area ratio of 2.7 at the exit plane.

3.2.3.2 72-Tube and 66-Tube/Annular Plug Suppressors

Acoustic Tests

The acoustic tests were conducted on the JENOTS hot-flow stand over a range of test conditions simulating a J6H2 engine operating line with ideal jet velocities varying from 1250 to 2930 ft/sec and nozzle pressure ratios ranging from 1.50 to 3.90. Figures 129 and 130 show multitube Models 1 and 2 installed on the JENOTS facility.

176
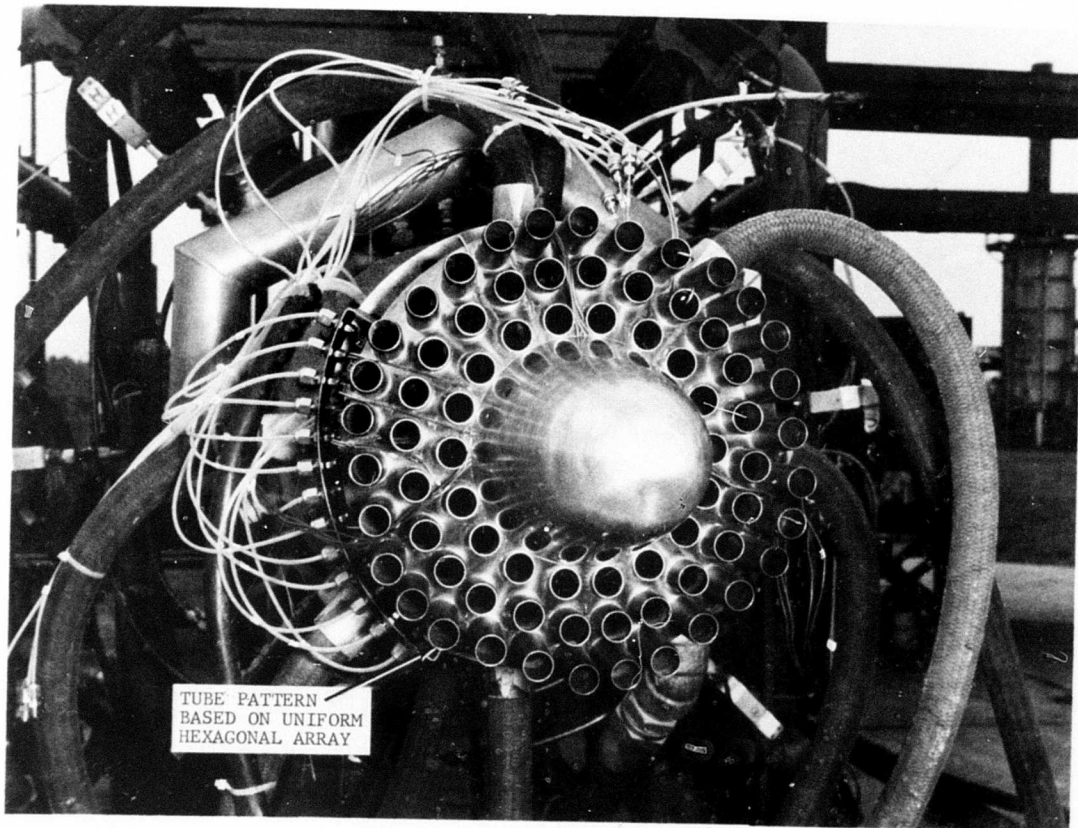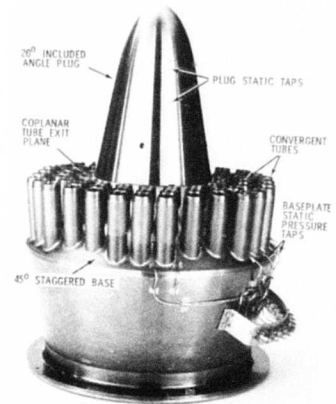
Figure 129.   72-Tube/Annular Plug Suppressor Model 1 at JENOTS (Area Ratio = 2.95).
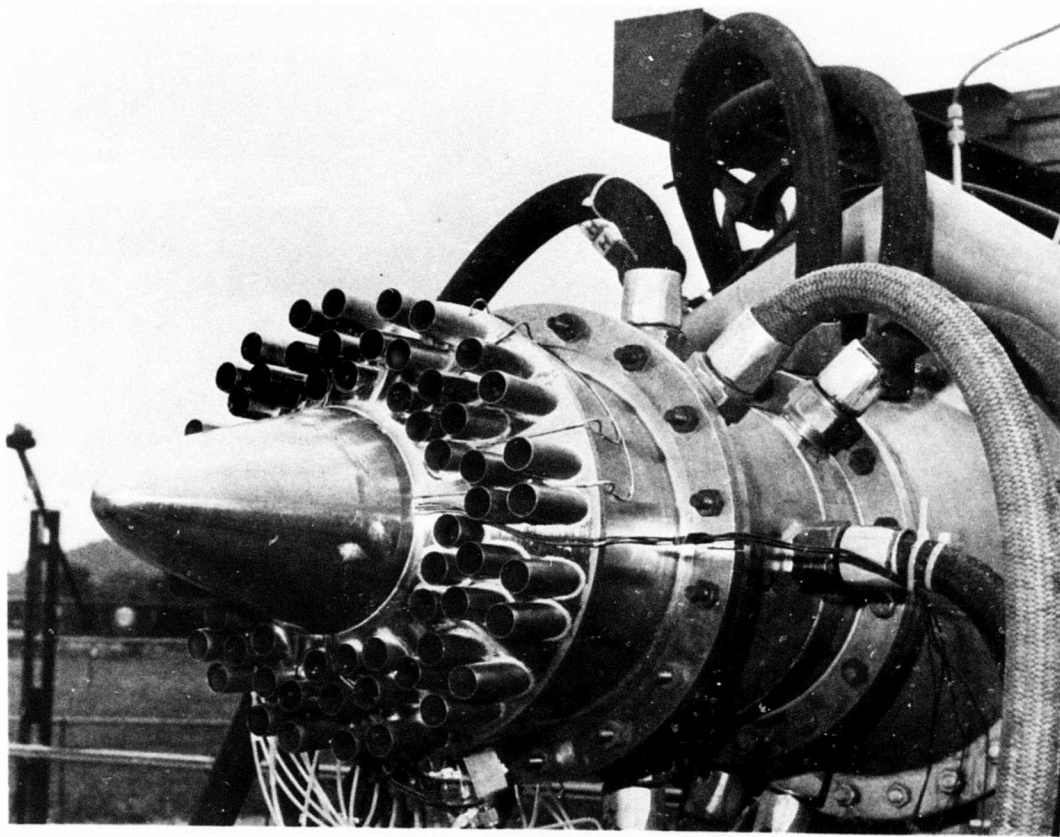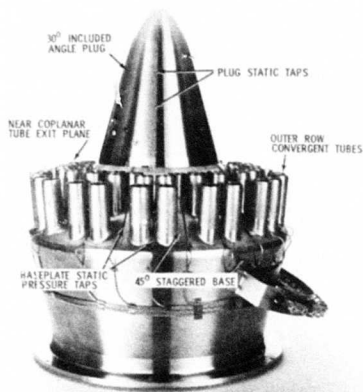
Figure 130. 66-Tube/Annular Plug Suppressor Model 2 at JENOTS (Area Ratio = 2.7).

178

Acoustic Results and Analysis

The acoustic data obtained from tests of the two multitube/annular plug suppressors and unsuppressed conical baseline nozzles were scaled by frequency and size to full-scale application using a scale factor of 8:1. All data presented in this section are, therefore, of simulated engine size and frequency range. Tabulations summarizing the acoustic results, at the conditions tested and for each configuration tested, are contained in Appendix C.

The results of the multitube/annular plug test series are presented as individual plots of normalized peak PNL at 300-, 1500- and 2128-foot distances, PNL directivity at the 2128-foot distance, and plots of 320-ft-arc spectral directivity at the design jet velocity ($\sim$2500 ft/sec) for the conical baseline and each of the two multitube models.

Comparison plots of the 2128-foot distance normalized peak PNL for Models 1, 2, and the conical nozzle are shown in Figure 131. The results show only about 1 dB difference between Models 1 and 2 over a velocity range from 2200 to 2950 ft/sec with little or no difference at lower velocities. Suppression levels relative to the conical nozzle also were about the same, 12 to 13 PNdB at V_j $\sim$2500 ft/sec, suggesting that the acoustic floor might have been reached.

Spectral comparisons of the multitube Models 1 and 2 along with the conical nozzle are shown in Figure 132. These results show no appreciable spectral differences between the Models 1 and 2 over the entire velocity range, within the limits of data measurement accuracy. The PNL directivity plots, Figure 133, show no significant differences between the two models.

3.2.3.3 66-Tube/Annular Plug Nozzle with Ejector

Part of the jet noise reduction task effort was to evaluate the effects of hardwall and treated ejectors on selected suppressor nozzles. A conical ejector shroud was designed, fabricated, and acoustically tested on the 66-tube nozzle mounted on the JENOTS facility. The purpose of the test was to see if additional suppression gains could be achieved by the use of an acoustically lined ejector nozzle over the 66-multitube/annular plug nozzle system. The 66-tube nozzle was selected for this test since it had achieved a higher level of aerodynamic performance (to be discussed later) than the 72-tube, and because the 66-tube design was more mechanically feasible.

Ejector Design

The conical ejector nozzle designed for this test was selected to be used on both the 66-tube and 36-chute nozzles (see Section 3.2.2). The design intent of this particular suppressor was that the ejector system was to induce a sufficient amount of secondary air to enhance mixing and improve the nozzle base pressurization. A bellmouth inlet was employed with the ejector to simulate the "ram" effect while undergoing static acoustic tests.

179
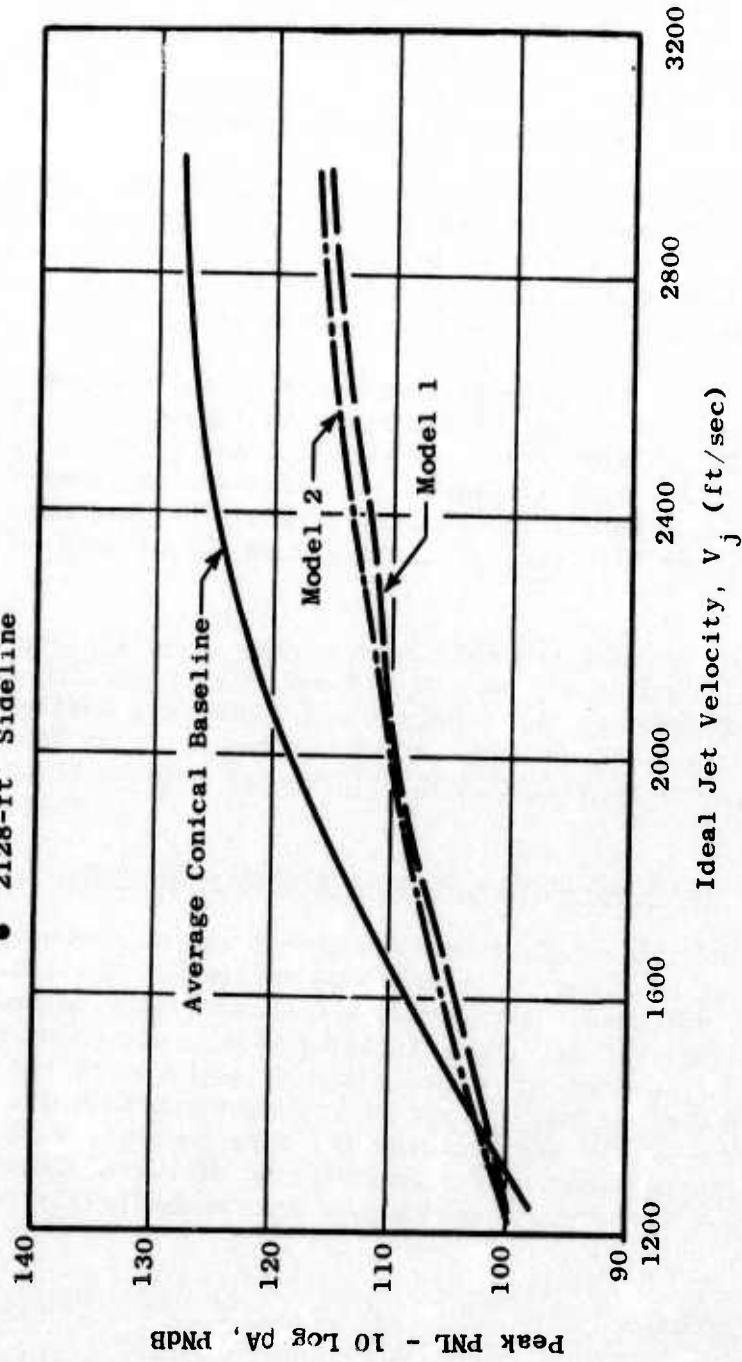
Figure 131. Peak PNL Comparisons of Multitube/Annular Plug Nozzle Models 1 and 2.

180
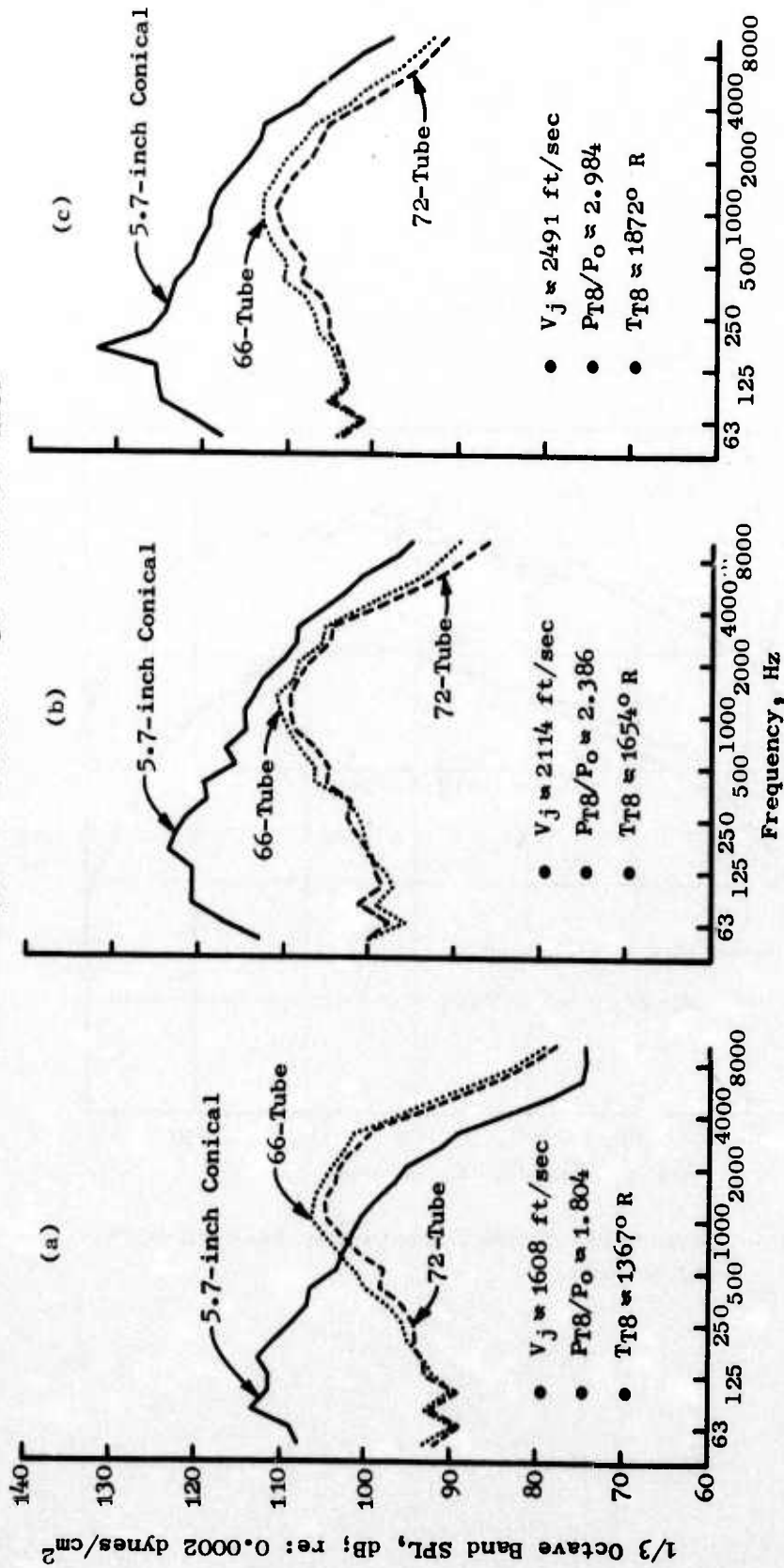
Figure 132. Peak Angle SPL Spectra Comparisons.

181
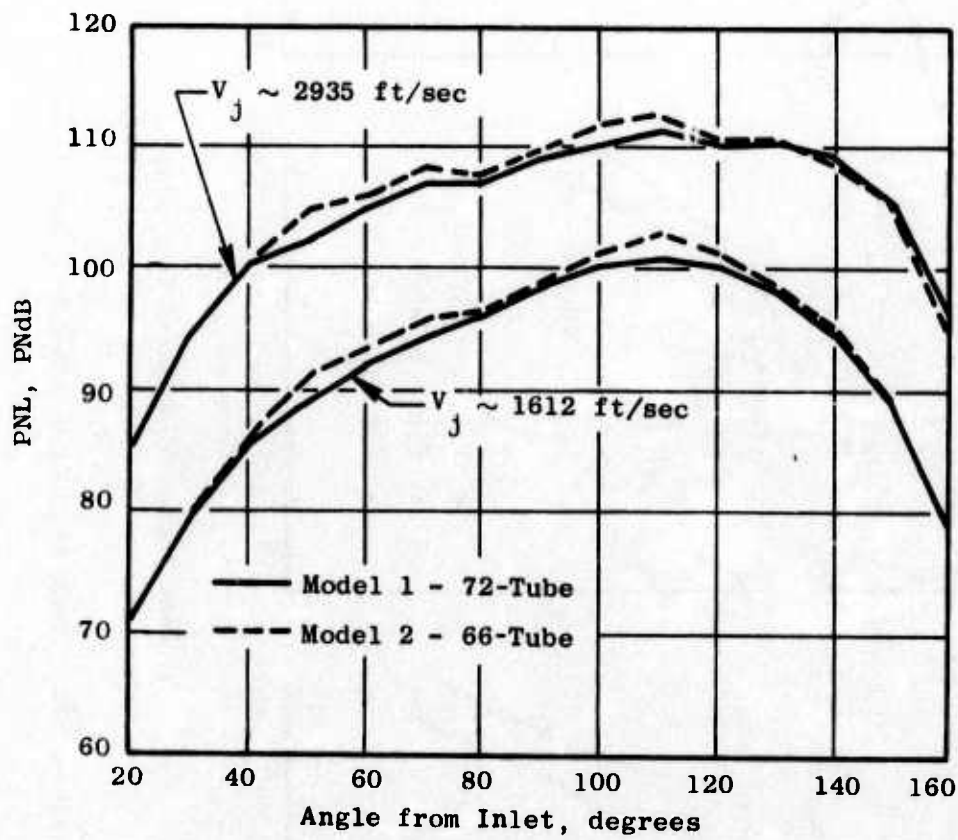
Figure 133. Comparison of PNL Directivity Between Multitube Suppressors.

182

Acoustic treatment used in the ejector was specified and designed as described in Section 3.2.2.

Acoustic Tests

The acoustic tests were conducted on the JENOTS hot-flow stand over the same test conditions previously described. Configurations tested included the 66-tube nozzle with hardwall and treated ejector. Figure 134 shows the model set up on the JENOTS facility.

Acoustic Results and Analysis

A summary of the acoustic test results for each test along with the test conditions is included in Appendix C.

The 66-tube/annular plug suppressor results with the hardwall ejector shown in Figure 135 indicate little or no suppression gain with the hardwall ejector. Scrubbing of the ejector wall with the hot primary flow was apparent along the aft half of the ejector length. This effect (which is believed to be due to the axial orientation of the tubes) may have been the cause of the minimal suppression effectiveness.

The SPL spectral comparisons illustrated in Figures 136a, b, and c show little difference between the 66-tube with and without hardwall ejector. This is true even for the high frequency (low wavelength) region where one would expect to get some reduction due just to the physical shielding aspects of the ejector.

The results of the treated ejector tests with the 66-tube suppressor, as shown in Figure 137, indicate approximately 2 dB suppression gain relative to the hardwall and suppressor alone at the velocities below 2000 ft/sec. No suppression difference was apparent among the three configurations at the higher jet velocities, (>2200 ft/sec).

The SPL spectra in Figure 138 for the 66-tube with hardwall and treated ejector show little difference between hardwall and no ejector. Apparent scrubbing of the primary flow on the ejector wall caused by the outward cant of the outer row of tubes may have been responsible for the neglegible suppression effect of the hardwall and treated ejectors at the higher velocities (>2200 ft/sec).

Aerodynamic Performance Tests

The static performance tests of the multitube models were performed in the Channel 12 static thrust stand at FluiDyne Engineering Corporation's Medicine Lake Laboratory. In addition, cold-flow testing was conducted at JENOTS to assess the effect on baseplate pressure due to the installation of an ejector shroud.

183

HARDWALL EJECTOR #2

66 TUBE/ANNULAR PLUG SUPPRESSOR
AREA RATIO = 2.7
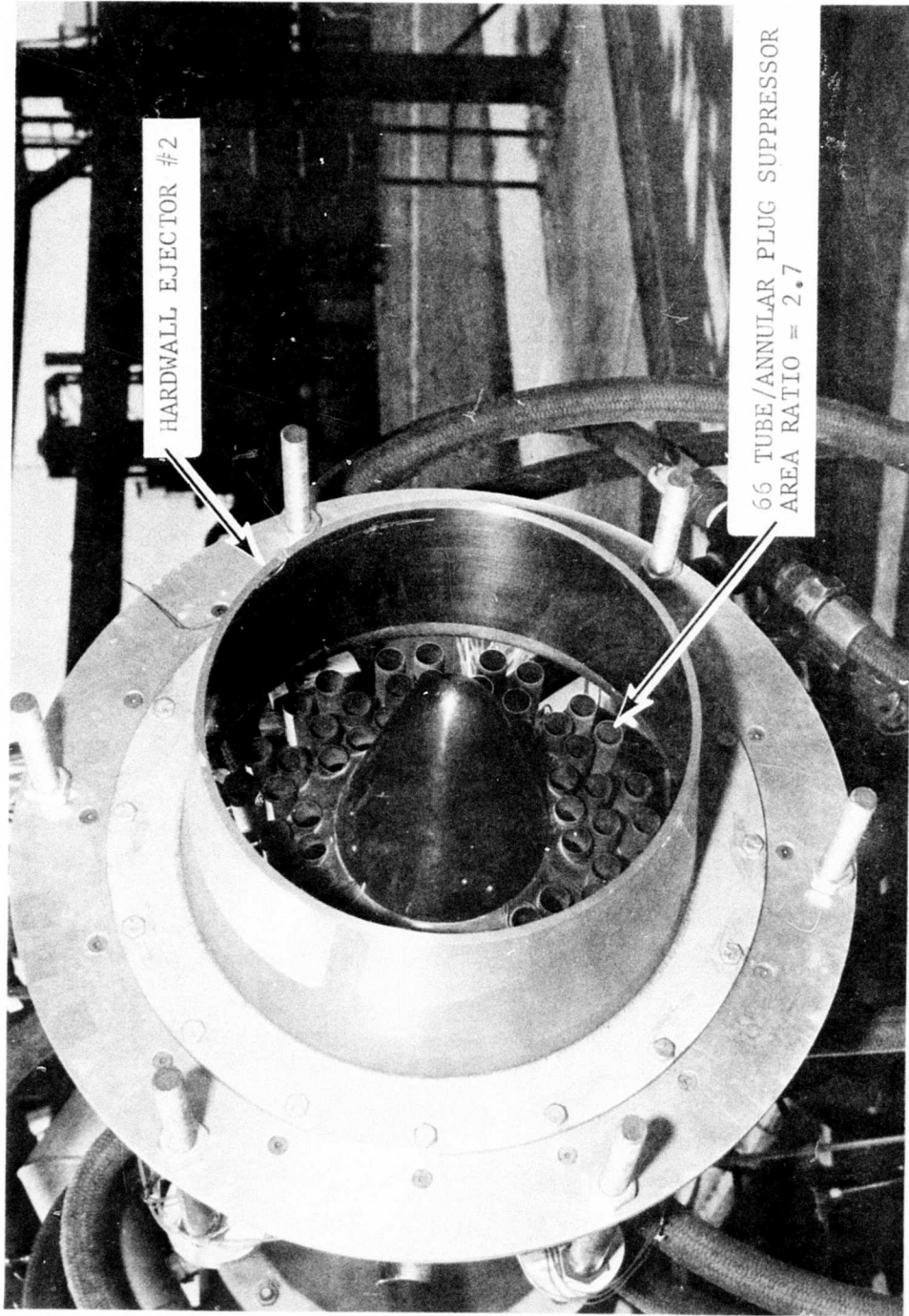
Figure 134. Multitube/Annular Plug Suppressor with Conical Ejector on JENOTS Facility.
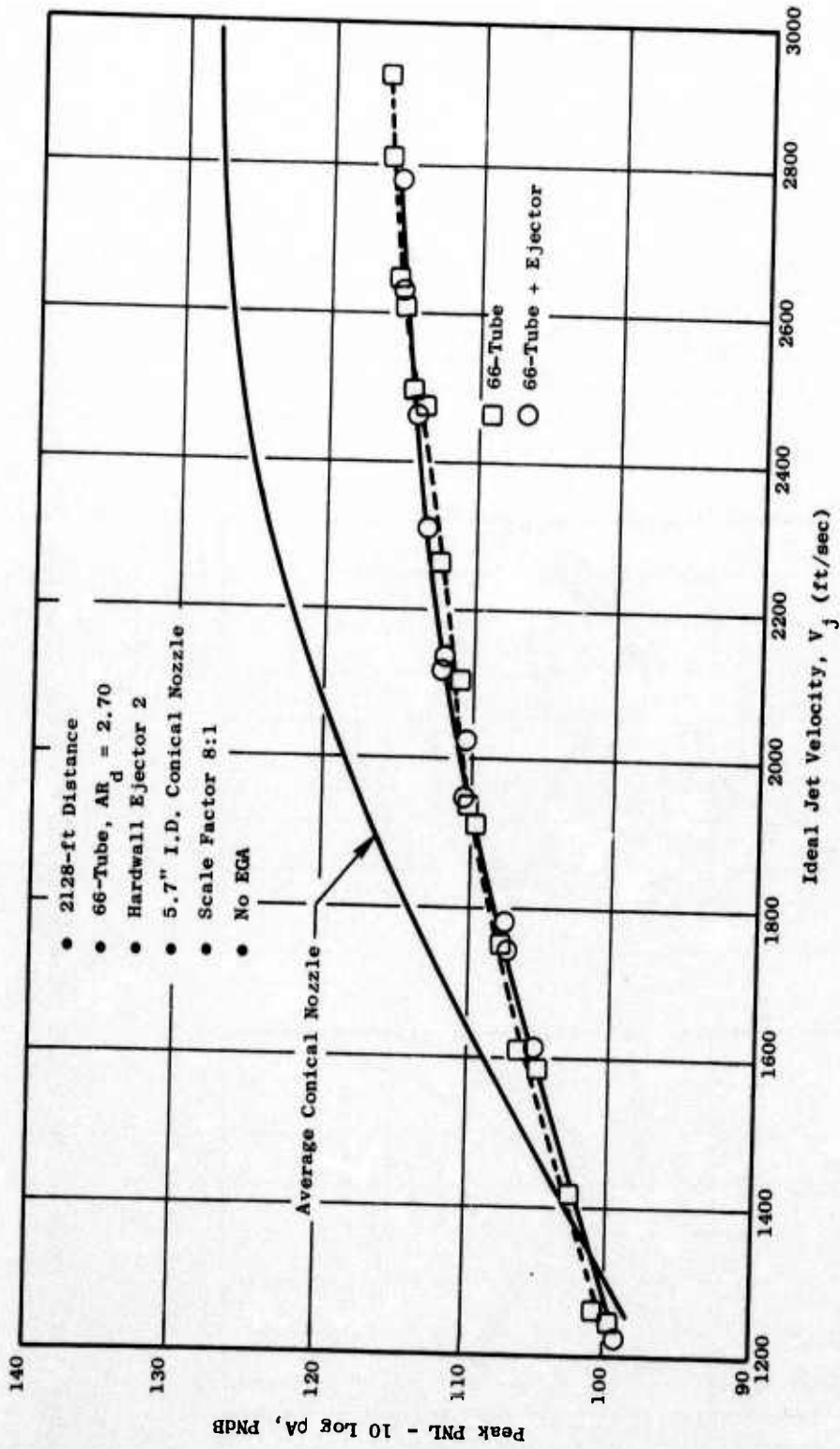
Figure 135. Peak PNL Comparison of Multitube/Annular Plug Suppressor with Teated Ejector.

185

Figure 136. Peak Angle Spectra Comparisons for Multitube/Annular Plug Suppressor with Ejectors.

300-ft Distance

- 5.7-in. ID Conical Nozzle
- 66-Tube and Hardwall Ejector No. 2
- 66-Tube, AR_d = 2.70
- Peak Suppressed Angle = 110° from Jet Inlet
- Peak Angle for Conical = 130° from Jet Inlet
- Scale Factor 8:1
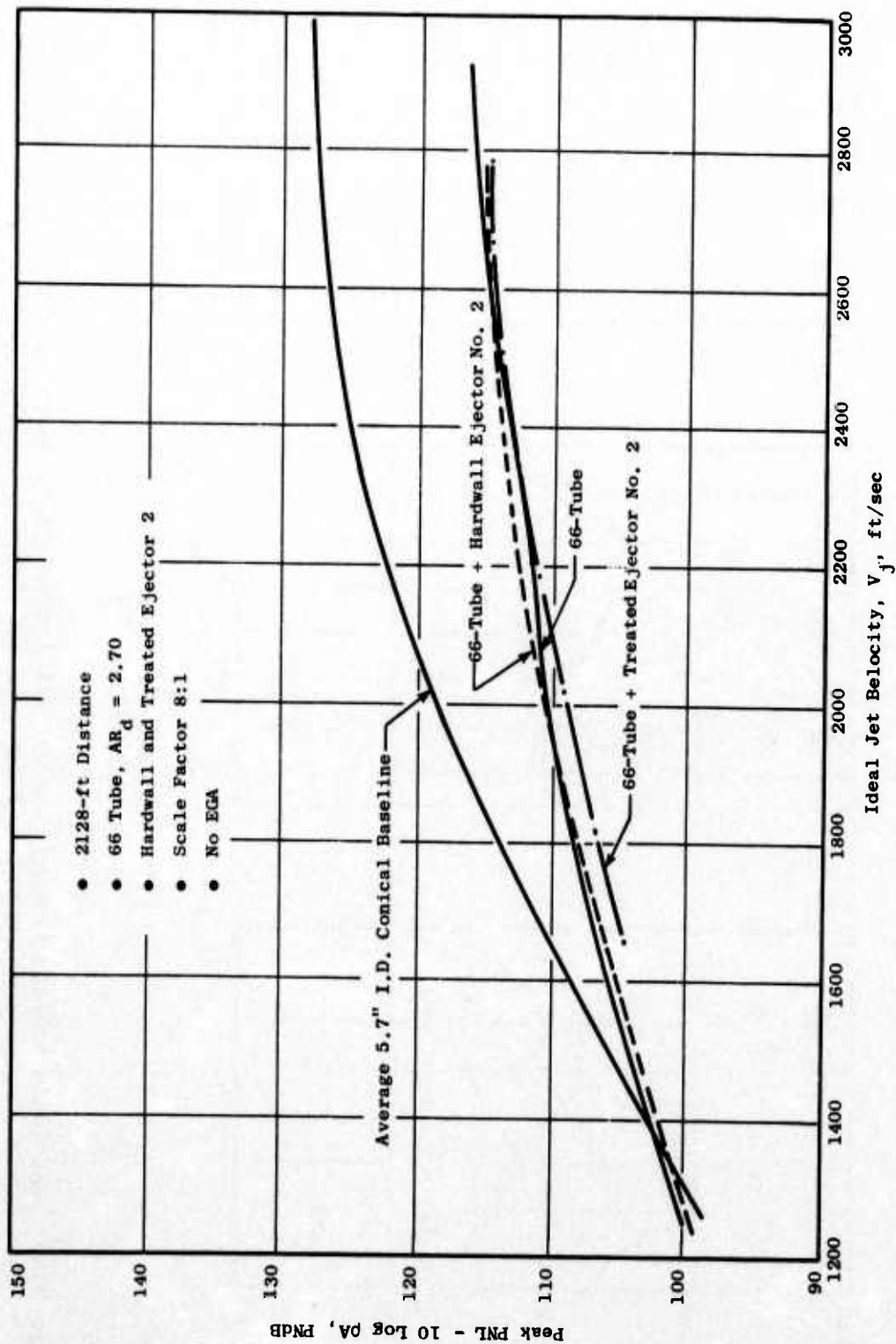
Figure 137. Peak PNL Comparisons of Multitube/Annular Plug Suppressor with Ejectors.

187

- 5.7" ID Conical Nozzle
- 66-Tube and Hardwall Ejector No. 2
- 66-Tube, AR_d = 2.70
- Peak Suppressed Angle = 110° from Jet Inlet
- Peak Angle for Conical = 130° from Jet Inlet
- Scale Factor 8:1
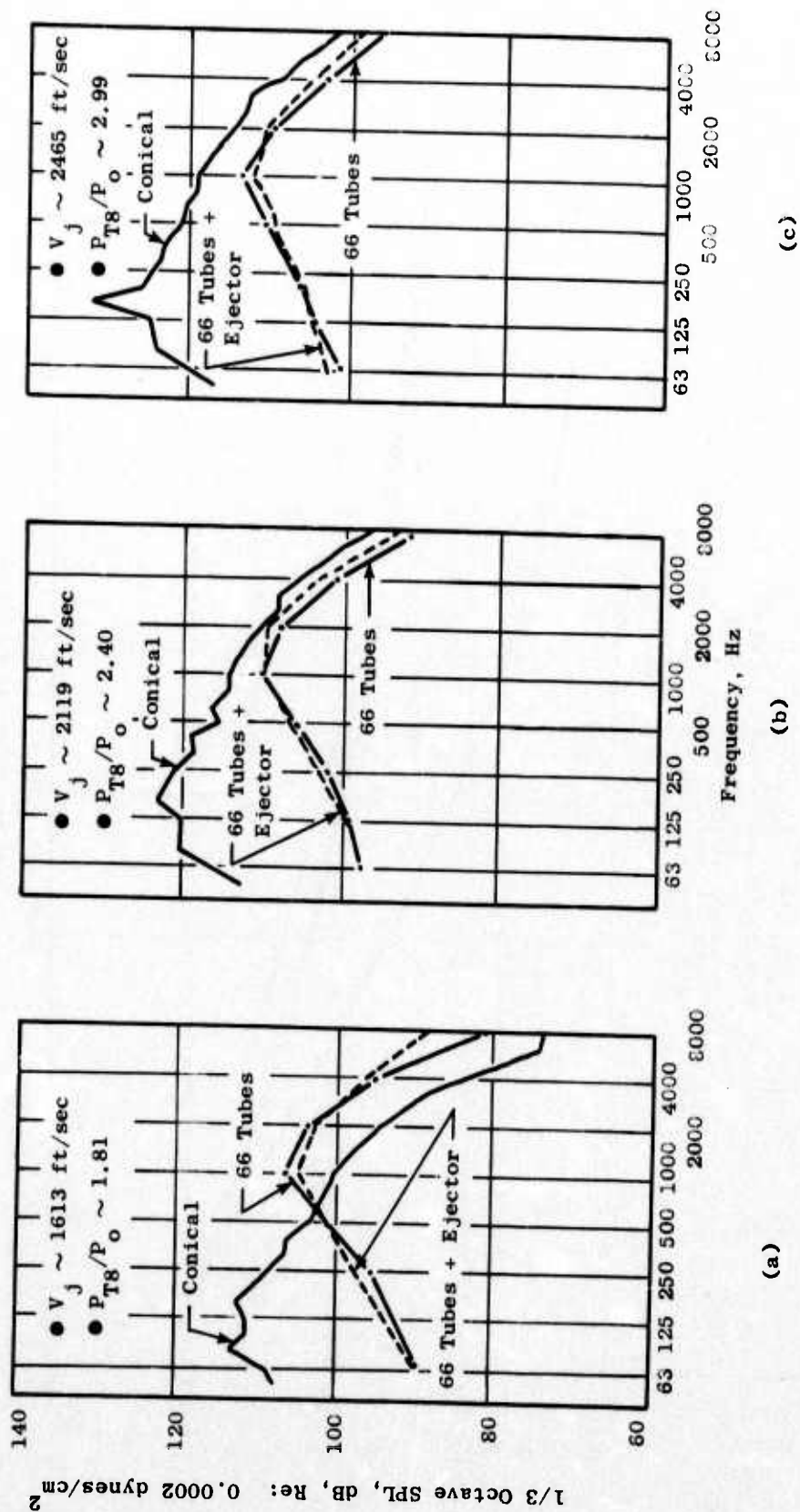
Figure 138. Peak Angle Spectra Comparisons for Multitube/Annular Plug Suppressor with Hardwall Ejector.

188

Assembly drawings of the two test models are presented in Figure 139. Figure 140 shows the model total-pressure instrumentation locations. Instrumentation consisted of static pressure taps on the plug and base plate and total pressure pitot tubes immediately upstream of the nozzle tube inlets and at the exit plane selected tubes.

The physical throat areas of the two models were determined by inspecting each tube exit individually with a hole gage. Two diameter readings 90° apart were made for each tube and then averaged to get the effective diameter. The variations in the two diameter readings for each tube were, in general, very slight; redundant checks on selected tubes proved the readings to be repeatable.

Aerodynamic Performance Results and Analysis

Test results of measured nozzle gross thrust coefficient and flow coefficient are presented in Figure 141. Values of C_{fg} at the take-off operating pressure ratio of 3.0 are 0.898 and 0.911 for Models 1 and 2, respectively.

The primary difference in performance levels between the two models was due to the higher baseplate pressure drag of Model 1 as compared to Model 2. Figure 142 shows both the average baseplate static pressure and the corresponding drag in terms of ΔC_{fg}. These values represent base area of the base plate only, which was instrumented with static pressure taps. They do not reflect additional projected base area which was not instrumented, such as tube lip thickness. Since Model 1 has more of this uninstrumented base area, the true difference in ΔC_{fg} due to base drag is expected to be even greater than that shown in Figure 142.

The increase in average base pressure of Model 2 over Model 1 was caused by the radial type array of Model 2 which allowed more direct ventilation of large segments of the baseplate than did the hexagonal stacking array of Model 1. Both models exhibited circumferential variations in static pressure and, while some of these were averaged out with radially redundant static taps, the pressure integrations should be considered only good approximations.

In order to evaluate any pressure drag on the center plug, both models were instrumented with plug static taps. Model 1 had a 10° half-angle plug and the inner row of tubes were canted downward along the plug in an effort to prevent pump-down of the plug. Model 2 had a 15° half-angle plug, and the inner two rows of tubes exited axially. The resultant average plug static pressures are shown in Figure 143. The Model 2 pressures were lower than those of Model 1, as would be expected, but the drag in terms of nozzle C_{fg} was not a very significant loss for either model. Lampblack pictures of the two models shown in Figures 144 and 145 illustrate differences in flow down the plugs. Model 1 is seen to maintain attached flow down to the tip of the plug while, on Model 2, the entire plug appears to be separated.

189

72-Tube

66-Tube
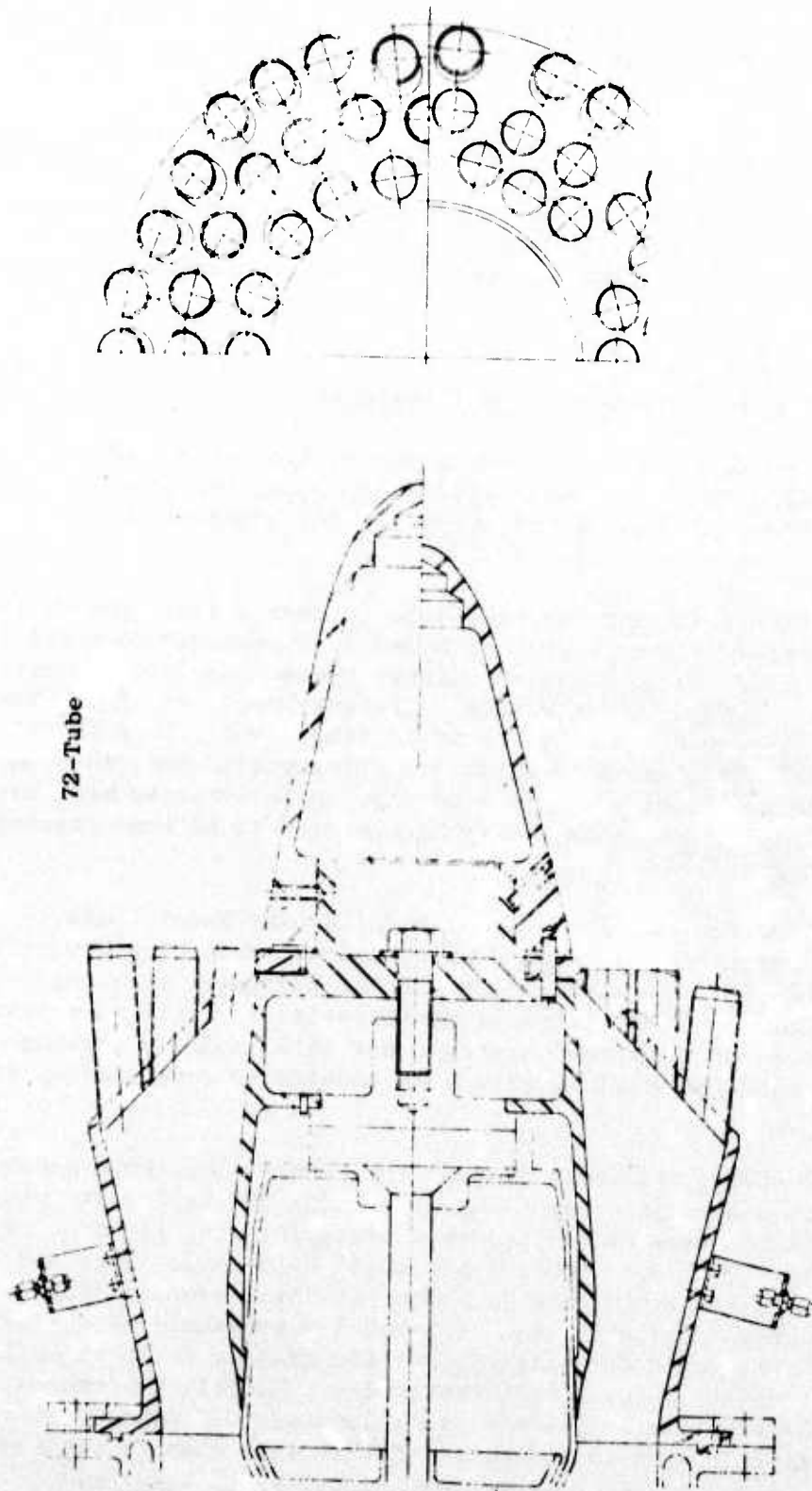
Figure 139. Multitube/Annular Plug Suppressor Schematic.
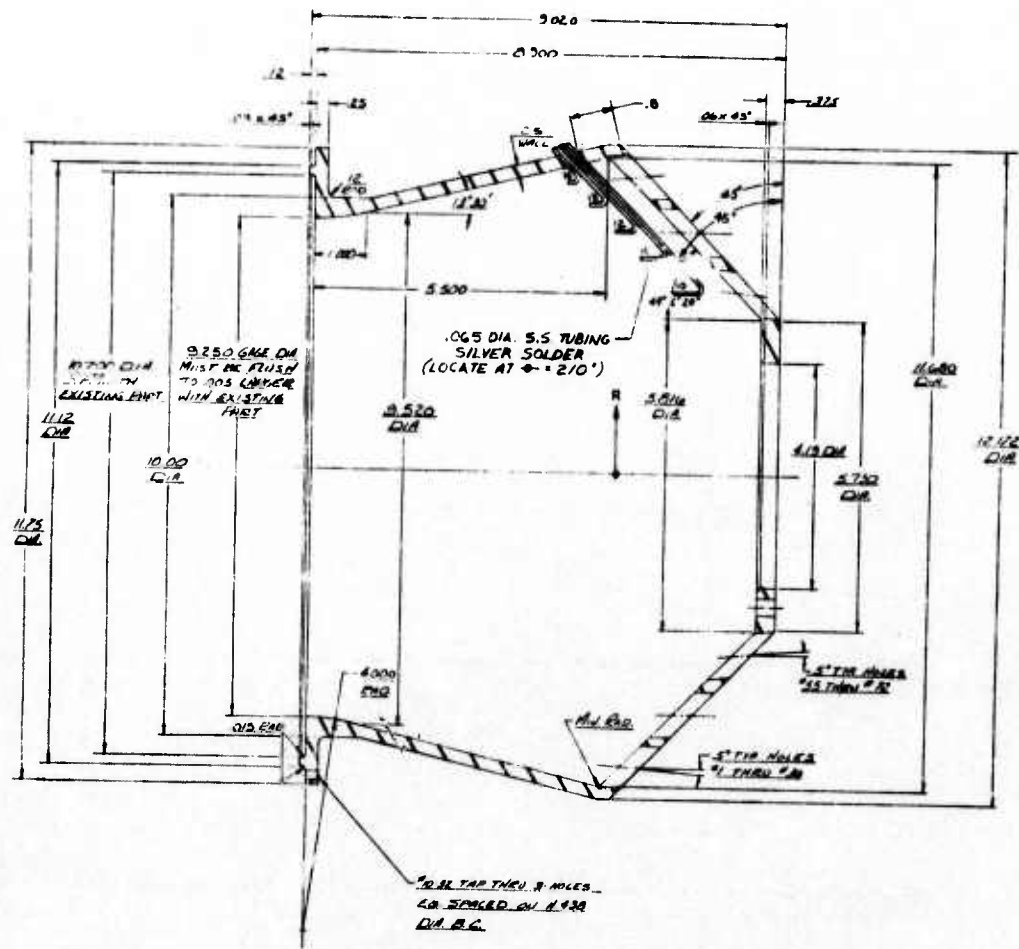
Figure 140. Multitube Suppressor Internal P_T Instrumentation.

191
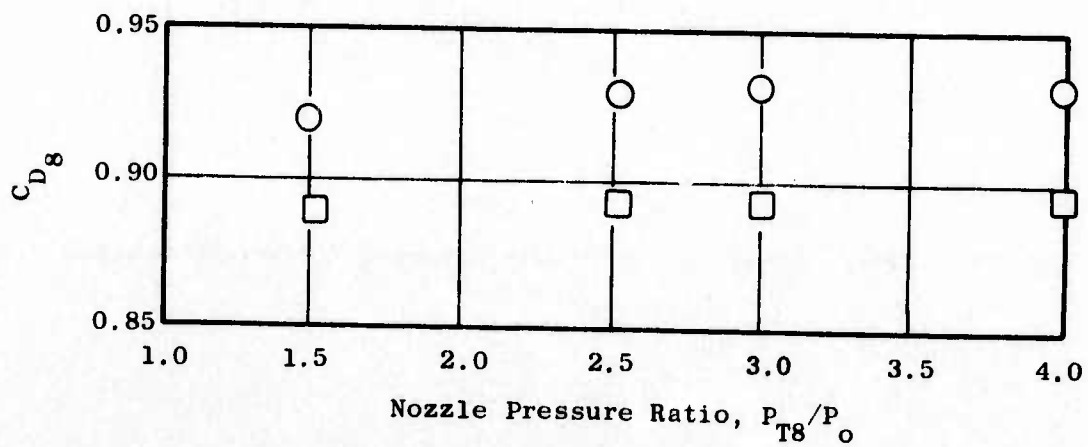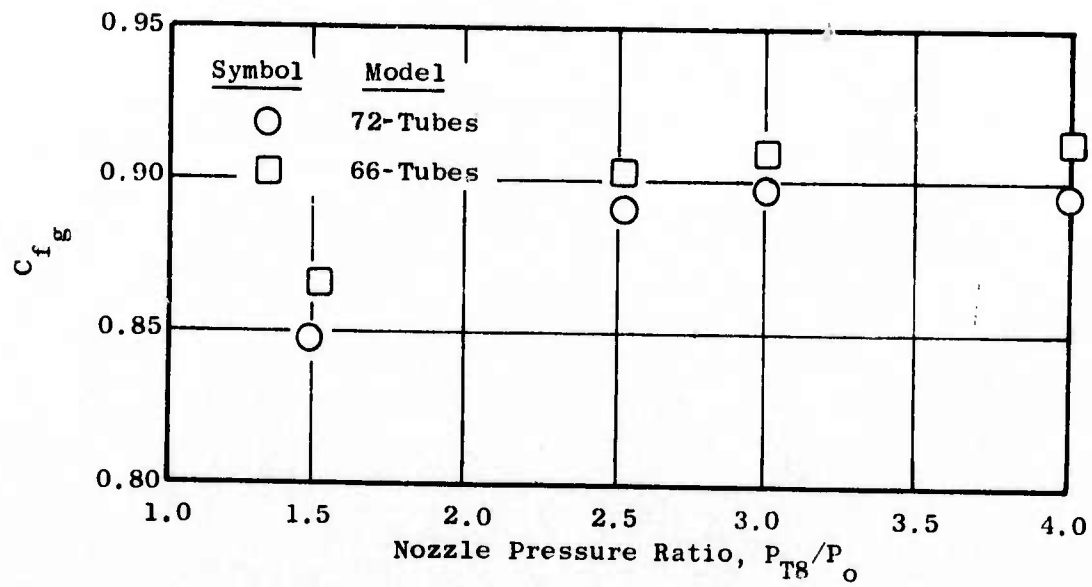
Figure 141. Static Thrust and Discharge Coefficients.
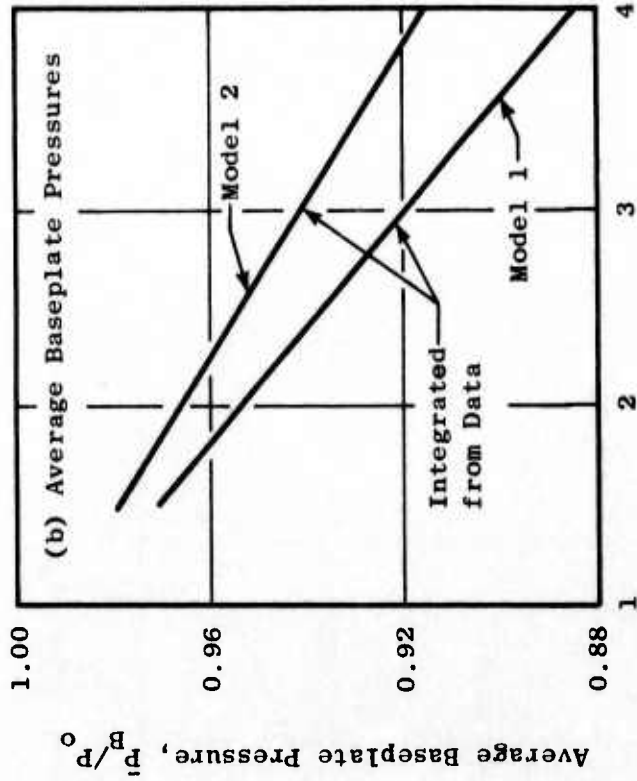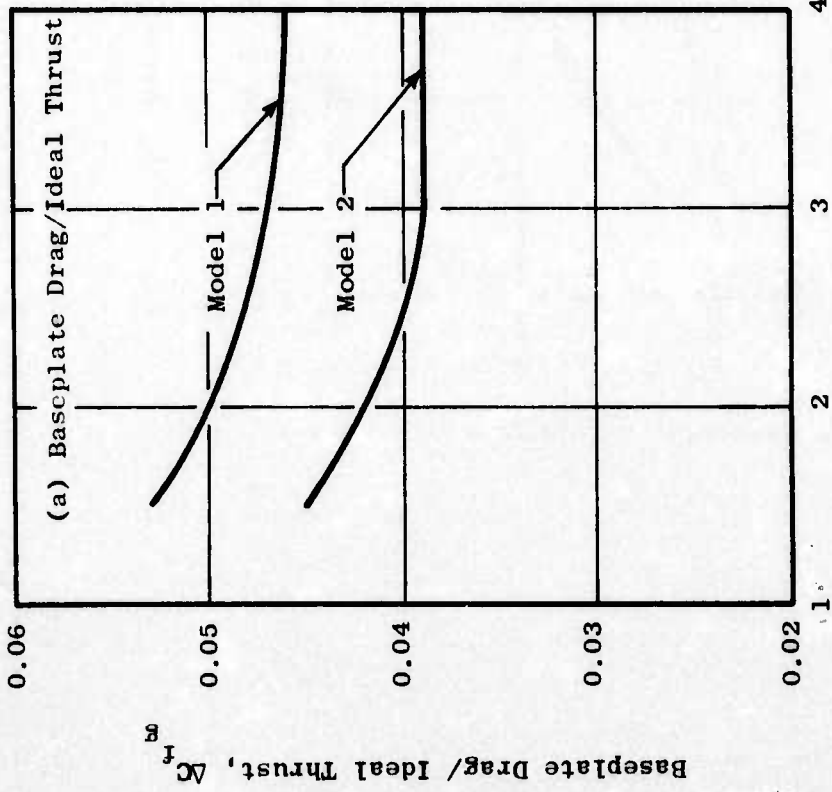
Figure 142. Integrated Base Pressure Effects.

193
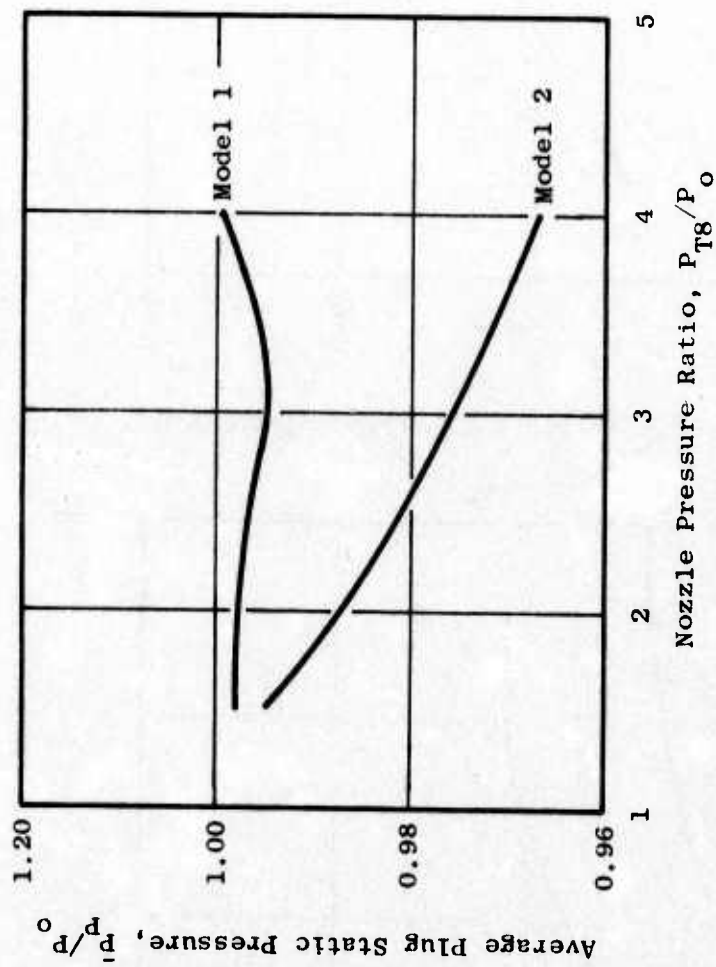
Figure 143. Average Plug Static Pressure.
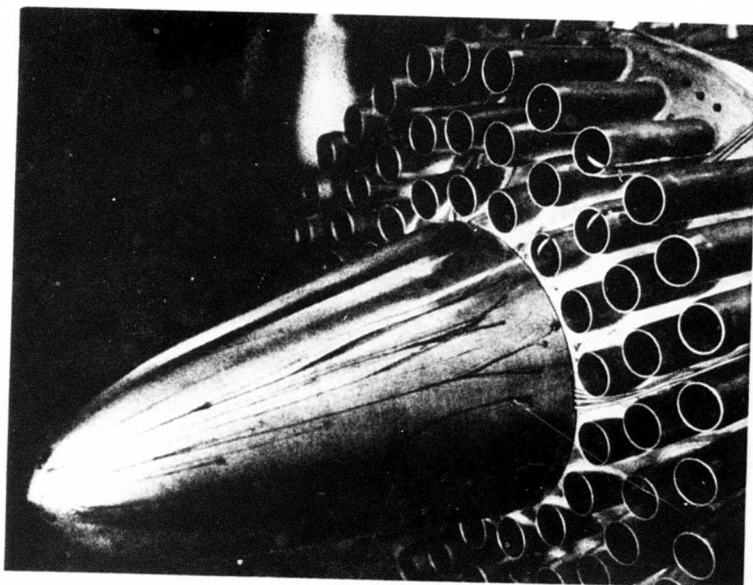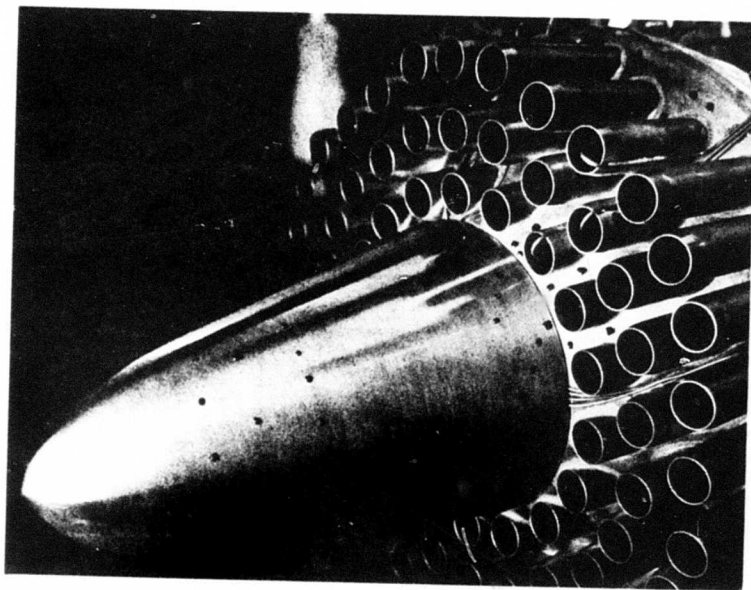
Figure 144. Model 1 Lampblack Photographs, P_{T8}/P_o = 3.0.
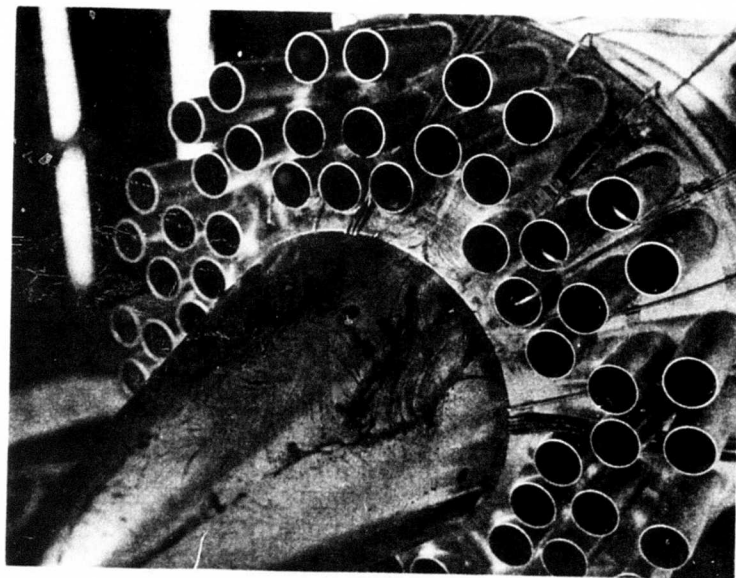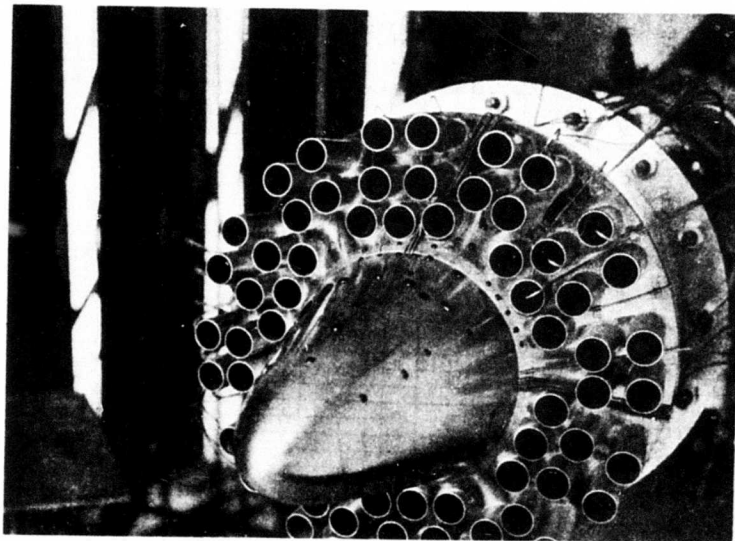
Figure 145.   Model 2 Lampblack Photographs, P_{T8}/P_o = 3.0.

An effort was made in the test to evaluate internal total pressure losses and profiles in the two models. The models were instrumented with a five-element P_T rake just upstream of the tube entrance and with pitot tubes on the centerline of several tube exit planes. The resultant measurements are shown in Figures 146 and 147. The flowpaths upstream of the tube entrance were identical for the two models and the measured internal P_T profiles were the same, as would be expected. However, the exit P_T values can be seen to be lower for Model 2 than for Model 1, indicating higher tube entrance and/or tube friction losses. These lower losses for Model 1 could be attributed to (1) the greater number of tubes having area convergence, thus reducing inlet Mach number, and (2) the even tube spacing providing more uniform flow contraction. This difference in tube entrance conditions can be more dramatically seen in the plots of flow coefficient in Figure 141, which shows Model 1 flow coefficients to be 3-4% higher than those of Model 2.

In an attempt to evaluate what these measured total-pressure profiles mean in terms of nozzle gross thrust coefficient, the single total pressure at each of the tube exits was mass-averaged to produce an average pressure loss and then converted to ΔC_{fg}. The results are shown in Figure 148. Since these exit measurements were made with pitot tubes located on the centerline of the tube exit plane, they do not reflect all the internal losses: specifically they cannot account for tube skin friction and possibly not all of the entrance losses.

Overall breakdowns of the loss mechanisms as determined from test pressure measurements are summarized on Figures 149 and 150. Some of the loss mechanisms obviously could not be accounted for by the model pressure analysis, the most notable being tube friction losses and tube projected area base drag.

An indication of the entrainment due to the addition of the ejector can be seen in Figure 151. Shown are plug base pressure profile differences at two V_j's with and without the hardwall ejector. The plug pressures with the ejector are considerably lower (5.6%) than those without ejector, indicating increased pumping effects which result in lower plug surface pressures.

Concept Evaluation

The results of the acoustic tests suggest that mechanical changes, such as nonuniform tube spacing, do not have as great a detrimental effect on suppression as previously thought.

Comparison of suppression levels achieved with Models 1 and 2 with those of previously tested multitube/annular plug suppressors show reasonable agreement (Figure 152) on a PNL basis but show marked differences in spectral shape which indicate this type of primary suppression system (multitube/annular plug) by itself, has a limited capability for increased suppression. Further increases in suppression were expected with the addition of acoustically treated ejectors. However, the results of the ejector tests indicated
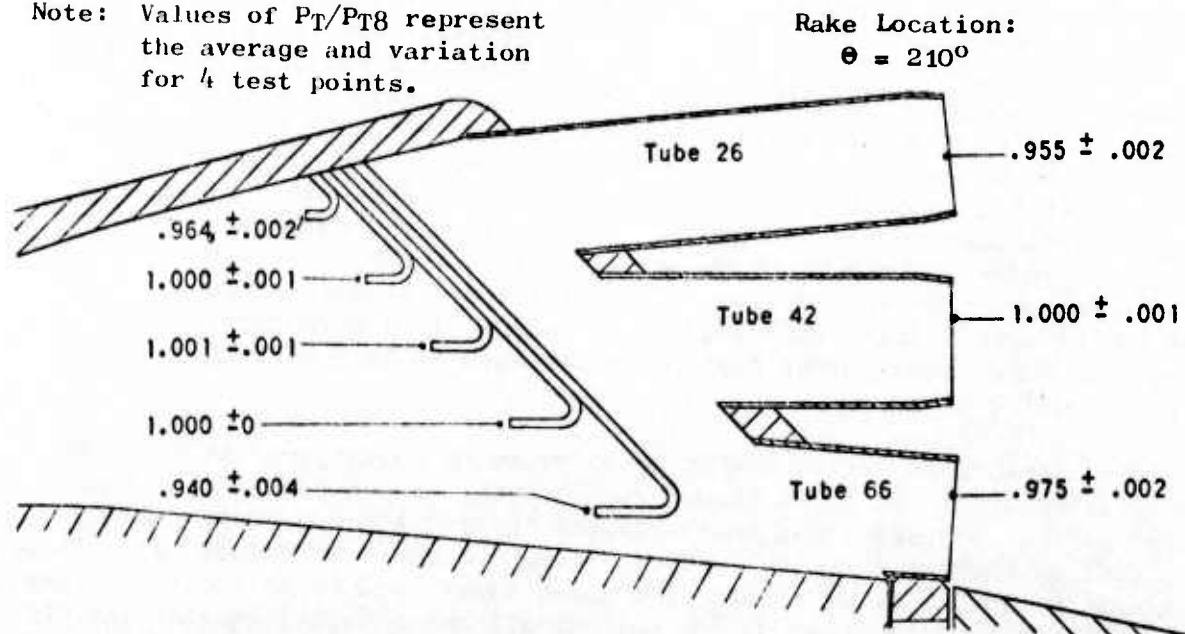
Figure 146. Nozzle Total Pressure Ratios at Indicated Stations and Model 1.
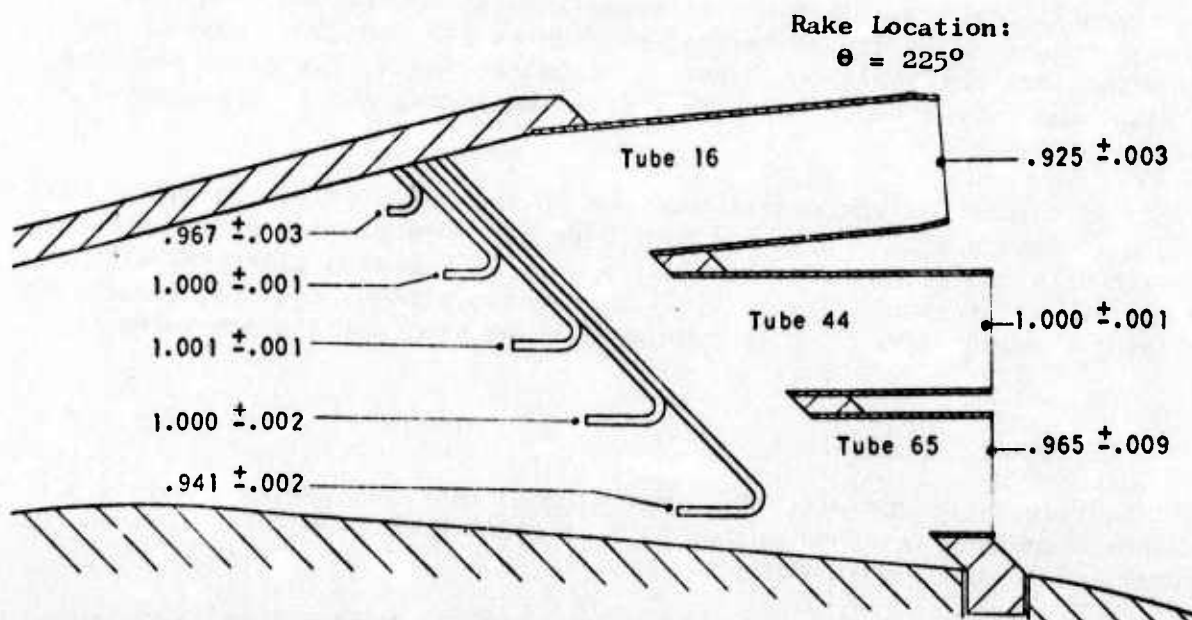
Figure 147. Nozzle Total-Pressure Ratios at Indicated Stations (Model 2).

198
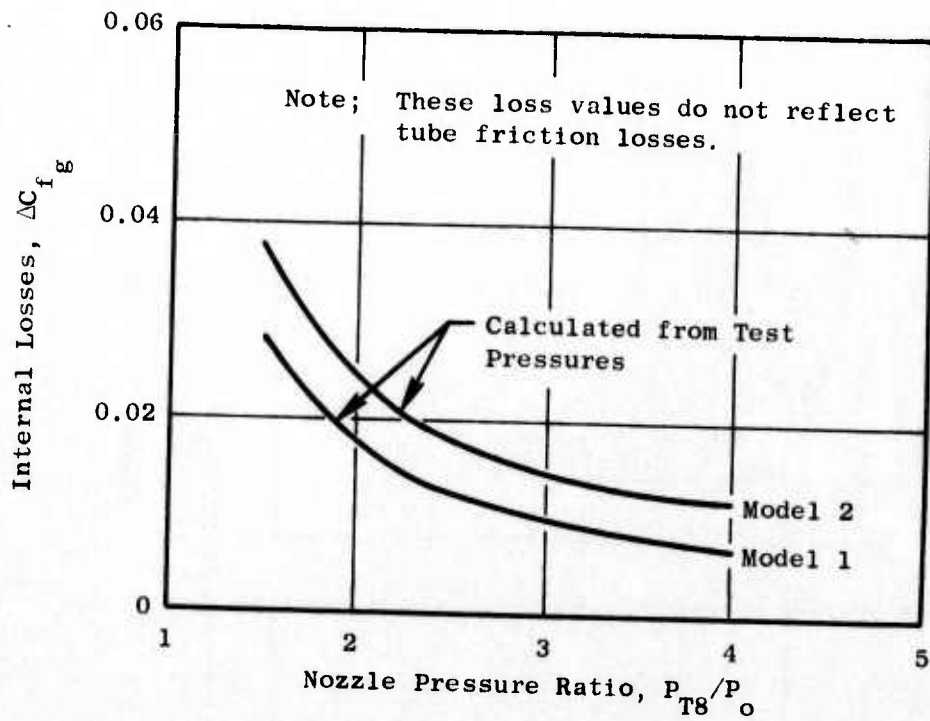
Figure 148.   Estimated Internal Loss Characteristics.
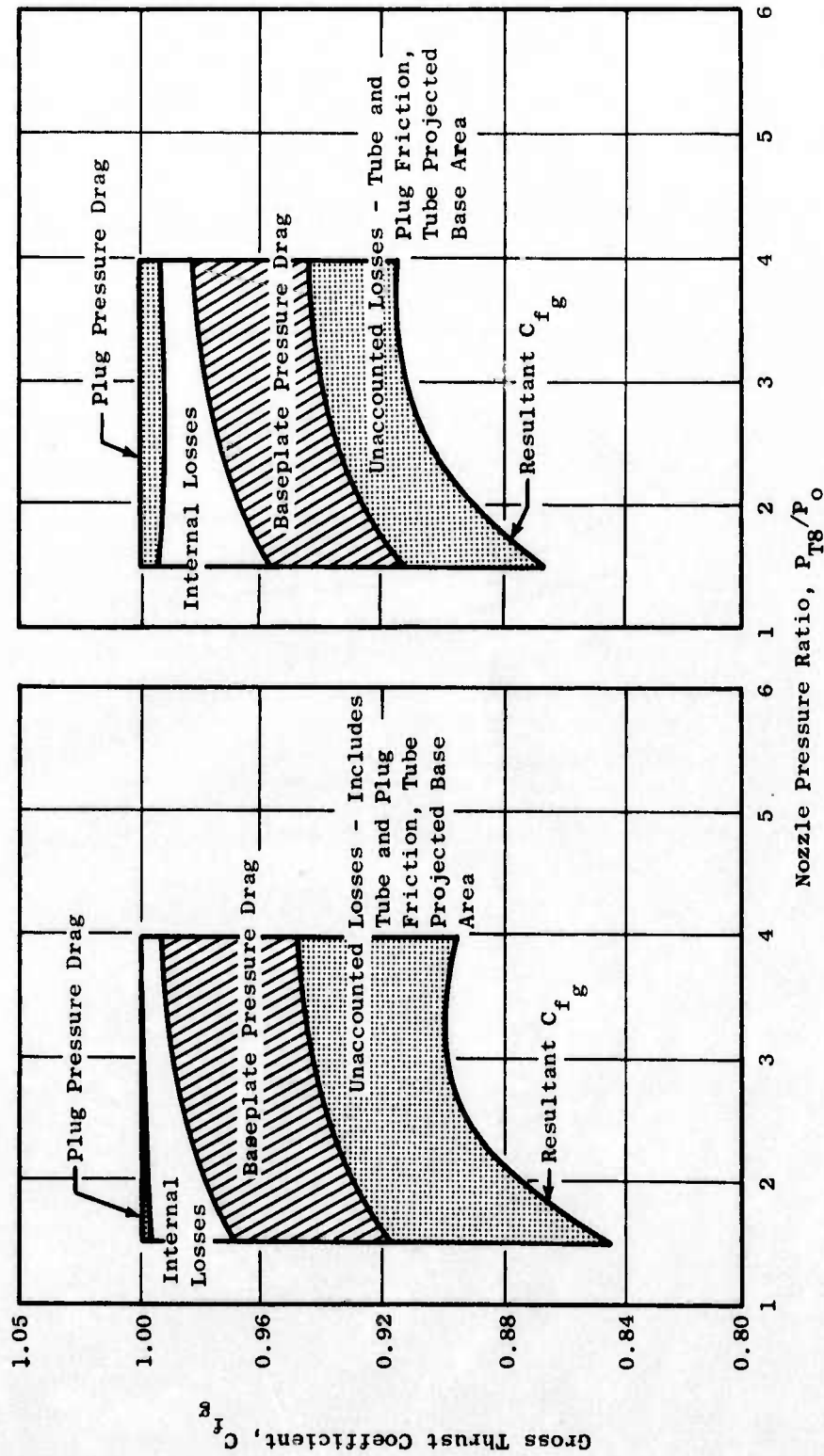
Figure 149. Loss Breakdown, Model 1.

Figure 150. Loss Breakdown, Model 2.
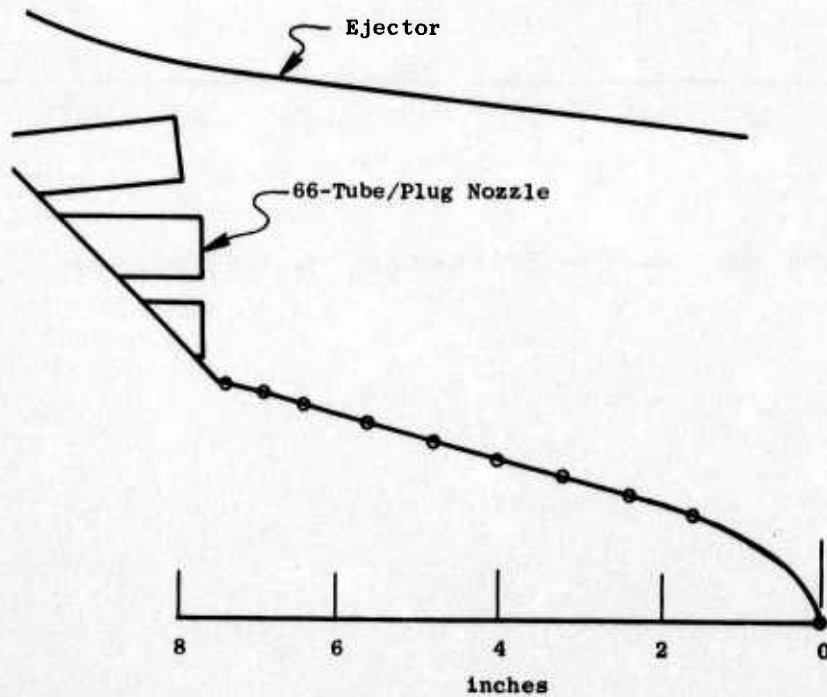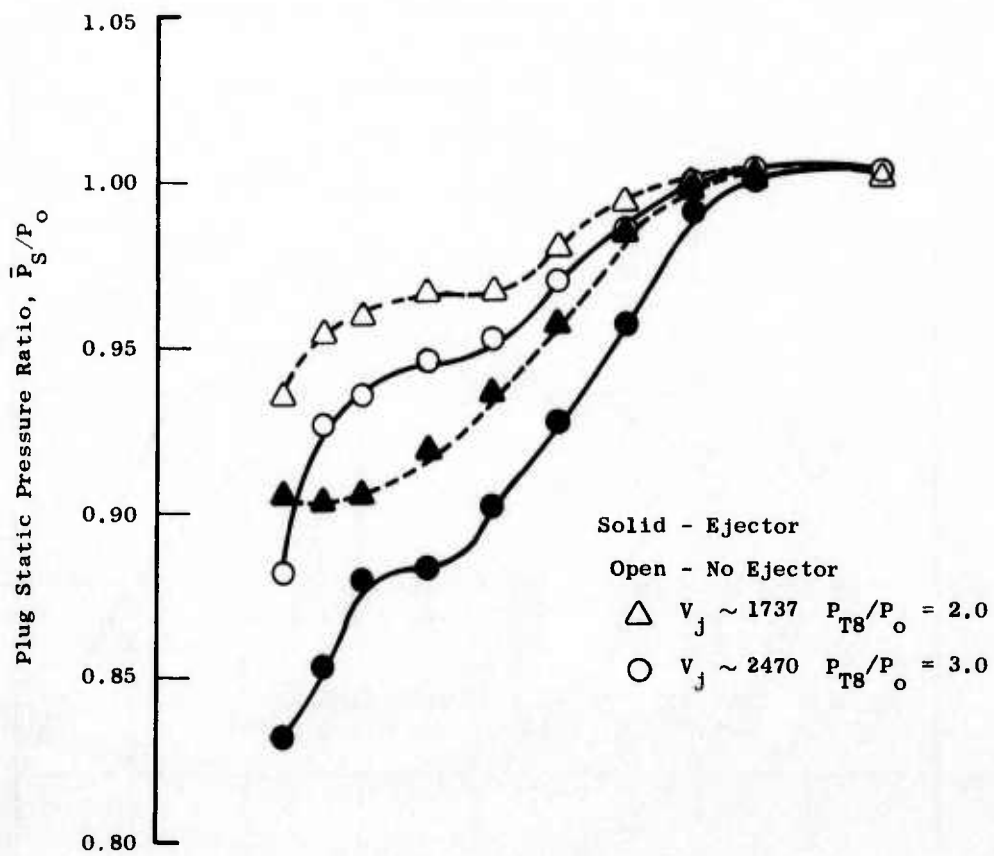
Figure 151.   Tube Suppressor Plug Pressures.

201
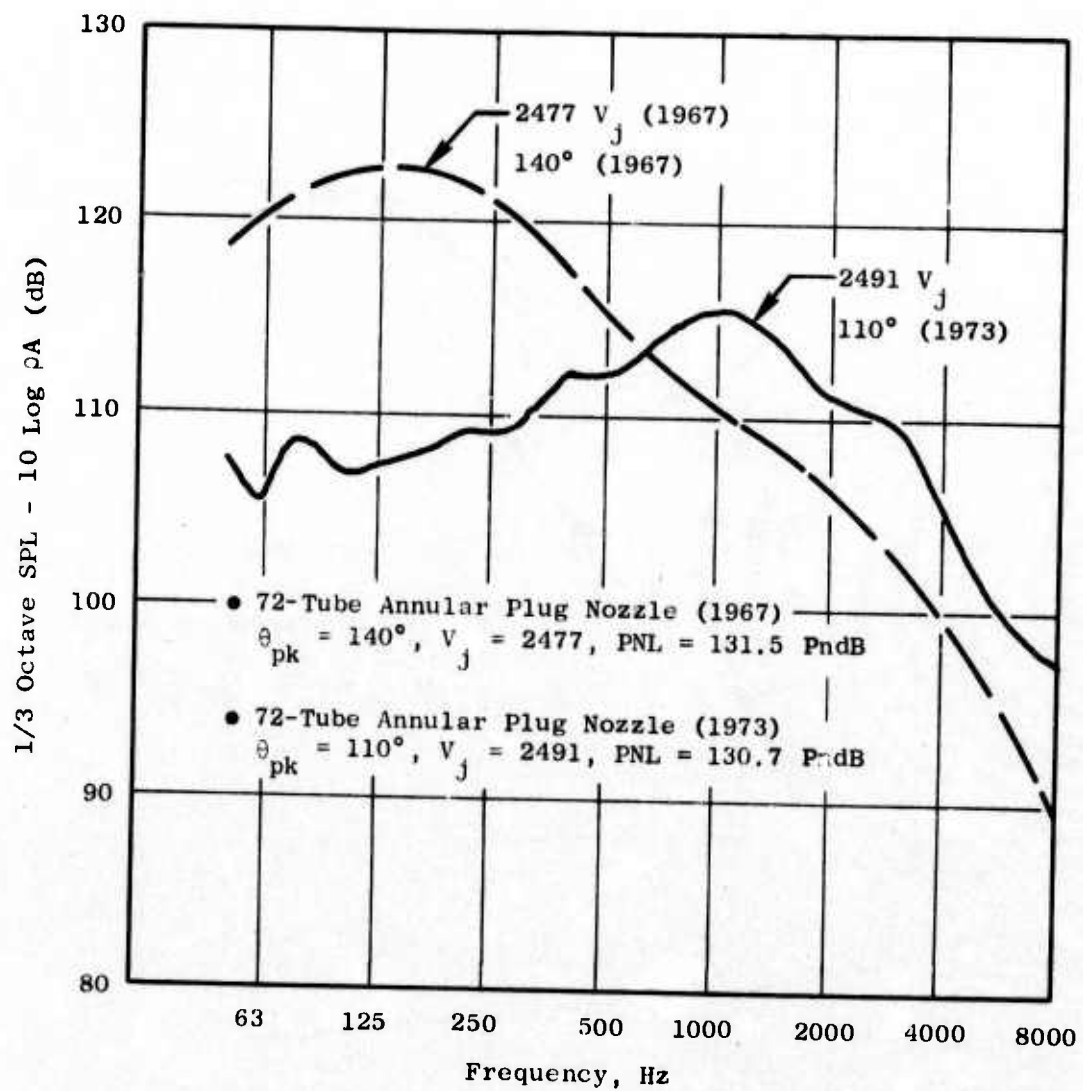
Figure 152. 300-foot Sideline SPL Spectra Comparison.

that additional suppression benefit from the ejector was minimal (2 dB) to essentially nonexistent at the high jet velocities (>2000 ft/sec) with the multitube configuration tested. The apparent scrubbing on the ejector may have negated the real gain possible with acoustic treatment; judicious design in the future may permit realizing these levels of suppression.

The multitube/annular plug suppressor nozzle designs demonstrated fair performance potential, relative to other multielement configurations. The thrust coefficient is largely insensitive to the existence and the geometry of the center plug. The major loss mechanisms are base drag and the combination of tube entrance and friction losses. The base plate drag is highly dependent on the tube array geometry, and the radial-type tube arrangement giving approximately a 0.5 - 1.0% increase in thrust coefficient. The convergent end tubes also give an increase in performance by minimizing tube entrance and friction losses.

Incorporation of favorable factors identified in previous testing and analysis did not raise existing performance levels by more than 1-2%. Additional fine tuning of multitube suppressors could be expected to yield only small further increases in performance.

To make the multitube nozzles attractive suppressor systems, higher levels of either suppression or suppression per thrust loss, must be achieved. Possible areas of investigation would be lower area ratio suppressors and radial tube arrays. These items would lower suppression levels somewhat but may be favorable on a suppression/performance basis.

Also, if multitube suppressors remain under consideration as viable systems, the in-flight thrust penalty, potentially high because of the large base areas involved, should be evaluated in wind tunnel tests. In addition, results to date have shown that unsuppressed flight effects are lower than classical V_R, especially at angles forward of the peak, and suppressor data, though limited, strongly suggest that the suppression to be realized during flight will be less than static levels.

3.2.4 Advanced Concepts

3.2.4.1 Preliminary Concept Review

Initial Studies

The advanced concept studies conducted during this task were designed to identify new suppressor concepts with possible high suppression capability. Several studies concerned with noise reduction resulting from turbulent mixing of the high velocity core with entrained ambient air were conducted on rotary nozzles, annular mixing nozzles, and hybrid nozzles (multitube/multispoke combinations). Suppression through fluid shielding was reviewed in studies of foam suppressors and coannular flow nozzles. Asymmetry and mechanical shielding effects on noise reduction were reviewed in initial evaluation of an asymmetric 2-D/over-the-wing nozzle concept. Another concept evaluated in

203

these studies was the "orderly structure" of the turbulent jet which was directed at determining if suppression could be achieved by the controlled disturbances of the ordered nature of the jet plume.

A review of some of these early suppressor concepts is presented in the following paragraphs.

Rotary Nozzle - A study of the possibilities of using a rotary jet flow ejector concept as a noise suppression device was conducted. The system was to operate by using a rotor with several nozzles which discharged the flow tangentially into an interaction duct. The exhausts formed spirals inside the interaction duct. This spiraling effect would result in a greater length over which viscous entrainment between the primary and secondary flows could occur. The increased mixing length of the spirals would increase the pumping over a comparable length ejector. A large amount of secondary (ambient) air could be interacted with the primary stream and provide a substantial augmentation ratio. The mixing of the flows should result in lower exit velocities which, in turn, could reduce the noise generated by the jet.

Two preliminary flowpath layouts were made. The first incorporated the suppressor concept into a translating 20° plug centerbody to vary A_8 and to block the nozzle exit for the rotary nozzle operation. The second had a variable flap and seal centerbody for A_8 variation and for the exit-blocking device. Preliminary aerodynamic estimates for the system indicated that supersonic cruise performance (M = 2.7, Alt = 60K ft, P_{T8}/P_0 = 28) should be in the C_{f_g} = 0.97 range internally, while the subsonic cruise (M = 0.9, Alt = 36K ft, P_{T8}/P_0 = 3.0) installed performance should be about 0.90 to 0.92.

Mechanical considerations of this concept, however, did not contribute favorably to implementation with a viable suppressor system.

Annular Mixing Nozzle - A second exhaust suppressor concept, again of the high mixing category, underwent aerodynamic and acoustic study. It was the annular-mixing ejector nozzle (AMEN) shown schematically in Figure 153. Initial analysis of the system indicated high net acoustic performance. Design considerations, hopefully leading to inherent low-noise/high-performance characteristics, included:

- A relatively long annular ejector, by design selection, can pump a large quantity of secondary air. This can mix with the primary air to effect a relatively low average jet velocity at A_9 and, therefore, a low jet noise generated external to A_9. The design objective would be to pump and mix, as fully as possible, from 40% to 50% secondary air. Selecting an annular, rather than a cylindrical ejector, should allow this design objective to be achieved without making the nozzle length impractical.

204
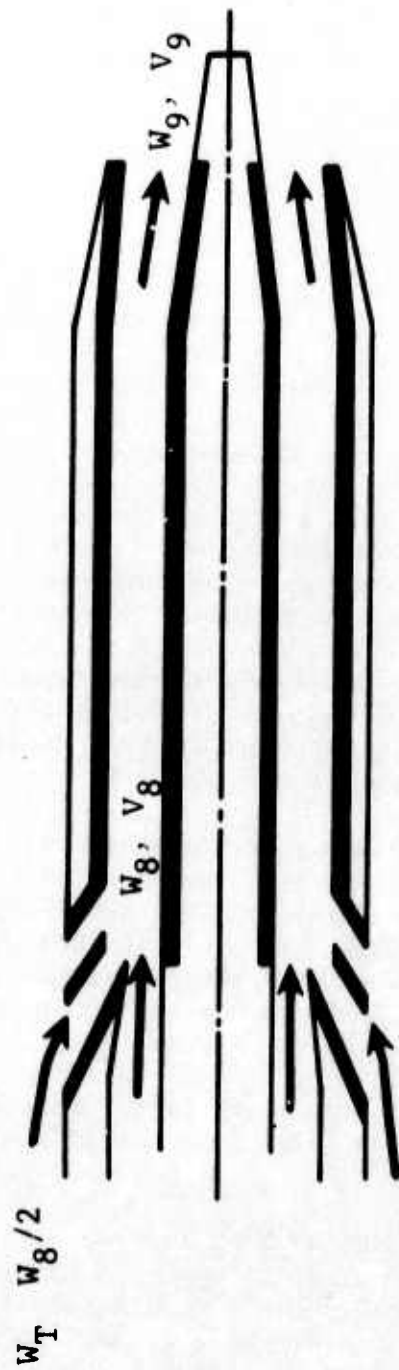
Figure 153. Schematic of Annular Mixing Ejector Nozzle.

- Noise generated internally to the ejector annulus through the mixing process of necessity, would be appropriately suppressed with high temperature acoustic lining material; otherwise, it would propagate outside and nullify the benefits associated with the low V_j jet noise generation. This applied both to the downstream-propagated noise, potentially escaping at the annular exit, and to the upstream-propagated noise which would escape through the secondary inlet passages.

- The treatment within the annular duct also would serve for turbo-machinery noise suppression to alleviate the major noise problem at approach and cut-back power settings.

- The suppression achieved through a combination of internal aero-dynamic mixing and physical shielding should not be drastically altered when an external velocity is applied. That is, the physical shielding may protect the primary noise suppression region from relative velocity influence, a factor which seems to cause a major loss of suppression for most conventional suppression mechanisms. The flow at the ejector exit is then essentially that of a low velocity conical nozzle, and should be able to capitalize on the V_R effect during flight. Pumping and internal aerodynamic mixing characteristics, however, may be altered and require evaluation as to their effects on source intensity and location.

Application of this system was evaluated on a forward-mounted over-the-wing engine installation. The wing would provide ground shielding and a place to stow suppressor hardware during unsuppressed flight modes. With retractable ejector, it would be possible to vary the L/D.

In addition to obvious wing and nozzle acoustic benefits, a by-product could be some powered lift during climb-out which would permit higher aircraft climb rates without advancing the throttle, thus shortening community noise exposure. The results of this study, combined with the current NASA-Langley AST aircraft programs dealing with the cruise drag aspects of the OTW concept, should provide some guidance as to how far to proceed with this type of installation.

Further variations to the concept include the use of multielements and combining nozzle asymmetry (which changes directivity) with the basic AMEN or multielement concept.

Hybrid Multitubes/Multispokes on Annular Plug Nozzles - This concept consisted of an axisymmetric plug nozzle with multitubes and multispokes. The objective of the combination was to retain the favorable base pressure characteristics of the spokes in the vicinity of the plug while taking advantage of the good ventilation characteristics exhibited by multitubes at the periphery of the nozzle. This concept proved difficult to assess because of the lack of data on the interaction region between tubes and spokes.

206

The hybrid design, consisting of various combinations of tubes and spokes on a plug nozzle, offered no apparent advantage over annular multitube or multichute suppressors tested and planned for testing. It was recommended that this design not be pursued.

Hybrid Multitubes/Multishrouds on Annular Plug Nozzle - This concept would consist of a multitube suppressor with individual shrouds (ejectors) on selected tubes. These individual shrouds entrain flow, mix it with the supersonic tube flow, and reduce the velocity at the shroud exit. Multitube suppressors of 50 and 191 tubes, with individual shrouds for each tube, were previously tested. Although power level reductions of 20 dB were recorded, the thrust losses were in the order of 25 - 30%. These losses, combined with the formidable mechanical implementation problem, discouraged further work on the concept. However, with an OTW installation, it is possible that by installing shrouds on selected tubes (e.g., inboard and outboard sides) the losses could be significantly reduced.

Coannular Nozzles - In all these previously mentioned concepts, the basic design approach was to reduce the velocity of the jet as quickly as possible, and the feasibility of the several methods depended upon the ability to achieve these reductions by aerodynamic design. Another configuration, however, achieves the velocity reduction by incorporating a normal shock in the flow downstream from the nozzle exit; a basic description of the approach and results of a preliminary experimental investigation are given in Reference 15.

Another approach investigated with the coannular dual-flow nozzles was to see if noise suppression could be achieved from aerodynamic shielding by the outer flow annulus on the high velocity core.

Orderly Structure - This concept was studied primarily to evaluate whether or not high velocity jet noise could be influenced from controlled manipulation of the jet plume envelope as proposed by J. Hardin of NASA-Langley (Reference 16). If so, another mechanism for suppression would have been identified which might be combined with classical turbulent mixing suppressor schemes to produce effective suppressor systems.

3.2.4.2 Selection of Three Concepts

To implement the work efforts for this task, three advanced suppressor concepts were selected for study based on preliminary estimates for the most promising suppression gains with new suppression schemes. They were 1) an over-the-wing mixing ejector nozzle concept, 2) a dual-flow suppressor concept, and 3) a suppression concept based on the "orderly" structure of turbulent jets. The following discussions review the work performed in the preliminary evaluation of these concepts.

207

Asymmetric 2-D Nozzles/Over-the-Wing

It was concluded from the initial studies that the over-the-wing (OTW) mixing-ejector nozzle installation was a true advanced concept for the AST. Including airframe implications, such a nozzle has the potential of delivering acceptable performance at unsuppressed cruise conditions. Advantages of this concept include possible shielding from the wing and from side-plates, or "fences." These side-plates are required for unsuppressed flight modes to guide the exhaust gas expansion and therefore, are integral to the design.

In addition, suppression devices considered impractical for axisymmetric podded engine installations (e.g., the mixing ejector nozzle), become feasible due to the availability of storage space. The OTW concept also readily lends itself to other suppression devices like spokes and tubes.

Several nozzle configurations were required to identify the suppression effects. The basic nozzle, depicted schematically in Figure 154a, consisted of a rectangular (two-dimensional) variable area throat, a 15° expansion ramp which faired into the wing, and a translating upper shroud to control exhaust gas expansion. Side walls extending to the nozzle exit plane prevent lateral expansion of exhaust gases as well as providing shielding.

A second configuration, depicted in Figure 154b, employed an area ratio of 2 and a 20-element, spoke suppressor. By nature of its geometry, the 2-dimensional spoke suppressor was thought to offer an aerodynamic advantage over previous annular spoke suppressors in that the ratio of the flow width at the base to the flow width at the shroud was equal to unity. It was shown that as the flow width ratio approached unity, base pressure, and thus performance, increased (see Section 3.2.2). The flow areas of both suppressed and unsuppressed nozzles were the same.

A third configuration was a 2-dimensional version of the AMEN, or annular mixing ejector nozzle. This configuration, shown schematically in Figure 154c, took advantage of the already present side walls. From an installation viewpoint, the top of the ejector might be formed by a section of the ramp which would be raised between the side walls. After takeoff, the ejector top would retract back onto the ramp. As envisioned, this concept would provide increased PNL suppression from entrainment of secondary air over a long mixing region.

Dual-Flow Exhaust Nozzle

This system also was considered applicable to the advanced concept studies. It is one which takes advantage of the possible fluid shielding effects of a low temperature duct stream interacting with a hot suppressed core stream. Current interest involving various separated-flow turbofan engine studies as part of the AST effort, also influenced the selection, since tests of the acoustic characteristics of the dual-flow nozzles would be of benefit for future AST studies.

(a) 2-D Unsuppressed Nozzle

Sidewall

20 Parallel
Spokes
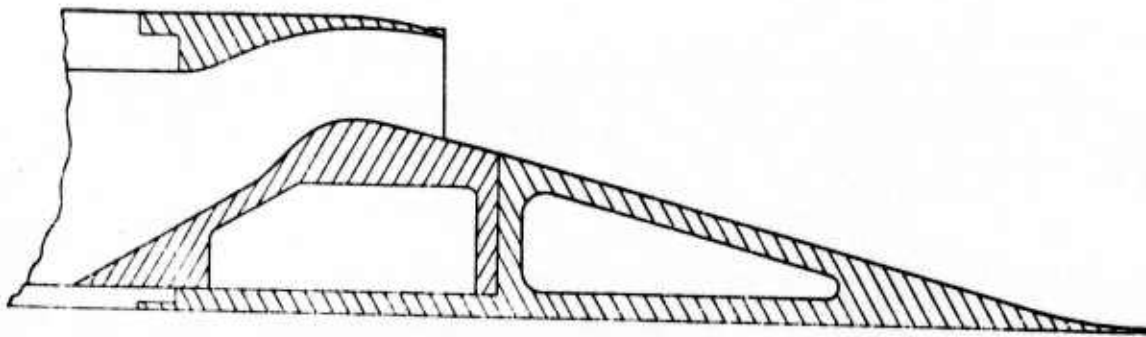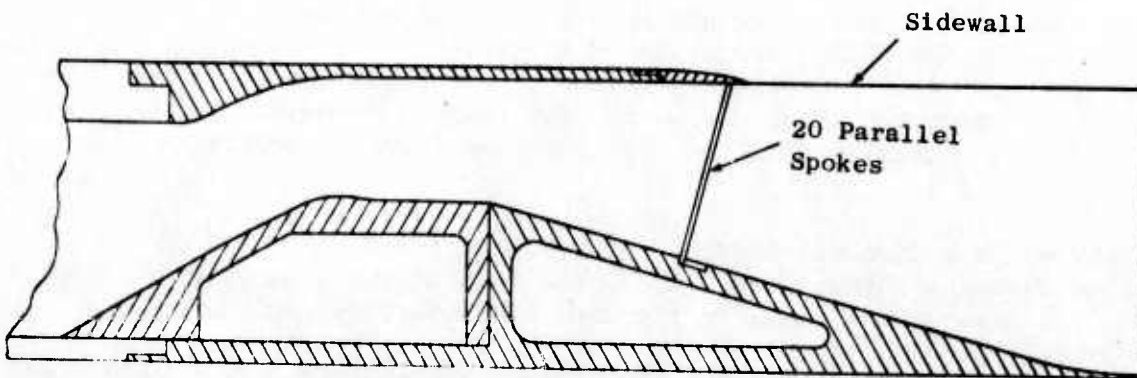
(b) 2-D Suppressed Nozzle With Sidewalls
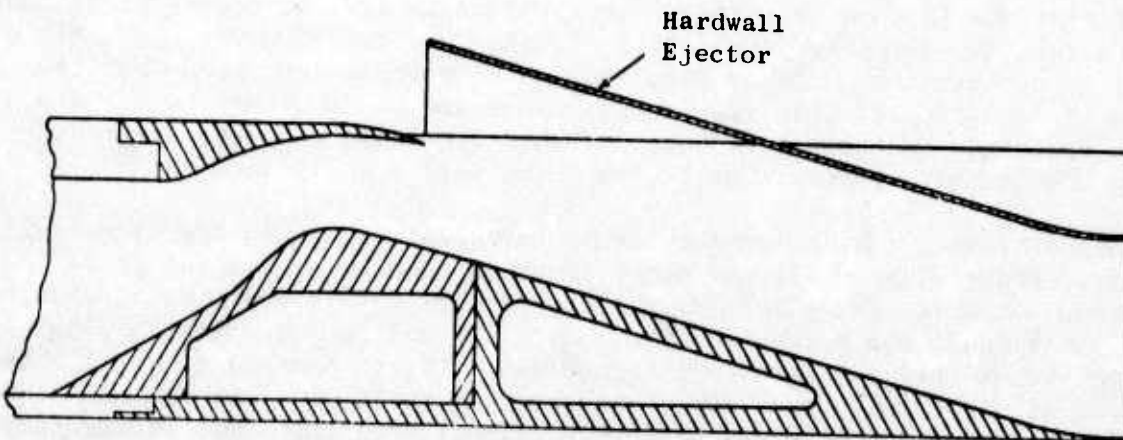
Hardwall
Ejector

(c) 2-D Unsuppressed Nozzle With Hardwall Ejector

Figure 154. Asymmetric 2-D Nozzle Configurations.

The dual-flow nozzle tests were designed to evaluate the suppression effects of a warm unsuppressed fan stream surrounding a hot suppressed core stream. The test configuration employed a nominal bypass ratio derived from the AST studies and was operated over an average operating line, again generated from AST cycle studies.

Orderly Structure of Turbulent Jets

Over the past two decades, a considerable amount of effort has been directed toward the understanding and quantization of the acoustic nature of turbulent jets. But, because of a lack of clear understanding and detailed mathematical and experimental specifications of the dominant noise producing agents, even for the most simple nozzles, only partial success has been met.

The Lighthill acoustic analogy theory of aerodynamically generated sound has been a dominating influence on the thinking of jet noise generation and suppression concepts. However, in the recent past, investigators have observed that there exists an "orderly" structure in turbulent jets. The results of these "orderly structure" studies are found in References 17 to 26.

Thus far, experimental evidence of such order has been confined to rather low Reynolds numbers (Re < 10^6), and most of the arguments for the "orderly" structure as a noise source have been heuristic in nature.

More recently, NASA-Langley's Hardin (Reference 16) has formulated the aeroacoustic nature of subsonic exhaust jets as a train of toroidal vortex rings which are formed near the jet exit and propagate downstream. Hardin's model is a reformulation of Lighthill's expression for the far-field acoustic density, which emphasizes the importance of the vorticity within the turbulent flow field. His results show that the noise production occurs mainly close to the jet exit and depends primarily upon temporal changes in the toroidal radii. Hardin's analysis suggested that, by inhibiting the radial growth of a jet's plume, noise reduction could be obtained. His analysis suggested that the process of formation of this regular structure was an important contribution to high frequency jet noise. To utilize this approach, concepts which help destroy the orderly structure would, in turn, reduce the noise.

On one hand, the noise production by turbulent mixing in the classical Lighthill/Ribner/Ffowcs-Williams sense is still clearly a dominant noise-generating mechanism for simple as well as complex suppressor nozzle concepts. On the other hand, the mechanism which helps "drive" the turbulent mixing noise may be the orderly structure of the jet. It was planned to examine the influence of destroying the orderly structure in turbulent jets on the acoustic suppression. This was performed primarily through very rudimentary experimental means.

This was the third suppression concept selected for evaluation under the advanced concepts activity.

3.2.4.3 Asymetric Two-Dimensional/OTW Nozzle System

Introduction

The exhaust nozzle under consideration for this phase of the study was a two-dimensional, over-the-wing, plug (ramp) nozzle with a translating shroud for exit area control and an expandable ramp for throat area variation. This asymmetric, over-the-wing nozzle system was attractive for two reasons. The first involves acoustic shielding inherent in a system in which the nozzle is positioned above the wing, the second reason being that the ramp can be used to store additional acoustic suppression devices.

The aeroacoustic preliminary performance estimates indicated that suppression gains could be realized due to the combination of nozzle asymmetry and wing shielding with relatively low thrust penalty potentially making the final $\Delta PNL/\Delta C_{fg}$ trade-off attractive for an SST application.

From an aerodynamic performance standpoint, the nozzle system appeared capable of delivering high efficiencies at unsuppressed flight points, e.g., supersonic and subsonic cruise.

Acoustic tests were conducted on this system at the JENOTS model test facility. Aerodynamic static performance tests were conducted at FluiDyne Engineering Corporation Facilities.

The suppressor concepts investigated are defined in the next few paragraphs including a short description of how each could be incorporated into the exhaust system when it is stowed. In addition, drawings are included of a full-scale nozzle incorporating the suppressor concepts. The full-scale, two-dimensional, ramp nozzle used in this study had an internal flow width equivalent to the internal diameter of the 900 lb/sec GE4/J6H2 nozzle. The height of the two-dimensional nozzle was set to accommodate the internal area ratio required for the supersonic cruise condition.

Shielded Exhaust Nozzle - Sidewalls (or plates) extend from the throat to the end of the ramp. These plates are permanently positioned, and the translating shroud rides on top of them.

Acoustically Lined Ejector Nozzle - A constant area mixing duct, in which the upper and lower surfaces are lined with acoustic treatment, is formed over the entire length of the ramp. At other power modes, the upper surface of the ejector is positioned on the ramp protecting both the upper and lower sets of treatment from the hot gases of the jet. The vertical movement of the ejector shroud is done on rails mounted in the sidewalls. In the stowed position, the ejector system does not interfere with the modulation of the throat and the translation of the shroud.

Shielded Spoke Nozzle - A 20-spoke suppressor with an effective area ratio of two is positioned normal to the ramp and forms the throat of the nozzle when it is deployed. The sidewalls extend the length of the ramp. The suppressor, when it is not in use, will be stowed in the ramp.

211

Acoustic Tests

Parameters that were evaluated acoustically included the effects of:

- Nozzle asymmetry (rectangular nozzle relative to a conical convergent nozzle)

- Acoustic shielding with nozzle sidewalls

- Wing shielding with and without primary suppression

- Wing-model spacing effect on scrubbing noises

- Hardwall ejector

The 2-dimensional (rectangular) model exhaust nozzle had an unsuppressed throat aspect ratio of 4. A schematic illustrating the geometric character-istics of the 2-D/OTW configuration is shown in Figure 155. The various model configurations are shown diagramatically in Figure 154, as previously discussed.

Acoustic testing of the asymmetric 2-D/OTW configurations covered a range of ideal jet velocities of 1250 to 2800 ft/sec at nozzle pressure ratios corresponding to 1.50 to 3.55. The 2-D/OTW configurations were tested in two orientations relative to the JENOTS facility 90° microphone plane as shown in Figure 156. The simulated ground sideline orientation (Figure 156a) was used to test the shielding effect of sidewalls and hardwall ejector configurations. The maximum effect of wing shielding was investigated in the simulated flyover orientation (Figure 156b).

Acoustic far-field measurements were taken with all configurations on an array of 14 microphones situated on a 40-foot arc in equal increments of 10° from 30° to 160° relative to the jet inlet. These measurements were scaled by frequency and size to typical SST full-scale applications using a scale factor of 8:1. All far-field data presented, therefore, are of simulated engine size and frequency range.

Near-field data were taken with some of the configurations (specifically in connection with the hardwall ejector evaluation, i.e. unsuppressed 2-D with and without hardwall ejector). The analysis of the near-field data was used to assist in the evaluation of the hardwall ejector performance in relation to the acoustically treated ejector selection.

The ejector test was conducted on the suppressed 2-D nozzle in the side-line orientation. Kulite transducer instrumentation mounted in the forward region of the ejector was used in conjunction with a linear array of seven near-field microphones to obtain an estimate of the SPL spectral distribution along the ejector axis. Figure 157 is a schematic illustration of the near-field microphone and Kulite locations with respect to the 2-D unsuppressed nozzle and ejector configuration.

- Aspect Ratio $\frac{b}{h} = 4$
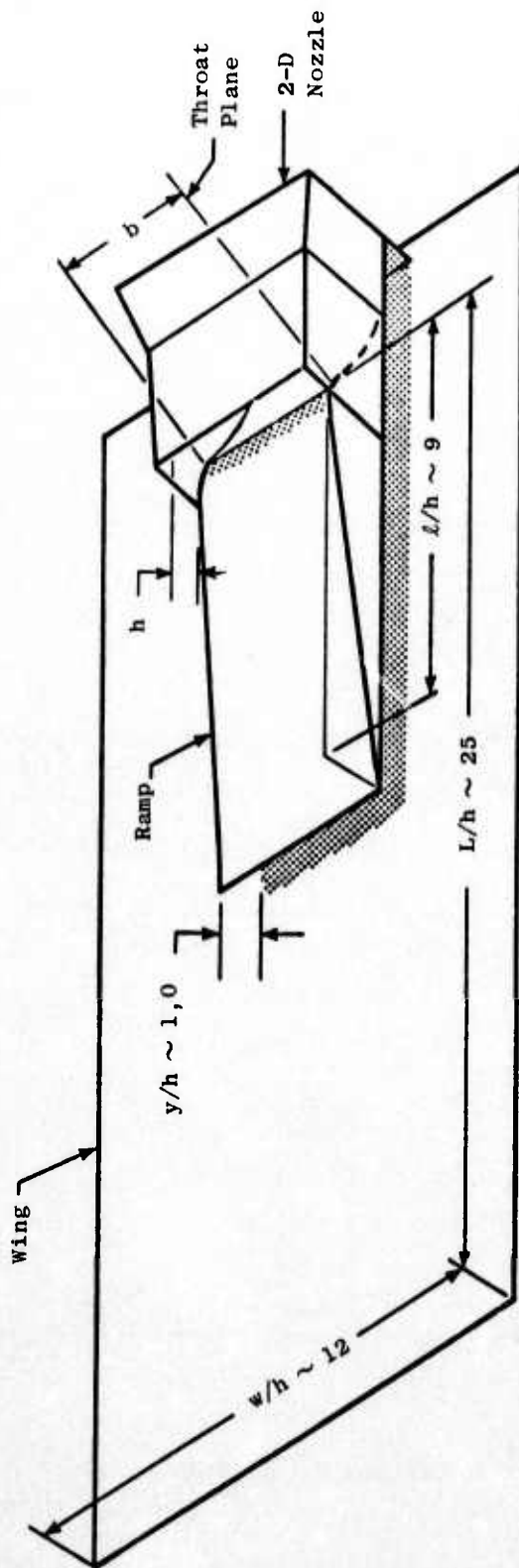
b = 2-D Nozzle Width
h = Unsuppressed Throat Height = 2.67"
ℓ = Ramp Height
L = Wing Length From Throat Plane
w = Wing Width
y = Model-Wing Spacing

Figure 155. Asymmetric 2-D/OTW Geometric Characteristics.

213

(a) Simulated Ground Sideline

90° Microphone

θ=16.5°

Microphone-Model Plane

16.5°

Wing

2-D Nozzle

JENOTS Axis

15.93'

Wing Extension

55"

Ground

(b) Simulated Flyover

90° Microphone

θ=16.5°

40' R.

16.5°+90°

Model-Wing Standoff, y

15.93'

h (Unsuppressed Throat Height)

Wing

Ground
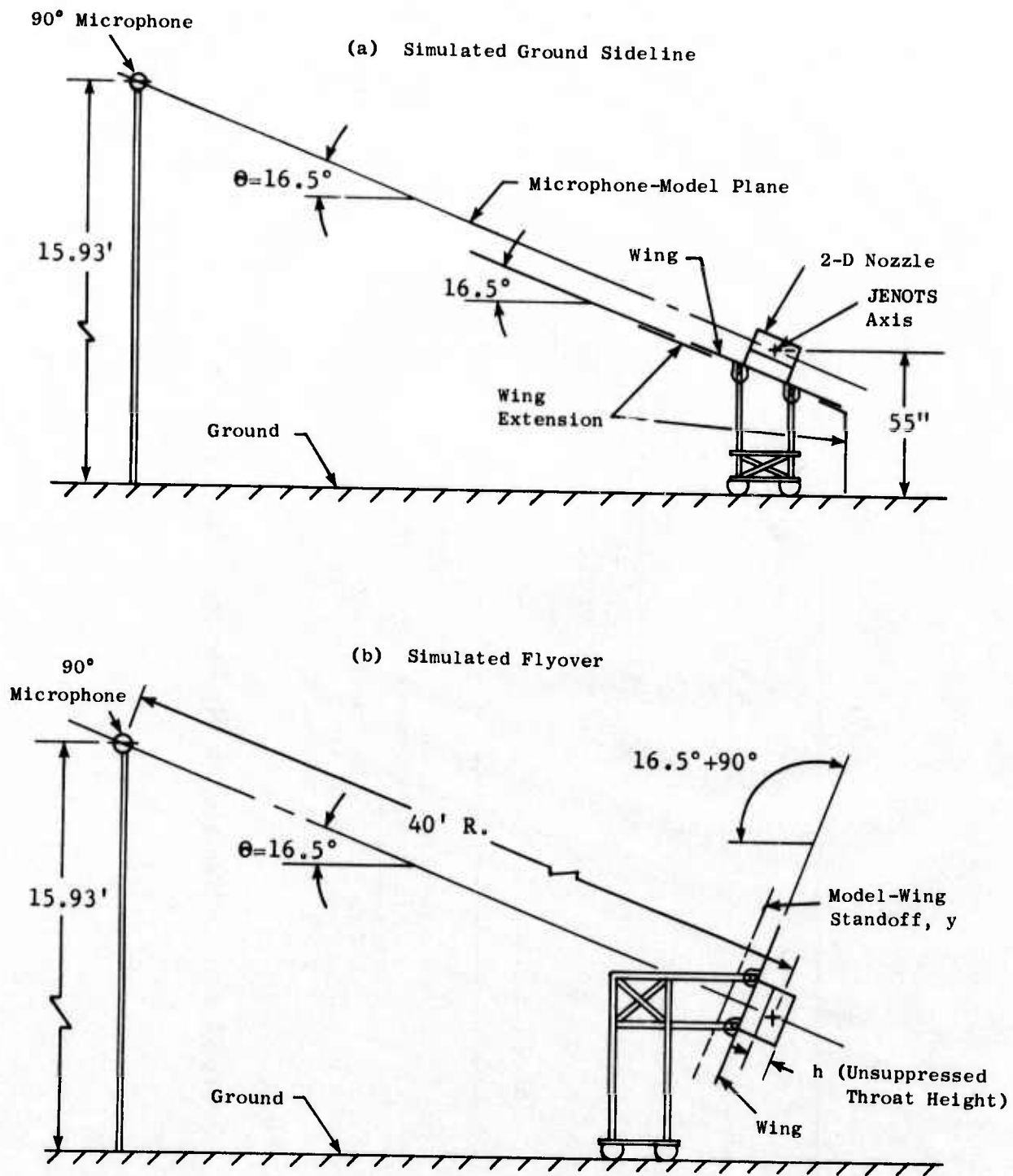
Figure 156. Asymmetric 2-D/OTW Nozzle Orientation.
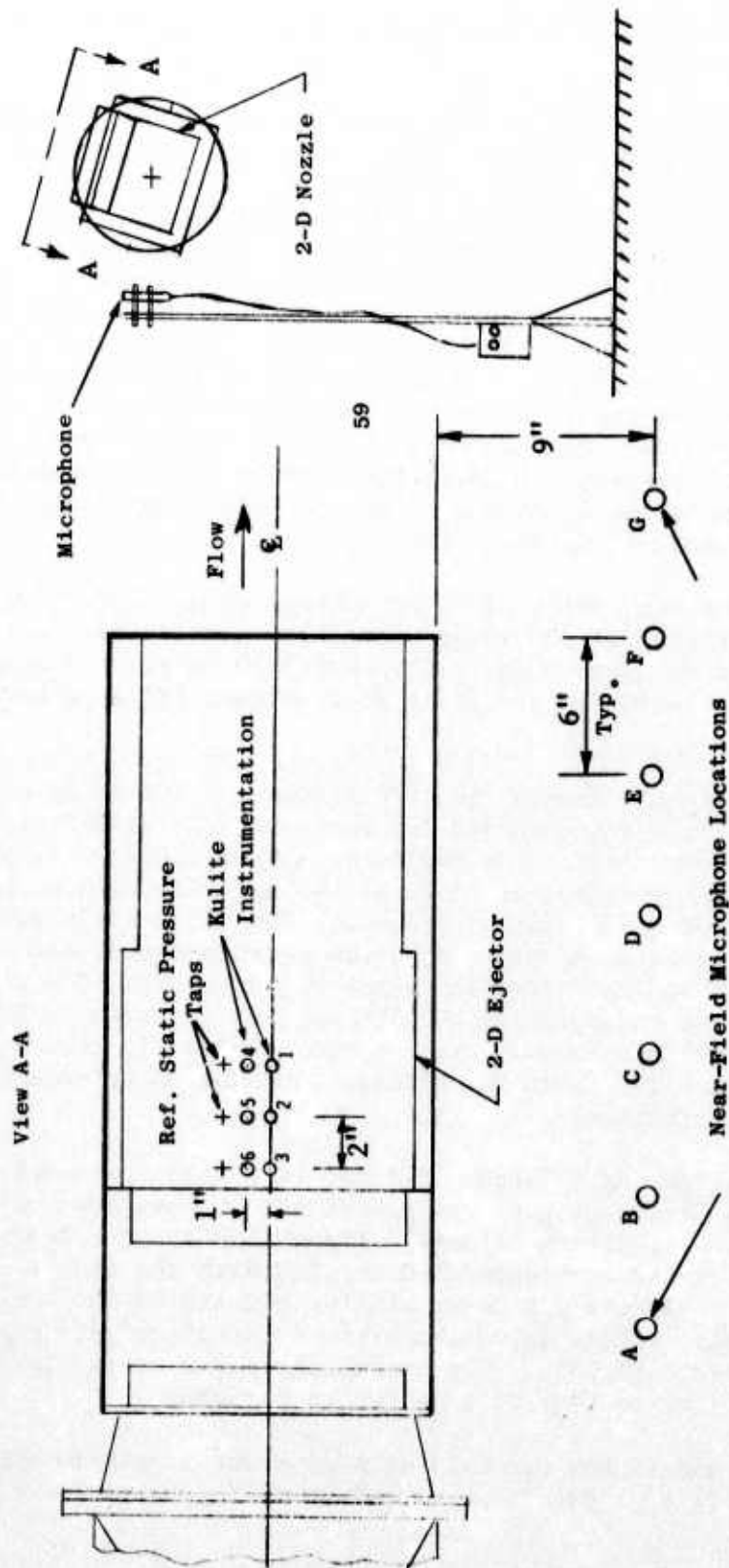
Figure 157. Near-Field Microphone and Ejector Kulite Instrumentation for the 2-D Hardwall Ejector Test.

215

Acoustic Results and Analysis

A tabulation summarizing the acoustic results obtained at each test condition is included in Appendix C.

Nozzle Asymmetry Effect - The effect of asymmetry on the unsuppressed 2-D nozzle is illustrated in Figure 158 by a comparison plot of normalized peak PNL at the 2128-foot distance for both sideline and flyover nozzle orientation positions, compared to a 5.7-inch I.D. conical nozzle. (The unsuppressed 2-D nozzle configuration is shown later in Figure 163, but without the wing.) The results show that the unsuppressed asymmetric nozzle, in both the sideline and flyover orientations, is noisier than its conical nozzle counterpart in the low to mid-range jet velocities. The unsuppressed "sideline" configuration is from 5.5 to 1.5 dB noiser than the conical from 1400 to 2000 ft/sec, while the unsuppressed "flyover" configuration is an average of 1.5 to 2.0 dB greater than the conical nozzle over the same velocity range. Above 2200 ft/sec, the "sideline" nozzle becomes somewhat quieter than the conical by about 1 dB; the "flyover" nozzle duplicates the conical nozzle PNL level above this condition.

Figure 159 illustrates the nozzle asymmetry effect on a 300-foot distance SPL spectra basis. Comparisons of the unsuppressed 2-D nozzle orientations are made at jet velocities of approximately 1600 and 1950 ft/sec. The spectra show that the "sideline" orientation yields slightly higher SPL's at both velocities.

Sidewall Shielding Effect - Figure 160 illustrates the shielding effect attributable to sidewalls on the suppressed 2-D nozzle at the 2128-foot distance in the sideline orientation. As can be seen from the figure, shielding of as much as 2 PNdB was attained at an ideal jet velocity of 2200 ft/sec and then gradually decreased as velocity increased. The decrease in suppression is probably due to the axial movement of noise sources downstream with increased velocity, and out of the sidewall region of influence. The effect of sidewall shielding on the unsuppressed 2-D SPL spectra is shown in Figure 161 and indicates only a minimum benefit which could be directly related to the sidewall length. Figure 162 shows the sidewalls on the unsuppressed 2-D nozzle in the sideline orientation.

Wing Shielding and Scrubbing Effects - The models tested are shown in Figures 163 and 164. The simulated wing was placed in two positions relative to the model to investigate scrubbing effects. Figure 165 shows comparative results of the unsuppressed and suppressed 2-D nozzles with the wing flush to the model surface, while Figure 166 shows similar results on the two configurations with the wing placed approximately one throat height (unsuppressed) away from the nozzle (Y/h∿1). The unsuppressed 2-D nozzle results without a wing are also shown on both figures for comparison.

The wing for these comparisons was held at a constant length-to-unsuppressed throat height ratio of about 25, measured from the unsuppressed throat plane.
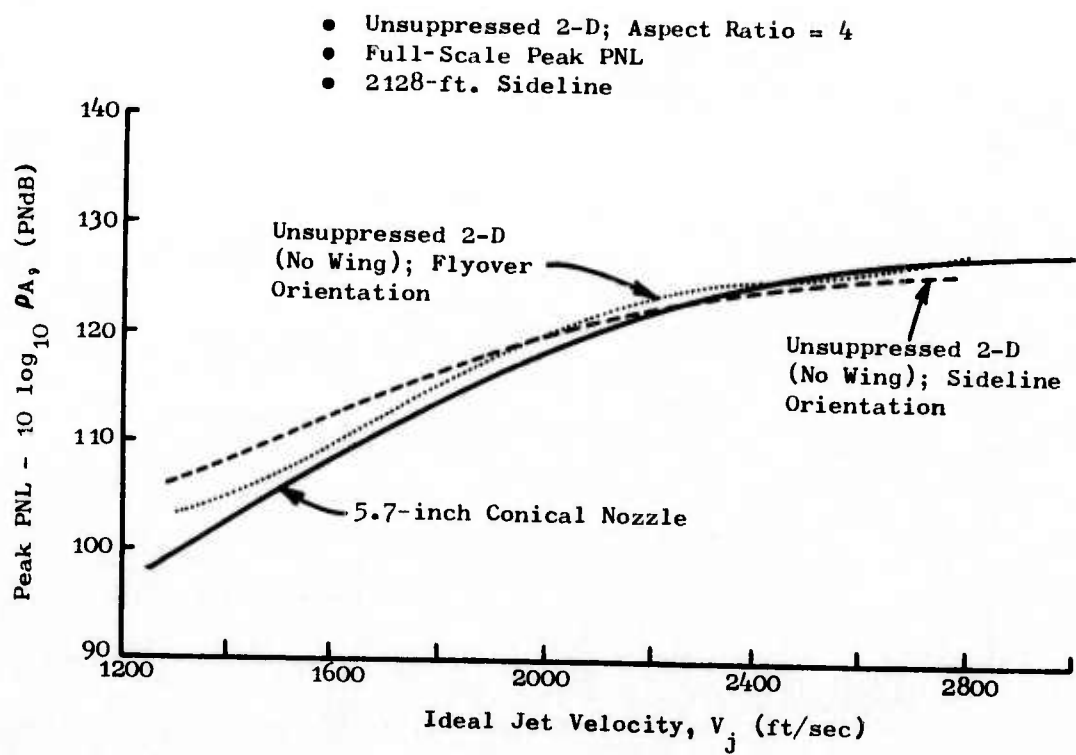
Figure 158. Effect of Nozzle Asymmetry on Peak PNL.
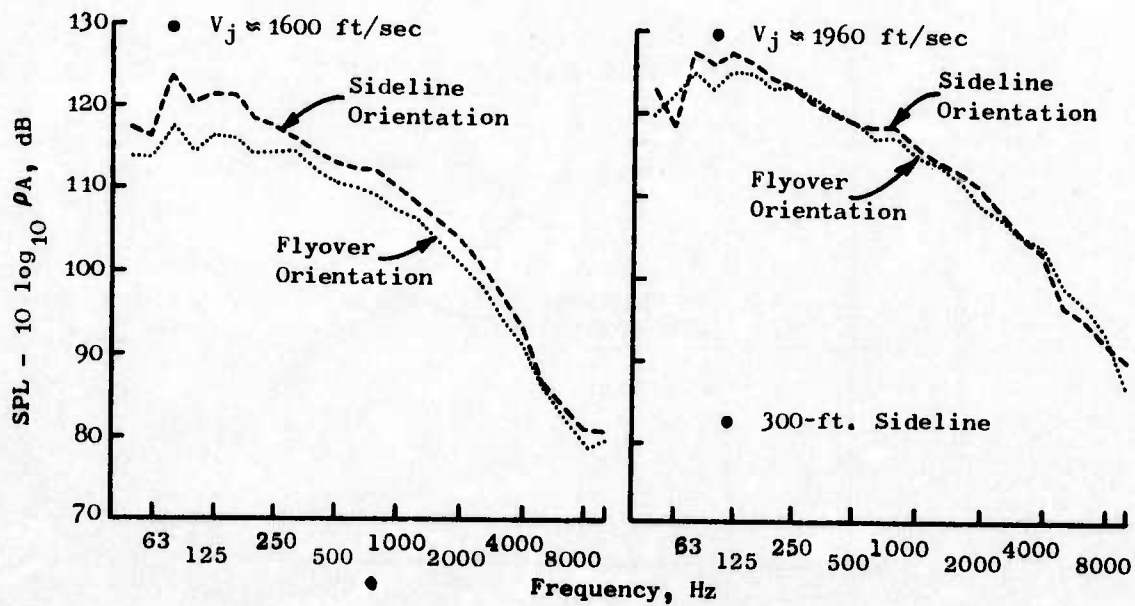
Figure 159. Effect of Nozzle Asymmetry on SPL Spectra.
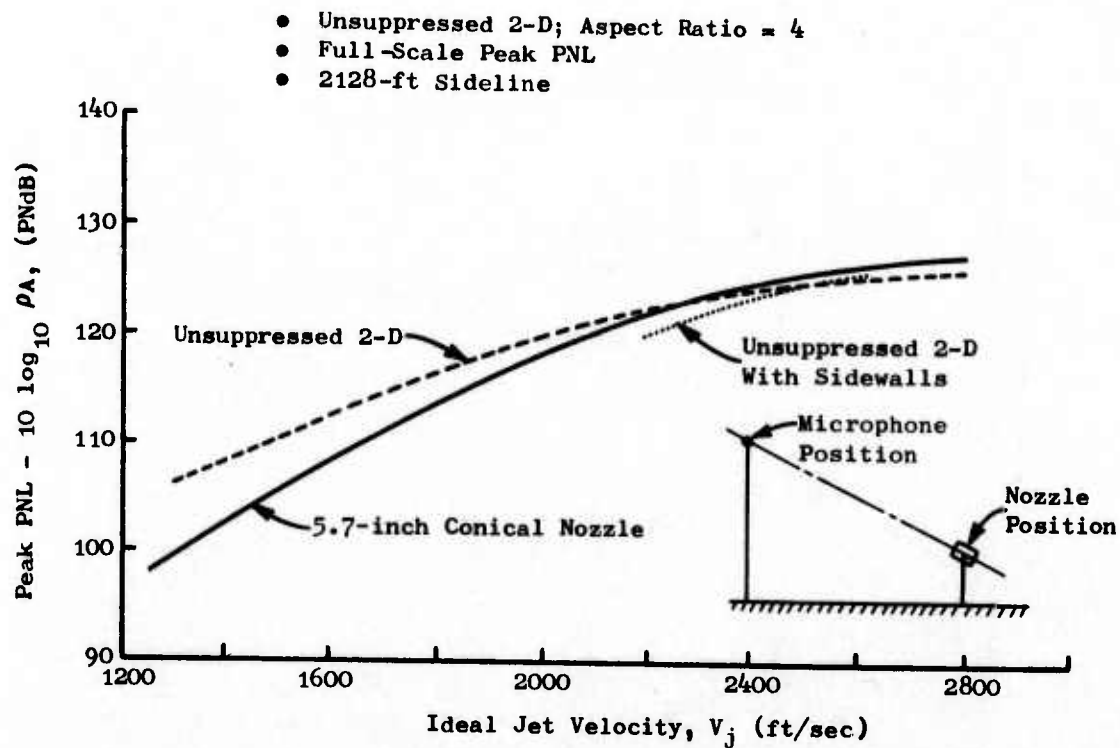
Figure 160. Effect of Nozzle Sidewall Shielding on Peak PNL.
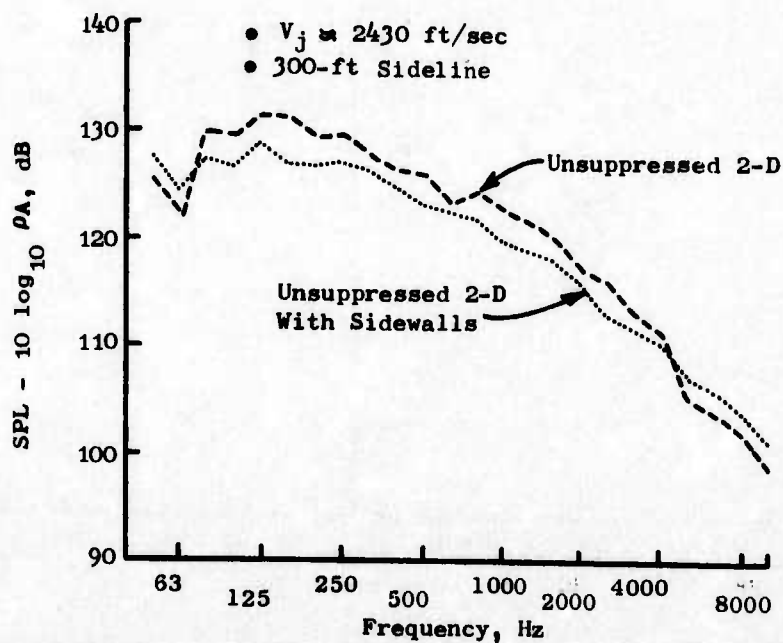
Figure 161. Effect of Nozzle Sidewall Shielding on SPL Spectra.

218

WATER-COOLED
TRANSITION
SECTION
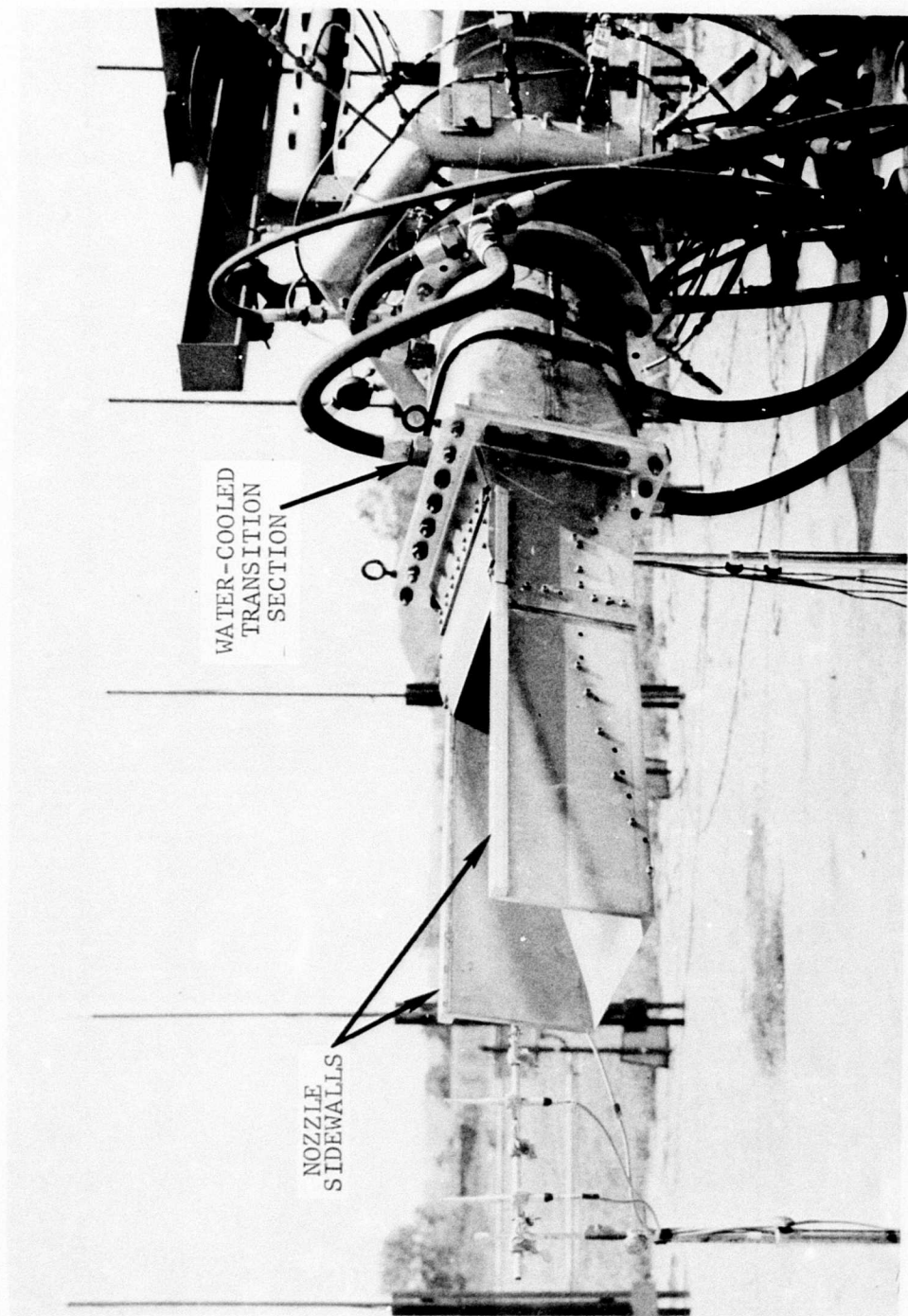
NOZZLE
SIDEWALLS

Figure 162. Unsuppressed Asymmetric 2-D Nozzle with Sidewalls; Sidewall Orientation.

2-D NOZZLE

SIMULATED WING
(OVER-THE-WING
INSTALLATION)
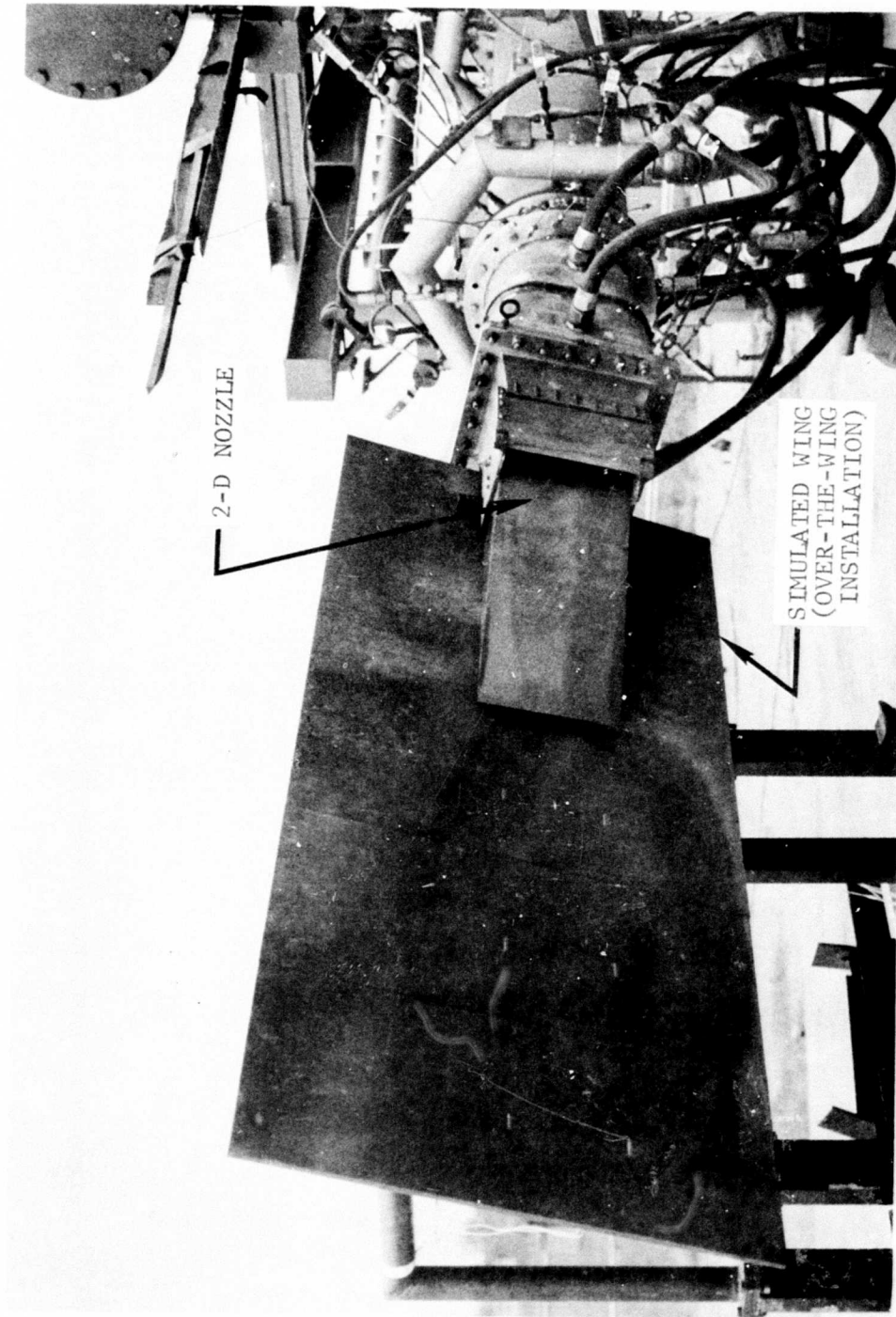
Figure 163. Unsuppressed Asymmetric 2-D Nozzle Mounted Over a Simulated Wing; Flyover Orientation.

WING FLUSH MOUNTED
TO 2-D NOZZLE

20 PARALLEL
SPOKE SUPPRESSOR
AREA RATIO = 2.0

THERMAL
SENSITIVE
PAINT
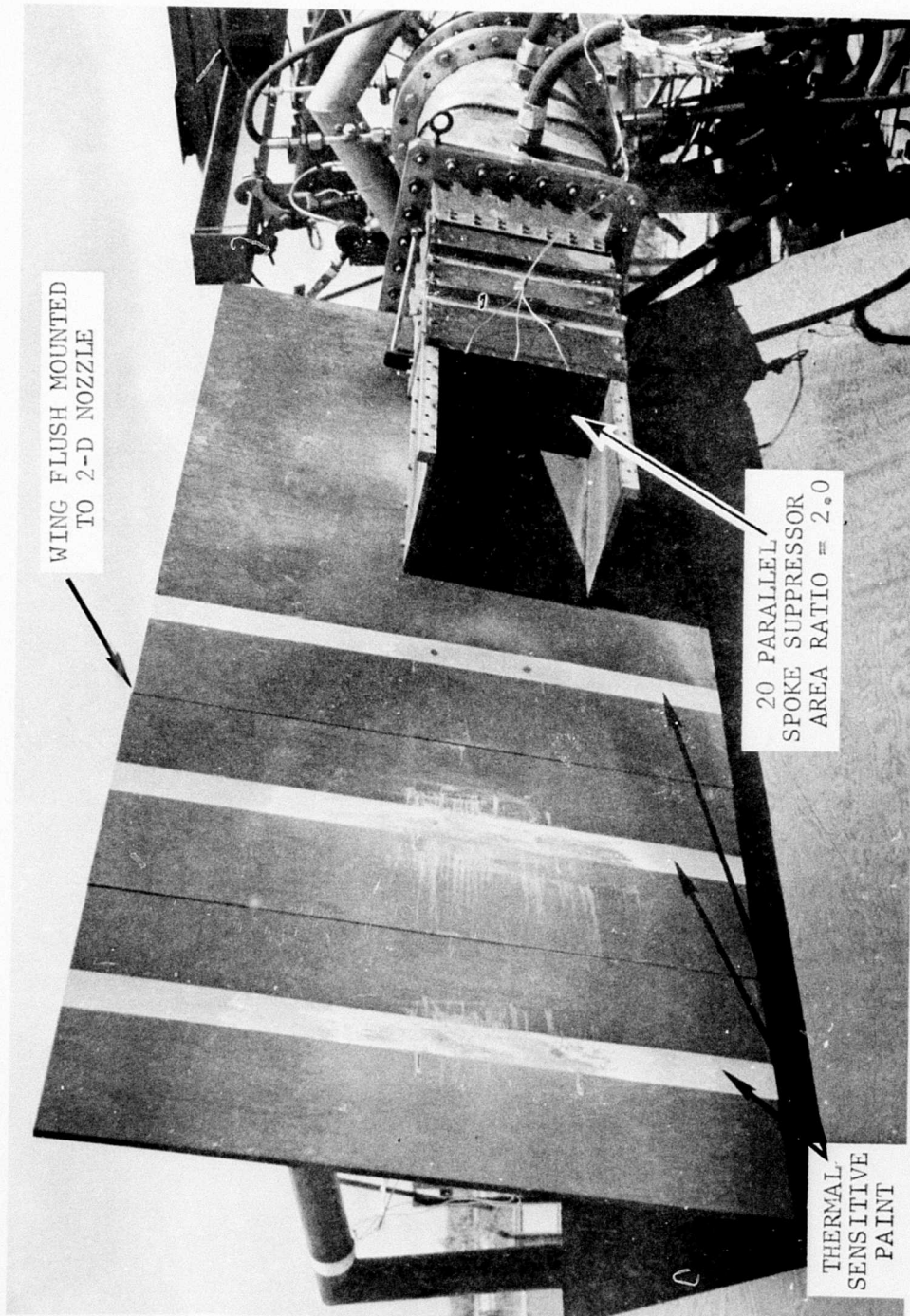
Figure 164. Suppressed Asymmetric 2-D Nozzle Mounted Over a Simulated Wing; Flyover Orientation.

221
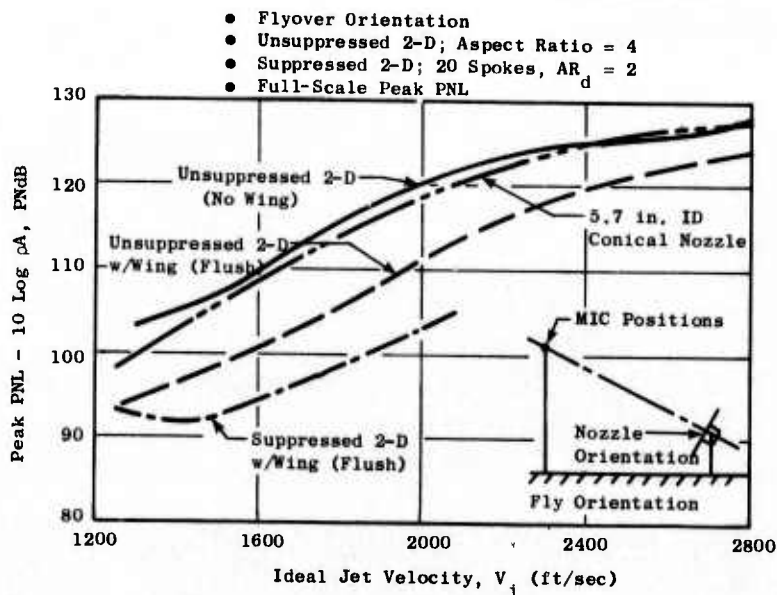
Figure 165. Effect of Wing (Flush)
Shielding on Peak PNL with
and without Suppression.

Figure 166. Effect of Wing (Y/h = 1)
Shielding on Peak PNL with
and without Suppression.

222

The suppressor used for this comparison consisted of a 20-parallel-spoke grid (normal to the plug ramp) with an area ratio of 2.0.

Figure 165 indicates a 9.0 to 4.0 PNdB reduction in noise with the wing flush mounted to the unsuppressed 2-D nozzle over the ideal jet velocity range tested. The suppression relative to a conical nozzle is seen to give a PNL reduction of 8-6 PNdB from 1600 to 2200 ft/sec. An additional suppression gain relative to a conical nozzle of 10 to 15 PNdB was incurred at velocities from 1400 to 2050 ft/sec with the 20-spoke suppressor in place.

With the wing at $Y/h \sim 1$, Figure 166, the unsuppressed 2-D nozzle noise levels were 8 to 10 PNdB lower than the same model without the wing over a velocity range of 1300 to 2300 ft/sec.

Suppression gains of 7 to 4.5 PNdB at velocities above 2300 ft/sec were obtained relative to the unsuppressed 2-D nozzle without the wing, and with the model and wing separated ($Y/h \sim 1$). This is about 0.5 to 1 dB greater ΔPNL than achieved with the flush-mounted wing over the same velocity range. This result demonstrates the effect of wing scrubbing which can be minimized to yield greater suppression.

When the suppressor grid was installed, an additional gain of 5 to 5.5 PNdB was obtained over the 1400 to 2050 ft/sec velocity range. The total suppression achieved was 10 to 16 PNdB, relative to the unsuppressed 2-D nozzle. The increase in noise level at the low velocity end (1250 ft/sec) with the 20-spoke suppressor is attributed to vortex shedding noise from the spokes at the condition.

Figures 167 and 168 illustrate the spectral effects of wing shielding and scrubbing. The figures show spectral comparisons at velocities of 1600 and 1950 ft/sec unsuppressed and suppressed nozzles with and without wing shields. The spectra show that the overall levels are 7 to 10 dB lower than with the wing at both conditions.

Hardwall Ejector Effect - A hardwall ejector (2-D) was tested in the sideline orientation on the unsuppressed 2-D nozzle with sidewalls. The model configuration is shown in Figure 169. The ejector employed an effective length-to-throat height ratio of about 9 which simulated a long aerodynamic mixing nozzle.

The results illustrated in Figure 170 show normalized peak PNL at the 2128-foot distance over the ideal velocity range of 1300 to 2800 ft/sec. The ejector gave a maximum of 3.5 PNdB suppression in the 2100 to 2300 ft/sec V_j range relative to the unsuppressed 2-D nozzle in the same orientation. At the lower velocities, only a 2-PNdB gain was realized due to low frequency noise dominating in the 315-Hz band which was apparent at pressure ratios up to about $P_{T8}/P_o \sim 2.2$ (corresponding to $V_j \sim 1950$ ft/sec). The cause of the "organ pipe" noise was attributed to the ejector inlet shape. In order to simulate the in-flight ejector acoustic performance in future tests, a bell-mouth shape would probably allow secondary air entrainment at low pressure ratios and thereby reduce or eliminate this dominant low frequency noise.
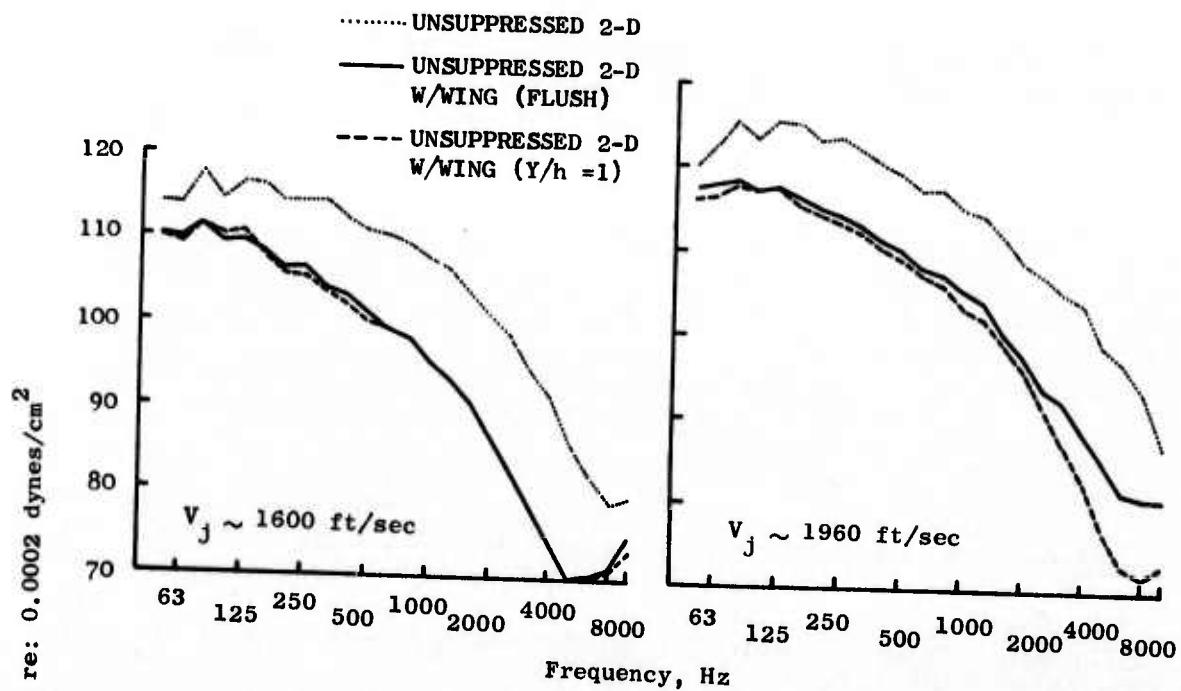
Figure 167. Effect of Wing Shielding on Unsuppressed 2-D Nozzle Spectra.
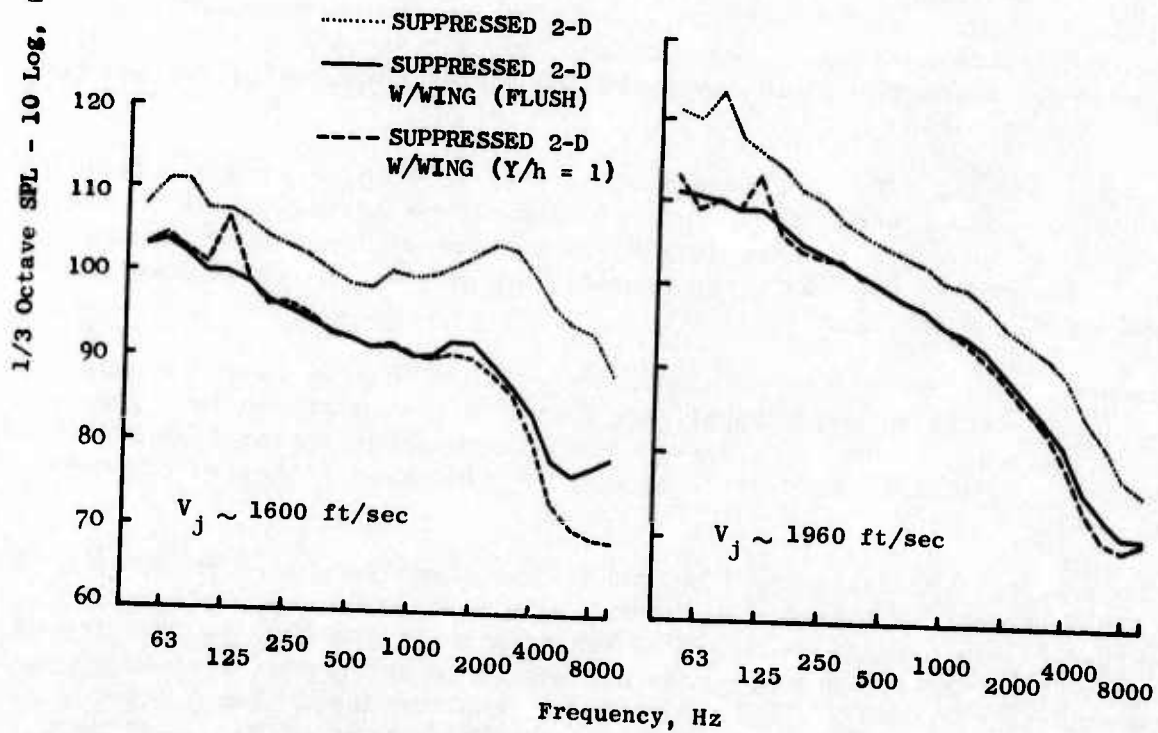
Figure 168. Effect of Wing Shielding on Suppressed 2-D Nozzle Spectra.
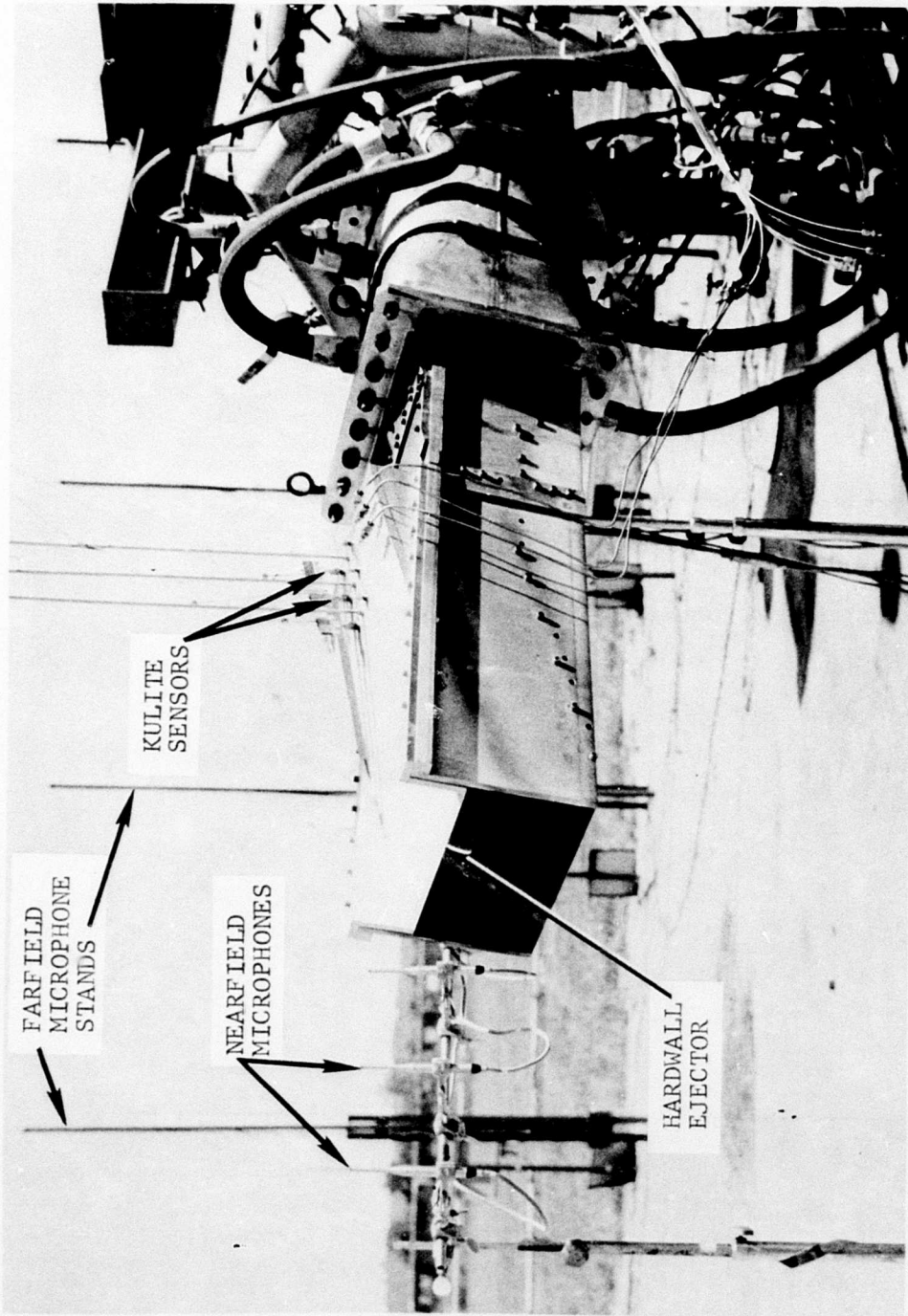
Figure 169. Unsuppressed Asymmetric 2-D Nozzle with Hardwall Ejector and Sidewalls; Sideline Orientation.

225
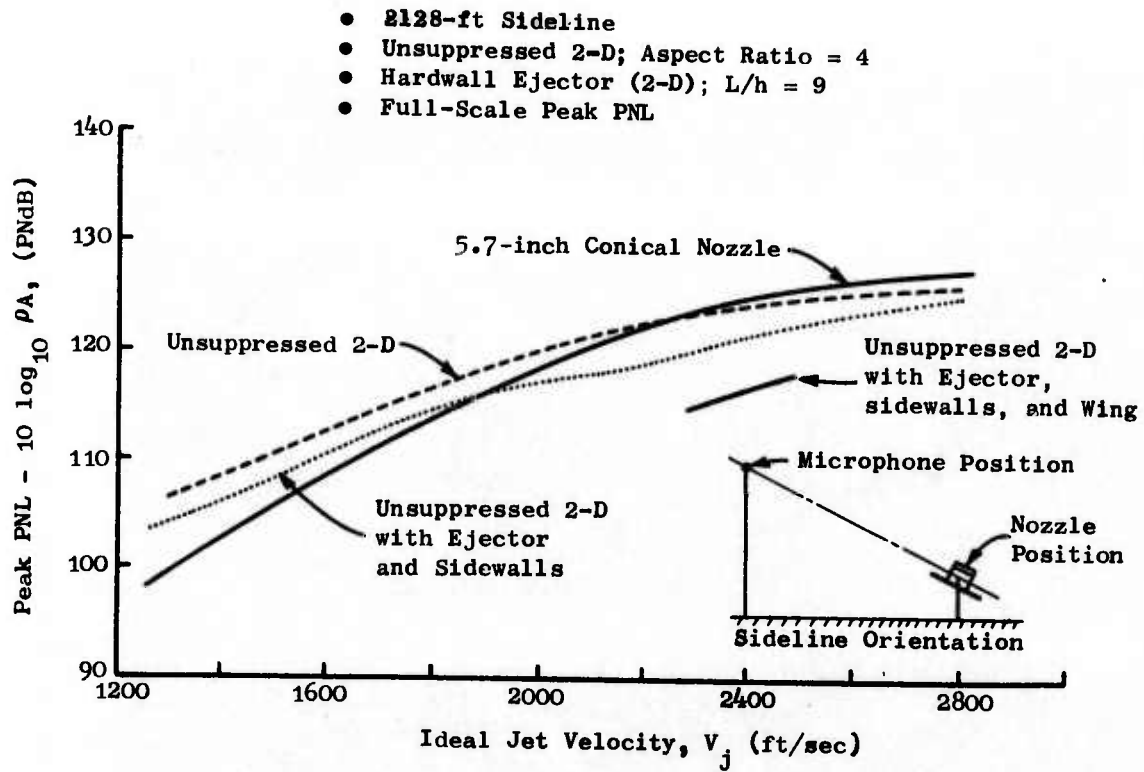
Figure 170. Effect of Hardwall Ejector on Peak PNL.
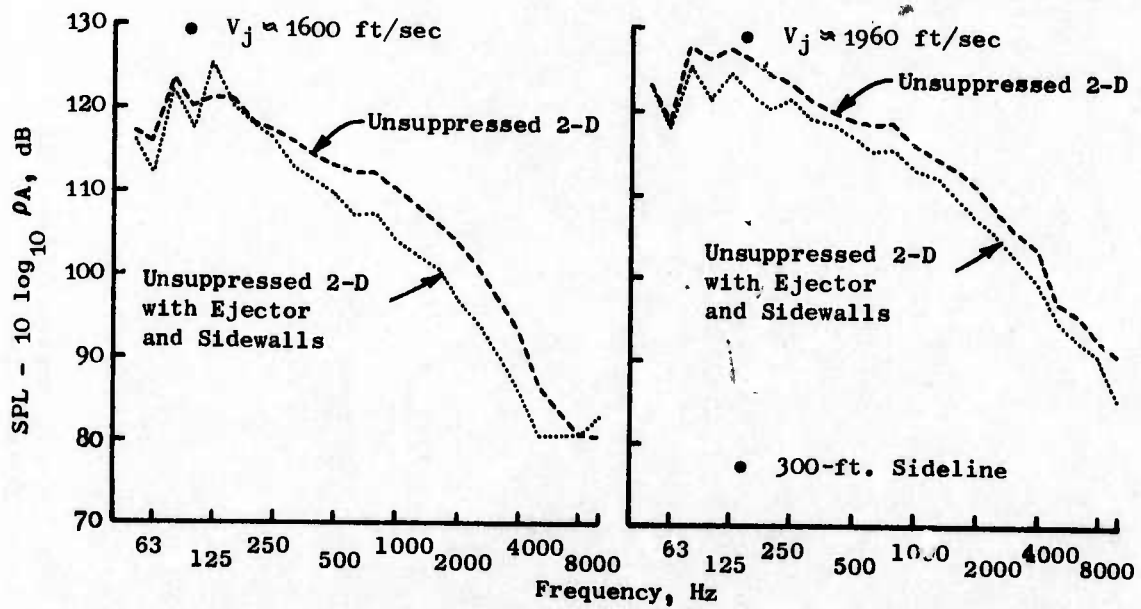
Figure 171. Effect of Hardwall Ejector on SPL Spectra.

226

The wing shielding effect with the ejector in the sideline orientation was demonstrated by placing the wing flush to the model surface; it provided a ΔPNL of 8.5 to 6.5 PNdB relative to the unsuppressed 2-D nozzle at velocities of 2300 to 2480 ft/sec.

The effects of the hardwall ejector can be seen on a spectral basis in Figure 171. These figures show comparisons between the unsuppressed 2-D nozzle with and without the hardwall ejector for jet velocities of 1600 and 1950 ft/sec. A uniform SPL reduction of 3-4 dB was observed with the ejector relative to the unsuppressed 2-D nozzle.

For purposes of evaluating the acoustic treatment design, one operating condition was selected (nozzle design point, V_J ~2350 ft/sec, P_{T8}/P_o~3.0). Figure 172 shows the as-measured model frequency spectral results of the near-field microphone measurements. The Kulite spectra for this operating condition are shown in Figure 173. Comparing the SPL contours for both the near-field microphone measurements and the Kulite instrumentation shows, in general, no dominant frequency tones, but suggests uniform noise level contours within the range of model frequencies of interest (1000 Hz to 80 KHz). The axial distribution of 1/3 octave band center frequencies is shown in Figure 174 and suggests an apparent near-constant noise level along the ejector axis for each frequency; strongly indicating that a broadband absorber was required for acoustic treatment. It also suggested that the predominant noise sources may have been generated downstream of the ejector region with the unsuppressed 2-D nozzle. The Kulites provided an estimate of the noise levels present inside the ejector, but did not give discernable data as to the spectral shape.

Comparisons (Figures 175 and 176) of near-field spectra were made with appropriate far-field test points for the unsuppressed 2-D nozzle with and without the ejector and also with data from a suppressed 2-D nozzle configuration. The far-field spectral shapes for the unsuppressed and suppressed 2-D nozzles exhibited much of the characteristics of an unsuppressed conical nozzle at that condition (V_j = 2350 ft/sec, P_{T8}/P_o = 3.0).

Rudimentary analyses suggest that the range of frequencies in the far-field that should receive the most attention with acoustic treatment should be from 125 Hz to 1000 Hz (full-scale). This could best be achieved by suppressing the near-field spectra between 1000 Hz to 4000 Hz (full-scale), as indicated by the NOY distribution curves for the near-field and far-field data, Figures 177 and 178.

This information and the results of annular plug nozzle tests with ejectors (Section 3.2.2) were used to specify the design of acoustic treatment to be employed in the model treated ejector tests.
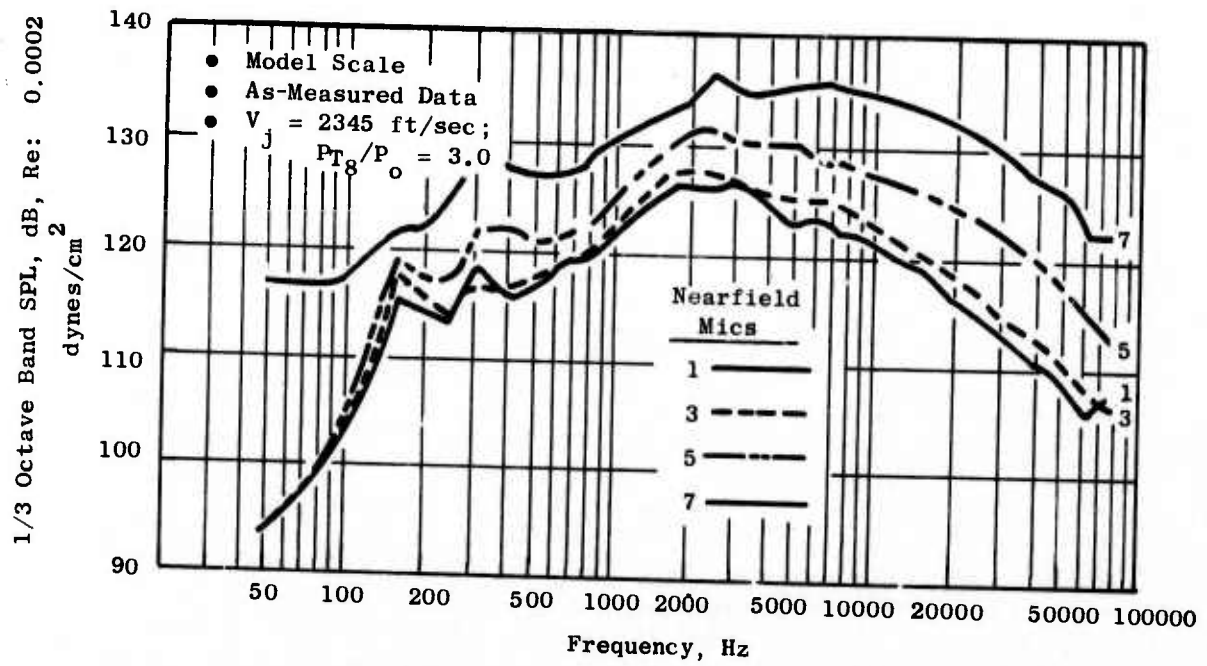
Figure 172. SPL Spectra from Near-Field Microphone Measurements.
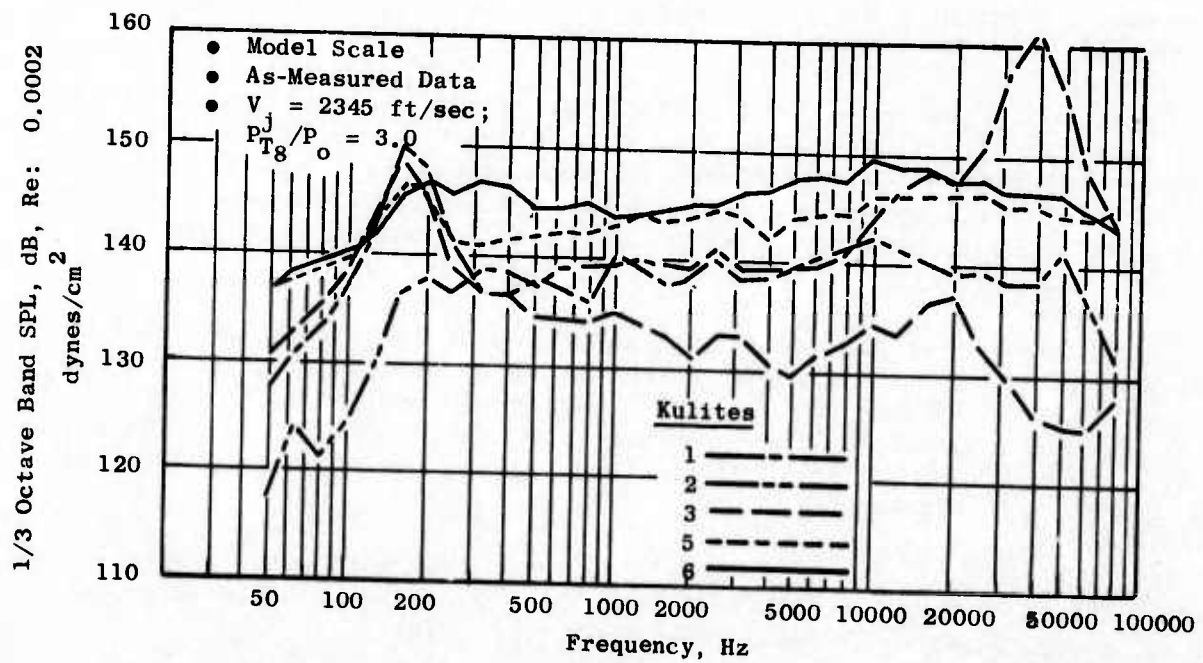
Figure 173. SPL Spectra from Ejector Kulite Measurements.
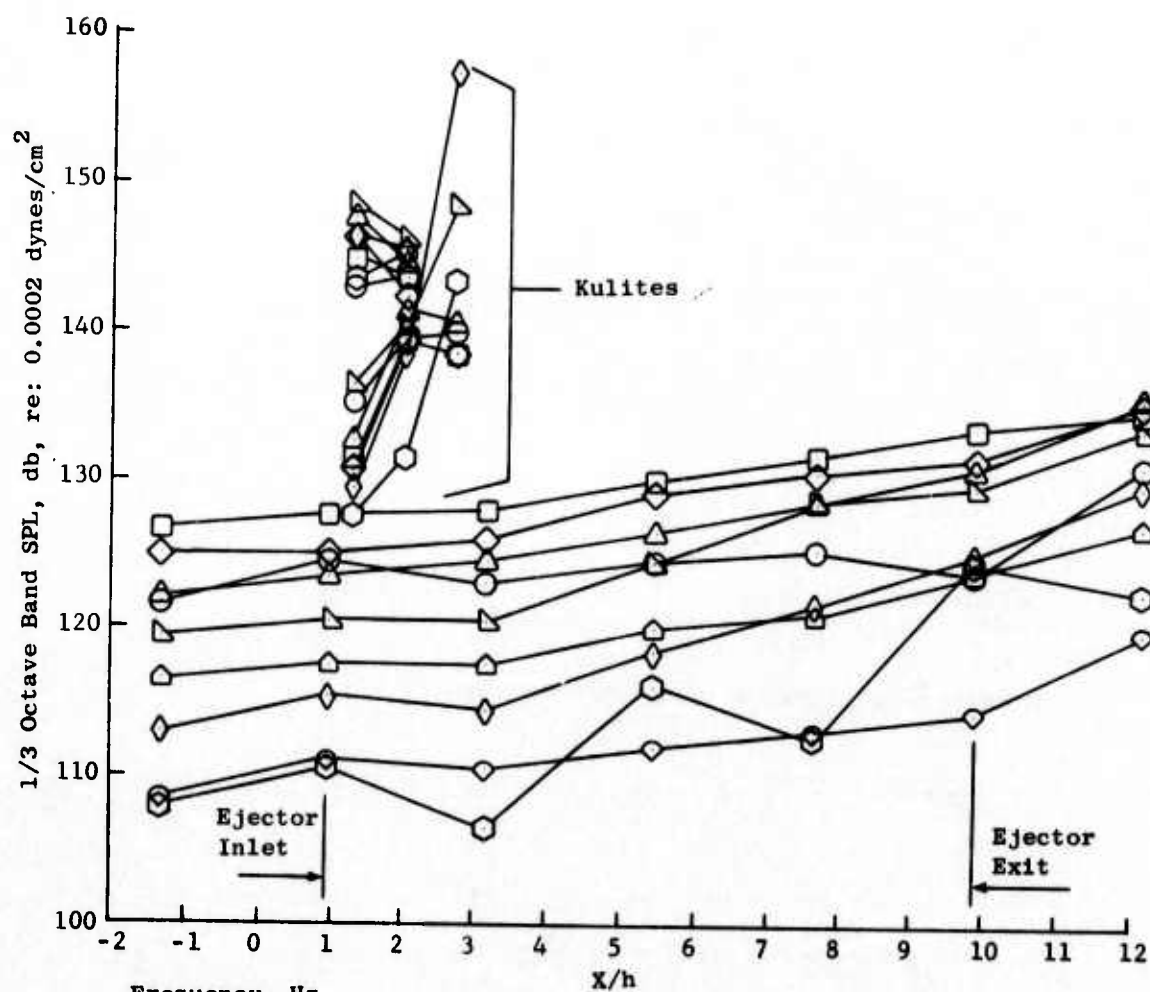
228
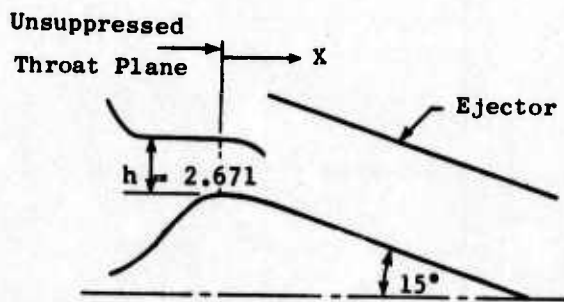
Figure 174. Axial Distribution of Near-Field Spectra.

Figure 176. SPL Spectra of Far-Field Acoustic Measurements.

Figure 175. SPL Spectra of Near-Field Acoustic Measurements.

230

Far-Field Measurement

○ Unsuppressed 2-D w/Ejector
□ Unsuppressed 2-D w/Sidewalls
  w/o Ejector
△ Unsuppressed 2-D w/o Ejector
◇ Suppressed 2-D w/o Ejector

● 1500-ft Sideline
● Peak Angle Spectra
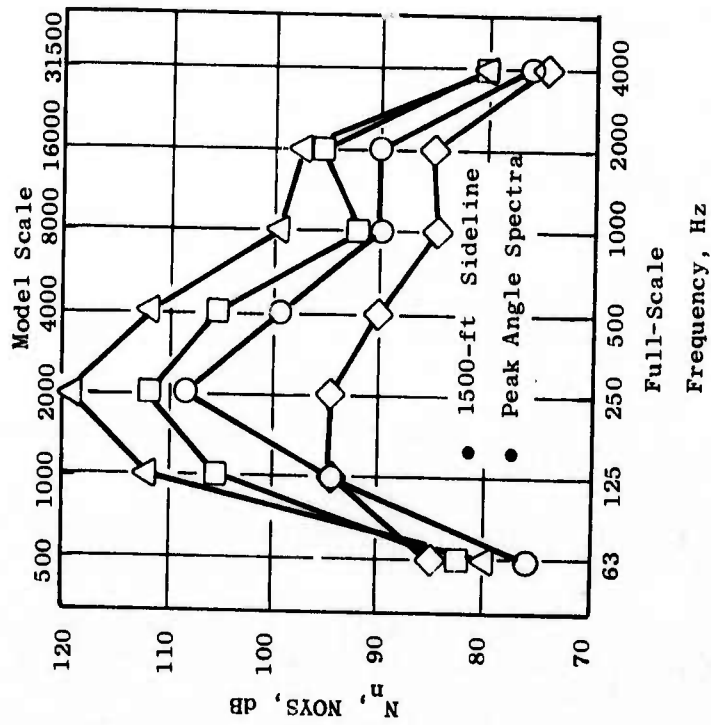
Figure 178. NOY-Weighted Spectra of Far-Field Acoustic Measurements.

Near-Field Measurement

── Inlet
── ── Exit

○ Unsuppressed 2-D w/Ejector
□ Unsuppressed 2-D w/Sidewalls w/o Ejector
△ Unsuppressed 2-D w/o Ejector

● As Measured Data

Figure 177. NOY-Weighted Spectra of Near-Field Acoustic Measurements.

231

Aerodynamic Performance Tests

Three acoustic suppressors were statically tested on a two-dimensional plug (RAMP) nozzle to determine thrust performance at take-off conditions. An unsuppressed plug nozzle and an ASME nozzle were also tested to determine baseline levels of thrust performance.

The objectives of the aerodynamic test program were:

- To determine the internal performance level of a baseline, unsuppressed, two-dimensional plug (ramp) nozzle at take-off conditions for the GE4/J6H2 cycle.

- To evaluate the effects of extended side plates on internal nozzle performance at take-off conditions.

- To determine the effects of a two-dimensional ejector shroud on uninstalled, nozzle performance at low nozzle pressure ratios.

- To investigate the performance levels of a two-dimensional nozzle with an effective area ratio of 1.94 spoke suppressor.

The nozzles tested in FluiDyne's Channel 7 dry air and room temperature, free jet, static thrust stand for this phase of the program included:

- A 4.5-inch ASME nozzle

- A Shielded Acoustic Suppressor Nozzle, Configuration 1

- A Baseline Nozzle, Configuration 2

- An Ejector Acoustic Suppressor Nozzle, Configuration 3

- A Spoke Acoustic Suppressor Nozzle, Configuration 4

Photographs of the individual models are presented in Figure 179. Table 7 contains a list of inspected throat and exit flow areas. The following paragraphs present a detailed description of the models tested:

ASME Nozzle - This reference nozzle has approximately the same throat area as the 2-D nozzles and provided a check of the facility force balance, metering nozzle, and seal combinations used in this test program.

Shielded Acoustic Suppressor Nozzle - Configuration 1 (Figure 179a was a small internal area ratio, two-dimensional plug nozzle with sidewalls which extended from the nozzle exit plane to the end of the plug. The shroud terminated at the nozzle exit plane which was 10.8% of the axial plug length downstream of the geometric throat.

232
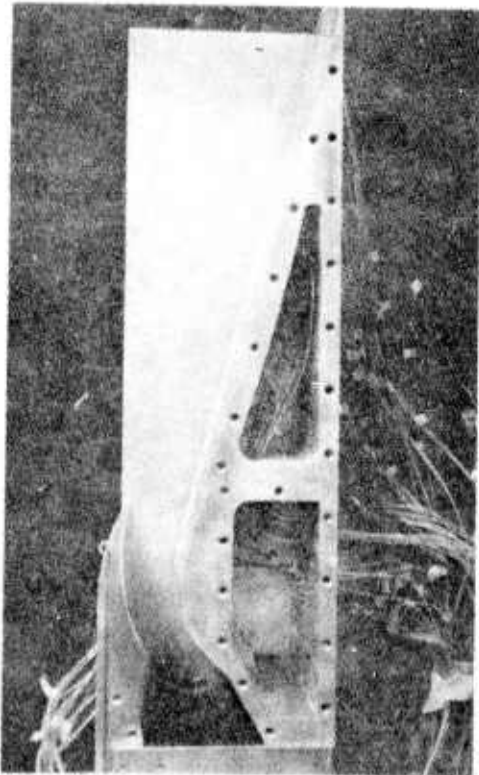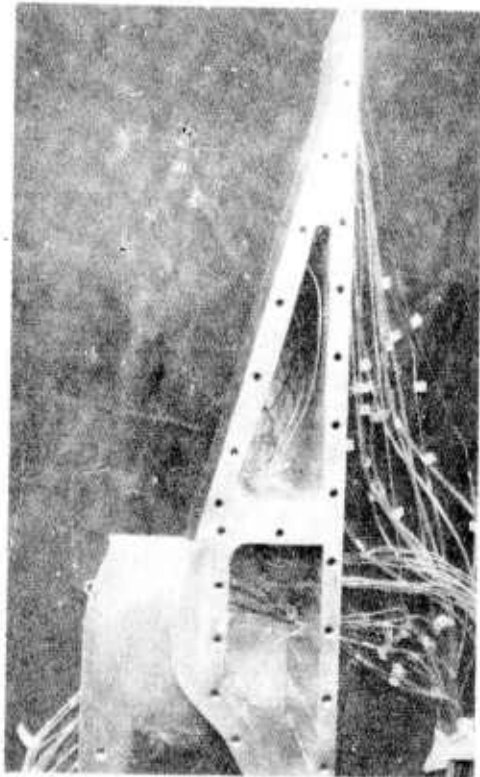
(a) Configuration 1
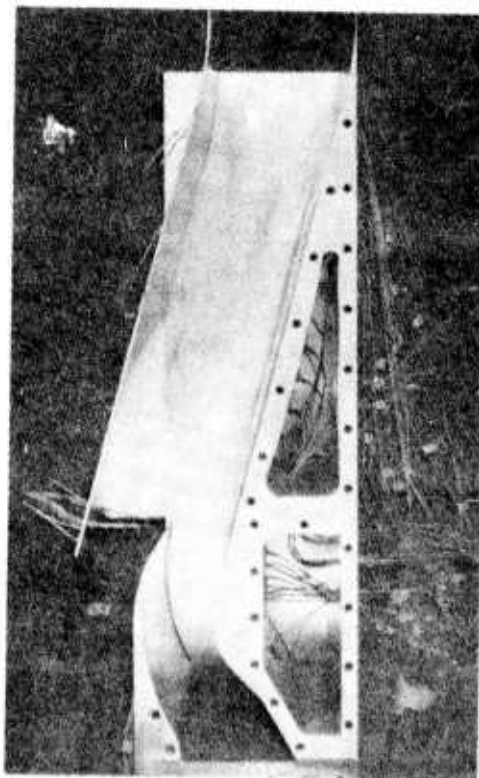
(b) Configuration 2
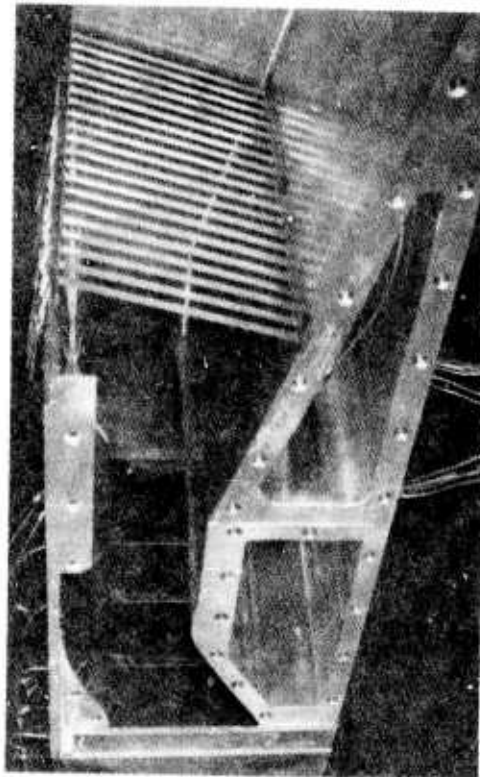
(c) Configuration 3

(d) Configuration 4

Figure 179. Model Photographs.

233

Table 7. Model Geometric Parameters.

Model	A_8	WI_8	H_8/HP	WI_8/H_8	Ri/H_8	Ro/H_8	L_p/H_8	$\left(\dfrac{A_9}{A_8}\right)_{int}$	$\left(\dfrac{A_9}{A_8}\right)_{ext}$	Area Ratio $(AR)_{eff}$
ASME	15.890	---	---	---	---	---	---	1.0	---	---
1	16.707	8.154	0.471	3.980	0.968	3.123	8.765	1.083	3.009	---
2	16.759	8.157	0.473	3.970	0.965	3.114	8.739	1.080	3.003	---
3	16.707	8.154	0.471	3.980	0.968	3.123	8.765	1.083	3.009	---
4	18.168	8.159	---	2.002	---	1.570	2.554	1.0	2.865	1.94

234
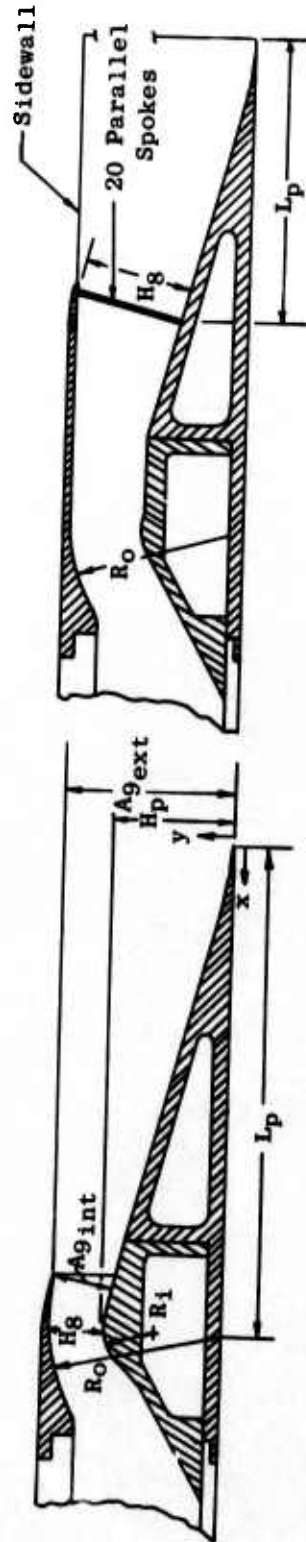
Baseline Nozzle - Configuration 2 (Figure 179b) was the same as Configuration 1 with the exception that the sidewalls terminated at the nozzle exit plane. The trailing edges of the sidewalls at the nozzle exit were normal to the model centerline and had the same external contour as the full-length sidewalls.

Ejector Acoustic Suppressor Nozzle - Configuration 3 (Figure 179c) was the same as Configuration 1 with the addition of an ejector shroud which was parallel to the plug and which extended from the primary nozzle exit plane to the end of the plug.

Spoke Acoustic Suppressor Nozzle - Configuration 4 (Figure 179d) was a 20-spoke, effective area ratio of 1.94, suppressor nozzle. The spokes were normal to the plug surface and had a solid triangular cross section. The width of a spoke at its trailing edge was constant from plug to shroud. The sidewalls were the same as those in Configuration 1.

Instrumentation - In addition to the facility instrumentation used to meter the flow and inlet momentum, the models were instrumented to obtain other pressure data. Model total pressure was defined as the numerical average of eight equal-area-weighted probes which were positioned on four, two-tube, rakes. The models were also equipped with static pressure taps to obtain the pressure distributions on the internal nozzle contours. Where applicable, static pressure distributions on the plug, shroud, sidewalls, ejector shroud, and spokes were obtained. For Configuration 3, the secondary or induced flow rate was also calculated, using the inspected area of the ejector inlet and an average inlet Mach number. The inlet Mach number was a function of the average of 10 total-pressure probes and the average of 4 static-pressure taps at the ejector inlet.

The model setup for this series was as described in the writeup of the FluiDyne Channel 7 static thrust stand in Appendix A.

Lampblack streak patterns also were obtained for the four two-dimensional nozzles. These streak patterns were made by placing discrete spots of a lampblack/glycerin mixture on the model surface prior to the test run. The streak patterns then were photographed after the run.

All model data were obtained in the nozzle pressure ratio range of 2.0 through 4.0.

Aerodynamic Performance Results and Analysis

The aerodynamic test results of the asymmetric 2-D nozzle configurations are summarized in Table 8.

A standard ASME long-radius metering nozzle was tested in Channel 7 over a range of five pressure ratios (2.0, 2.5, 3.0, 3.5, and 4.0) and flow rates to demonstrate facility data accuracy. The experimental ASME thrust coefficients, discharge coefficients, and stream thrust parameter were required to

Table 8. Aerodynamic Test Result Summary for Asymmetric 2-D Nozzles.

Configuration	Run No.	P_{T8}/P_o	C_{D_8}	$C_{D_8}A_8$	C_{f_g}	f_9	W_{ej}/W_8
4.5 in. ASME	1	1.978	0.9904	15.738	0.9935	1.2557	---
	2	2.480	0.9895	15.723	0.9942	1.2553	---
	3	2.963	0.9909	15.745	0.9916	1.2569	---
	4	3.458	0.9902	15.735	0.9866	1.2561	---
	5	3.969	0.9906	15.740	0.9815	1.2569	---
1 Shielded Unsuppressed 2-D Nozzle	6	1.994	0.9644	16.113	0.9666	2.2235	---
	7	2.994	0.9623	16.078	0.9771	1.8886	---
	8	3.981	0.9625	16.080	0.9585	1.7103	---
2 Baseline Unsuppressed 2-D Nozzle	9	2.003	0.9685	16.232	0.9654	2.2179	---
	10	2.980	0.9658	16.187	0.9753	1.8911	---
	11	3.970	0.9677	16.218	0.9637	1.7203	---
3 Unsuppressed 2-D Nozzle with Ejector	12	1.995	0.9646	16.116	0.9701	2.2259	0.210
	13	2.983	0.9659	16.137	0.9795	1.8965	0.114
	14	3.975	0.9668	16.153	0.9714	1.7283	0.108
4 Suppressed 2-D Nozzle	15	1.995	0.9053	16.456	0.6724	1.9032	---
	16	2.984	0.9119	16.568	0.7656	1.6152	---
	17	3.986	0.9124	16.576	0.8535	1.5247	---

236

agree within 0.25% of the semiempirical values before the facility was considered accurate and ready for testing. This criterion was satisfied.

Configurations 1, 2, 3, and 4 were run statically at three nozzle pressure ratios (2, 3, and 4). The results (thrust, discharge coefficients, and stream thrust parameter) of these four nozzles are presented in Table 8. The thrust coefficient, discharge coefficient, and stream thrust parameter, as functions of nozzle pressure ratio, are plotted in Figures 180a, b, and c, respectively. Nondimensional pressure distributions on the model surfaces are presented in Figures 181 through 184. These results show the Configurations 1, 2, and 3 to be nearly equal in static performance, while the shielded-spoke nozzle shows a drastic performance loss over the P_{T8}/P_O range as a result of a large base drag caused by poor spoke ventilation.

Lampblack photographs were made for each of the four two-dimensional configurations at a nozzle pressure ratio of three. The lampblack streak patterns are presented in Figures 185a through 185d and give an indication of flow patterns characteristic of each configuration.

This data analysis consisted of the following quantities: thrust coefficient, discharge coefficient, stream thrust parameter, static pressures on the internal surfaces, and ejector inlet total pressures. From the above quantities, other parameters, such as, peak thrust coefficient, fully flowing discharge coefficient, thrust loss due to pressure drag on the spokes, and ejector entrained flow were calculated. The above parameters, which are important in understanding a nozzle's performance, were determined as described in Appendix B.

Pertinent results of the analyses are presented below.

Shielded Acoustic Suppressor Nozzle (Configuration 1) - The peak thrust coefficient of Configuration 1 was calculated to be 0.981 at a nozzle pressure ratio of 2.7. The fully flowing discharge coefficient (C_{D8}) was 0.962. From the lampblack photo, Figure 185a, it can be seen that the nozzle flow downstream of the throat has been turned and directed down the plug at a nozzle pressure ratio of three.

Baseline Nozzle (Configuration 2) - The baseline nozzle has a calculated peak thrust coefficient of 0.980 at a nozzle pressure ratio of 2.7 and a fully flowing discharge coefficient of 0.967. From lampblack photo, Figure 185b, it appears that the primary flow downstream of the throat was turned down from the plug and that there was little lateral spillage off the plug from the shroud exit plane to a region halfway down the plug. This strongly suggests that, at $P_{T8}/P_O = 2.7$, the sidewalls were not required.

Ejector Acoustic Suppressor Nozzle (Configuration 3) - The peak thrust coefficient of the ejector nozzle was calculated to be 0.982 at a pressure ratio of 2.6. The fully flowing discharge coefficient of Configuration 3 is 0.966, which is almost equal to the discharge coefficient of Configuration 1. Numerical equivalency of the fully flowing discharge coefficients of Configurations 1 and 3 is expected since the ejector model is Nozzle 1 with

237
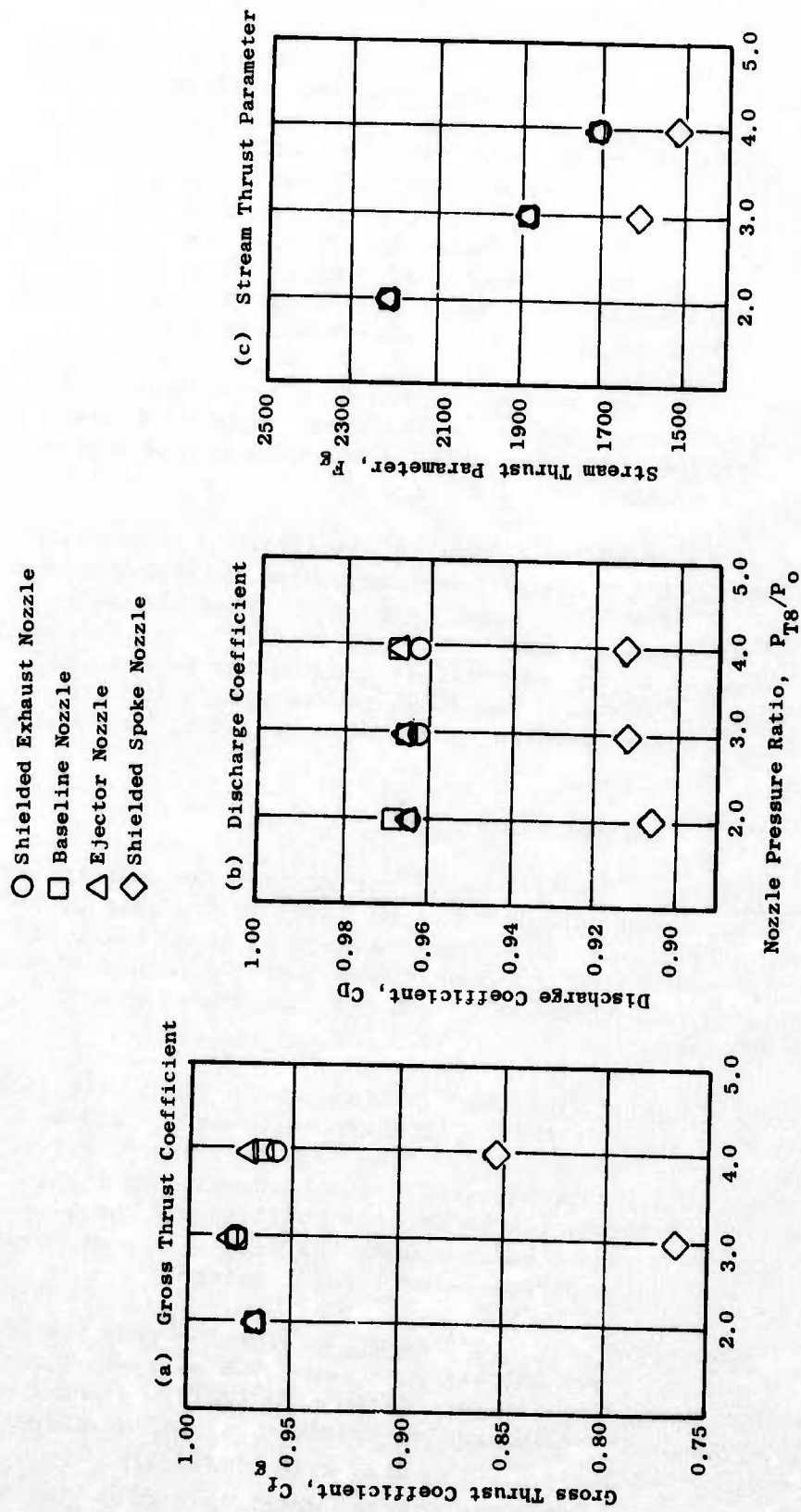
Figure 180. Asymmetric 2-D Nozzle Aerodynamic Performance Results.

238
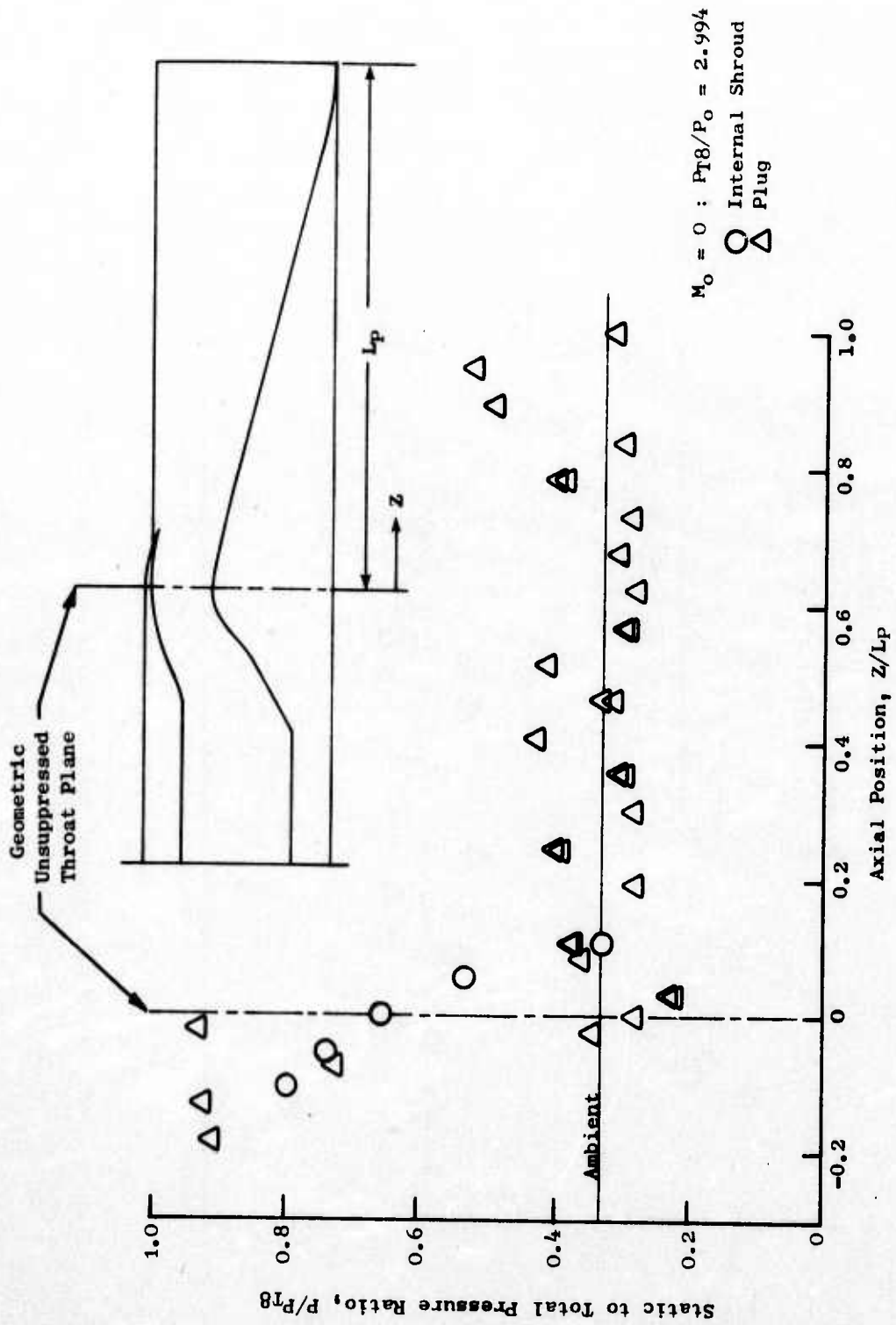
Figure 181. Unsuppressed 2-D Nozzle with Sidewalls; Surface Pressures.

239
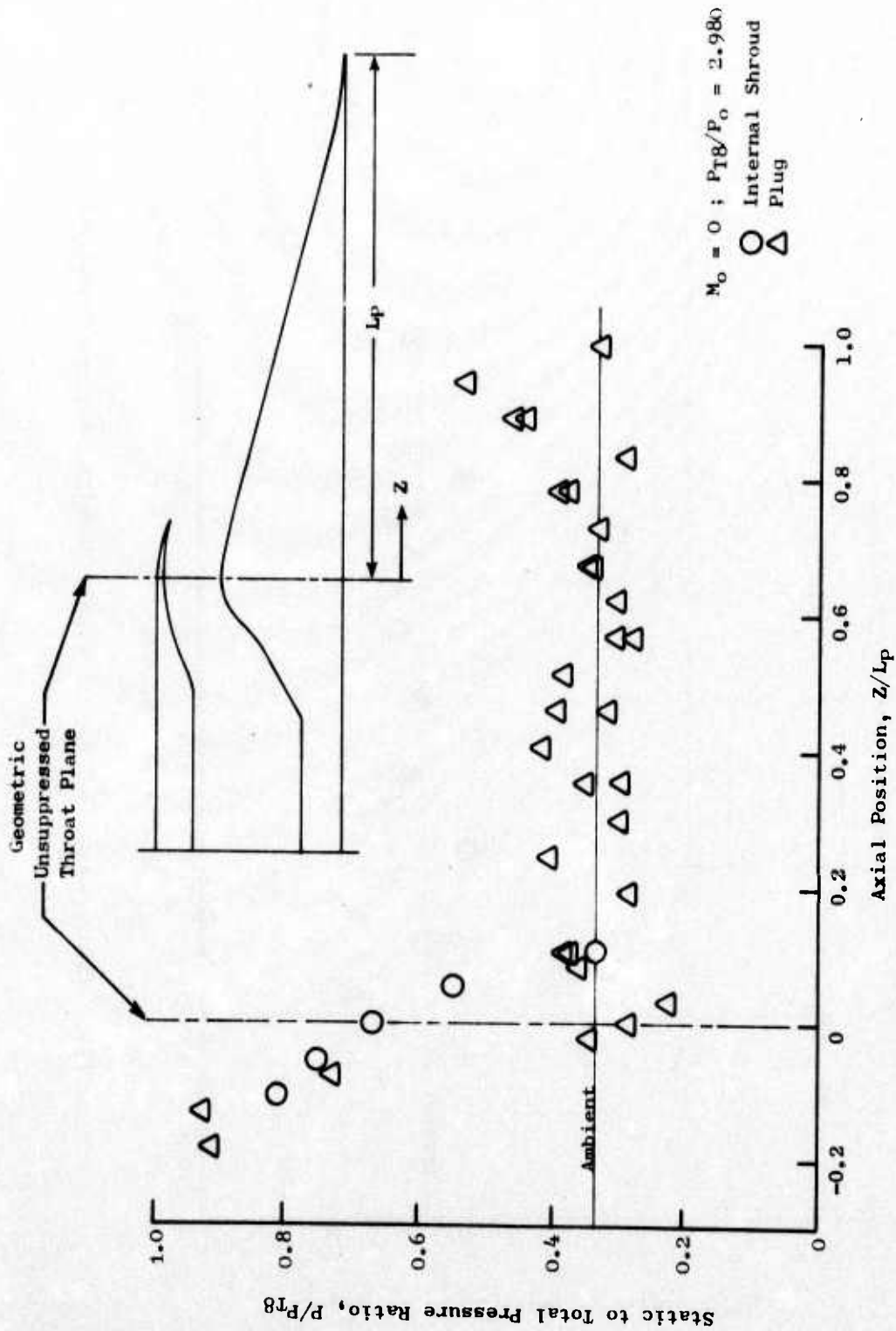
Figure 182. Unsuppressed 2-D Nozzle Surface Pressures.

240
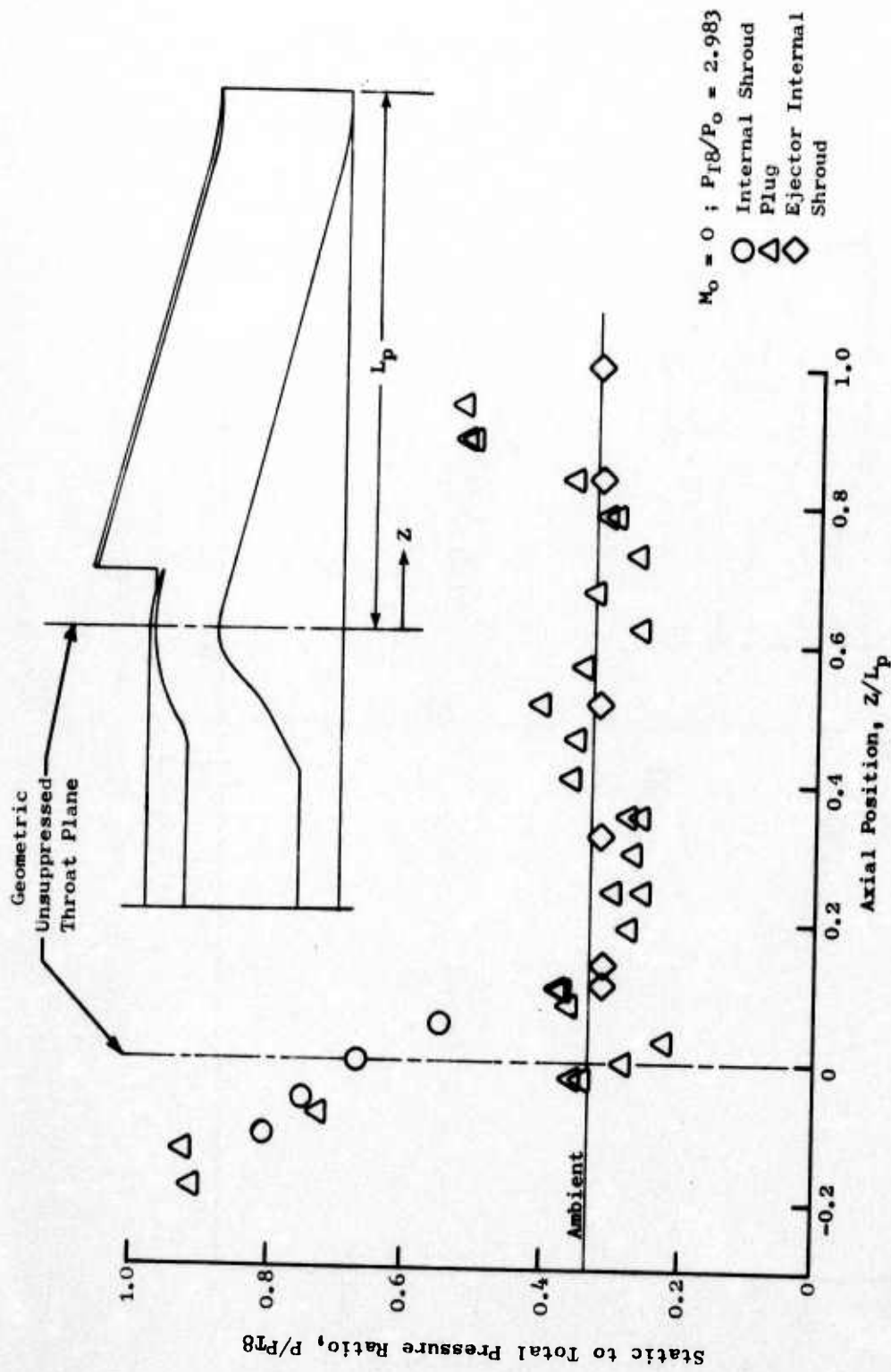
Figure 183. Unsuppressed 2-D Nozzle with Ejector Surface Pressures.

241
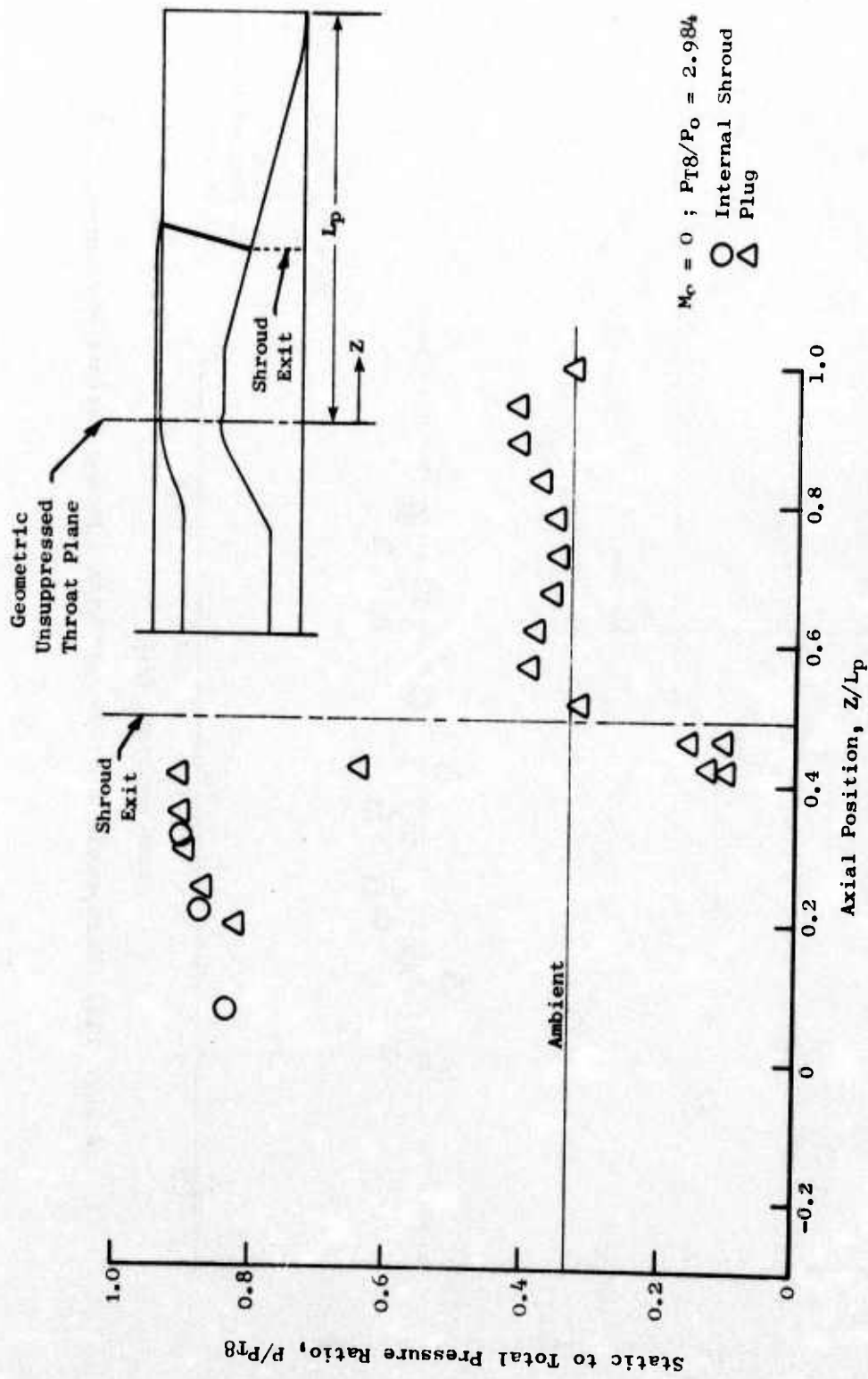
Figure 184. Suppressed 2-D Nozzle Surface Pressures.

242
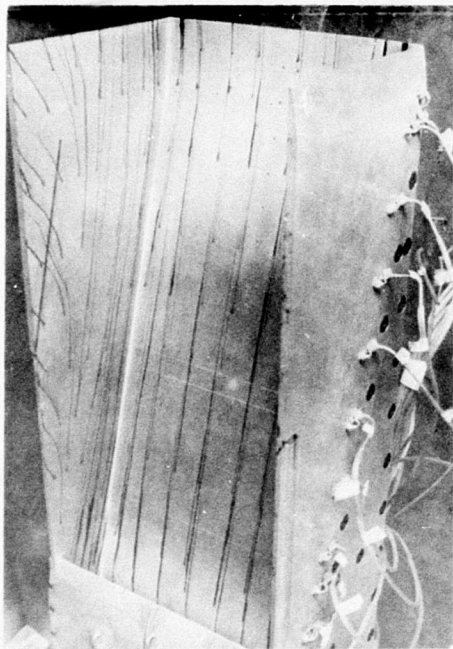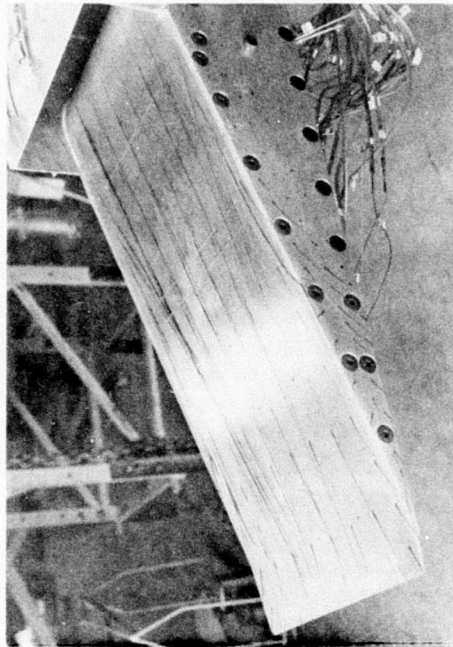
(a) Configuration 1
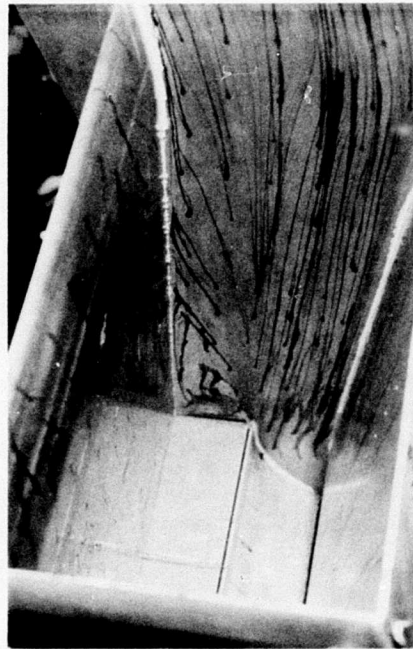
(b) Configuration 2
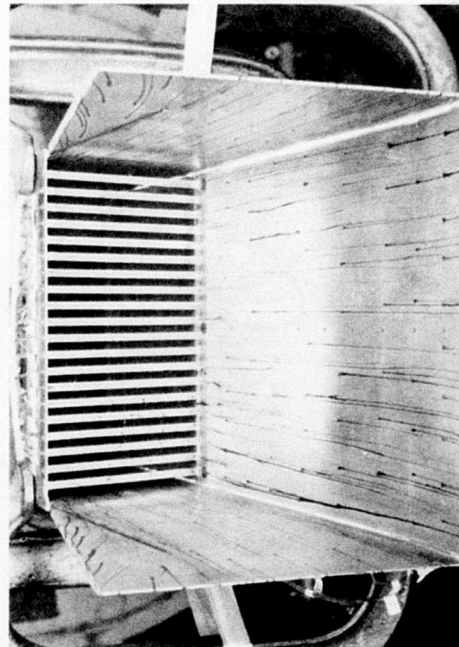
(c) Configuration 3

(d) Configuration 4

Figure 185. Model Photographs of Lampblack Test Results.

243

the addition of an ejector shroud. The induced flow rates of the ejector were calculated from the measured pressures and are presented below:

P_{T8}/P_o	Wej/W_8
1.995	.210
2.983	.114
3.975	.108

The secondary flow rate is a small percentage of the primary flow, considering that the flow areas of the ejector inlet and the primary throat are 16.772 in.^{2} and 16.707 in.^{2}, respectively. The reason for this low entrained flow rate is tthat the ejector had a flight-type inlet during this static test. In Figure 185c, it is apparent that there were large regions of separation around the inlet perimeter resulting in recirculation and reverse flow on the surfaces. Under forward velocity conditions, it is expected that this inlet would be filled.

Spoke Acoustic Suppressor Nozzle (Configuration 4) - The thrust coefficient versus nozzle pressure ratio distribution for Configuration 4 did not peak in the nozzle range investigated. The maximum thrust coefficient was 0.854 at a nozzle pressure ratio of 3.986. The fully flowing discharge coefficient for this configuration was 0.912. The thrust loss due to spoke base pressure drag and the ratio of average spoke base pressure to ambient pressure are presented below for each of the three nozzle pressure ratios tested:

P_{T8}/P_o	P_B/P_o	$\% \Delta C_{f_{g}SPOKE}$	$\% \Delta C_{f_{g}Total}$
1.995	.550	27.86	---
2.984	.367	21.27	$\sim$>90%
3.986	.477	11.92	---

The geometric and effective spoke area ratios are 1.768 and 1.938, respectively. It is interesting to note that the ratio of the static surface pressure to the nozzle total pressure on the backside of the spoke, and on the plug immediately downstream of the spokes, is constant once the nozzle is choked. This ratio, P/P_{T8}, varies on these surfaces from 0.10 to 0.13, which corresponds to an area ratio, A/A^*, from 1.93 to 1.67, respectively (which, in turn, corresponds to the effective and geometric spoke area ratios). This area ratio inequality would indicate that an overexpansion of the primary flow has occurred with the spoke base pressures being pumped down resulting in very low thrust performance.

244

Concept Evaluation

The baseline unsuppressed nozzle and both the shielded and the ejector acoustic suppressor nozzles exhibited high internal performance, $C_{fg} = 0.981$. It was recommended that these three two-dimensional plug nozzles should be tested in a wind tunnel under take-off conditions (M = 0.36) to investigate the external flow effects on thrust performance. This work would be carried out under the parametric refinement task.

A deep-chute suppressor for the two-dimensional plug nozzle also should be designed, built, and tested to determine if chute backside pressures can be increased. Another possible solution to low backside chute pressures would be to partially open the sidewalls downstream of the chute exit plane in order to ventilate this overexpanded region.

The acoustic characteristics of the asymmetric over-the-wing nozzles are shown in Figure 186. It illustrates the significance of the system with gains in PNL suppression relative to an unsuppressed conical nozzle due to combined effects of wing shielding and suppressed jet flow.

Suppressor tuning has the potential of increasing overall suppression at the higher V_j end. Additional gains might be achieved by the application of an acoustically treated ejector on the suppressed stream. Minimizing the wing scrubbing effect also would contribute favorably to the overall suppression of the system.

In summary, the asymmetric over-the-wing nozzle concept appears to be a potential mechanically feasible system which shows promise of significant gains in jet noise suppression with reasonable aerodynamic performance. Further investigation of this concept was continued under the Aeroacoustic Refinement tests.

3.2.4.4 Dual-Flow Exhaust Nozzle Systems

Acoustic Tests

The dual-flow exhaust nozzle tests conducted under this phase were designed to give a preliminary evaluation of the relative merit of the dual-flow concept in affecting jet noise suppression. Hot-jet acoustic tests were conducted on the JENOTS Facility setup for dual-flow operation as described in Appendix A. Cold flow testing also was conducted for aerodynamic measurements of core base pressure.

The dual-flow exhaust nozzle configuration selected for this initial test was a coannular, non-coplanar system consisting of an unsuppressed fan bypass stream and a suppressed core stream comprised of a 24-tapered-spoke, area ratio of 2.0, suppressor. The core-to-fan physical area ratio was 1.32, and the design bypass ratio was 1.5. The suppressor was instrumented with static taps to obtain base pressure measurements during cold flow test runs. A schematic illustration of the dual-flow configuration is shown in Figure 187.

245
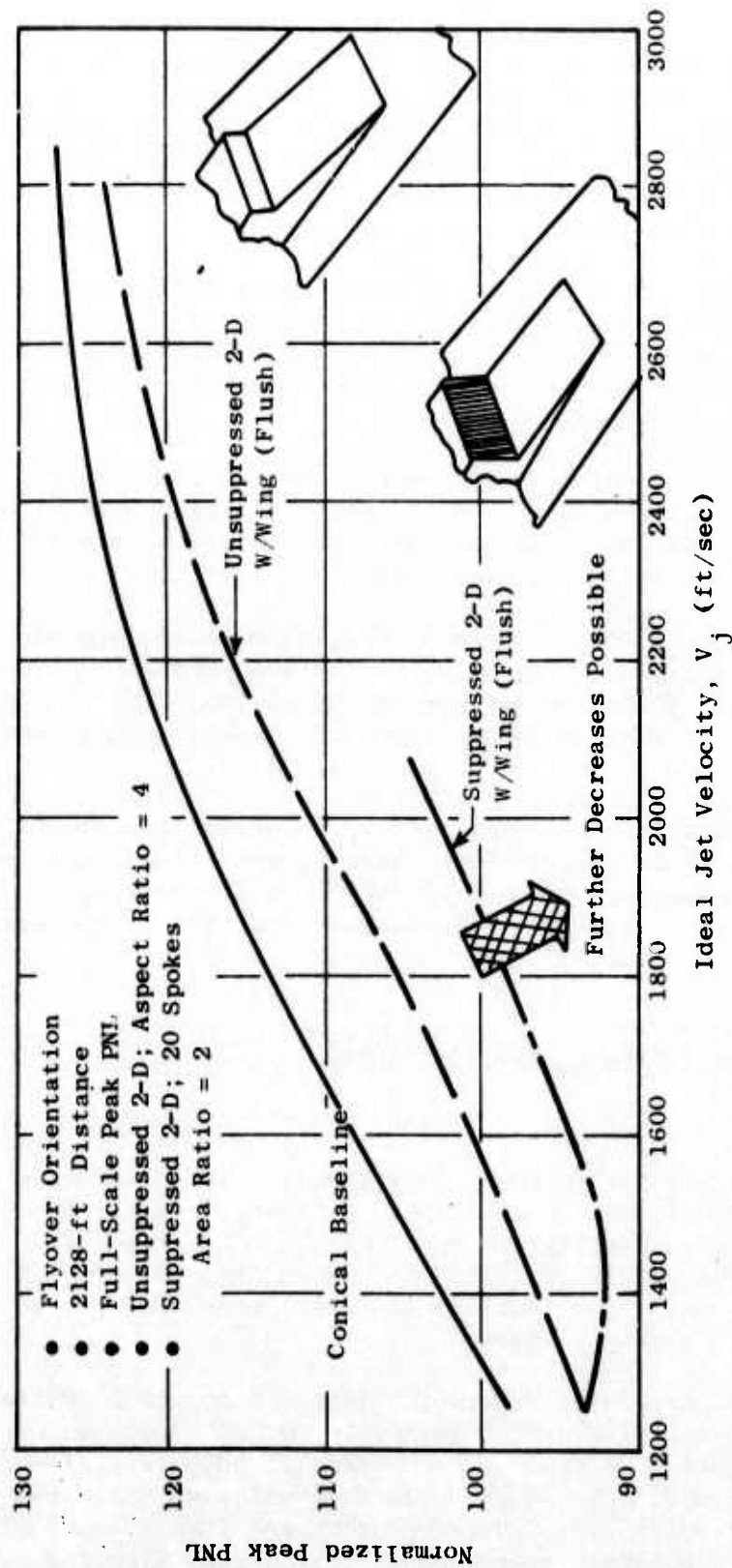
Figure 186. Asymmetric Over-the-Wing Nozzle Acoustic Characteristics.

246
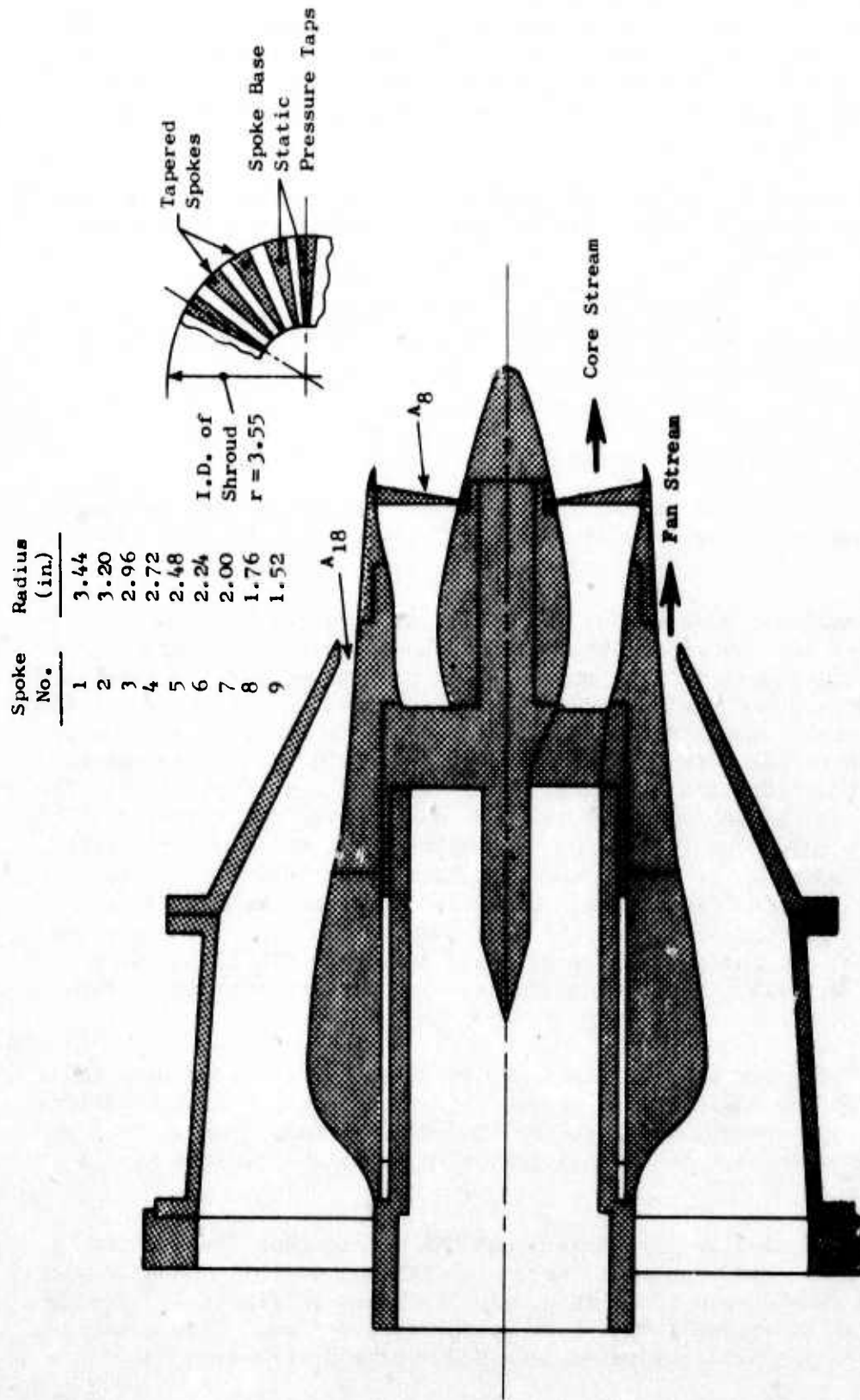
Figure 187. Schematic of Dual-Flow Exhaust Model with 24-Spoke Suppressor, AR_d = 2.0, in Core Stream.

247

Acoustic testing was conducted with single flows in the core and fan bypass alone, and with dual-flow (combined core and fan) operation. Conditions of dual-flow operation covered a range of ideal jet velocities from 1384 to 2422 ft/sec on the core with fan bypass velocities varying from 1255 to 1700 ft/sec, which simulated an average operating line derived from current AST engine studies.

Tests conducted with single flows ranged from fan stream ideal velocities of 600 to 1600 ft/sec and a corresponding range of core stream velocities from 600 to 2350 ft/sec.

Figure 188 is a photograph of the dual-flow exhaust nozzle configuration on the JENOTS facility. All acoustic data will be presented in simulated engine size and frequency range.

Acoustic Results and Analysis

The acoustic results of the dual-flow exhaust nozzle and single-core and fan flow tests are summarized in Appendix C along with the test conditions set.

Plots of normalized peak PNL at the 2128-foot sideline are shown versus ideal jet velocity for the suppressed core and unsuppressed fan bypass in Figure 189. Averaged data from an unsuppressed conical nozzle (5.7-inch I.D.) also are shown as a basis for comparison. The suppression attributed to the core with the 24-spoke suppressor (having an area ratio of 2) is as much as 10.5 PNdB at 2200 ft/sec. At velocities of 1300 to 1400 ft/sec, no change in PNL was observed between the conical nozzle and the suppressed core. The core directivity in Figure 190 shows that the peak angles shift from 110° to 140° from the jet inlet for increasing jet velocities. The fan directivity, although not included due to high winds, indicated that peak noise occurs around 110° over the operating range. PNL directivity at the 2128-foot distance is shown in Figure 191 for the dual-flow nozzle over the operating range of interest. Comparison of the core and dual-flow PNL directivity shows a marked similarity, indicating the core nozzle predominance of the jet noise.

Spectral directivity on a 320-foot arc is shown for the core only in Figure 192 and for the dual-flow in Figure 193 at the design point condition. The results show the spectra for both the core and the dual-flow to be low-frequency-dominated at high jet velocities, similar to the conical nozzle spectra.

A plot of the dual-flow normalized peak PNL versus ideal net thrust is shown in Figure 194. The suppressed core peak PNL and dual-flow nozzle peak PNL are compared on a common ideal core velocity basis in Figure 195 and show a reduction in PNL of around 4 PNdB between the core and dual-flow nozzle over an ideal core jet velocity range from 1700 to 2400 ft/sec.

248

24 SPOKE SUPPRESSOR
AREA RATIO = 2.0

FAN/CORE β = 1.5
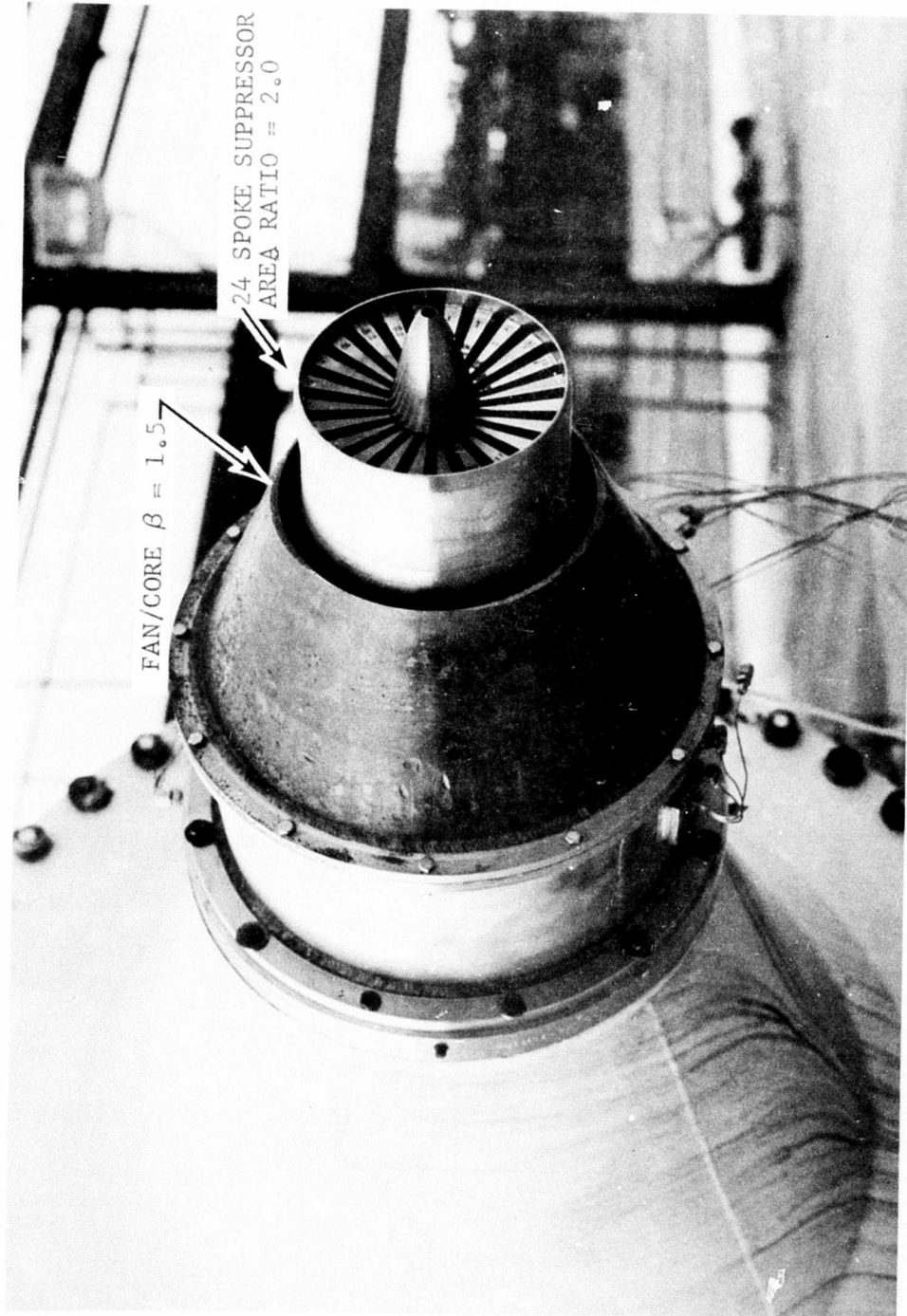
Figure 188. Dual-Flow Exhaust Nozzle Tested for Advanced Concepts.

249
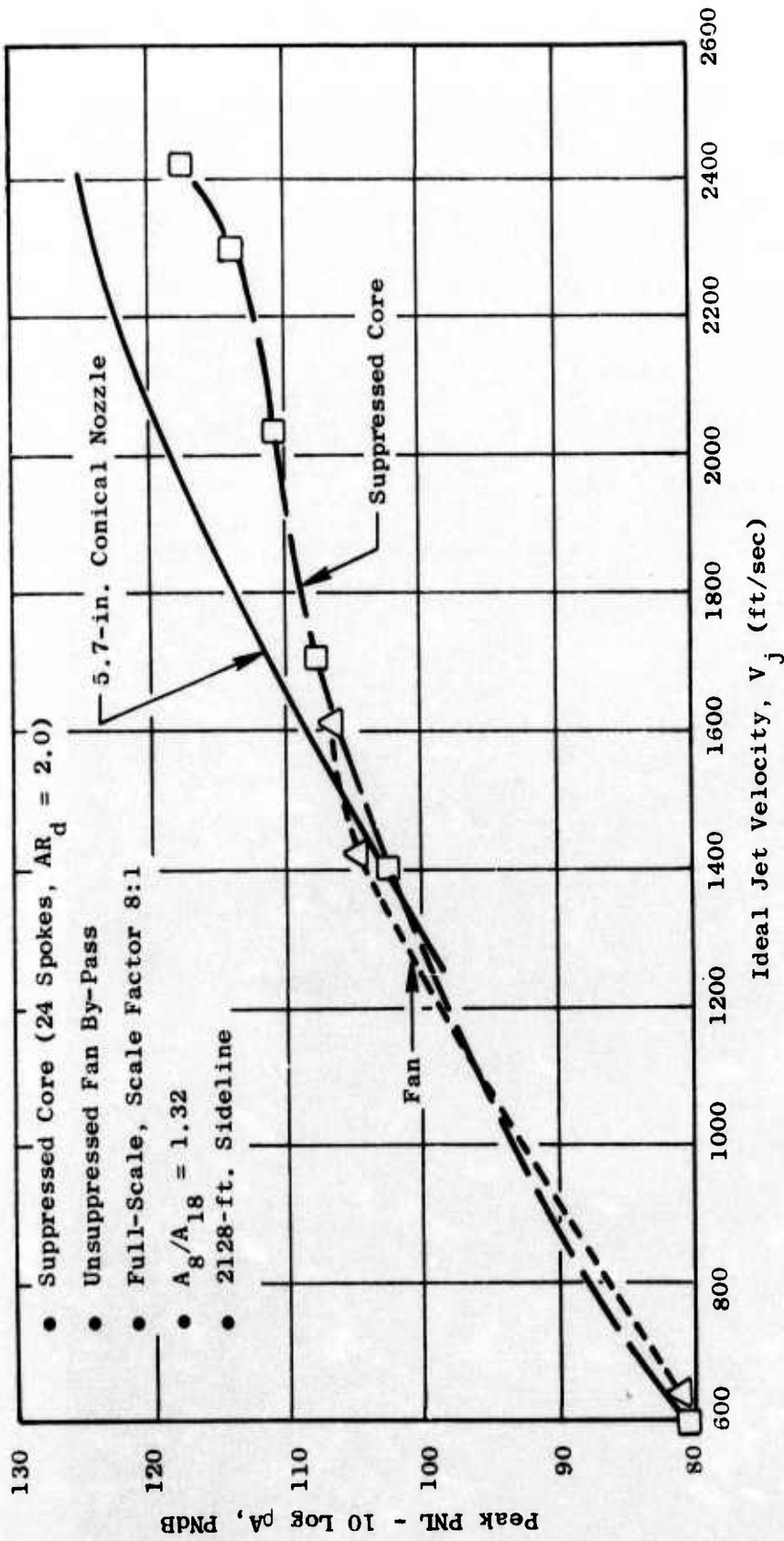
Figure 189. Peak PNL Comparisons of Dual-Flow Exhaust Nozzle Components.

250
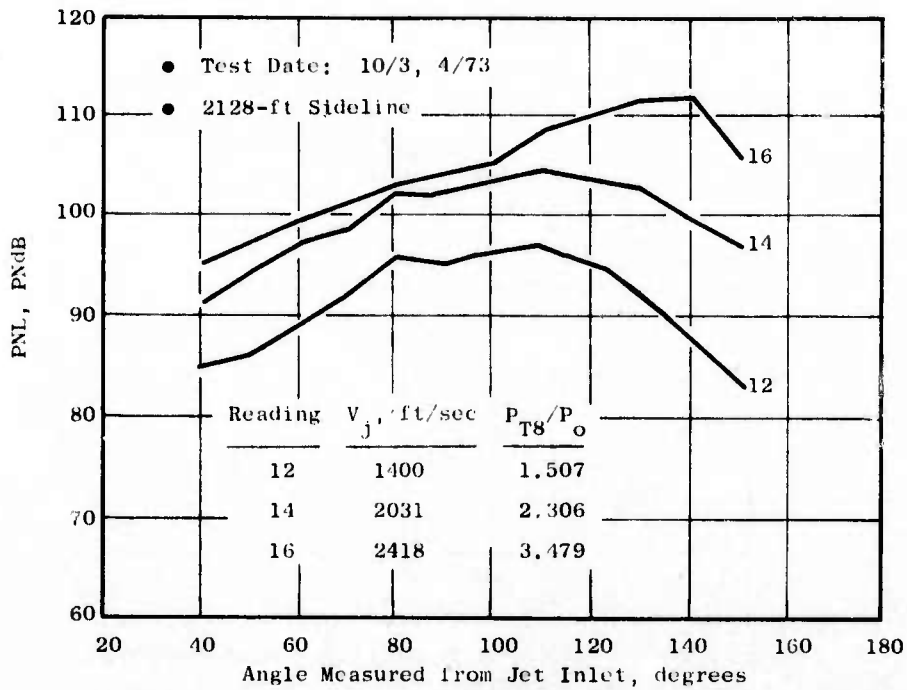
Figure 190. PNL Directivity for Suppressed Core Only.

The chart includes:
- Test Date: 10/3, 4/73
- 2128-ft Sideline

Reading	V_j, ft/sec	P_{T8}/P_o
12	1400	1.507
14	2031	2.306
16	2418	3.479
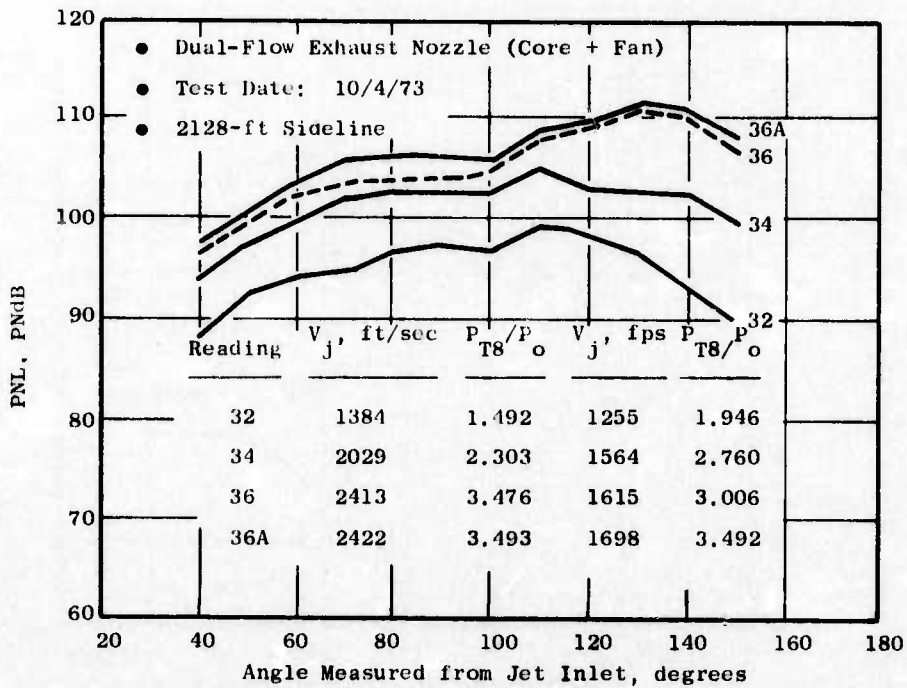
Figure 191. PNL Directivity for Dual-Flow Nozzle.

The chart includes:
- Dual-Flow Exhaust Nozzle (Core + Fan)
- Test Date: 10/4/73
- 2128-ft Sideline

Reading	V_j, ft/sec	P_{T8}/P_o	V_j, fps	P_{T8}/P_o
32	1384	1.492	1255	1.946
34	2029	2.303	1564	2.760
36	2413	3.476	1615	3.006
36A	2422	3.493	1698	3.492

251
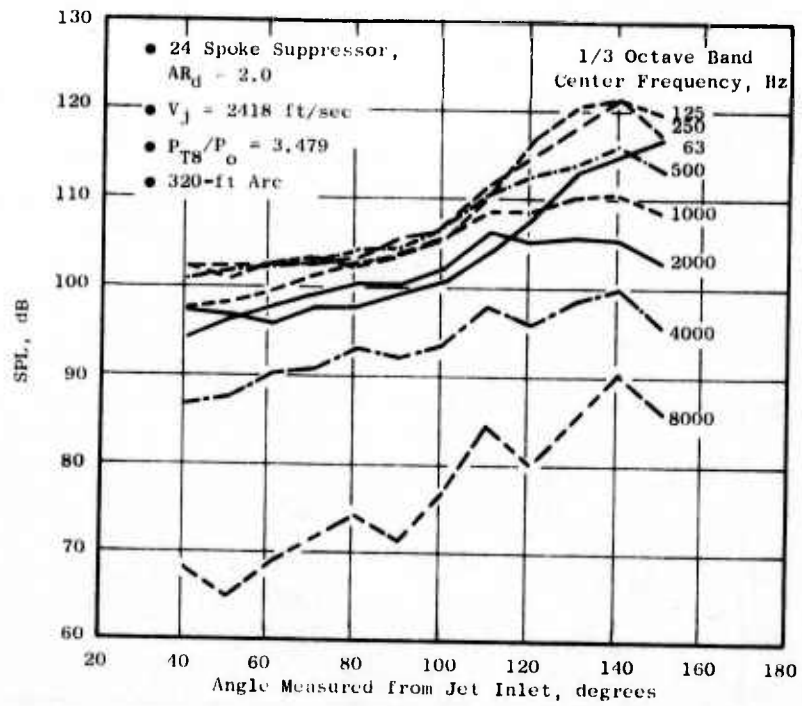
Figure 192.   Spectral Directivity for Suppressed
Core Only.
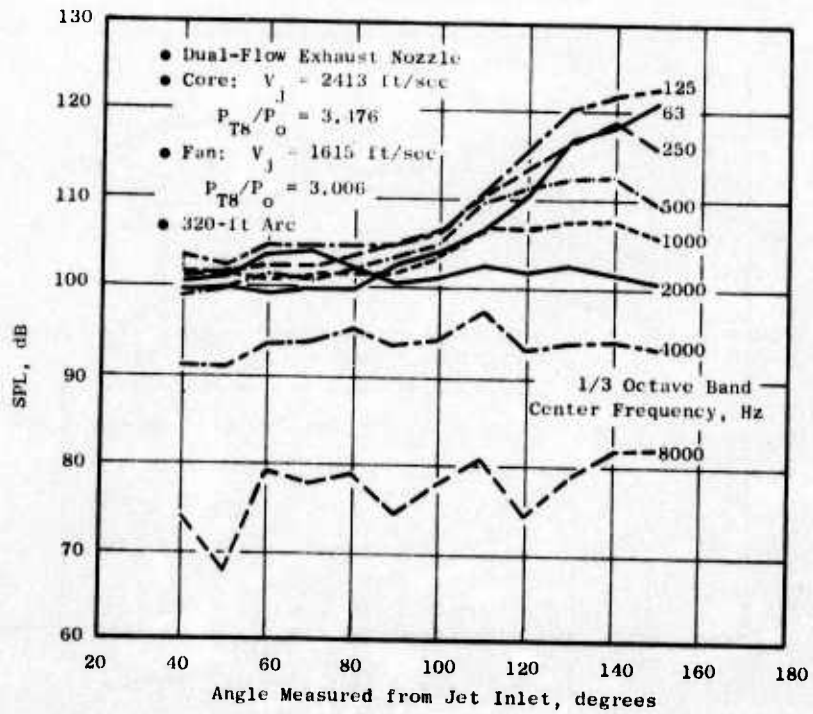
Figure 193.   Spectral Directivity for Dual-Flow
Nozzle.

252
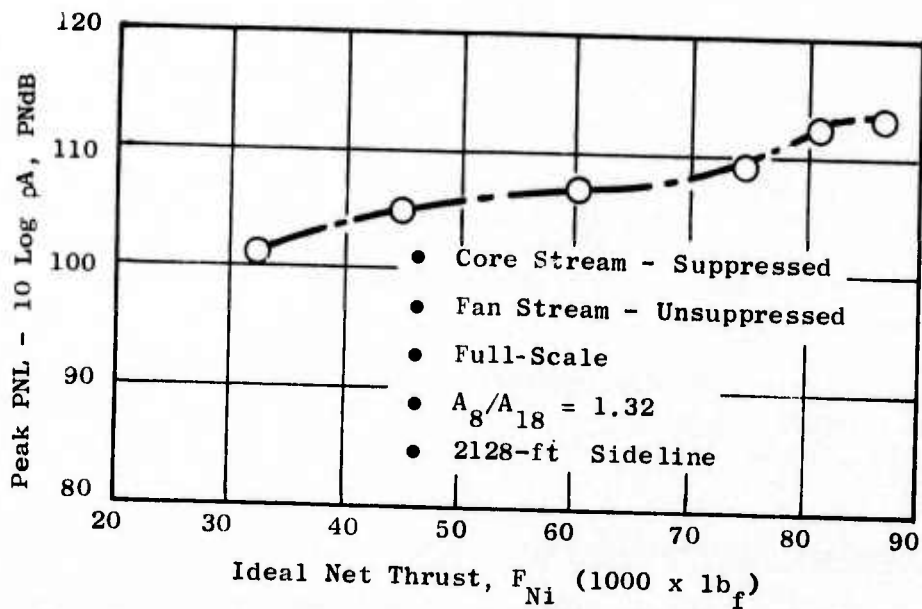
Figure 194. Peak PNL for Dual-Flow Nozzle as a Function of Ideal Net Thrust.
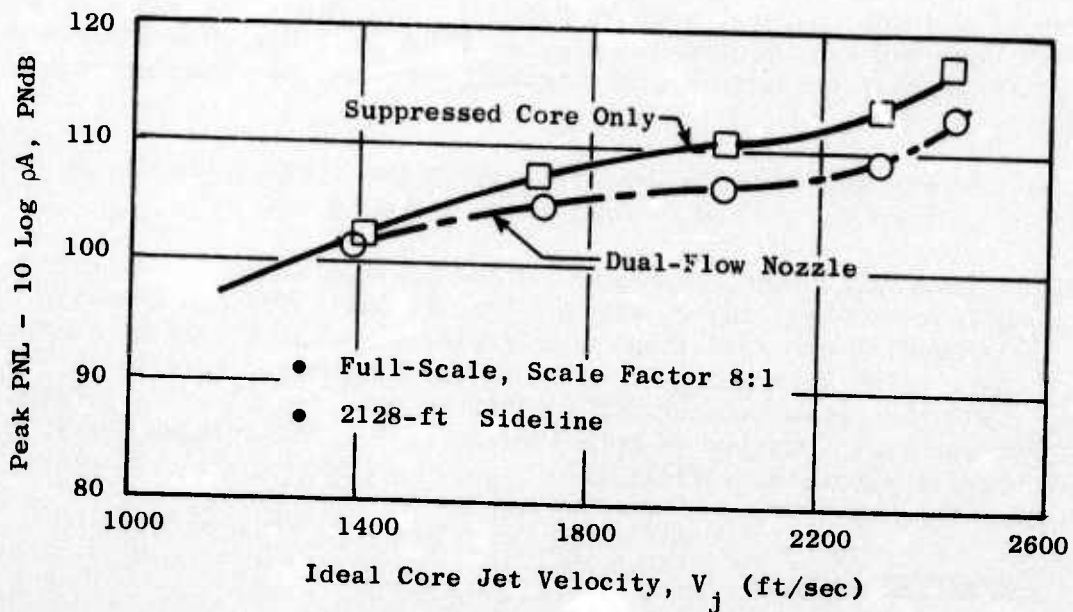
Figure 195. Peak PNL Comparison of Dual-Flow Nozzle with Suppressed Core.

An SPL spectral comparison between the suppressed core and dual-flow is shown in Figure 196 at the representative conditions, a conical nozzle spectra is included for reference purposes. The spectra show that, at the highest condition, both the dual-flow nozzle and the suppressed core alone exhibit conical nozzle characteristics, although the dual-flow spectra are from 6 to 8 dB lower than the suppressed core at frequencies above ∿125 Hz. At the lower condition, the dual-flow and suppressed core are more high frequency dominated. The dual-flow nozzle is again approximately 3 to 4 dB lower than the suppressed core alone at the frequencies above 650 Hz. In both cases, the effect of the fan flow is to primarily reduce the high frequency contribution of the suppressed core.

These data suggest that the addition of a secondary stream on suppressed core flows can provide a fluid shield which, in turn, permits noise levels to be lower than the sum of the two streams.

Aerodynamic Performance Evaluation

Aerodynamic performance estimates were prepared for the dual-flow/core suppressed exhaust nozzle. These estimates were based on previous dual-flow, unsuppressed nozzle data and previous spoke suppressor/plug nozzle data. The bulk of the nozzle static thrust losses can be attributed to spoke base pressure. Analysis of spoke base pressure data taken prior to acoustic testing, therefore, was used to check pretest estimates and as an indicator of the overall performance level of the dual-flow nozzle.

The base areas of the 24-spoke, area ratio = 2.0 suppressor were instrumented with nine static taps at various radii and the model was run with cold flow in both core and fan at JENOTS. Figures 197a, b, and c show the static pressure profiles that occurred for the several fan and core pressure ratios that were run.

Figures 198 and 199 show the drag translated into thrust coefficient, both in terms of core thrust and overall (core + fan) thrust.

The most important item illustrated in the profile is that the base pressure drag is very high; the reason for this is that the high velocity fan stream surrounding the core suppressor prevents any ventilation of the base area. This is an inherent deficiency of the suppressed core/unsuppressed fan concept, and the potential for improvement is questionable. In general, the base pressure is a function of both fan and core nozzle pressure ratios, making performance predictions difficult.

Concept Evaluation

Initial evaluation of the dual-flow concept as a suppression mechanism seemed favorable based on this limited amount of test results and suggested the merit of further investigation of this concept under the aeroacoustic parametric refinement task.
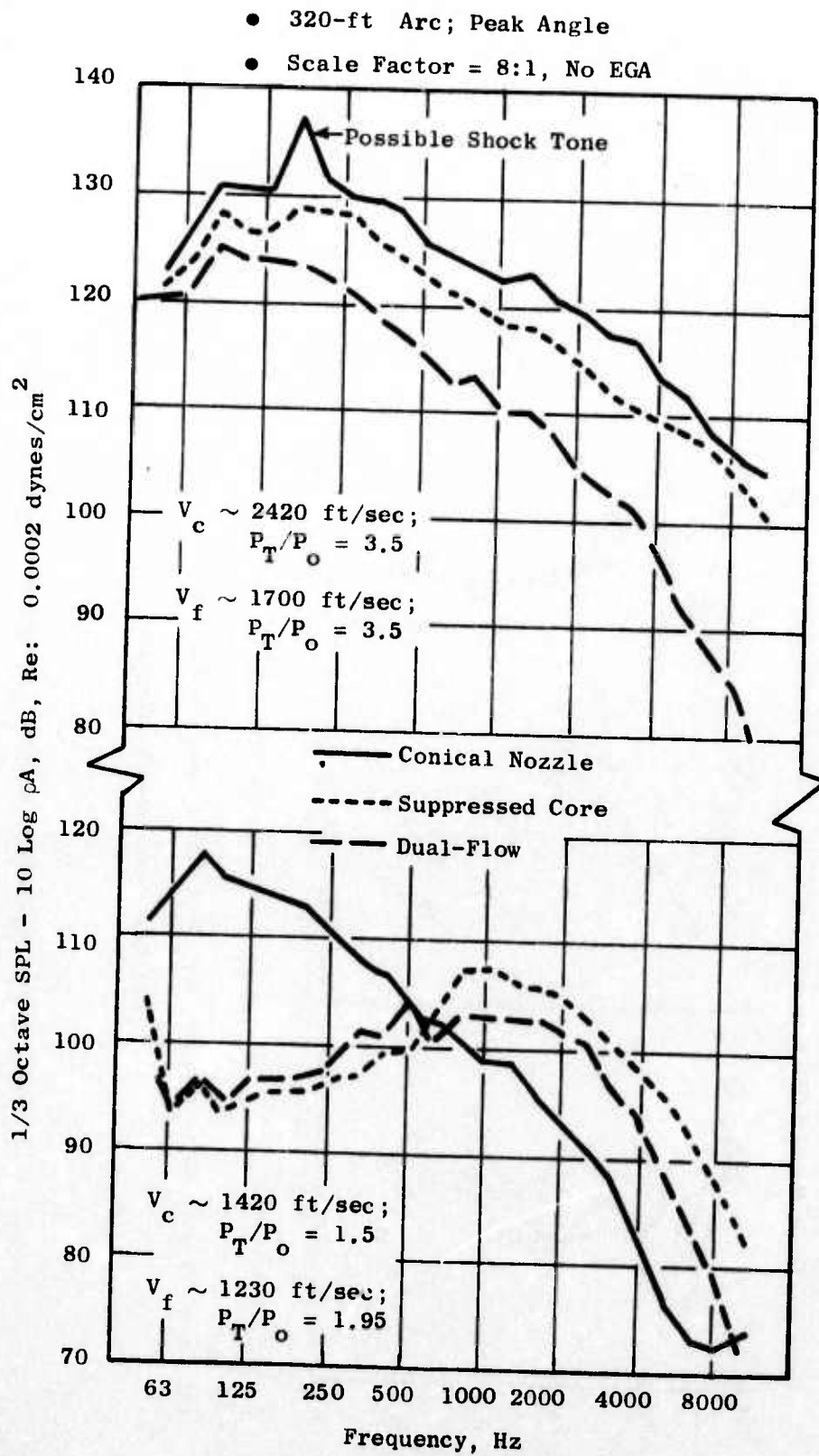
Figure 196. Comparison of SPL Spectra.
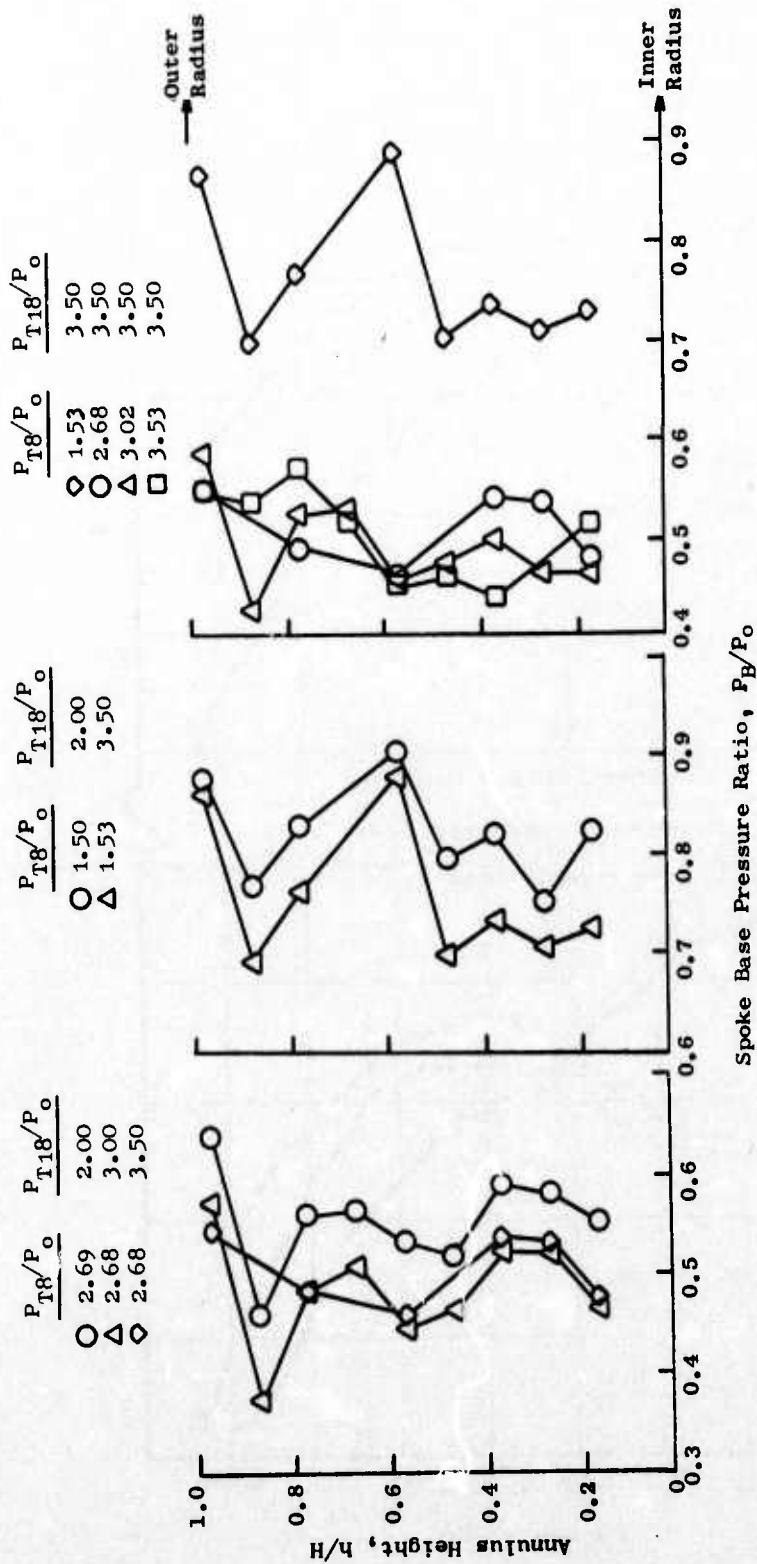
255

Figure 197. Dual-Flow Nozzle Static Pressure Profiles.
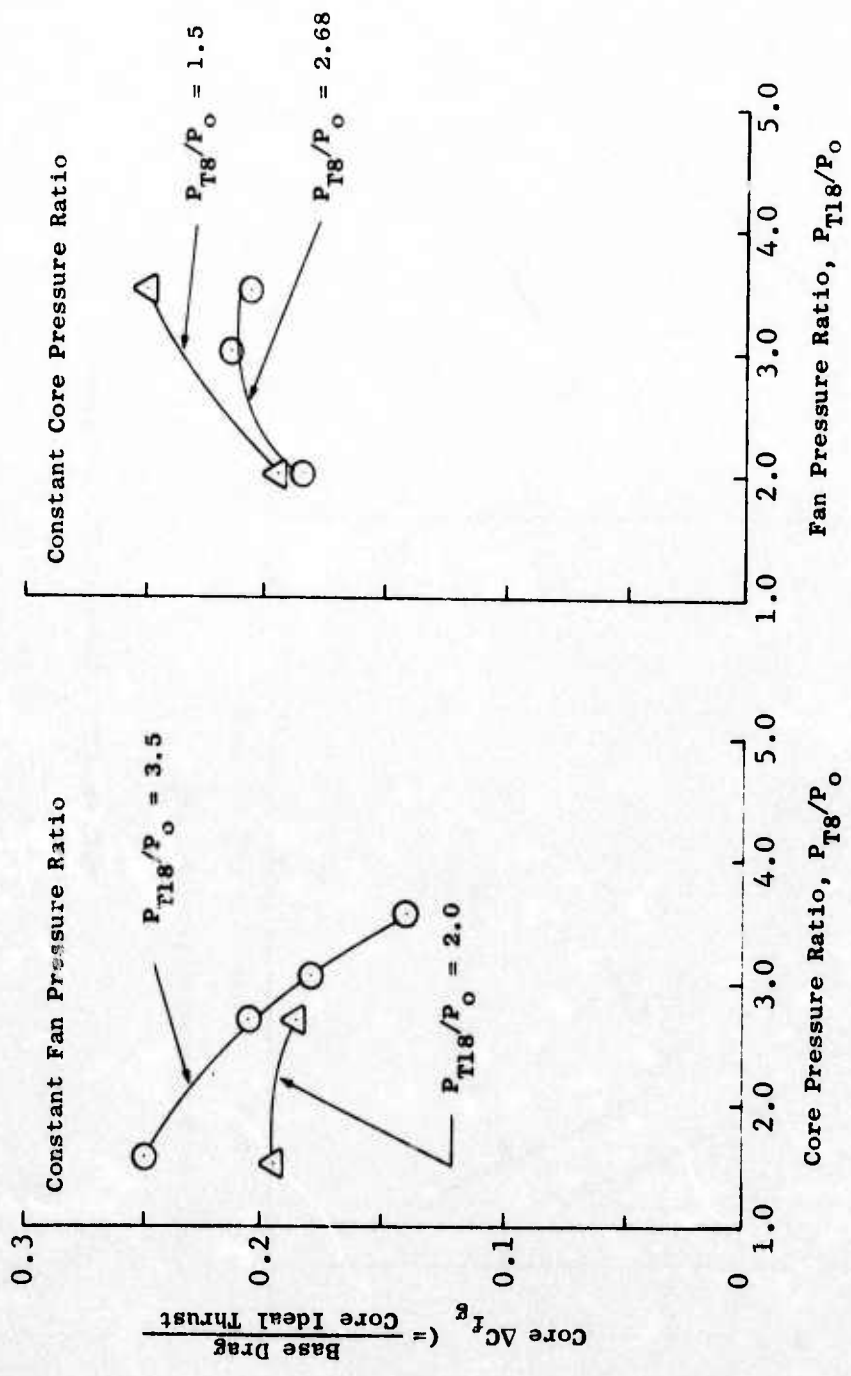
Figure 198. Core Thrust Loss.

257

Constant Core Pressure Ratio

$A_{e8}/A_{e18} = 1.23$

$P_{T8}/P_0 = 2.68$

$P_{T8}/P_0 = 1.5$

Fan Pressure Ratio, $P_{T18}/P0$

Constant Fan Pressure Ratio

$A_8/A_{18} = 1.32$

$P_{T18}/P_0 = 2.0$

$P_{T18}/P_0 = 3.5$

Core Pressure Ratio, P_{T8}/P_0

Overall ΔC_{fg} $\left(= \dfrac{\text{Base Drag}}{\text{Core Ideal + Fan Ideal Thrust}} \right)$
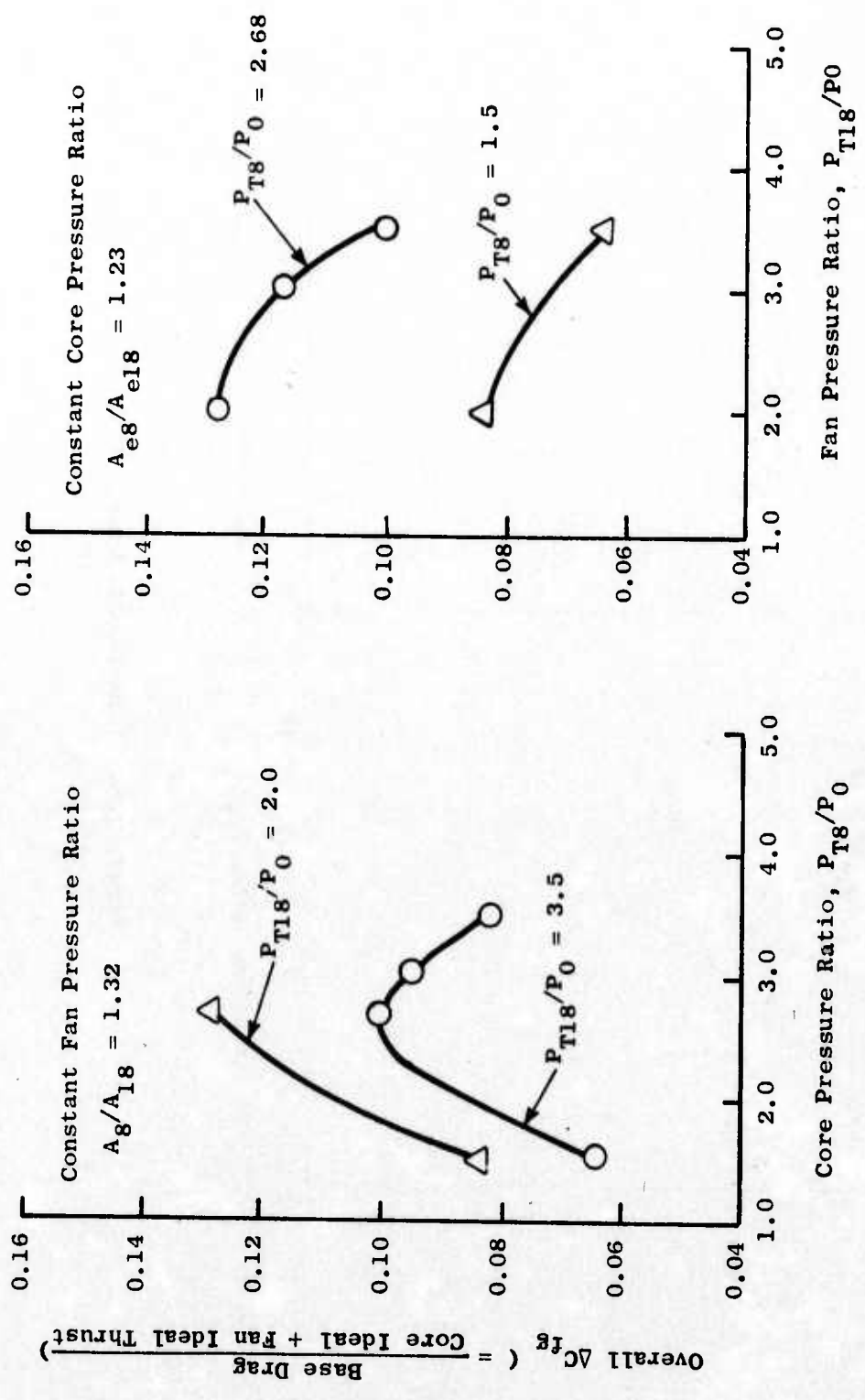
Figure 199. Overall Thrust Loss.

258

3.2.4.5 Orderly Structure of Turbulent Jets

Experiments were designed and executed to examine the concept of reducing jet noise through the destruction or control of a jet's hypothesized "ordered structure." The emphasis of these controlled experiments was to utilize the concepts formulated by J. Hardin (Reference 16). The primary thrust of the experiments was to utilize the influence of a jet's vorticity distribution as a noise-generation mechanism.

Acoustic Tests

Figure 200 is a schematic of the experimental setup used to test the concept of orderly structure. Several core jet flow rates were tested. At each flow condition radial injection of air was superimposed to inhibit the jet's radial growth. A convergent/divergent nozzle designed for shock-free operation at $M_j \sim 1.5$ was used as the basic core jet. Figure 201 shows the full test apparatus at General Electric's JENOTS facility.

The baseline nozzles tested were a 4.3-inch-diameter convergent nozzle for the subsonic test cases and a 4.3-inch-throat-diameter convergent/divergent nozzle for shock-free supersonic jet operation. The external air injection rig consisted of seven tubes at each of eight axial locations. The axial planes were spaced one core jet diameter apart starting at one diameter downstream.

The test setup included the 4.31-inch I.D. throat C-D nozzle plus adapters, surrounded by the orderly structure test apparatus illustrated in the schematic of Figure 200.

The orderly structure test apparatus was an arrangement of so circular rings with eight 1/4-inch radial tubes equally spaced around each ring. The rings were located at seven axial stations equally spaced in one-nozzle-diameter increments from the nozzle exit. External air was blown radially through the tubes at different rates to interact with the jet plume. The tube penetration depth was adjustable to simulate the plume expansion angle for subsonic and supersonic jet test conditions.

The range of test conditions covered subsonic to sonic jet Mach numbers ($M_j \sim 0.5$, 0.8, and 1.0) at ambient temperature, and subsonic to supersonic Mach numbers between 0.5-1.5 for $T_{T8} \sim 1500°$ R and $2500°$ R.

For each test condition, three external weight flows were run through the tubes. The weight flows of the 56 (8 X 7 tubes) tubes were 16, 20, and 30% of the core jet weight flow.
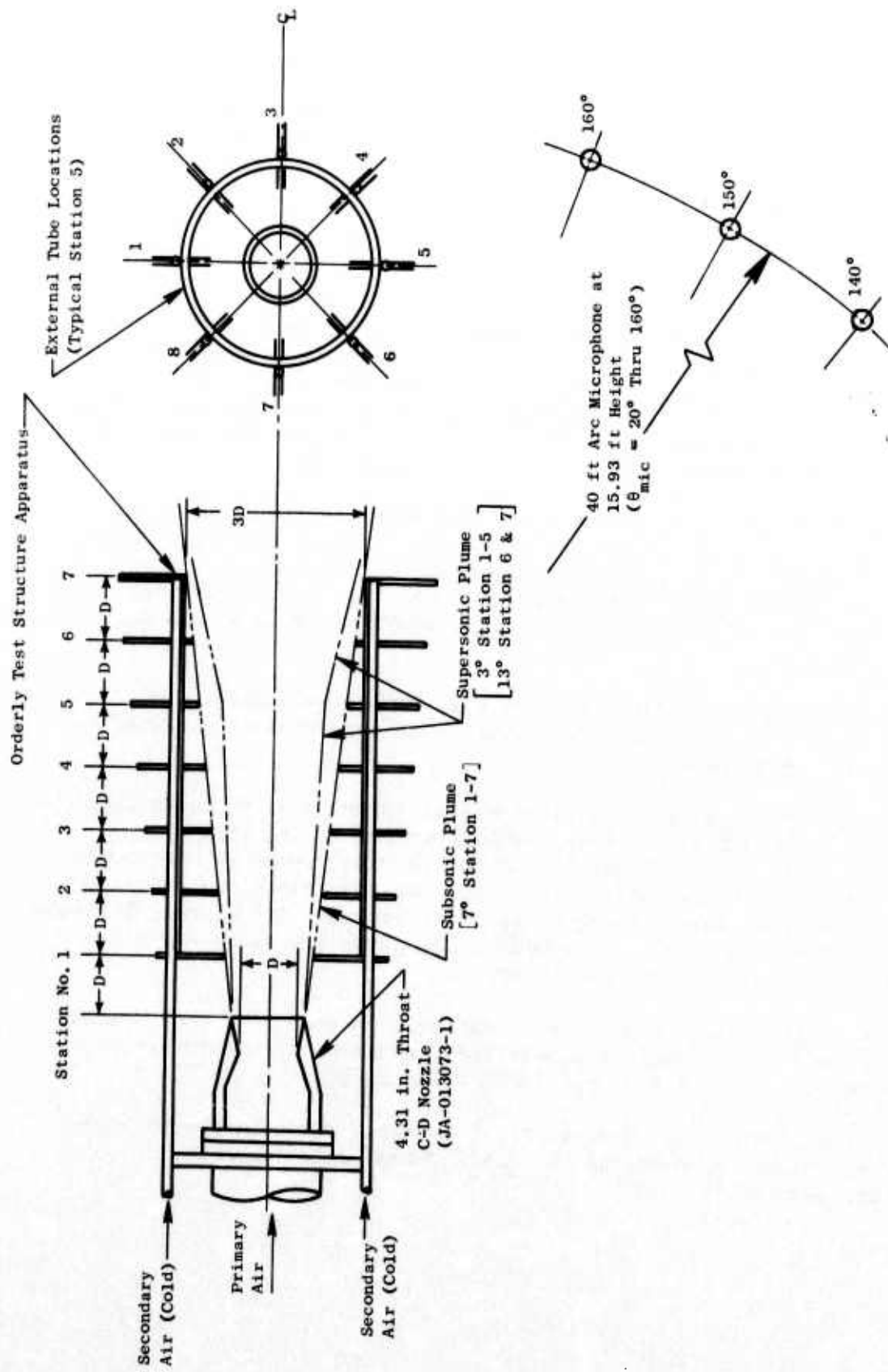
Figure 200. Test Setup and Sound Field Schematic for Orderly Structure Experiment on JENOTS.

FARFIELD MICROPHONE
ARRAY

ORDERLY STRUCTURE
TEST APPARATUS

4.3" THROAT
C-D NOZZLE
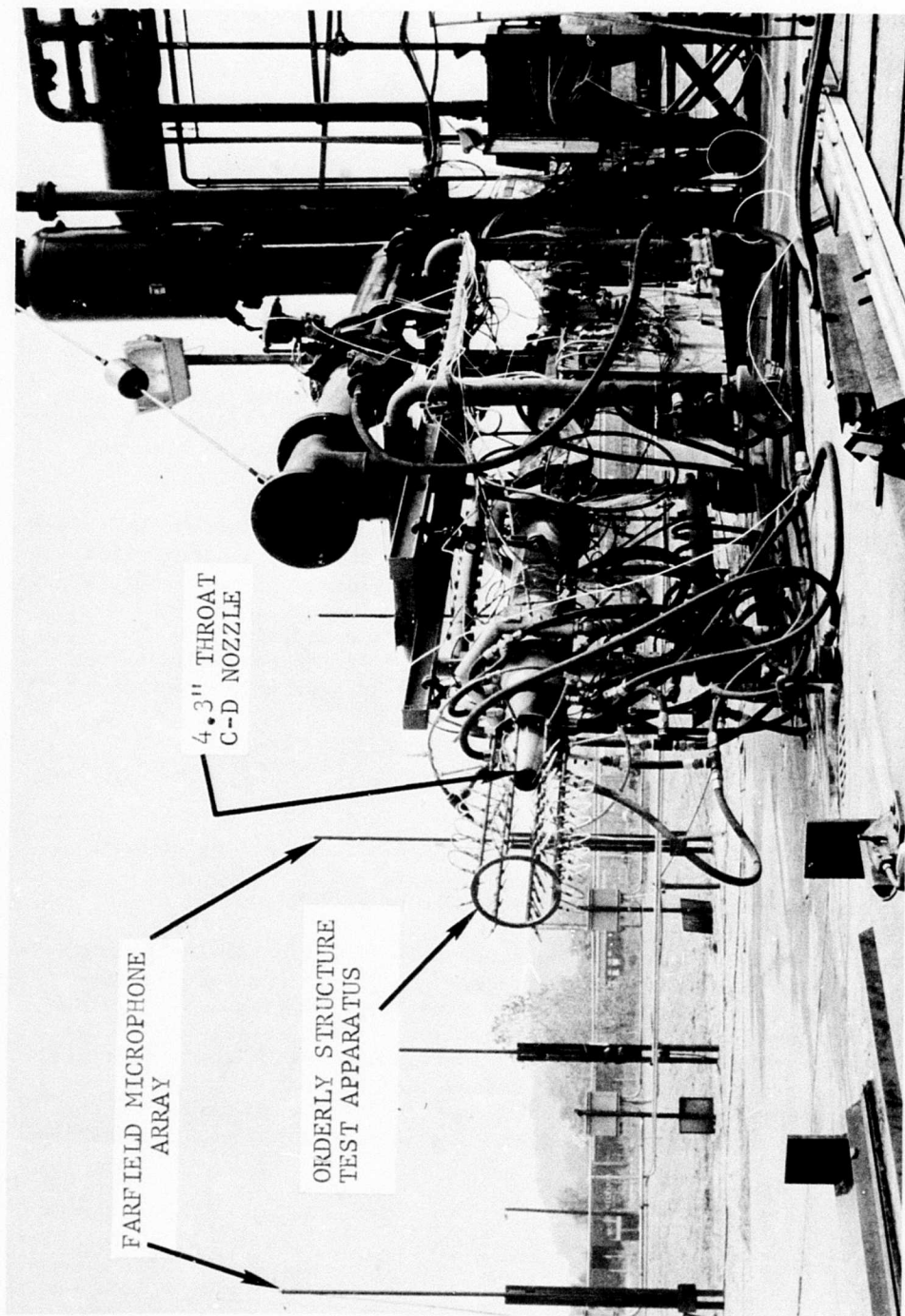
Figure 201. Jet "Orderly Structure" Test Setup at JENOTS.

Acoustic Results and Analysis

The acoustic data presented in the following figures are scale model 1/3 octave band data corrected for standard day conditions.

Figures 202 and 203 show the effects of increasing secondary flow in OASPL for a subsonic and supersonic exhaust jet. For the subsonic jet, suppressions in the order of 2.5 dB are experienced at the peak jet noise angles while, at the larger jet angles, corresponding increases in OASPL are observed. The same general trends are observed for the high Mach number case illustrated in Figure 203.

Figures 204 and 205 show the effects of secondary air injection on SPL spectra at the peak jet noise angle for a subsonic and supersonic jet. Figure 204 shows that the secondary air injection reduces the low frequency noise (but includes noise up to and in excess of the peak Strouhal Number), while the high frequency noise is only moderately increased. Figure 205 again shows some low frequency noise reduction, but high frequency noise also was somewhat reduced.

The results of these preliminary experiments have shown that, by inhibiting the radial growth of the jet's plume through air injection, suppression of 2.5 dB OASPL is obtained at the peak jet noise angles.

These results suggest the possibility of using the orderly structure method for a secondary suppressor. Such a secondary suppressor could act on the jet plume after the exhaust has been acted upon by a primary suppressor such as a multitube or multichute suppressor.

Concept Evaluation

Although these experiments suggested that Hardin's concept might have merit, the preliminary test results have shown that, for high levels of suppression, this concept, most likely, would not be sufficient.

The "orderly structure" suppression concept is probably the least understood of all the basic "suppression principles." Although the results discussed above have indicated that an "orderly structure" suppression principle may exist, a clear understanding of what has taken place is still to be formulated. One question still unanswered, for example, is whether the radial injection increased the mixing rates and entrainment to such a degree as to yield suppression due to other causes. Only more refined examination of the flow and acoustic source distributions occurring in such a process can resolve such understanding.
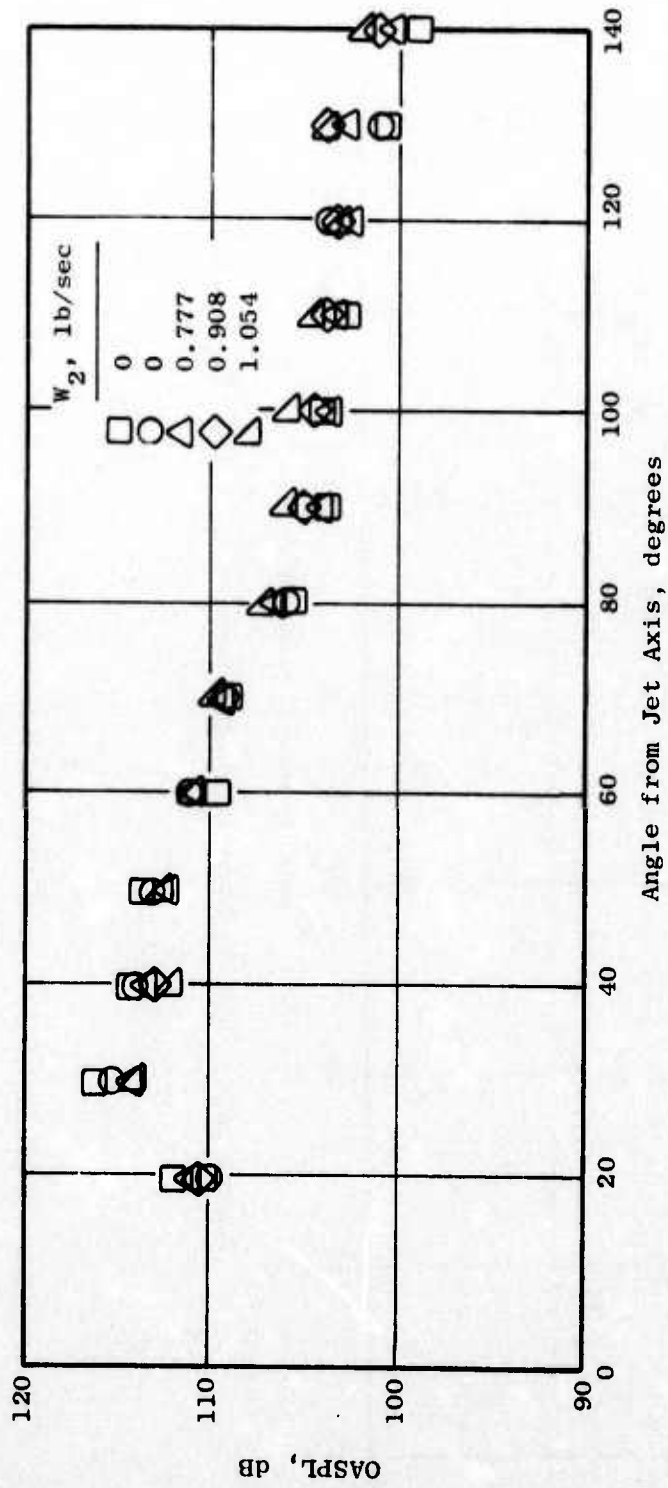
Figure 202. Orderly Structure Experiments, $M_j = 0.8$, $T_{T8} = 1500°$ R.

263
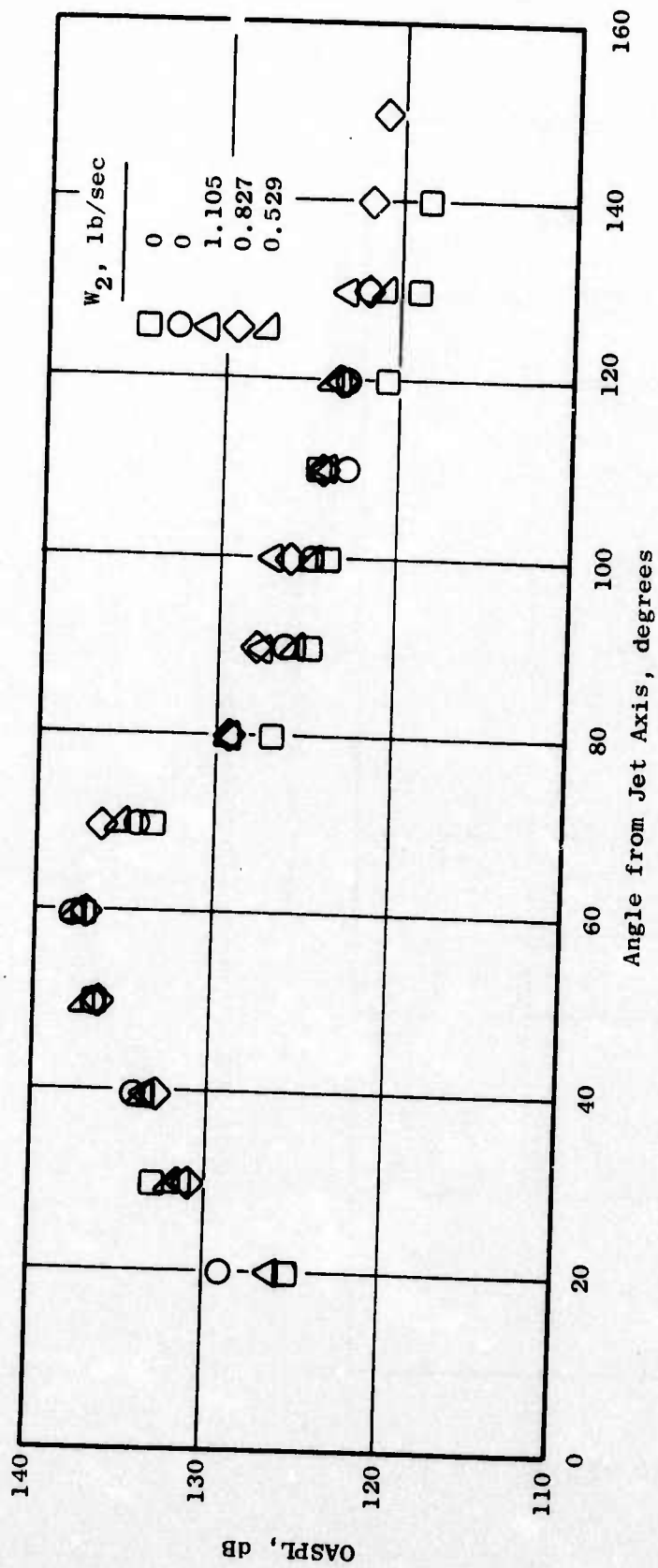
Figure 203. Orderly Structure Experiments, $M_j = 1.6$, $T_{T8} = 2400°$ R.
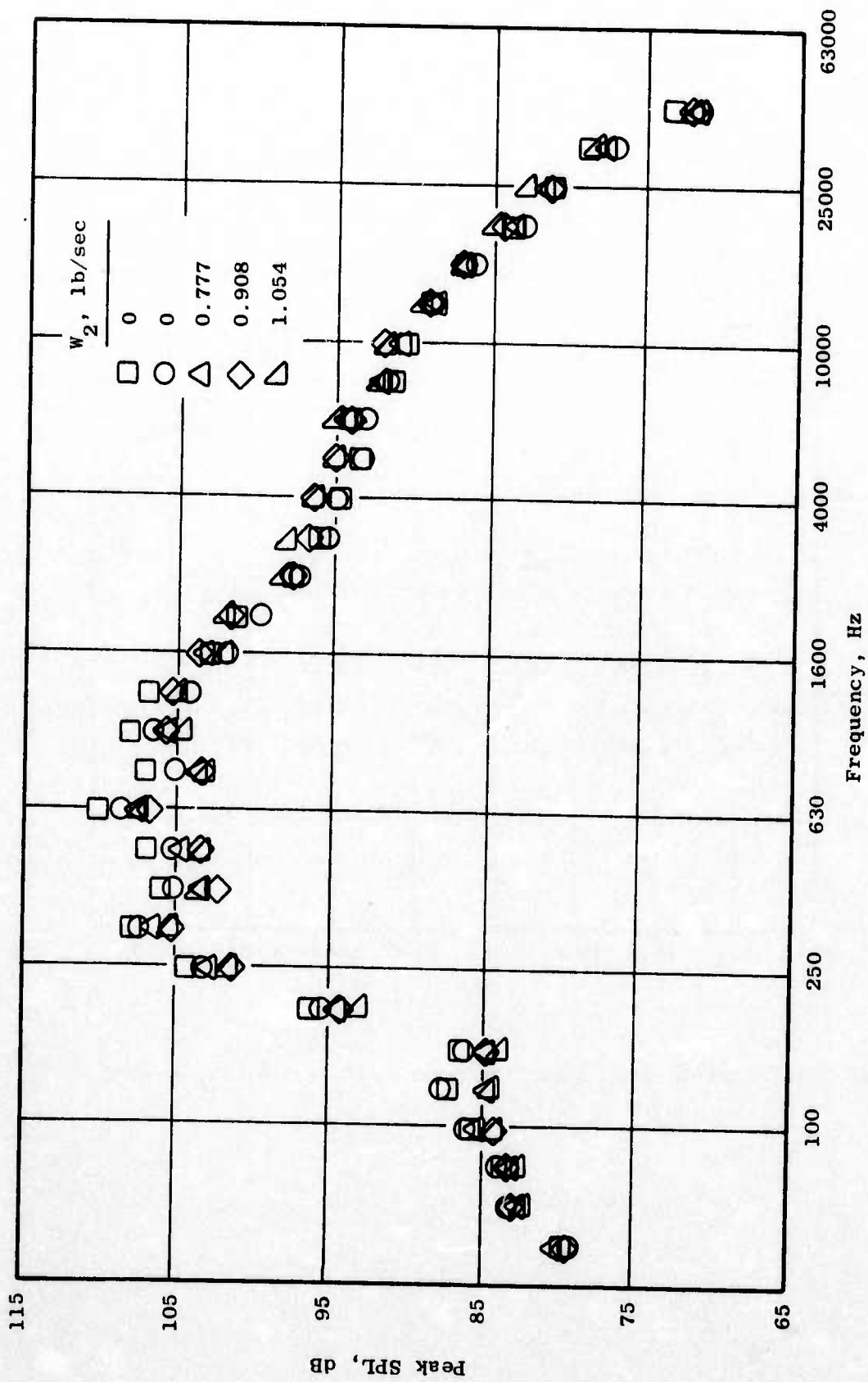
Figure 204. Orderly Structure Experiments, $M_j = 0.8$, $T_{T8} = 1500°$ R.
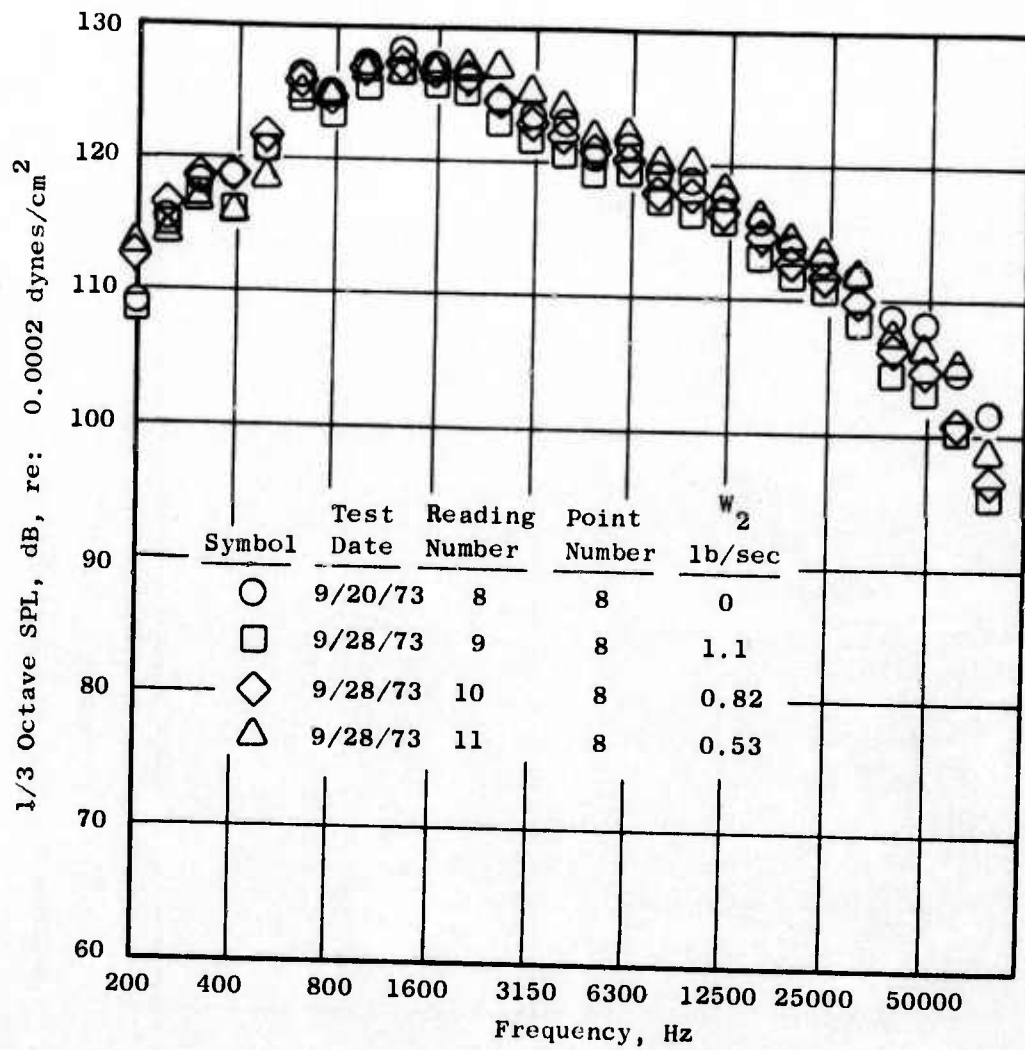
Figure 205. Orderly Structure Experiments, $M_j = 1.5$, $T_{T8} = 2500°$ R.

266

3.2.5 Parametric Refinements

The parametric refinement task of this program was conducted for the purpose of continued aeroacoustic refinement of two nozzle systems which appeared to have potential as candidates for possible final suppressor systems. Parametric tests were conducted to further identify suppression characteristics of the nozzle systems. The systems included 1) the dual-flow exhaust nozzles which showed that some suppression could be obtained from the unsuppressed fan stream by fluid shielding of the suppressed core, and 2) the asymmetric 2-D nozzle systems which showed potential for high suppression gains through mechanical shielding and aerodynamic mixing.

The parametric refinements to these systems were designed, in the case of the dual-flow exhaust nozzles, to identify geometric characteristics in relation to their effect on suppression. The effects of core/fan area ratio and coplanar-to-non-coplanar exit plane were investigated. Refinements to the asymmetric 2-D nozzle systems were similarly selected to identify a maximum suppression level that could be achieved with a system of this type, while attempting to improve the system aerodynamic performance. The parametric refinements to this system consisted of suppressing the primary stream with a multichute nozzle and evaluating the added effect of a long treated (and hardwall) ejector shroud.

3.2.5.1 Dual-Flow Exhaust Nozzle Systems

Acoustic Tests

The tests of the dual-flow exhaust nozzle configurations were conducted on the JENOTS test facility to investigate core/fan area ratio effects and non-coplanar and coplanar fan-core exit plane effects on acoustic suppression. The facility was set up for dual-flow operation as described in Appendix A. Figure 206 shows, schematically, the dual-flow configurations that were tested. Each dual-flow configuration underwent cold flow tests for aerodynamic base pressure measurements, and hot flow tests for acoustic measurements.

The non-coplanar fan shroud model (A_8/A_{18} = 1.0, 1.5) is shown in Figure 207a, while the dual-flow coplanar model (A_8/A_{18} = 1.5) is seen in Figure 207b. Both types of model configurations used the 24-spoke, area ratio of 2.0, annular plug core suppressor, which was instrumented with spoke base static pressure taps.

Acoustic testing was conducted with single flow in the suppressed core alone and with dual-flow operation (hot suppressed core, warm unsuppressed fan bypass). Conditions of dual-flow operation covered a range of ideal jet velocities from 900 to around 2430 ft/sec in the core with fan bypass velocities varying from 950 to 1700 ft/sec. Figure 208 shows the fan, core operating lines for the hot flow tests which stimulated typical low bypass turbofan engine studies.
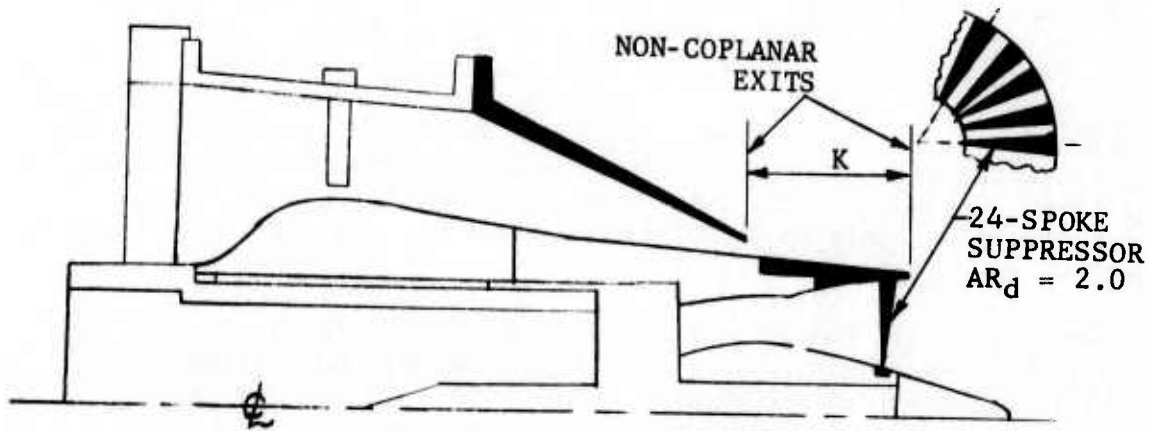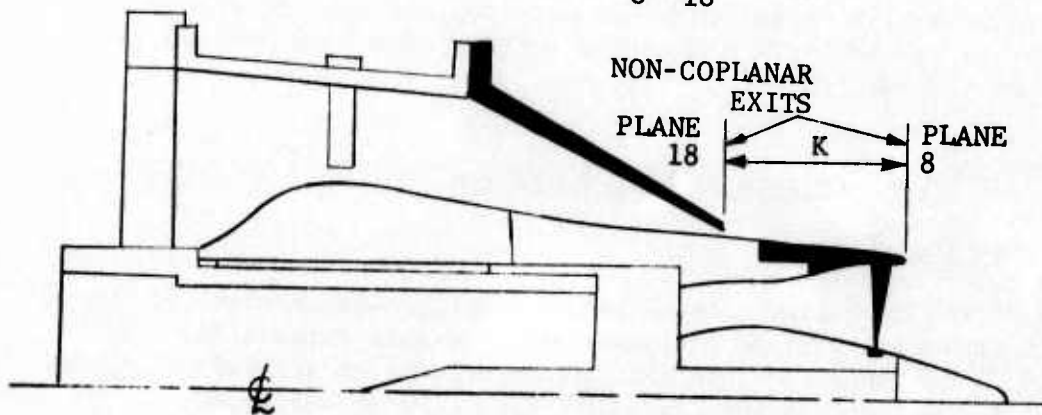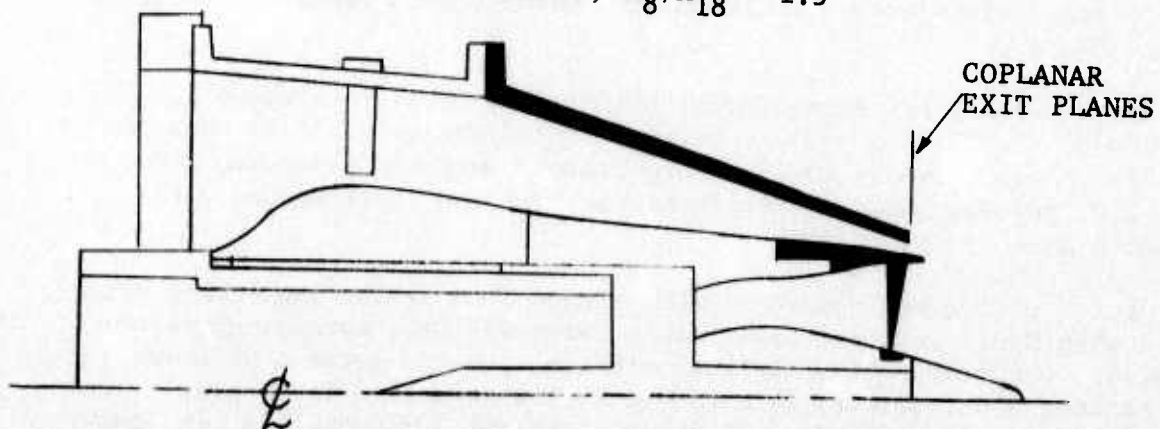
Figure 206. Parametric Refinements to the Dual-Flow Exhaust Nozzles.

NON-COPLANAR FAN SHROUDS,
$A_8/A_{18} = 1.0$ AND 1.5

24 SPOKE SUPPRESSOR
AREA RATIO = 2.0

COPLANAR FAN SHROUD,
$A_8/A_{18} = 1.5$

24-SPOKE SUPPRESSOR
AREA RATIO = 2.0
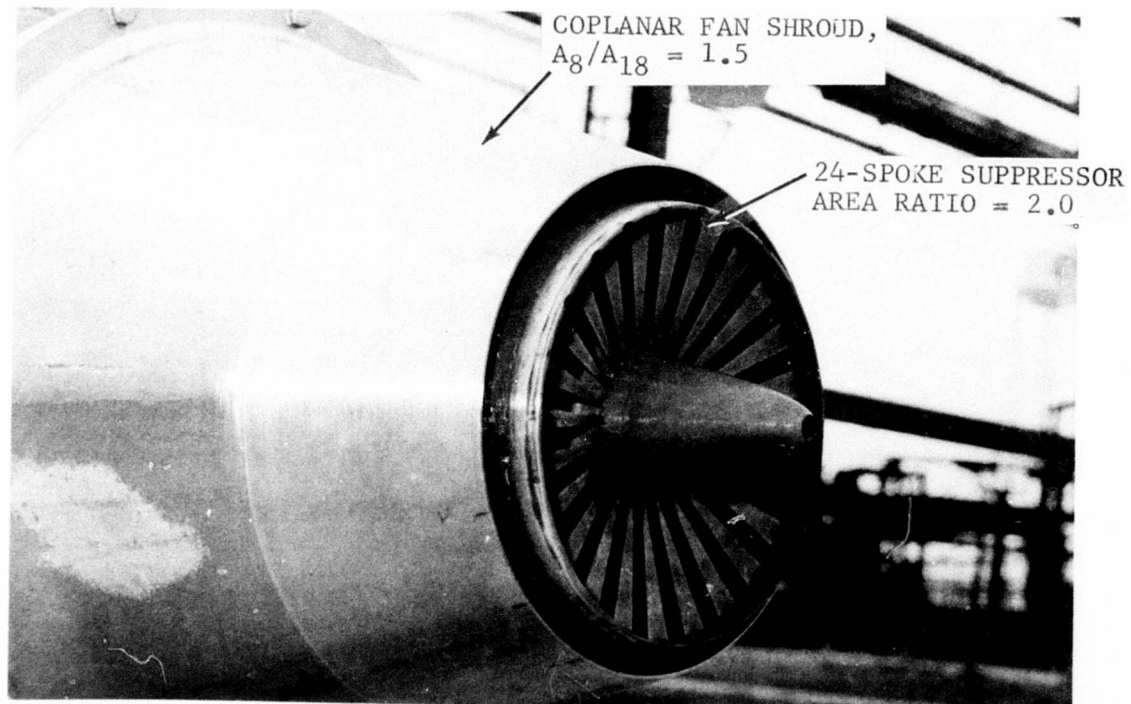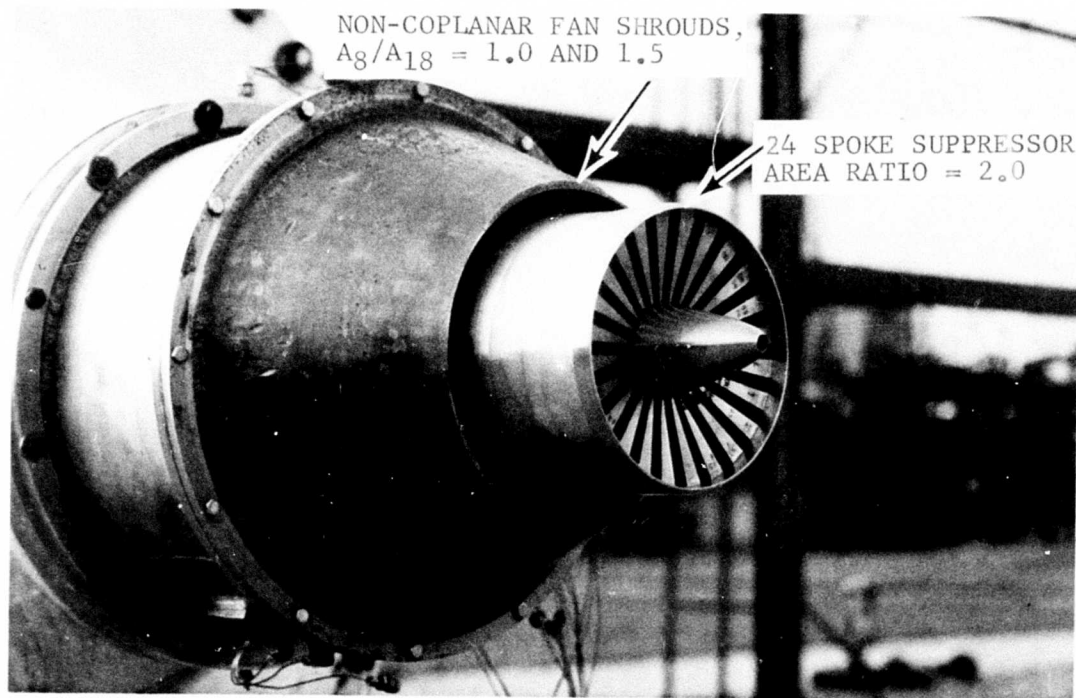
Figure 207.   Dual-Flow Exhaust Nozzle Parametric Test.
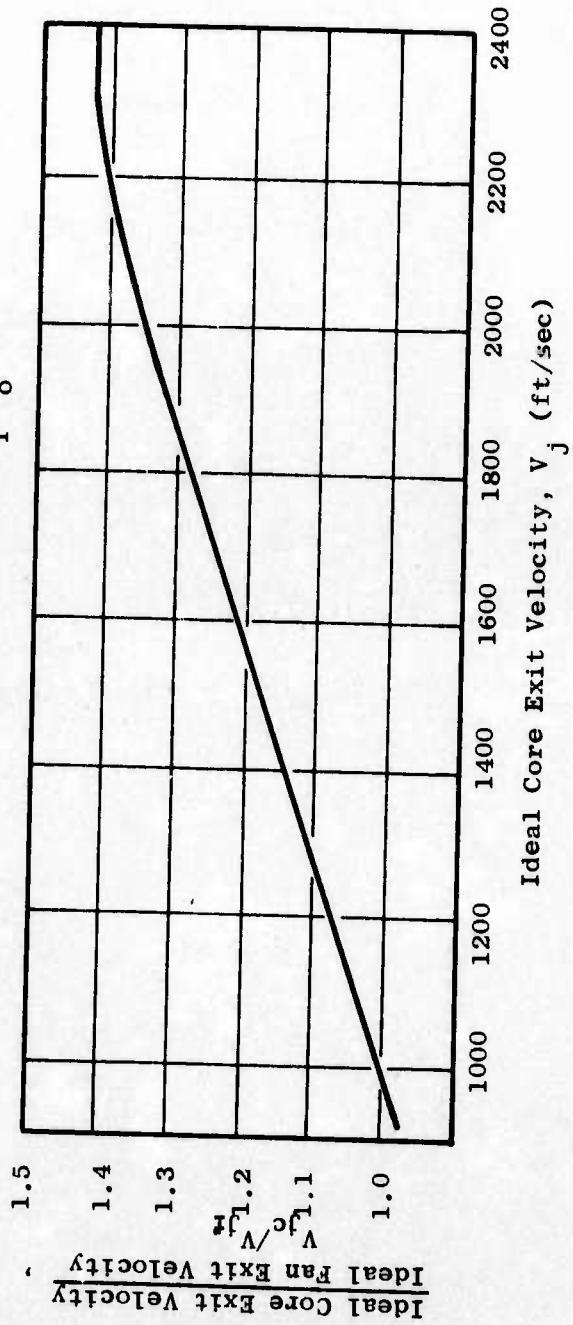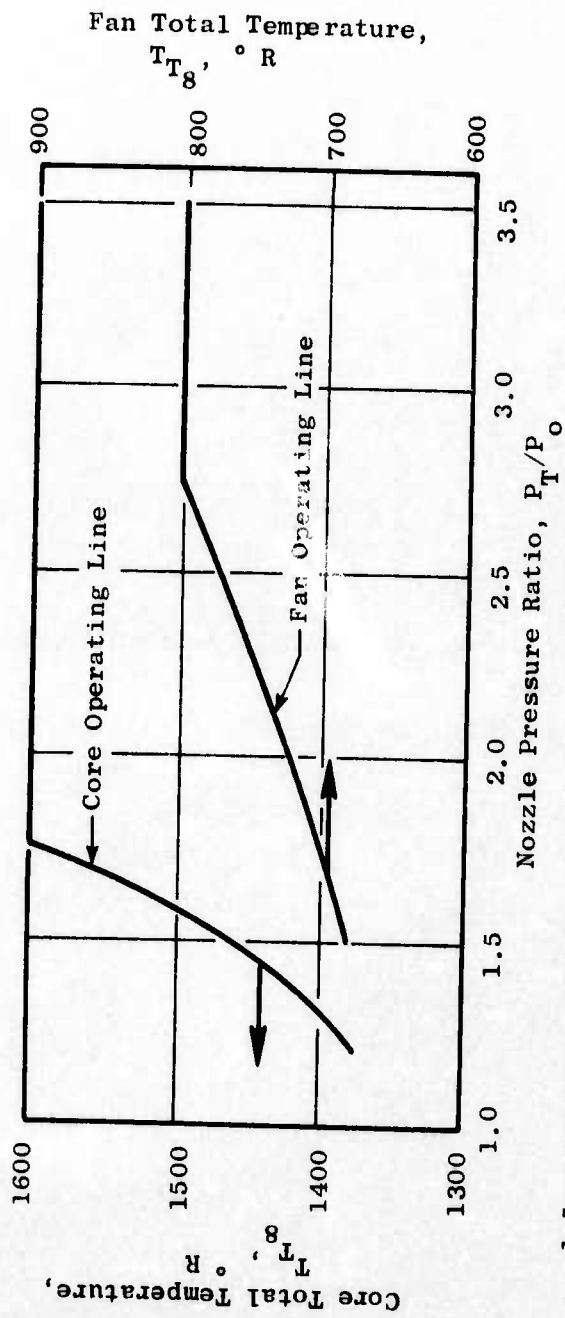
Figure 208. Dual-Flow Exhaust Nozzle Operating Lines.

270

Far-field acoustic measurements were obtained on each model. The sound field consisted of 15 microphones equally spaced around a 40-foot arc from 20° to 160° from the jet inlet. Acoustic measurements were scaled to full-scale application by frequency and size using a diametrical scale factor of 8:1.

Previous tests of the dual-flow nozzle system were conducted, as described in Section 3.2.4 of this report, with an $A_8/A_{18} = 1.32$ non-coplanar fan shroud. Comparisons with the earlier test results also are presented.

Acoustic Results and Analysis

The results of the acoustic tests are summarized in Appendix C. The results of the core alone are shown in the plot of normalized peak PNL over the core jet velocity range at the 2128-foot sideline (Figure 209). The PNL directivity for the core is shown in Figure 210. A comparison with similar data (Figure 209), obtained from the earlier tests conducted under the Advanced Concepts, shows good agreement.

The non-coplanar dual-flow nozzle results are shown in Figures 211 through 216. The plots of normalized peak PNL versus the ideal core jet velocity for $A_8/A_{18} = 1.0$ and 1.5 fan shrouds are shown in Figures 211 and 212, respectively. PNL directivity in Figure 213 ($A_8/A_{18} = 1.0$) and Figure 214 ($A_8/A_{18} = 1.5$) show relatively similar contours with the angle of peak noise occurring at 80° from the jet inlet for the mid-to-high pressure ratio range and moving to 130° - 140° with increasing fan and core pressure ratios. The SPL spectra directivity on the full-scale, 320-foot arc is seen at the high fan and core pressure ratio condition for $A_8/A_{18} = 1.0$ in Figure 215 and for $A_8/A_{18} = 1.5$ in Figure 216. The low frequencies are dominating the spectra at the peak angles for both configurations, but the $A_8/A_{18} = 1.5$ appears to have somewhat lower low frequency SPL.

The coplanar model ($A_8/A_{18} = 1.5$) results are similarly illustrated in Figures 217, 218, and 219. A review of the PNL and spectral directivities with the non-coplanar models shows similar results as far as peak noise angle and PNL contours.

Comparison of the SPL spectral directivities between $A_8/A_{18} = 1.5$ non-coplanar (Figure 216) and coplanar (Figure 219) show low frequency noise to be lower for the non-coplanar model.

The comparison of normalized peak PNL for all of the dual-flow nozzles tested in the program is shown in Figure 220 as a function of ideal net thrust. These indicate that, on a constant thrust basis, an increase in the core/fan area ratio, A_8/A_{18}, tends to increase in system noise.

A comparison of the unsuppressed conical nozzle, suppressed core, and dual-flow PNL noise levels is shown in Figure 221 illustrating the effect of the secondary stream on PNL suppression. All of the dual-flow nozzles
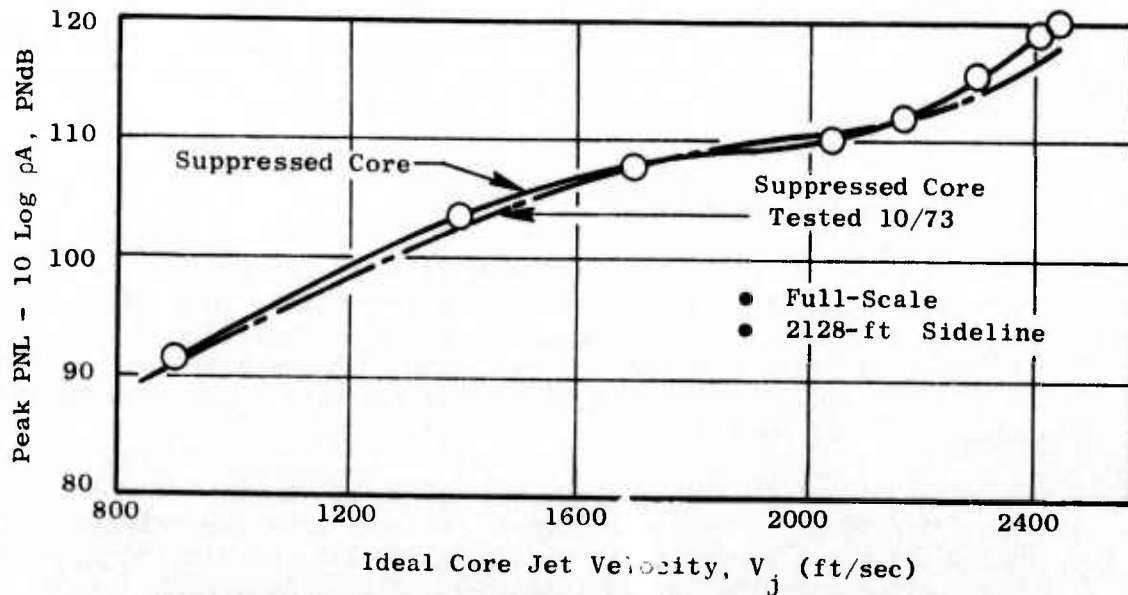
Figure 209. Peak PNL Variation for Suppressed Core Only.
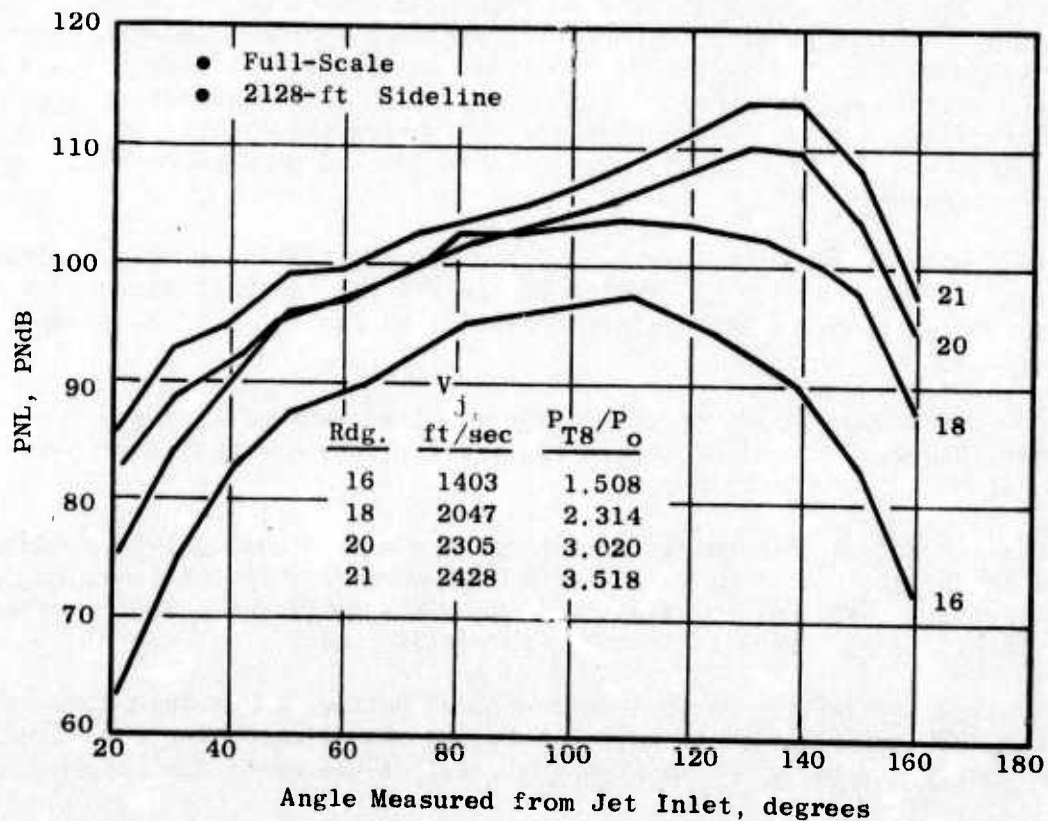
Figure 210. PNL Directivity for Suppressed Core Only.

272
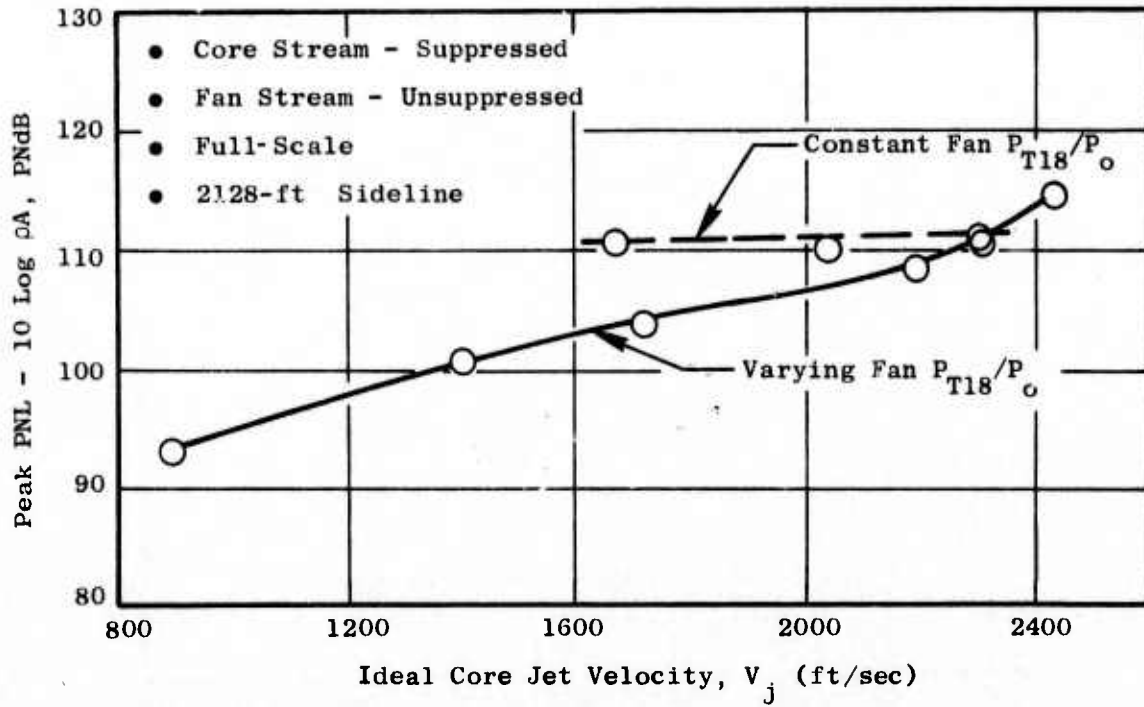
Figure 211. Peak PNL Variation for Dual-Flow Nozzle, $A_8/A_{18} = 1.0$
Non-coplanar.
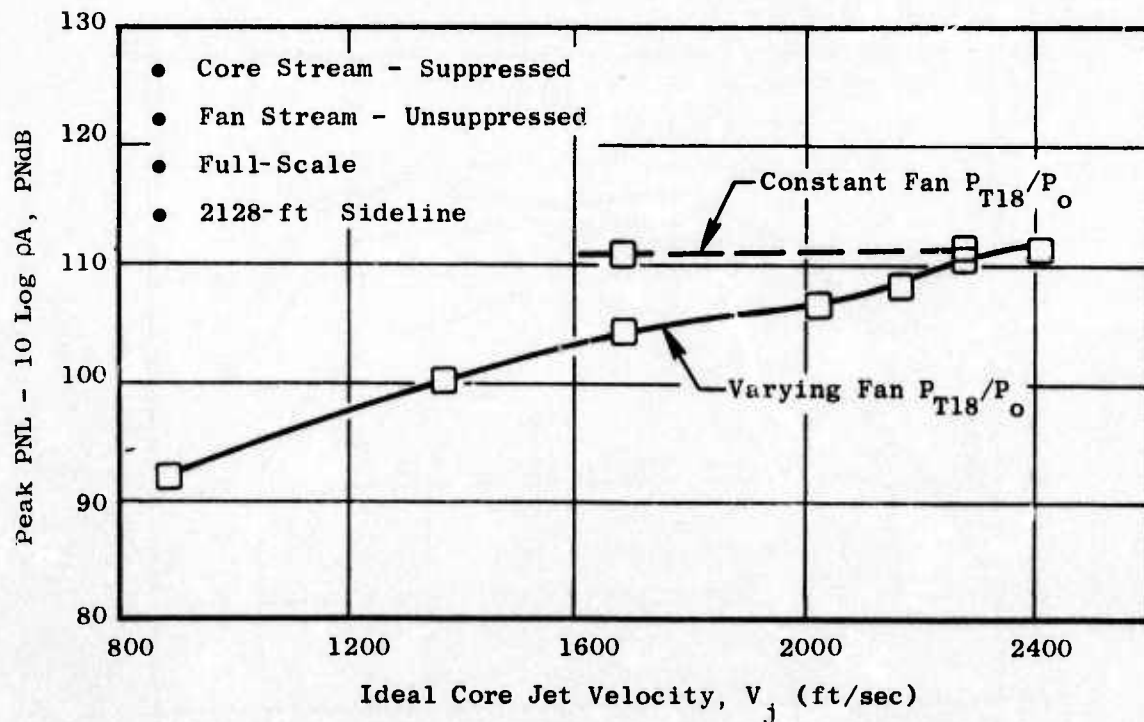
Figure 212. Peak PNL Variation for Dual-Flow Nozzle, $A_8/A_{18} = 1.5$
Non-coplanar.
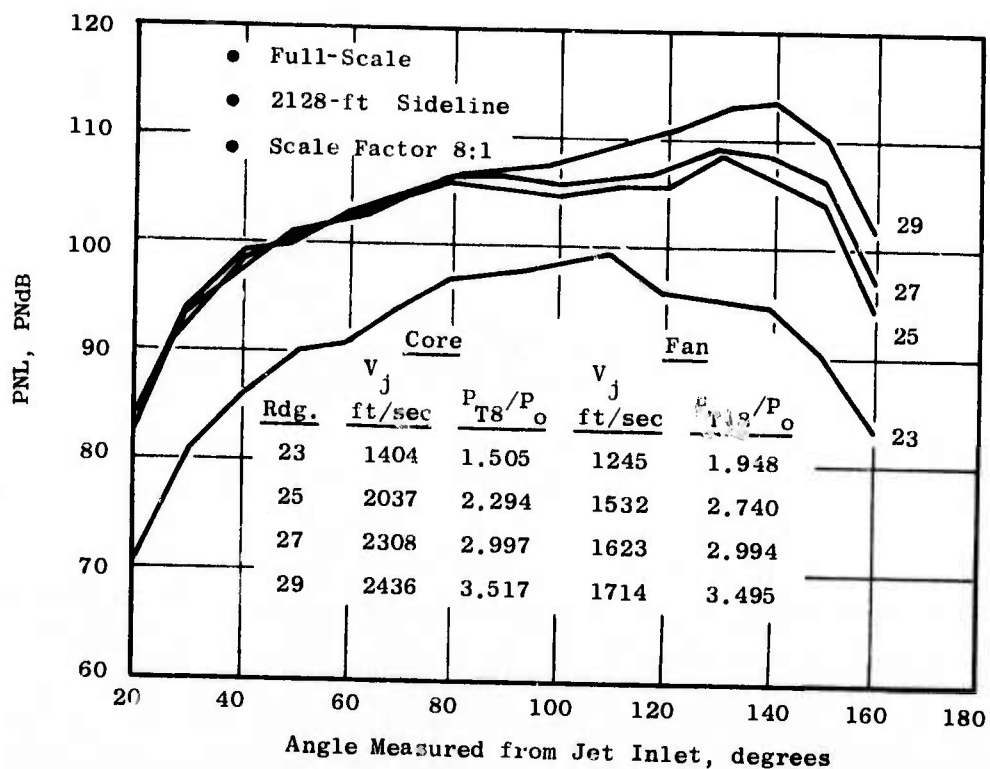
Figure 213. PNL Directivity for Dual-Flow Nozzle, $A_8/A_{18} = 1.0$ Non-coplanar.
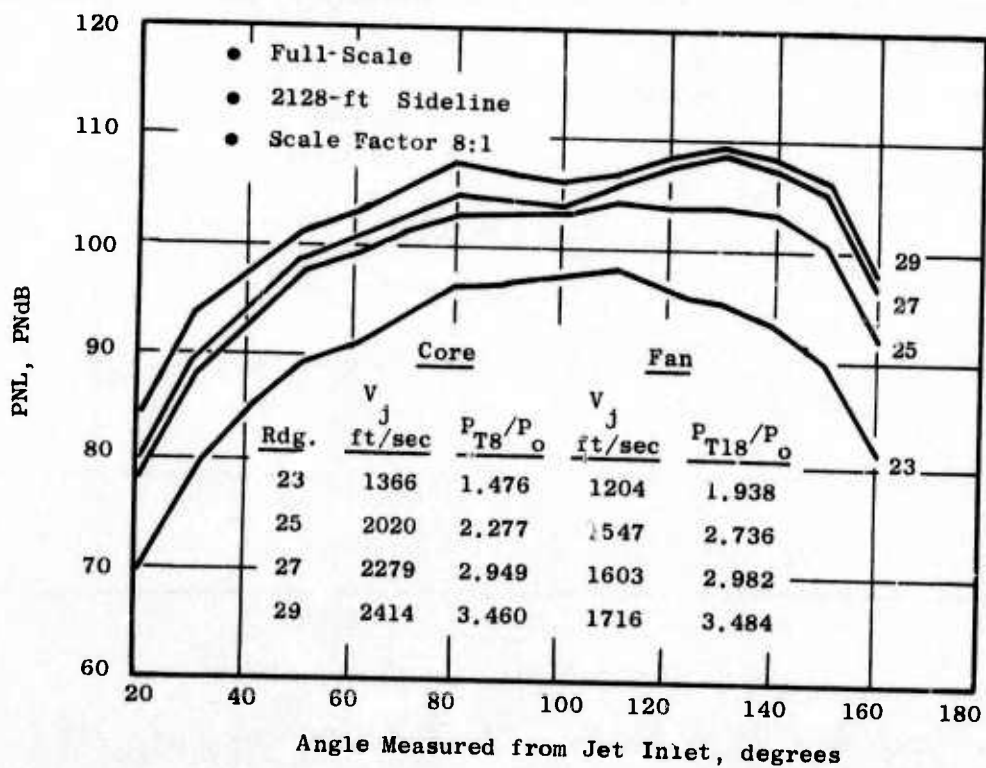
Figure 214. PNL Directivity for Dual-Flow Nozzle, $A_8/A_{18} = 1.5$ Non-coplanar.

274
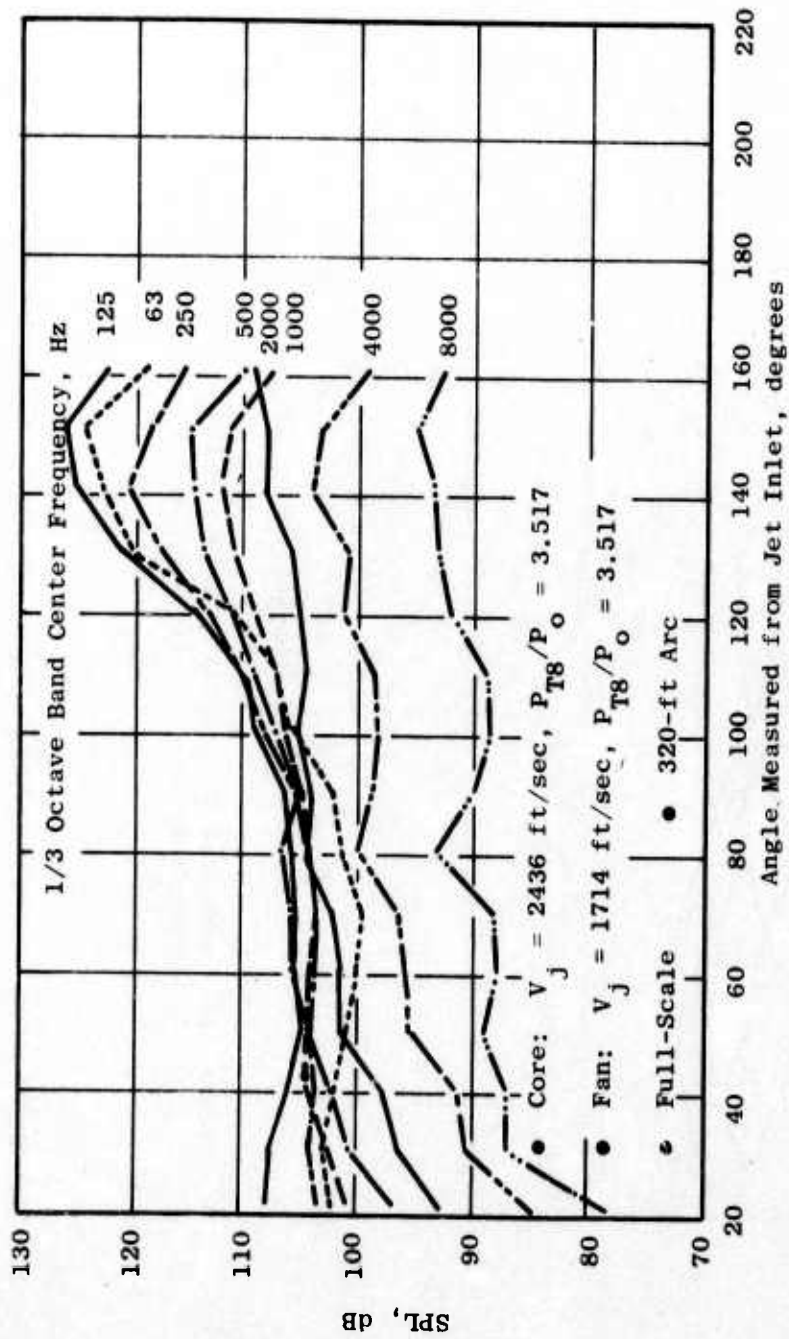
Figure 215. Spectral Directivity for Dual-Flow Nozzle, $A_8/A_{18} = 1.0$ Non-Coplanar.

275
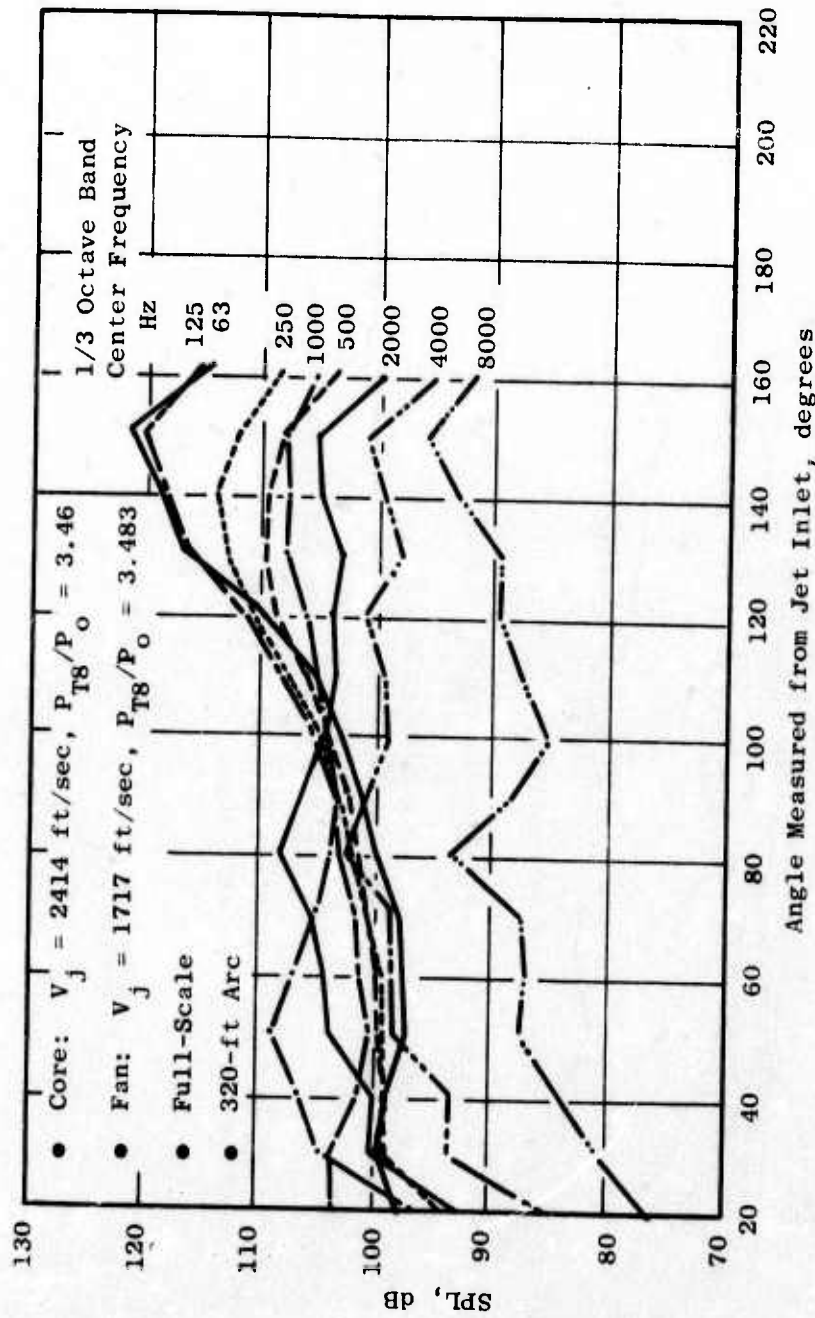
Figure 216. Spectral Directivity for Dual-Flow Nozzle, $A_8 A_{18} = 1.5$ Non-Coplanar.
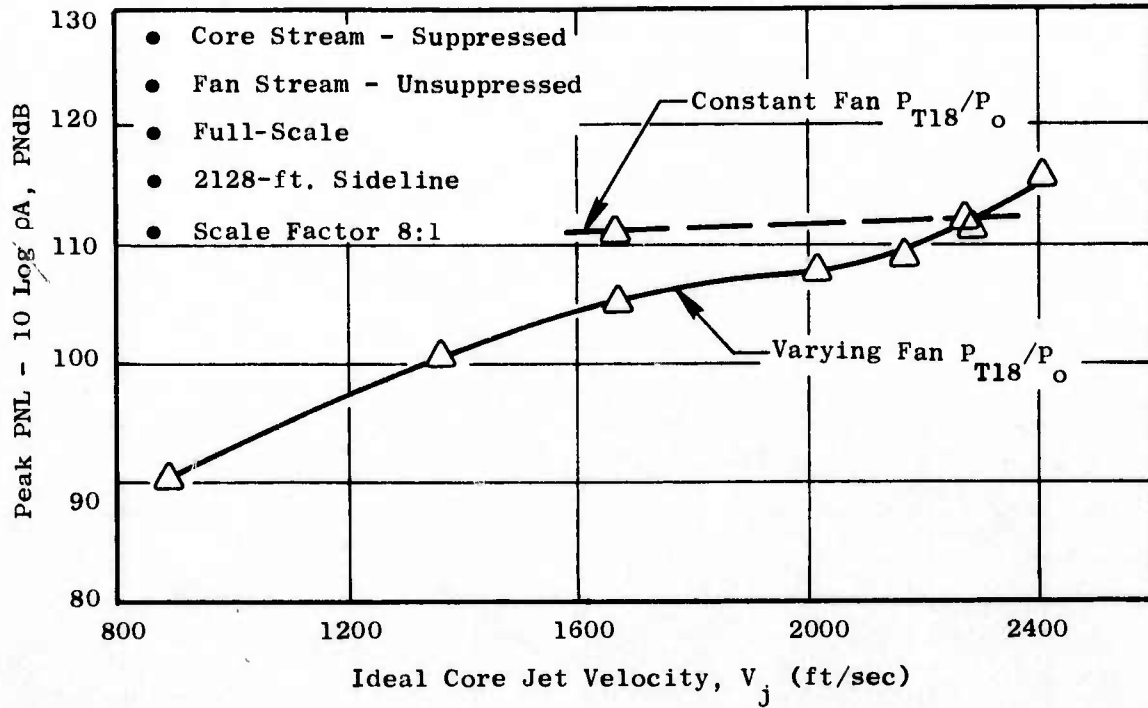
Figure 217. Peak PNL Variation for Dual-Flow Nozzle, A_8/A_{18} = 1.5 Coplanar.
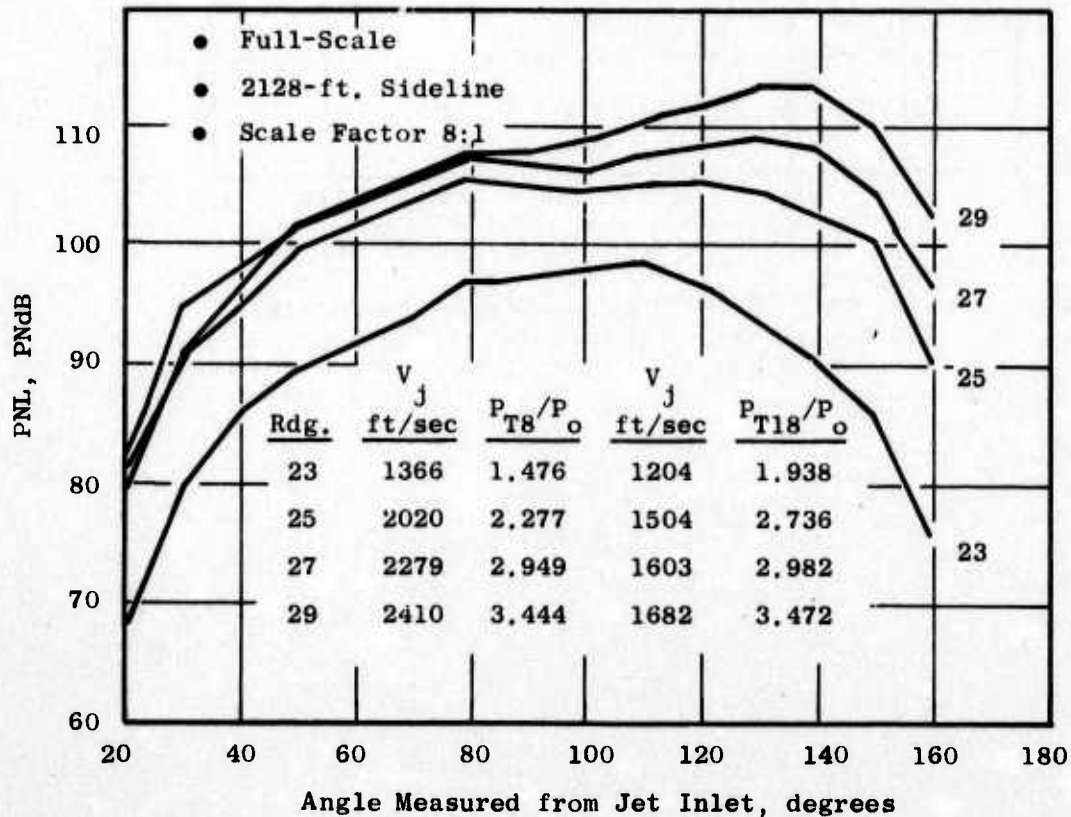
Figure 218. PNL Directivity for Dual-Flow Nozzle, A_8/A_{18} = 1.5 Coplanar.

277
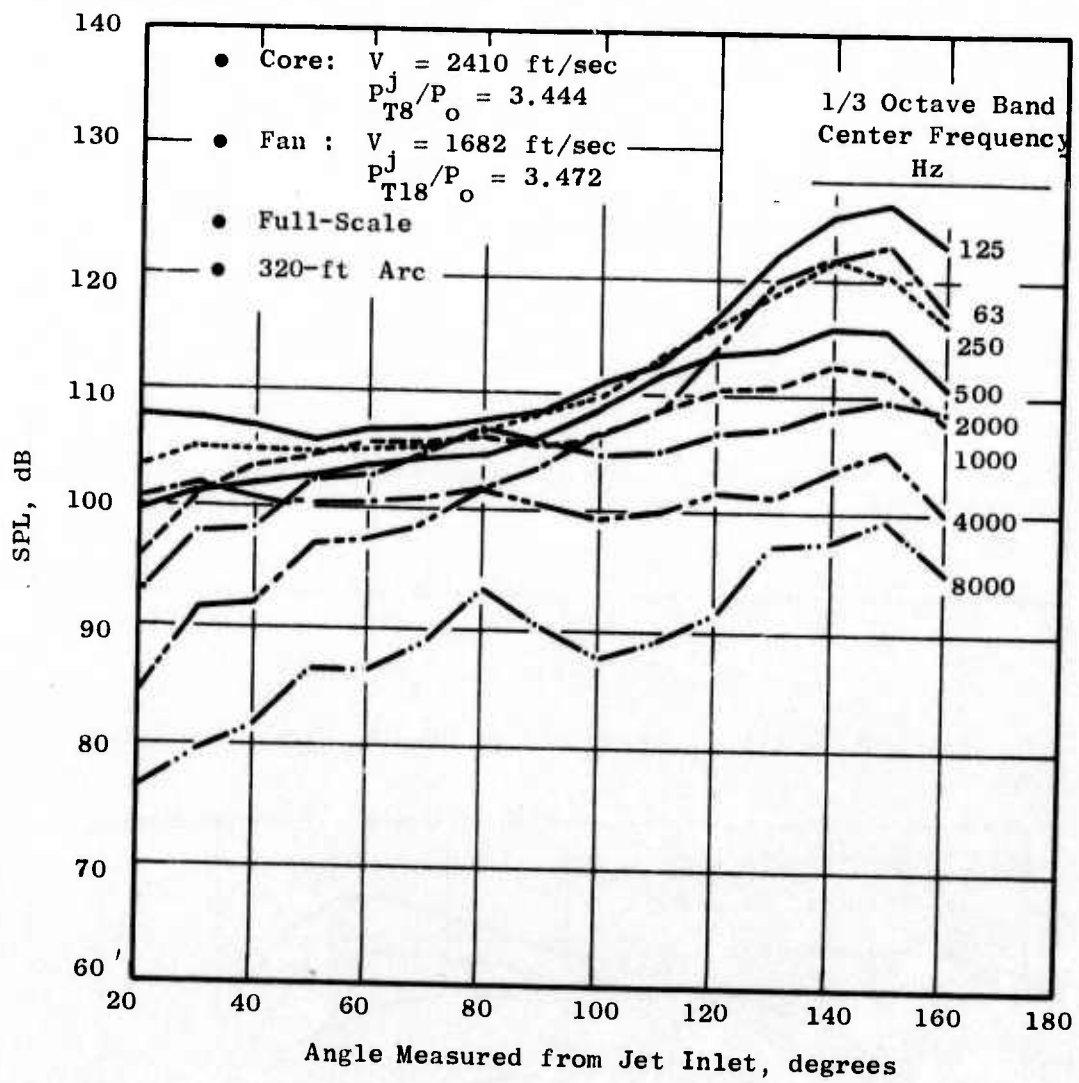
Figure 219. Spectral Directivity for Dual-Flow Nozzle, A_8/A_{18} = 1.5 Coplanar.

278
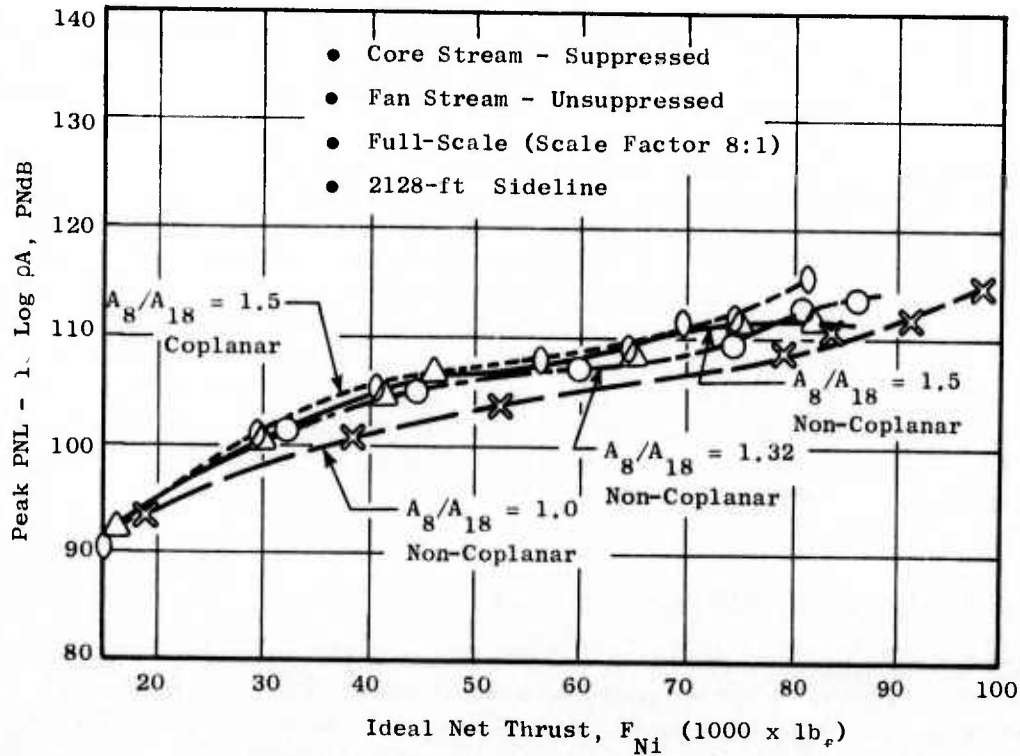
Figure 220.   Peak PNL for Dual-Flow Nozzle as a Function of Ideal Net Thrust.
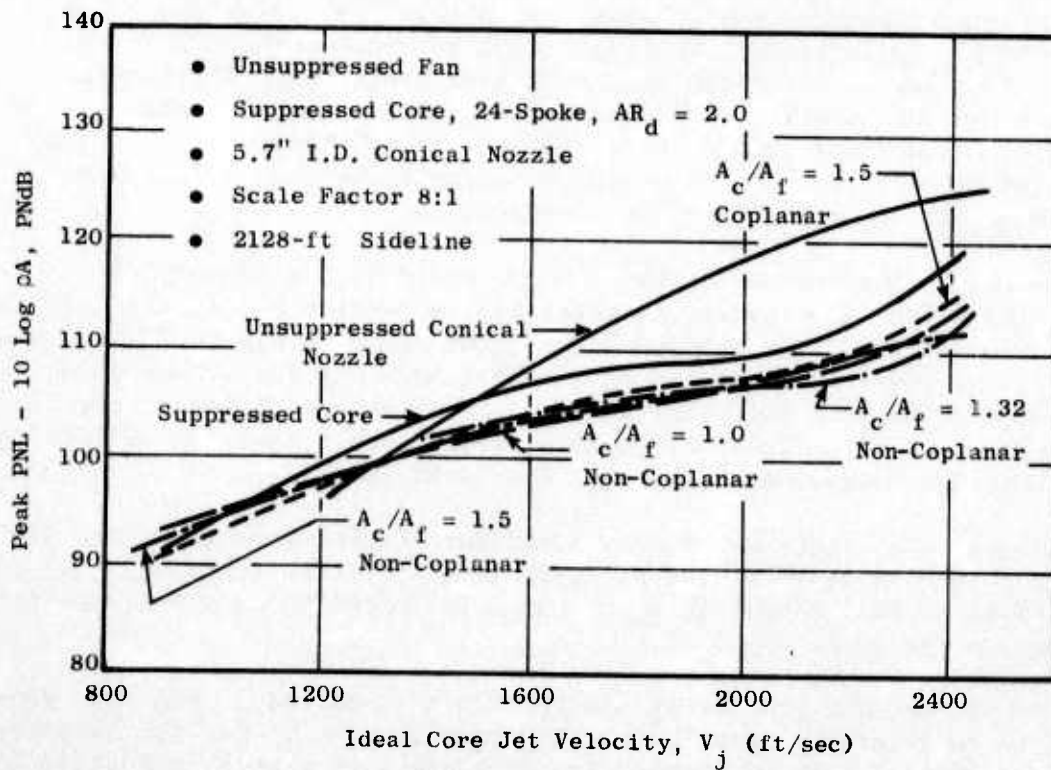
Figure 221.   Peak PNL Comparison of Dual-Flow Nozzle with Suppressed Core.

279

exhibited similar noise characteristics and showed some suppression through-
out the velocity range relative to the suppressed core alone. The effect of
coplanar versus non-coplanar fan/core streams on peak PNL was not significant.

Figure 222 shows the effect on the spectra of varying core-to-fan area
ratio at representative velocities over the range investigated. The coplanar
versus non-coplanar exit effect appears insignificant, with little or no
difference noted for the dual-flow configurations as illustrated in Figure
223. The non-coplanar dual-flow nozzle, $A_8/A_{18} = 1.5$, generally maintained a
lower spectrum level than the other configurations in the frequencies below
1000 Hz for the fan and core high jet velocity condition. It also should be
noted that during subsonic fan and core operation (Figure 223a) the addition
of fan flow reduces the high frequency (>500 Hz) content in much the same way
exhibited in the coplanar jet noise activity during the FAA/DOT Core Engine
Program (Contract No. DOT-FA72WA-3023), References 27-29.

Aerodynamic Performance Evaluation

An aerodynamic evaluation of the dual-flow exhaust nozzle systems was
made from core suppressor base pressure measurements and from comparisons
to unsuppressed coannular nozzle results obtained from previous tests.

During the preliminary evaluation of the advanced concepts and further
parametric refinement tests of the dual-flow systems, the configurations
with suppressed core were run at JENOTS with cold flow to record the static
pressure on the spoke bases. The base areas of the 24-spoke, area ratio
of 2.0, suppressor were instrumented with nine static taps distributed
across the annulus on centers of equal areas. Readings were taken over a
range of core and fan nozzle pressure ratios. A schematic and photograph of
the configuration tested in the Advanced Concepts (Section 3.2.4) are
presented in Figures 187 and 188 of that section.

Refering to the results of the initial tests of the non-coplanar,
$A_8/A_{18} = 1.32$, dual-flow nozzle as described in Section 3.2.4, the integrated
average values of the base pressures are shown again in Figure 224. Because
the core suppressor is buried inside the high velocity fan stream (and,
therefore, isolated from any ventilation with ambient conditions), the base
pressures are all quite low. The base pressures are a function of both core
and fan pressure ratio, as can be seen in Figure 224.

The base drag, relative to core ideal thrust, is shown in Figure 225
while Figure 226 shows this drag relative to the overall (core and fan) ideal
thrust. This overall thrust loss is obviously dependent on the thrust ratio
of the fan to the core.

These curves show the thrust loss penalties incurred by the core sup-
pressors to be generally quite high. The base drag is by far the largest
thrust loss mechanism in the system and thus provides a good indication of
relative performance level. Single-flow spoke suppressor tests run in the
past have shown that additional thrust losses due to friction and pressure

280
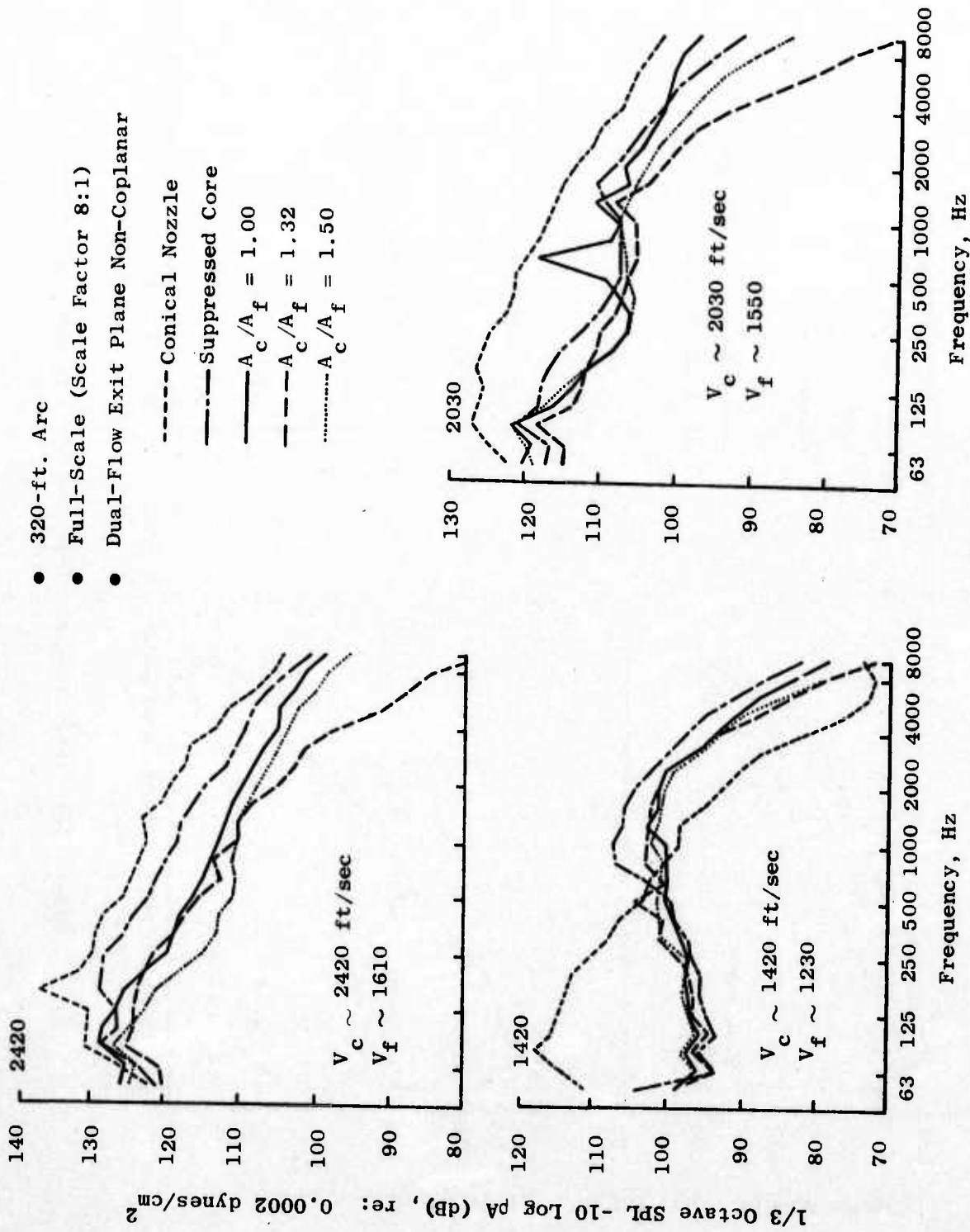
Figure 222. Effect of Area Ratio Variation on Dual-Flow Nozzles.

281
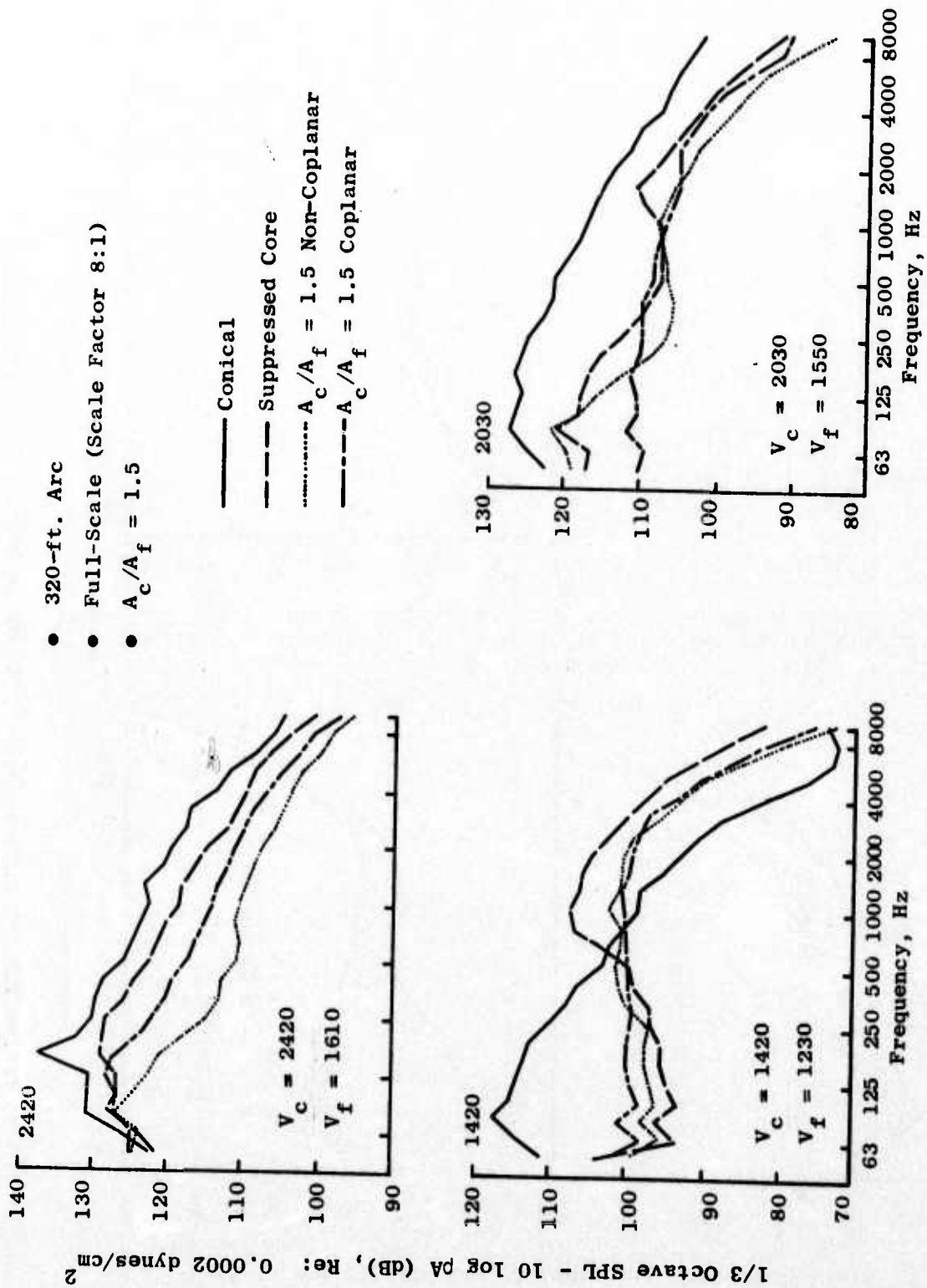
Figure 223. Effect of Non-Coplanar and Coplanar Exit Planes.

282
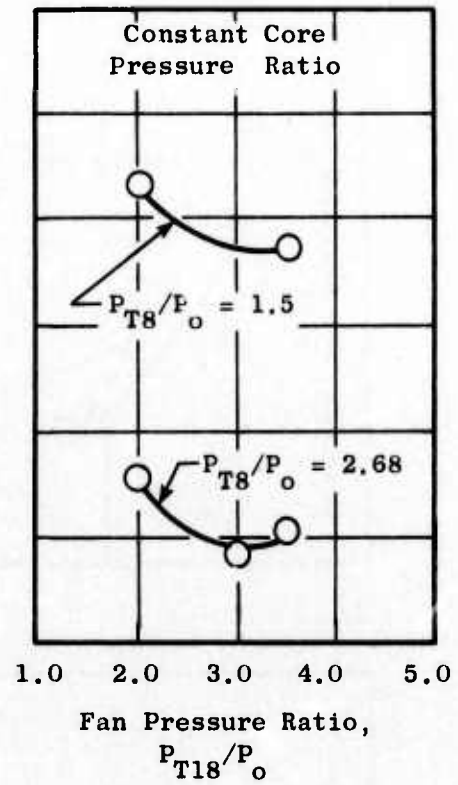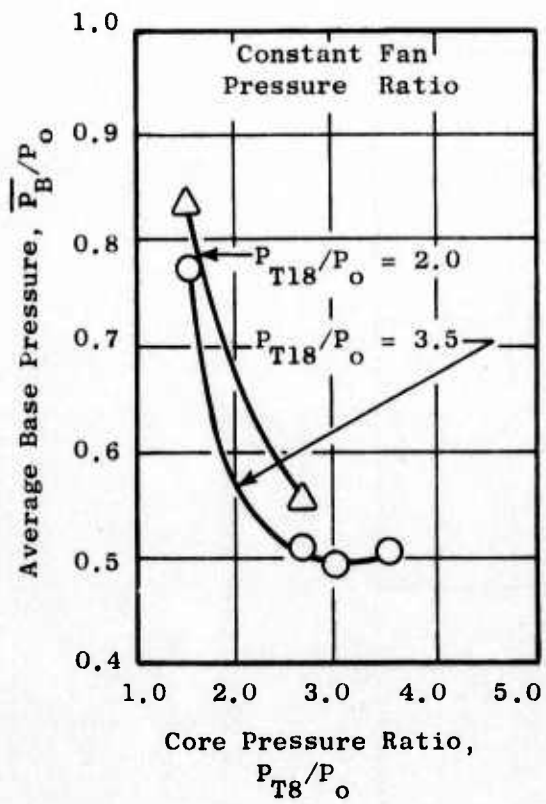
Figure 224. Integrated Average Base Pressures.
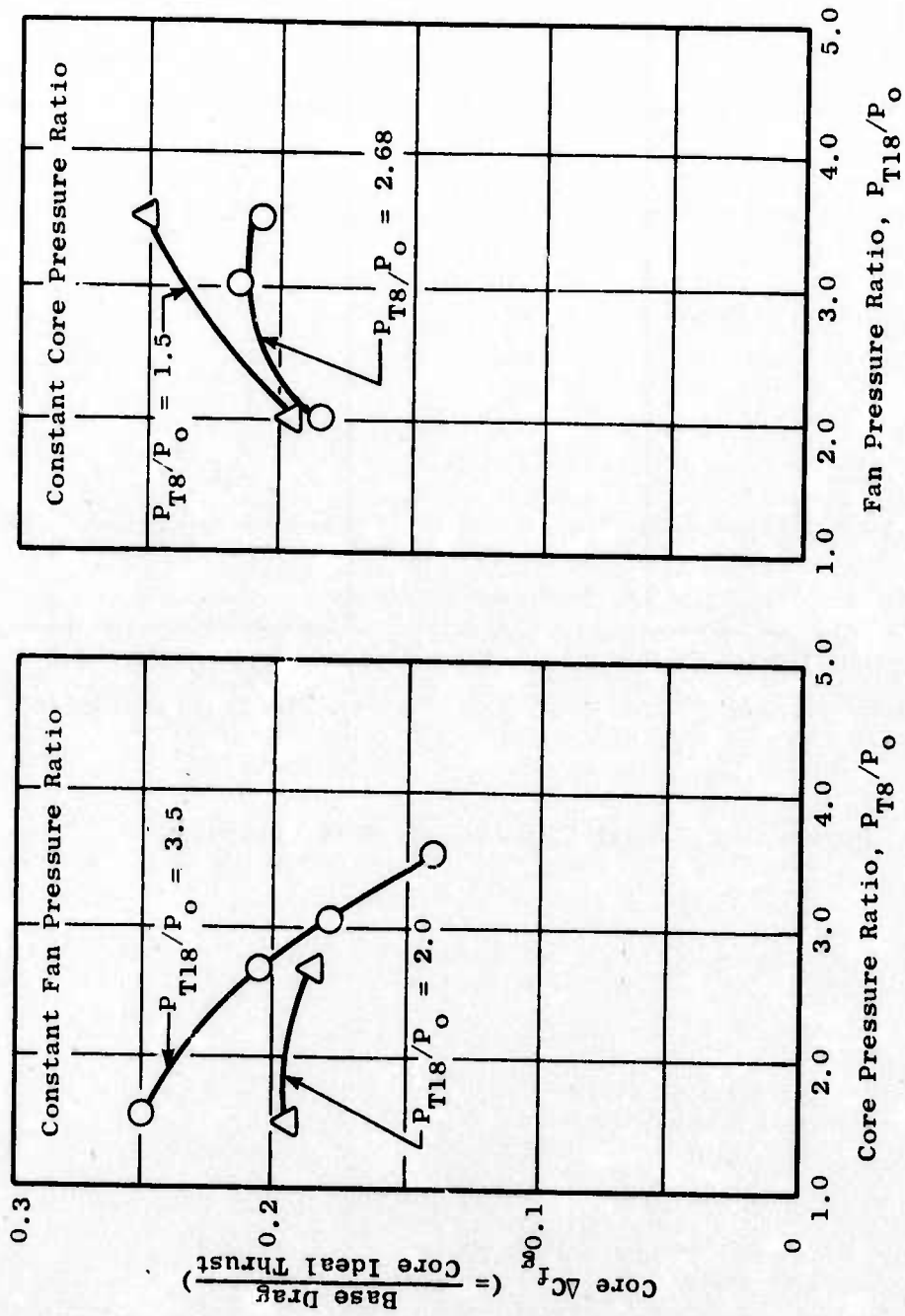
Figure 225. Core Thrust Loss.

284
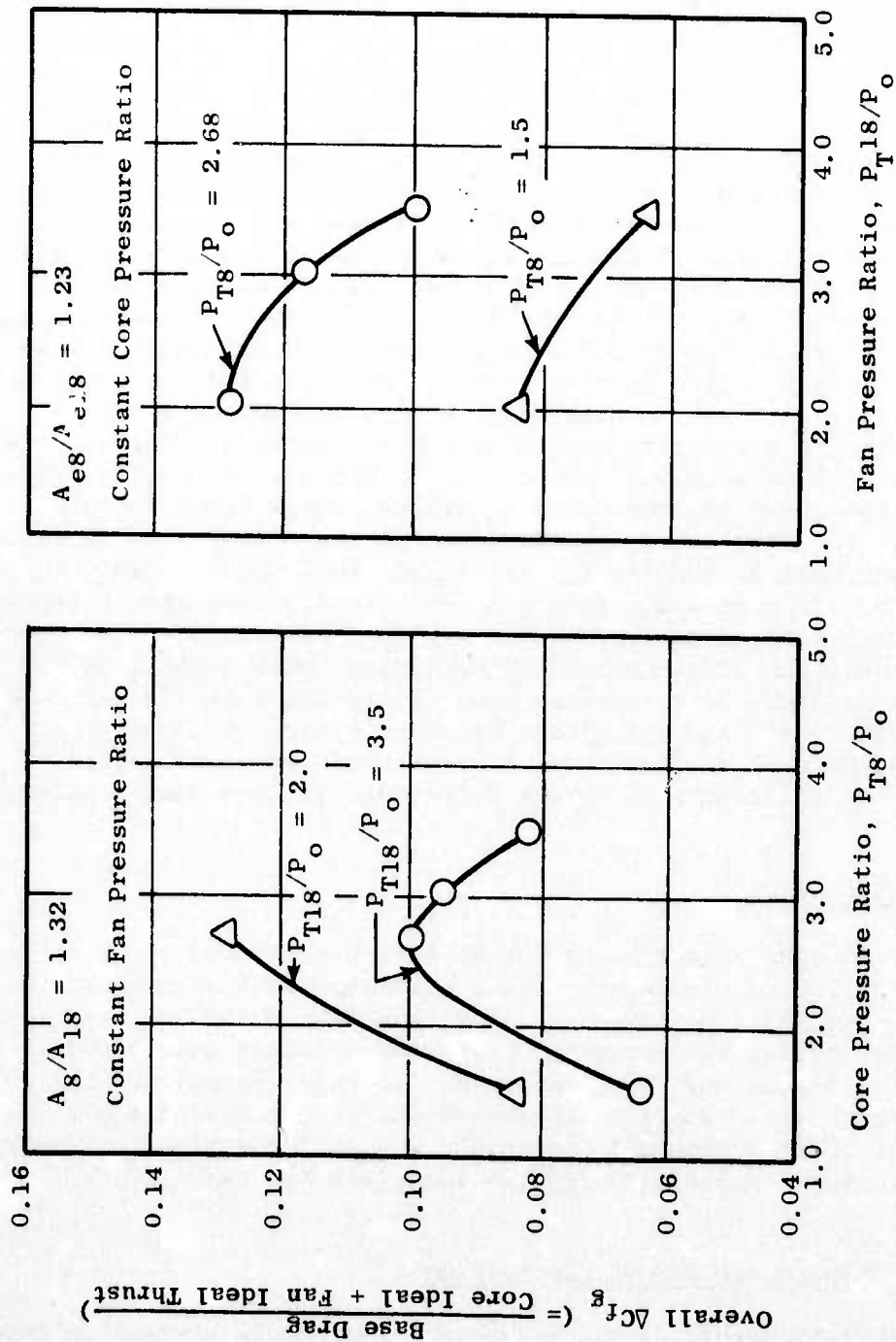
Figure 226. Overall Thrust Loss.

drags are fairly constant and predictable. Figure 226 shows total overall thrust loss versus core and fan pressure ratios based on single-flow thrust data. Integrated base drag ΔC_{f_g}'s were subtracted from total thrust loss for single-flow configurations similar to the core suppressor of the dual-flow system. This resultant ΔC_{f_g} was then added to the dual-flow base drags to produce the total thrust loss.

During the Parametric Aeroacoustic Refinement task, the effects of core/fan area ratio and non-coplanar, coplanar fan-core exit planes were investigated. The nozzle thrust losses from spoke base pressure drag for the three configurations tested are tabulated in Table 9 with the corresponding core and fan nozzle pressure ratios. The thrust losses are presented in two forms: 1) as a percentage of core ideal thrust and 2) as a percentage of total (fan and core) ideal thrust. The nozzle thrust loss decrement from core, spoke-base pressure drag between the flow and no-flow secondary nozzle conditions are presented in Figure 227 as a function of core nozzle pressure ratio. The thrust loss in these figures is based on the ideal, core nozzle thrust. With the exception of the data point at the highest core nozzle pressure ratio, the ratio of primary to secondary total pressures, P_{T8}/P_{T18}, for the remaining data fell between 0.78 and 0.89. In Figures 227a and b, the effect of primary-to-secondary area ratio is presented for the non-coplanar dual-flow nozzles. For core nozzle pressure ratios less than or equal to 2.0, the thrust decrement is smaller for the larger area ratio ($A_8/A_{18} = 1.5$) nozzle. For core nozzle pressure ratios greater than 2.0, the thrust losses for the two different area ratio nozzles are within 1 percent of each other. The effect of the position of the secondary exit plane with respect to the primary exit plane on spoke-base pressure drag is presented in Figures 227b and c. The positioning of the exit planes has more effect at lower core nozzle pressure ratios than at higher. For core nozzle pressure ratios greater than 2.3, the difference in thrust decrements is less than 1 percent.

System Evaluation

The dual-flow nozzles investigated during this task proved to be difficult to implement from a systems viewpoint. The suppression gain attributed to the fluid shielding of the cold unsuppressed fan stream around the hot suppressed core annulus did not offset the estimated performance losses attributed to the suppressed core. Additional considerations for this concept may be possible (e.g., suppression from hot suppressed fan stream around a hot unsuppressed core). This approach is presently undergoing evaluation under the NASA-Lewis Duct-Burning Turbofan Program (Contract No. NAS3-18008).

3.2.5.2 Asymmetric 2-D Nozzle Systems

The parametric refinements of the asymmetric 2-D nozzle systems included investigation of a suppressed primary nozzle with and without a long rectangular ejector (hardwall and full treated). Hot flow acoustic tests and cold flow aerodynamic wind-on performance tests were conducted to identify and evaluate the effects of these parametric refinements.

Table 9. Aerodynamic Evaluation of Dual-Flow Parametric Results.

Non-Coplanar A_8/A_{18} = 1.0				Non-Coplanar A_8/A_{18} = 1.5				Coplanar A_8/A_{18} = 1.5			
P_{T8}/P_o	P_{T18}/P_o	(Core) $\%\Delta C_{fg}$*	(Core + Fan) $\%\Delta C_{fg}$†	P_{T8}/P_o	P_{T18}/P_o	(Core) $\%\Delta C_{fg}$	(Core + Fan) $\%\Delta C_{fg}$	P_{T8}/P_o	P_{T18}/P_o	(Core) $\%\Delta C_{fg}$	(Core + Fan) $\%\Delta C_{fg}$
1.20	1.0	20.8	20.8								
1.52	1.0	19.3	19.3								
2.02	1.0	17.1	17.1								
2.32	1.0	16.6	16.6								
2.68	1.0	16.2	16.2								
3.03	1.0	14.7	14.7								
3.52	1.0	11.6	11.6								
1.21	1.5	30.5	8.9	1.20	1.51	29.2	10.6	1.20	1.50	19.2	6.7
1.51	1.94	27.0	9.2	1.52	1.95	--	---	1.51	1.94	23.7	10.0
2.03	2.53	26.5	10.2	2.03	2.50	24.0	11.3	2.03	2.50	26.2	12.0
2.34	2.74	27.3	10.8	2.35	2.76	26.4	13.2	2.32	2.74	28.4	13.5
2.68	2.99	24.2	10.7	2.68	3.01	23.5	12.2	2.69	3.00	24.0	12.3
3.05	3.50	20.5	8.6	3.04	3.51	19.8	10.1	3.03	3.49	20.1	10.0
3.54	3.49	15.6	7.2	3.55	3.51	14.8	8.4	3.54	3.49	14.8	8.6

* $\%\Delta C_{fg}$: Calculation based on integrated spoke base pressures and ideal core thrust.

† $\%\Delta C_{fg}$: Calculation based on integrated spoke base pressures and combined ideal thrust of fan and core.

287
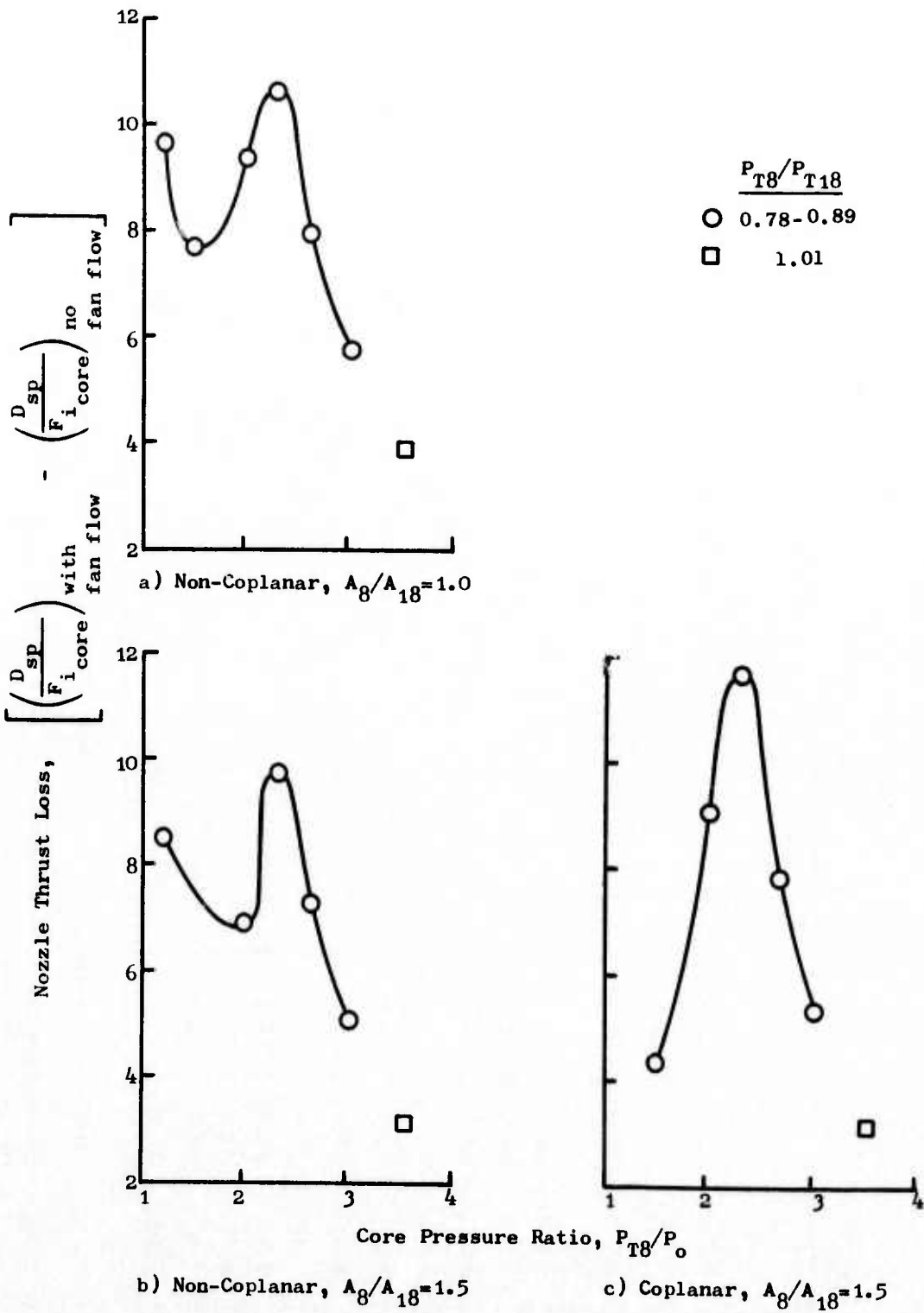
Figure 227. Nozzle Thrust Loss from Spoke-Base Pressure Drag with Fan Flow.

Acoustic Tests

The acoustic tests of the asymmetric 2-D nozzle systems were conducted on the JENOTS hot jet test facility. The facility was set up for single-flow operation as described in Appendix A.

Five nozzle configurations were tested in this series:

- Unsuppressed 2-D nozzle (comparison with previous test)

- Unsuppressed 2-D with hardwall ejector and ramp assembly (comparison with previous test; effect of ejector bellmouth)

- Unsuppressed 2-D with fully treated ejector and ramp assembly (comparison with unsuppressed 2-D with hardwall ejector; for treatment effect)

- Suppressed 2-D with hardwall ejector and ramp assembly (comparison with unsuppressed 2-D with hardwall ejector; for suppressor effect)

- Suppressed 2-D with fully treated ejector and ramp assembly (comparison with suppressed 2-D with hardwall ejector; for treatment effect)

The suppressor for these configurations consisted of 12 parallel-sided chutes with an area ratio of 2.0. The suppressed throat plane was located approximately 4.5 inches downstream of the unsuppressed throat plane, just inside the inlet to the ejector. Moving the suppressed exit plane forward of its original position, when it was tested in the Advanced Concepts task (Section 3.2.4), allowed for a greater effective ejector length (L/H~3-4), where "L" is ejector length aft of the suppressed core exit plane and "H" is the ejector height. This also resulted in an increased linear scale factor of 10:1 (previously 8:1), since the overall flow area of the suppressor was reduced but the area ratio remained at 2.0. Figure 228 schematically illustrates the differences in the suppressed plane location for the advanced concepts and parametric refinement tests. The suppressed 2-D nozzle was designed with the capability to vent the sidewalls in order to pressurize the sidewalls downstream of the suppressor exit, thus reducing drag. Tests were conducted with vents open and closed.

Treatment was incorporated into the ejector, sidewalls, and nozzle exit ramp for acoustic tests of a long treated 2-D ejector with a suppressed primary stream simulating a long aerodynamic mixing nozzle. The treatment design criteria and material selection is described in Section 3.2.4 of the Advanced Concepts.

The unsuppressed 2-D nozzle was the same as had been previously tested in the Advanced Concepts task. The nozzle aspect ratio was 4 to 1 and the flow area was 1/64th of the full-scale size.

Section of 12-Chute Suppressor
Used in Parametric Refinements

$L/h_1 \sim 5$

h_1

Suppressor Exit Plane
(Parametric Refinements)

H

15°

● Suppressed 2-D with Ejector (L/H ~ 3)

$L/h_2 \sim 2.3$

h_2

Suppressor Exit Plane
(Advanced Concepts)

15°

● Suppressed 2-D with Sidewalls, No Ejector
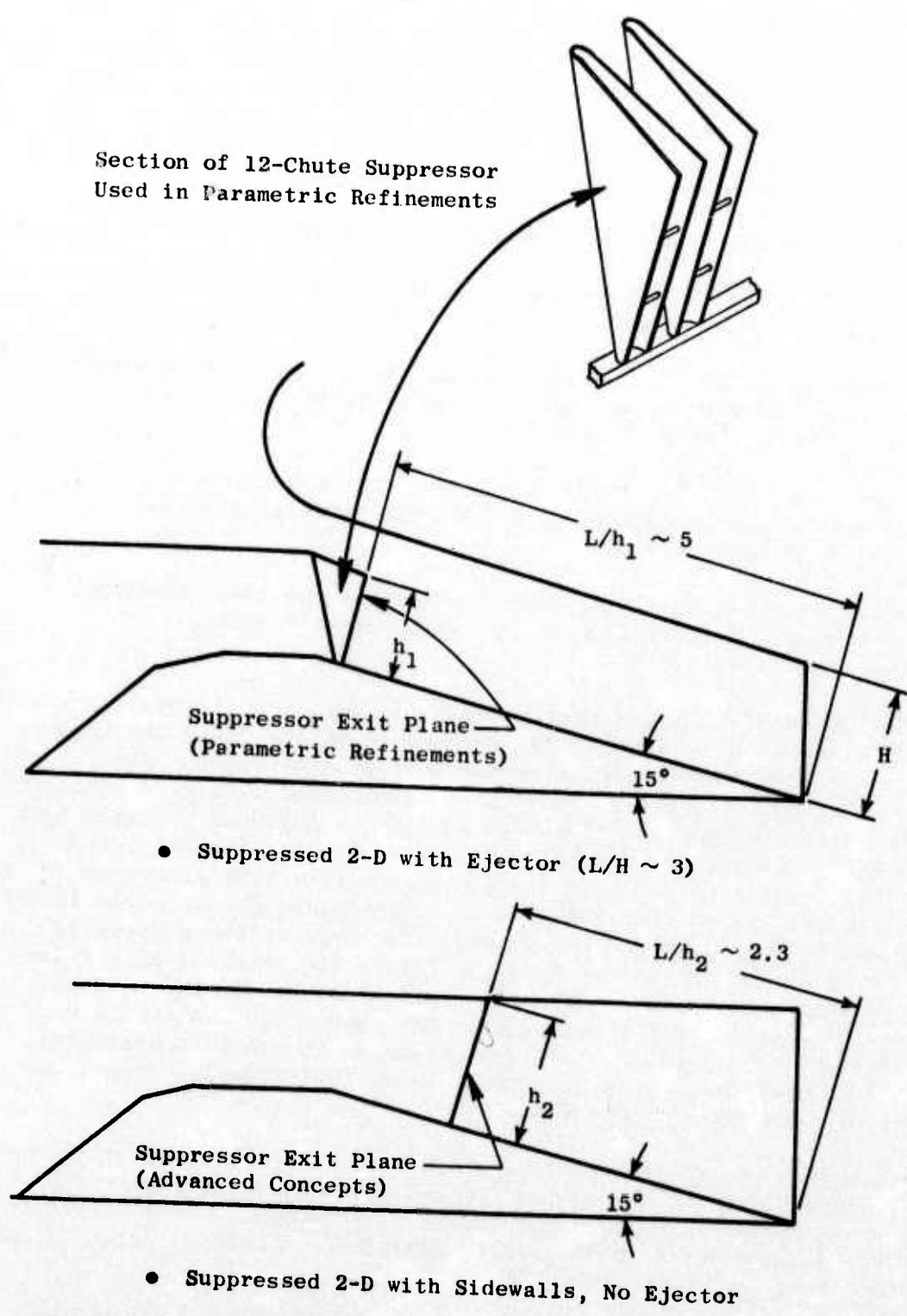
Figure 228. Comparison of Suppressed 2-D Exit Plane Locations.

Far-field acoustic measurements were obtained on each configuration. All of the 2-D model configurations tested in this series were positioned in the "sideline" orientation. This meant that the long axis in the exit plane of the rectangular nozzle was parallel to the plane of the 90° microphone position – jet axis. A full description of the setup is found in Advanced Concepts, Section 3.2.4.

The acoustic measurements obtained in this fashion were scaled by frequency and size to full-scale application. The unsuppressed 2-D nozzle results were scaled by a factor of 8:1, while the suppressed 2-D results were scaled by a factor of 10:1. The differences in scaling were normalized for purposes of data comparison.

Acoustic Results and Analysis

The individual test configuration results are summarized in tables which can be found in Appendix C. The tables include a list of acoustic results for the actual test conditions observed.

The unsuppressed 2-D nozzle 2128-foot sideline test results are shown in comparison to a previous test of the same configuration in Figure 229. The variation between the 1973 and 1974 results is within the ±1.5 dB tolerance band established at JENOTS and indicate good data repeatability with the asymmetric nozzle. An unsuppressed conical nozzle line also is included for reference. The PNL directivity (Figure 230) On the 2128-foot sideline and the 300-foot sideline spectral distribution (Figure 231) also show good agreement with the previous test. Peak PNL remains at 120° for the entire range of velocities, while peak frequency also remains constant (~125 Hz) in this same velocity range.

Acoustic results of the 2-D unsuppressed nozzle with hardwall ejector are shown in Figures 232 through 234. The peak PNL at the 2128-foot sideline is shown in Figure 232 over the ideal jet velocity range. PNL directivity is illustrated in Figure 233 for the 2128-foot sideline. Spectral distributions at the 300-foot sideline are presented in Figure 234 over the operating range. These figures illustrate the acoustic characteristics of this configuration.

The data comparison of the test results on the unsuppressed 2-D nozzle with the hardwall ejector (Figure 235) showed the data to repeat reasonably well with earlier tests conducted in the Advanced Concepts phase. The only difference in the hardwall ejector configuration was the addition of the ejector bellmouth inlet. The effect of the hardwall ejector on the unsuppressed spectra is shown in Figure 236.

The unsuppressed 2-D nozzle with treated ejector results are shown in Figures 237 to 248. The photograph of the model configuration (Figure 237) shows the ejector bellmouth which was used for all ejector test configurations. The treatment is observed to have little or no influence on the PNL for the unsuppressed 2-D nozzle as shown in Figure 238. This is most

291
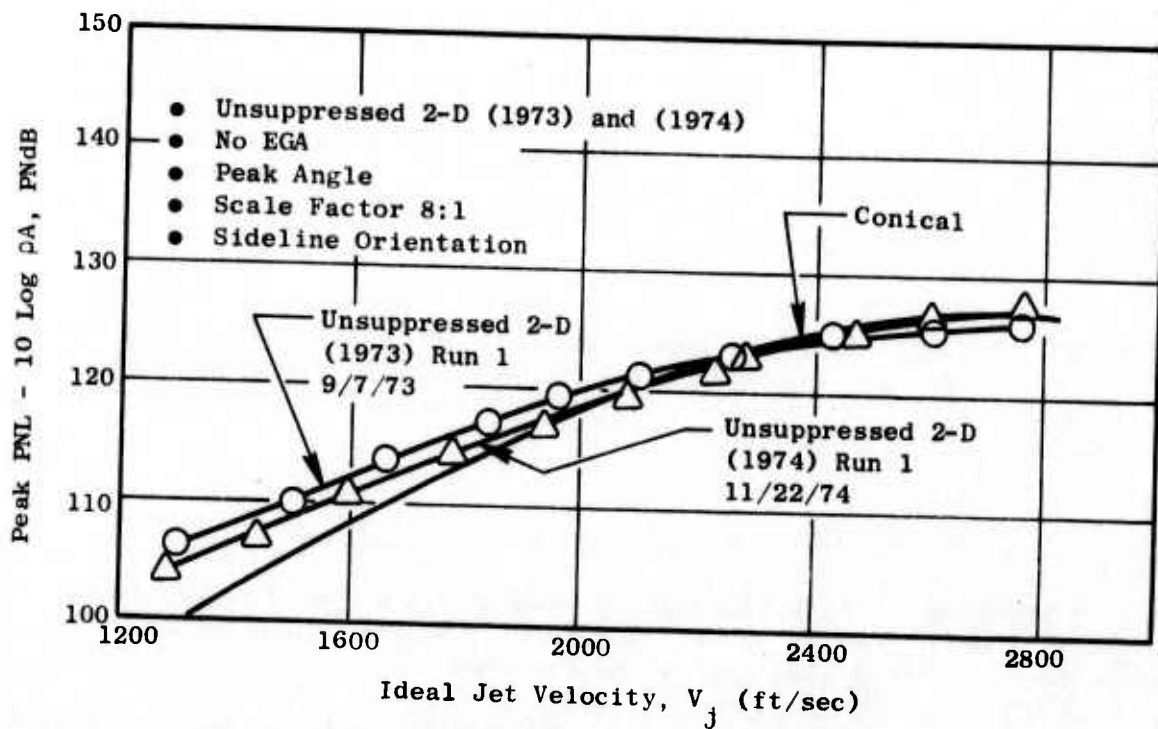
Figure 229. 2128-Foot Sideline PNL Comparison.
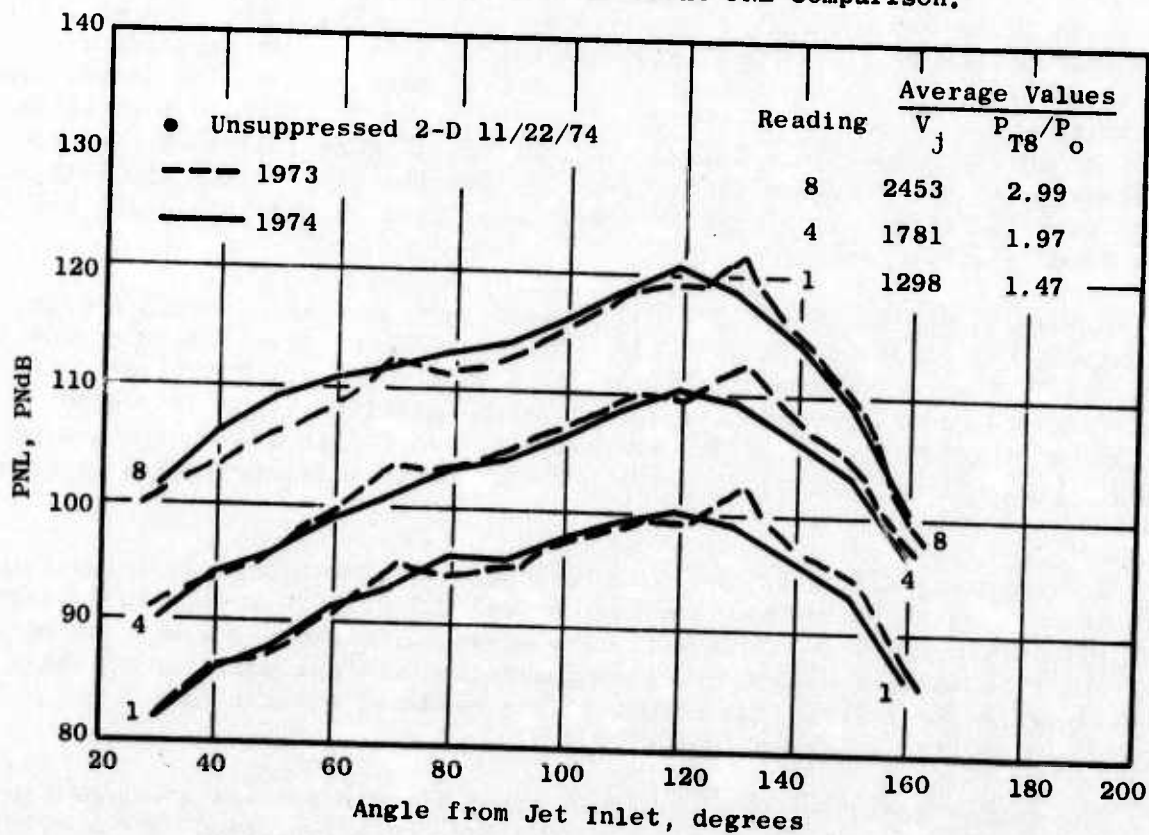
Figure 230. 2128-Foot Distance PNL Directivity.
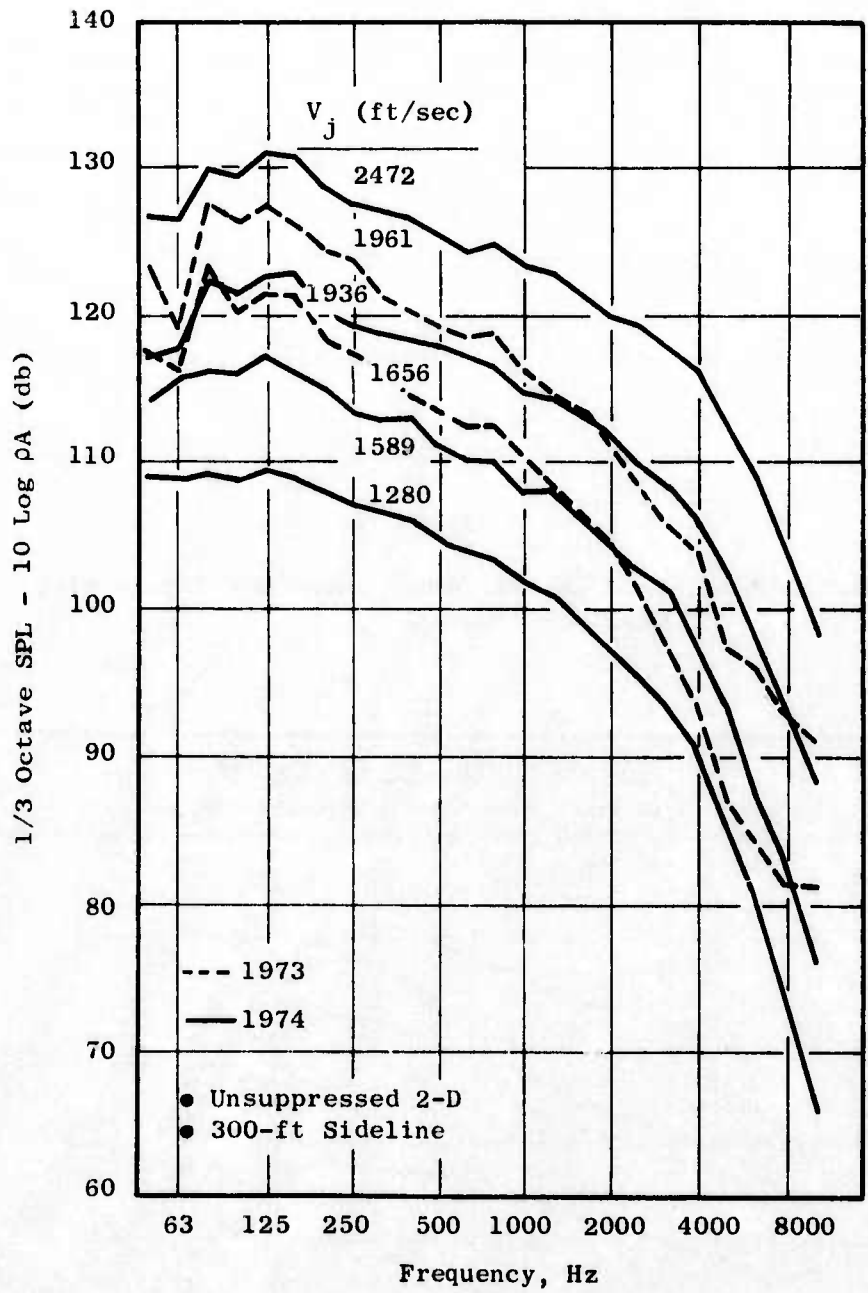
Figure 231. 300-Foot Sideline Peak Spectra.
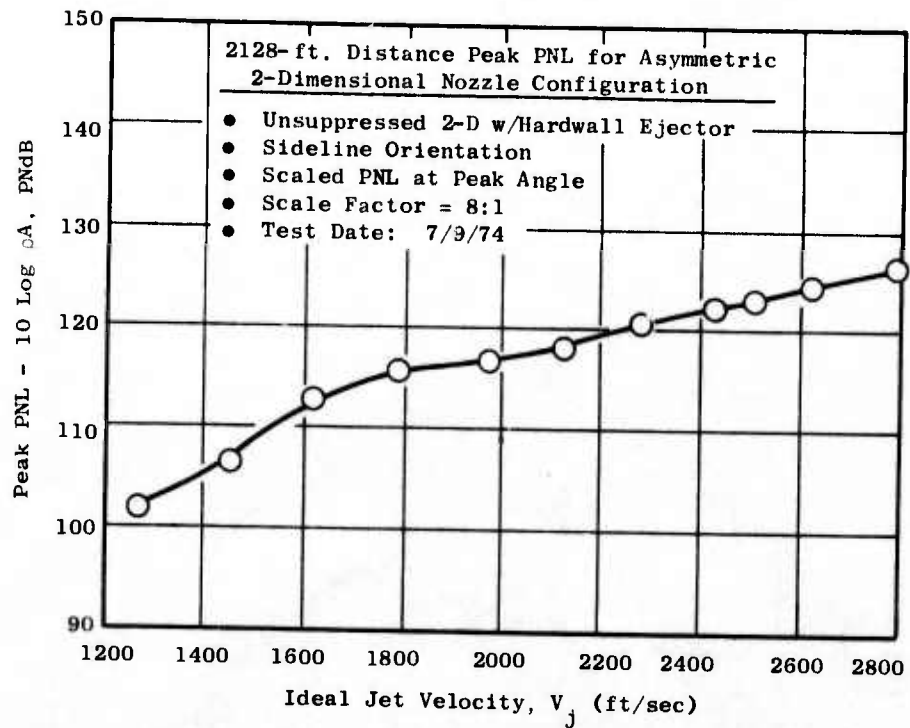
Figure 232.   Peak PNL of Unsuppressed 2-D Nozzle with
                Hardwall Ejector.
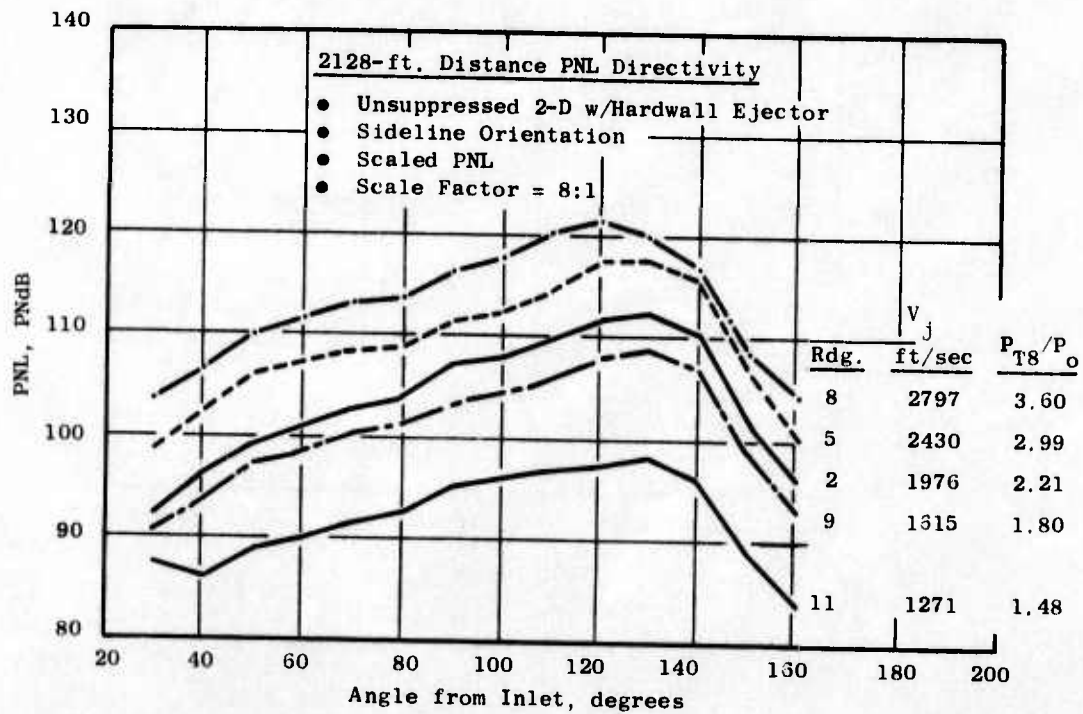
Figure 233.   PNL Directivity of Unsuppressed 2-D Nozzle with
                Hardwall Ejector.

294
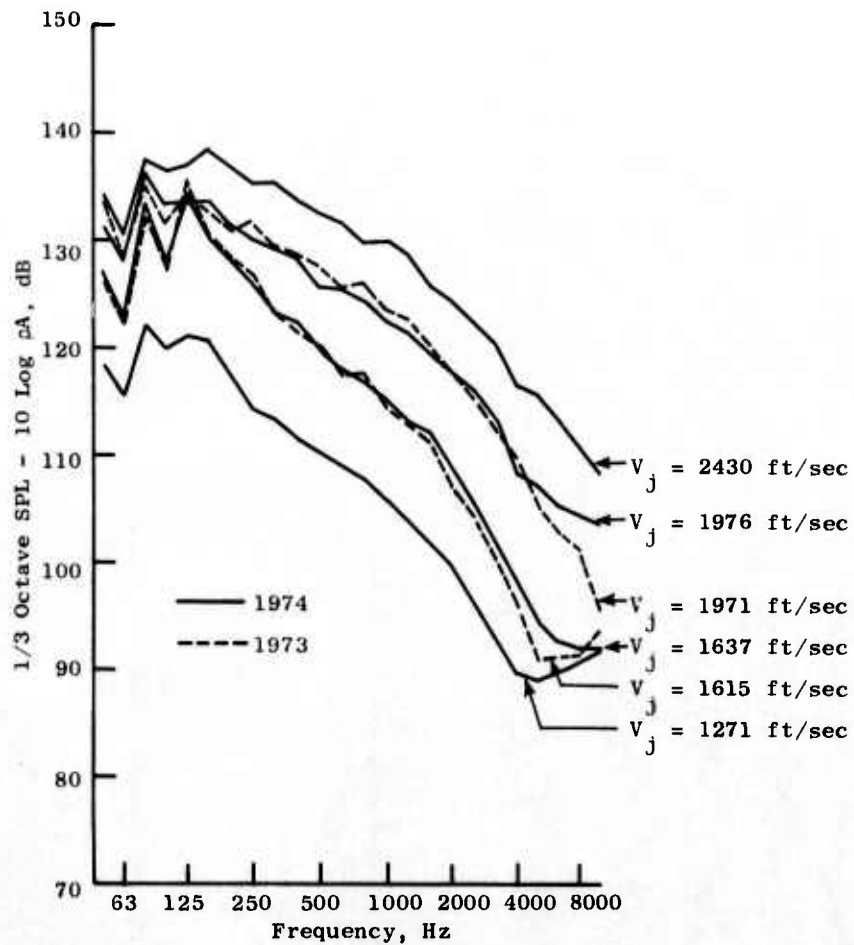
Figure 234. Spectral Comparison of Tests with Unsuppressed 2-D Nozzle with Hardwall Ejector.
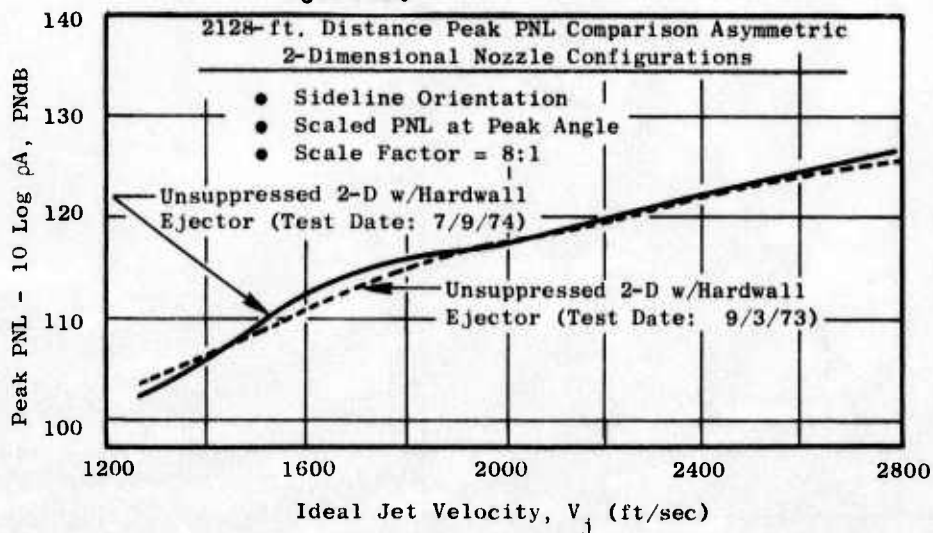
Figure 235. Peak PNL Comparison of Unsuppressed 2-D Nozzle with Hardwall Ejector.

295
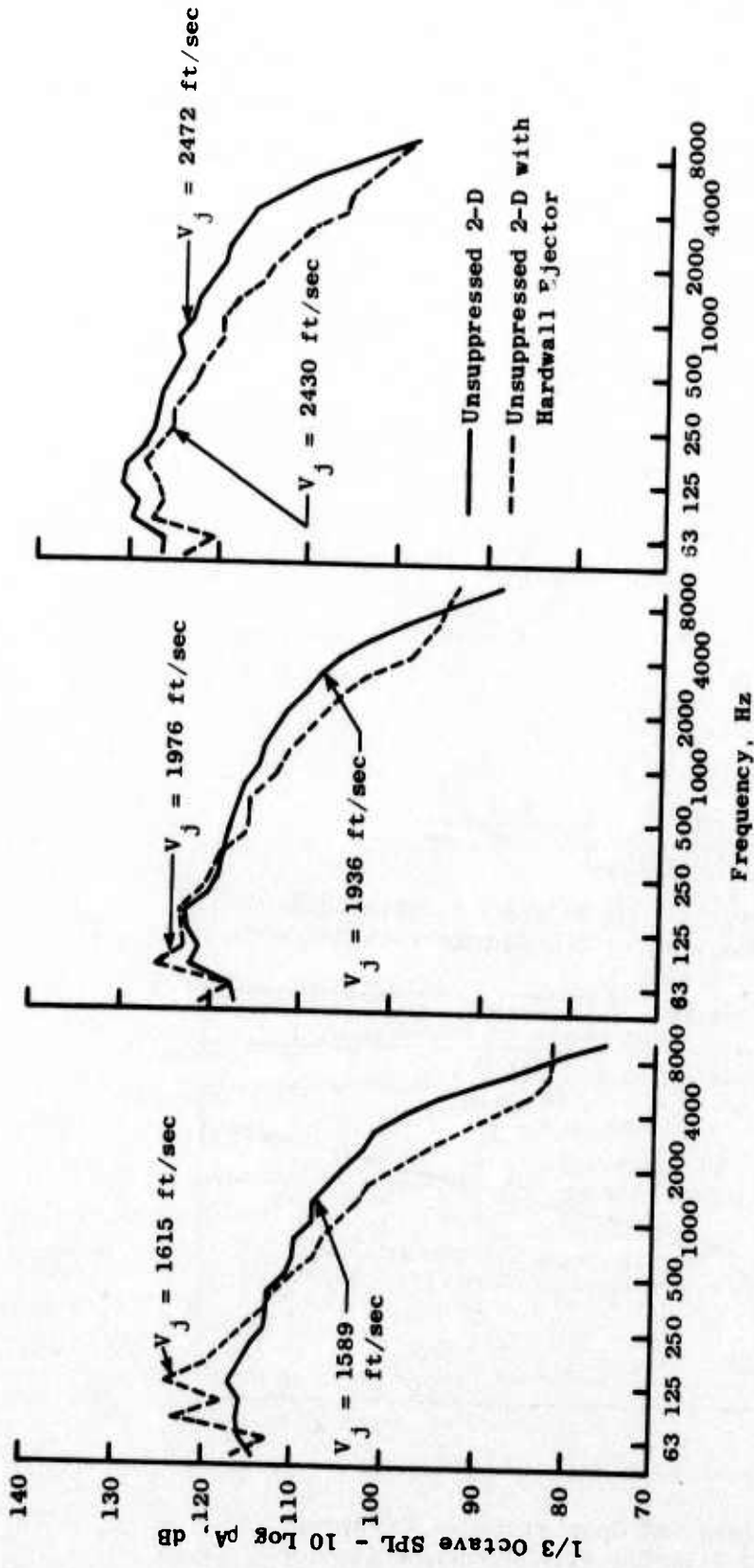
Figure 236. Effect of Hardwall Ejector on Unsuppressed 2-D Nozzle, 300-foot Sideline.

TUFTS

EJECTOR BELLMOUTH
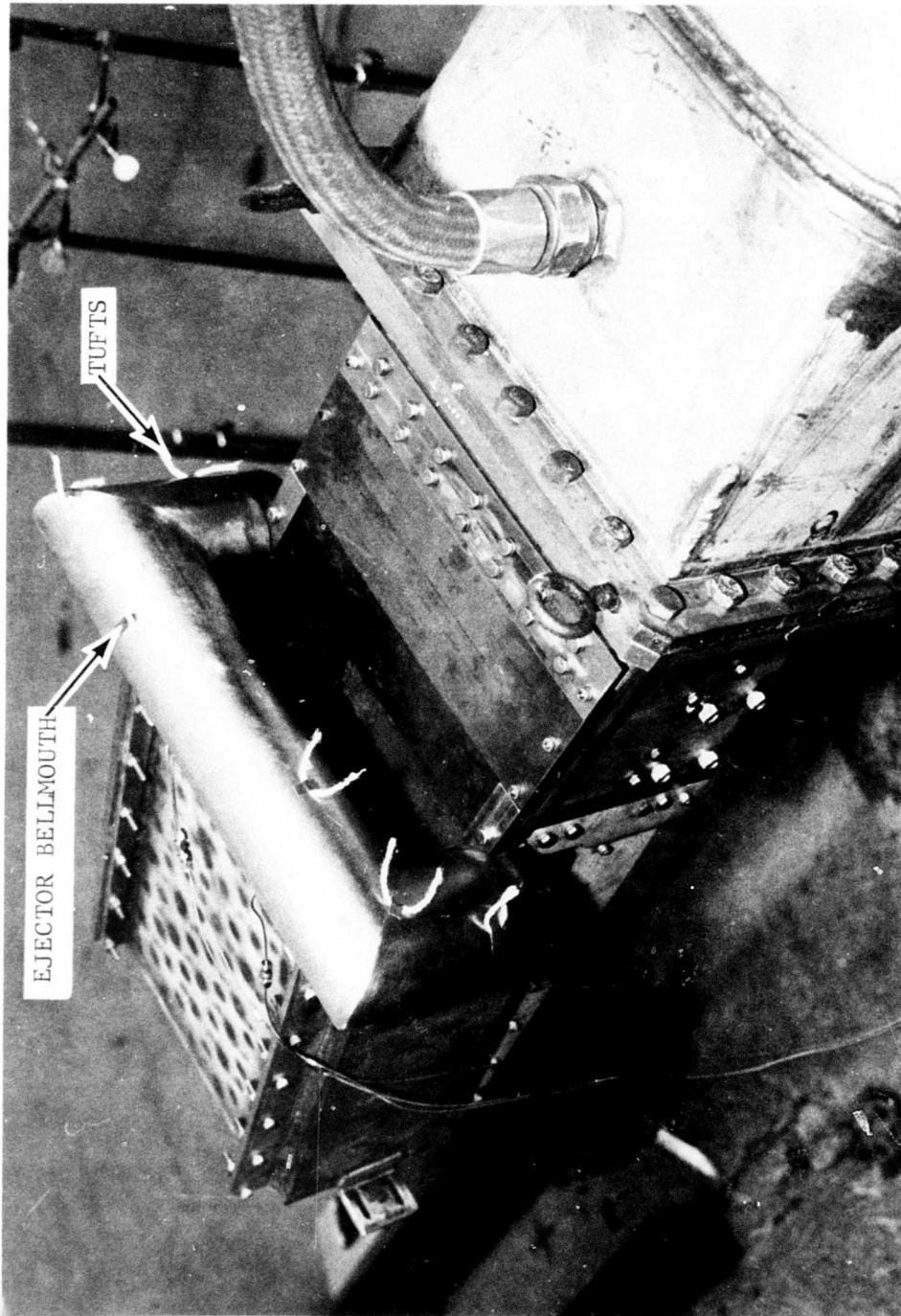
Figure 237. Unsuppressed 2-D Nozzle with Treated Ejector and Ramp Assembly.

297
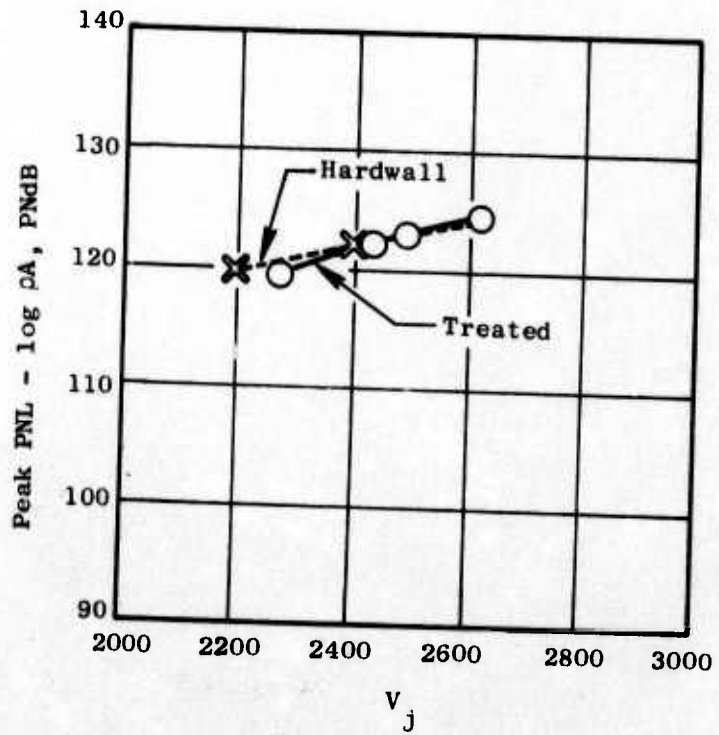
Figure 238.   Effect of Treatment with
Unsuppressed 2-D Nozzle
+ Ejector.

298
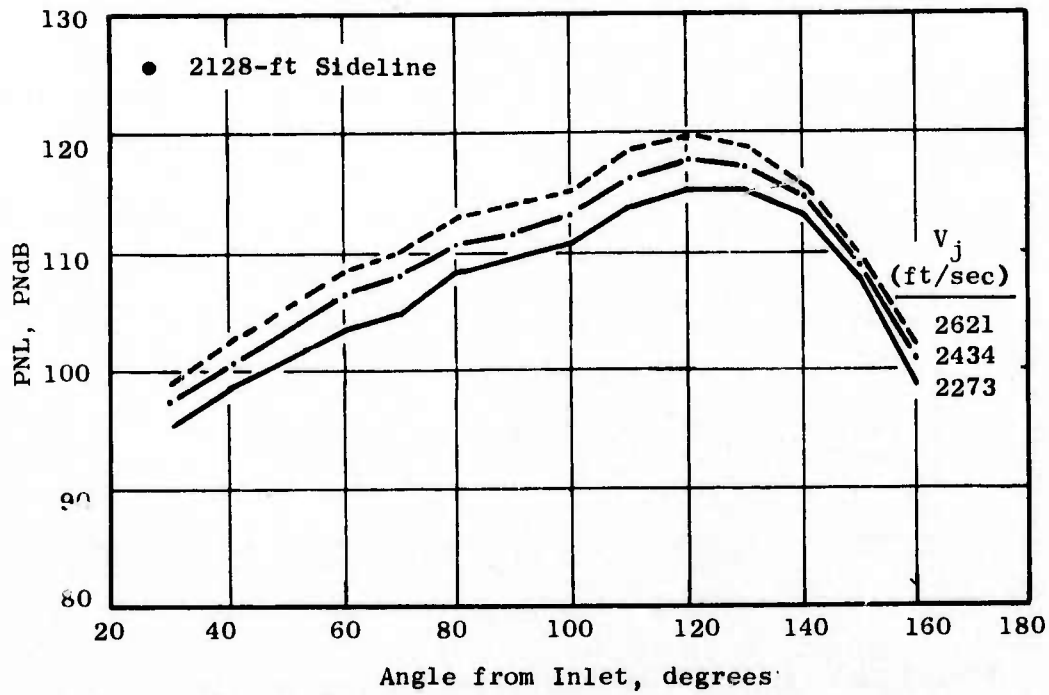
Figure 239. PNL Directivity.
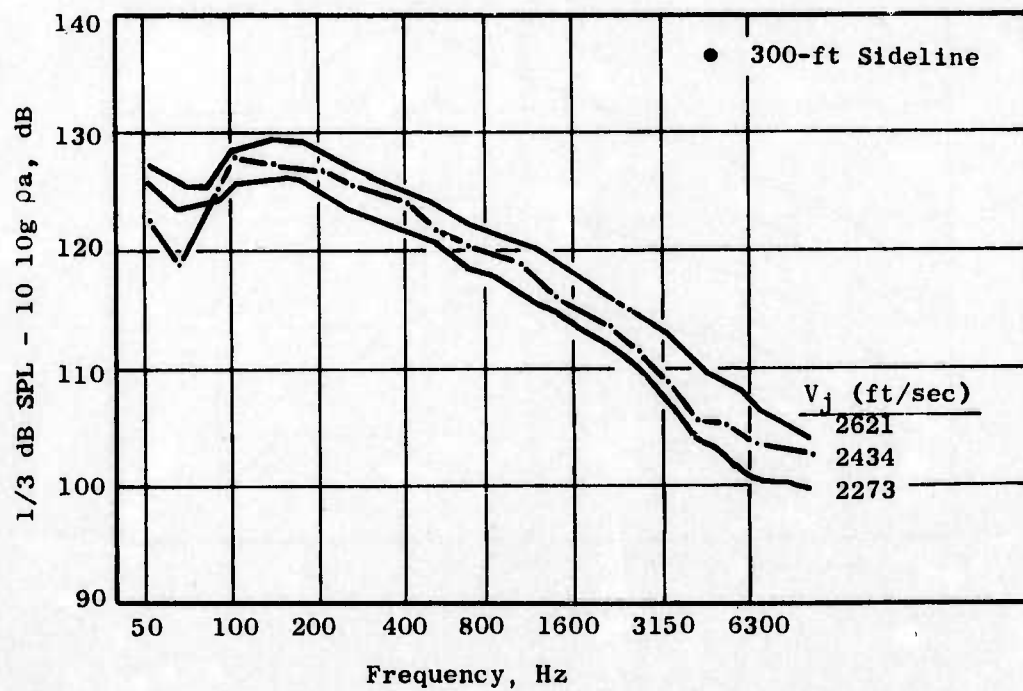
Figure 240. SPL Spectra.

299
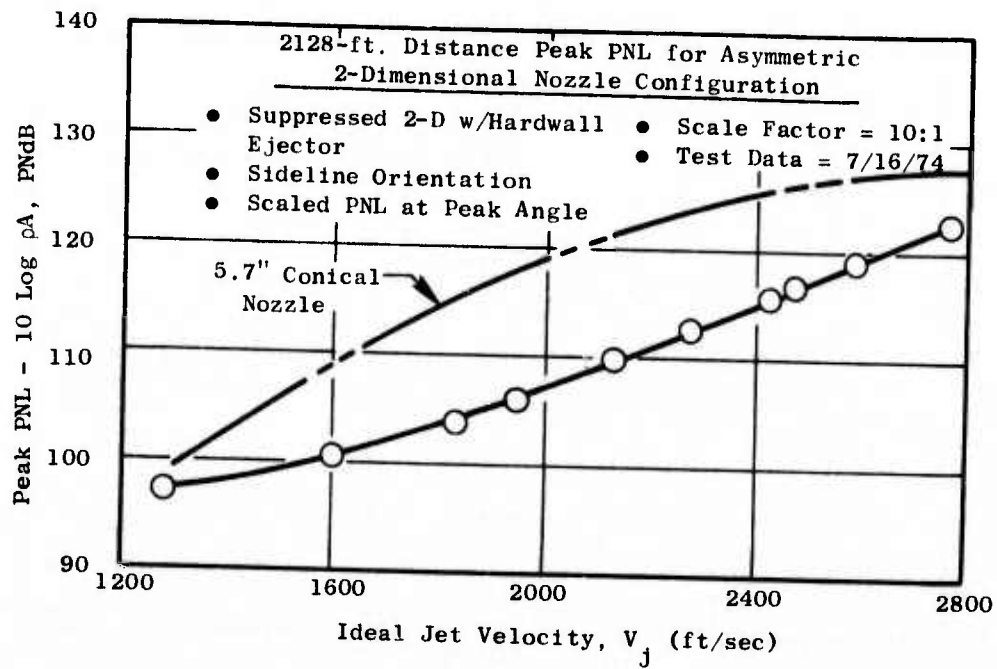
Figure 241. Peak PNL of Suppressed 2-D Nozzle with the Hardwall Ejector.
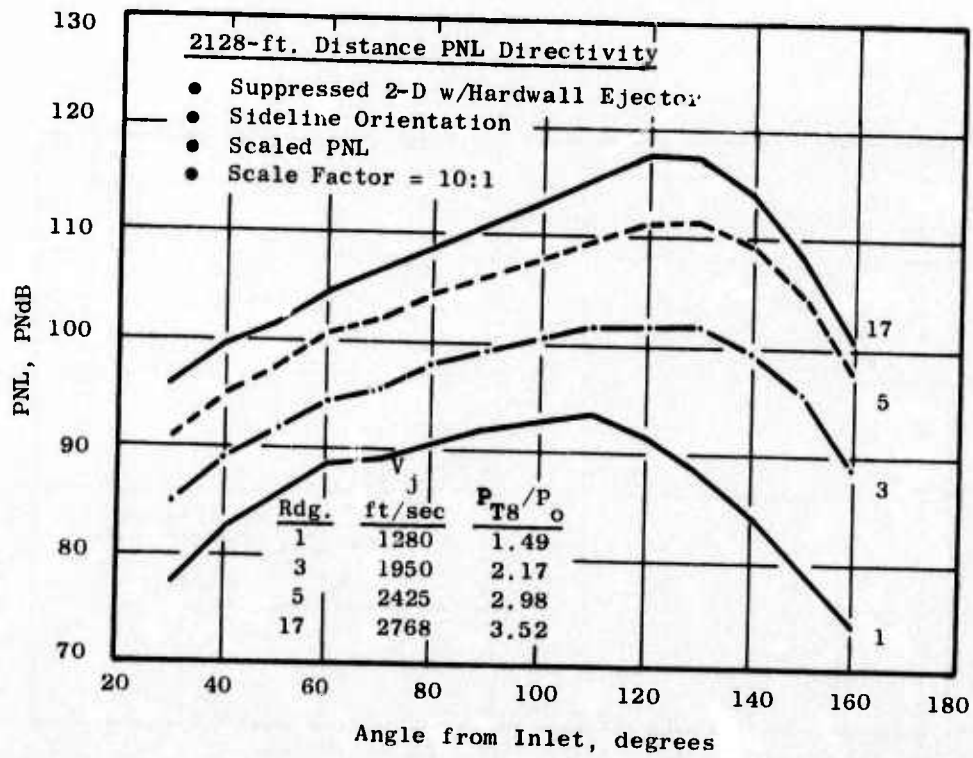
Figure 242. PNL Directivity of the Suppressed 2-D Nozzle with the Hardwall Ejector.

300
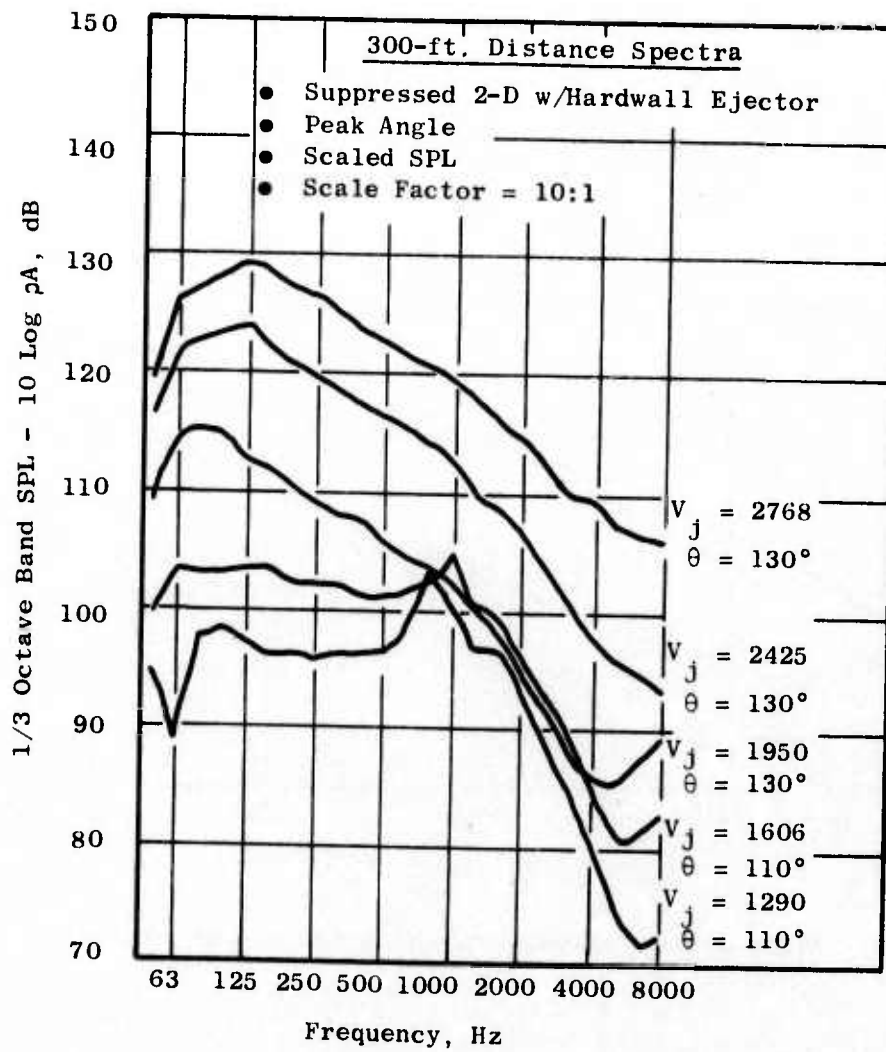
Figure 243. SPL Spectra for the Suppressed 2-D Nozzle with the Hardwall Ejector.
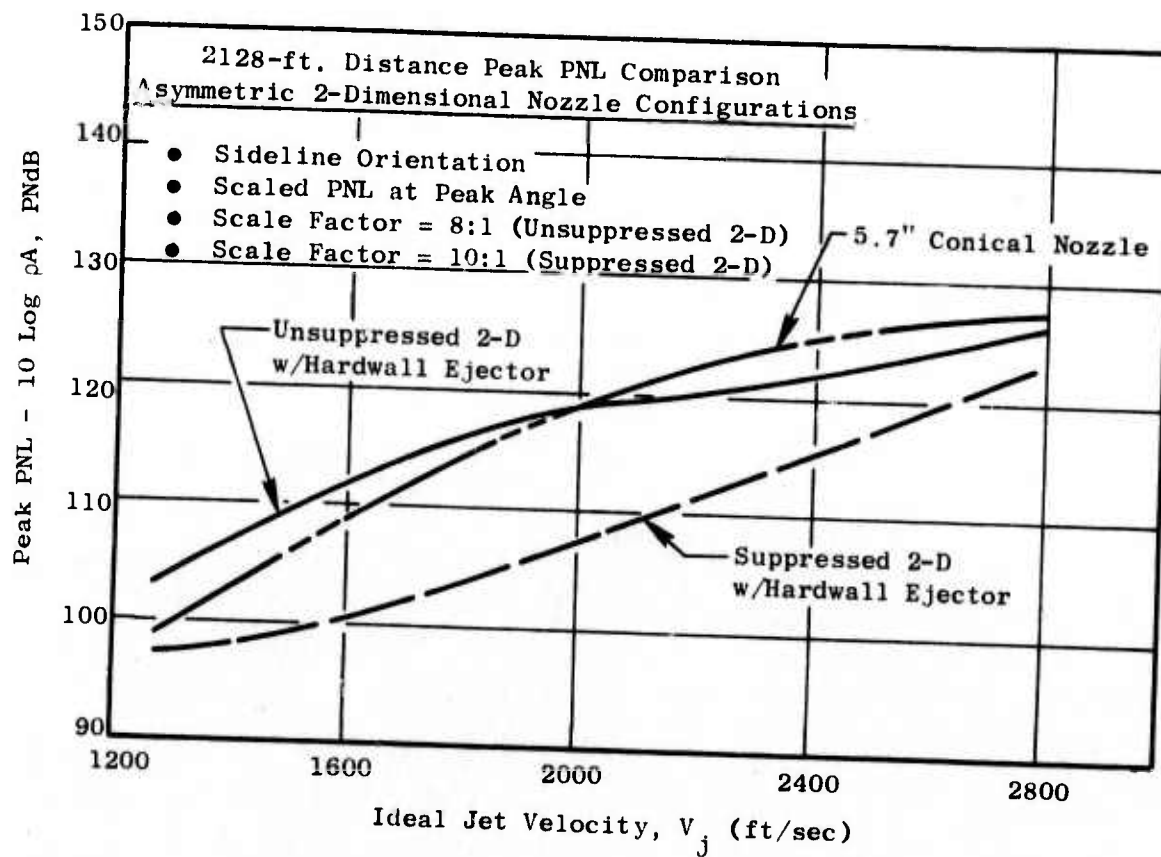
Figure 244. Effect of Suppressed Primary on the 2-D Nozzle with Ejector.
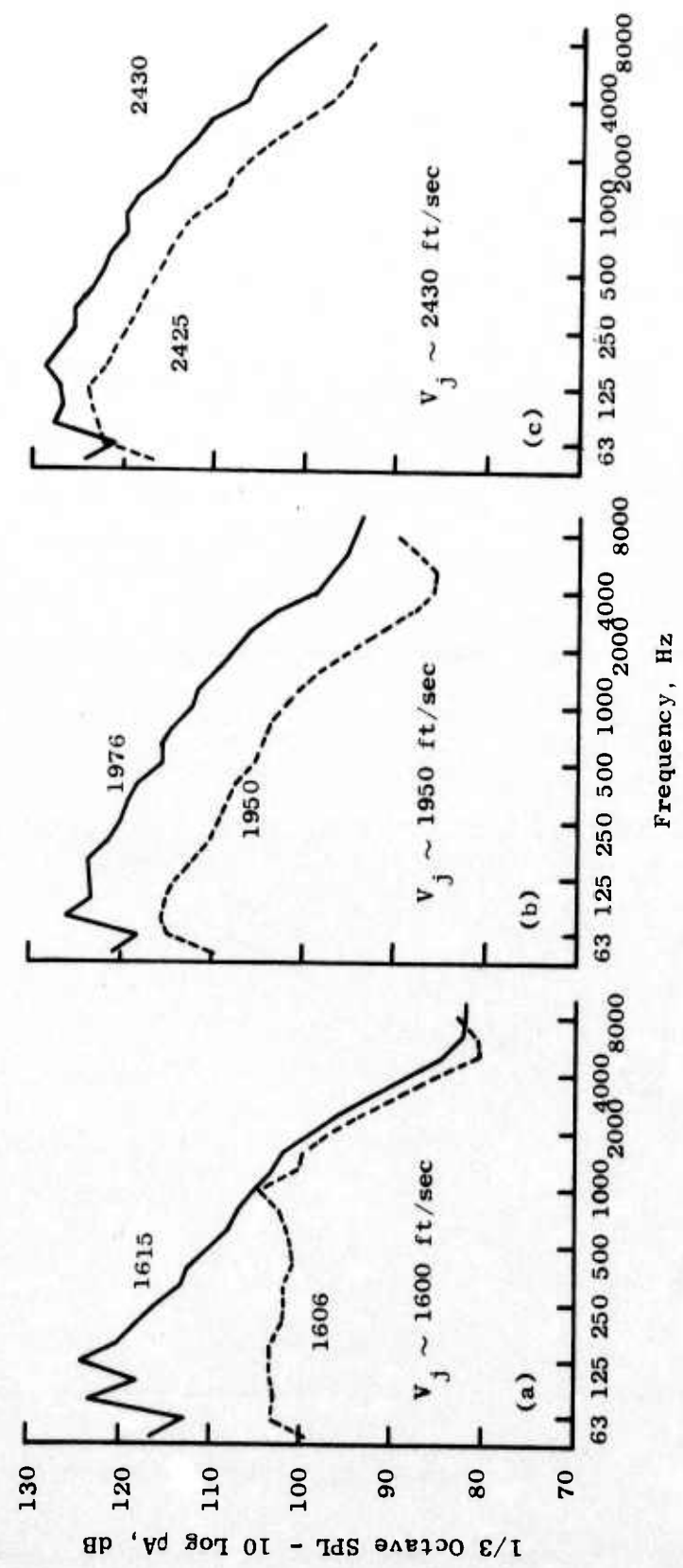
Figure 245. Effect of Suppressor on 2-D Hardwall Ejector Configuration, 300-foot Sideline.
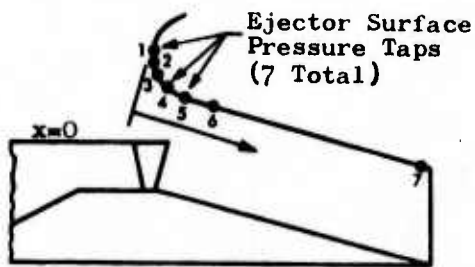
303
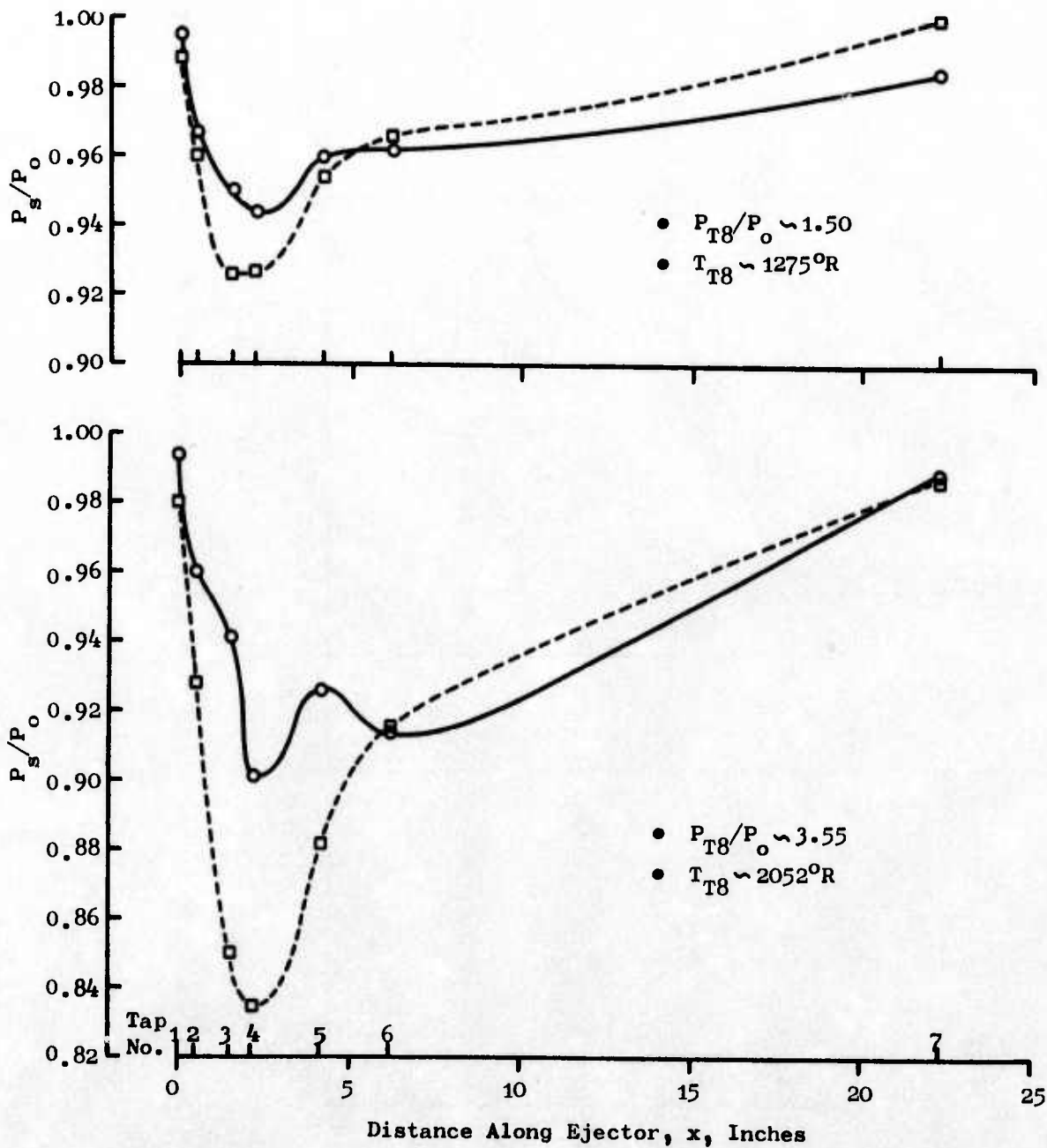
Figure 246.   Ejector Surface Static Pressure Distributions.
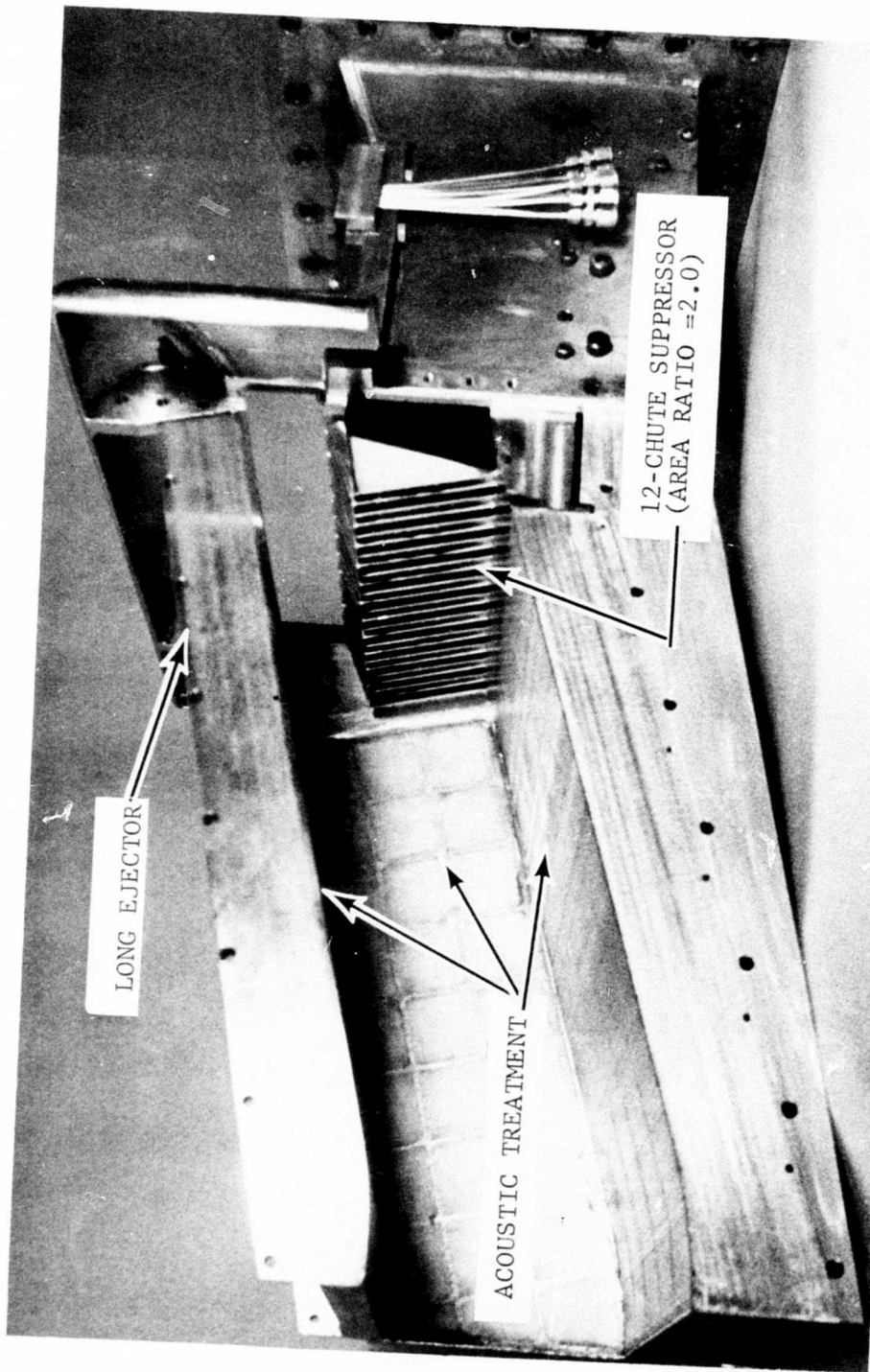
Figure 247. Suppressed 2-D Nozzle with Treated Ejector.

305
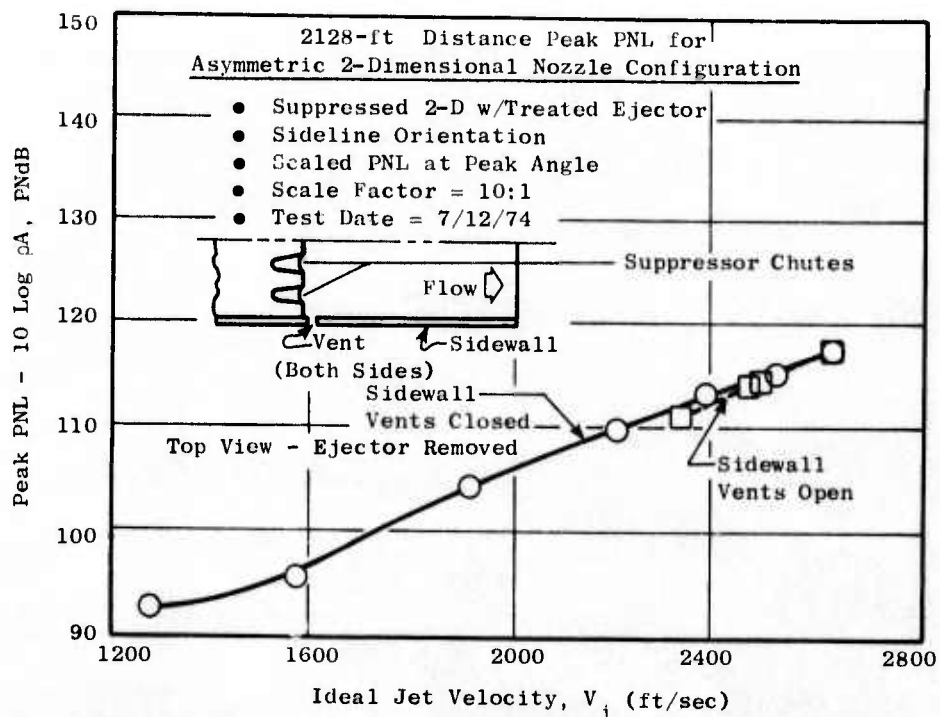
Figure 248. Peak PNL of Suppressed 2-D Nozzle with Treated Ejector.
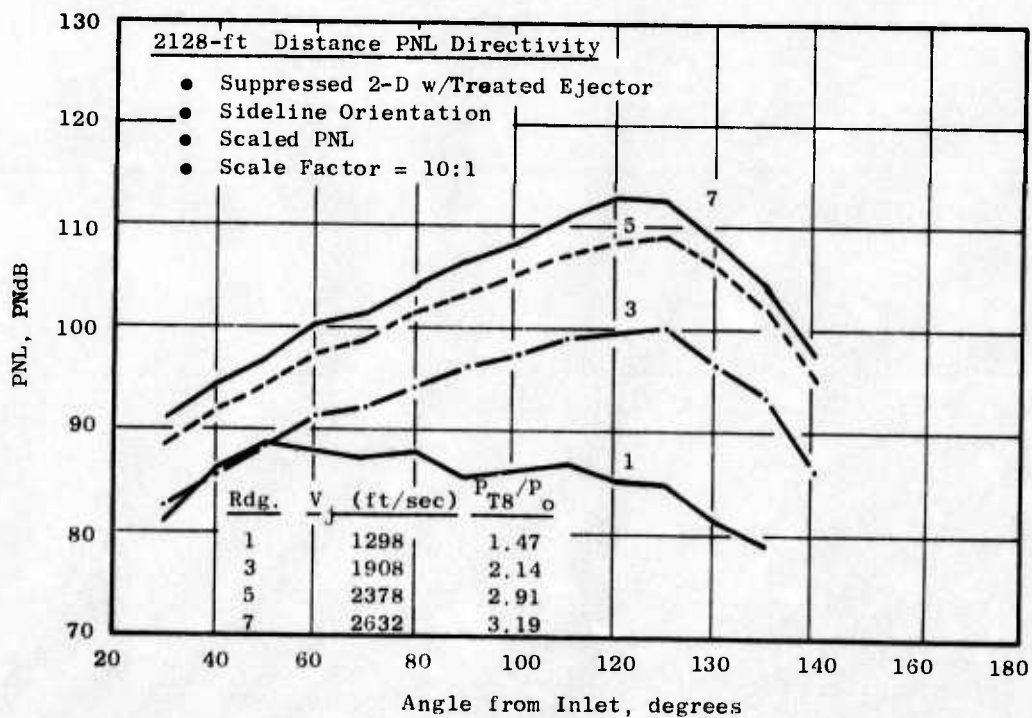
Figure 249. PNL Directivity of Suppressed 2-D Nozzle with Treated Ejector.

probably due to the elongated distribution of noise sources typical of unsuppressed nozzles, in which the low and mid-frequencies to be attenuated by the treatment are outside the ejector region and, therefore, not affected by the treatment. The peak angle is shown to be 120° (Figure 239) while low frequencies dominate the spectra in Figure 240.

In an attempt to gain additional suppression from the 2-D system, hardwall and acoustically treated ejectors were tested with a suppressed primary. The suppressor was a 12-chute (area ratio of 2.0) configuration with parallel-sided jet flow elements normal to the 15° ramp. The peak PNL variation with ideal jet velocity is shown in Figure 241 for the suppressed 2-D nozzle with hardwall ejector. The data are presented on a 2128-foot sideline, as is the PNL directivity shown in Figure 242. The 300-foot sideline SPL spectra are illustrated in Figure 243 over the velocity range of interest and show the low frequencies to become dominant at $V_j \sim 1950$ ft/sec indicating coalescence of the suppressed jet elements.

A comparison of the suppressed 2-D nozzle with the unsuppressed 2-D nozzle with hardwall ejector configurations is shown in Figure 244, The effect of the suppressor is shown to give an additional 1 PNdB suppression over the unsuppressed configuration at 2400 ft/sec. A spectral comparison of these configurations is presented in Figure 245 which illustrates the effect of the suppressor on the hardwall ejector configuration.

The effect of the bellmouth on the ejector surface pressures with unsuppressed and suppressed 2-D nozzles is shown in Figure 246 for nozzle pressure ratios of 1.5 and 3.55. The curves indicate bellmouth separation which would act to close the ejector inlet area down and reduce the amount of entrained flow available for mixing with the primary stream and, hence, limit the suppression gained from turbulent mixing.

The asymmetric 2-D suppressed primary nozzle tested with the fully treated long ejector is shown in Figure 247. Comparisons between treated and hardwall ejector results show that the treated ejector gave an additional suppression gain of 1-1.5 PNdB over most of the velocity range relative to the hardwall ejector. At velocities below 1600 ft/sec, a 3-4 PNdB suppression gain was observed. This comparison was made with the suppressed 2-D sidewall vents closed. Figure 248 shows the 2128-foot sideline peak PNL variation of the suppressed 2-D nozzle with treated ejector. The PNL directivity at the 2128-foot sideline is found in Figure 249, while Figure 250 presents the 300-foot sideline SPL spectra. The tone in the spectrum at $V_j = 1278$ appears to be a vortex shedding tone off the 12-chute suppressor.

A comparison of vented with unvented sidewalls was made on the suppressed primary nozzle with the treated ejector configuration. The limited results indicate that a slight (1 dB) suppression gain was obtained with the vents as seen in Figure 248. However, measured vent wall static pressure distributions were greater than ambient for the jet velocities above 1600 ft/sec (Figure 251) ($P_{T8}/P_o > 1.75$), indicating a possible outward flow through the vents (instead of flow entrainment) resulting in additional thrust loss.
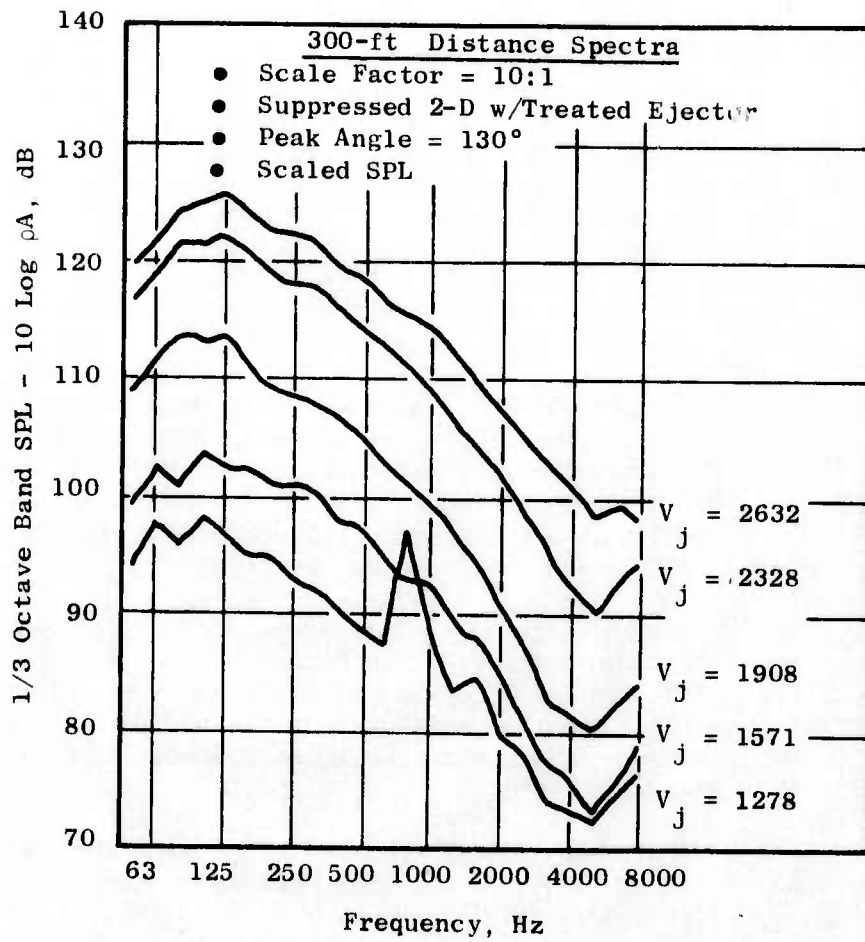
Figure 250.   SPL Spectra of Suppressed 2-D Nozzle with
Treated Ejector.
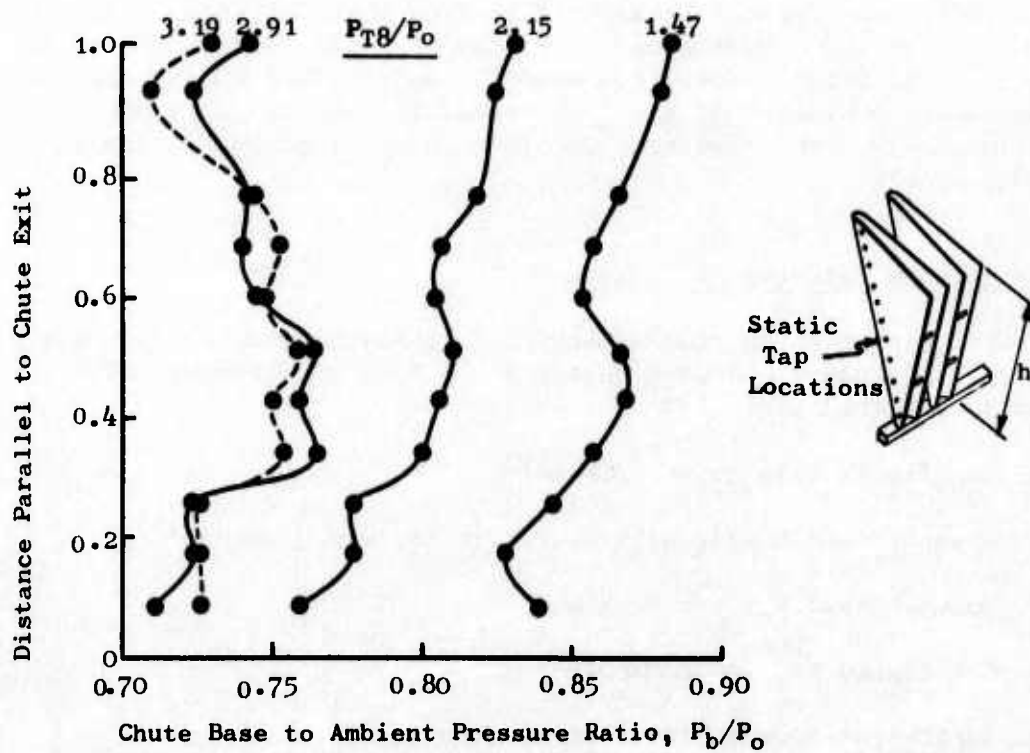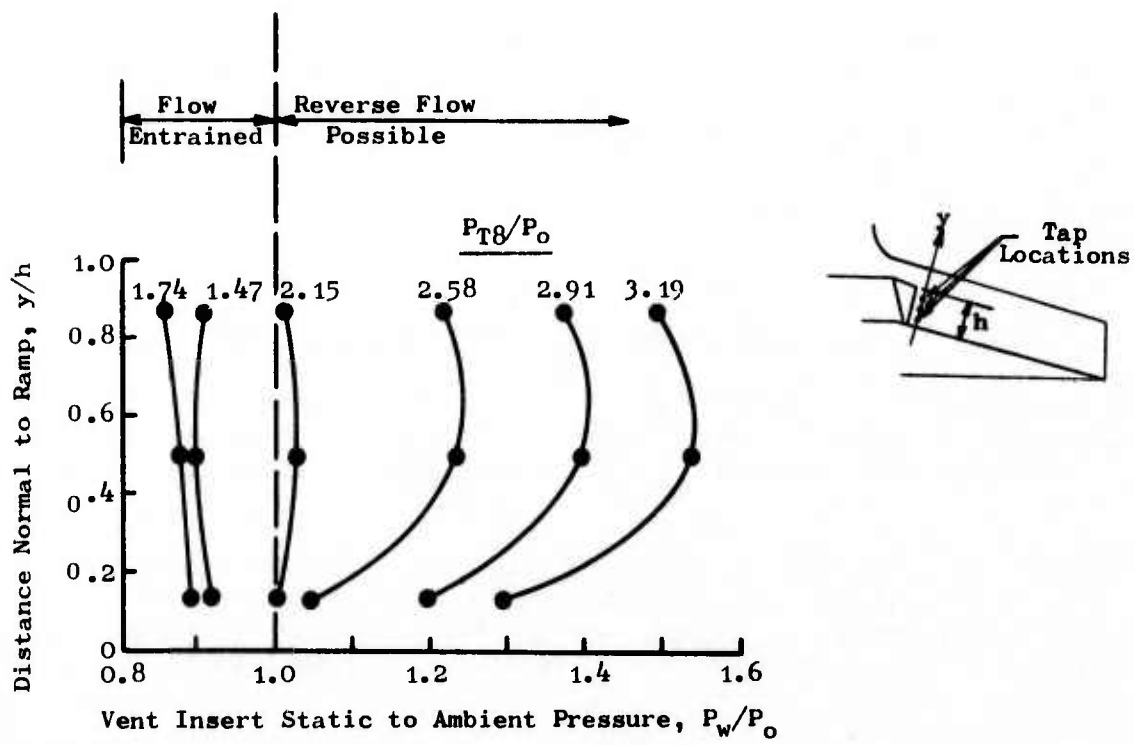
Figure 251. Vent Insert and Chute Base Pressure Distributions.

A peak PNL comparison between the suppressed 2-D nozzle with hardwall ejector and the suppressed 2-D nozzle with treated ejector is shown in Figure 252. The results indicate that ΔPNL's of 14 to 10 dB were achieved over most of the operating range (V_j's from 1300 to 2200 ft/sec).

The effect of the treatment on the ejector configurations with unsuppressed and suppressed 2-D nozzles is illustrated in Figure 253.

Laser Velocimeter Measurements on the Two-Dimensional Nozzle

In order to obtain an understanding of the exhaust plume velocity field for the two-dimensional, 12-chute, suppressor nozzle with hardwall ejector, a series of velocity measurements was taken with General Electric's laser velocimeter.

The resultant mean velocity profiles obtained for two test conditions: $P_{T8}/P_O = 2.2$, $T_T \sim 1565°$ R and $P_{T8}/P_O = 2.65$, $T_T \sim 1740°$ R, are shown in Figure 254. Also shown on the figure is a schematic drawing of the nozzle configuration. The ejector aspect ratio (width/height) is 1.73:1; the nozzle length-to-height ratio is 8:1.

Figure 254 shows the mean velocity profiles at axial locations $x/h_O =$ 0, 2, 5, and 8.5. At the exit plane of the ejector, the peak mean velocity is observed to have been reduced by several hundred feet per second from the ideal isentropic velocity. Additionally, a "ramping" effect is observed in the mean velocity trajectory after it leaves the exit. This may be the result of the Prandtl-Meyer expansion of the flow around the end of the ramp. For both of the cases shown, the flow profiles look fully developed at the x/h_O location of 8.5.

Aerodynamic Performance Tests

Aerodynamic testing of the two-dimensional, over-the-wing nozzles was conducted in the NASA-Lewis Research Center 8 × 6 foot wind tunnel. The asymmetric nozzles tested included:

● 2-D Baseline Nozzle (unsuppressed)

● 2-D Unsuppressed Nozzle with Sidewalls (shielded nozzle)

● 2-D Unsuppressed Ejector Nozzle

● 2-D Suppressed Nozzle (nonvented)

● 2-D Suppressed Nozzle With Slots (vented)

● 2-D Suppressed Ejector Nozzle (nonvented)

● 2-D Suppressed/Ejector Nozzle With Slots (vented)
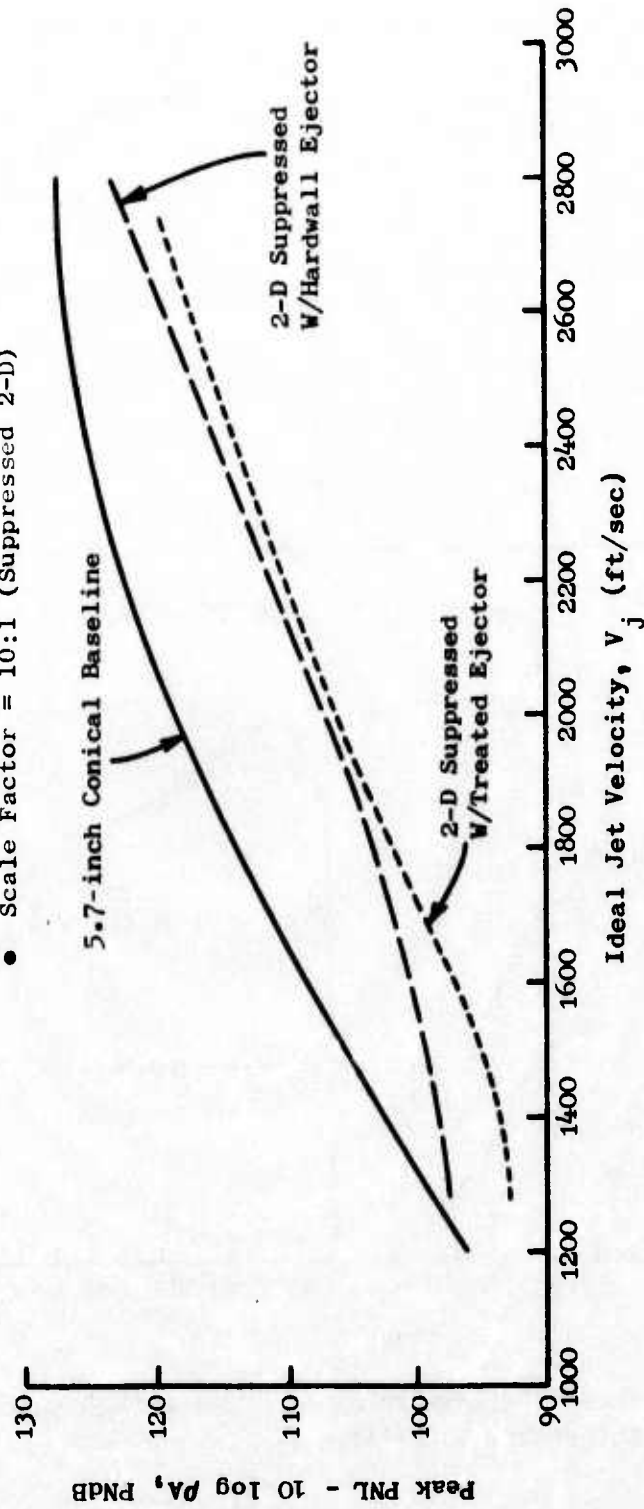
Figure 252. Effect of Treated Ejector with Suppressed Primary.

311
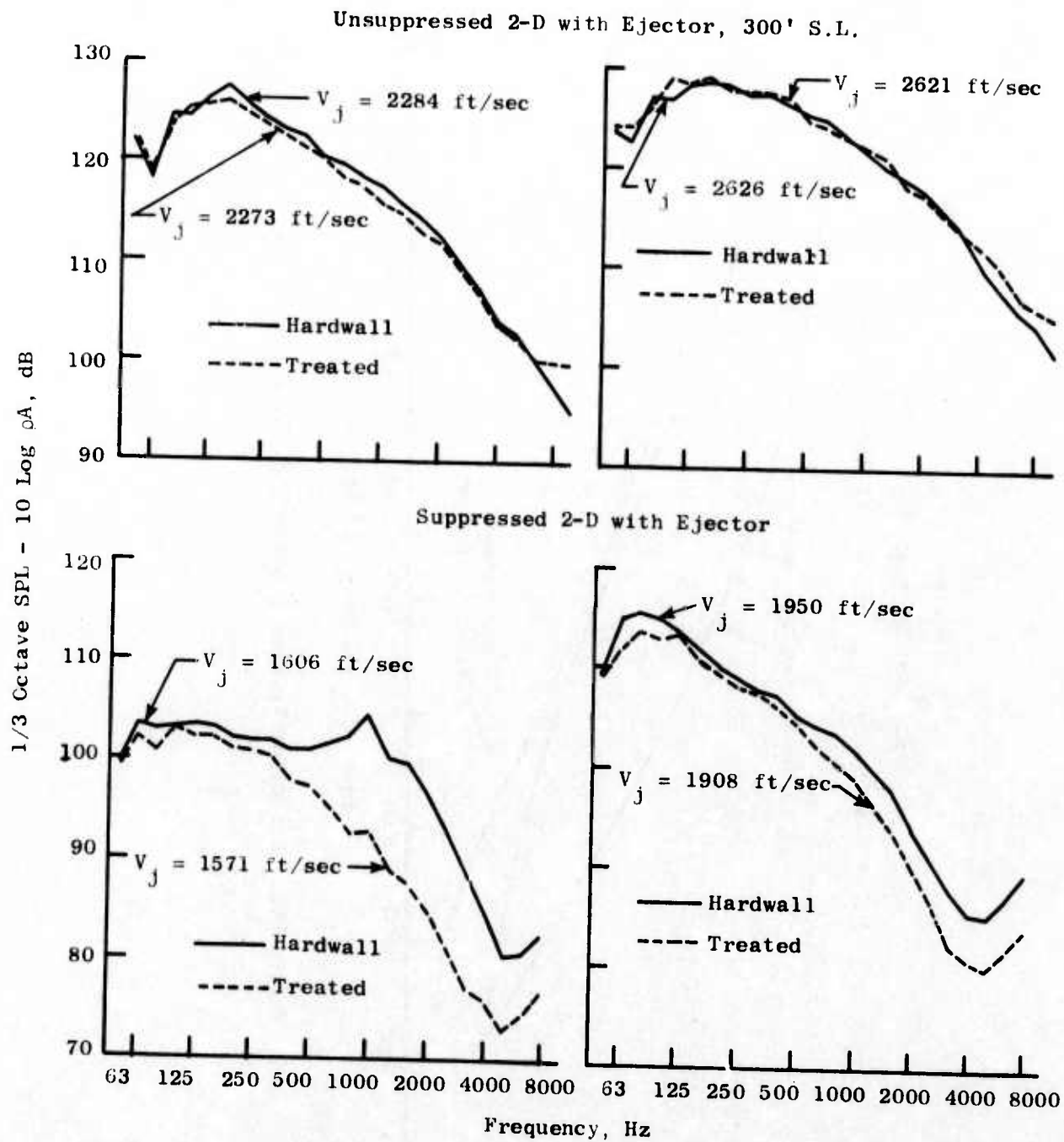
Figure 253. Effect of Treatment on Ejectors with Unsuppressed and Suppressed 2-D Primaries.

312
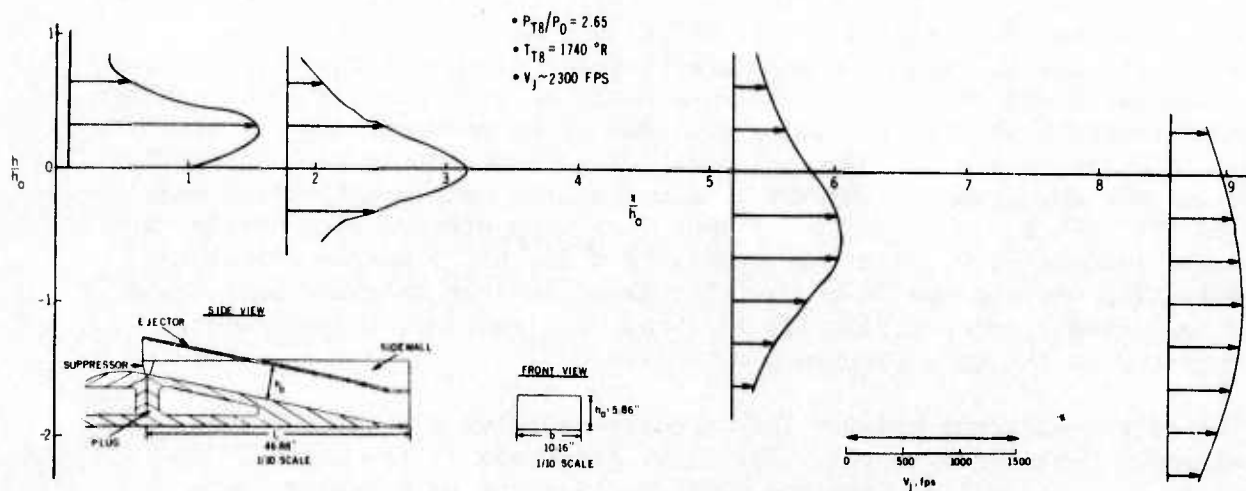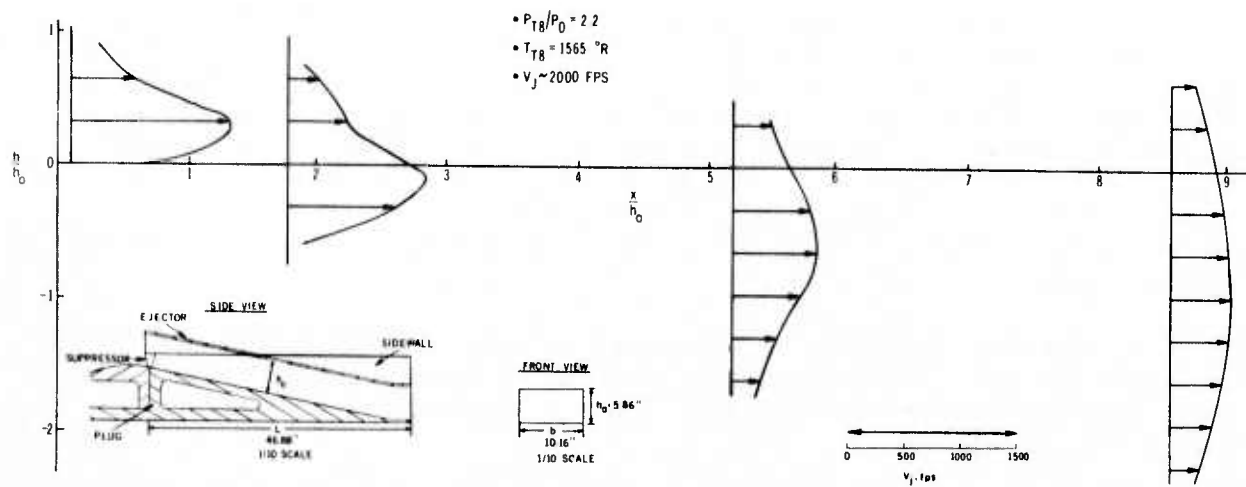
Figure 254. Mean Velocity Profiles of Suppressed 2-D Nozzle with Hardwall Ejectors.

313

In Figure 255 the basic, two-dimensional, unsuppressed plug nozzle is shown in the wind tunnel. The shielded nozzle is shown in Figure 256. In a further attempt to reduce the jet noise, the two acoustic suppression techniques of mixing and acoustic treatment were incorporated. This new model, the unsuppressed ejector nozzle, Figure 257, reduced the high velocity of the primary flow by mixing with it the low velocity entrained flow. The second suppressive technique, acoustic treatment of the internal surfaces, was not incorporated in the aerodynamic model since its only effect would be to increase the surface friction drag, which is a function of the porosity of the treatment faceplate.

The two-dimensional multichute suppressor nozzle was tested with and without downstream ventilation slots and is shown in Figure 258 with the slots open. The suppressed/ejector nozzle with the ventilation slots closed is presented in Figure 259.

Aerodynamic Performance Results and Analysis

Nozzle efficiencies of the unsuppressed plug nozzle, the shielded exhaust nozzle, and the unsuppressed ejector nozzle are presented as a function of nozzle pressure ratio in Figure 260. For static conditions, the unsuppressed ejector nozzle had the highest nozzle efficiency at pressure ratios less than 3.0. Statically, the peak nozzle efficiency of the aforementioned configuration was 0.979 at a nozzle pressure ratio of 2.5. The shielded exhaust nozzle exhibited a nozzle efficiency of 0.963 at an assumed take-off pressure ratio of 3.0 and at a Mach number of 0.36. This same nozzle with an ejector shroud was the unsuppressed ejector nozzle, and its nozzle efficiency was 0.958 at the assumed take-off conditions. The unsuppressed plug nozzle, at a pressure ratio of 3.0 and a Mach number of 0.36, had a nozzle efficiency of 0.961. The differences in nozzle efficiency for the shielded nozzle and the unsuppressed ejector nozzle are +0.2 and -0.3 percent, respectively, when compared to the unsuppressed plug nozzle.

The only difference between the unsuppressed plug and the shielded exhaust nozzles was side length. The level and shape of the nozzle efficiency curves for the above two nozzles, over the Mach number range investigated, were the same through a nozzle pressure ratio of 3.0. Between a nozzle pressure ratio of 3.0 and 3.5, the model with the longer sidewalls (the shielded exhaust nozzle) experienced a 1 to 1.6 percent greater nozzle efficiency loss than did the shorter sidewall model (the unsuppressed plug nozzle). However, the shielded exhaust nozzle recovered to a nozzle efficiency level equal to or greater than that of the unsuppressed plug nozzle at a nozzle pressure ratio of 4.0. Statically, the nozzle efficiency curve of the unsuppressed ejector nozzle had the same shape as the unsuppressed plug nozzle curve but a different level. With external flow the nozzle efficiency curve of the unsuppressed ejector nozzle was flat between a nozzle pressure ratio of 2.5 and 3.0 and increased from 3.0 to 4.0.

314
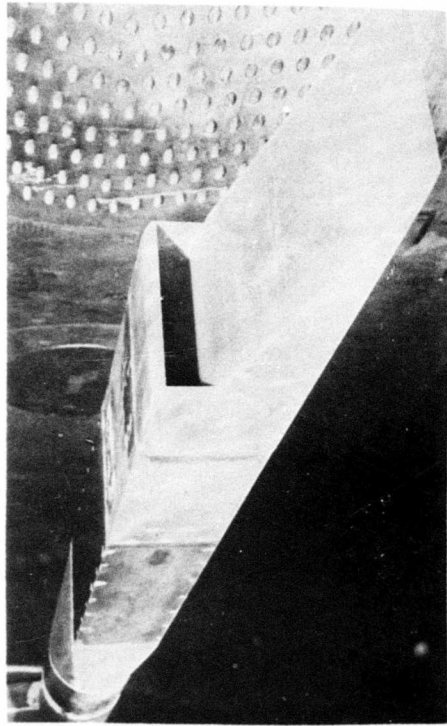
Figure 255. Wind Tunnel Setup of Unsuppressed 2-D Plug Nozzle.
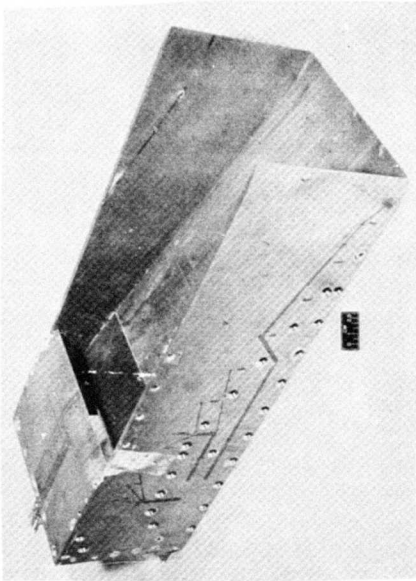
Figure 256. Unsuppressed 2-D Plug Nozzle Aerodynamic Model Hardware with Sidewalls.
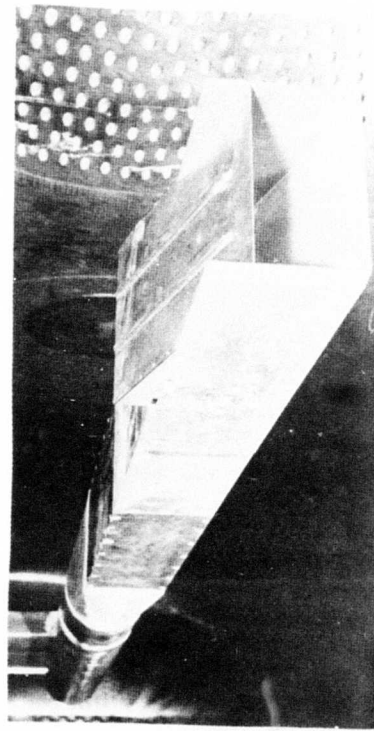
Figure 257. Unsuppressed 2-D Ejector Nozzle Wind Tunnel Configuration.

315
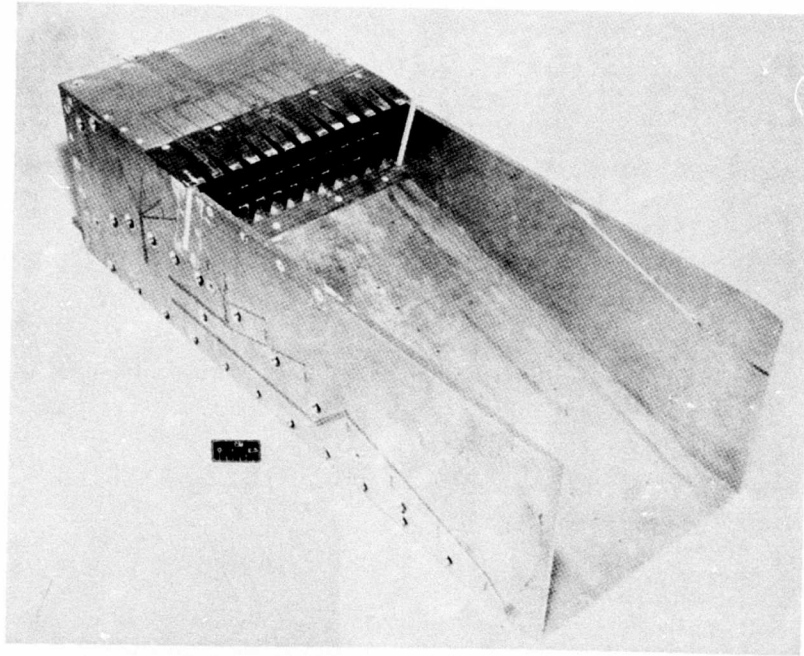
Figure 258. Suppressed 2-D Nozzle with Vented Sidewalls.
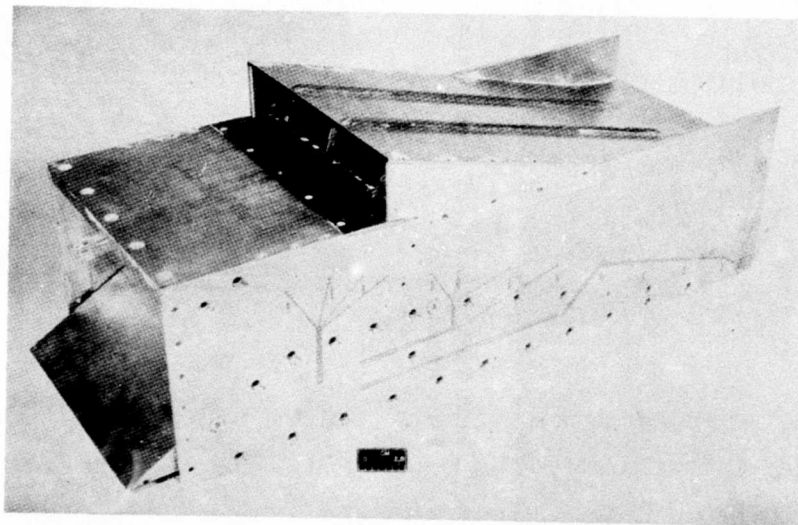
Figure 259. Suppressed 2-D Nozzle/Ejector Aerodynamic Model
Hardware.
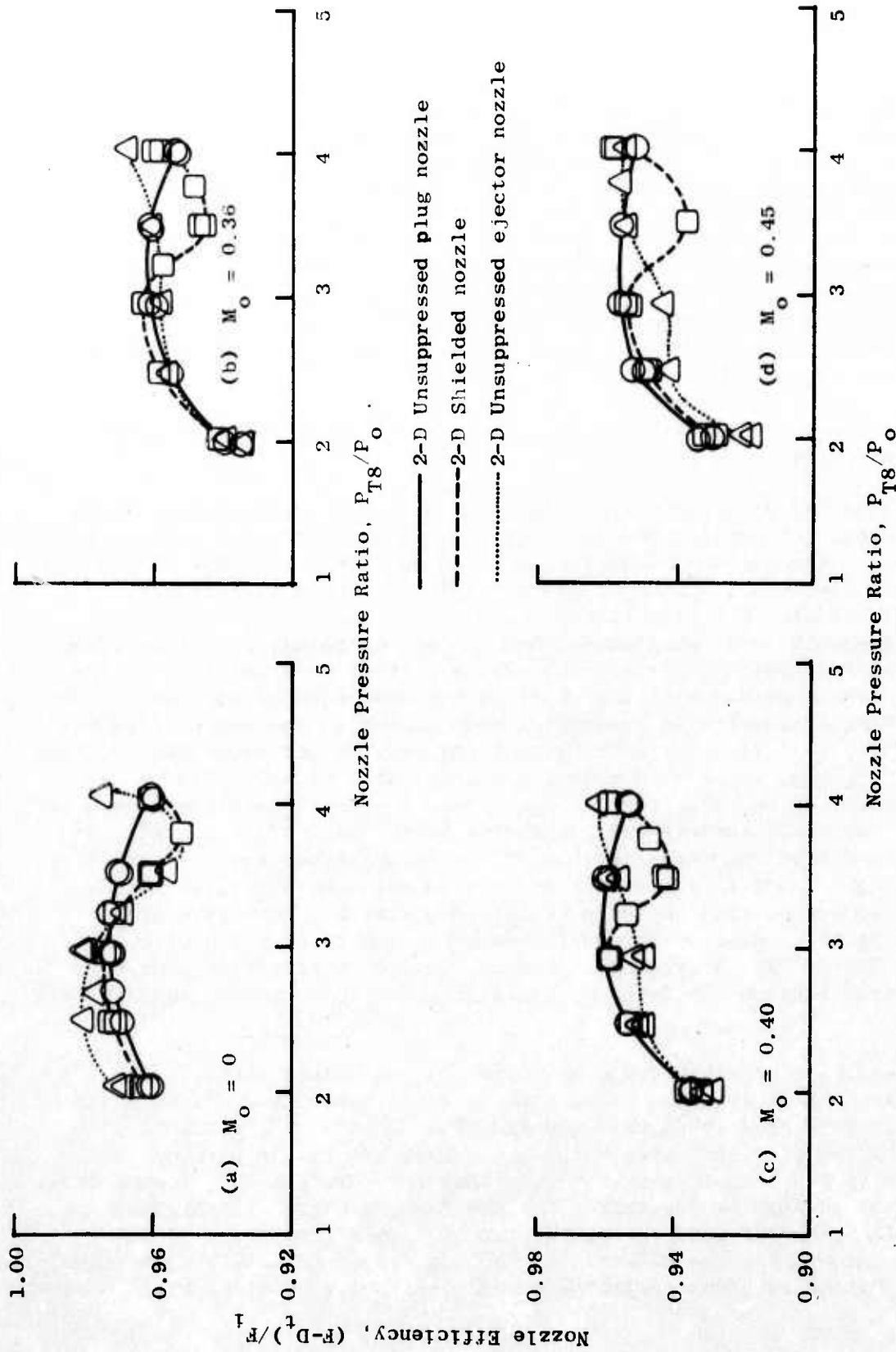
Figure 260. Unsuppressed 2-D Nozzle Performance Comparisons.

317

Nozzle efficiencies of the suppressor nozzle, with and without an ejector shroud and sidewall vent slots, are presented with the efficiency of the unsuppressed plug nozzle as a function of nozzle pressure ratio in Figure 261. For the Mach number range tested, the efficiency curves of the four suppressed configurations were monotonically increasing with nozzle pressure ratio. Over the Mach number and nozzle pressure ranges investigated, the suppressor nozzle had the highest nozzle efficiency of the acoustic suppressor configurations. At the assumed take-off conditions, the suppressor nozzle without an ejector shroud and sidewall vents had a nozzle efficiency of 0.809. Opening the sidewall vent slots under these same conditions caused a reduction in efficiency to 0.805. The efficiencies of the suppressor/ejector nozzle, with and without sidewall vents and at the assumed take-off conditions, were 0.788 and 0.792, respectively. The decrements in nozzle efficiency for the suppressor nozzle with and without sidewall slots are 0.152 and 0.156, respectively, when compared with an unsuppressed plug nozzle. The nozzle efficiency decrements for the suppressor/ejector nozzle with and without sidewall slots are 0.173 and 0.169, respectively.

The integrated plug pressure forces for the unsuppressed plug nozzle, the shielded exhaust nozzle, and the unsuppressed ejector nozzle are presented in Figure 262. The pressure integration extended from the throat to the end of the plug. The resulting thrust component is presented as a fraction of nozzle ideal thrust. The plug thrust component of the unsuppressed plug nozzle was insensitive to Mach number and was approximately 2 percent from a nozzle pressure ratio of 3.0 to 4.0. The effect of external flow on the plug thrust component for both the shielded and unsuppressed ejector nozzles was a reduction in level with increasing Mach number in the nozzle pressure region from 2.5 to 3.75. For both nozzles the plug thrust component recovered to a relatively high level at a nozzle pressure ratio of 4.0. The nozzle thrust component of the plug for the unsuppressed ejector nozzle was negative, a drag, for each Mach number/nozzle pressure ratio combination tested. It can be inferred from the inconsistency of the unsuppressed ejector nozzle having the highest nozzle efficiency and the lowest plug pressures that a favorable interaction with the ejector shroud occurred. This interaction resulted in positive ejector shroud forces being generated which offset the plug drag. Statically the plug of the unsuppressed ejector nozzle experienced a step-function increase in force at a nozzle pressure ratio of approximately 2.55.

The chute-base pressure drag, as a fraction of nozzle ideal thrust, for the suppressor nozzle with and without the ejector shroud and the sidewall vent slots is presented in Figures 263 and 264. This nozzle thrust loss was a strong function of nozzle pressure ratio. Over the nozzle pressure ratio range of 2.0 to 4.0, the thrust loss resulting from chute-base pressure drag was reduced by as much as two-thirds for the four suppressor configurations. At the assumed take-off conditions, the thrust losses for the suppressor nozzle with and without the sidewall slots are 0.139 and 0.141, respectively. In the case of the suppressor/ejector nozzle with and without sidewall vents

318

Figure 261. Comparison of Performance for the 2-D Unsuppressed Plug Nozzle and the 12-Chute Suppressor Nozzle Configurations.

319

○ Unsuppressed Plug Nozzle

□ Suppressed Nozzle With Sidewalls

△ Suppressed Nozzle With Slotted Sidewalls

◇ Suppressed/Ejector Nozzle

⬠ Suppressed/Ejector Nozzle With Slotted Sidewalls
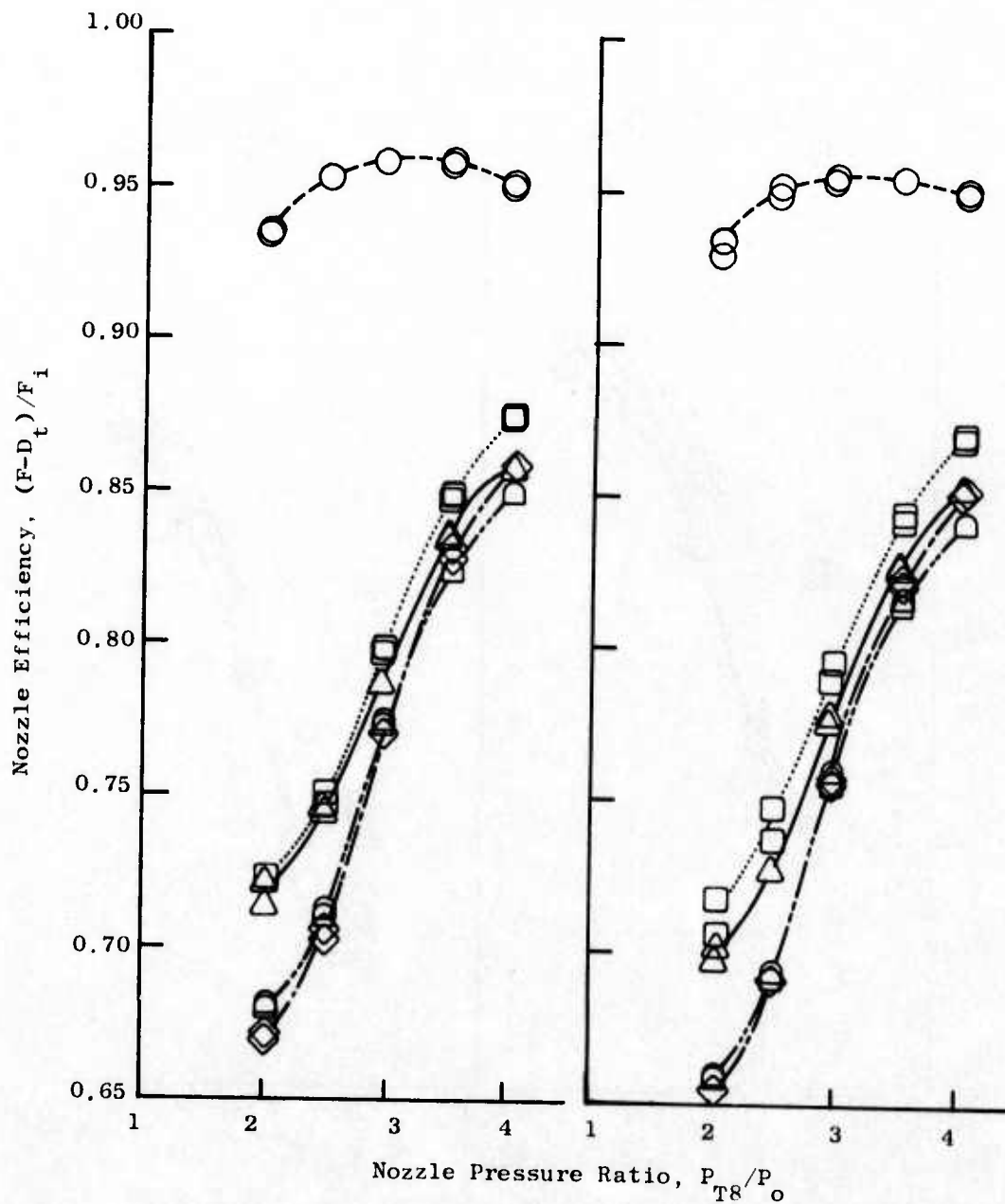
(c)   Free-Stream Mach No., 0.40 (d)   Free-Stream Mach No., 0.45

Figure 261.   Comparison of Performance for the 2-D Unsuppressed
Plug Nozzle and the 12-Chute Suppressor Nozzle
Configurations (Concluded).

320
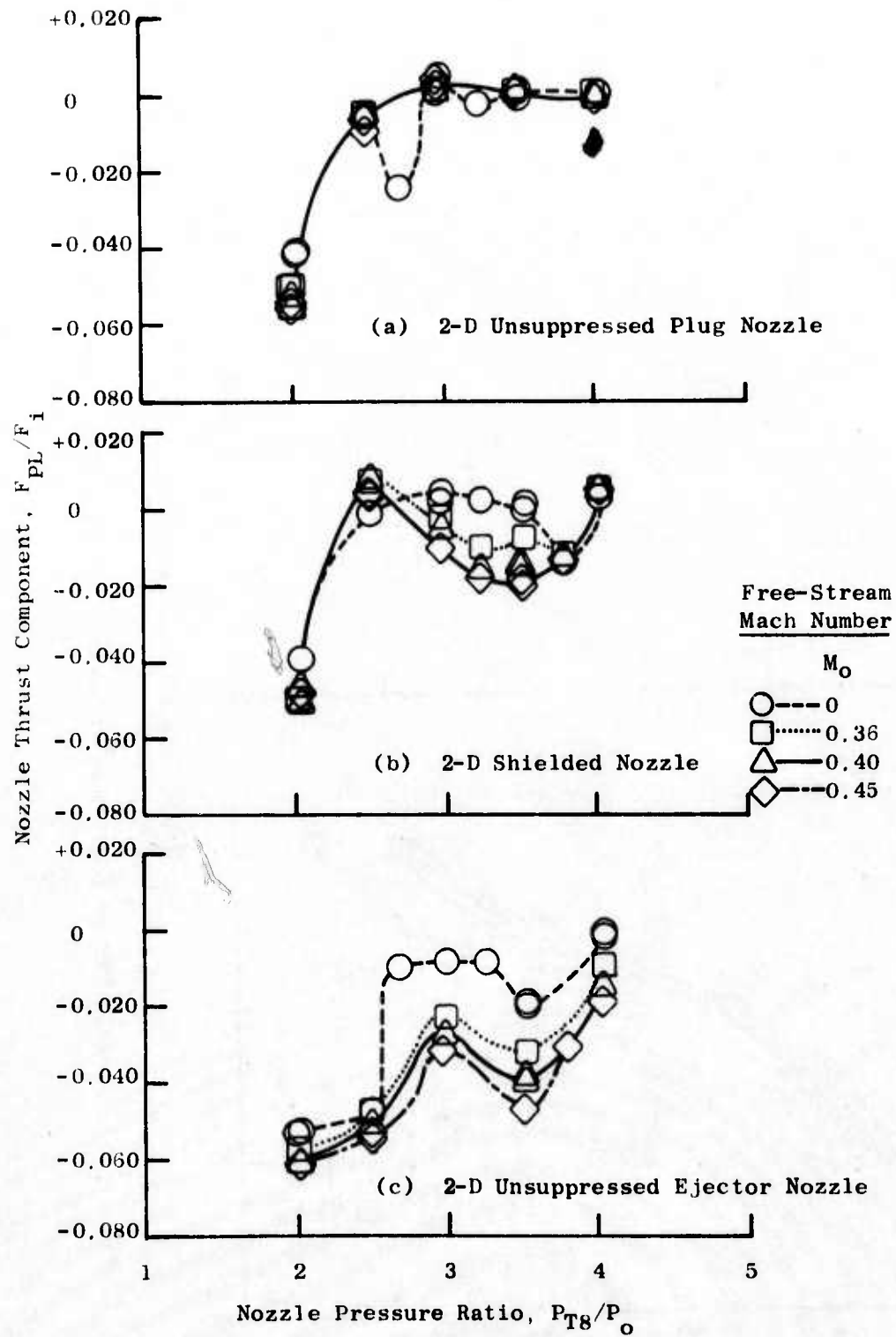
Figure 262. Unsuppressed 2-D Nozzle Thrust Components from the Integrated Plug Pressures.

321
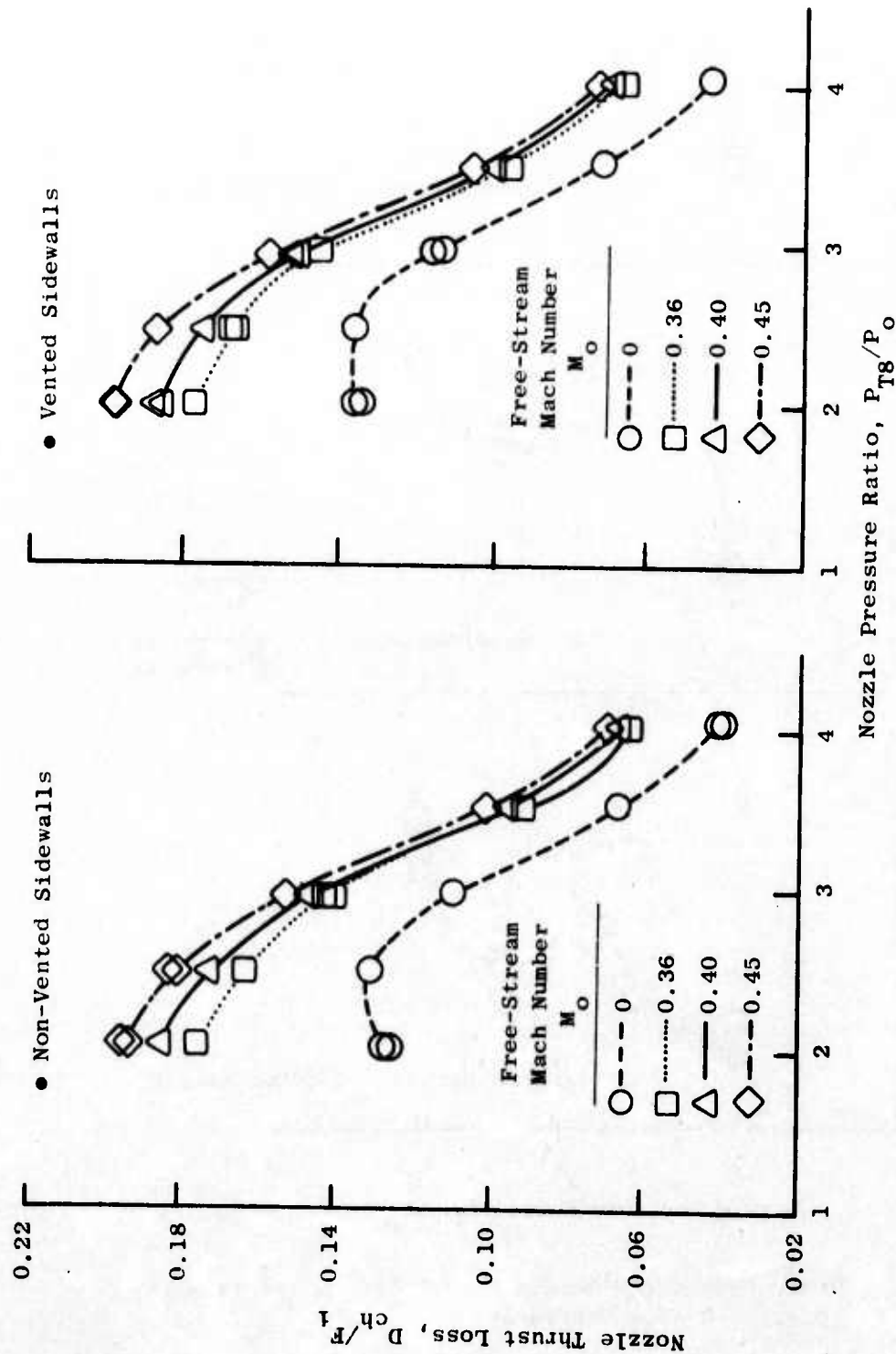
Figure 263. Nozzle Thrust Loss from Chute-Base Pressure Drag, 2-D Nozzles.

322
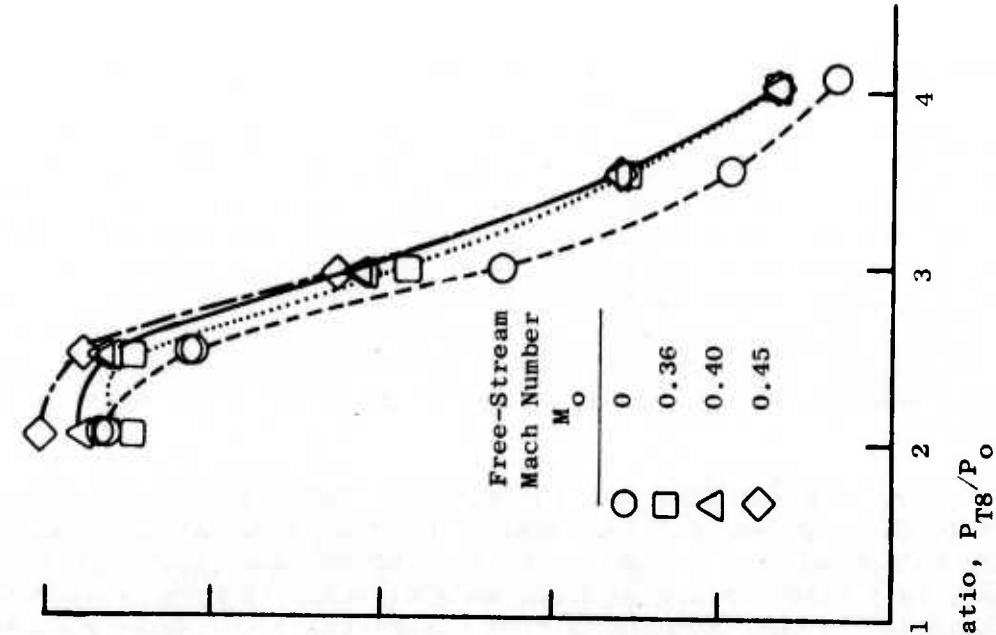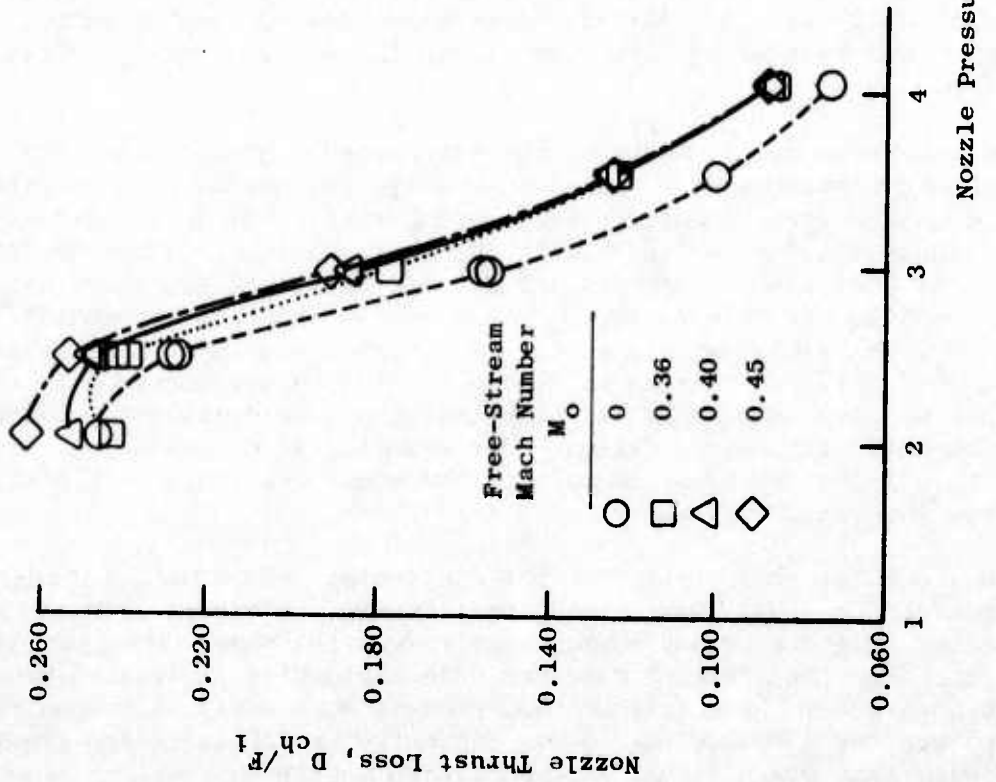
Figure 264. Nozzle Thrust Loss from Chute-Base Pressure Drag, 2-D/Ejector Nozzles.

323

(Figure 264), the nozzle thrust losses at the same conditions are 0.174 and 0.172, respectively. The variation with Mach number in chute-base-related, thrust losses for the four multichute configurations was greater at the lower nozzle pressure ratios than at the higher.

In Figure 265 the effect of external flow on nozzle efficiency at a pressure ratio of three is presented. The unsuppressed plug and shielded exhaust nozzles have approximately the same nozzle efficiency with external flow. Both of the aforementioned nozzles experienced a thrust loss of 0.6 percent over the Mach number range 0.36 to 0.45. The unsuppressed ejector nozzle had lower nozzle efficiency than either of the preceding two configurations; and, the nozzle efficiency loss over the above Mach number range was 0.014. Over the Mach number range investigated, 0.36 to 0.45, the nozzle efficiency losses for the suppressor nozzle with and without sidewall vents were 0.013 and 0.025, respectively. The nozzle efficiency losses for the suppressor/ejector nozzle with and without sidewall vent slots over the same Mach number range were 0.024 and 0.027, respectively.

The entrained ejector flow rate was measured for the unsuppressed ejector nozzle with P_T-rake instrumentation mounted in the ejector inlet region. The entrained flow parameter, a ratio of the entrained flow to the primary flow, is presented in Figure 266 as a function of primary nozzle pressure ratio at the Mach numbers tested. Statically, the entrained flow rate was approximately 11.5 percent of the primary flow in the nozzle pressure ratio range from 3.0 to 4.0. At the assumed take-off conditions, the entrained flow ratio was 23.2 percent. At each Mach number tested, the entrained flow parameter was reduced by over one-half in the nozzle pressure ratio range from 2.0 to 4.0.

Nozzle discharge coefficients of the unsuppressed plug nozzle, the shielded exhaust nozzle, and the unsuppressed ejector nozzle are presented in Figure 267a as a function of nozzle pressure ratio. Since the throat geometry of these methods was physically the same, their discharge coefficients were considered equivalent. The discharge coefficients of the above nozzles were plotted not as discrete points but as a band. This band represents the upper and lower limits within which all the data for these nozzles fell. The largest spread for these data was 1.0 percent at a nozzle pressure ratio of 3.0. This scatter would only slightly affect nozzle performance because of the thrust measuring system design. For example, at a nozzle pressure ratio of 3.0, a 1-percent error in weight flow would result in only a 0.3-percent error in nozzle efficiency.

Nozzle discharge coefficients of the suppressor nozzle with and without ejector shroud and sidewall vent slots are presented in Figure 267b. The throat geometry of the four suppressor nozzles was the same; consequently, the model discharge coefficients were equivalent and were plotted as bands. The largest spread for these data was 2.0 percent at a nozzle pressure ratio of 3.5. The greater data scatter in the discharge coefficients for the multichute configurations was a result of the flexure in the chutes.
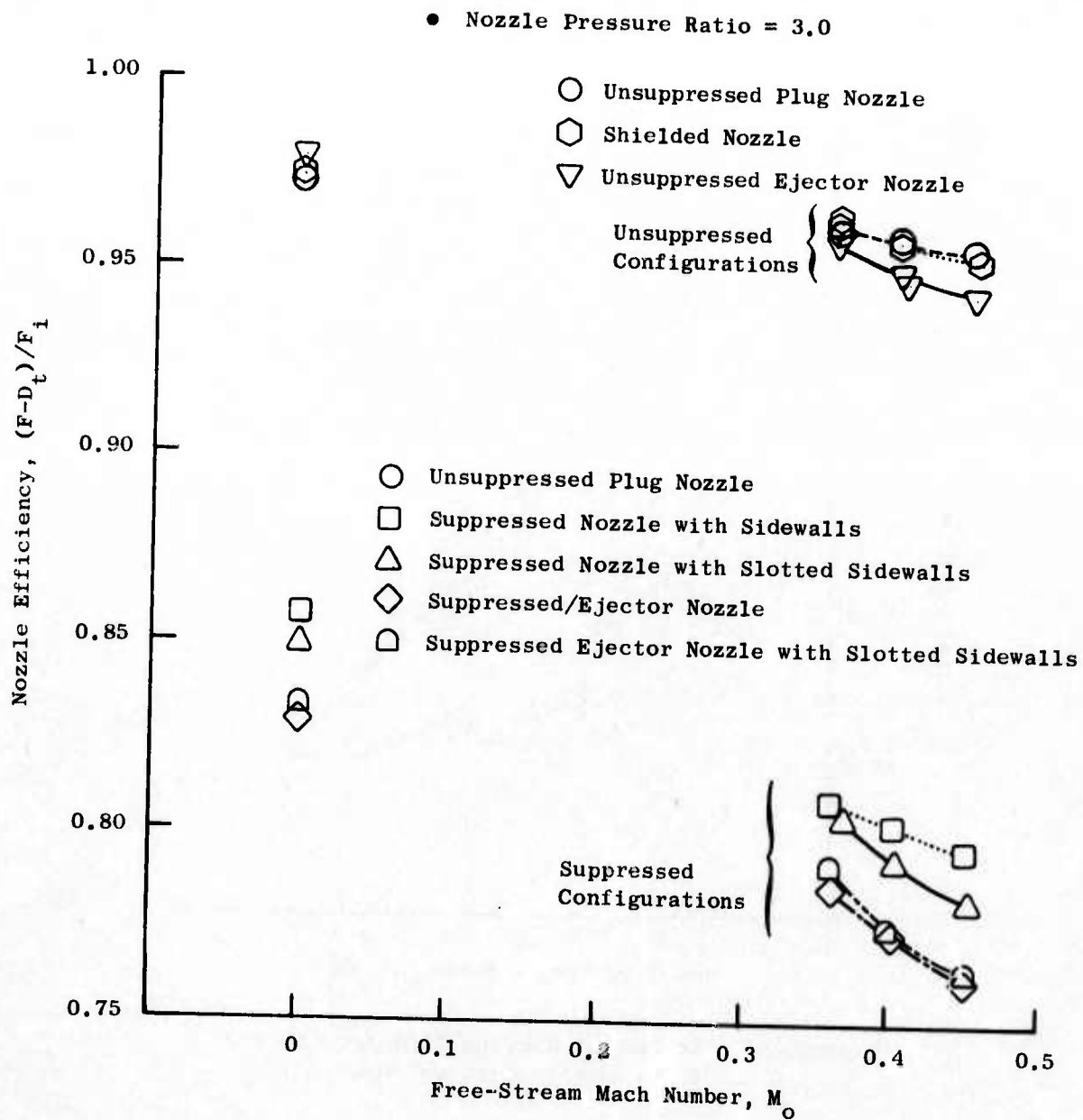
Figure 265. External Flow Effects on 2-D Unsuppressed and Suppressed Nozzle Performance.

325
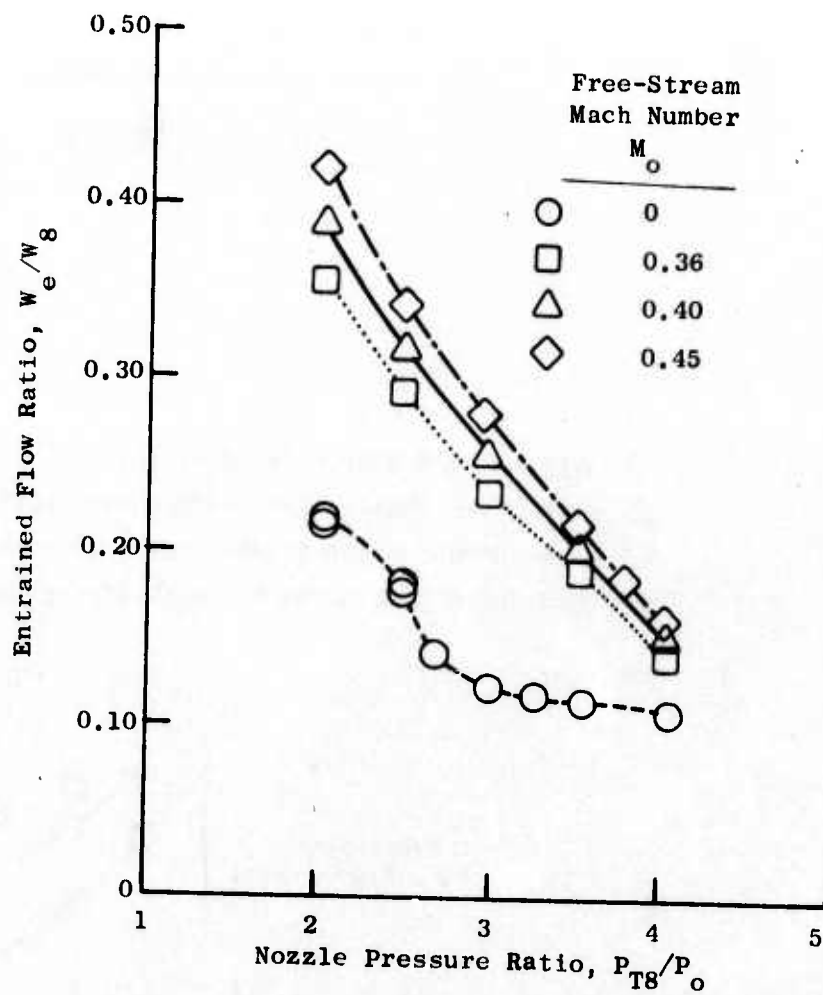
Figure 266. Entrained Ejector Flow for the 2-D
Unsuppressed Ejector Nozzle.
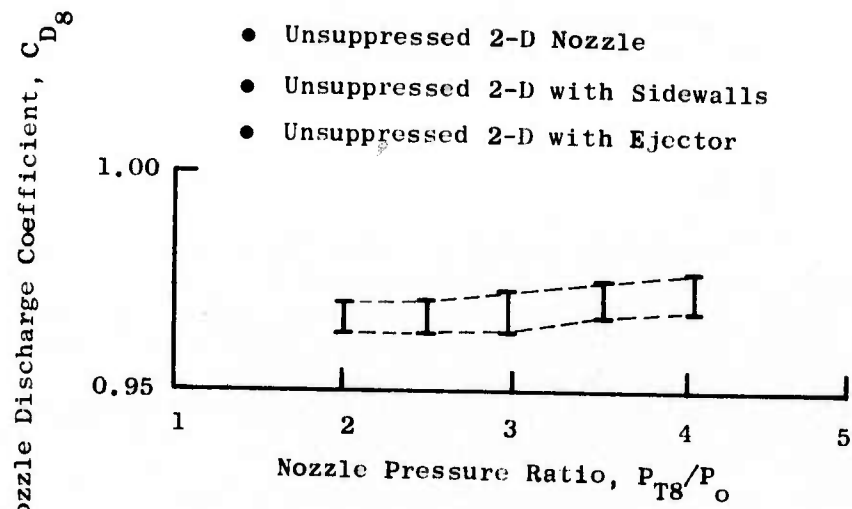
(a) Unsuppressed 2-D Nozzle Configuration
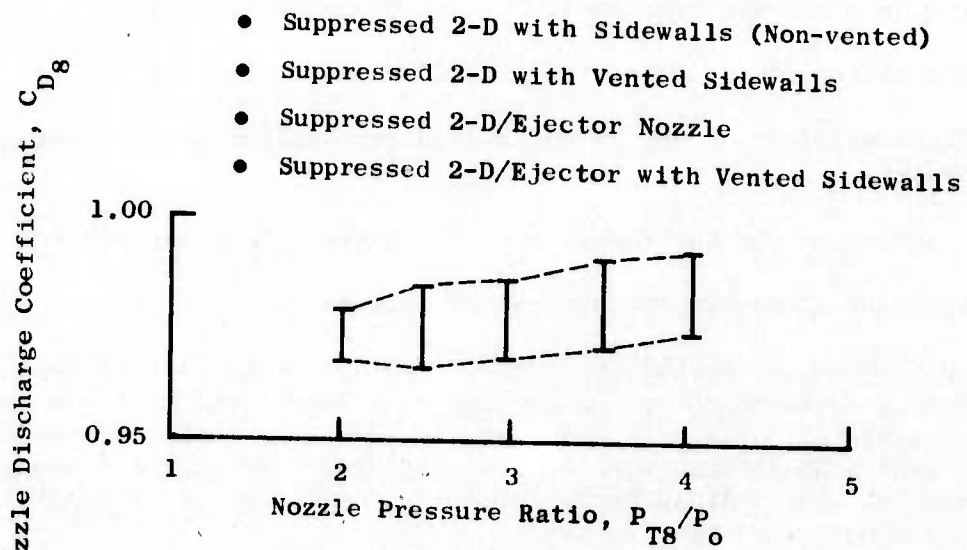
(b) Suppressed 2-D Nozzle Configuration

Figure 267. Effect of Nozzle Pressure Ratio on 2-D Nozzle Discharge Coefficient for the Freestream Mach Number Range of 0 - 0.45.

327

The chute-base pressure profiles for $M_O = 0$ and 0.36 are presented at pertinent nozzle pressure ratios in Figures 268 through 271 for the suppressed configurations tested and indicate the entrainment characteristics of the nozzle configurations.

System Evaluation

The asymmetric 2-D suppressed nozzle systems tested in this program gave relatively good suppression but at the expense of aerodynamic performance as shown in Figure 272. The complexities of the system are such that it is highly configuration-oriented, requiring considerably more effort than that envisioned in the original scope of this program. This investigation should provide the background for further work on these systems to be conducted in any new program ventures.

3.3 FINAL CONFIGURATION SELECTION

3.3.1 Selection Criteria

The selection of the final suppressor configuration to be tested in both model and engine scale was made based on the following criteria:

- Identification of type of engine flow system (engine cycle)

- Considerations of system mechanical feasibility with aeroacoustic trades

- A review of the suppressor systems tested during the program

- Application to current technology systems

The types of engine cycles considered for application during the latter stages of this program consisted of low bypass turbofan and turbojet cycles which were essentially single-flow systems. These engine cycles were attractive from a system viewpoint, more so than the dual-flow cycles (nonaugmented fan stream) which have a disadvantage of large thrust loss on a suppressed core due to the poor base ventilation.

Another consideration which weighed quite heavily in selecting the final suppressor configuration was the mechanical applicability and feasibility of the system design. The asymmetric over-the-wing nozzle systems had demonstrated attractive suppression levels with reasonable aerodynamic performance trades (unsuppressed), but the mechanical complexities of the system (aircraft installation, etc.) required refinements which were beyond the scope of the program. Application of such a suppressor system without benefit of the detailed aircraft/engine mechanical design effort might seriously jeopardize the overall results of the system.
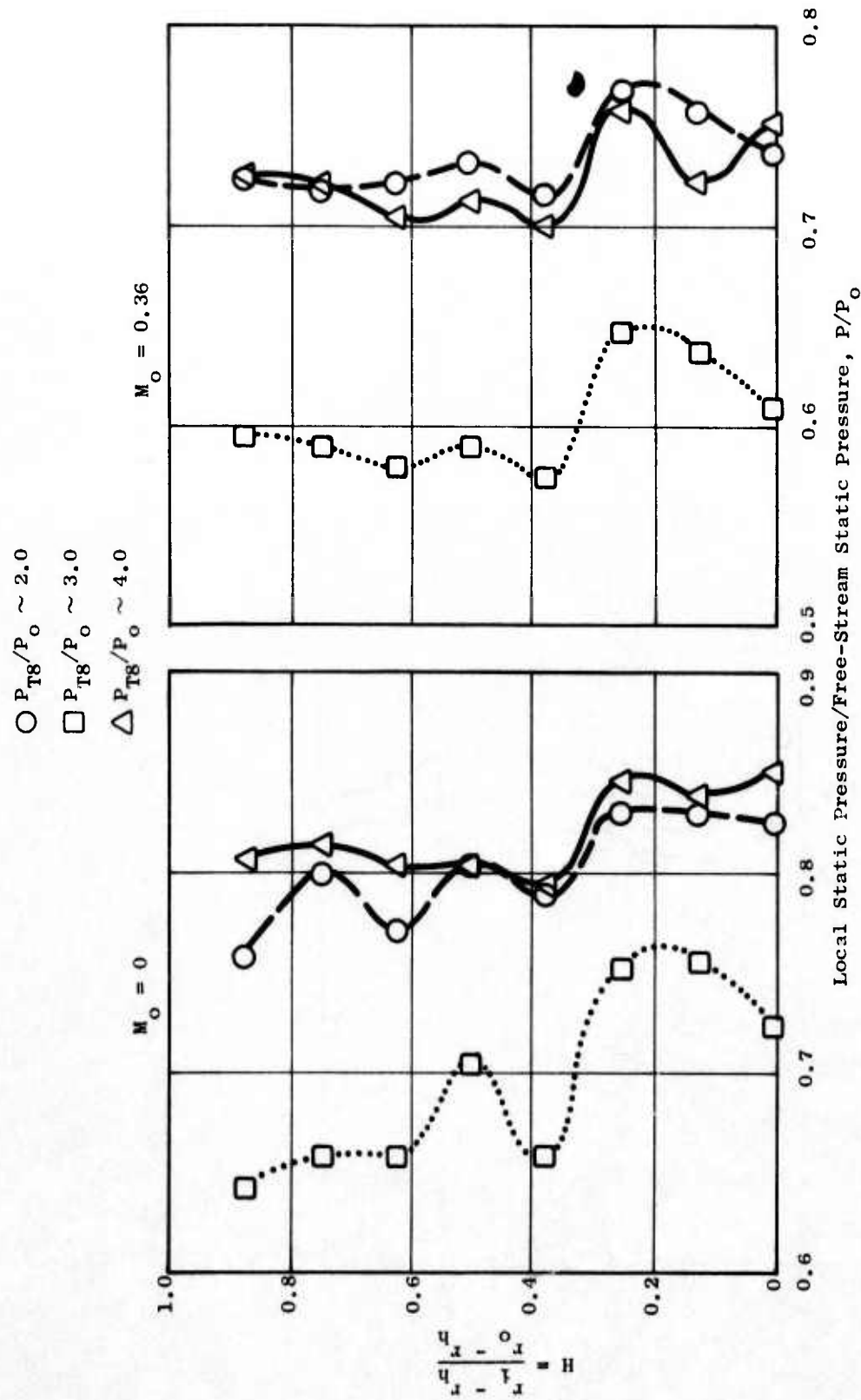
Figure 268. Chute Base Pressure Profiles of 2-D Suppressor with Sidewall Slots.

329
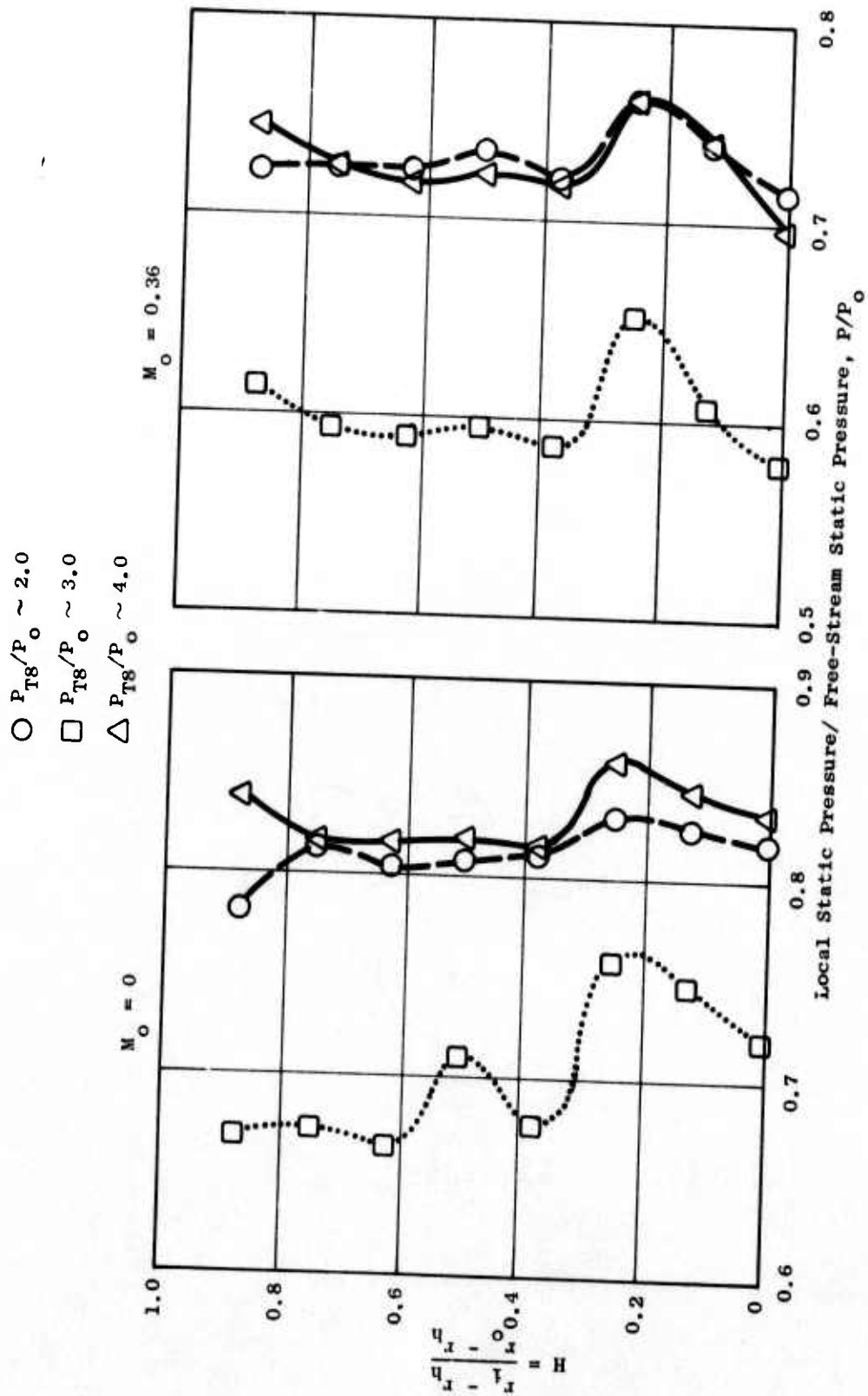
Figure 269. Chute Base Pressure Profiles of 2-D Suppressor without Sidewall Slots.
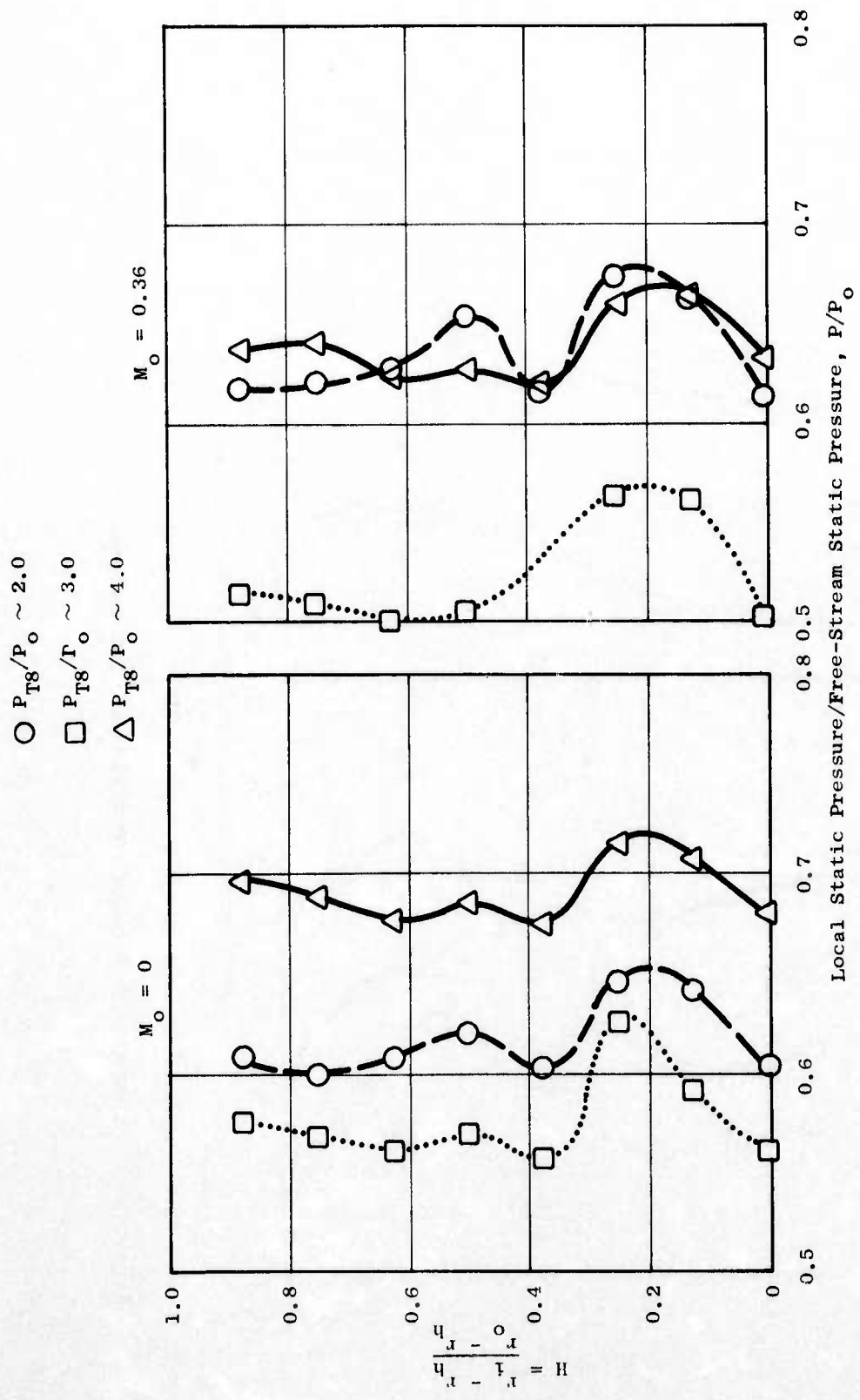
Figure 270. Chute Base Pressure Profiles of 2-D Suppressor-Ejector with Sidewall Slots.

331
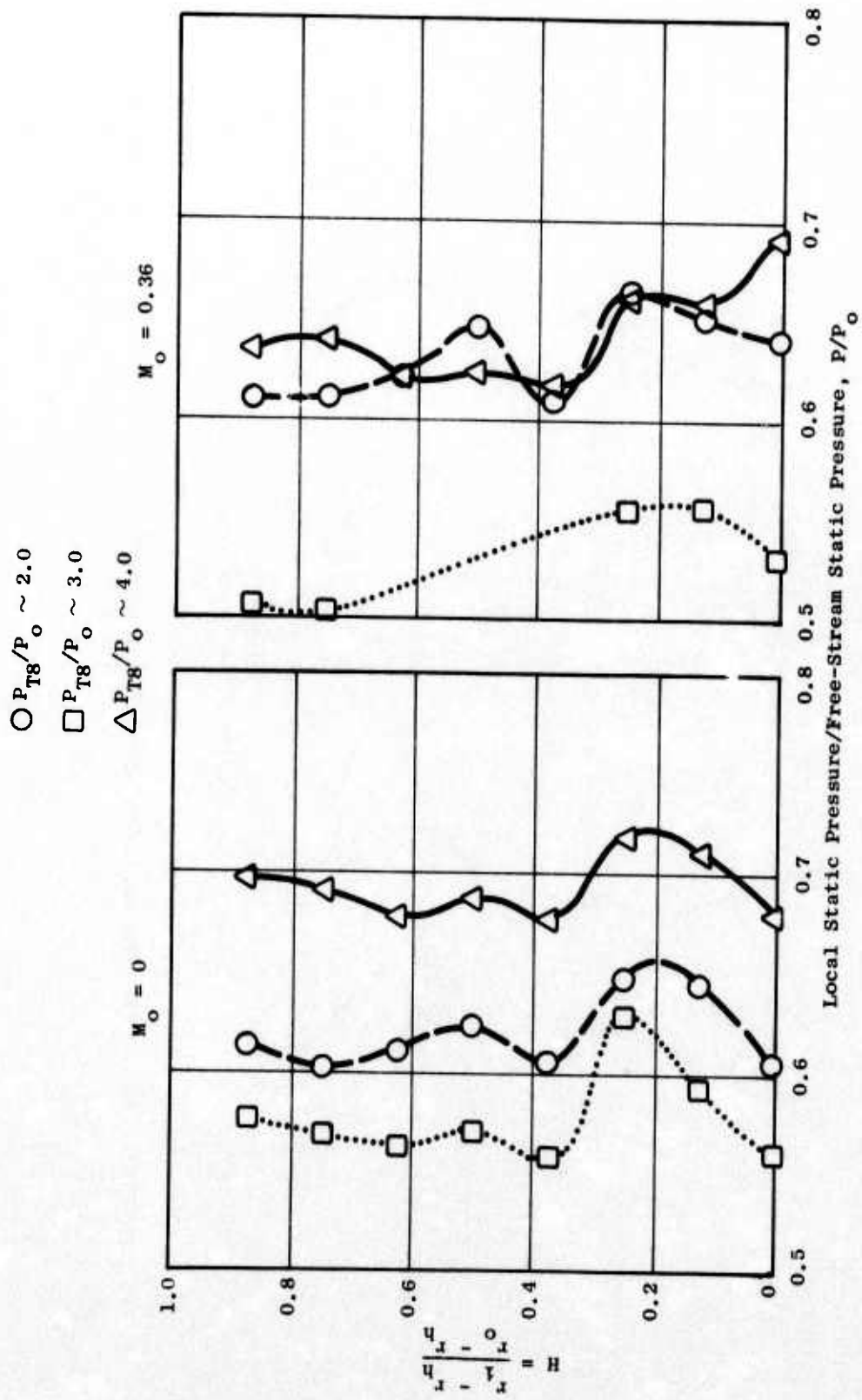
Figure 271. Chute Base Pressure Profiles of 2-D Suppressor-Ejector without Sidewall Slots.

332
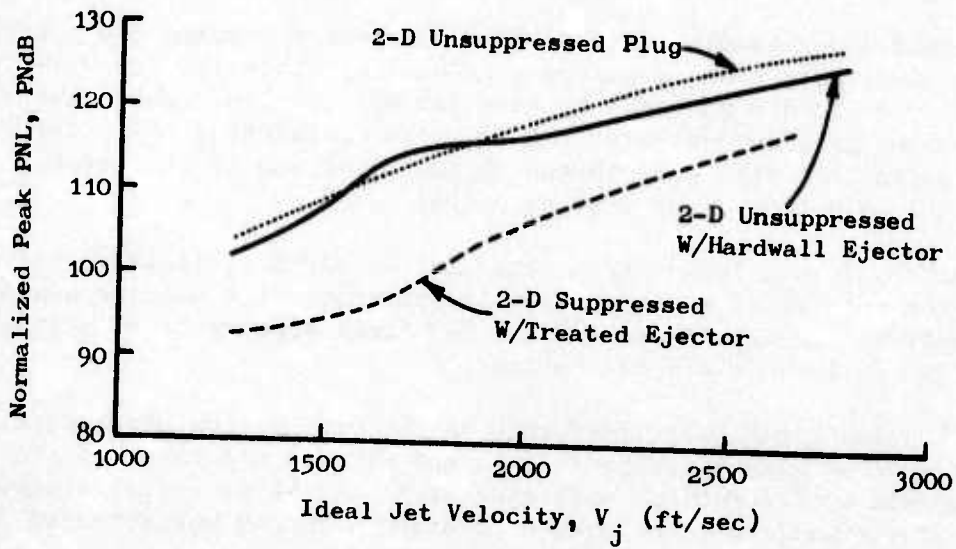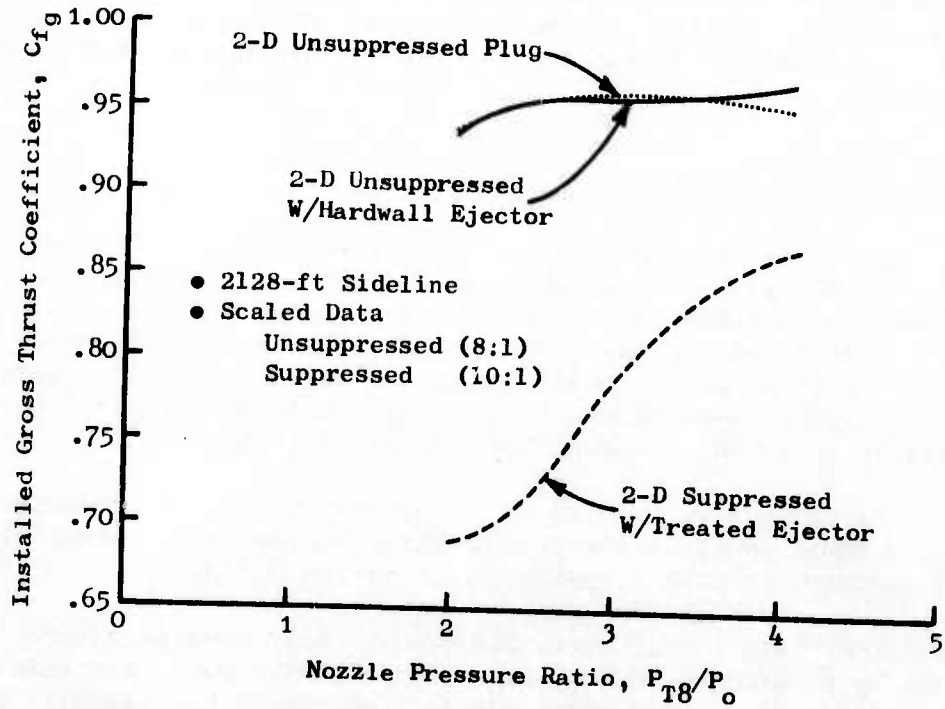
Figure 272. 2-D Nozzle System Aeroacoustic Evaluation.

The review of the individual suppressor systems included the comparison of the acoustic PNL suppression, rudimentary ΔEPNL estimates as well as an evaluation of the mechanical design implementation, and application to current technology systems.

3.3.2 Overall Review of Model Series Results

The multichute/annular plug nozzle systems were identified as having the most potential for viable system application. Results of individual nozzle tests showed that the multichute/annular plug system was capable of high suppression (40-chute) and also high aerodynamic performance (36-chute). The system selected for final engine/model demonstration was to exhibit good acoustic and aerodynamic performance which blended well with several mechanical schemes applicable to advanced technology engines (see Section 3.2.2).

The multitube suppressor systems on annular plugs were not selected on the basis of the added complexities of the multitubes and the aeroacoustic limitations inherent with such a system (see Section 3.2.3).

The suppressed 2-D primary nozzle and acoustically treated ejector system offered attractive suppression gains but aerodynamically poor performance (due to the inability to sufficiently ventilate the suppressor base area). The extensive aircraft engine mechanical systems integration effort required, however, was the main contributor in the rejection of such a system for the final suppressor configuration (see Section 3.2.4).

The present understanding of dual-flow suppressor systems did not lend itself to an acceptable final suppressor selection, since the nonaugmented fan dual-flow fixed cycle did not show promise for application. The relatively minor suppression gain demonstrated and the poor ventilating characteristics of the suppressed core also contributed to the rejection of this system for the final model selection (see Section 3.2.4).

A comparison of simulated ΔEPNL (calculated) and ΔC_{f_g} (tested) values obtained on the suppressor systems investigated under this program was conducted to evaluate the best trade-off for the final suppressor selection and, ultimately, the full-scale J79 engine test.

The EPNL calculations were performed on the single-flow systems (i.e., multielement/annular plug suppressors with and without ejectors and the asymmetric 2-D nozzle configurations with ejectors) and the dual-flow systems (i.e., dual-flow exhaust nozzles with suppressed core and unsuppressed fan flows).

The EPNL calculations were based on PNL values determined from acoustic data obtained at an ideal jet velocity of 2500 ft/sec (2300 ft/sec for the 2-D nozzles) from the static, hot-jet tests. A level flyover at an altitude of 2128 feet and an aircraft velocity of 422 ft/sec was assumed. No adjustments

334

for relative velocity (V_R) effects on PNL suppression were assumed due to the complexity of the problem and the current lack of generalized procedures for suppressed exhaust systems.

Table 10 lists the results of the ΔEPNL and ΔC_{f_g} comparisons for the suppressor systems tested. The acoustic baseline reference for the multielement annular suppressors and the dual-flow nozzles is an unsuppressed conical nozzle. The reference nozzle for the asymmetric configurations is the unsuppressed 2-D nozzle. The ΔC_{f_g} values listed are for old flow static and wind tunnel performance with the single-flow systems. The ΔC_{f_g} for the dual-flow systems was based on cold flow base pressure measurements on the suppressed core nozzle.

The selection of the single flow, multielement/annular plug suppressor system for the final model and engine suppressor test was based on the best overall compromise between aeroacoustic performance and mechanical feasibility for a viable suppressor system.

3.3.3 Final Configuration Selection

The final suppressor configuration selection for the J79 engine test at Edwards Flight Test Center and the JENOTS scale model test was a multielement annular plug suppressor system with treated ejector. The annular suppressor system appears to give the best trade-offs mechanically, aerodynamically, and acoustically and shows the most potential for a viable engine system. The addition of the treated ejector was thought to give greater overall suppression to the system.

A review of multichute suppressors was conducted to evaluate and compare favorable (acoustic) characteristics while identifying the unfavorable ones, in order to specify the final suppressor design. The annular plug suppressors in this comparison included the 36- and 40-chute suppressors tested under Task I of the DOT Phase II program, and the 32-chute, area ratio of 2.0 suppressor, tested under Phase I.

A summary of the aeroacoustic test results is found in Figure 273. The details of the data analysis are described in Section 3.2.2.

Figure 274 illustrates the acoustic effectiveness of the three multichute suppressors tested on a spectral basis. The SPL spectra are presented on a 320-foot arc at 140° from the jet inlet. The data are full-scale. The results show that the 40-chute nozzle maintains a double-hump characteristic with primarily the high frequencies dominating the spectra at the 2300 ft/sec ideal jet velocity. The 36-chute nozzle has a more pronounced low-frequency-dominated spectral shape at this velocity, similar to the conical nozzle. The 32-chute nozzle spectra fall between those of the 40- and 36-chute nozzles. These results indicate that the 36-chute primary flow elements merged sooner, and at a higher velocity, than either the 32- or 40-chute elements and was further substantiated by the laser velocimeter tests. The 40-chute aerodynamic performance from previous testing was undesirable from a systems viewpoint, while

335

Table 10. Summary of Estimated EPNL and C_{f_g} Tradeoffs.

1. Single-Flow Systems	$V_j = 2500$ ft/sec $P_{T8}/P_o = 3.0$ EPNL	ΔEPNL	$M_O = 0.0$ $P_{T8}/P_o = 3.0$ C_{f_g}	ΔC_{f_g}	$M_O = 0.36$ $P_{T8}/P_o = 3.0$ C_{f_g}	ΔC_{f_g}
● Acoustic Baseline Conical Nozzle	122.3	---	0.994	---		---
● Unsuppressed 2-D Nozzle	118.8	---	0.972	---	0.961	---
● Aero Performance Baseline Unsuppressed Plug Nozzle	---	---	0.978	---	0.981	---
● 40-Spoke/Annular Plug	115.5	6.8	0.835	0.143	0.839	0.142
● 40-Chute/Annular Plug	110.8	11.5	0.839	0.139	0.832	0.149
● 36-Deep-Chute/Annular Plug	114.3	8.0	0.972	0.006	0.941	0.040
● 36-Deep-Chute/Annular Plug + Ejector 1	113.6	8.7	1.000	-0.022	0.946	0.035
● 36-Deep-Chute/Annular Plug + Ejector 2	114.4	7.9	0.968	0.010	0.927	0.054
● 72-Tube/Annular Plug	110.3	12.0	0.898	0.080	---	---
● 66-Tube/Annular Plug	111.4	10.9	---	---	---	---
● 66-Tube/Annular Plug + Ejector 2	109.4	12.9	---	---	---	---
● Unsuppressed 2-D + Sidewalls + Wing	114.2	4.6	0.974	-0.002	0.963	-0.002
● Unsuppressed 2-D + Ejector	117.2	1.6	0.977	-0.005	0.958	+0.003

2. Coannular Dual-Flow Systems	$P_{T8}/P_o = 3.5$ $P_{T18}/P_o = 3.5$ EPNL	ΔEPNL	Core ΔC_{f_g}*	Core + Fan ΔC_{f_g}**
● Suppressed Core of Dual-Flow	---	---	0.116	---
● Dual-Flow, Non-Coplanar, $A_{core}/A_{fan} = 1.0$	113.2	9.0	0.156	0.072
● Dual-Flow, Non-Coplanar, $A_{core}/A_{fan} = 1.32$	114.2	8.1	---	---
● Dual-Flow, Non-Coplanar, $A_{core}/A_{fan} = 1.5$	113.2	9.1	0.148	0.084
● Dual-Flow, Coplanar, $A_{core}/A_{fan} = 1.5$	114.6	7.7	0.148	0.083

* C_{f_g} calculation based on integrated spoke-base pressures and ideal core thrust.

** C_{f_g} determined from ideal thrust of combined core + fan flows.

- $M_o = 0.36$

- $P_{T8}/P_o = 3.0$

- $V_j = 2500$ ft/sec

- Peak PNL at 2128-ft Sideline

- Relative Velocity Effects not Included on Suppression
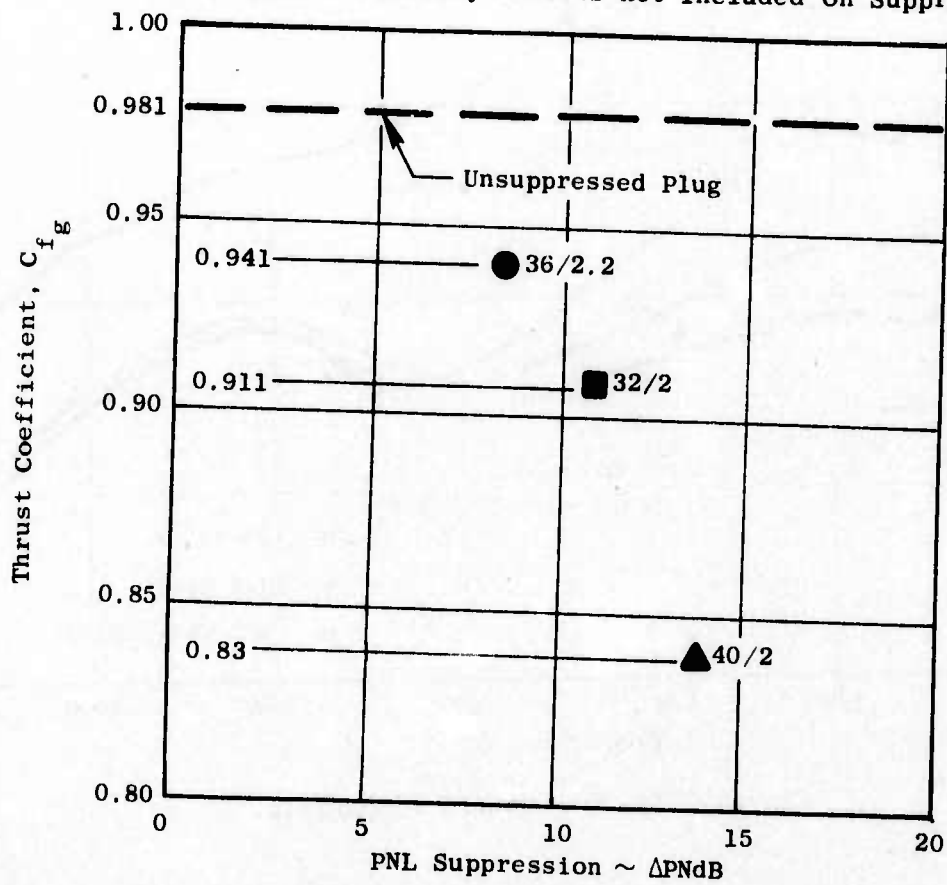
Figure 273. Multichute Suppressor Aeroacoustic Summary.
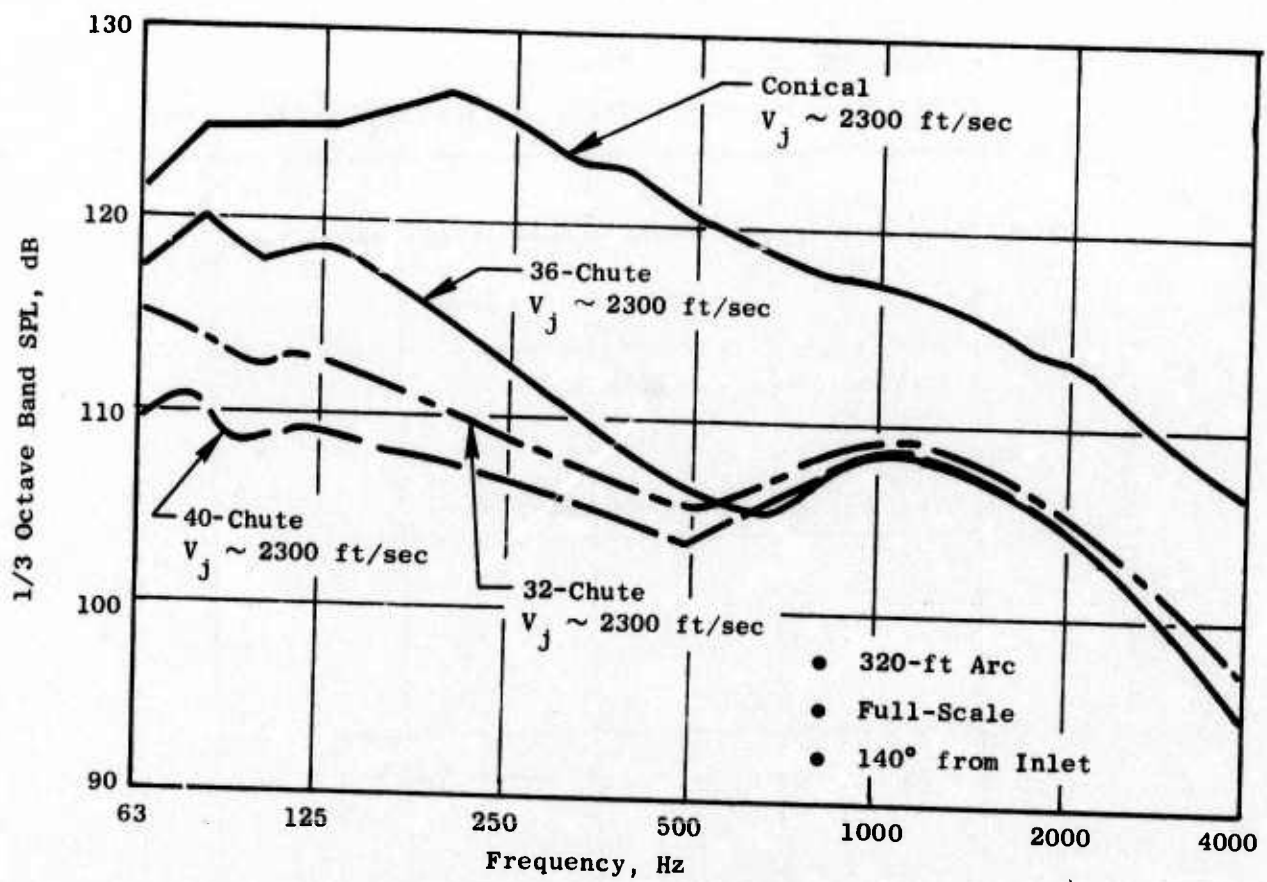
Figure 274. SPL Spectra Comparison.

the 32-chute performance exhibited a favorable combination of aeroacoustic performance trades. The planform of the 32-chute model did not converge the primary flow elements as rapidly as the 36-chute model.

The design of the final multichute suppressor was based on results and conclusions drawn from the series of tests on the 40-, 36-, and 32-chute suppressors. A review of the planform geometries on all three nozzles was conducted in order to correlate the nozzle geometric parameters with suppression and performance. The flow-width ratio, and a parameter identified as the hub spacing ratio, were plotted as functions of ΔC_{f_g} and ΔPNL as shown in Figure 275.

The flow-width ratio (ratio of primary flow element hub-to-tip spacing) controls the flow distribution across the annulus, influences the amount of mixing of entrained air with the primary elemental flows, and is a strong factor in maintaining proper chute backside ventilation which reduces thrust loss.

The hub-spacing ratio, defined as the ratio of the blocked (chute) to open (primary flow) spacing at the hub, defines a parameter for that region which has the greatest influence on the coalescence of the individual flows off the plug (see Section 3.2.2) and which consequently controls the magnitude of the noise suppression. The objective of any multielement nozzle is to segment the primary flow for a sufficient length downstream of the exit to allow entrained low-velocity flow to mix with and decay the high-velocity stream to a value low enough to achieve the desired noise reduction.

It can be seen from Figure 275 that reducing the thrust loss, ΔC_{f_g}, increases the flow-width ratio and decreases the hub-spacing ratio. Increasing the ΔPNL suppression requires a decrease in flow-width ratio and an increase in hub-spacing ratio.

From the trends on Figure 275, the planform geometry design region for flow-width and hub-spacing ratios between 0.7 and 1.0 was considered acceptable. This region was defined as most reasonable from a viable system approach, since the aeroacoustic-mechanical constraints seemed to affect the best trades.

A trade-off of geometric characteristics was reached with the selection of a 32-element, deep-chute ($AR_d \sim 2.1$) configuration with a primary flow-width ratio (hub/tip) of 1.0 and exit plane cant angle of 5° on a 15° plug (e.g., 100° between plug surface and exit plane, which would be amenable with a conical ejector). Figure 276 is a photograph illustrating the geometric features of the 32-deep-chute suppressor configuration selected for the "optimum type" nozzle. This design was expected to give peak PNL suppression between 11 - 14 PNdB while improving the wind-on performance at design to C_{f_g}'s more like the 36-chute model previously demonstrated (0.93 - 0.94 class).
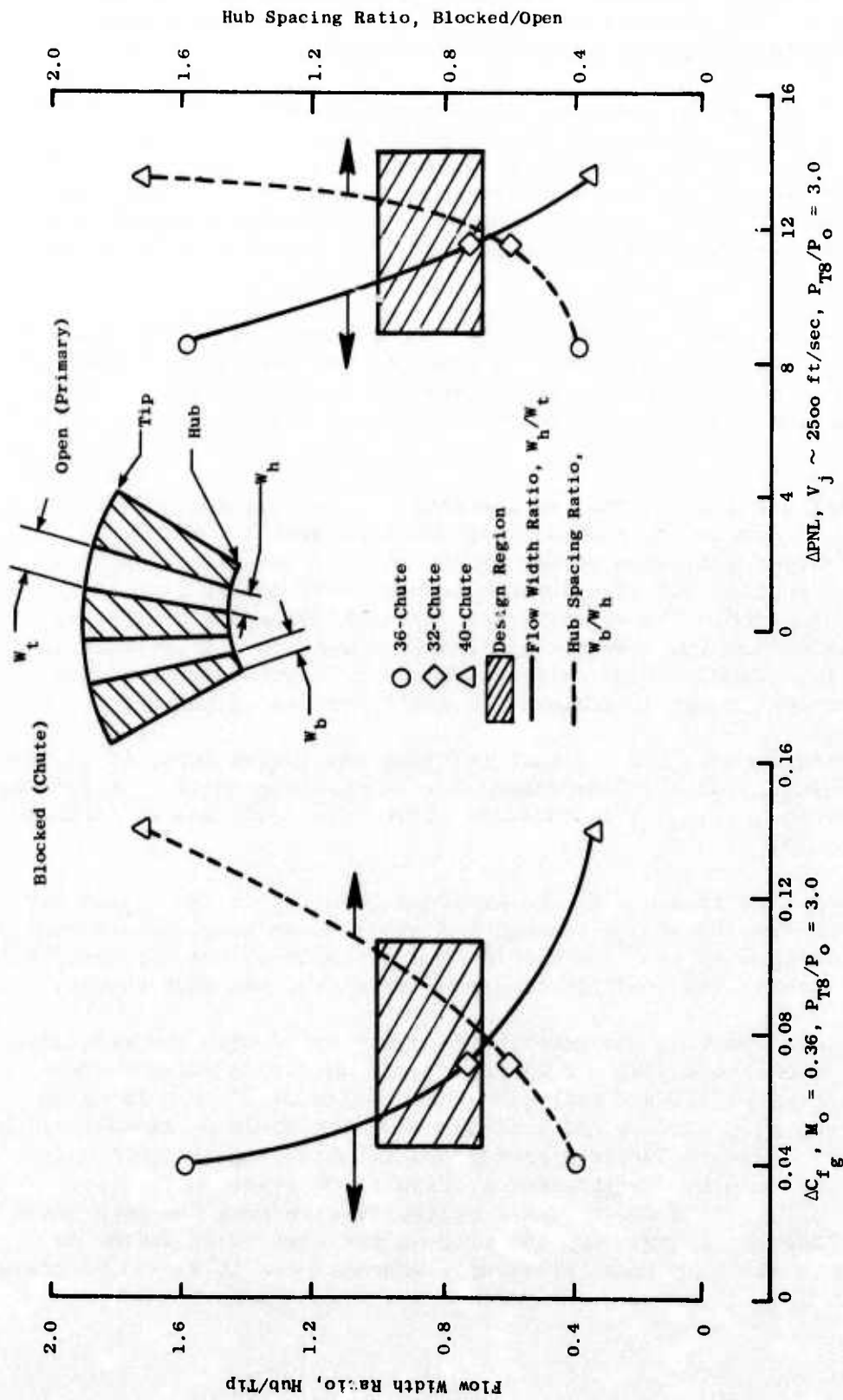
Figure 275. Multichute/Annular Plug Suppressor Planform Geometry Correlation.

5° CANT

⊥ TO AXIAL
℄

AREA RATIO = 2.1
$\left(\dfrac{\text{TOTAL ANNULUS AREA}}{\text{PRIMARY FLOW AREA}} \right)$

PARALLEL SIDED
PRIMARY FLOW
PASSAGES

32 DEEP
CHUTES
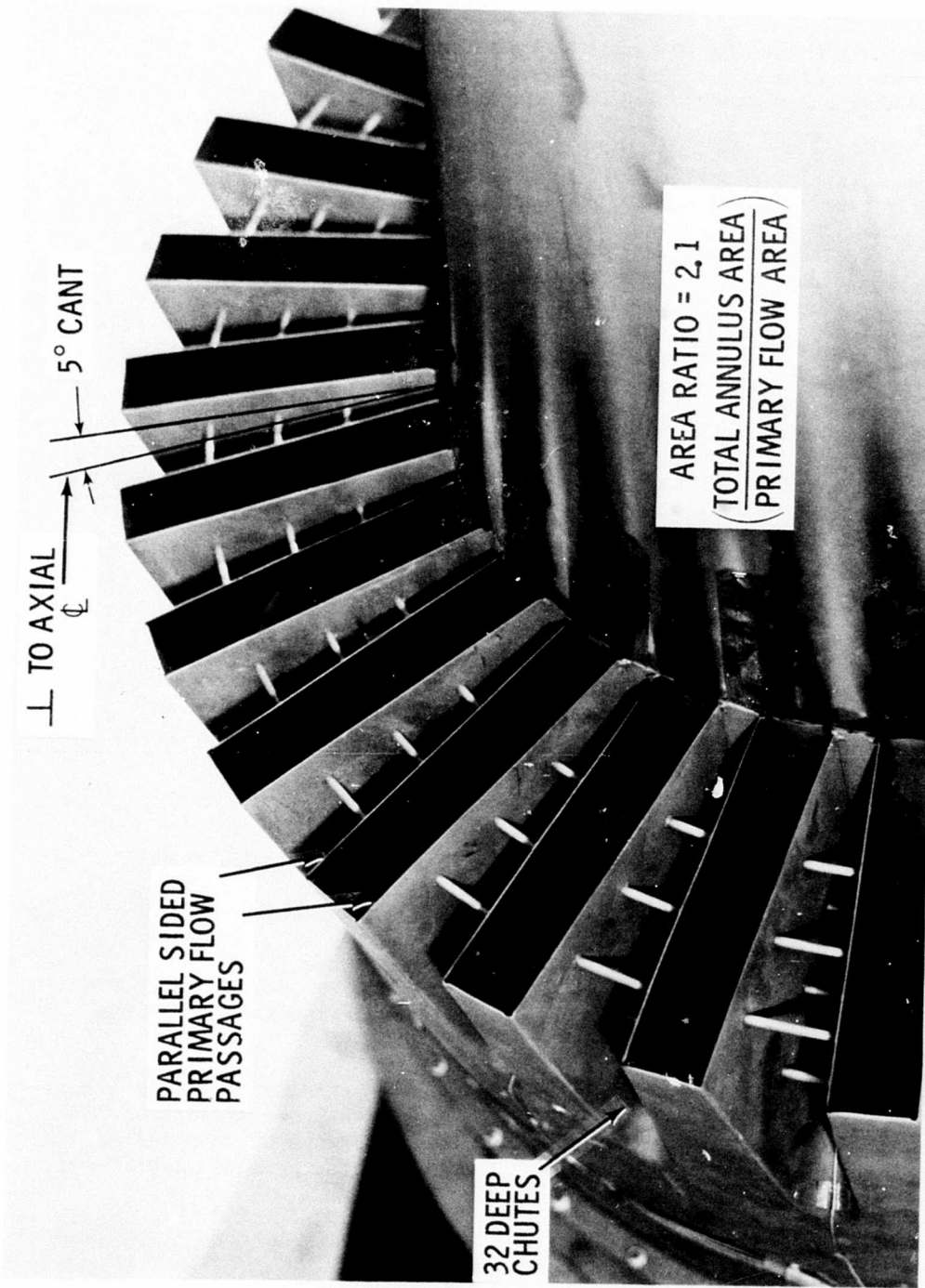
Figure 276. Multichute Candidate for "Optimum" Nozzle.

341

3.4 FINAL MODEL AND ENGINE SUPPRESSOR TESTS

The testing of the "optimum type" suppressor configuration was per-
formed in both model and large engine scales for the purpose of comparing
acoustic results and demonstrating model/engine scaling of a viable suppres-
sion system.

The model testing consisted of hot-jet acoustic tests to determine PNL
suppression relative to a conical baseline; laser velocimeter measurement
of the jet plume to identify mean and turbulent velocity profiles and distri-
butions, and aerodynamic wind-on performance tests to determine the installed
thrust. (Ellipsoidal mirror-microphone surveys also were conducted with the
hot jet to determine noise source locations in connection with Task 1 of the
DOT High Velocity Jet Noise Source Location and Reduction Program, Contract
No. DOT OS-30034.)

Large-scale engine tests were performed on a specially prepared acoustic
arena and a supersuppressed J79-8/15 engine. (Complete details of the setup
of sound field and engine are found in Reference 6). Acoustic tests were
conducted for comparison with model results. In addition, laser and ellip-
soidal mirror-microphone measurements were obtained for use in the DOT High
Velocity Jet Noise Program.

3.4.1 Final Model Suppressor Tests

Scale model acoustic and aerodynamic (wind-on) performance tests of
the "optimized" final suppressor were conducted for comparison with acoustic
and aerodynamic results from previous scale model tests. They were also
used for comparisons with the J79 engine test results to illustrate model-to-
engine data scaling.

Acoustic Tests

The hot-jet acoustic tests of the conical baseline and final config-
uration with and without a treated ejector were conducted on the JENOTS
facility over a simulated J79 and SST combined operating line, covering a
range of pressure ratios from 1.2 to 3.85 and temperatures from 1030° R
to 2115° R which yielded ideal jet velocities from 900 to 2900 ft/sec. The
model test setup was the same for all configurations tested and is described
in Appendix A.

Photographs of the 32-deep-chute annular plug suppressor alone and
with treated ejector mounted on the JENOTS facility are shown in Figures 277
and 278, respectively. Figure 279 is a posttest photograph of the treated
ejector which shows the apparent impingement areas of the primary flow around
the ejector circumference.

342
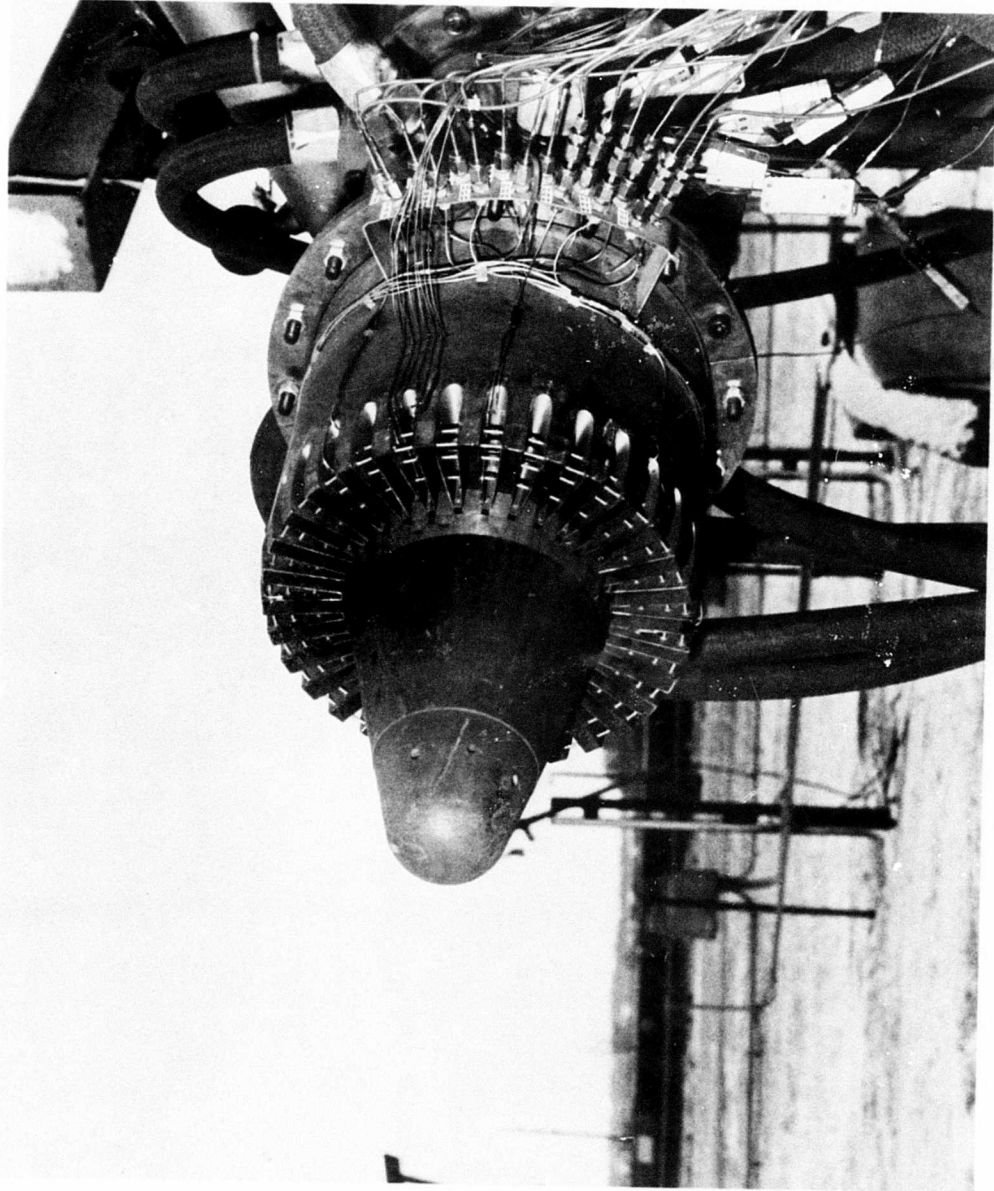
Figure 277.   32-Deep-Chute/Annular Plug Suppressor on JENOTS.
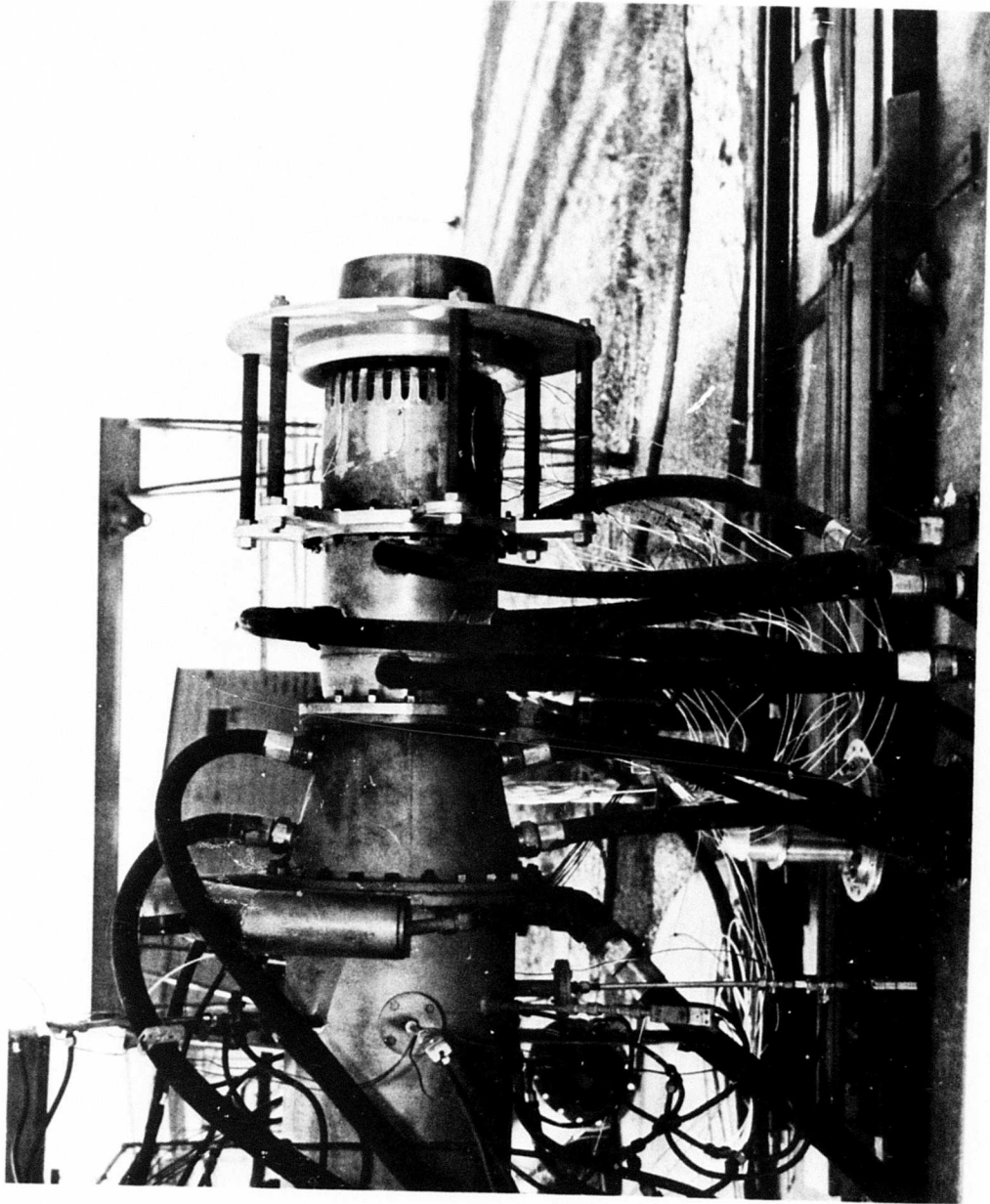
Figure 278. 32-Deep-Chute Nozzle with Conical Ejector on JENOTS.

Regions of
Nozzle
Impingement
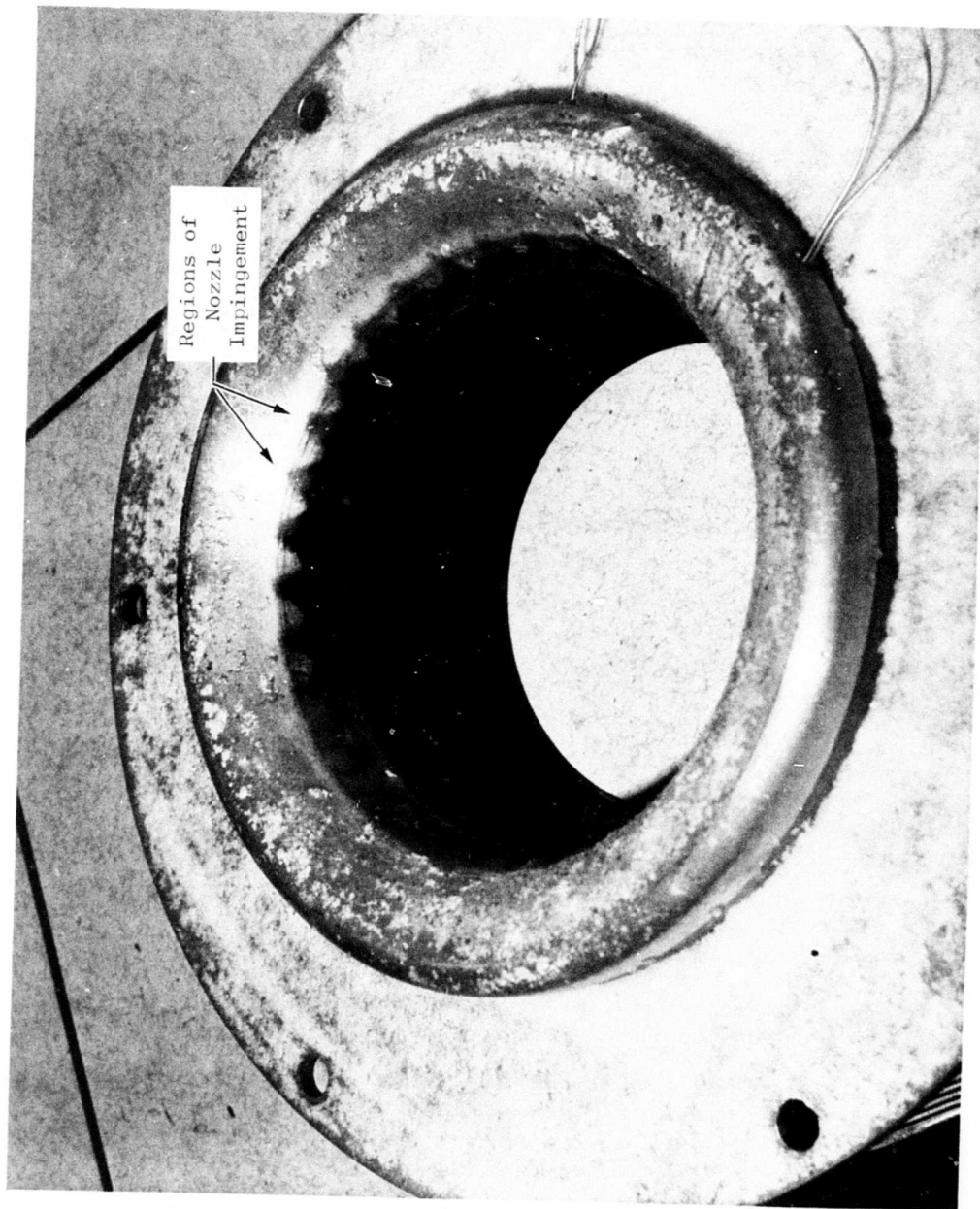
Figure 279. Treated Conical Ejector Used with 32-Deep-Chute Suppressor.

345

Acoustic Results and Analysis

All acoustic data were corrected to standard conditions of 59° F and 70% R.H. The data were scaled by frequency and size to full-scale engine application. Results of the acoustic model tests on the 32-chute suppressor with and without hardwall and treated ejectors are reported in the following paragraphs. The acoustic results of each model and the range of test conditions are contained in Appendix C.

Test results of the conical nozzle were compared with conical nozzle data obtained earlier in the year. A comparison of the full-scale peak PNL on the 300-, 1500-, and 2128-foot sidelines is shown in Figure 280 for the two sets of conical nozzle data along with the average conical line established from a previous history of data obtained on numerous conical nozzle tests. The results of this comparison indicate that the data compare well with previous data as shown in Figure 280. PNL directivity over the velocity range is shown in Figure 281. Shock noise is apparently affecting the PNL directivity at the high jet velocities in both aft and forward angles. The peak angle SPL spectra in Figure 282 also exhibit shock noise effects (broadband and tonal) at high velocity. Corrections (smoothing primarily) for the shock tones appearing in the SPL spectra were made at the high velocity points, and the PNL recomputed to bring the fixed area data more in line with shock-free nozzle operation with variable exit area setting capability.

Peak PNL comparisons of the 32-deep-chute suppressor and conical nozzle baseline are presented in Figure 283, along with the results of the earlier test of the 32-chute (Phase I) model. The evaluation of the 32-deep-chute suppressor indicated the suppressor matched or exceeded earlier results of the older 32-chute model tested as part of the multichute suppressor evaluation series in this program. The acoustic suppression, in terms of full-scale peak ΔPNL at the 2128-foot sideline without EGA, was 12 PNdB from 2300 to 2500 ft/sec ideal jet velocity.

A check of the full-scale, peak angle SPL spectra at the 300-foot sideline in Figure 284 indicated the suppressor maintained its high frequency domination through 2494 ft/sec up to 2574 ft/sec, where the postmerged and premerged regions are about equal. The spectra becomes low-frequency-dominated at 2735 ft/sec. These characteristics are born out by the directivity (Figure 285) which shows peak angle at 110° to 120° for the velocities below 2574 ft/sec. The peak angle at 2735 ft/sec is 140°, which is indicative of the aftward shift (toward axial) of the noise from a coalesced jet. Comparison of 32- and 36-chute peak angle spectra at ∿2500 ft/sec in Figure 286 shows that suppression of the low frequencies was achieved with the 32-chute design.

The conical ejector results with hardwall and acoustically treated liners are shown in Figure 287 on a peak PNL comparison basis at the 2128-foot sideline. The results indicate a 2.0 to 1.0 dB reduction in noise over the hardwall results for an overall PNL suppression of 12-13 dB from 2000-2500 ft/sec.

Figure 280. Peak PNL Comparisons.

Figure 281. PNL Directivity, 2128-foot Sideline.

- Full Scale
- Scale Factor 8:1
- 2128-ft Distance PNL Directivity
- 5.7" ID Unsuppressed Conical

348
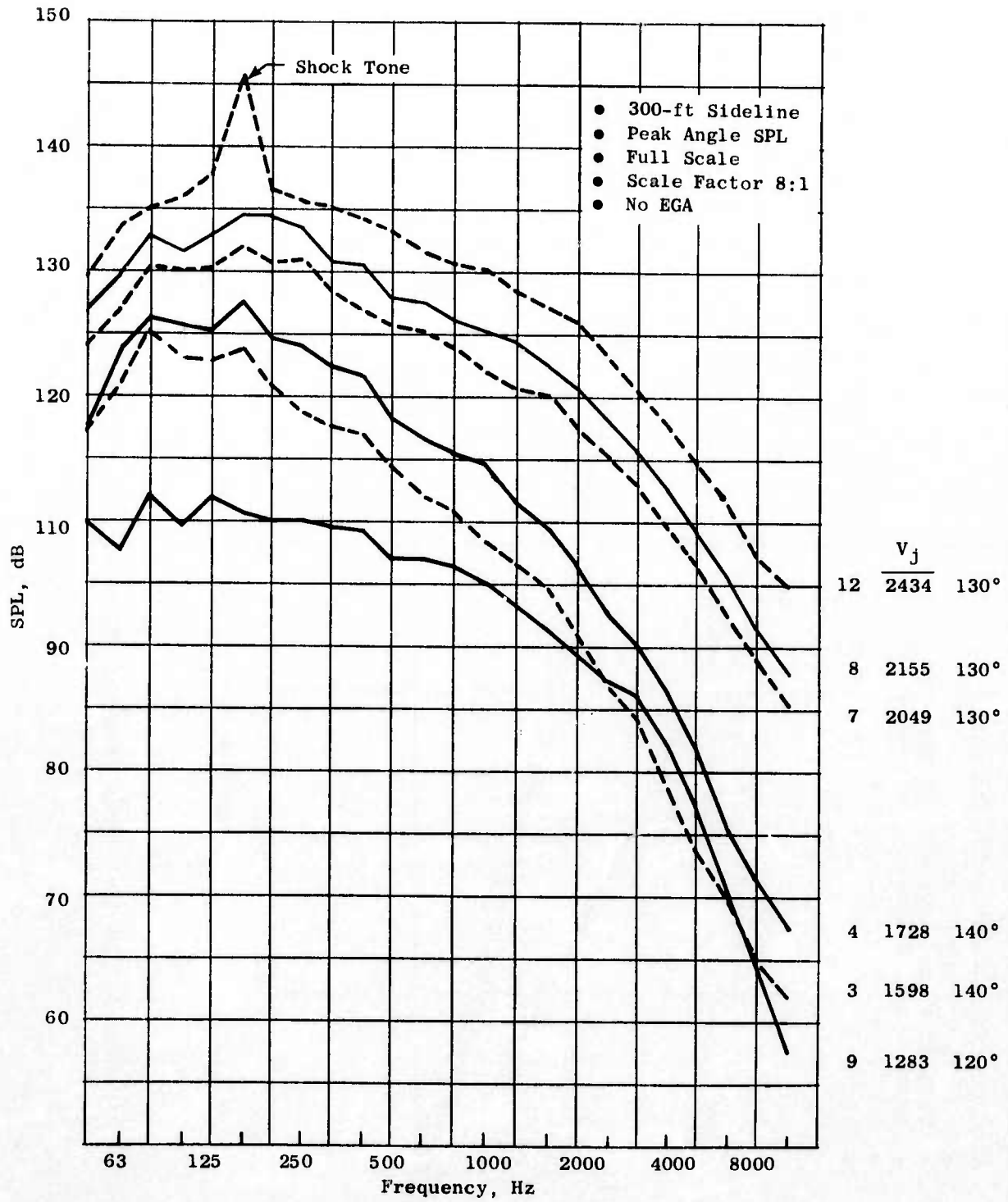
Figure 282. Conical Nozzle Spectra.

349
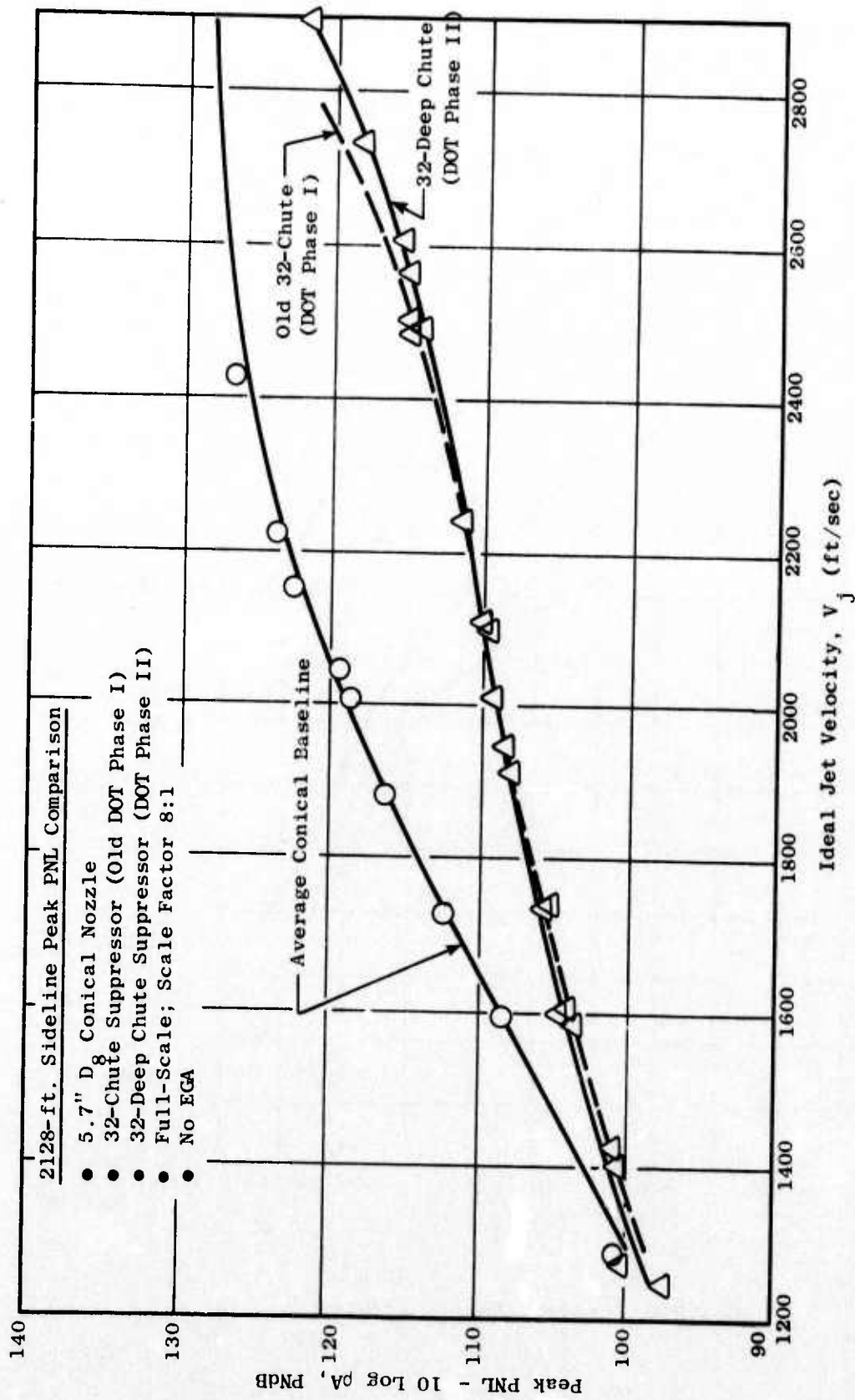
Figure 283. 32-Chute-Model Annular Plug Suppressor PNL Comparison.

350
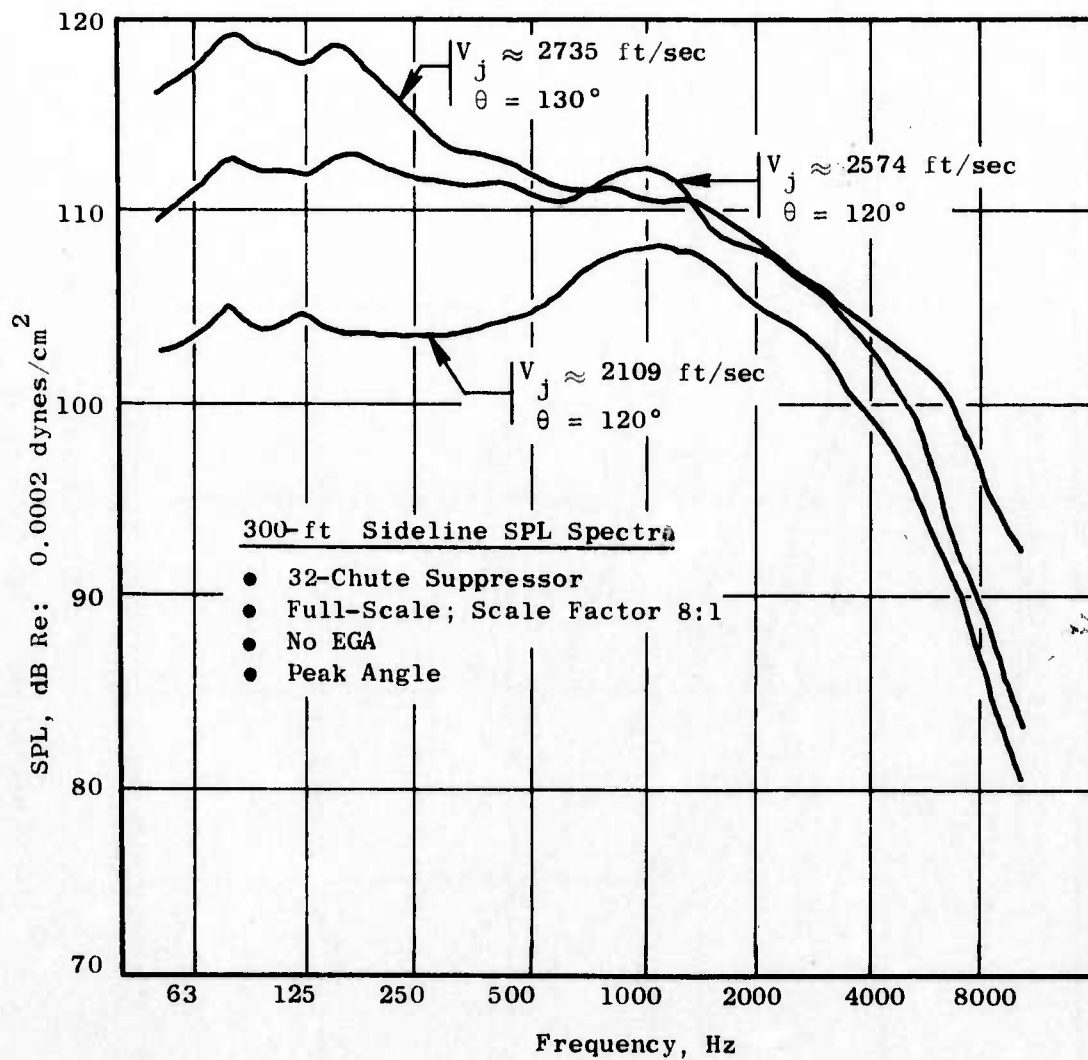
Figure 284. SPL Spectra, 300-foot Sideline.
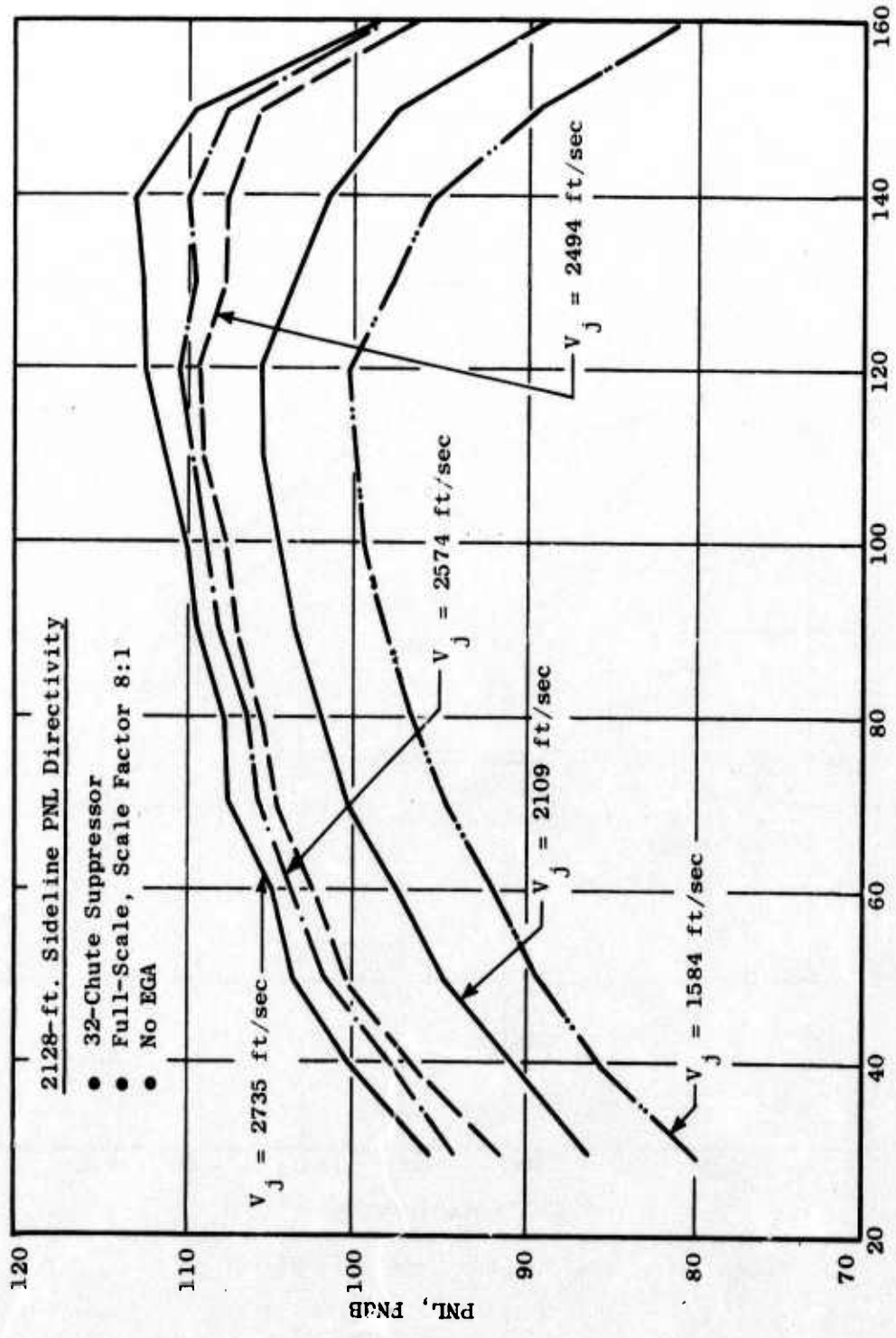
Figure 285. PNL Directivity, 2128-foot Sideline.
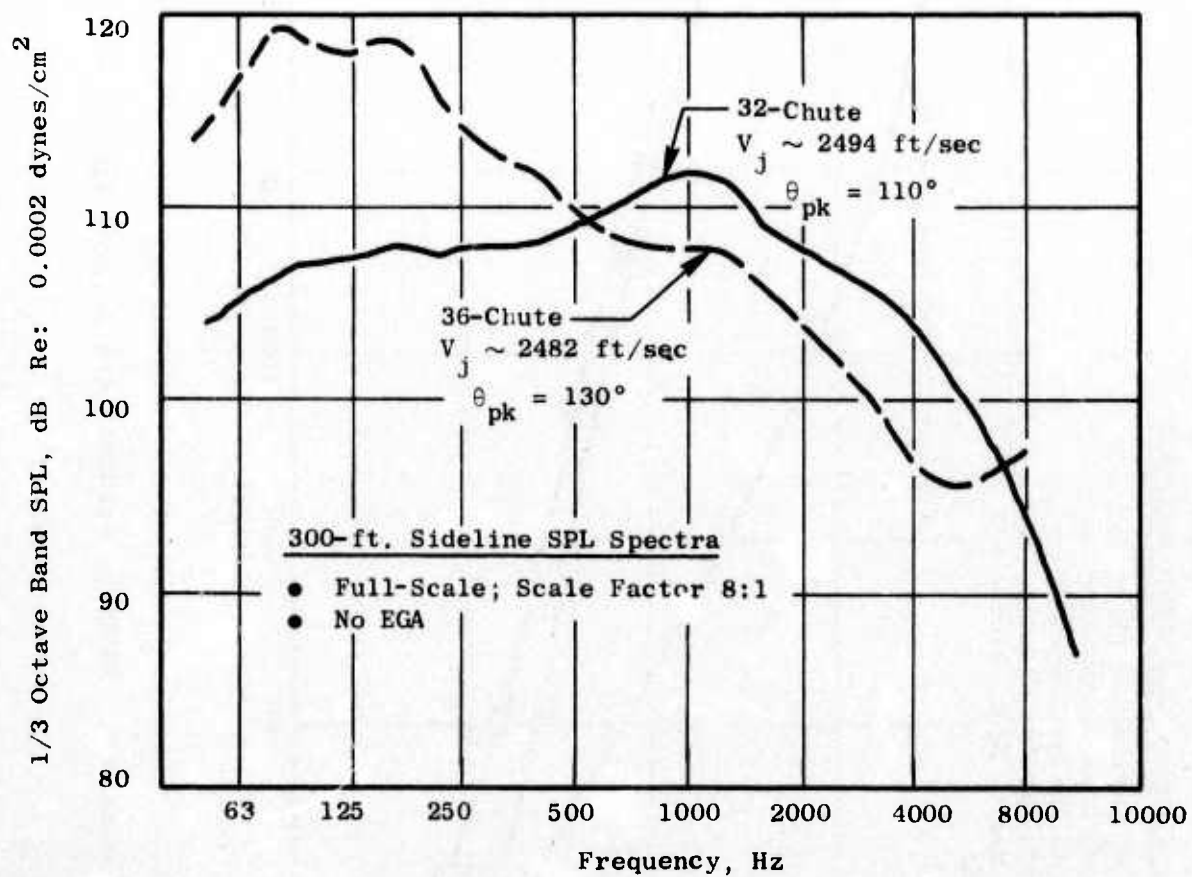
Figure 286. SPL Spectra, 300-foot Sideline.
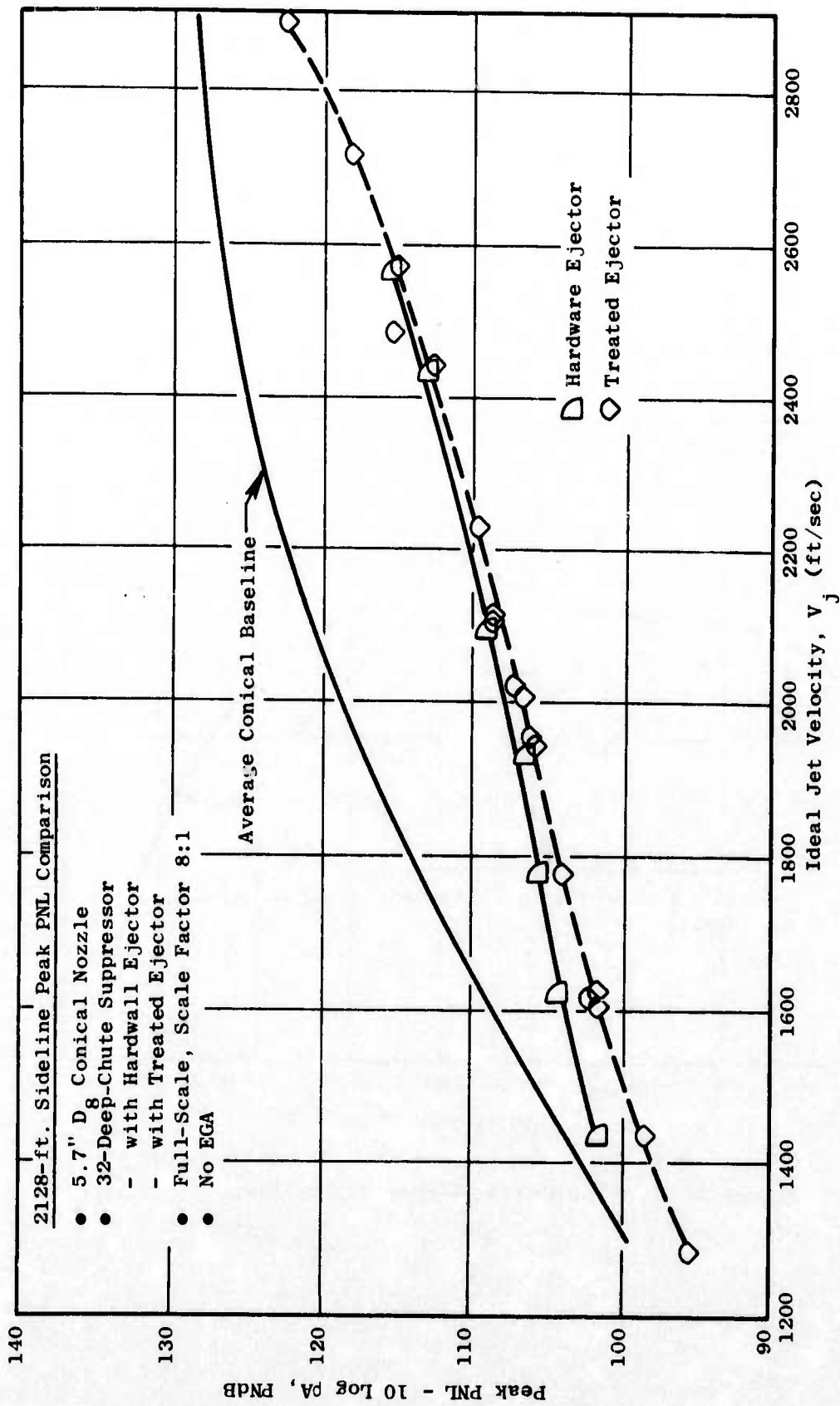
Figure 287. 32-Chute Hardwall and Treated Ejector PNL Comparison.

354

The PNL directivity shown in Figure 288 illustrates an aftward shift of peak angle from 110° to 140° at jet velocities above 2100 ft/sec, which indicates the early coalescence of the primary flow elements, possibly brought about, in part, by the mechanical constraints of the conical ejector which tend to force the entrained and primary flows along the plug, merging them to a smaller diameter at the ejector exit.

The SPL spectra at peak angle (300-foot sideline) shows, in Figure 289, that the ejector system maintained a relatively flat spectral shape up to 2444 ft/sec and then became completely dominated by the low frequency at 2574 ft/sec. This low frequency domination also is indicated by the shift in the peak angle.

Comparisons of the 32-chute and 32-chute with treated ejector shows an improvement in PNL suppression (Figure 290) of 2.5-1.5 dB over the 32-chute at velocities below 2200 ft/sec and above 2400 ft/sec. The ejector effectiveness is gone and even becomes detrimental at higher velocities.

The PNL directivity comparison of the above nozzle configurations in Figure 291 shows the aftward shift of peak angle at the higher velocity, indicating a more rapid directivity shift with the ejector nozzle than with the suppressor alone.

Figure 292 compares the SPL spectra for both suppressor configurations and illustrates the effect of the treatment on the high frequencies (>500 Hz). The reason for the minimal suppression with the ejector at the higher velocity (~2574 ft/sec) is seen to be due to the increase in low frequency SPL's as a result of the shifting of the noise generation sources downstream of the ejector.

Laser Velocimeter Test Results on Final Model Suppressor

Plume surveys for mean and turbulent velocity distributions were conducted on the 32-deep-chute suppressor at selected test conditions consistent with the requirements of the DOT High Velocity Jet Noise Program and this program. Conditions set for the Phase II program evaluation consisted of ideal jet velocities of 1600 and 2300 ft/sec. Axial traverses along the nozzle centerline were obtained from 1 to 20 nozzle diameters downstream. Radial traverses at an X/D_o of 1, just aft of the end of the plug, were taken to observe the radial distribution of mean velocity at both test conditions.

The 32-deep-chute suppressor model test results for these test conditions are shown in Figure 293. Trends of the mean velocity axial traverses are shown in Figure 293a for both 1600 and 2300 ft/sec jet velocities. The curves illustrate the trend toward rapid axial decay of the jet velocity by some 300 ft/sec at 4-5 X/D from plug end. Comparison of the earlier axial decay trend established with the original 32-chute suppressor (Phase I) and discussed in Section 3.2.2 shows good agreement.
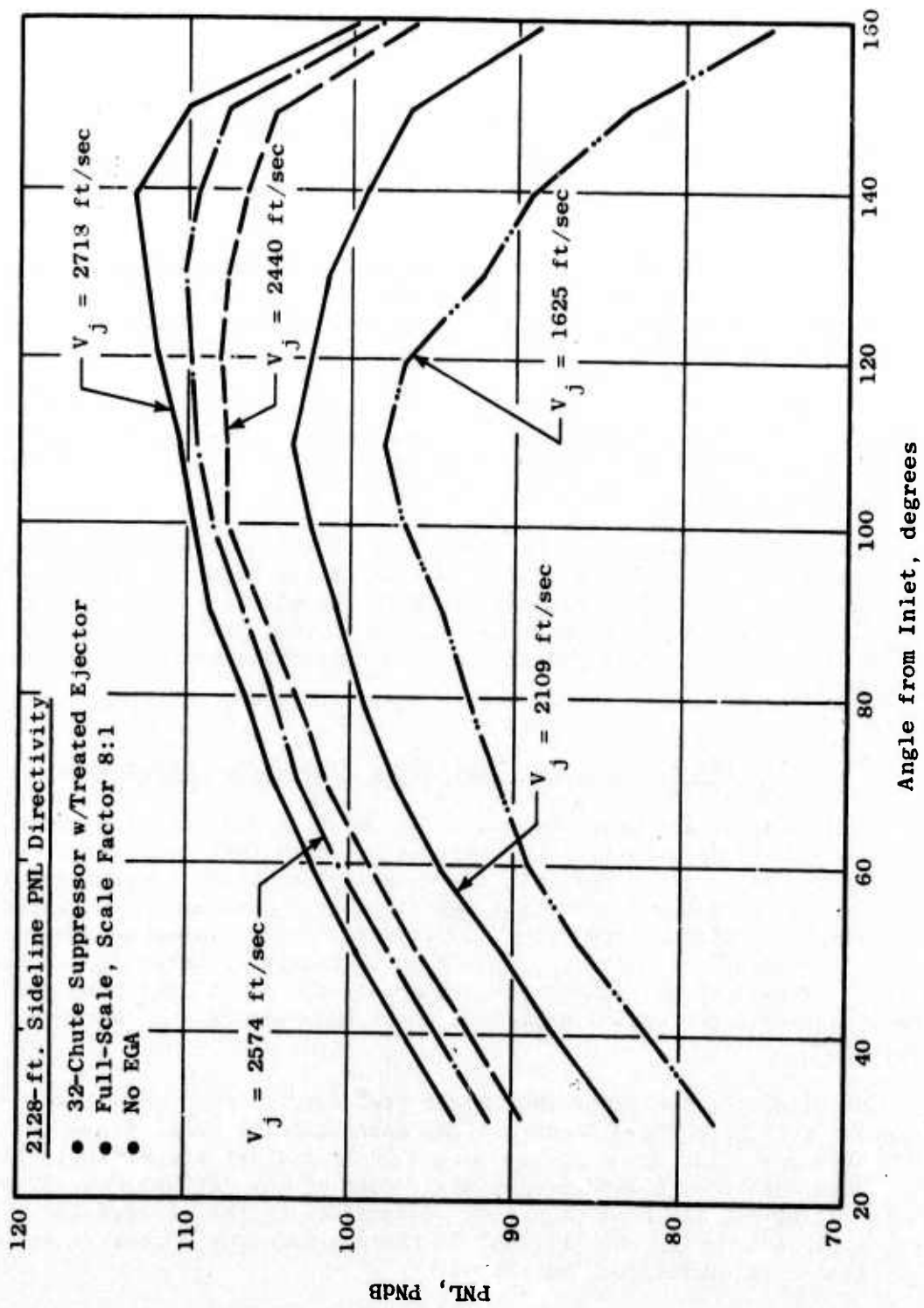
Figure 288. PNL Directivity at the 2128-foot Sideline.

356
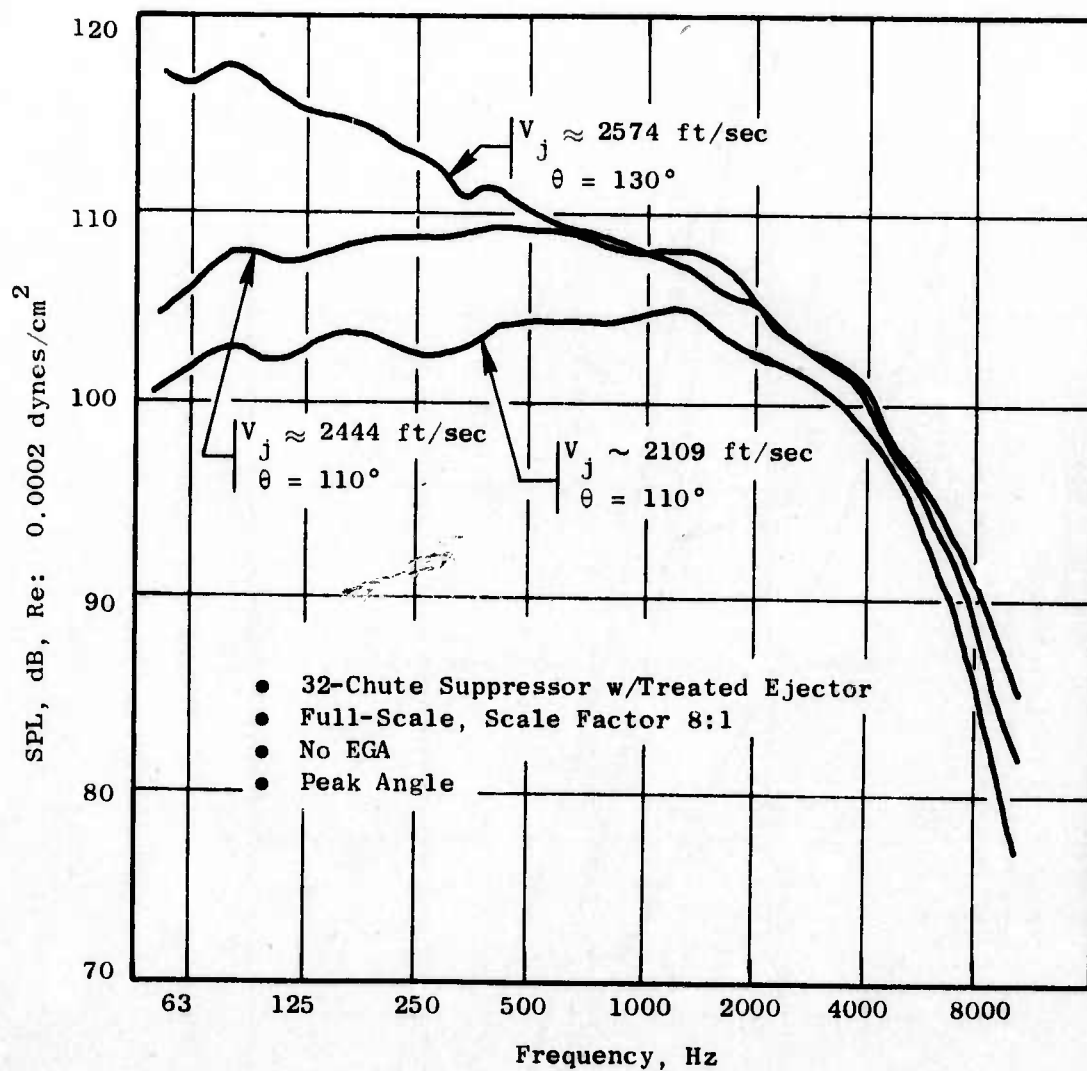
Figure 289. SPL Spectra, 300-foot Sideline.

357
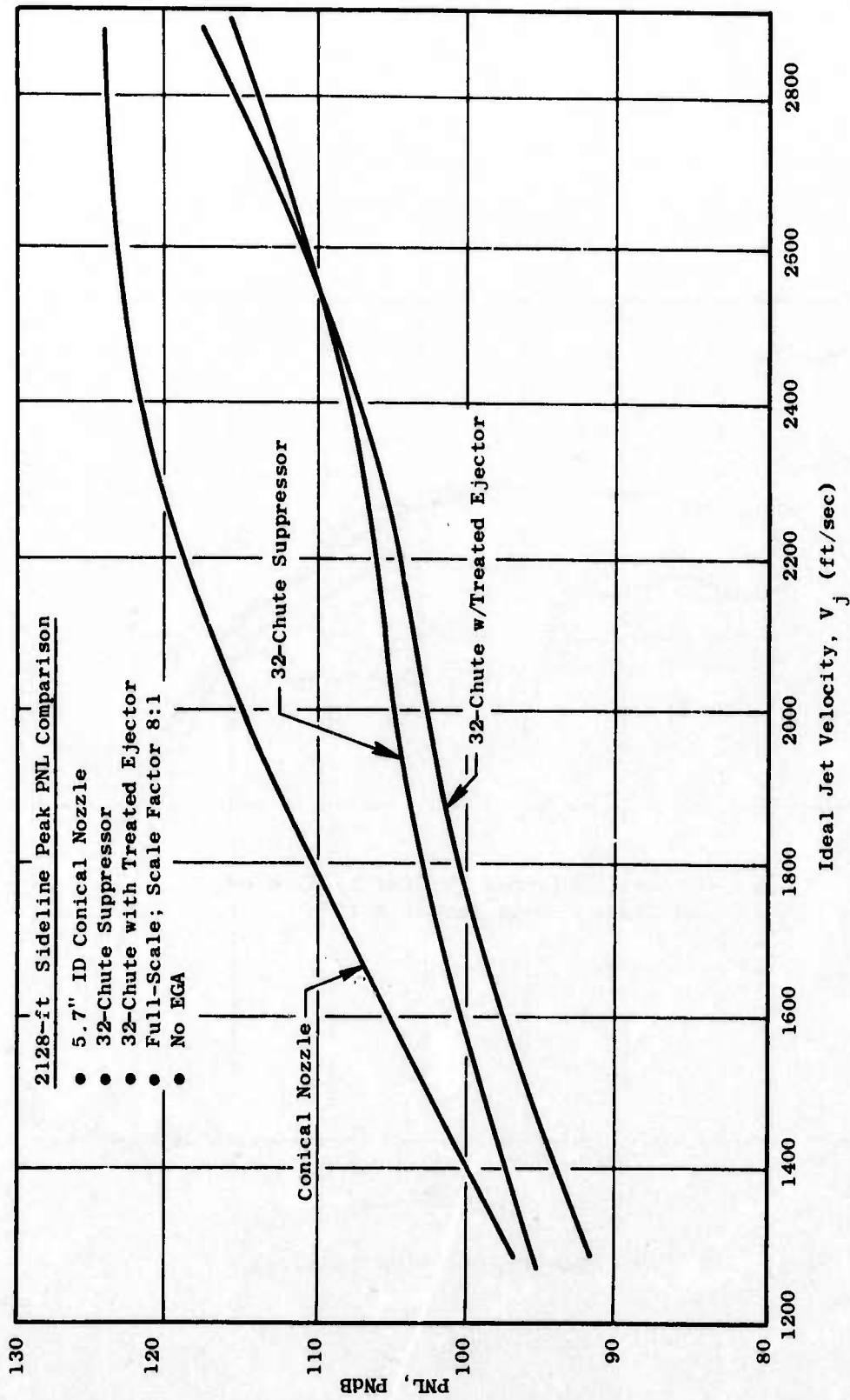
Figure 290. Peak PNL Comparison, 2128-foot Sideline.
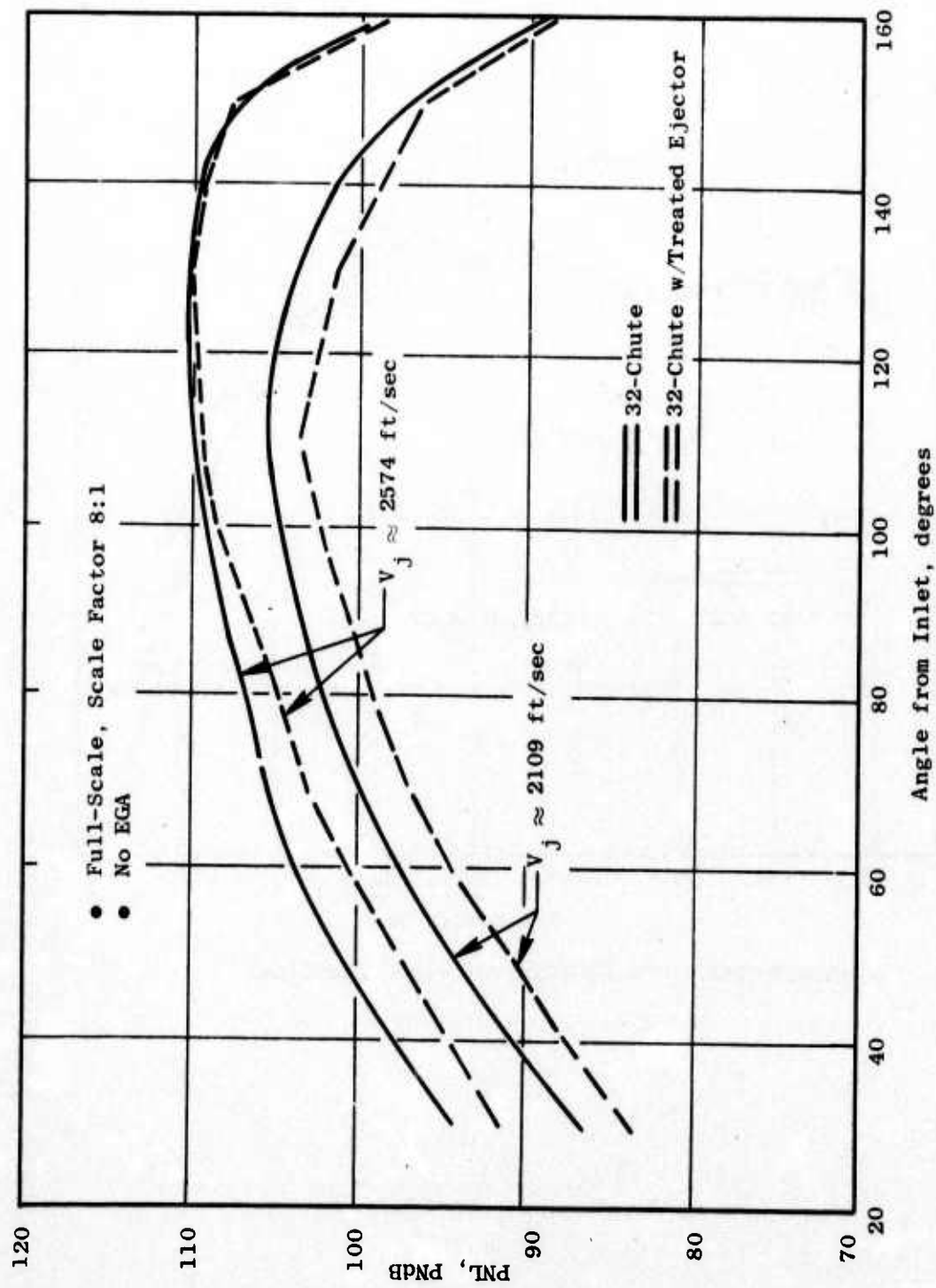
Figure 291. PNL Directivity, 2128-foot Sideline.

359
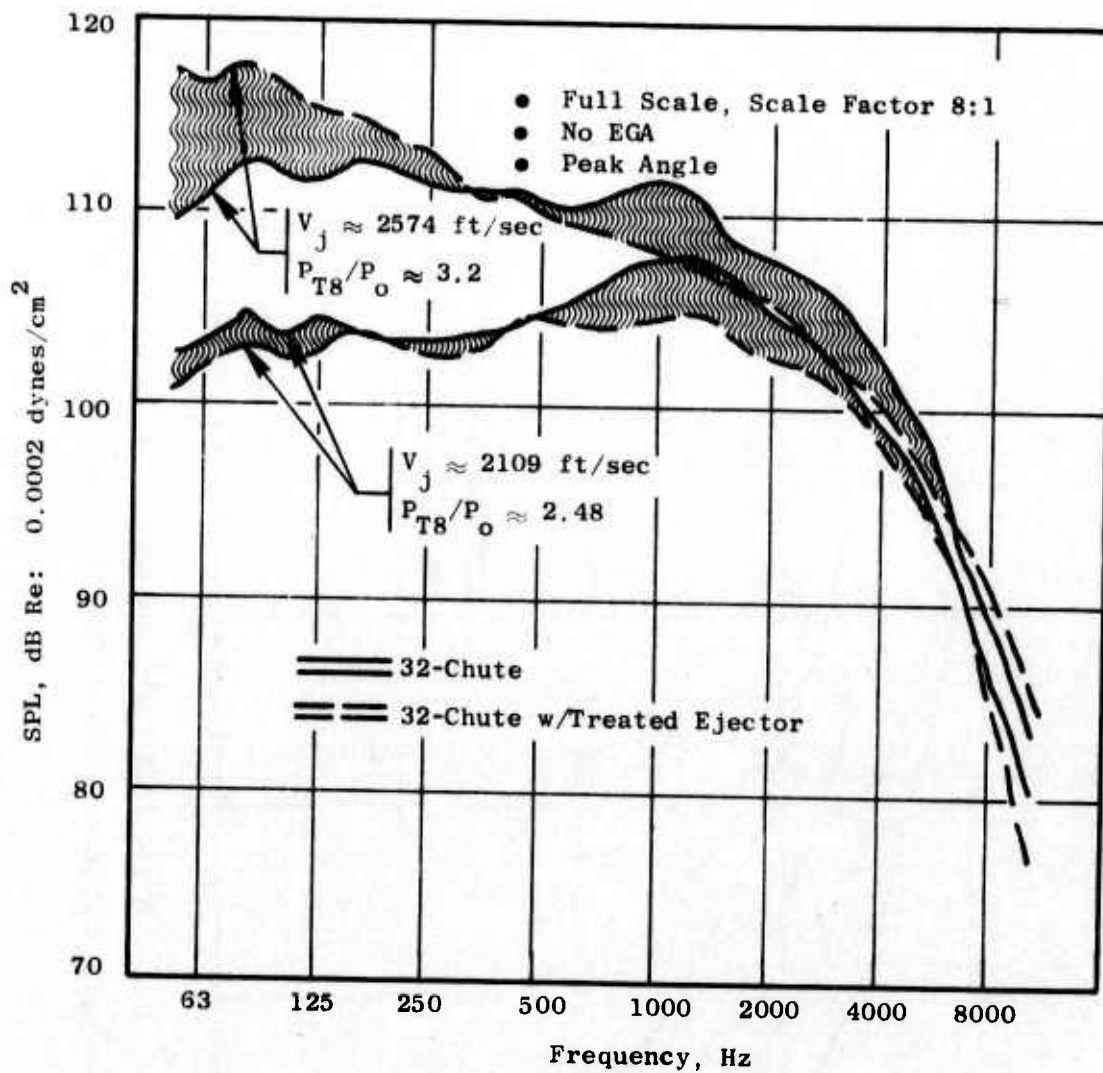
Figure 292. SPL Spectra, 300-foot Sideline.
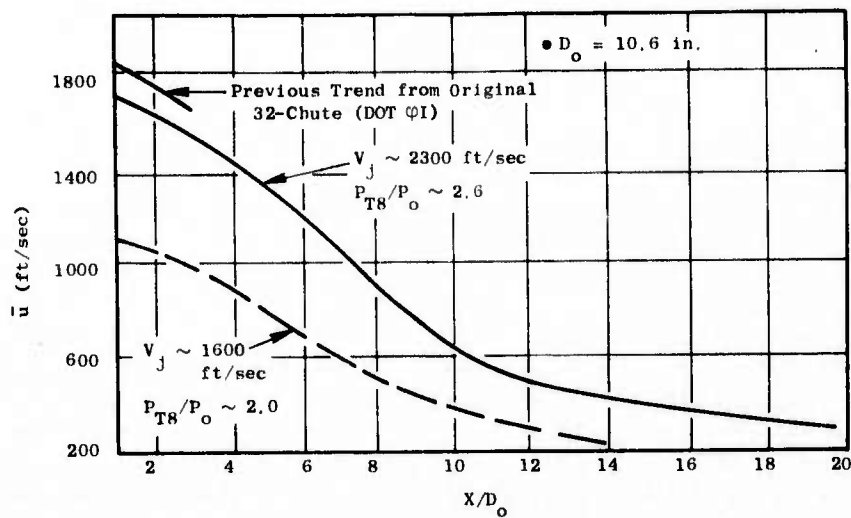
(a) Axial Decay Trends of Mean Velocity
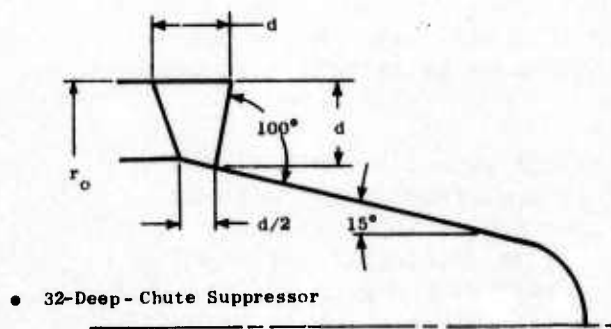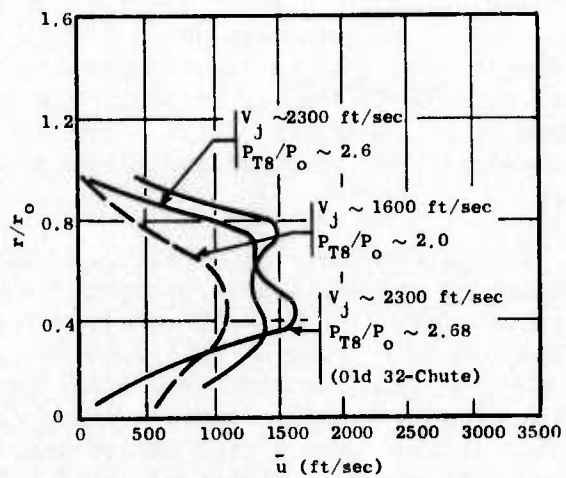
(b) Radial Distribution of Mean Velocity

Figure 293. Mean Velocity Profiles from LV Measurements.

361

The radial profiles of mean velocity are presented in Figure 293b at an X/D of 1. A relatively smooth, nearly flat profile is apparent at the higher jet velocity, very similar to the results of the earlier 32-chute nozzle mentioned above.

Aerodynamic Performance Tests

The model aerodynamic performance tests were performed in the Channel 10 Transonic Wind Tunnel at FluiDyne's Medicine Lake Aerodynamic Laboratory (see Appendix A for facility description).

Performance data were obtained at free-stream Mach numbers of 0 and 0.36 and at nozzle pressure ratios of 2.5, 3.0, and 3.5. In addition, a standard ASME long-radius metering nozzle was tested statically over the nozzle pressure range from 2 to 4 to demonstrate facility data accuracy. Dry air at approximately tunnel total temperature was supplied to the nozzles in this test. Angle of attack of the model was maintained at 0°. The Reynolds number per foot for the 0.36 Mach number runs was 2.21×10^6.

An assembly drawing and photographs of the deep-chute plug nozzle, with and without a setback ejector shroud, are presented in Figures 294 and 295. Both configurations had a 15° half-angle plug. During takeoff and climb-out with this nozzle, chutes are deployed for jet noise suppression. After climb-out from the airport, the chutes are retracted either into the shroud or the plug for cruise. The nozzle then will take on the general appearance of an unsuppressed plug and should have relatively high performance.

The deep-chute plug nozzle also was tested with a setback ejector, (similar to the small conical ejector tested acoustically but without a bellmouth inlet). The setback ejector shroud had an inlet diameter of 7.334 inches, an exit diameter of 6.106 inches, and an inclination of 8°30' to the horizontal. The flow area distribution between the plug and the shroud is convergent. The ejector was attached to the nozzle by eight struts which were parallel to the engine centerline. The purpose of the ejector was to promote the internal mixing of the low velocity external flow with the high velocity primary jet. This mixing is intended to reduce the jet noise through the reduction of the primary jet velocity.

Aerodynamic Performance Results and Analysis

The major test results of the ASME and the two suppressor nozzles are tabulated in Table 11.

Nozzle efficiencies of an unsuppressed plug nozzle (Reference 2) and the 32-chute suppressor nozzle, with and without the setback ejector, are presented as a function of nozzle pressure ratio at Mach numbers of 0 and
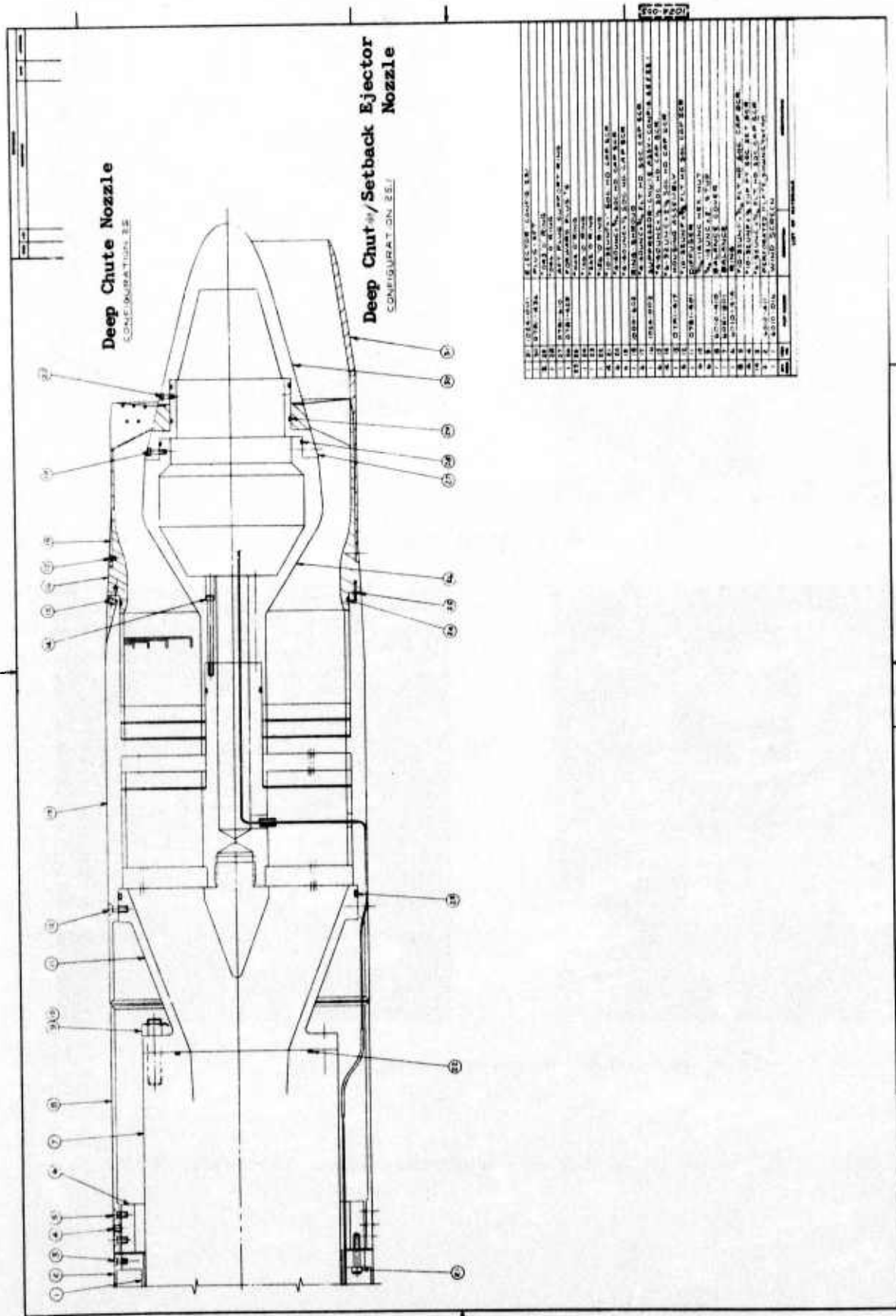
Figure 294. Model Assembly, Configurations 25 and 25.1.

363

(a) 32-Deep-Chute Suppressor
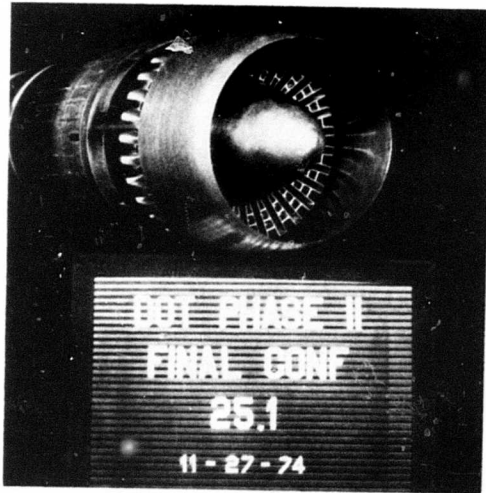
(b) 32-Deep-Chute Suppressor with Ejector.

Figure 295. Photographs of Installed Aerodynamic Final Suppressor Models.

Table 11. Aerodynamic Performance Summary of 32-Deep-Chute Nozzle Tests.

Configuration	Run No.	Mach No.	P_{T_8}/P_o	C_{fg}	C_{D_8}	f_g
4.5 ASME	1.2	0	1.992	0.9937	0.9892	1.2548
	2.1	0	2.482	0.9956	0.9910	1.2578
	3.1	0	2.966	0.9923	0.9917	1.2583
	4.1	0	3.467	0.9868	0.9904	1.2565
	5.1	0	3.960	0.9811	0.9897	1.2556
32-Deep-Chute	6.3	0	2.512	0.9645	0.9778	2.1916
	7.3	0	3.014	0.9631	0.9781	2.0289
	8.3	0	3.521	0.9607	0.9789	1.9136
	9.0	0.363	2.564	0.9191	0.9773	2.1324
	10.0	0.363	3.054	0.9250	0.9764	1.9817
	11.0	0.363	3.534	0.9290	0.9788	1.8800
32-Deep-Chute with Ejector	12.3	0	2.520	0.9805	0.9762	2.2006
	13.3	0	3.021	0.9918	0.9775	2.0528
	14.3	0	3.533	0.9796	0.9790	1.9297
	15.0	0.363	2.566	0.9039	0.9748	2.1163
	16.0	0.363	3.047	0.9324	0.9775	1.9913
	17.0	0.363	3.534	0.9350	0.9757	1.8829

0.36 in Figures 296a and b, respectively. The discharge coefficients of the suppressor nozzle, with and without the ejector shroud, also are presented.

The unsuppressed plug nozzle, which was not tested during this program, is presented in this report for comparative purposes. Under static conditions, and over the nozzle pressure ratio range investigated (2.5 to 3.5), the nozzle efficiency curve of the unsuppressed plug nozzle fell between the efficiency curves of the deep-chute/setback-ejector nozzle, which had the highest performance, and the deep chute nozzle. At a nozzle pressure ratio of three, the static nozzle efficiencies of the deep-chute/setback-ejector nozzle and the deep-chute nozzle were 0.992 and 0.963, respectively. At an assumed take-off pressure ratio of 3.0 and Mach number of 0.36, the unsuppressed plug nozzle had a baseline nozzle efficiency of 0.981. At the same conditions, the nozzle efficiencies of the deep-chute nozzle and the deep-chute/setback-ejector nozzle were 0.924 and 0.931, respectively. The nozzle efficiency decrements for the deep-chute and deep-chute/setback-ejector nozzles, when compared with the unsuppressed plug nozzle, are 0.057 and 0.050, respectively.

The chute-base pressure drag for the 32-deep-chute suppressor nozzle, with and without the setback-ejector shroud, are presented at Mach numbers of 0 and 0.36 in Figure 297. This drag component is presented as a fraction of nozzle ideal thrust. At both Mach numbers the ratio of chute-base pressure drag to nozzle ideal thrust for the two suppressor nozzles decreased with increasing nozzle pressure ratio. This loss mechanism constitutes a significant part of the nozzle efficiency decrement between the unsuppresssed plug nozzle and the deep-chute suppressor nozzles. At an assumed take-off Mach number of 0.36 and pressure ratio of 3.0, the chute-base pressure drag of the 32-deep-chute suppressor nozzle without an ejector was 4.7 percent of nozzle ideal thrust. This loss is equal to approximately 82 percent of the efficiency decrement incurred by the above nozzle when compared with the unsuppressed plug. At the assumed take-off conditions, the chute-base pressure drag of the deep-chute suppressor nozzle with the setback-ejector has a chute component thrust loss of 0.053 which exceeds the suppressor thrust decrement (0.050) when compared with an unsuppressed plug nozzle. It can be inferred from this inconsistency that a favorable interaction with the ejector shroud occurred resulting in positive ejector shroud forces being generated. These positive forces offset a portion of the chute-base pressure drag.

The effect of external flow on the nozzle efficiencies of the deep-chute and deep-chute/setback-ejector nozzles was significant. At a nozzle pressure ratio of 3.0, the losses in nozzle efficiency between a Mach number of 0 and 0.36 for the deep-chute and the deep-chute/setback-ejector nozzles were 0.039 and 0.061, respectively.

The nozzle discharge coefficients of the deep-chute and the deep-chute/ setback-ejector nozzles, as described previously, are presented in Figure 296. By definition the discharge coefficients of the suppressor, with and

366

Legend (top left):
○ Unsuppressed Plug Nozzle
□ Deep-Chute Nozzle
△ Deep-Chute/Setback-Ejector Nozzle

(a) Free-Stream Mach No., 0

(b) Free-Stream Mach No., 0.36

Axis labels:
Nozzle Efficiency, $(F-D_t)/F_i$
Nozzle Discharge Coefficient, C_{D8}
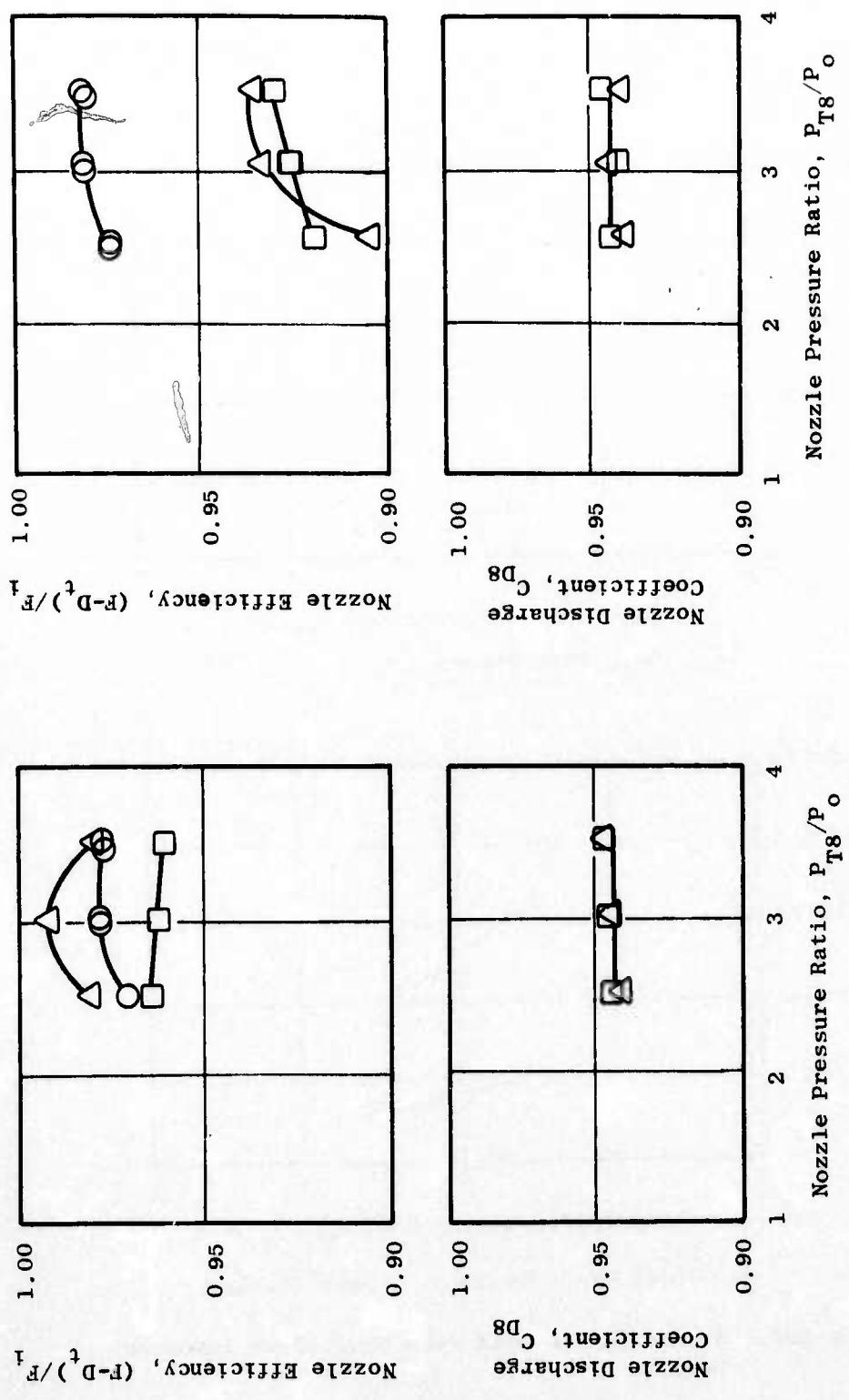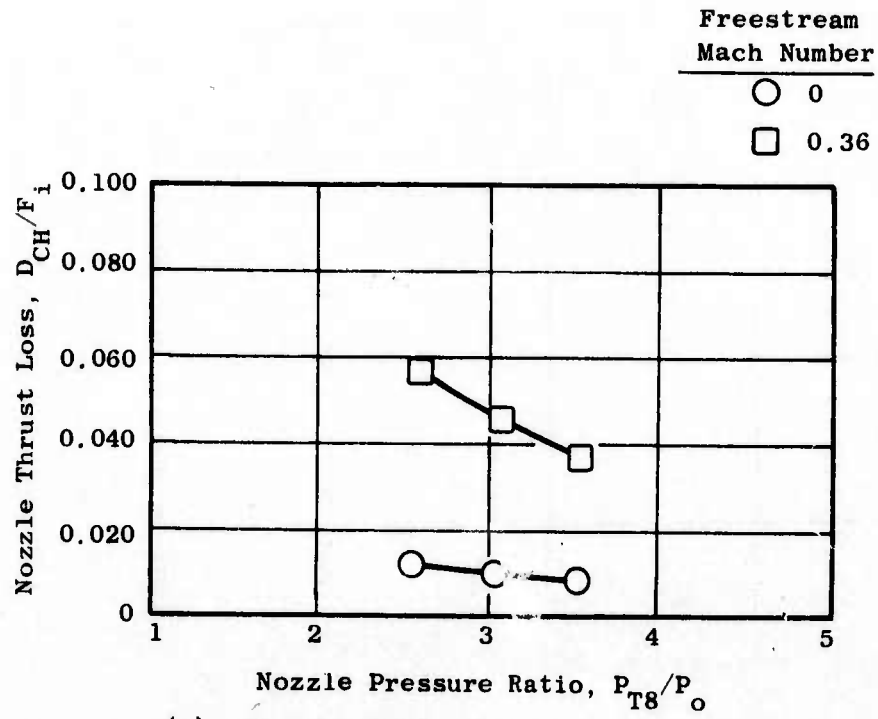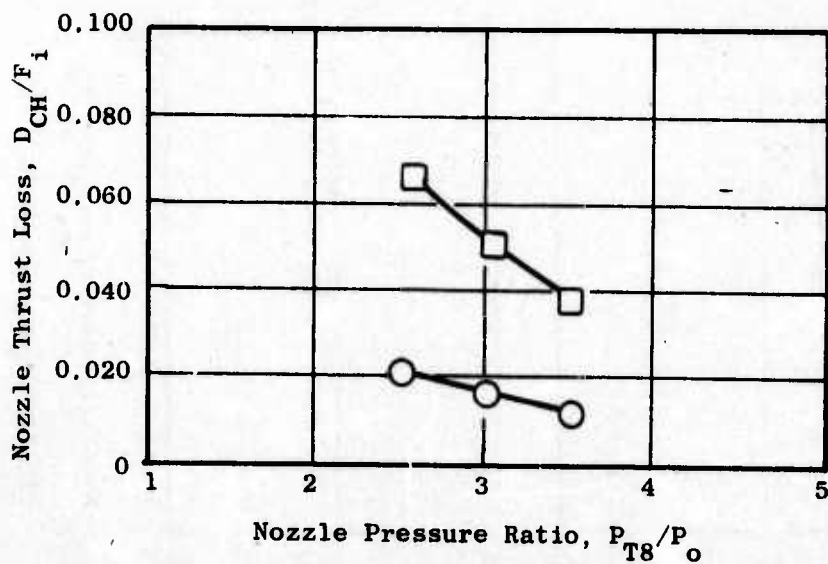Nozzle Pressure Ratio, P_{T8}/P_o

Figure 296. Comparison of Performance for Unsuppressed Plug Nozzle and 32-Deep-Chute Suppressor Nozzle with and without Ejector Shroud.

367

(a) Deep Chute Nozzle

(b) Deep Chute/Setback-Ejector Nozzle

Figure 297. Nozzle Thrust Loss from Chute-Base Pressure
Drag.

without an ejector, should be the same since the internal flowpath and exit area were the same.

The chute-base pressure distributions for the deep-chute and the deep-chute/setback-ejector nozzles are shown in Figures 298 and 299. The aerodynamic performance results obtained from this series of tests did indeed substantiate the pretest prognosis that the 32-deep-chute/plug suppressor nozzles would be a good performer.

3.4.2   Final Engine Suppressor Tests

Acoustic Tests

The tests of the 32-deep-chute suppressor at the Edwards Flight Test Center, North Site, were conducted on a J79-8/15 dry turbojet engine which had been prepared along with the sound field to minimize and effectively eliminate turbomachinery and other engine noise sources from radiating to the far-field. Preparation of the facility and testing of the nozzle configurations was a highly coordinated activity of both this program and the DOT High Velocity Jet Noise Source, Location and Reduction Program. The test site was prepared as part of the Task 1 effort specified in the DOT High Velocity Program. Figure 300 is a photograph of the sound field and engine test stand. The sound field consisted of 13 microphone (mic) positions equally spaced around the 160-foot measurement arc from 40° through 160° from the inlet. The acoustic arena was completely leveled and rolled to produce a smooth surface around the measurement arc. A dual-microphone system was employed at each angular station which consisted of a high mic located at the engine centerline (12 feet) and a low mic positioned 2 feet off the ground. The dual-mic system was used to correct out the ground reflections inherent in the acoustic measurements by superimposing portions of the SPL spectra for the respective mics where high confidence in the ground reflection corrections are known. From this a composite spectrum was obtained which approached free-field conditions.

The engine employed a calibrated bellmouth and treated inlet section with splitters to reduce forward-radiated noise. A treated housing, mounted over the engine as shown in Figure 300, was used to minimize the casing-radiated noise. A turbine exhaust suppressor section was used to eliminate aft-radiated engine noise. The desired net effect from the full engine treatment was to obtain, effectively, a gas generator for the jet exhaust nozzle acoustic testing. It was found that the contamination to the 1/3 octave jet noise from the turbomachinery noise was less than 1 dB (worst case). (See Appendix A for facility description details.)

The engine setup included instrumentation systems to measure inlet weight flow, total pressure and temperature aft of the turbine exhaust suppressor (used to calculate ideal jet velocity), suppressor base static pressure, and chute surface temperature. Static thrust measurements also were obtained from the calibrated engine thrust stand built into the test facility.
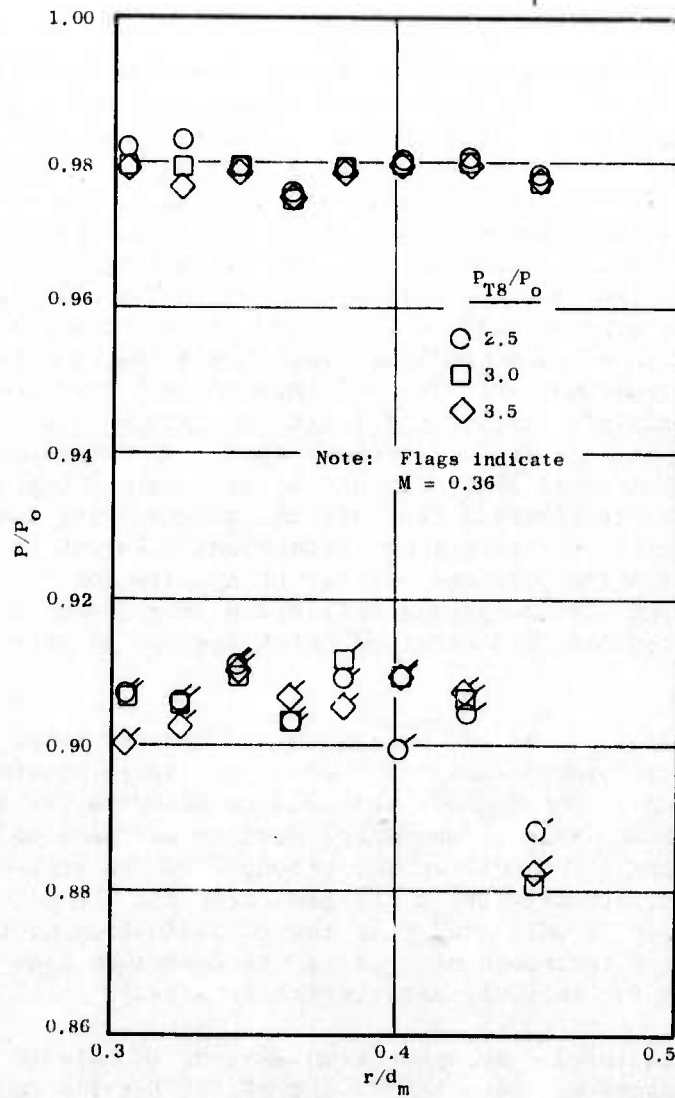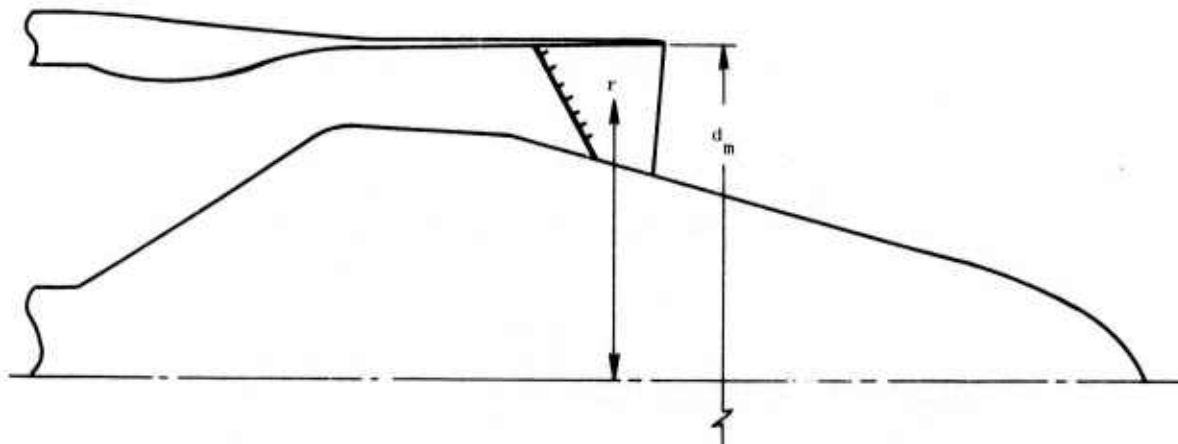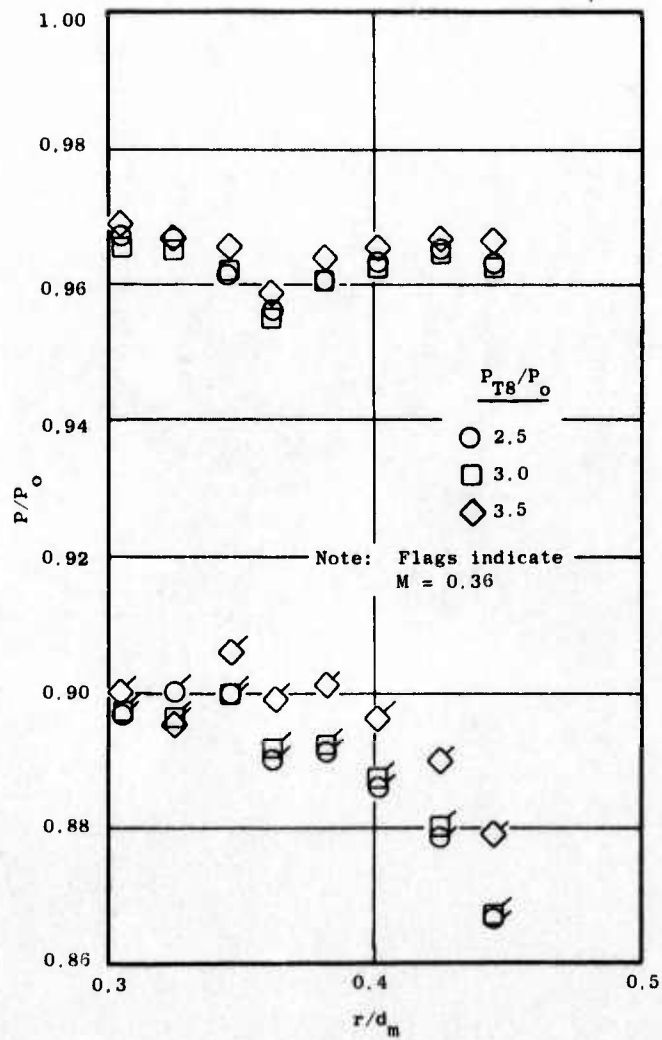
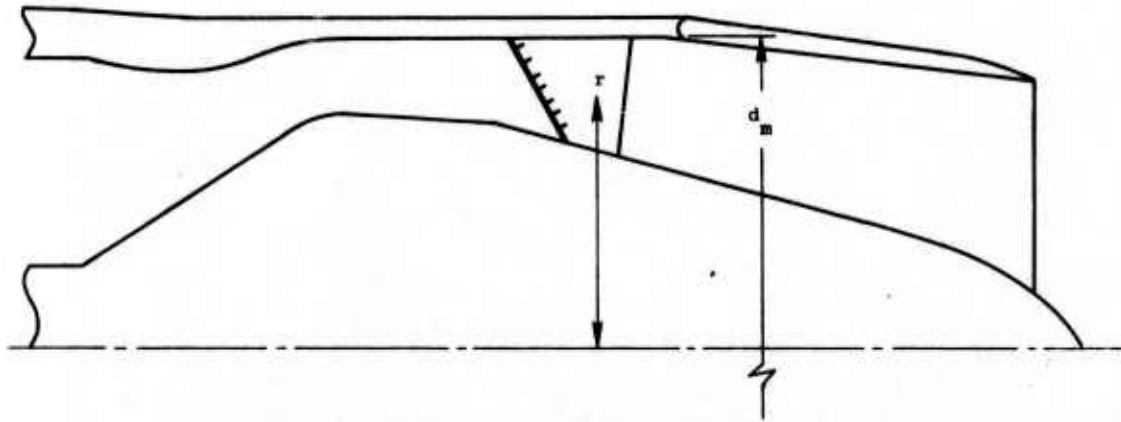Figure 298. Chute Static Pressure Distribution, 32-Chute.

Figure 299. Chute Static Pressure Distribution, 32-Chute with Ejector.

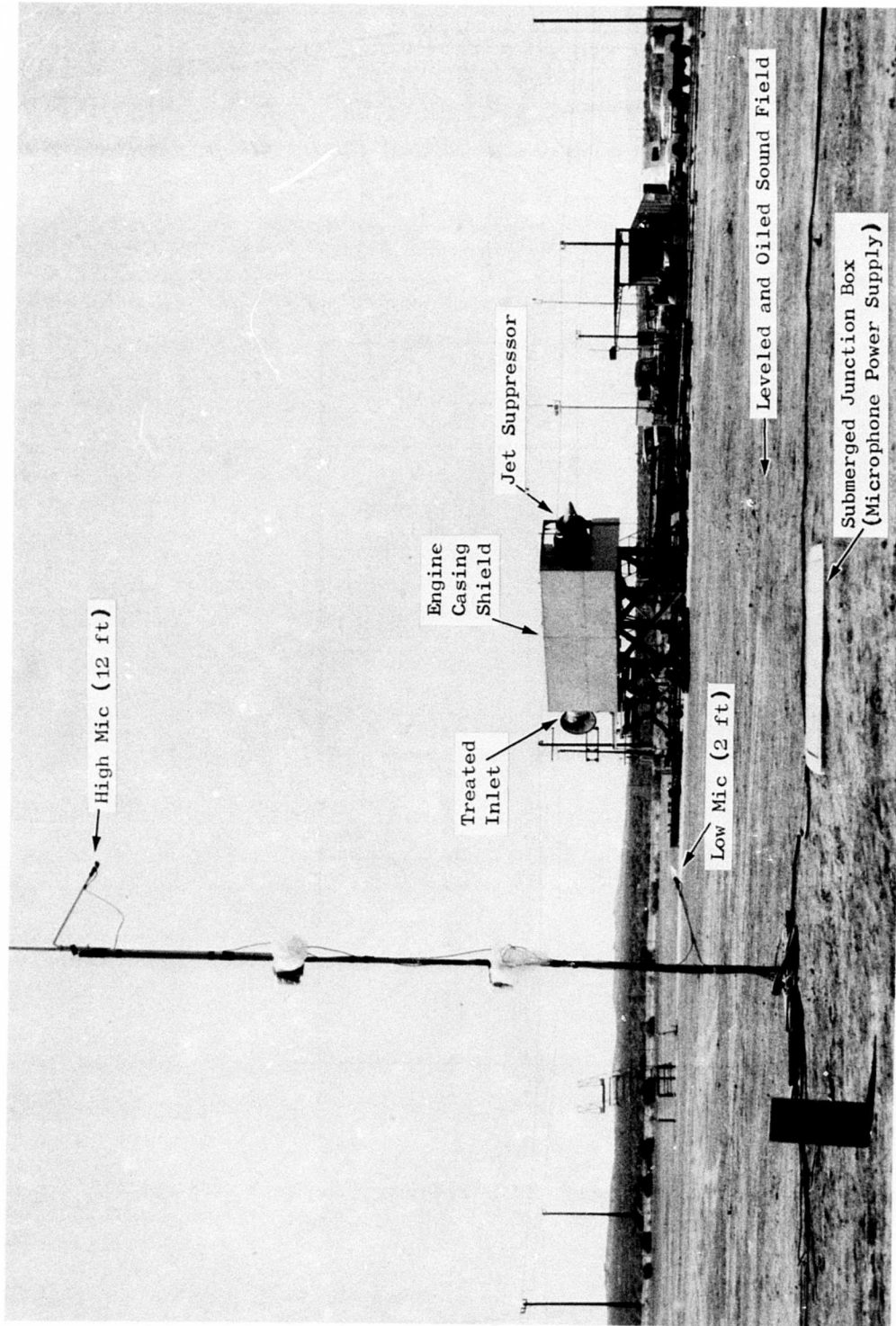Figure 300. Edwards Sound Field and J79 Engine Facility.

High Mic (12 ft)

Treated Inlet

Engine Casing Shield

Jet Suppressor

Low Mic (2 ft)

Leveled and Oiled Sound Field

Submerged Junction Box (Microphone Power Supply)

Figure 301 shows the final suppressor configuration mounted on the J79 engine. It was a multielement suppressor consisting of 32 deep chutes equally spaced around the 30° included-angle plug centerbody. The ratio of total exit area (blocked area plus primary flow) to the primary flow area alone was 2.1. The chutes formed parallel-sided primary-flow passages which were canted 5° aft toward the plug surface. The details of the suppressor selection and design are described in Section 3.3.

The treated ejector mounted on the multichute suppressor and J79 engine is shown in Figure 302. The ejector had a slight converging area with the ratio of ejector inlet to exit area of 1.07. The overall ejector length-to-nozzle overall diameter, L/D_0, was 0.55. The acoustically treated ejector liner, specified from model treated ejector tests, consisted of a single layer of foam metal (0.16 inch thick, 90-95% porosity, MTL: Nickel-Chrome) and 2 inches of high temperature ceramic fiber (3 lbs/ft^3/in thickness, MTL: Boron-Silicon). The liner material (ceramic fiber and foam metal) was compressed to fill the 1-inch cavity depth of the ejector surface. A perforated sheet metal faceplate (24 ga., 37% open, 0.045-inch-dia holes, MTL: 304 SS) was used to contain the treatment in the ejector. (See Section 3.2.2 for acoustic treatment design details.)

The baseline nozzle for these configurations was a 20.82-inch-diameter unsuppressed conical nozzle with an effective exit flow area of 338 in^2. Figure 303 shows the baseline nozzle mounted on the J79 engine. Tests were conducted over the J79-8/15 operating line from ideal jet velocities of 520 to 2190 ft/sec at nozzle pressure ratios of 1.08 to 2.58.

Acoustic Results and Analysis

The acoustic data obtained on the J79 engine configurations with the high and low microphone systems underwent corrections for the free field as described in Reference 6. Corrections for turbomachinery tones and facility reflections were made to the data along with adjustments for electronic noise. The resultant J79 size combined (high and low mic) spectra on the 160-foot measuring arc were corrected to standard day conditions of 59° F, 70% relative humidity. The data were scaled to the full engine size arc (320 ft) and frequency range (63-10,000 Hz) using a diametrical scale factor of 2:1. The data were then extrapolated to sideline distances of 300, 1500, and 2128 feet for data presentation purposes. A summary of the acoustic results for each configuration is contained in Appendix C along with pertinent engine parameters determined for each test condition.

Figure 304 illustrates this peak PNL suppression at the 2128-foot sideline attributed to the 32-chute suppressor and shows approximately 10 dB suppression at the high velocity point. Figure 305 shows the normalized peak PNL for the 32-chute suppressor with the treated ejector. A comparison with conical nozzle results shows PNL suppression levels of 11 to 12 dB above 1800 ft/sec. A typical PNL directivity pattern for the conical nozzle is shown in Figure 306a at the 2128-foot sideline over the velocity range
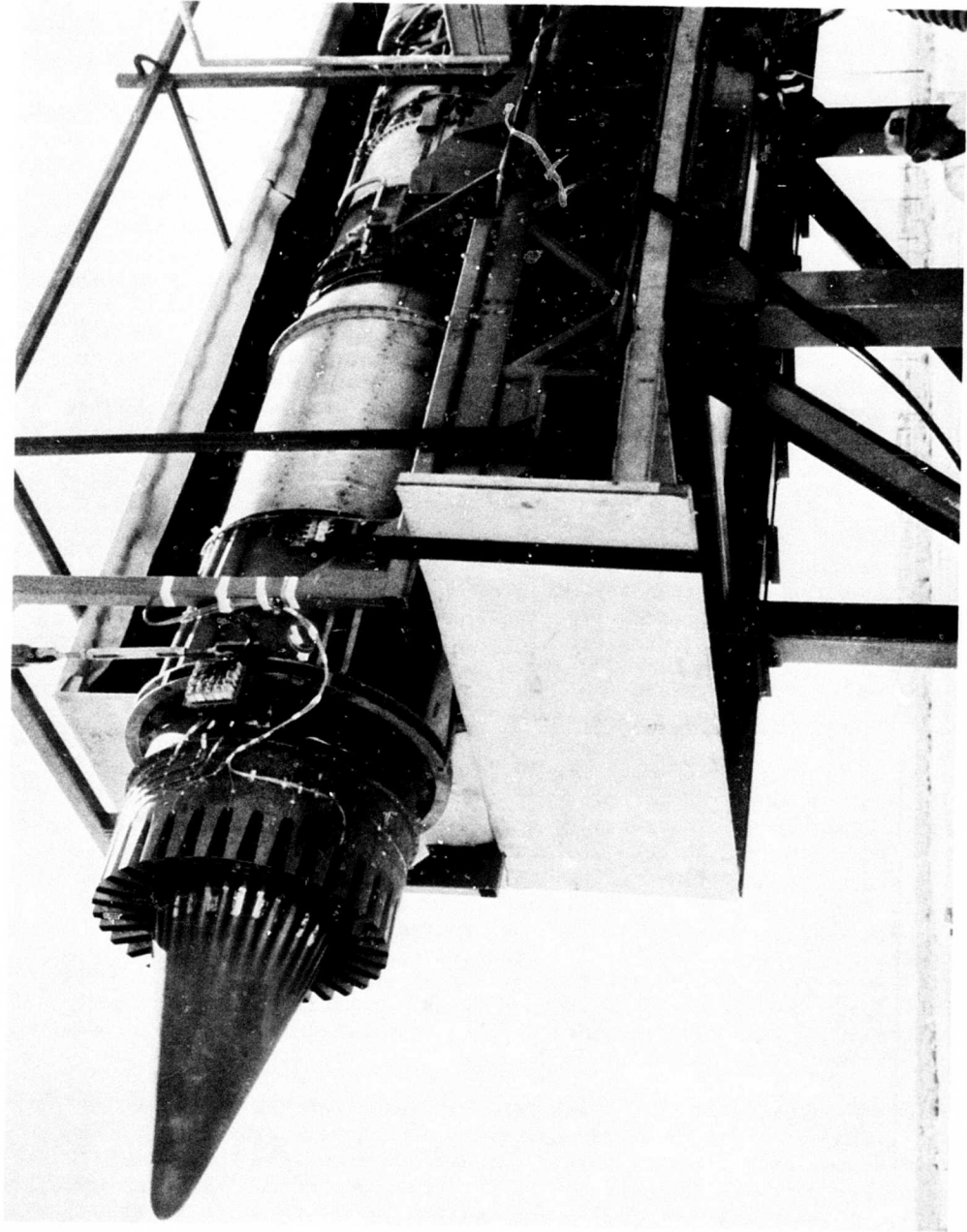
Figure 301. Multichute Compressor Mounted on J79 Engine.
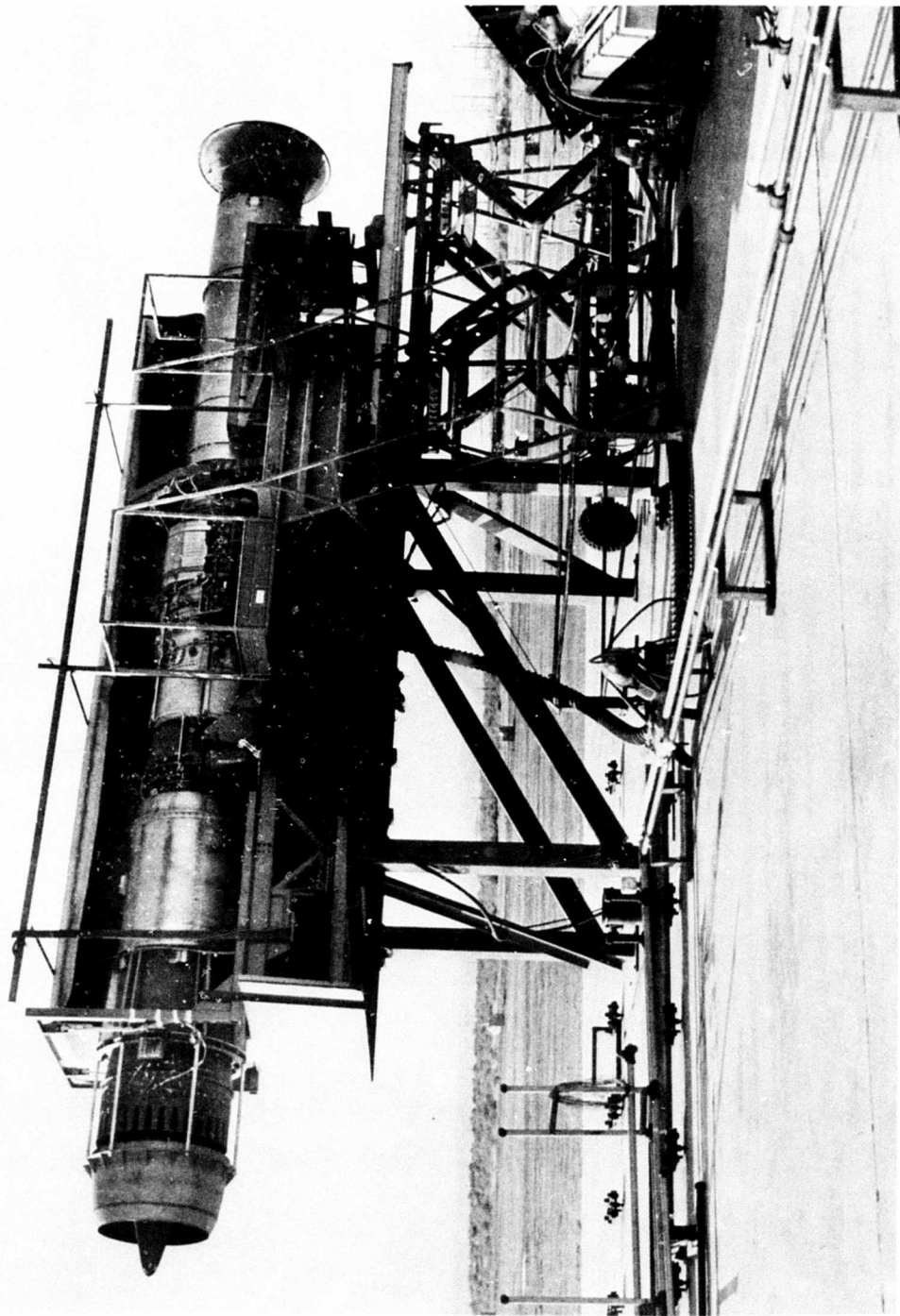
Figure 302. J79 Engine with Multichute Suppressor and Ejector.
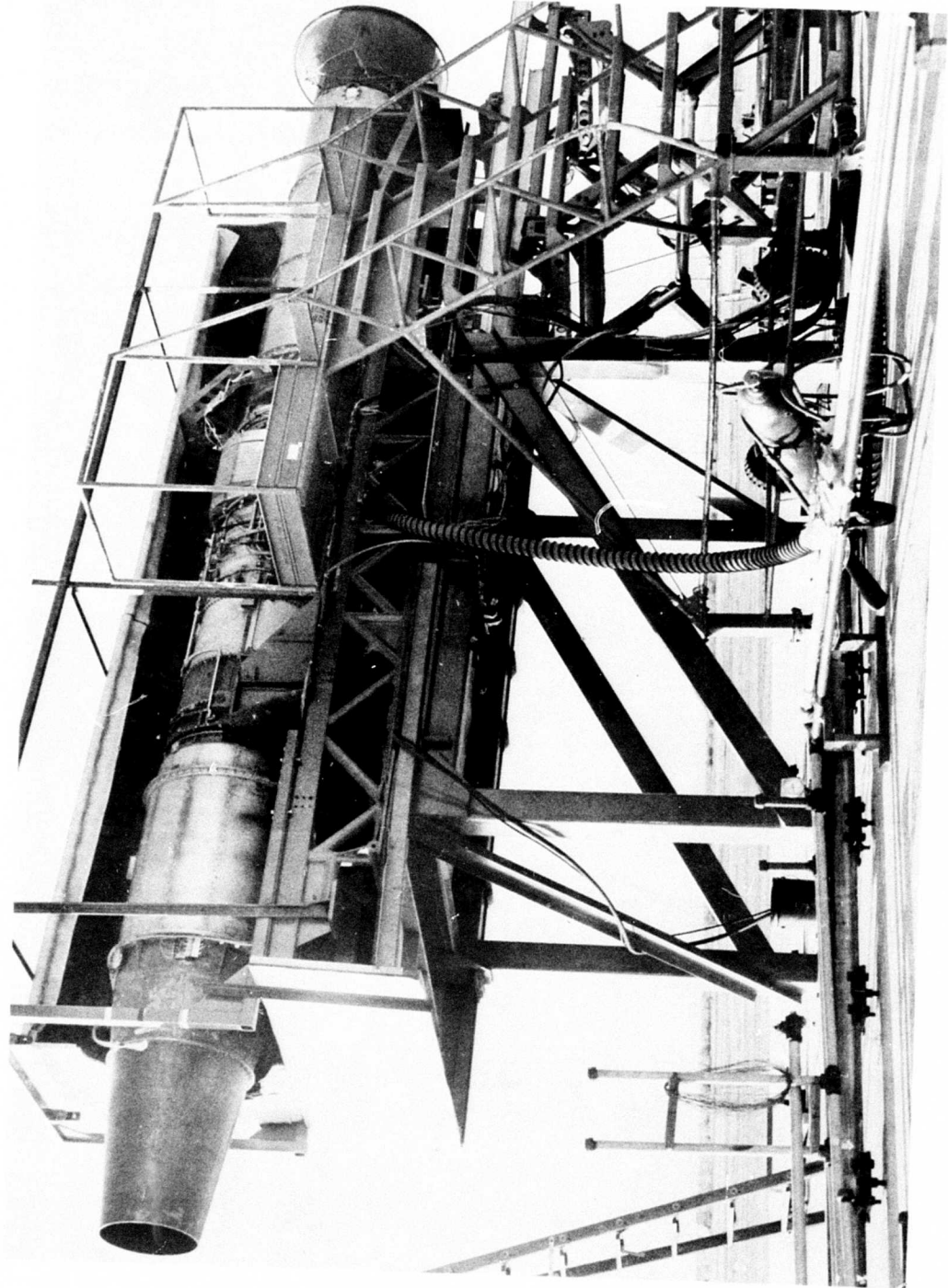
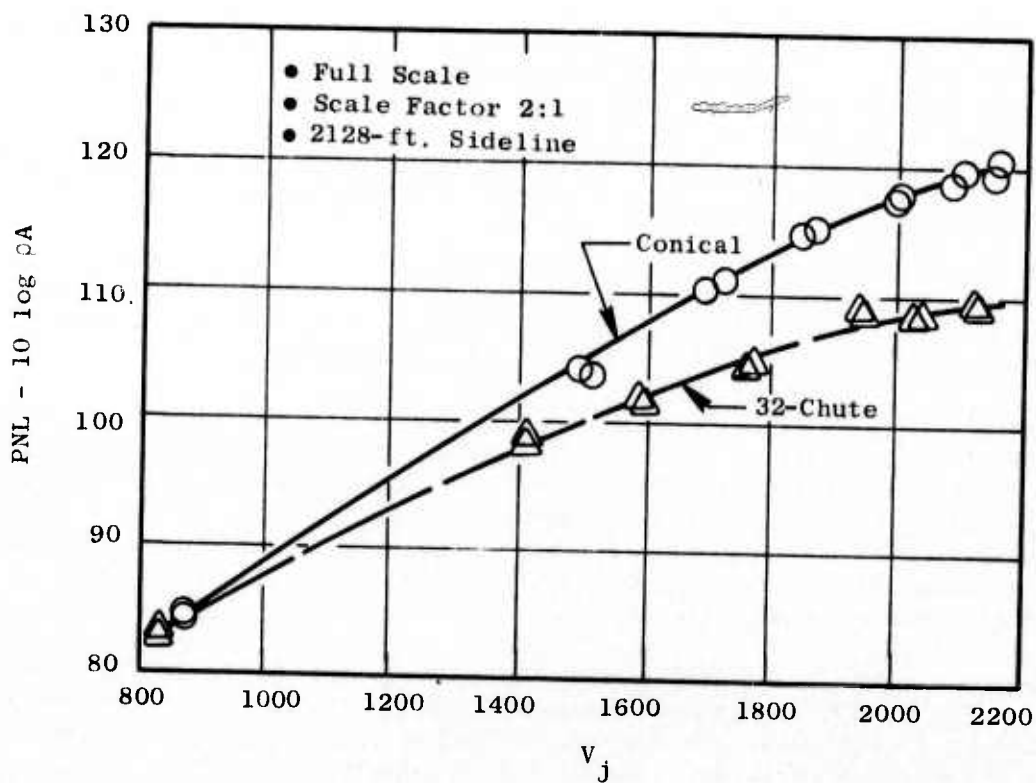Figure 303. Baseline Nozzle Mounted on the J79 Engine.

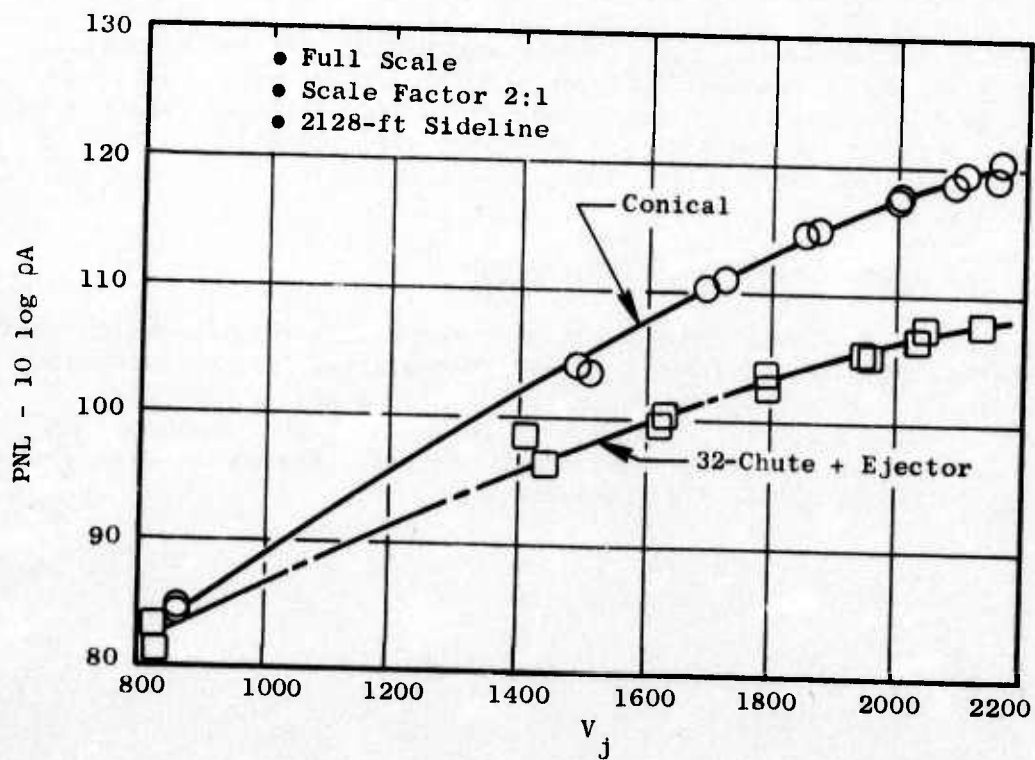Figure 304.   Peak PNL Comparison of Suppressor and Baseline Nozzles.

Figure 305.   Peak PNL Comparison of Suppressor with Ejector and
Baseline Nozzles.

377

tested. The peak angles for all speeds are between 130° and 140° from the inlet. The influence of shock in the forward and aft angles also is noted at the higher velocity points (V_j = 2008 and 2159 ft/sec) as shown in the angular distributions of PNL for these conditions. The PNL directivity for the 32-chute suppressor is similarly displayed in Figure 306b and illustrates a nearly uniform peak angle of 110° to 120° from the inlet.

The 32-chute suppressor with treated ejector results gave a PNL directivity as shown in Figure 306c which indicates that, although this peak angle is still at 110°, the directivity is more pronounced with a more rapid decrease in PNL on either side of the 110° position.

The 300-foot sideline normalized SPL spectra at peak angle for the three test configurations are shown in Figures 307a, b, and c. Figure 307a shows conical nozzle spectra while the 32-chute suppressor and 32-chute suppressor with treated ejector are shown in Figures 307b and c, respectively. The suppressed spectra are predominately high-frequency-weighted over the entire operating range of the J79 engine indicating that coalescence of the suppressed primary flow elements had not occurred.

The effect of the treated ejector is illustrated in Figures 308, 309, and 310. Figure 308 compares the peak PNL distributions of the conical nozzle and suppressor configurations over the velocity ranges tested. A nearly uniform suppression increase of about 2 dB is observed for the treated ejector configuration relative to the suppressor alone. The PNL directivity comparison for the suppressor configurations shown in Figure 309 suggests that the ejector was more effective at angles other than peak 110°.

Spectral comparisons of the 32-chute suppressor with and without the treated ejector are presented in Figure 310 for two velocity conditions, V_j ∿1600 and 2130 ft/sec. The comparison shows 2-3 dB SPL suppression over the frequency range for the treated ejector at 1600 ft/sec and 1 to 2 dB suppression above 400 Hz at 2130 ft/sec.

Aerodynamic Performance Assessment

Aerodynamic assessment of the J79 measured static thrust results show that a static C_{fg} level of 0.964 to 0.968 was obtained for the 32-chute suppressor at a nozzle pressure ratio of 2.5. This performance level is slightly less than that of the 36-deep-chute nozzle tested earlier, and about the same level as the 32-chute model results. Ejector results show a lower C_{fg} (∿0.939) at the 2.5 pressure ratio.
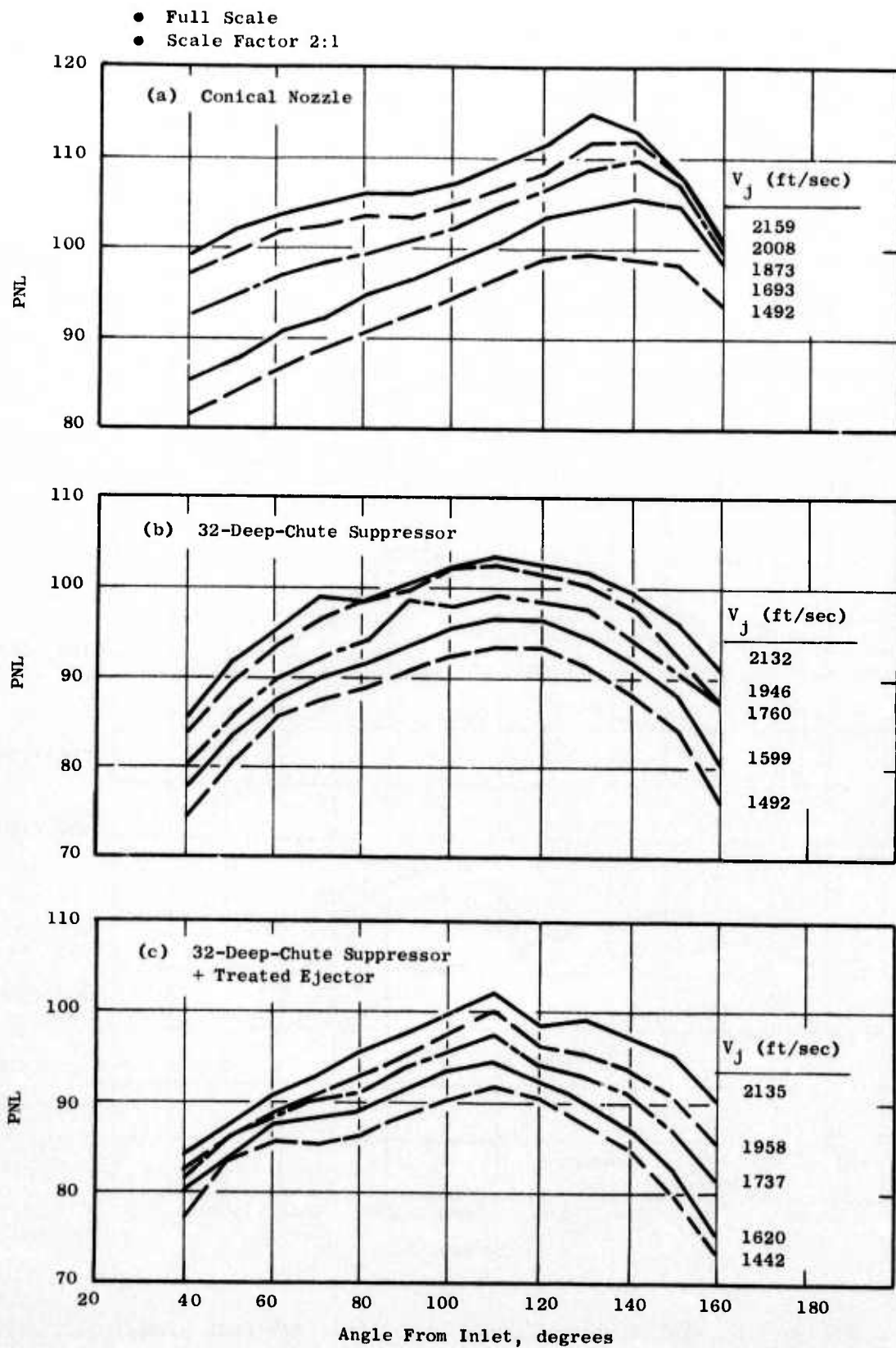
378

Figure 306. PNL Directivity Comparisons at the 2128-foot Sideline.
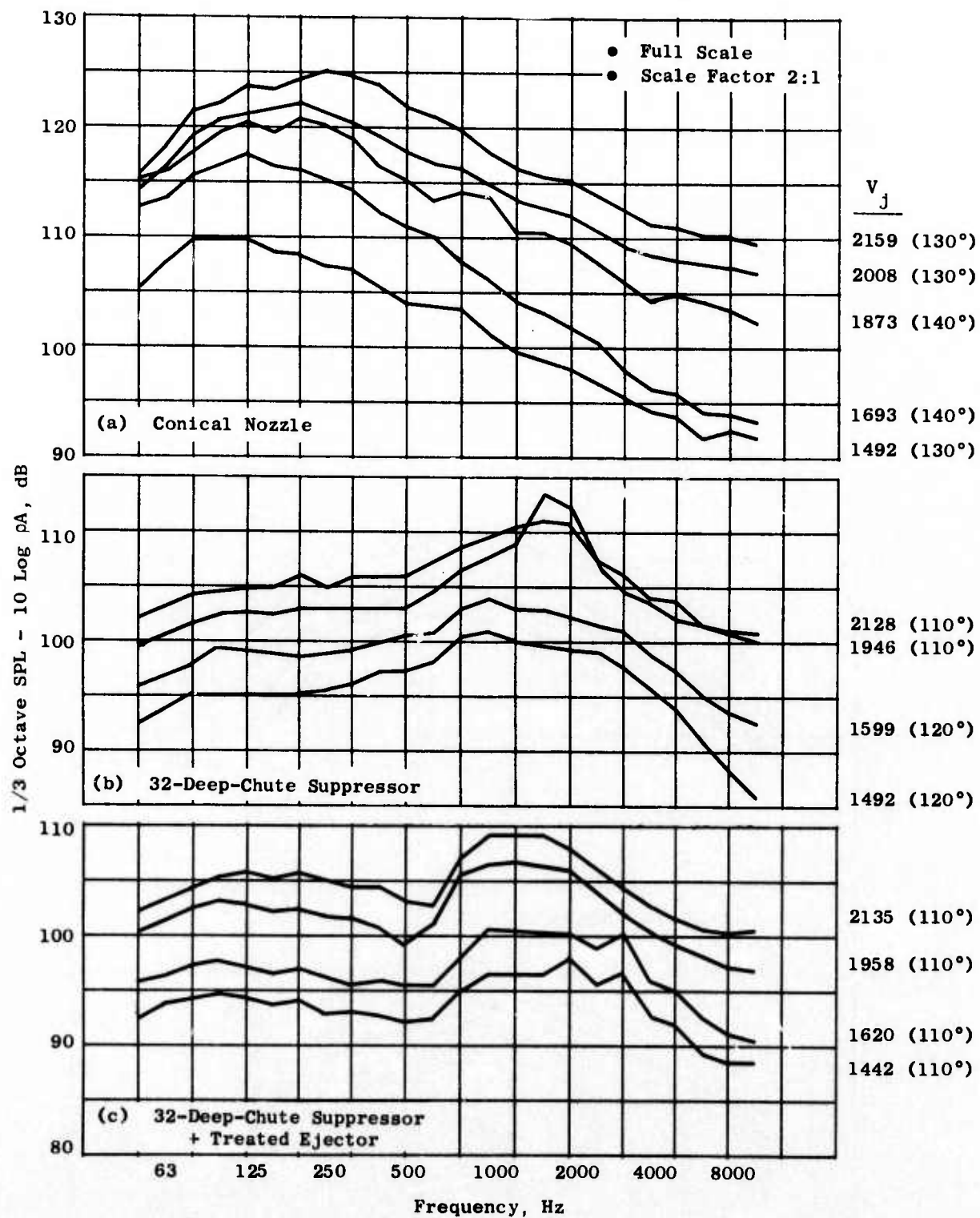
379

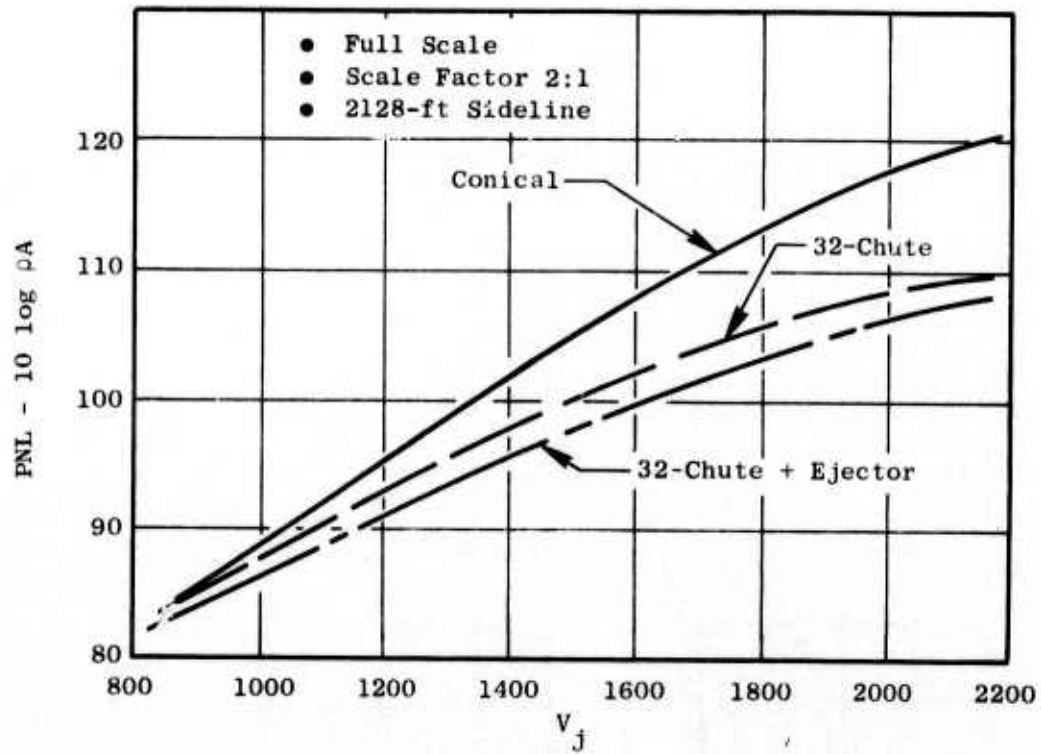Figure 307. SPL Spectra Comparison at the 300-foot Sideline.
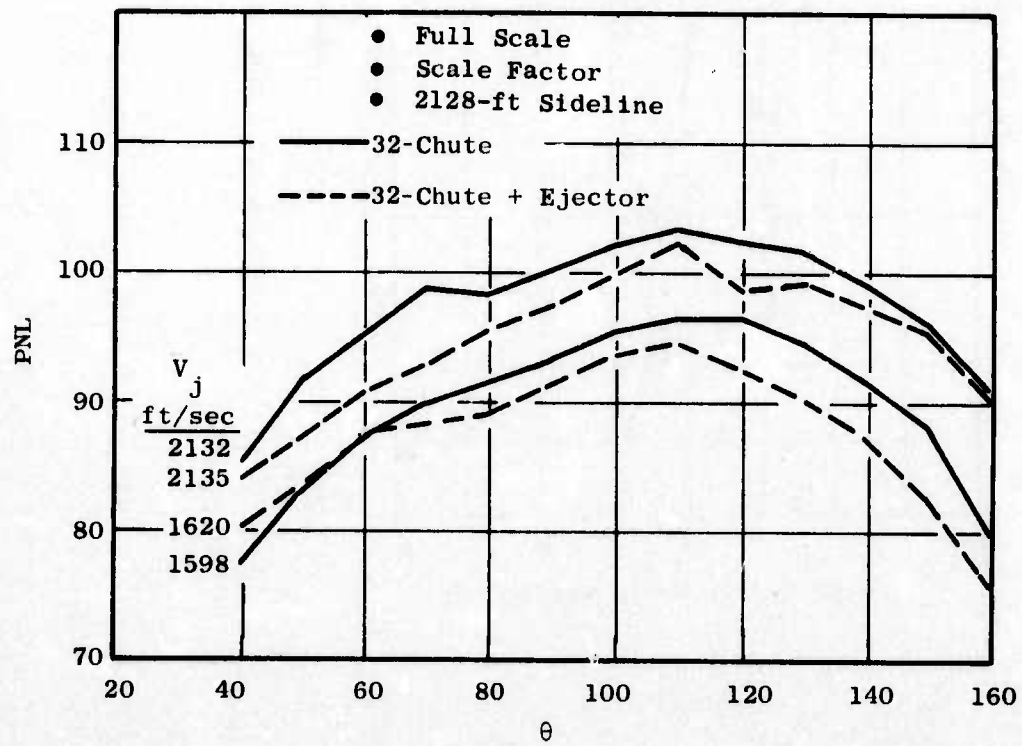
Figure 308. Peak PNL Comparisons.

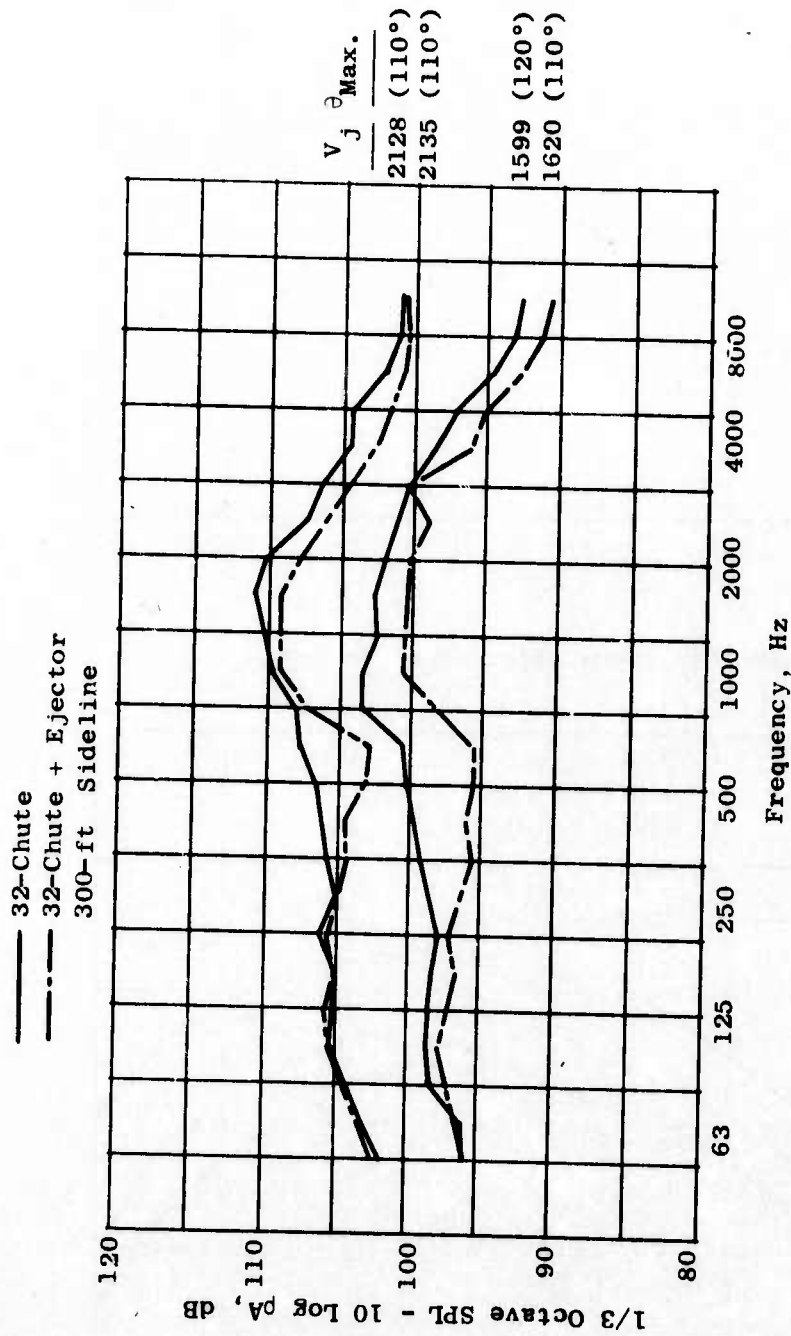Figure 309. PNL Directivity Comparisons.

381

Figure 310. SPL Spectra Comparisons.

Laser Velocimeter Tests on the Engine Suppressor

Mean and turbulent velocity measurements were obtained from jet plume surveys taken with the laser velocimeter on the J79 engine nozzle configurations for evaluation in the DOT High Velocity Jet Noise Source Location and Reduction Program. A comparable test matrix was employed for both model and engine LV tests. Results from specific test conditions ($V_j \sim 1650$ ft/sec, $P_{T8}/P_O \sim 2.0$) were used in this program to compare with similar results obtained with the model suppressor (see Section 3.4.3). The test setup on the J79 32-chute suppressor is shown in Figure 311 with both the LV and ellipsoidal mirror microphone mounted on the actuation cart. (The ellipsoidal mirror microphone was used exclusively in the DOT High Velocity Jet Noise Program to document noise source locations.)

3.4.3 Model and Engine Data Comparison

Acoustic Data Comparison

Comparisons of model and J79 engine data show good agreement on a peak PNL basis. Both the conical nozzle and the 32-deep-chute suppressor were compared on a 2128-foot sideline, all data (J79 and model) scaled to typical SST size and frequency range, and corrected to free-field and standard day conditions as shown in Figure 312. The high velocity condition with the conical nozzle was corrected for shock tones. The peak PNL was normalized by 10 log ρA to account for discrepancies in full-scale physical nozzle exit areas compared to the design intent, and to account for slight density changes resulting from variations in setting test conditions.

A similar comparison of the treated ejector configurations is shown in Figure 313. PNL directivity comparisons at the 2128-foot sideline of model and engine configurations are shown in Figures 314a, b, and c for the conical nozzle, 32-deep-chute suppressor, and suppressor with ejector nozzles, respectively. The directivity comparisons show that, for the engine conical nozzle (Figure 314a, the peak angle is at the 130 - 140° location, consistent with the model results. Comparison of model and engine directivity for the suppressor alone is quite good in Figure 314b and reflects the fact that both model and engine suppressors maintained the same suppressed directivity characteristic with peak angles at 110° to 120° from inlet.

The ejector directivity comparison illustrated in Figure 314c indicates the same peak angle for both model and engine (110°) at the velocities shown, but the engine directivity has a more peaked distribution.

Spectral comparisons of these nozzle configurations are shown in Figures 315, 316 and 317 for the conical nozzle, 32-chute suppressor alone, and with treated conical ejector, respectively. The comparisons were made for representative velocities over the operating range at peak angle PNL on a 300-foot sideline. The model and engine spectra agree reasonably well.
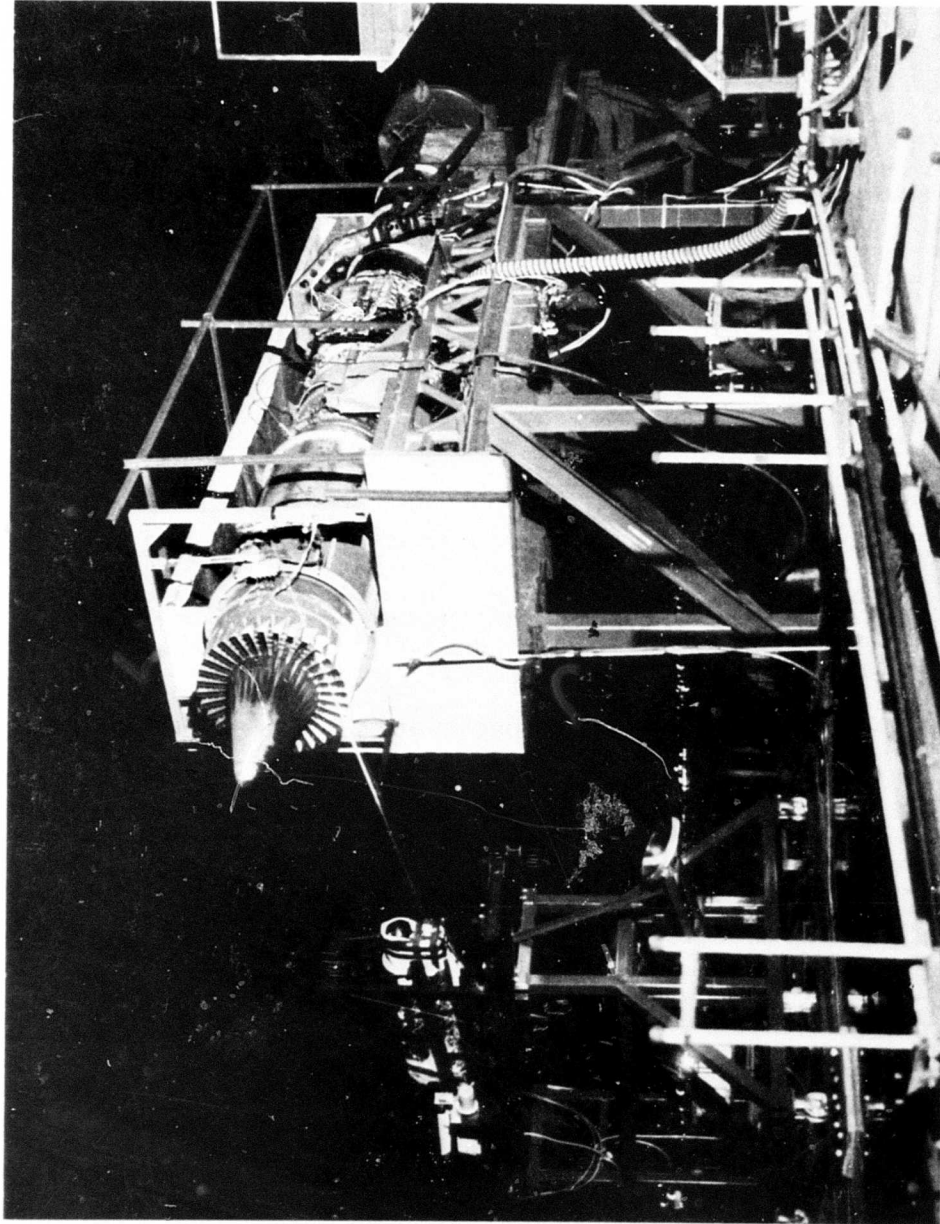
Figure 311. Laser Velocimeter Setup with the J79 Engine Suppressor.
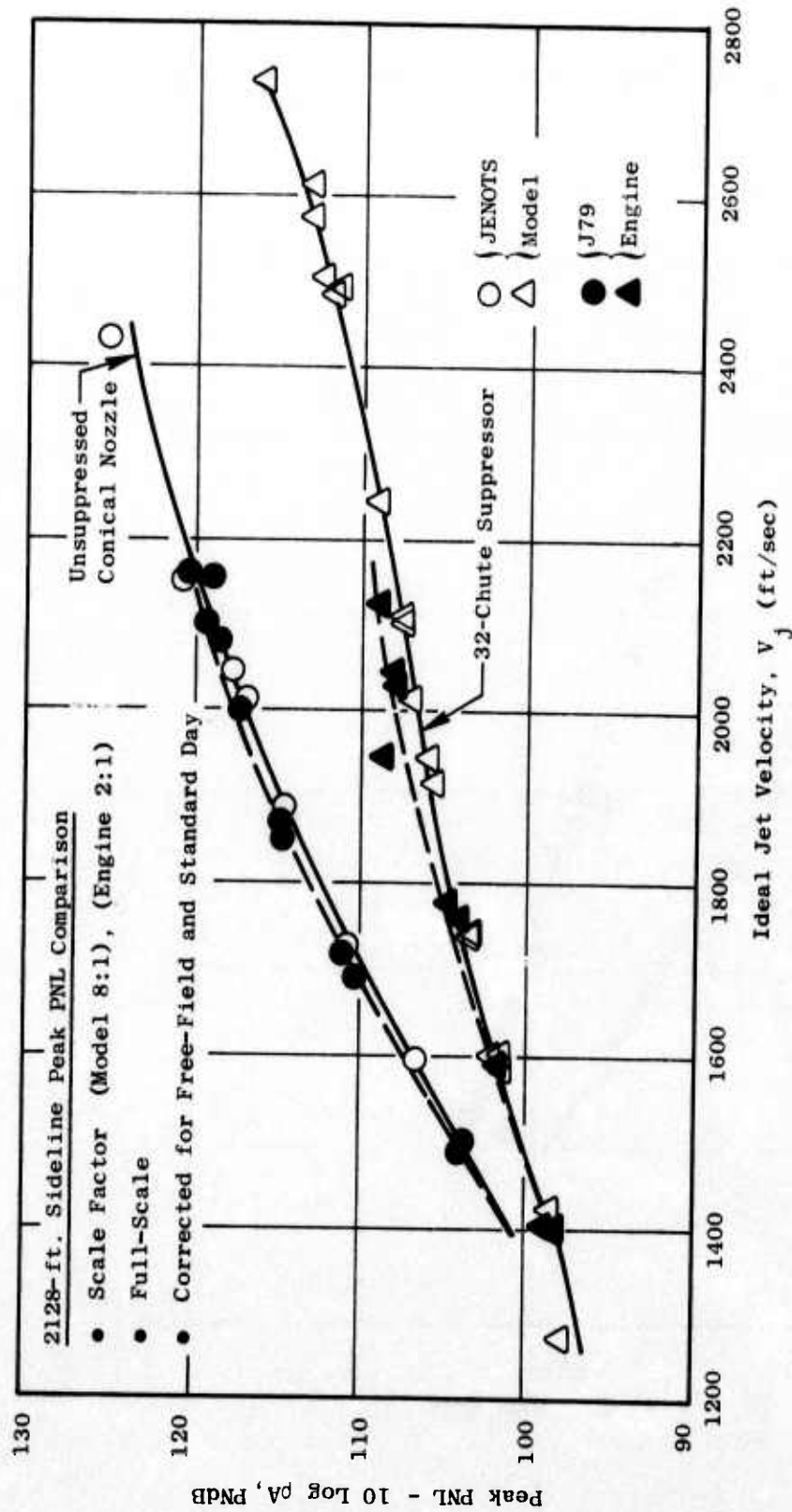
Figure 312. Model-to-Engine PNL Comparison with Suppressor and Baseline Nozzles.

385
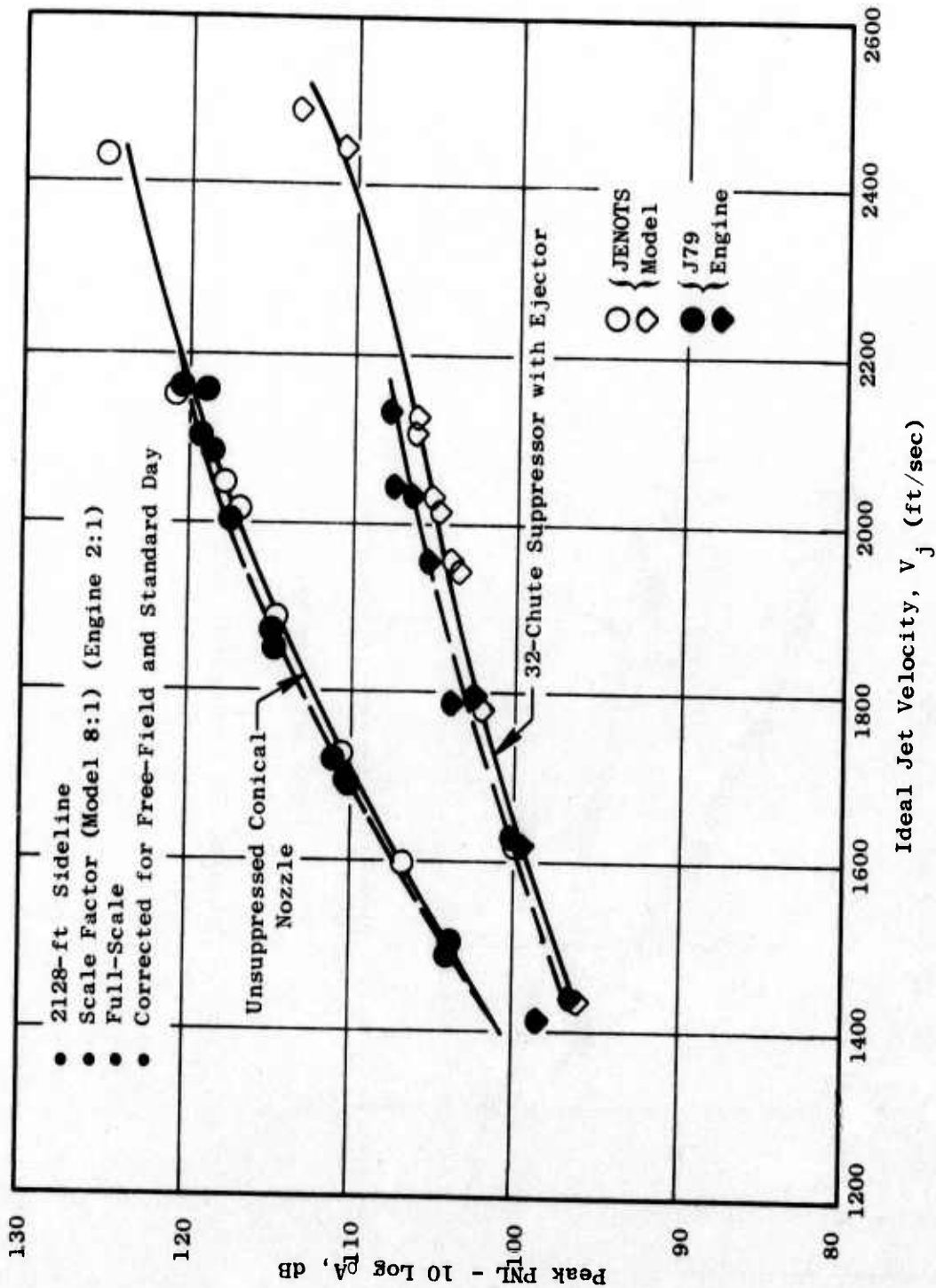
Figure 313. Model-to-Engine PNL Comparison with Treated Ejectors and Baseline Nozzles.

386
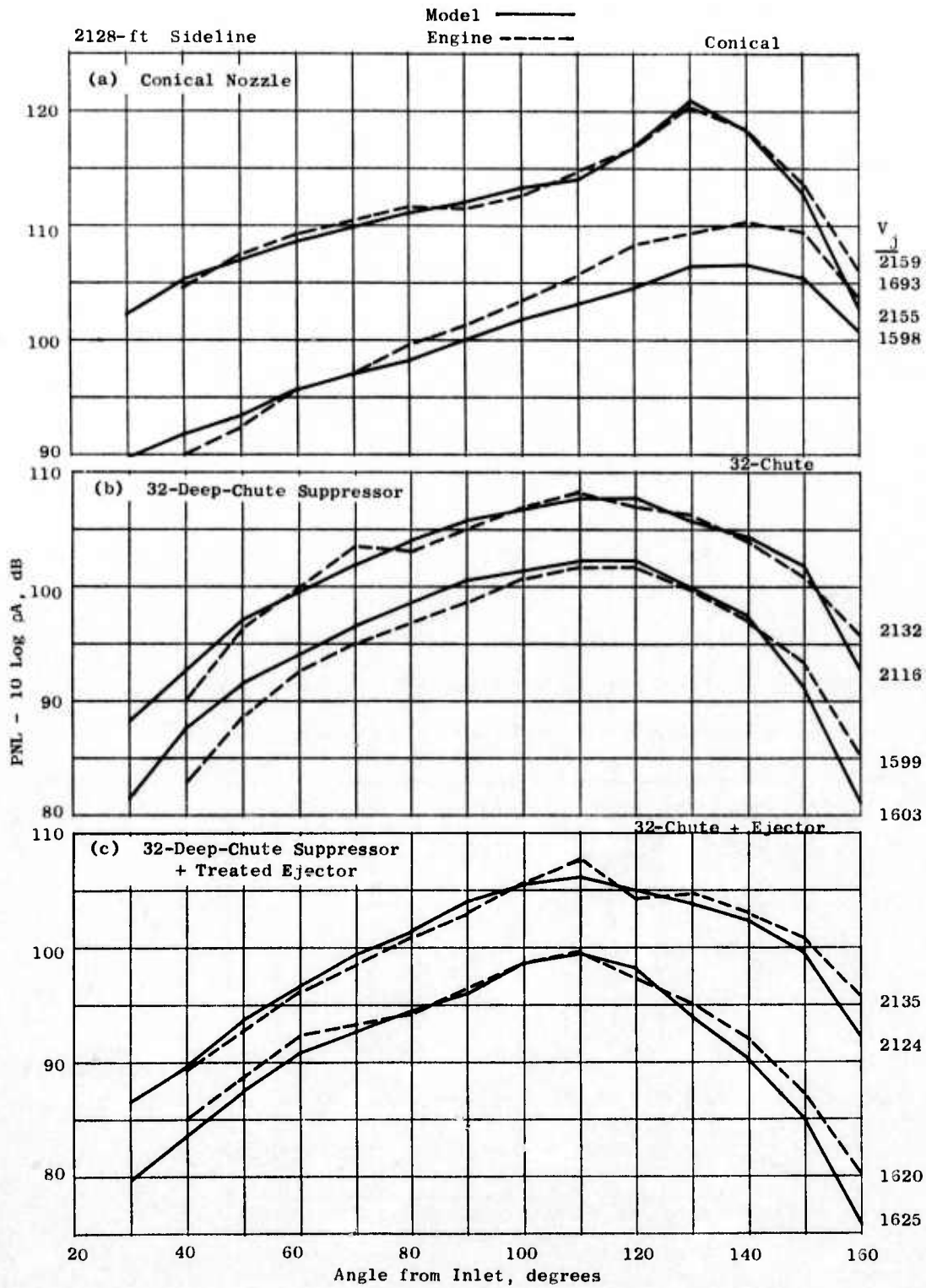
Figure 314. Model-to-Engine PNL Directivity Comparisons.
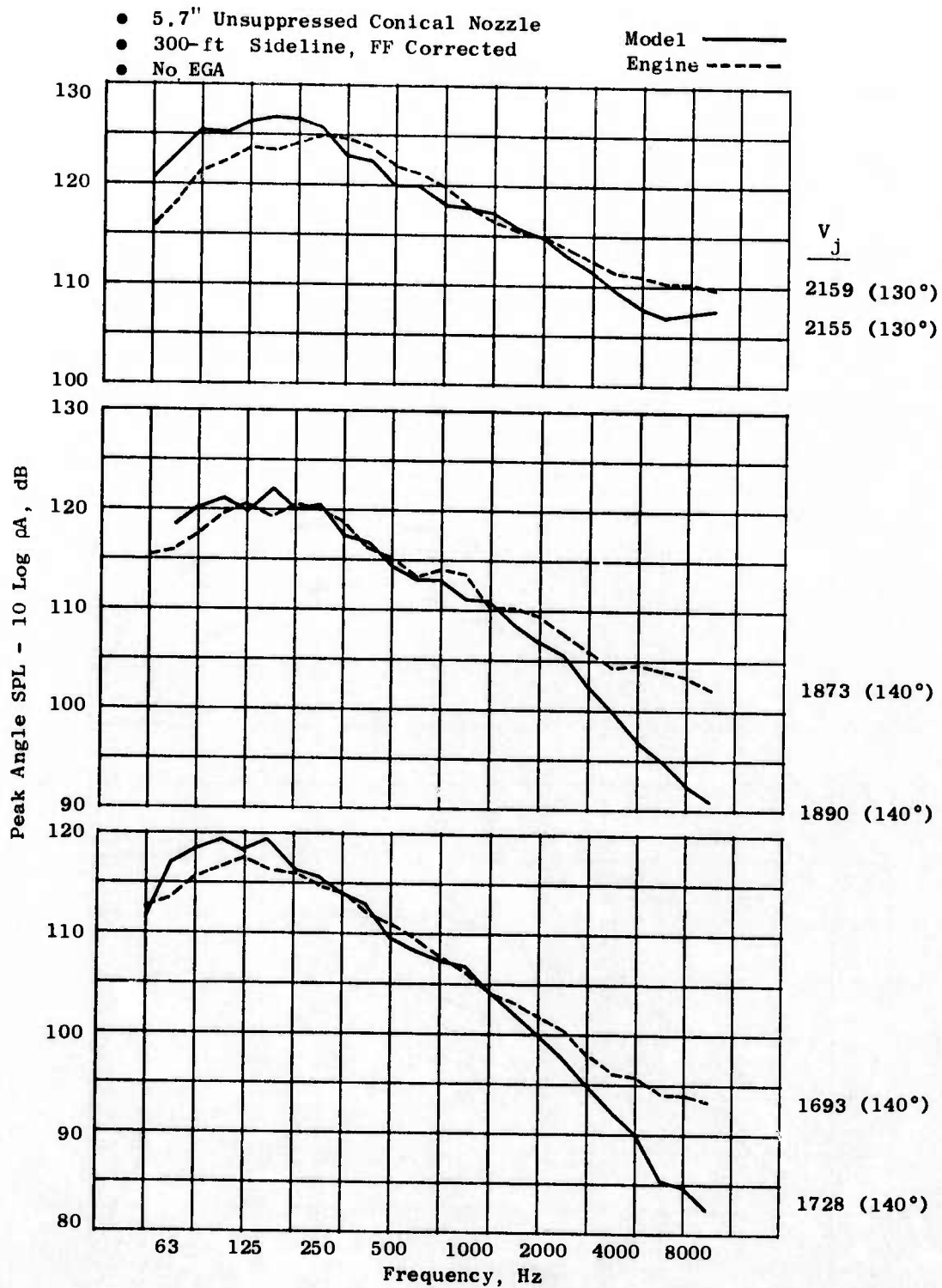
Figure 315. Model-to-Engine Conical Nozzle SPL Spectra
Comparisons.

388
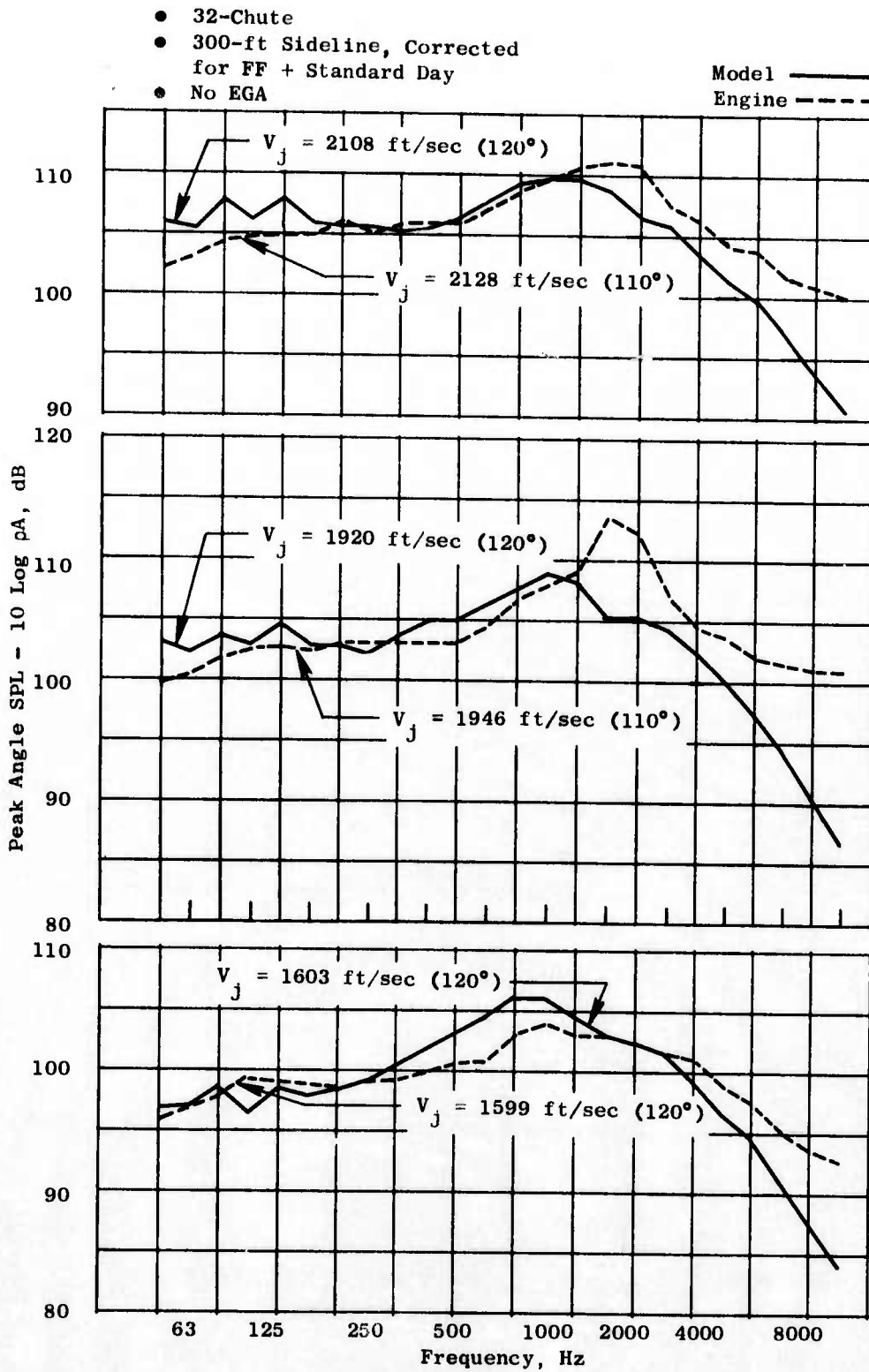
Figure 316.   Model-to-Engine 32-Deep-Chute Suppressor
SPL Spectra Comparisons.

389
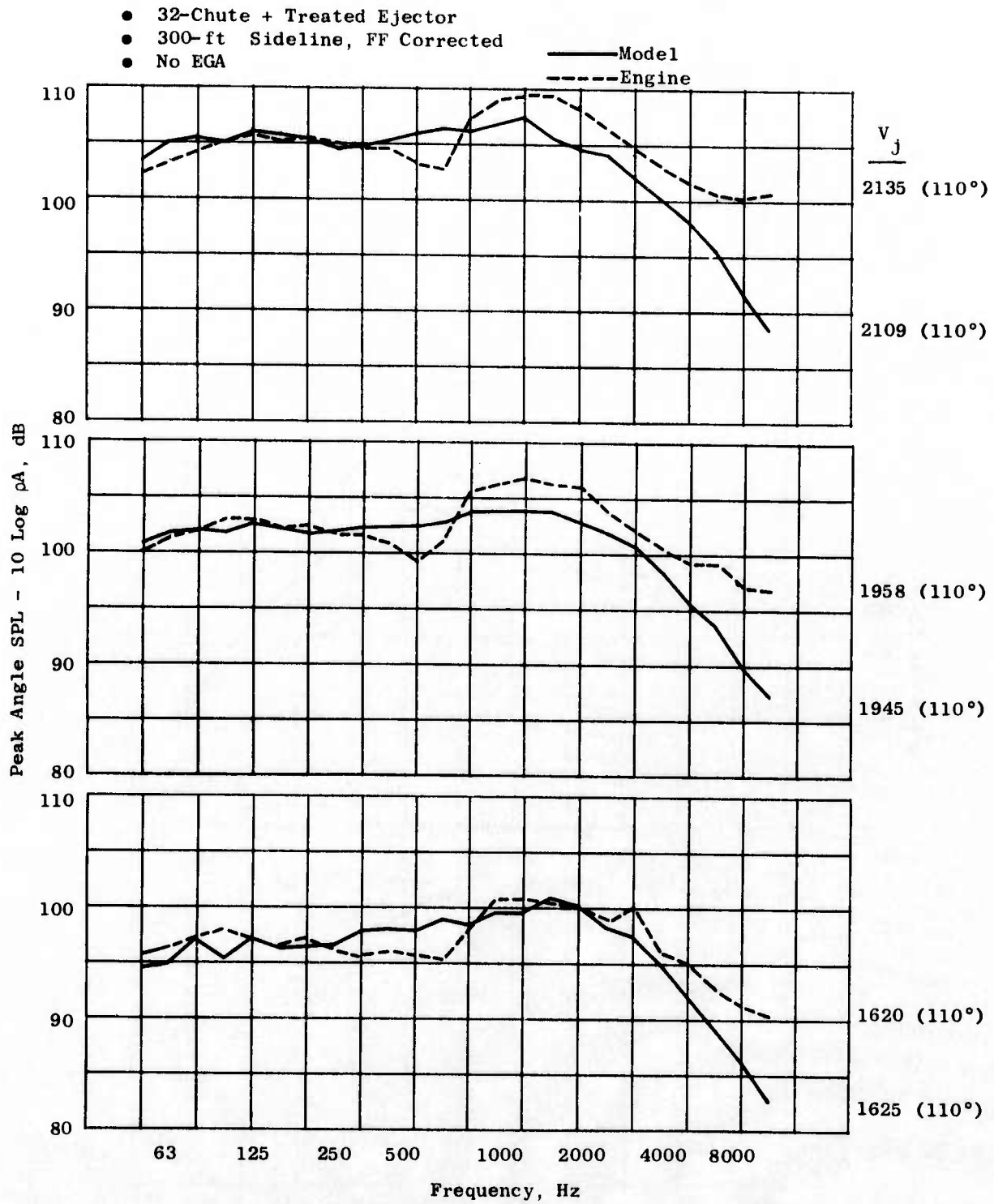
Figure 317. Model-to-Engine 32-Deep-Chute Suppressor + Treated
Ejector SPL Spectra Comparison.

390

Aerodynamic Performance Comparisons

The static performance comparisons of the model suppressor and J79 engine tests are shown on Figure 318. The 32-chute suppressor model results cover a range of nozzle pressure ratios from 2.5 to 3.5, while the engine results cover a range from 1.2 to 2.5. The 32-chute static performance curve is continous through both engine and model data.

The ejector performance comparison shows the cold flow model hardwall configuration to be about 4-4.5% higher in C_{fg} than the J79 suppressor with treated ejector at a pressure ratio of 2.5. Approximately 1.5 to 2.0% C_{fg} loss can be attributed to the scrubbing effect on the perforated treatment ejector lining as shown in Reference 30. The additional 2% thrust difference in part, may be attributed to the geometric differences of the aerodynamic model ejector and the treated ejector used in the J79 testing. The aerodynamic model had smooth internal and external flow lines, while the large scale treated ejector had a 2-inch flange just aft of the ejector inlet which was used for mounting the ejector to the suppressor shroud. The drag on this flange may have been a significant factor in the additional thrust loss with the engine ejector. Temperature effects also might be a part of the performance differences.

Comparisons of the chute-base pressure and chute-surface temperature distributions for the J79 engine and aerodynamic and acoustic models are shown in Figures 319 and 320. Figure 319 presents the model and engine base pressures and chute-surface temperatures for the 32-chute suppressor, while Figure 320 shows similar distributions for the ejector configurations. The comparison indicates that close agreement was obtained from the model and engine measurements.

Laser Velocimeter Mean Velocity Comparison

Hot-jet plume surveys were conducted on both model and engine suppressors with the laser velocimeter (see Appendix A for LV description). Radial profiles of mean velocity were obtained at several axial locations (X/D's). A comparison of the 32-chute suppressor model and engine mean velocity profiles at an X/D of 1, just aft of the end of the plug centerbody, is shown in Figure 321, for conditions of V_j ~1650 ft/sec and P_{T8}/P_o ~2.0. Close agreement in profile shape is observed for both suppressors. The overall results of the laser surveys will be presented as part of the Task 3, DOT High Velocity Jet Noise Program effort (Contract No. DOT OS-30034).
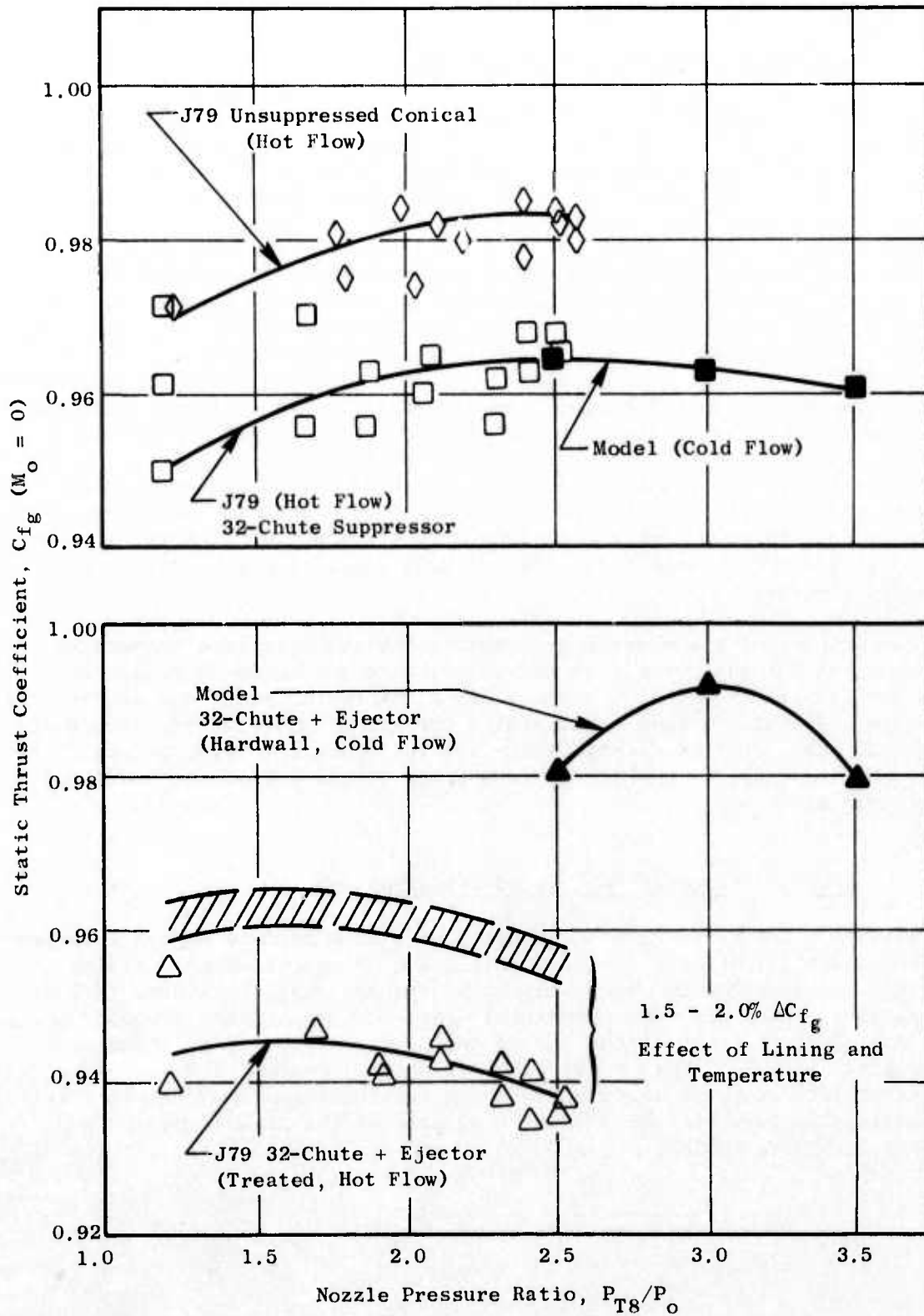
Figure 318. Static Performance Comparisons of Model and Engine Comparisons.
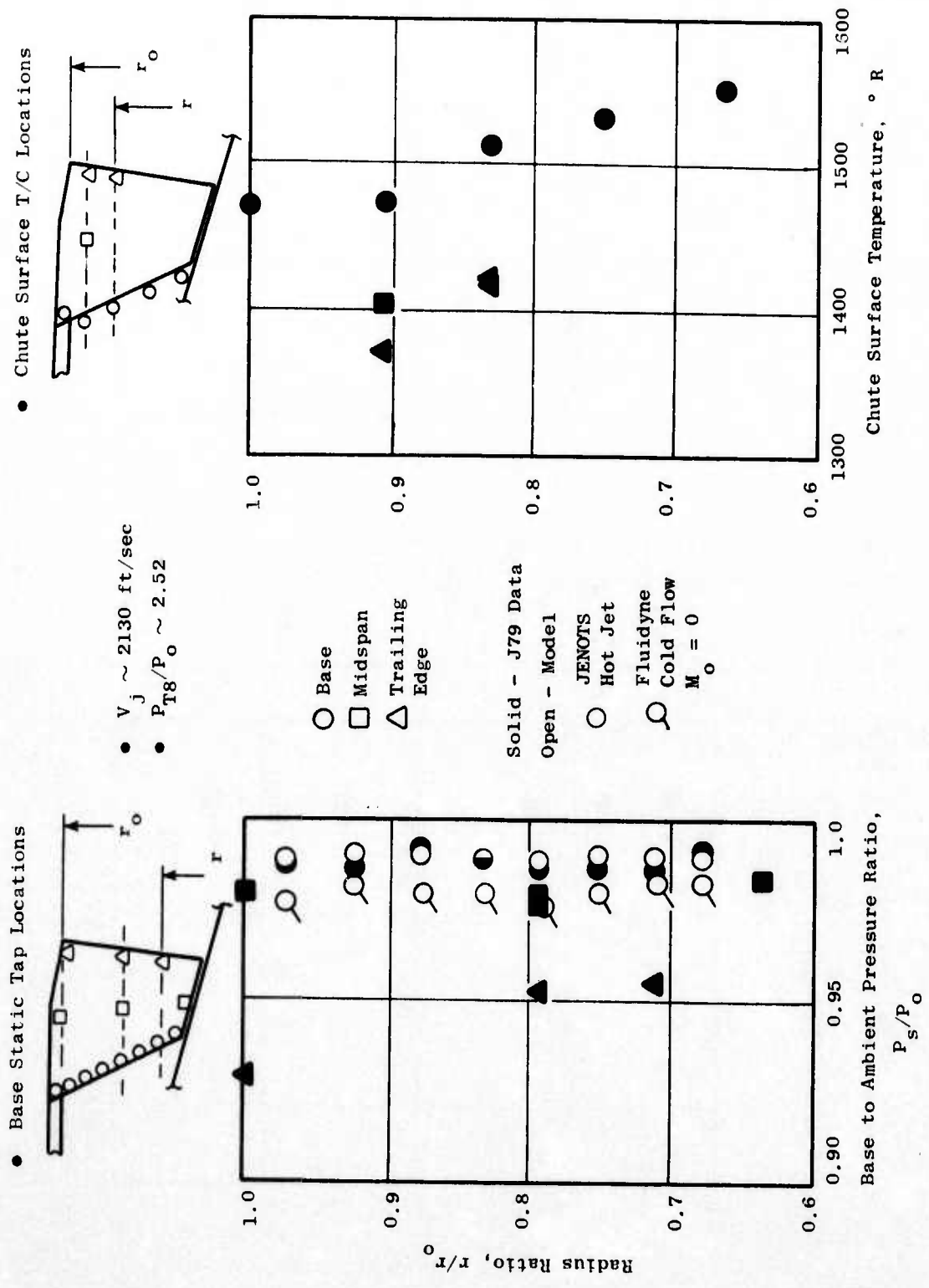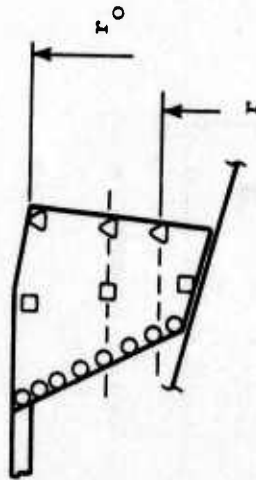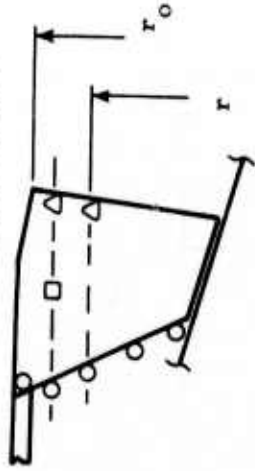
392

Figure 319. 32-Chute Suppressor Base—Pressure and Surface Temperature Distributions.

393
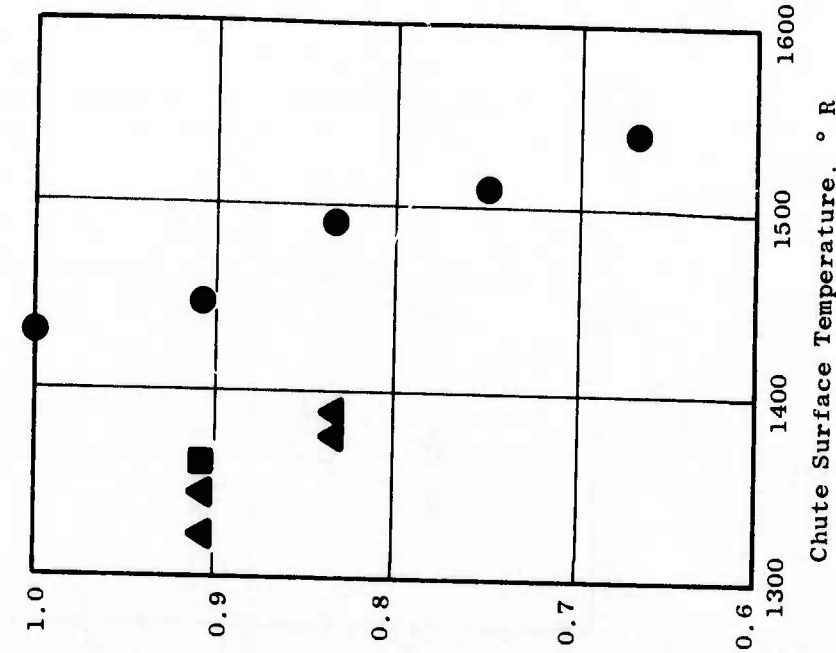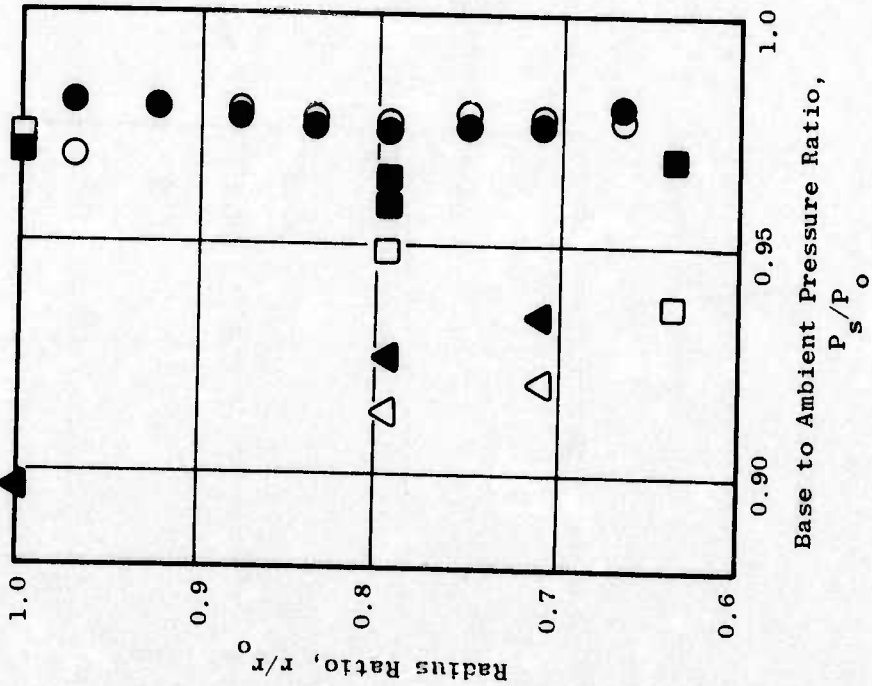
Figure 320. 32-Chute Suppressor + Treated Ejector Base-Pressure and Surface Temperature Distributions.
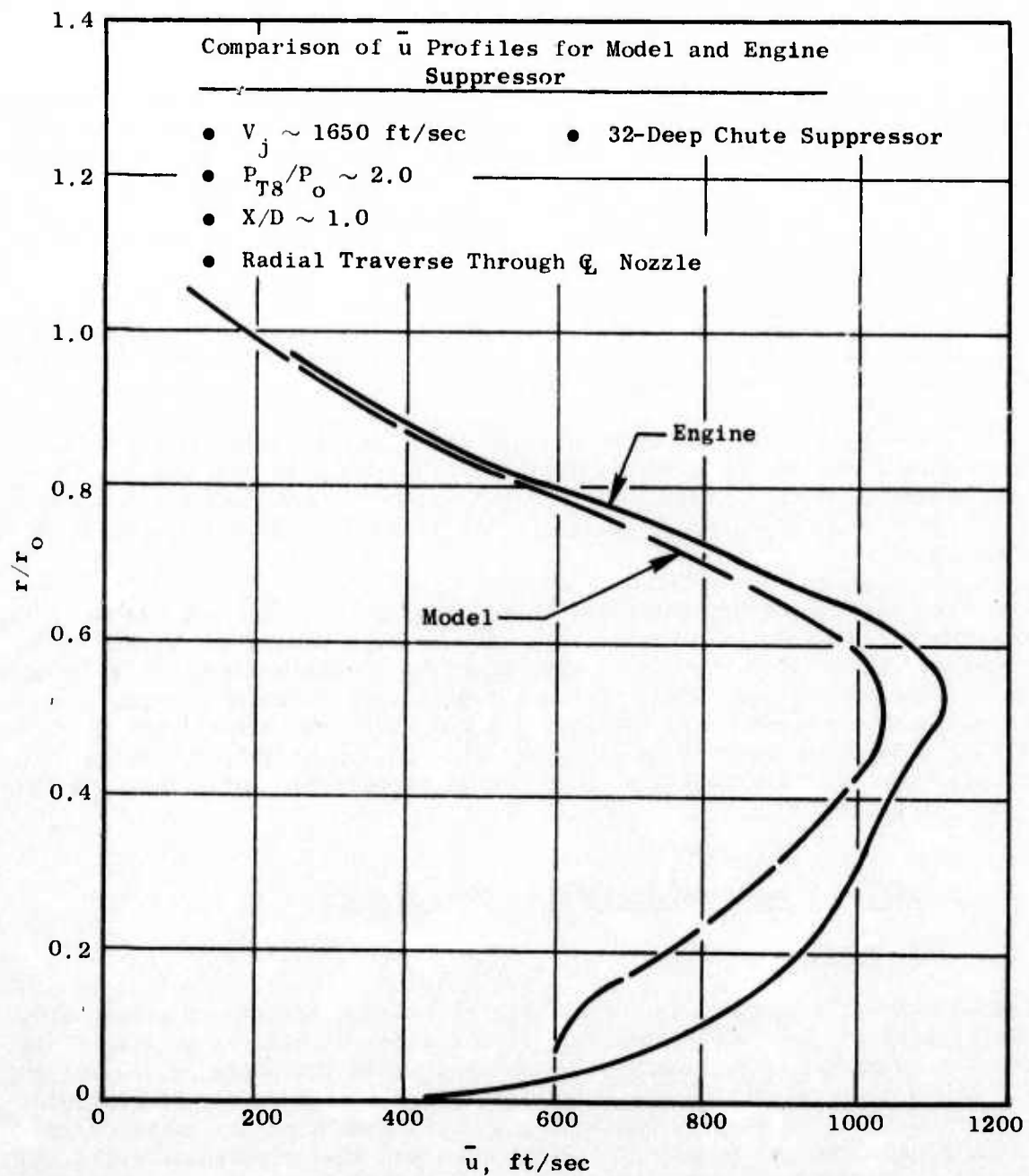
Figure 321. Comparison of Mean Velocity Profiles for Model and Engine Suppressors.

System Evaluation

The tests of the large scale suppressor on the J79 engine were among the first of their kind which enabled a one-to-one comparison of scale model and engine results on an identical suppressor system. This multichute/annular plug suppressor system exhibited reasonable suppression (12 dB at a 2128-foot SL) and good aerodynamic performance (0.924 C_{fg} at $M_O = 0.36$), coupling these with a viable mechanical configuration which could be applied to advanced technology engine suppressor systems.

The integration (and effects) of such a suppressor system into a typical advanced technology aircraft/engine cycle, along with the turbomachinery suppression schemes, is the subject of Section 5.0, the aircraft systems integration.

3.5 RELATED TECHNOLOGY

In an effort to lend some further insight on the acoustic and aerodynamic results discussed in the main body of the report, several rudimentary experimental/analytical studies were undertaken.

One investigation conducted at the General Electric Corporate Research and Development Center under Dr. R. Kantola (Reference 31) made in-jet fluctuating static pressure measurements and attempted to cross-correlate these with the far-field acoustic pressures for two typical scale model annular/plug suppressors.

Another area of study, which was stimulated by the shock studies of Harper-Bourne and Fisher (Reference 31), was directed toward an assessment of the far-field acoustic signature as influenced by nozzle underexpansion (e.g., pressure ratio and temperature). Several rudimentary diagnostic tests were conducted in an effort to identify its far-field characteristics especially around the forward quadrant wherein, during flight, the shock contribution (tone and broadband) may exert an undesirable influence (possibly no V_R effect benefit).

3.5.1 Jet and Suppressor Correlation Measurements

Introduction

An experimental program was undertaken to explore the acoustic and aerodynamic aspects of jet noise suppressor flow fields, as well as the far-field noise. The suppressors studied were of the spoke and the chute annular plug types. One principal aim of this study was to try to find a way of characterizing the far-field noise from single-point measurement of the unsteady pressure fluctuations of the plume. The motivation was that suppressor evaluation then could be simplified, since the need for detailed far-field measurements would be reduced.

396

Results and Discussion

Plume Mean Aerodynamic Data - These experiments were conducted on an outdoor test facility with cold air exhausting through suppressor models (scaled versions of the 40-spoke and 40-chute suppressors discussed in Section 5.2.2) with effective flow areas approximately equivalent to a 2-inch diameter convergent nozzle. The 40-element suppressors were fed by a 12-inch-diameter plenum equipped with straightening screens and honeycomb, which was, in turn, fed by a long 4-inch line. The actual models used can be seen on Figures 322 and 323, with the details of the exit plane geometries given on Figure 324. The chute and spoke suppressors were 3.62 and 3.71 inches in diameter, respectively. The models were run at a nozzle pressure ratio of 3.0. At this ratio of upstream total pressure to ambient pressure, the flow field was highly underexpanded and consisted of shock-expansion patterns in both the radial and circumferential directions.

The complex flow field for both suppressors is given on Figures 325 and 326. On these figures are a series of radial distributions of the maximum and minimum points of the pitot pressure variation in the circumferential direction as taken at various axial positions. Close to the exit plane, the circumferential variation dominates. For the chute suppressor, a two-jet annular system is apparent, and the circumferential peaks and valleys persist further downstream than for the spoke suppressor. For both suppressors, the jet plume attempts to follow the centerbody surface by contracting slightly in the downstream direction, as the centerbody becomes smaller in diameter.

The effect of the centerbody is to cause a velocity deficit in the center of the plume. This is the cause of the hump in the radial profiles which persists in the suppressors' plumes until about six diameters downstream. After this distance, the suppressor plumes decay with distance like those of a round jet. Typical radial pressure profiles shown in Figures 327 and 328 illustrate this trend.

Plume Unsteady Pressure Field

Pressure Probe Selection - The probe selection had to be very carefully done to adequately measure the fluctuating pressure within the jet plume and not cause extraneous readings in the in-jet pressure measurement, and in the cross-correlation of the in-jet pressure to far-field measurement. A 1/8-inch condenser microphone was selected as the in-jet pressure probe. This microphone was fitted with an aerodynamically shaped noise cone and a long 90° (3/16" diameter) probe support to align the probe with the flow.

Static Pressure Fluctuations - At each downstream station, a radial distribution of the overall average (rms) jet pressure (static) level, OAJPL, was plotted on an x-y recorder. Typical plots are shown in Figures 329, 330, and 331. The OAJPL profiles are very peaked near the exit plane and gradually transition to more uniform profiles with increasing downstream distance. The spoke suppressor transition occurs a little earlier than that of the chute suppressor. From the mean total-pressure distributions, discussed earlier,
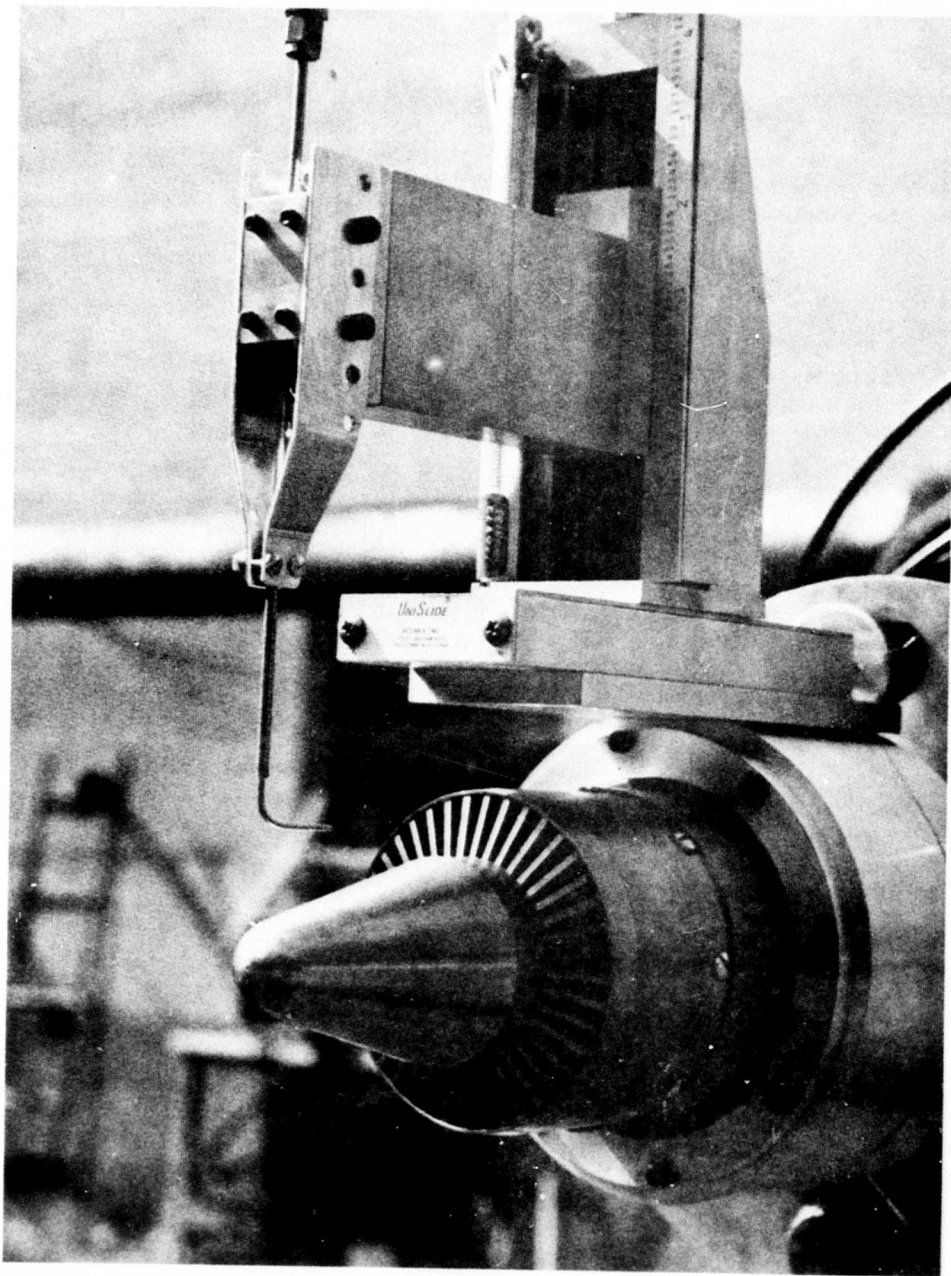
Figure 322. 40-Spoke Suppressor and Axisymmetric Traversing Mechanism.

398
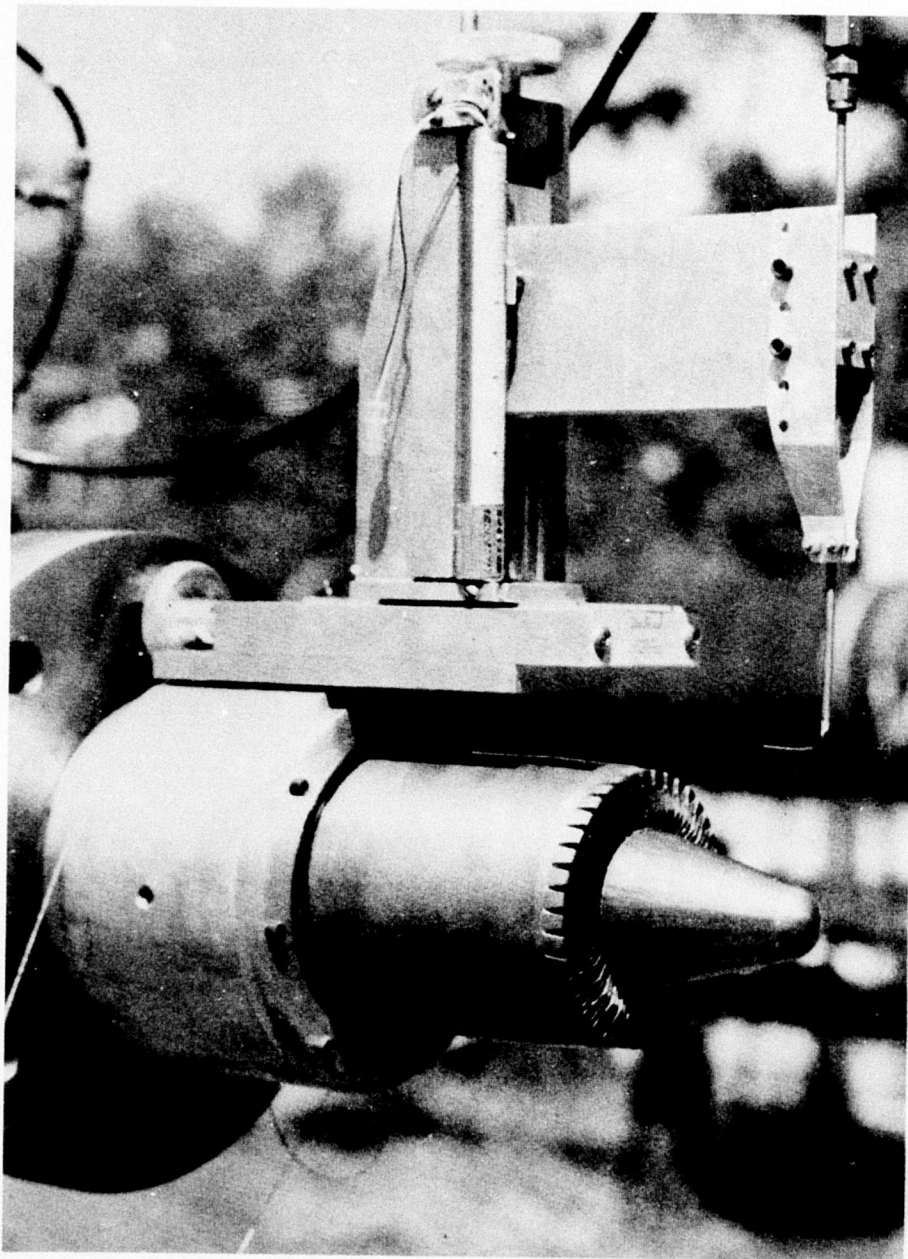
Figure 323. 40-Chute Suppressor and Axisymmetric Traversing Mechanism.

399
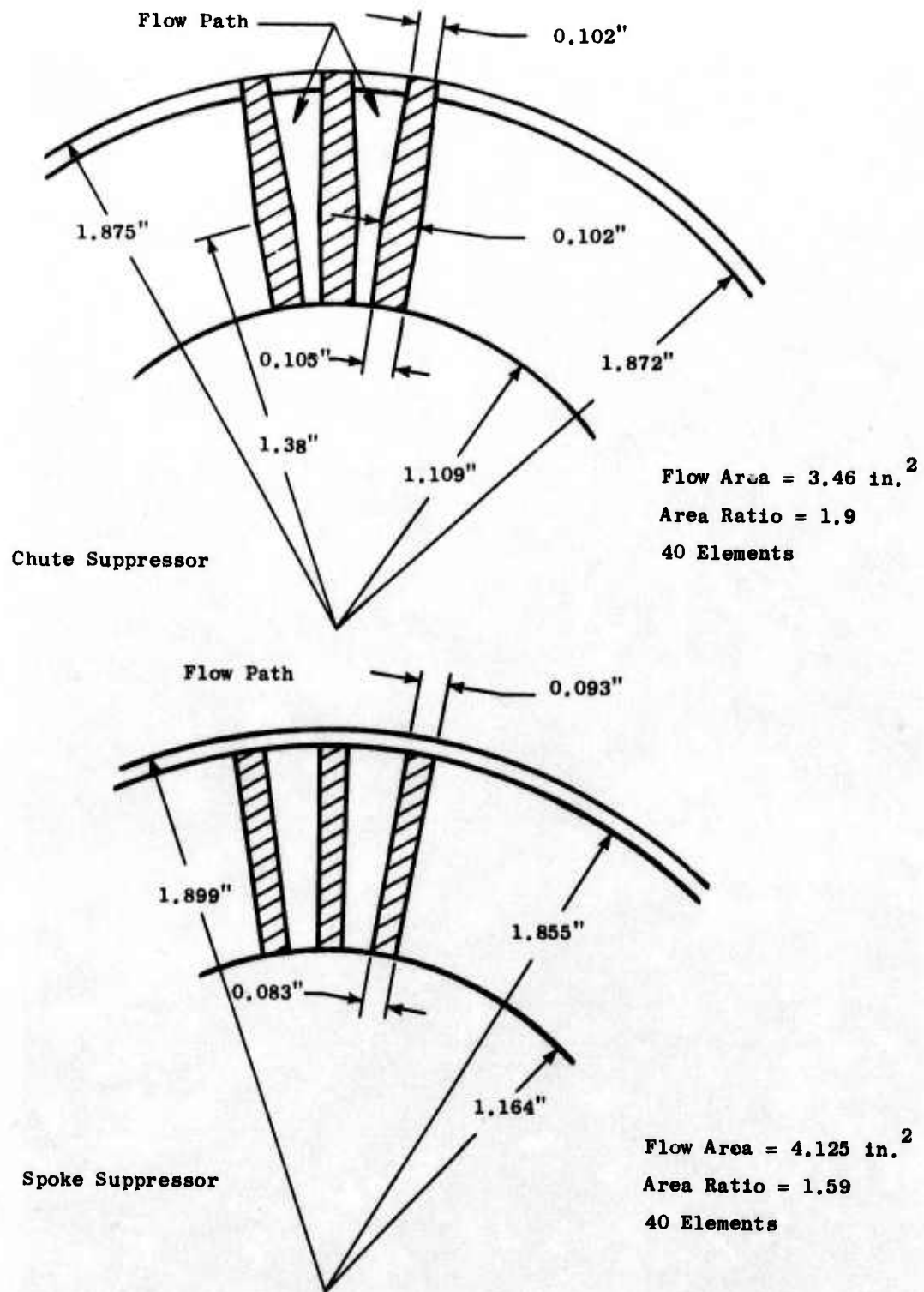
Figure 324. Suppressor Exit Plane Geometry.
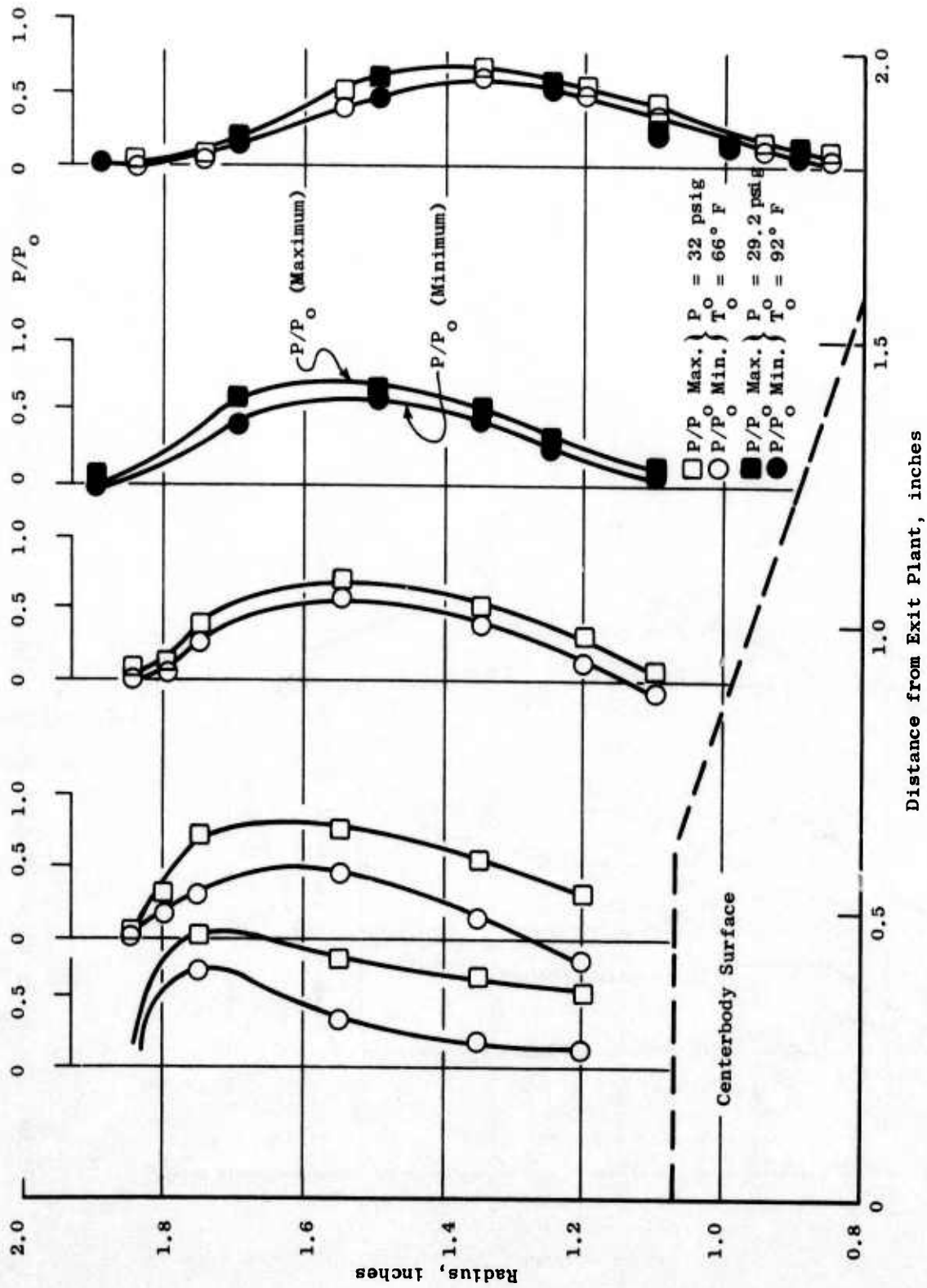
Figure 325. Circumferential Variation in Pitot Pressure, 40-Spoke Suppressor.

401
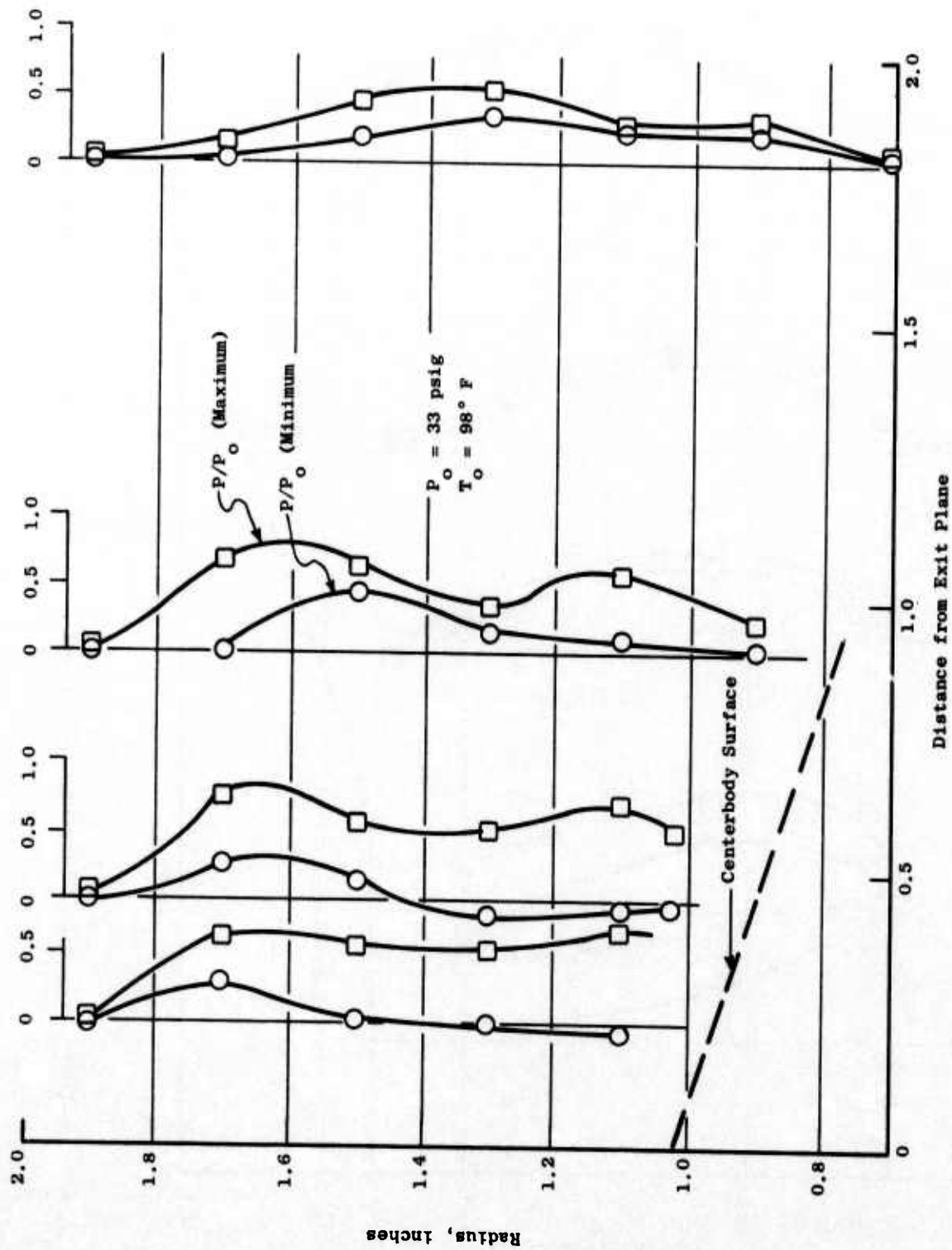
Figure 326. Circumferential Variation in Pitot Pressure, 40-Chute Suppressor.

402
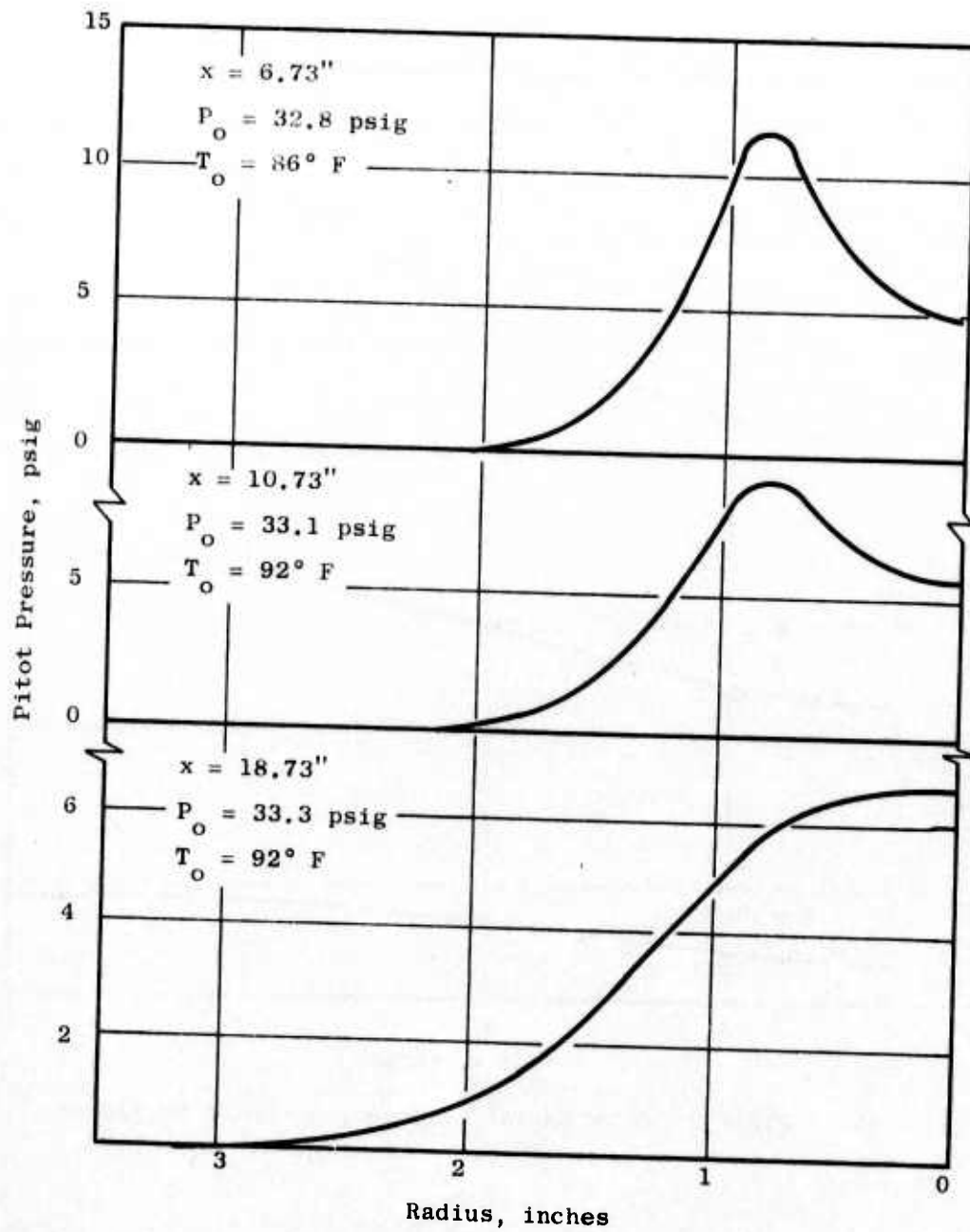
Figure 327. Pitot Pressure Radial Traverse, 40-Chute Suppressor.
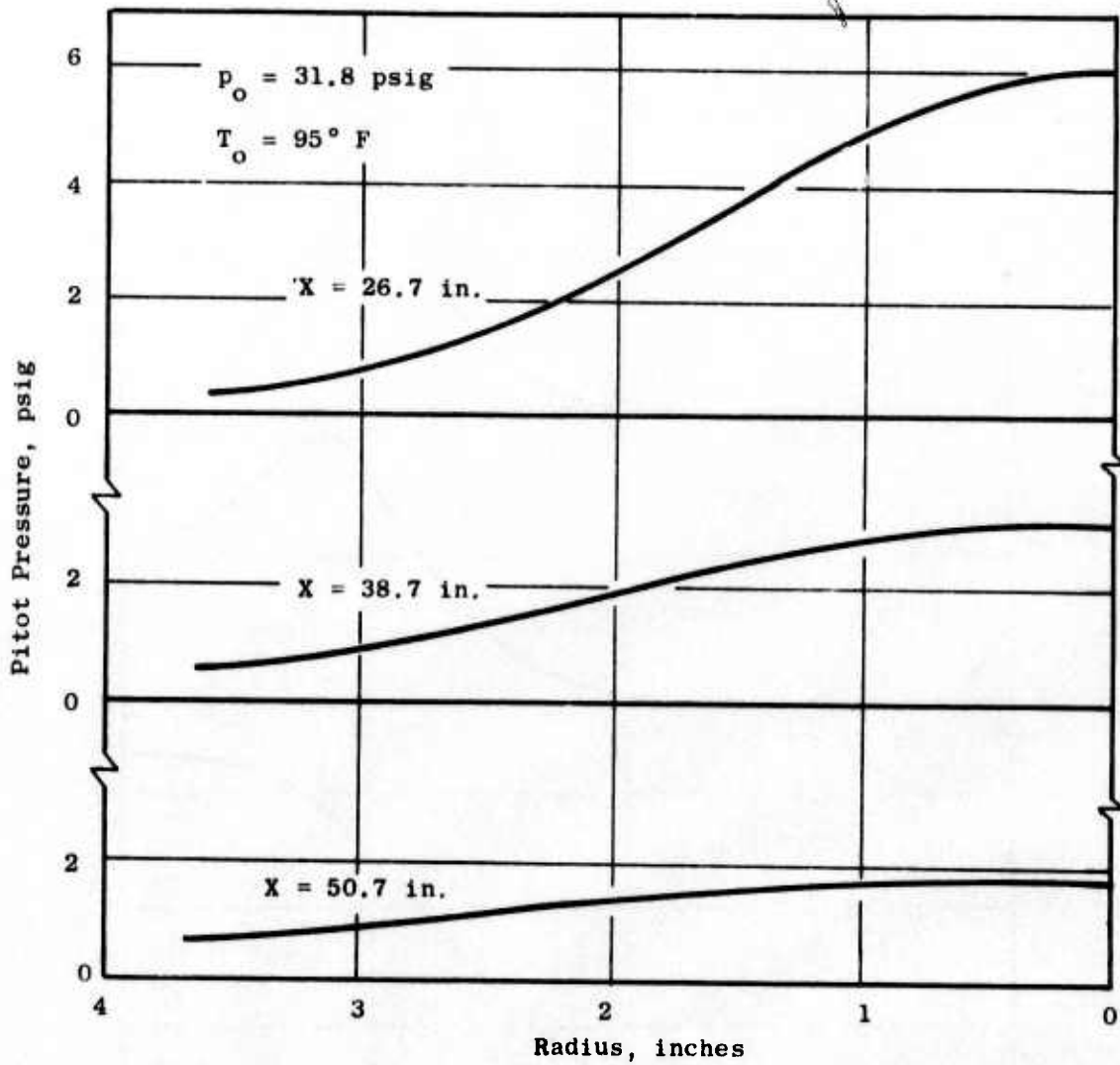
Figure 328. Pitot Pressure Radial Traverse, 40-Chute Suppressor.
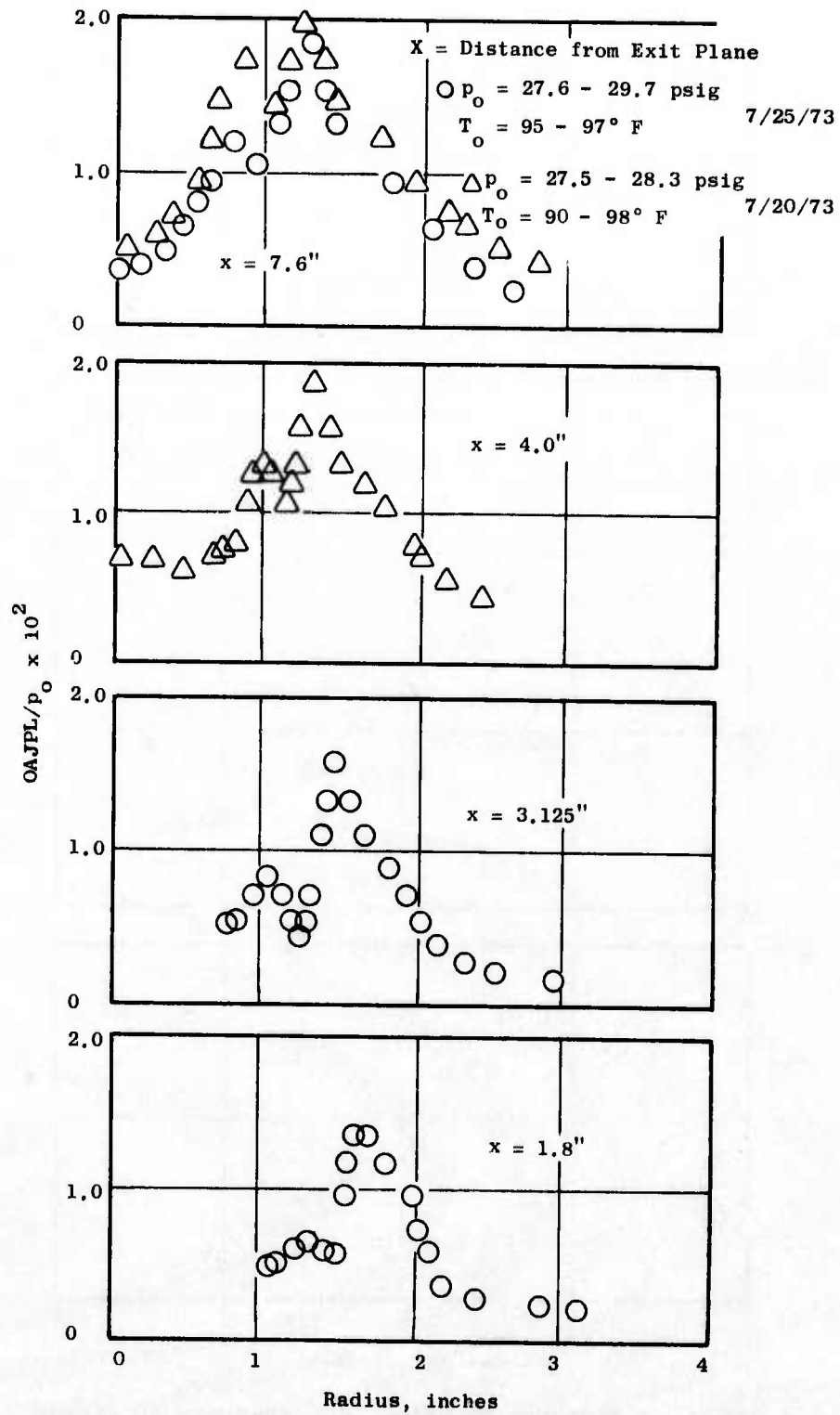
Figure 329.   Jet Pressure Distribution, 40-Spoke
Suppressor.

405
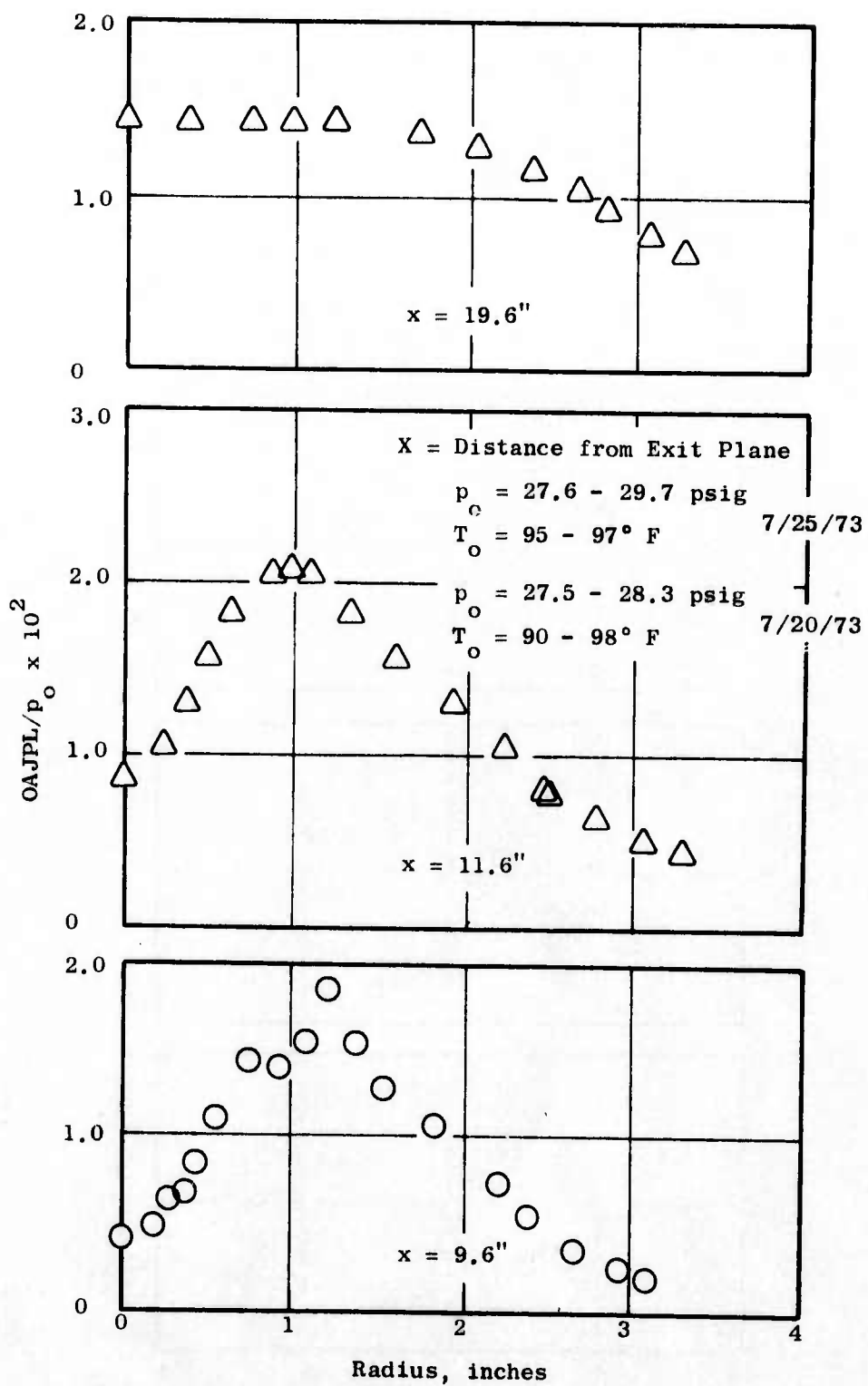
Figure 330. Jet Pressure Distribution, 40-Spoke Suppressor.
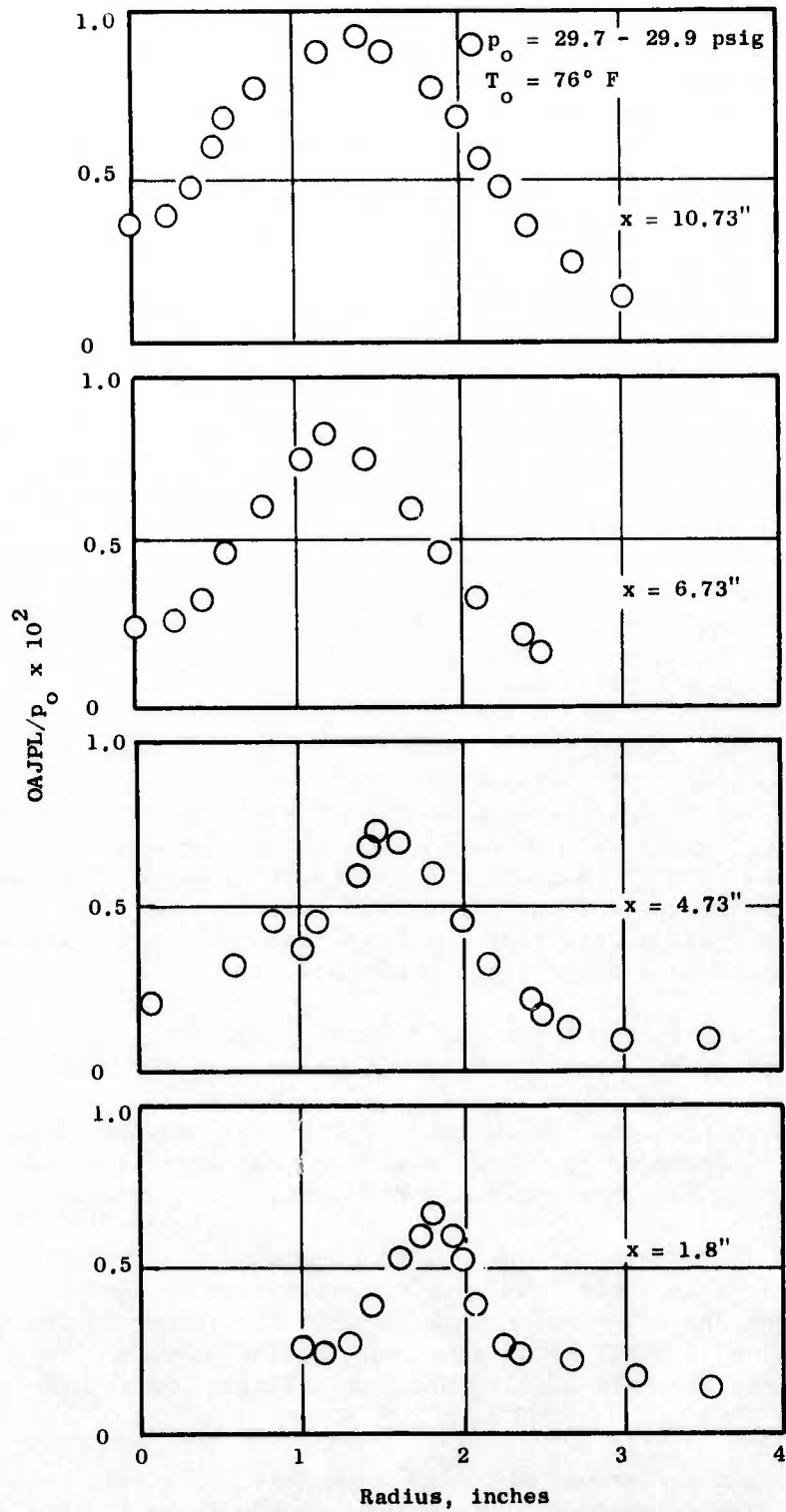
Figure 331. Jet Pressure Distribution, 40-Spoke Suppressor.

the suppressor flow was seen to become like that of a round jet at about 6 diameters downstream. The OAJPL traverses showed a similar trend. These distributions are somewhat like those of turbulent intensity for subsonic jets; but, unlike the turbulence which peaks at a radius equal to or greater than the nozzle lip, the peak value of the radial OAJPL distributions is located inside the suppressor outer lip. The axial distributions of these peak values of OAJPL are shown on Figure 332. The absolute maximum OAJPL is seen to occur at about 2 diameters for the spoke suppressor and at about 3 diameters for the chute suppressor. In a round convergent jet, measurements of this type show a peak at about 7 to 8 diameters downstream. The much smaller axial extension of suppressor plumes is due to the breaking up of the jet into many smaller jets which then decay in a much shorter distance.

Figure 333 shows that the average of Strouhal frequency with axial distance was virtually identical for both suppressors and different than that of the round convergent nozzle. The suppressors have a more rapid decrease of the peak frequency with axial distance. This points out that the action of the suppressor is to force the eddies to be of small physical scale such that the growth and decay history of the eddies occurs over a shorter length, which enhances the high frequency content of the sound. The increased flow frequency content far downstream is due to the increased broadening of the plume when compared to an equivalent round jet.

Far-field Acoustic Results - The far-field acoustic measurements were conducted on the outdoor test facility as described in Appendix A. The jet axis was parallel to a grass-covered ground plane at a height of 5.5 feet. Far-field acoustic signals were measured with a 1/2" Bruel and Kjaer microphone which was traversed on a 10-foot arc (in a horizontal plane containing the jet axis) over the angular range from 19° to 146° from the jet axis. In-jet and far-field acoustic signals were fed to a tape recorder and processed through a mini-computer, real time analyser, and a correlator.

The temperature difference between the jet total temperature and the ambient temperature ranged from 15° F to a maximum of 39° F with the ambient temperature ranging from a low of 53° F to a maximum of 78° F. The ambient noise level for this facility was quite low, with the background OASPL ranging from 65 to 67 dB (referenced to 0.0002 μbar) and the far-field OASPL ranging from 100 to 118 dB. Thus, the ambient contamination was very low.

Far-field acoustic data, as well as simultaneous measurements of unsteady jet pressure, were taken. The far-field directivities of the two suppressors are shown on Figure 334. The difference between the spoke and the chute suppressors is quite constant with angle and remains between 5 to 6 dB. This difference is nearly the same result that was indicated by the in-jet OAJPL measurements.

By assuming that the ground plane is a perfect reflector, the acoustic power level, PWL, was calculated. These results are shown in Figure 335. As would be expected from the previous results with a 5-6 dB difference between suppressors of both the OAJPL and the far-field OASPL, the difference in the peak far-field 1/3-octave PWL of the two suppressors is 4.8 dB. Since the spectrum shapes are similar, the difference in overall average power level,

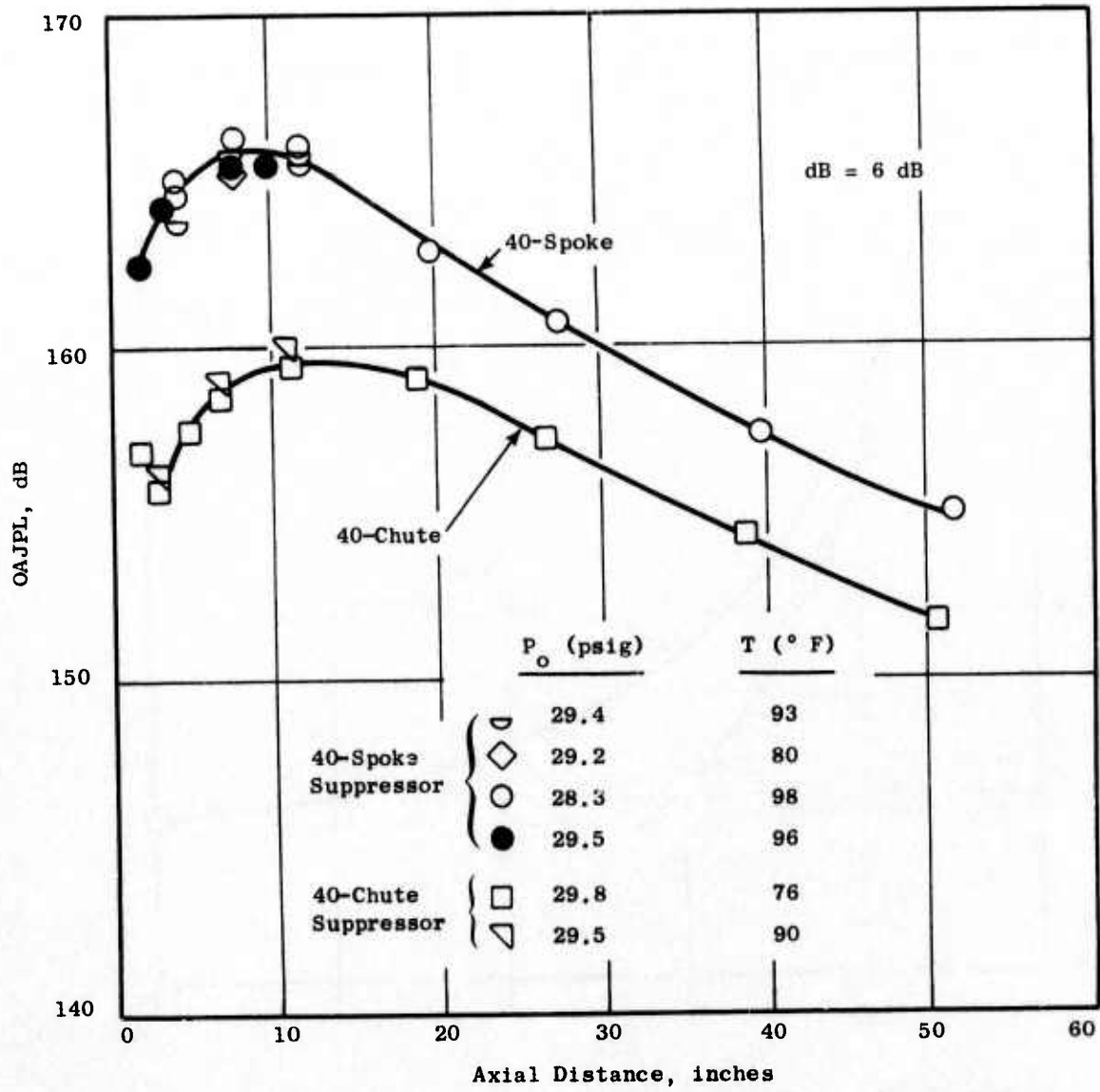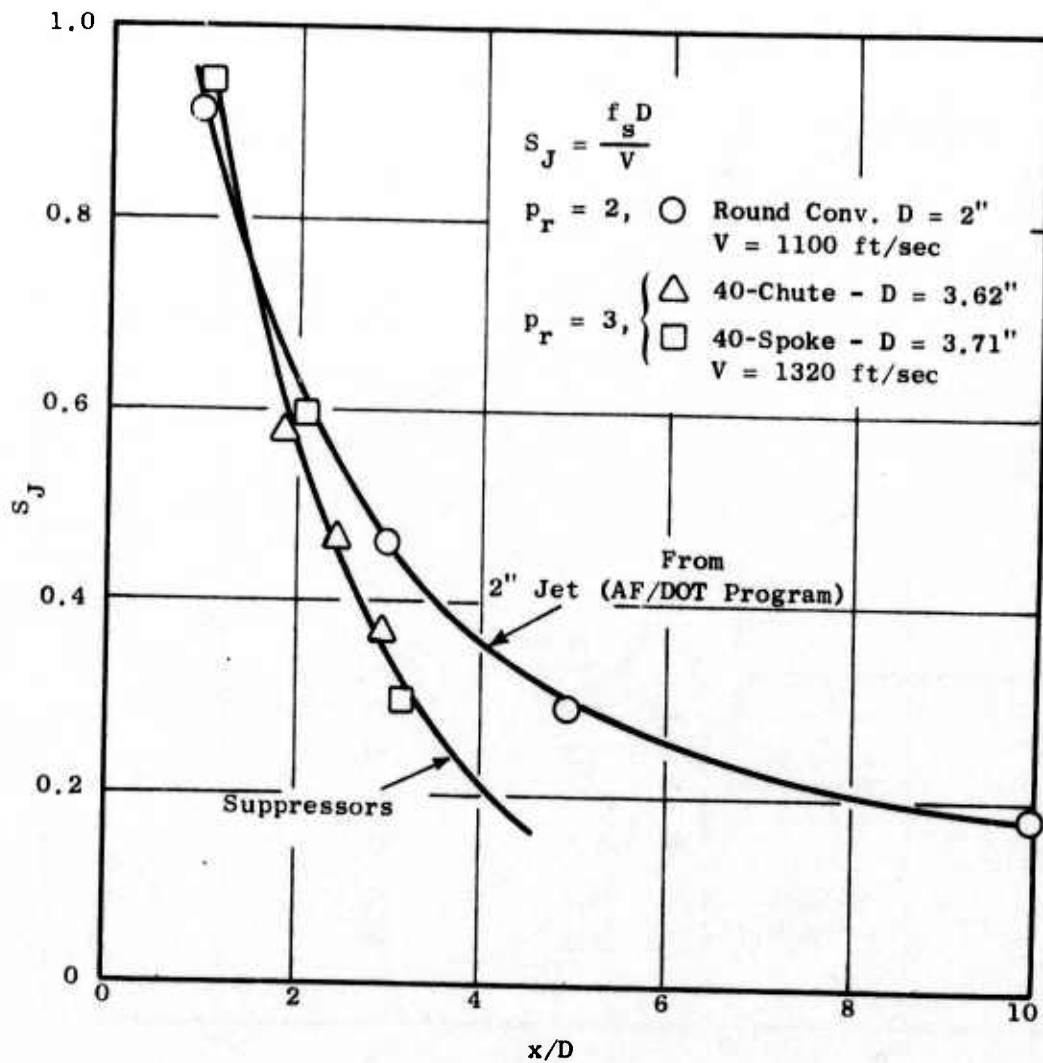Figure 332. Maximum OAJPL Axial Distribution.

409

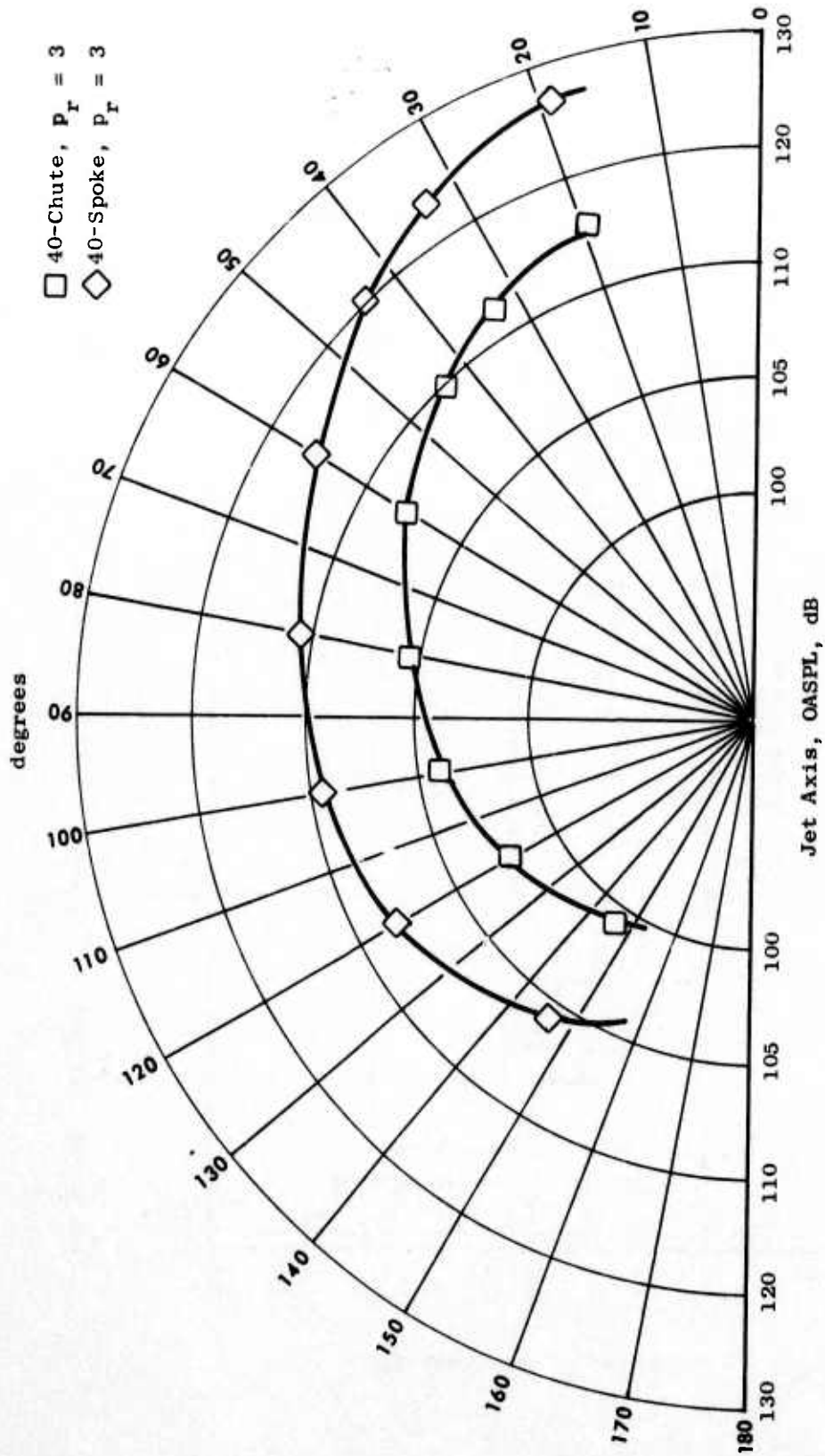Figure 333. In-Jet Strouhal Number, S_J, Axial Distribution.

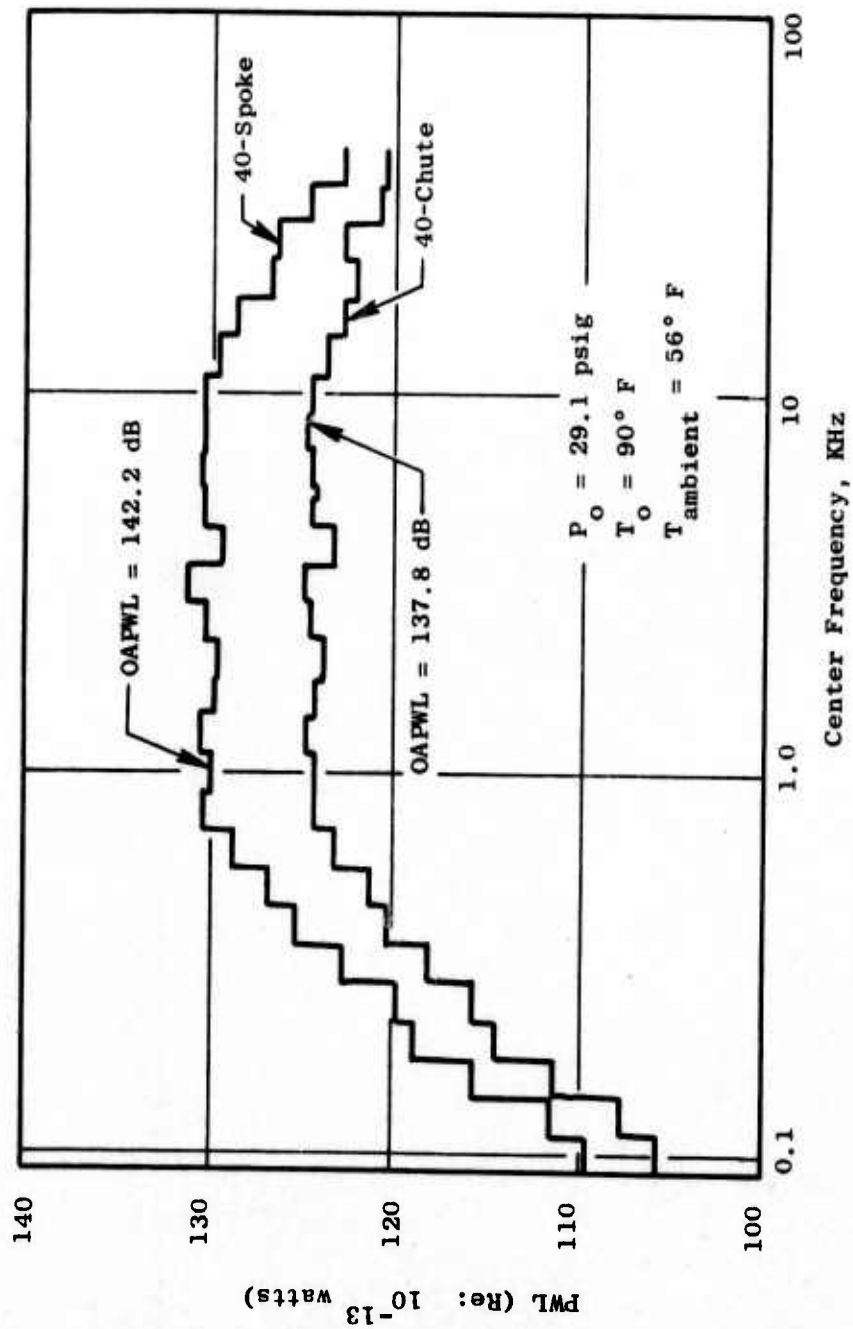Figure 334. Far-Field Directivity Characteristics.

411

Figure 335. Suppressor Acoustic Power Level (PWL) in 1/3-Octave Bands.

412

OAPWL, is nearly the same, 4.4 dB. These power spectra also show evidence of the typical two-humped spectra of suppressors. The high-frequency hump at 8-10 KHz is due to the individual jets with their small scale eddies. The lower frequency hump at about 0.8 to 1 KHz is due to the large eddies that are formed as the individual jets are merged into a single large jet. This can be seem by comparing these suppressor spectra to that of a 2-inch round jet which has the same centerline velocity in the fully developed region, as shown in Figure 336. Here the Strouhal peak is about 1.3 KHz and the falloff is somewhat more rapid for the higher frequency bands.

Cross-Correlation of Fluctuating Static Pressure with the Far-field
Acoustic Pressure - Considerable research activity in the area of jet noise has been (and still is) involved with the cross-correlation of the unsteady pressure in the jet plume with the far-field acoustic signal. The application of these techniques to suppressor flows is further discussed in Reference 33.

At the start of this study there existed in the available literature only five references on the cross-correlation of in-jet measurements of the far-field sound (References 33, 34-37). Unfortunately, none of these prior investigators carried out a reasonably complete variation of the in-jet position with various far-field microphone positions.

In view of the lack of basic information necessary to evaluate the applicability of this technique as a noise source location method, it was decided that in this study as well as in the round jet work[Ref 36], a major goal would be to quantify the effects of in-jet position and far-field microphone locations. In this investigation, the in-jet microphone was placed on the radial point of the local maximum overall jet pressure level, OAJPL, for three axial stations $x/D \simeq 1$, 2, and 3. The in-jet microphone signal was then cross-correlated with several far-field microphones at positions ranging from 20° to 100° from the jet axis. A 1/8" B&K microphone mounted on a 90° probe support was used as the in-jet probe with a 1/2" B&K microphone used to measure the far-field signal. These correlations for the most part, were processed using a Saicor correlator, Model SAI-43A, and checked with a Hewlett-Packard fourier analyser and minicomputer.

Figure 337 shows the results for unfiltered normalized cross-correlations. When the in-jet probe was close to the jet exit plane and the far-field microphone was at large angles to the jet axis, the correlation shapes were completely obscured by noise. Generally, the measurements at the greater distances from the suppressor exit plane have a higher correlation coefficient. This is clearer when the correlations are not normalized, as shown in Figure 338. When the probe is further downstream, it encounters a larger scale of turbulence and should yield a better correlation, since the contribution of each source to the far-field sound is then more significant. However, in suppressors, the axial extent of the source region is very short (Reference 38). This is indicated in Figure 338, where the correlation levels at $\Theta = 33.6°$ are peaked between 2 to 3 diameters downstream of the exit.

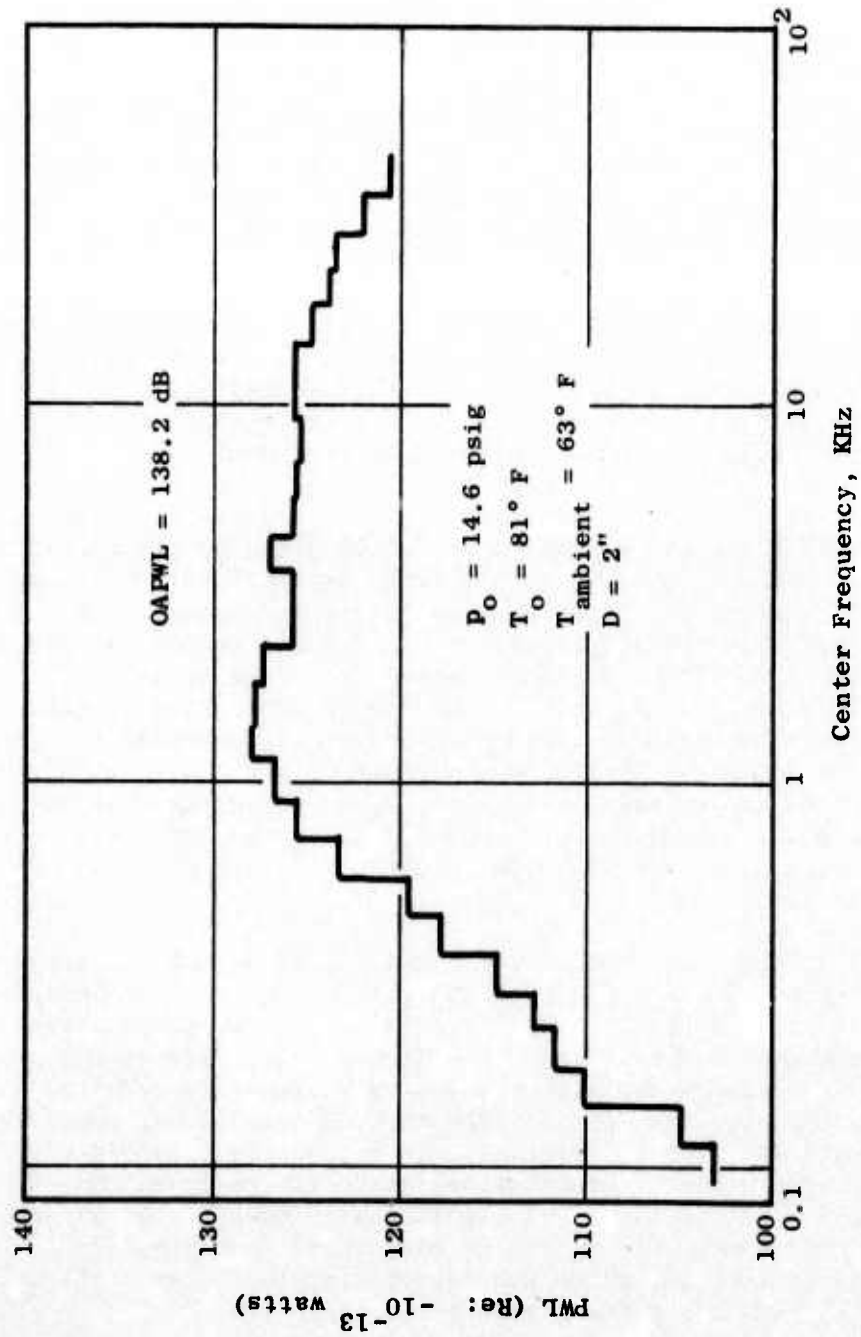In round jet flows, the axial extent of the noise source region is larger;

413

Figure 336. Round Jet Acoustic Power Level in 1/3-Octave Bands.
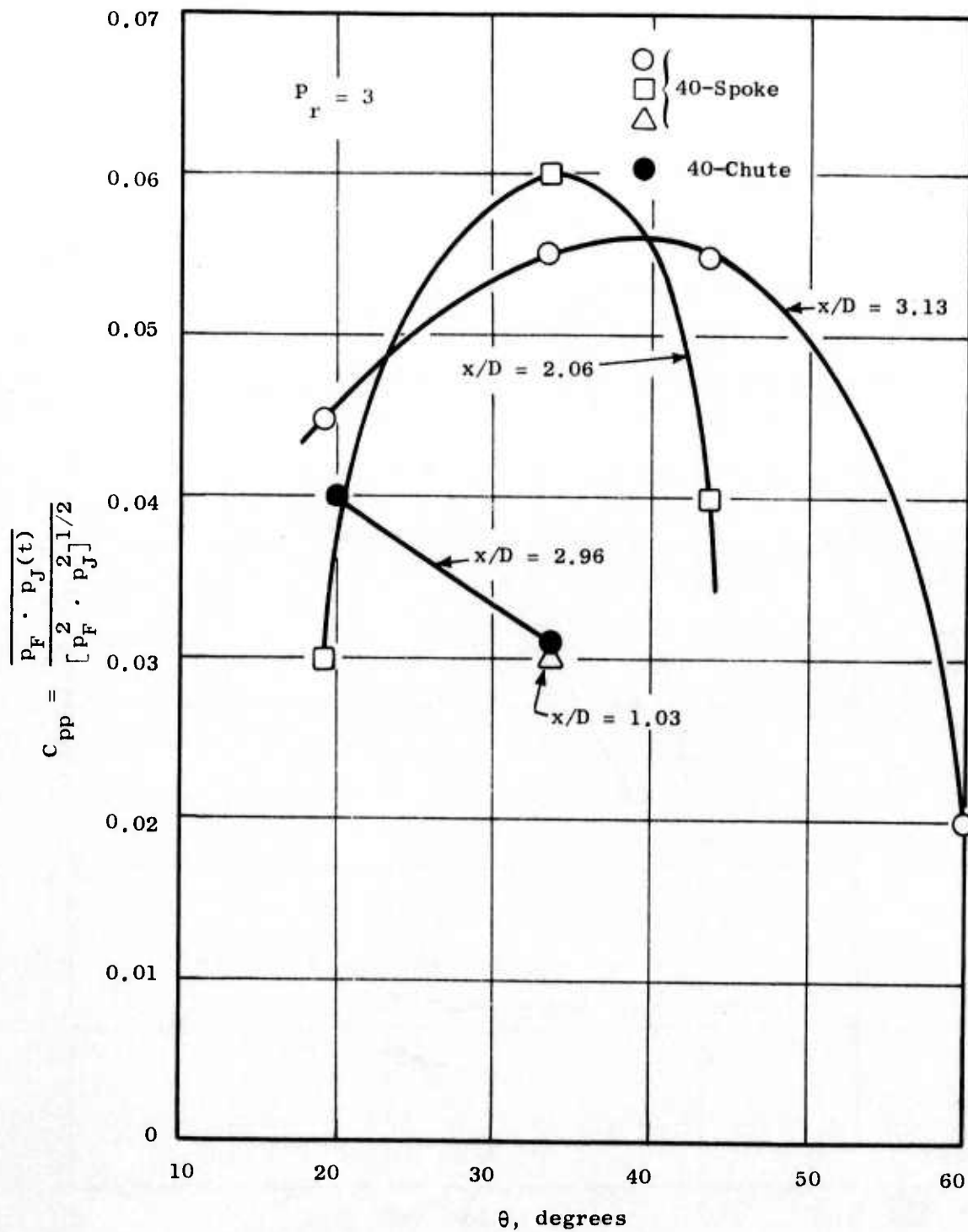
414

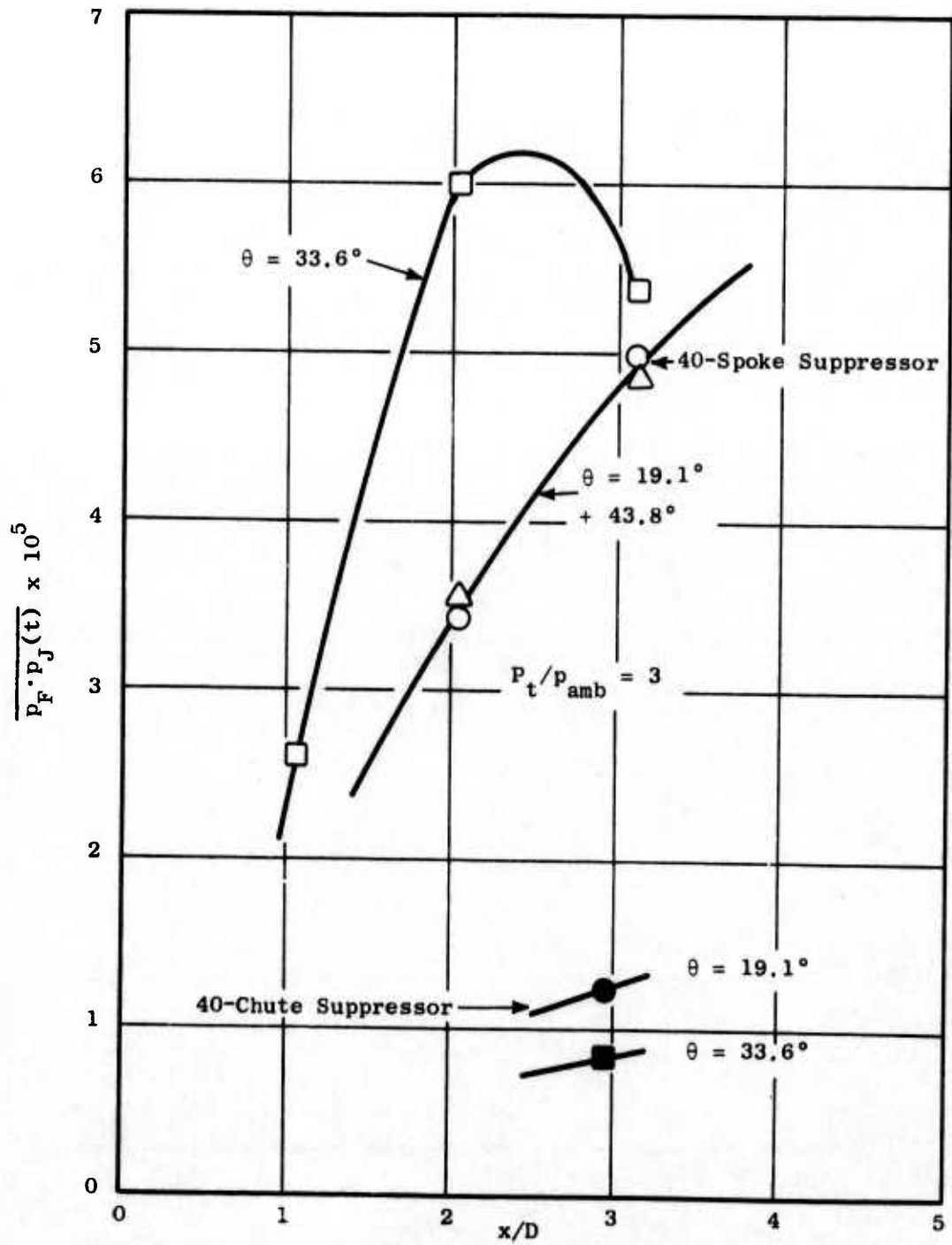Figure 337. Normalized Cross-Correlation, In-Jet to Far-Field.

Figure 338. Cross-Correlation of In-Jet to Far-Field.

416

and, at the far downstream distances, the round jet has a larger turbulent scale and a much higher level of correlation.

Noise source location methods as suggested by Meecham and Hurdle[36], Rakl[33], and Siddon[37] require the complete mapping of the correlation function for the entire jet plume. Also, the second time derivative of these correlations must be carried out. The correlation functions themselves, without differentiation, range from fairly definitive to very marginal with respect to signal-to-noise ratios. Band-pass filtering of the signals prior to correlating was done to try to clarify the correlation functions. Figures 339 and 340 show an unfiltered correlation function and a filtered correlation function, respectively. For the filtered correlation function, a 1 KHz to 10 KHz band-pass filter was used on both signals. Regretably, amplitude modulation at the filter frequency showed up before any significant reduction in "hash" occurred. This was done for a number of correlations with the same result. Apparently the "hash" is due to the correlator itself and, therefore, filtering of the signals did not help.

Hard clipping of the signals also did not improve the clarity of the correlation functions to any significant degree. The cross-correlation of the chute suppressor remained hidden in the noise, except at the largest downstream distance and the shallowest angles.

On the basis of the tenuous nature of this process, an attempt was made to estimate the source function without carrying out the double-time differentiation. A first approximation to the source function can be obtained by estimating the effect of the double differentiation by assuming that the second derivative can be replaced by the frequency squared term. This frequency squared method was applied to the spoke suppressor by multiplying the unnormalized cross-correlations by the square of the Strouhal number of the plume measurements. Figure 341 shows that the source distribution of the spoke suppressor is peaked very close to the exit plane. McGregor and Simcox[38] came to a similar conclusion on multitube suppressors, using the "hole-in-the-wall" technique, indicating at least qualitative agreement with the results from the current study.

At the present time, the use of cross-correlations of in-jet pressure to the far-field acoustic pressure as an _axial_ noise source location method does not appear to be very attractive, as it requires a very tedious and marginal procedure. For the determination of the radial location of sources, the in-jet-to-far-field cross-correlation technique appears necessary. Newer developments of nonintrusive sensing, such as a Laser Velocimeter or an acoustic lens, may offer means of measuring the in-jet fluctuations.

3.5.2 Observations on Shock Noise

The phenomena of "shock screech," which is associated with underexpanded supersonic low temperature jets, has been known for many years.
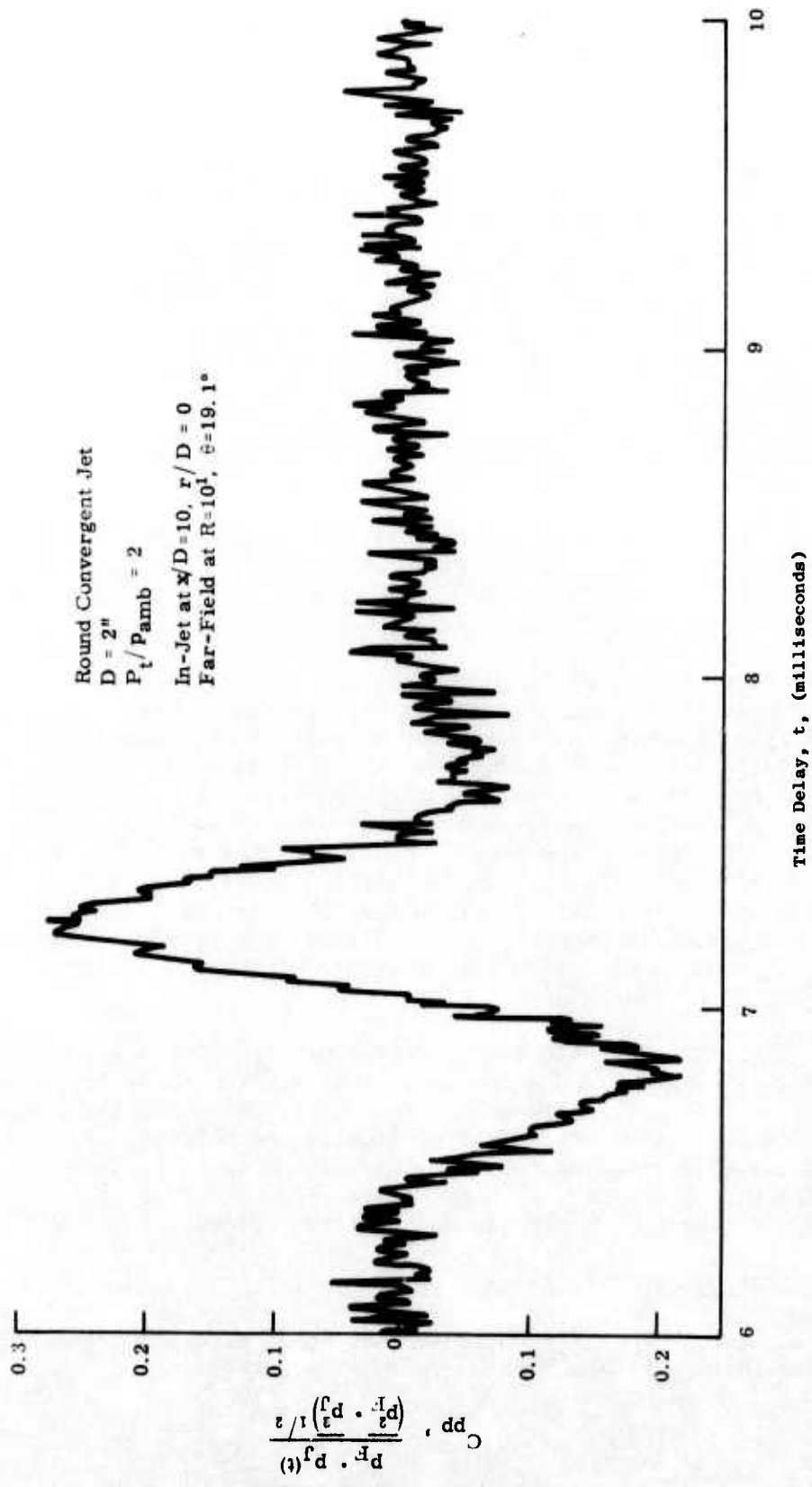
Figure 339. Cross-Correlation Function, Filter Band 10 Hz to 80 KHz.

Round Convergent Jet
$D = 2''$
$P_t/P_{amb} = 2$

In-Jet at $x/D = 10$, $r/D = 0$
Far-Field at $R = 10^1$, $\hat{\theta} = 19.1°$

Time Delay, t, (milliseconds)

C_{pp}, $\dfrac{\overline{P_F \cdot P_J(t)}}{\left(\overline{P_F^2} \cdot \overline{P_J^2}\right)^{1/2}}$

418
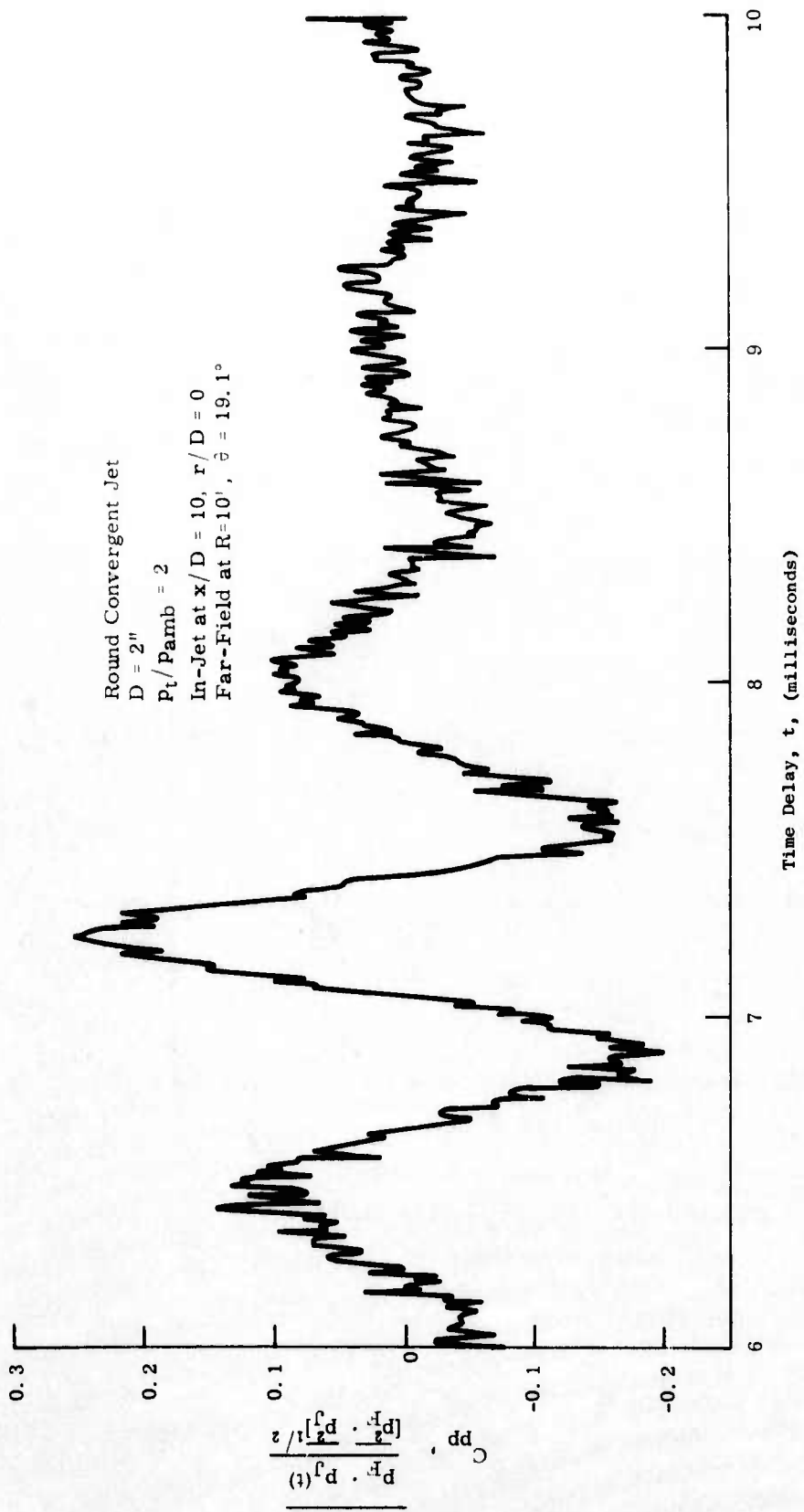
Figure 340. Cross-Correlation Function, Filter Band 1 KHz to 10 KHz.

Round Convergent Jet
$D = 2''$
$P_t / Pamb = 2$
In-Jet at $x/D = 10$, $r/D = 0$
Far-Field at $R=10'$, $\hat{\theta} = 19.1°$

Time Delay, t, (milliseconds)

$C_{pp}, \dfrac{\overline{p_F \cdot p_J(t)}}{[p_F^2 \cdot p_J^2]^{1/2}}$

Figure 341. Source Function Distribution.

Powell (Reference 39) did considerable work in contributing to the under-
standing of this acoustic feedback mechanism; however, up until recently,
little work was directed to the broadband contribution associated with this
same source (e.g., the shock structure). Most recently, Harper-Bourne and
Fisher have attempted to synthesize a model which can be used to predict the
broadband shock-related noise in addition to that due to turbulent mixing.
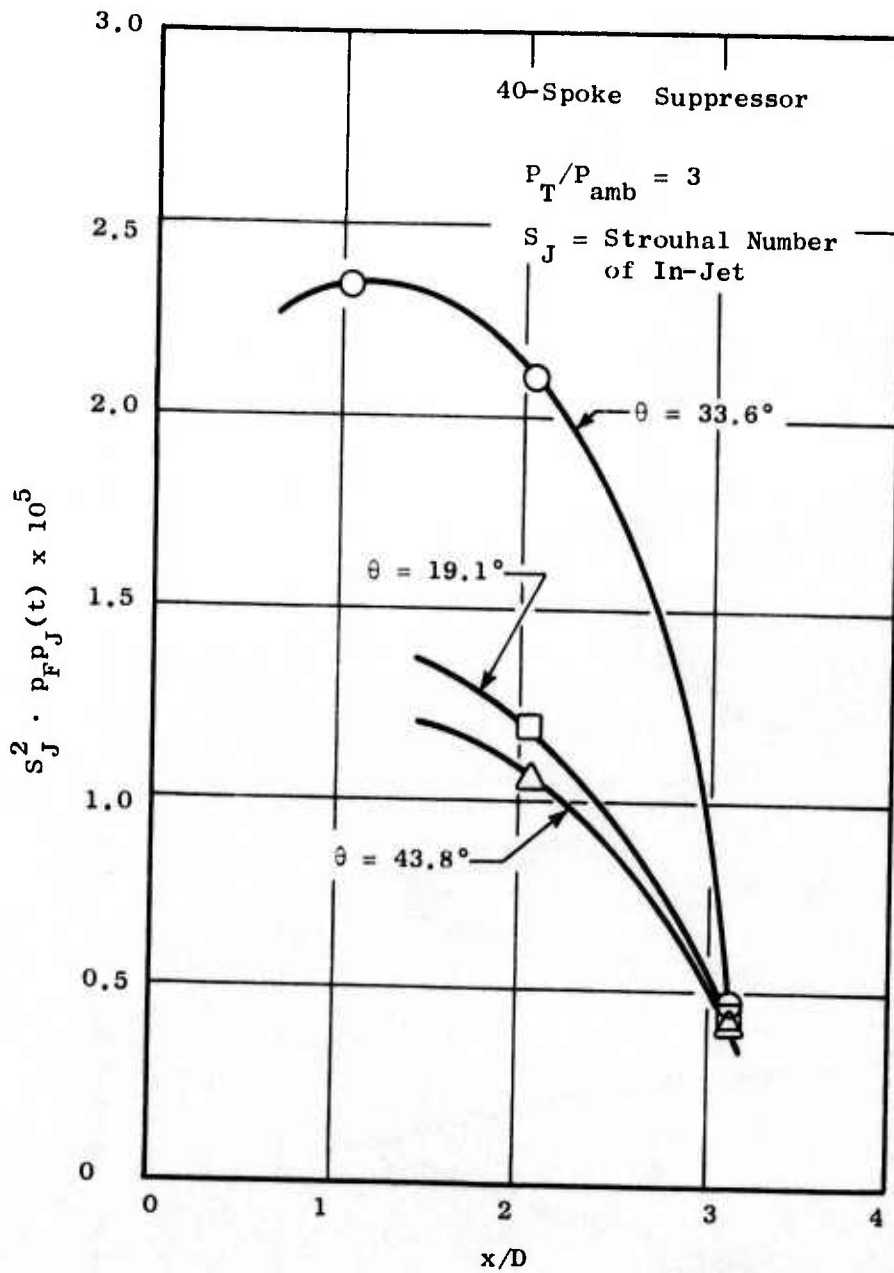This work serves as the basis for the shock cell noise document (Reference 40)
under review by the SAE A21 Jet Noise Subcommittee.

In the 1973 Harper-Bourne and Fisher paper, they indicated that shock
noise intensity was only a function of pressure ratio and independent of jet
stagnation temperature. Although their initial observations were based on
unheated jets, nevertheless, they concluded that as pressure ratio was in-
creased the noise field became less directional especially in the forward arc.
SNECMA-NGTE (Hoch, Cocking, et al) (Reference 41) work on the influence of
density on jet noise also included considerable data in the supercritical
regime. Figure 342 from their 1972 paper shows that the shock-associated
noise becomes more and more pronounced in the forward quadrant as the pressure
ratio is increased. They summarized their findings thusly: "the forward arc
is essentially governed by the jet pressure ratio, if the latter is super-
critical, while the jet velocity and density remain the predominant factors in
the rear arc." They also cautioned the reader that any prediction technique
to be evolved must recognize the existence of these complicated phenomena.
Indeed, the present SAE A21 proposal prediction technique on shock noise
attempts to blend these phenomena, resulting in the directivity plot (OASPL
versus θ_i) shown in Figure 343. Comparison of measured data with total pre-
dicted level is quite good. Also noted is the fact that the shock noise com-
ponent is essentially invariant with angle.

In the course of this program, a considerable number of excursions was
made from the standard operating line test matrix in an attempt to qualita-
tively assess the effect of either pressure ratio or temperature at a given
velocity on the peak noise (primarily the aft angles). In light of the
current interest on the role shock noise plays on total noise angular varia-
tion (e.g., directivity), some of the results were perused in the hopes of at
least qualitatively substantiating the trends observed by the others previ-
ously mentioned.

The results presented in the next few paragraphs are based on observa-
tions primarily from conical nozzles, with some peripheral data on suppres-
sors.

The first series of data, scaled up PNdB (Figure 344) attempts to verify
the fact that the noise level loses its directionality characteristics in
the forward quadrant with increasing pressure ratio. In order to more vividly
exhibit this effect, Figure 344 was plotted as a function of relative noise
level ($\theta_{max} - \theta_i$) for different supercritical pressure ratios and essentially
constant temperature. Examination of Figure 344 conical nozzle data apparently
supports the previous findings, since the absence of shocks would show little
or no change in ΔPNL (θ_{Ii}) with increasing pressure ratio. This is further
substantiated by the pure jet noise prediction (proposed/revision to SAE-AIR
876) at $\theta_{Ii} \doteq 40°$, also shown in Figure 344.

P_j/P_o	T_j (°K)	P_j (kg/m³)
3.23	446	1.14
2.94	401	0.99
2.39	575	0.78
2.28	579	0.77
2.06	663	0.65
1.88	762	0.55
1.51	1150	0.34

$V_j \approx 500$ m/s
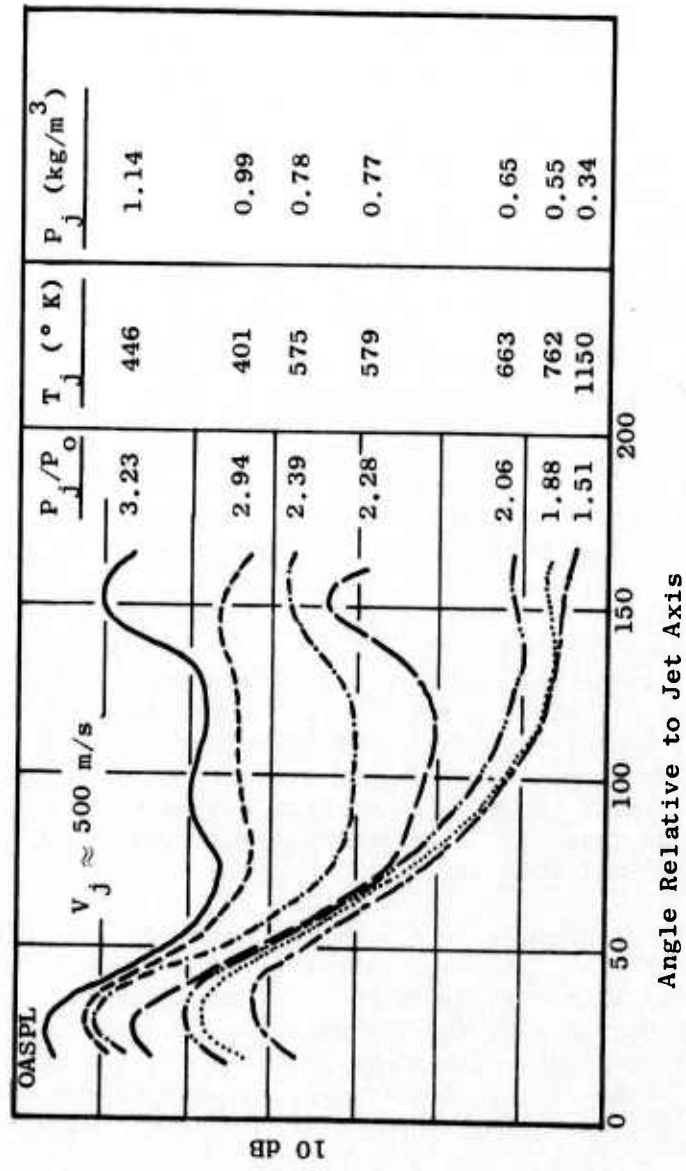
OASPL

10 dB

Angle Relative to Jet Axis

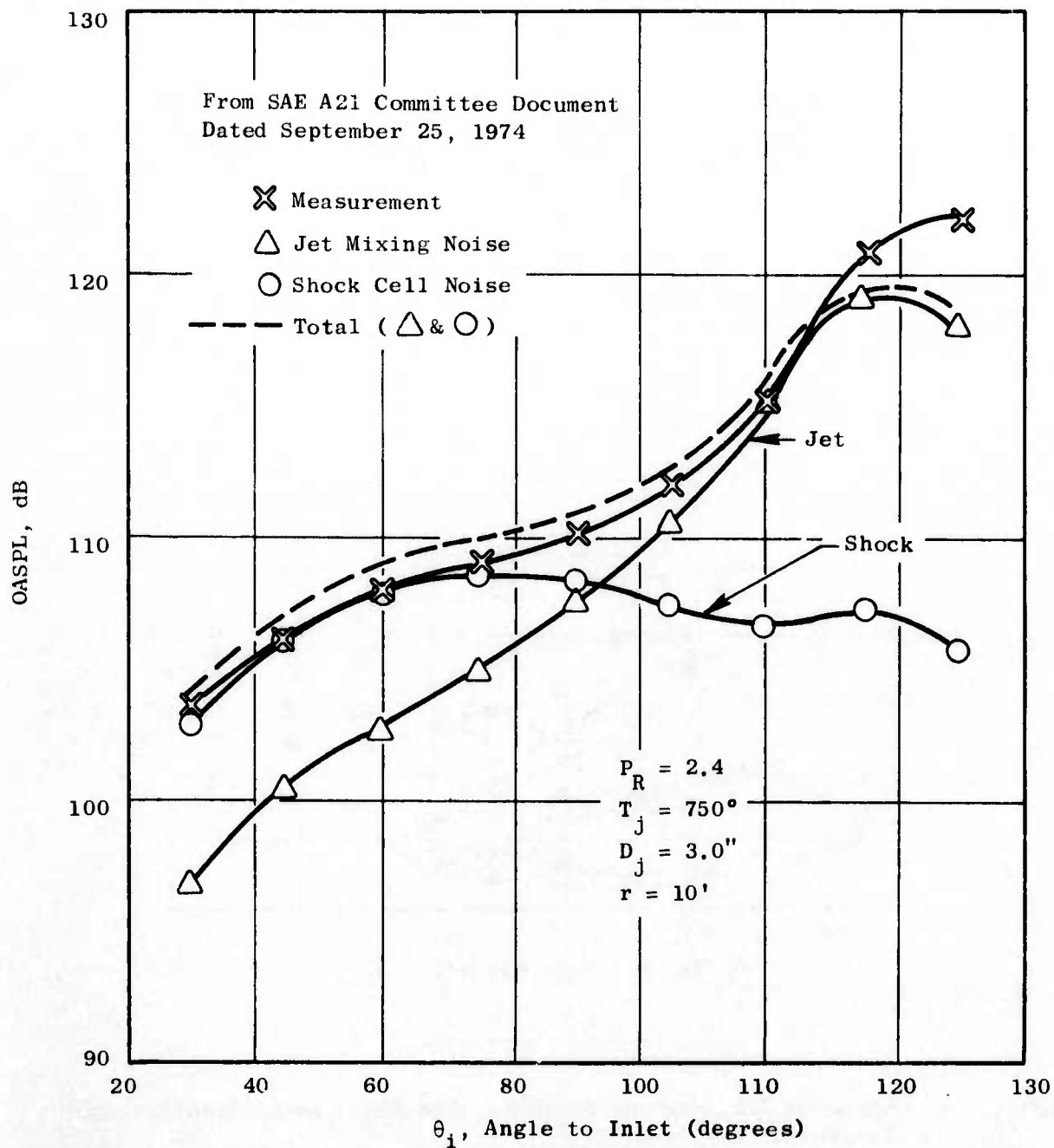Figure 342. Field Shapes, Effect of P_j/P_o at Constant V_j.

422

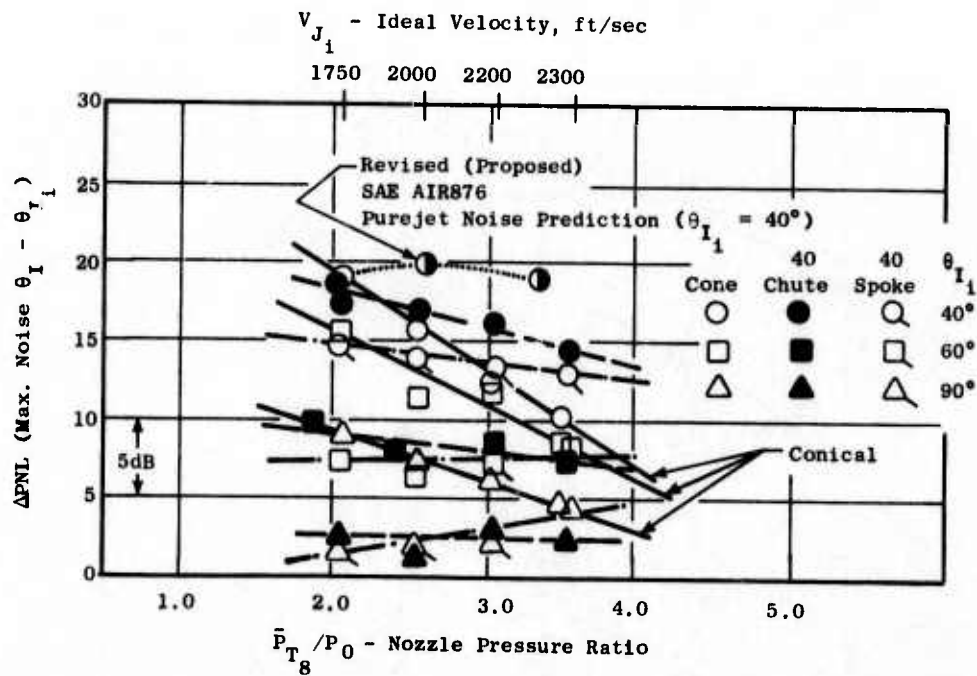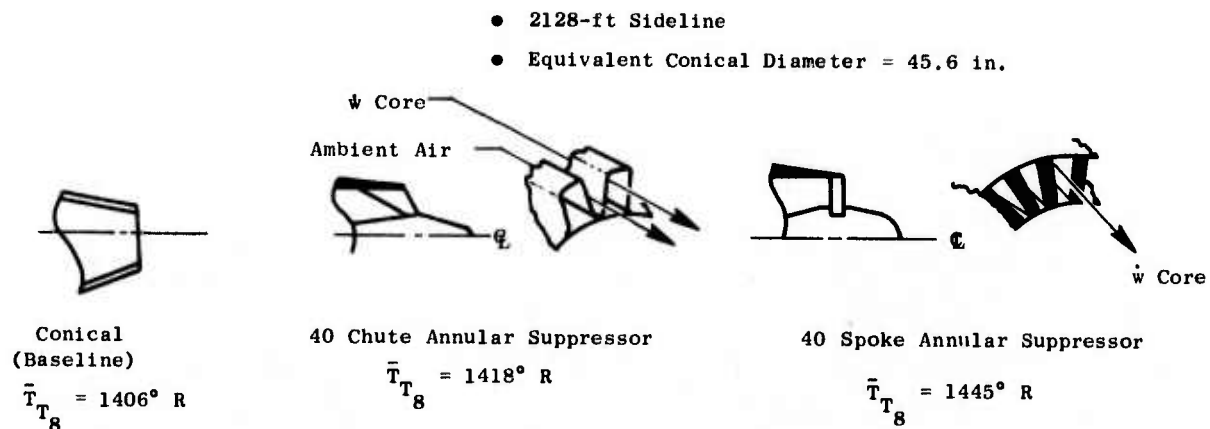Figure 343. Supersonic Jet Noise, Comparison of Measured Data with Jet Mixing Noise and Shock Cell Noise.

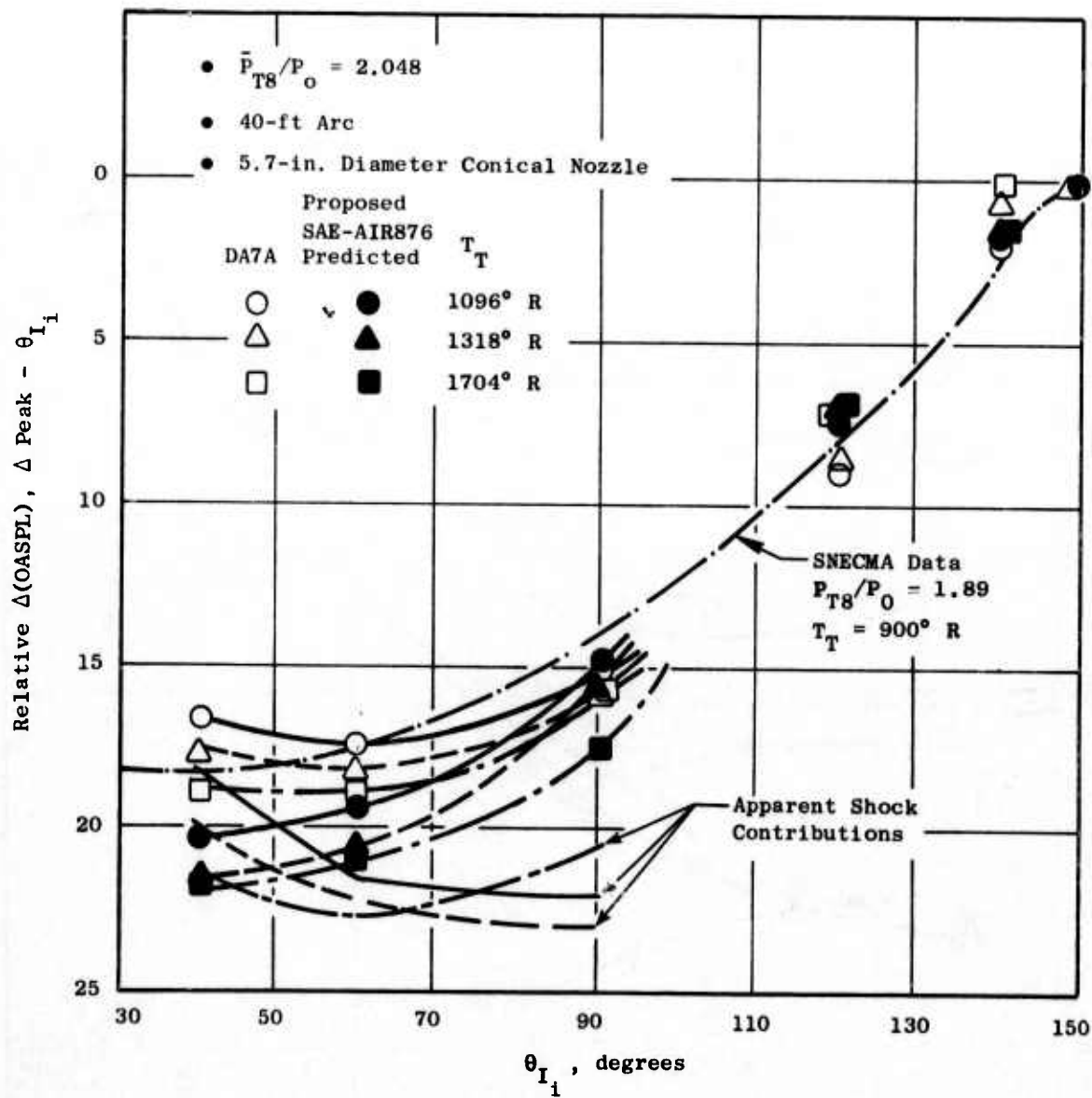Figure 344.   Apparent Influence of Shock-Related Noise Among Baseline and Suppressor Nozzles.
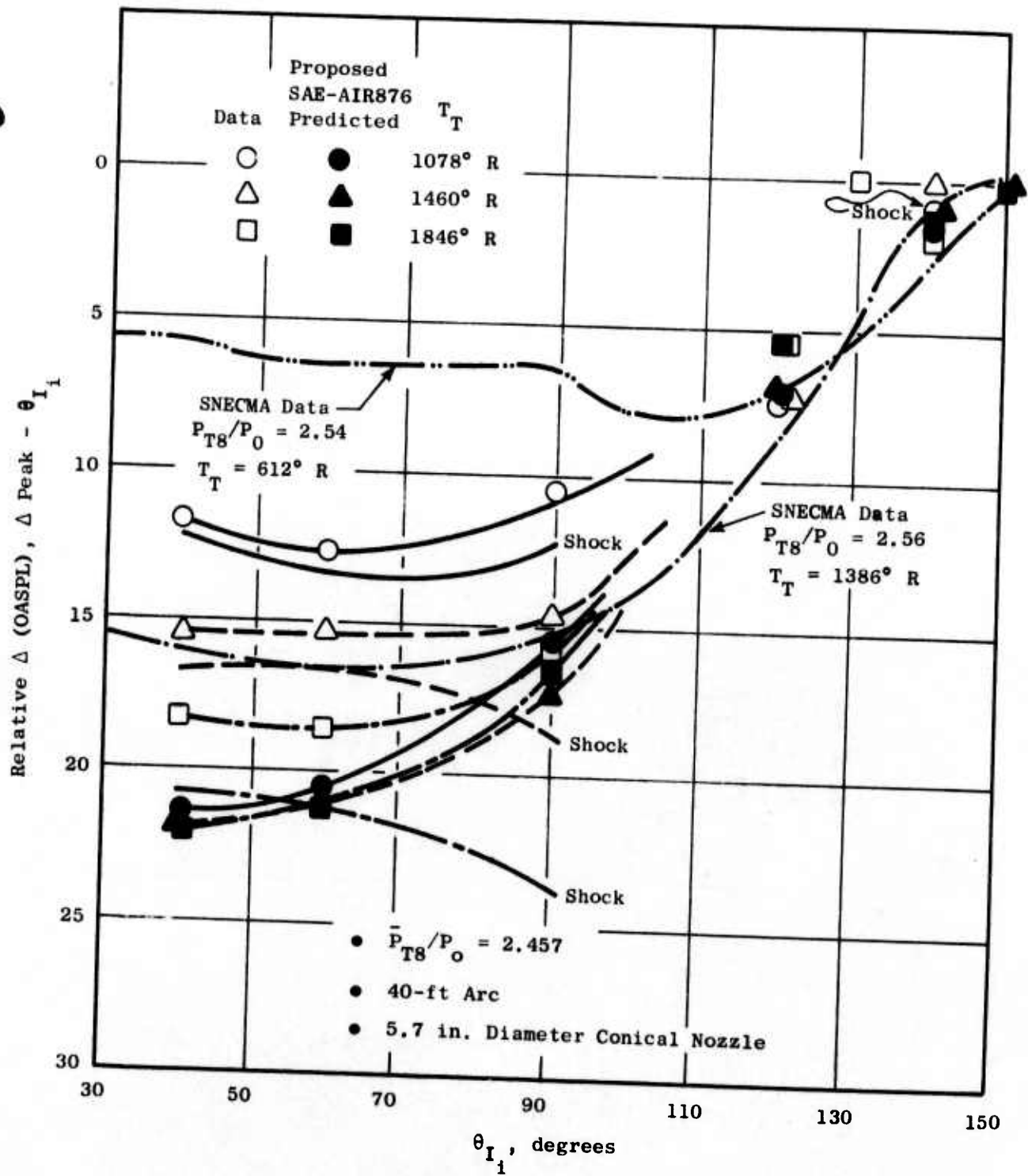
424

Figure 345. Relative ΔOASPL Versus Inlet Angle, P_{T8}/P_o = 2.048.

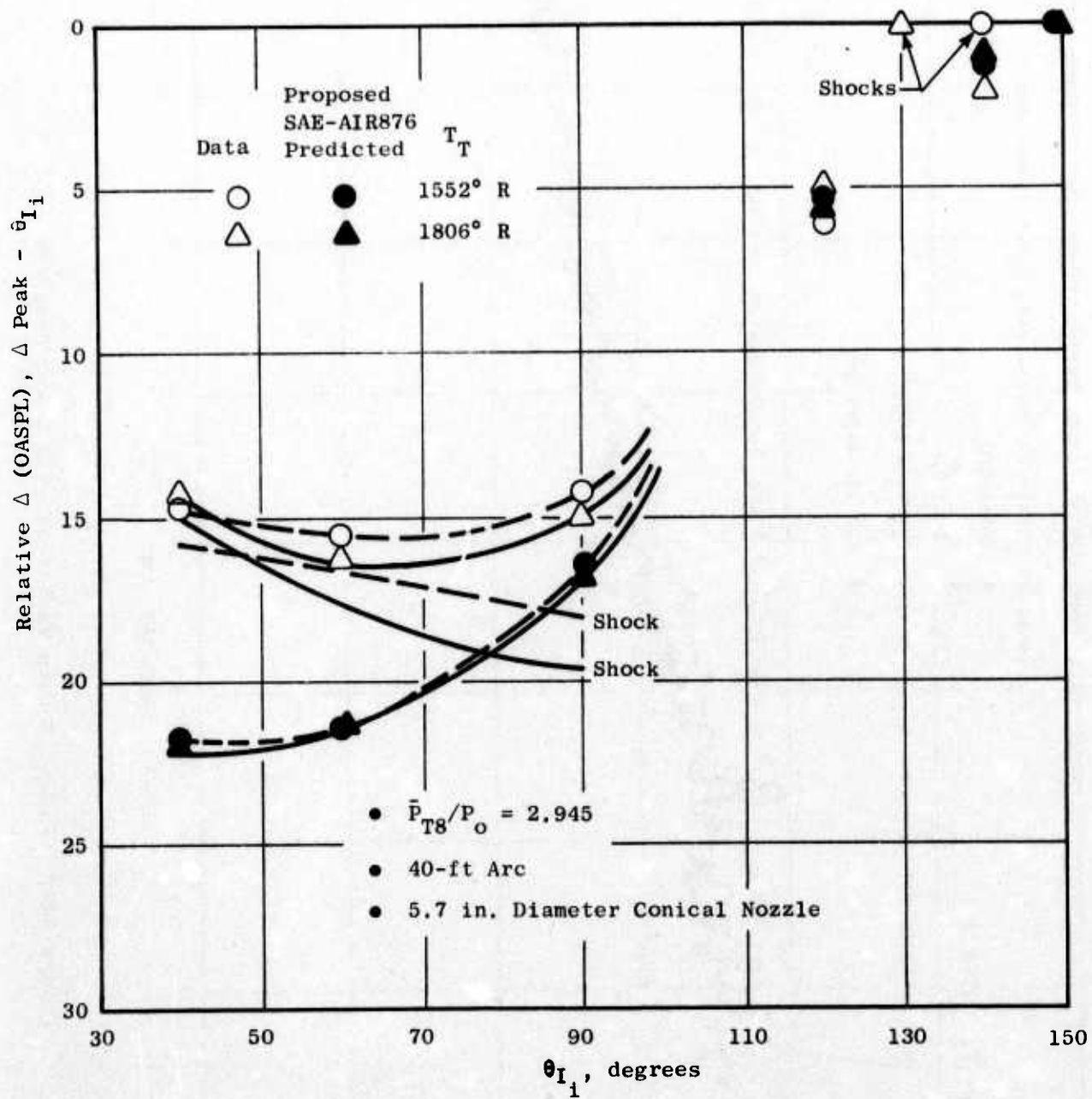Figure 346. Relative ΔOASPL Versus Inlet Angle, $P_{T8}/P_o = 2.457$.

426

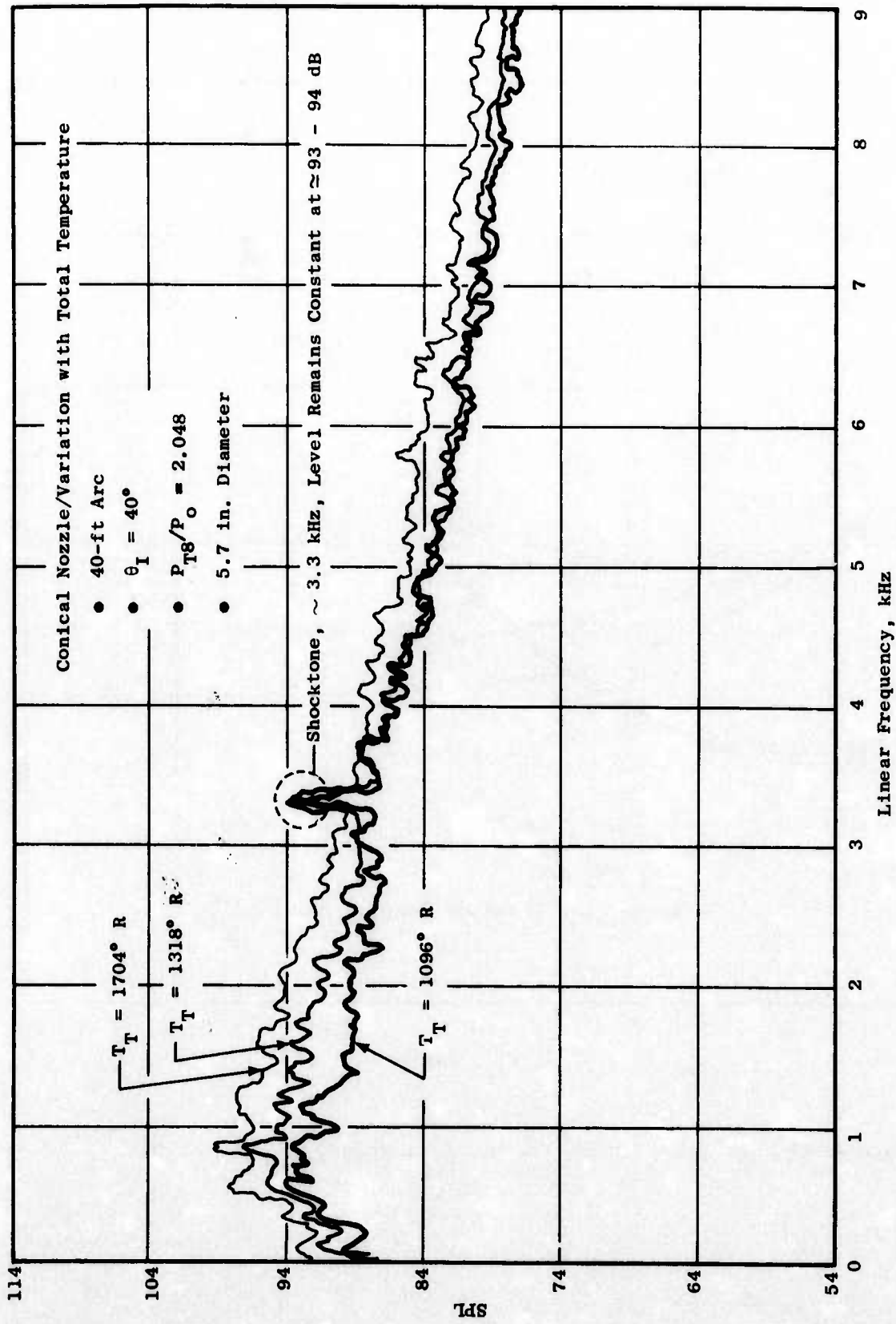Figure 347. Relative ΔOASPL Versus Inlet Angle, P_{T8}/P_o = 2.945.

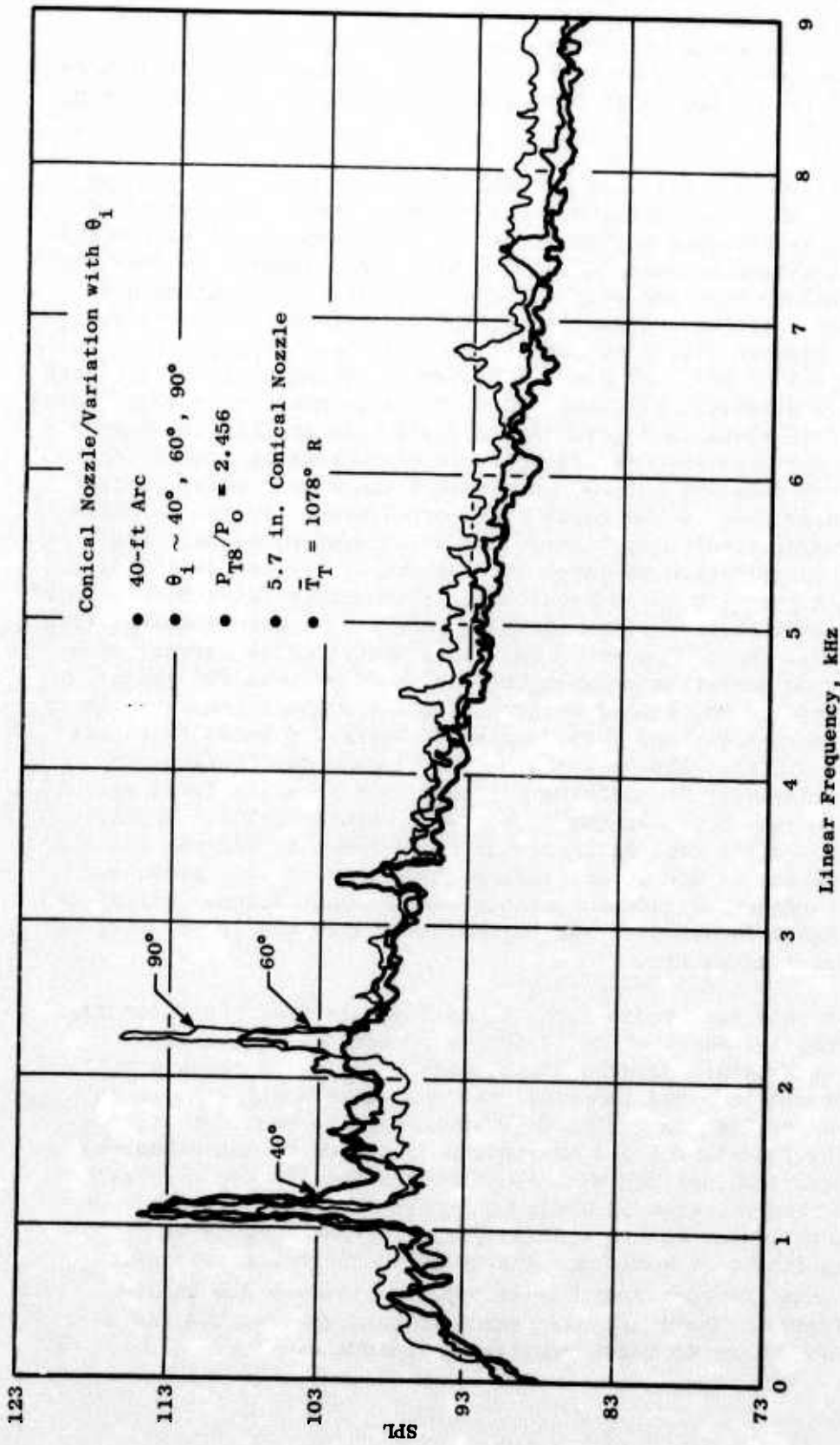Figure 348. Conical Nozzle Variation with Total Temperature.

Figure 349. Conical Nozzle Variation with θ_i.

In contrast, the ΔPNL characteristics of the 40-spoke and 40-chute annular/plug suppressors (Section 3.2.2) show little dropoff with pressure ratio, suggesting that the shock structure of the small suppressor elements tend to reduce the shock-related noise either through accelerated viscous dissipation and/or shielding of the inner jet by the outer portion of the element flow.

As a result of these observations, a small shock matrix for the conical nozzle was included in the final model suppressor tests previously described in Section 3.4.1. Three pressure ratios at two or more temperature excursions were included in this parametric exercise. The data are presented in "as-measured" (scale model) 40-foot arc data. Where possible, pertinent results from other sources are included wherever possible to substantiate the validity of the data trends. Figures 345, 346, and 347 present $\Delta OASPL/\theta_{peak} - \theta I_i$ for pressure ratios of 2.048, 2.457, and 2.945. The apparent influence of pressure ratio, even at the low pressure ratio condition, is quite evident in the forward angles. The SNECMA data shown in Figures 345 and 346 also exhibit the same trends. All the figures show the dramatic effects of increasing stagnation temperature (at a given pressure ratio), namely that the mixing noise contribution assumes a greater role in the total noise as witnessed by the increase in ΔOASPL with increasing total temperature. In an attempt to extract the equivalent broadband contribution of shock-related noise, Figures 345, 346, and 347 also include a pure jet noise prediction (proposed/revision SAE-AIR 876) from which the shock contribution lines shown in each figure were obtained (i.e., logarithmic difference). As can be seen, the shock contribution curves essentially show little or no deviation between the angles of 40° and 90° again verifying the Harper-Bourne and Fisher observations for a given pressure ratio. The only contrary observations from these series of tests are noted in Figure 346 (pressure ratio = 2.457). Although the shock-related contribution for each temperature is relatively insensitive to angle, the absolute level varies considerably more than that noted at the other two pressure ratios. Typical narrowbands obtained in the course of these tests are shown in Figures 348 and 349. Figure 348 shows the effect of increasing temperature (e.g., broadband increase) while the fundamental and/or harmonic remains unaffected. Figure 348 illustrates how the shock fundamental and harmonics (number and level) vary as the angle from the inlet moves aft.

The results from this very rudimentary study suggests that the currently proposed SAE techniques for shock noise do indeed appear to reflect the phenomenological observations. However, considerably more work appears to be in order not only for simple round (conical) nozzles but for suppressors as well. The question of scaling must also be answered in the near future, e.g., how does one scale the fundamental and harmonic(s) relative to the broadband - does it follow Strouhal scaling, and what is the effect during the all-critical wind-on flight mode? Indeed, even if a simple suppressor were to exhibit no discernible shock contribution during static operation, there would be no guarantee that during flight it would not emerge as a critical factor (with the assumption that only the turbulent mixing noise is reduced due to the relative velocity effect). There are also some indications that the non-U.S. SST has already observed some of these perplexing phenomena.

430